Fluid-rock interactions during blueschist and greenschist metamorphism in the Aegean area of Greece

Hazel Mary Barr

Thesis submitted for the degree of

Doctor of Philosophy
Edinburgh University
1989

Kastri, north-west coast, Syros

"I do not know what I may appear to the world, but to myself I seem to have been only like a boy playing on the sea shore, and diverting myself in now and then finding a smoother pebble or a prettier shell than ordinary, whilst the great ocean of truth lay all undiscovered before me."

Sir Isaac Newton

Acknowledgements

I would like to thank my research supervisors, John Dixon, and Colin Graham, for all their guidance, help, and encouragement, both in Edinburgh and in the field.

There are a vast number of people in the department who must be thanked for their help and expertise, particularly; Kenny Cameron, Eddie Clark, and Christine Lawley, for producing countless thin-sections, and probe slides; Pete Hill, John Craven and Stuart Cairns, for teaching me how to use the electron microprobe, and for all their efforts which keep the system running so smoothly; Yvonne Cooper and Diane Baty, for help with photography; Leo Harrison, for always producing my sought-after item from the depths of the stores; Heather Hooker, Denise Wilson and Helena Jack, for help with innumerable things, and a special thank-you to Heather for undertaking some 'very-last-minute' typing.

In East Kilbride, I would like to thank Tony Fallick, for his help and encouragement, and for running an excellent stable isotope lab. Thanks too to Alison, Julie and Terry, who made working there so trouble-free, and enjoyable. I am deeply indebted to Judy Kinnaird, St. Andrews University, for freely giving so much of her time and expertise to help me with the fluid inclusion work. Thanks also to Andy Rankin and Barry Foster, Imperial College, for providing expert advice on data interpretation, and sample preparation.

In the department I would like to thank all the other postgraduate students and research workers who have encouraged and helped me, in particular; Andy Baker, who smoothed so many of my computing problems; Steve Elphick, who initiated me into ultra-high quality polishing techniques, and Mark Welch, for many useful discussions on amphiboles. Thanks also to Claire Linklater, Ed Follows and Andy Poole, for being such good fun, and livening up the Grant Institute.

A huge thank-you must go to all my room-mates, who between them, have put up with a great deal over the years, and have always remained cheerful and good humoured. To Pete Winterburn, Pete Dymoke (thanks especially to them for all the bike maintenance !), Tracy Watson, Nana Kolocotroni, and Dave Whitmarsh, a big thank-you.

A very special thank-you goes to Sue Wallis, for being such a super friend, and flatmate, and sharing so much of the 'Edinburgh Experience'.

To all the friends outside the department, who have reminded me that there is more to life than geology. Special thanks to Frances Ritchie, all the teachers and kids at Mayfield primary Sunday school, especially Hilary, Nancy and Andy, and to Tina Lehmbeck, and Carson and Amanda Bergstrom for being such loyal friends

Financial support was provided by the Natural Environment Research Council, and the Department of Health and Social Security, and this is gratefully acknowledged.

This thesis is dedicated to my family, who have always supported, encouraged and loved me. To Niall, who was such a wonderful field assistant on Syros (Ποσ ειναι!), to Lorna, who has always been there when I needed a hug, and to my parents, who have done, and given so much that I can never hope to repay them.

ABSTRACT

The island of Syros, in the Attico-Cycladic metamorphic belt, is an excellently preserved blueschist terrain, consisting of alternating marbles and schists, with subsidiary meta-tuffs and metabasites. Blueschist metamorphism took place under P-T conditions of 14 to 19 kbars, and 470±30 °C. During uplift the blueschists were sporadically overprinted by greenschist assemblages, with the development of chlorite, calcite, albite and actinolite.

Petrographic study led to the idenification of stable blueschist and greenschist mineral assemblages. Schreinemakers analysis, and equilibrium thermodynamic calculations, using an internally consistent data-set, led to the construction of T-X_{CO2} sections, from which the composition of the fluid in equilibrium with the blueschist mineral assemblages could be determined. The fluid composition was found to be very water-rich, with less than 0.1 mol% CO_2 present. This conclusion was reinforced by preliminary fluid-inclusion data, which only detected aqueous fluids in quartz and garnets from blueschist samples. Samples collected on an outcrop scale enabled the relative roles of fluid buffering and infiltration to be assessed. Individual rocks record difference in the equilibrium fluid composition, even at outcrop scale. This suggests that the rock layers have buffered the coexisitng fluid composition and very little, if any, fluid communication and exchange has occurred between layers.

$\delta^{18}O$ analyses of whole rocks and mineral separates from the blueschists show a close approach to isotopic equilibrium. However, isotopic homogenization has not occurred between heterogeneous layers, and values of $\delta^{18}O_{qtz}$ from schist layers, collected on a scale of 1.5 metres, range from 17.5 to 20‰. It appears that the isotopic composition of the fluid, as well as the CO_2/H_2O ratio, has been buffered internally during blueschist facies metamorphism.

The conclusion of closed system behaviour in the blueschists does not explain the common occurrence of lawsonite, a feature which appears to require large-scale infiltration of H_2O-rich fluid. This paradox remains unresolved, but genesis of lawsonite may involve a process of C-burning in graphite-bearing schists.

The blueschist to greenschist transformation involves hydration and carbonation reactions, and both heat and fluid are required to drive the alteration process. In

the majority of the greenschist rocks isotopic evidence suggests that the volume of infiltrating fluid involved is low, with fluid-rock ratios around 0.05 to 0.01. In these rocks the infiltrating fluid has had little effect on the isotopic composition of the rocks, as the buffering capacity of the rock units has not been exceeded. High fluid-rock ratios (F/R ratios up to 4:1) have been identified in a few outcrops, where zones of channellized flow have produced much larger fluid fluxes. In these outcrops an approach towards $\delta^{18}O$ homogenization is demonstrated by the small isotopic variations found on an outcrop scale bewteen mafic, pelitic and carbonate rocks, despite the original isotopic differences which would have existed prior to infiltration.

The results of this study are consistent with the peak metamorphic event having occurred in a subduction zone. Although subduction zones are sites of high fluid flux, the Syros blueschists have experienced a limited fluid flux during the primary event. This may reflect the channellized nature of fluid flow in the subduction environment, which allows some rocks to experience infiltration, while others, isolated from fluid channelways, 'see' very little external fluid (e.g. Syros). The infiltrating fluid required for the greenschist alteration was probably generated at depth within the subduction zone, and channelled up-dip into the overlying wedge, along planes of structural weakness. The fluid could then interact with the uplifting blueschists, causing alteration.

CONTENTS

CHAPTER 1

INTRODUCTION

TABLE OF CONTENTS

1.0 OUTLINE AND AIMS OF THE PROJECT

This chapter discusses the aims of the project, and outlines the contents of the thesis. It also aims to provide a brief summary of the published literature on fluid-rock interaction studies, which are of relevence to this thesis.

This thesis aims to provide important comparative data on fluid-rock interactions under high-pressure, low-temperature conditions. Previous studies have largely considered greenschist and amphibolite facies terrains, and very little work has been undertaken on blueschists. There is a need for a unified model of fluid generation and transport in blueschist facies rocks because the P-T conditions experienced, and the tectonic regimes required to generate these conditions are very different to anything encountered during normal Barrovian metamorphism.

To set the scene, the following section briefly compares the tectonic settings of greenschist/amphibolite and blueschist facies rock.

The basic characteristics of greenschist-amphibolite facies metamorphism can be explained by the action of collision events, causing crustal thickening (England & Thompson 1984, Thompson & Ridley 1987), followed by uplift and erosion. After the thickening event, the rocks heat up, partly through the generation of internal heat, and partly through the conduction of heat from below. The extent of the temperature rise, will depend on a number of factors, i.e. the rate of internal heat production, thermal conductivity, length of time before onset of erosion, rate of erosion etc. (England & Thompson 1984). Partial melting may occur in the deeply buried rocks (<35km, England & Thompson 1984), which are subjected to higher temperatures. These *in-situ* melts are more or less granitic in composition, and may coalesce and rise through the crust driven by buoyant forces. As the rocks approach the surface, the loss of heat to the surface exceeds that generated internally, and they will cool down. This cycle of burial and steady-state exhumation produces the familiar clockwise path on P-T-t diagrams.

As mentioned above, blueschist facies rocks require very different tectonic regimes for their formation. Two problems exist: firstly, how to generate the high-pressure, low-temperature conditions to form the blueschists; secondly, how to preserve them and transport them back to the surface. It is now recognised that the thermal conditions for blueschist metamorphism commonly occur at convergent plate margins where oceanic crust is transported into the mantle depressing the regional isotherms. However, blueschist metamorphism can occur in other situations, such as the tectonic

loading of a continental plate, as is the case for the blueschists of the Seward peninsula, Alaska (Forbes *et al.* 1984). Thermal models (England & Thompson 1984; Ridley 1982; Thompson & Ridley 1987), suggest that blueschists could also form during the early stages of a collisional event. However, these rocks are unlikely to be preserved during uplift.

Many models have been put forward to explain the generation of blueschists based on the inferred processes occurring in subduction zones. Most of these involve the repeated addition of cold material to the base of the overlying accretionary prism (Draper & Bone 1981, Platt 1986, Ridley 1982). The continual addition of cold material effectively prevents the rocks from heating up, and so low temperatures can be maintained, even at great depths.

Having generated the blueschists, the problem becomes how to preserve them during uplift. As soon as subduction ceases the rocks will begin to increase in temperature, and if uplift is not sufficiently rapid, the blueschist assemblages will be prograded to greenschist or amphibolite facies. Uplift models fall into two camps, those considering post-subduction uplift, and those considering synsubduction uplift.

Examining the latter case first, Ernst (1974, 1988) proposed a mechanism of return-flow, whereby material is underthrust back up the subduction zone. As subduction is still occurring, the rocks are kept cool during their return journey to the surface by the continuing addition of cold material to the descending slab. Although this model satisfies the thermal constraints, it is difficult to envisage Ernst's mechanism for return-flow working in practice. However, high-grade blueschists *appear* to have been exhumed in circum-Pacific terrains, such as the Franciscan, without the apparent involvement of collision, unless missing, obliquely-impacted microcontinents are involved. Peacock's model (1987) incorporates an inverted metamorphic gradient in the early accreted material, caused by the conduction of heat from the hanging wall down into the top of the descending slab. This inverted gradient is preserved by the continued subduction of oceanic lithosphere which removes heat from the hanging wall. Peacock suggests synsubduction uplift (isobaric cooling) as a mechanism to return the blueschists to the surface intact, while allowing geologically reasonable uplift rates of $<1 mm yr^{-1}$. The problem with Peacock's "refrigeration" model is that it does not appear to consider internal heat production. Certainly, while subduction is proceeding and cold material is being added at depth, the temperature might not increase significantly with depth, but even in a subduction zone, the temperature will tend to increase downwards, and heat will still be supplied from below. In Cloos'

model (1982, 1984), flowing mud-matrix mélanges are generated in a "flow-channel" beneath the accretionary wedge. The upwelling mélange can remove blocks of blueschist and eclogite facies rocks accreted at an early stage of subduction, and transport them back to the surface. This convection-like system would tend to obliterate all structures, and while such a model may explain the mélange units commonly associated with blueschist terrains, it is not a general model which can be applied to the uplift of structurally coherent, regional blueschist terrains, such as occur in the Aegean area.

If uplift is viewed to occur as a post-subduction event, then it must be extremely rapid to prevent a significant rise in temperature.

Draper and Bone (1981) examined the rates of erosion needed to successfully return blueschists to the surface. The rates required are obviously dependent on the heat producing capacity of the rocks, but assuming an average heat-production rate (~4-5 $calgm^{-1}yr^{-1}$ Draper and Bone 1981), erosion rates would have to be extremely fast, $0.14cmyear^{-1}$ to exhume the rocks more or less isothermally. It seems fair to comment that for the majority of situations, the proposed rate of uplift is greater than that which could be produced by erosion alone, and therefore some form of tectonic uplift is required. Platt (1986) suggests that underplating of material at the base of the accretionary wedge, accompanied by stabilizing extension higher up, is the driving mechanism behind the uplift of high P, low T rocks. This is an extension of the "critical wedge theory" of Chapple (1978), as expounded for foreland thrust belts by Dahlen *et al.* (1984). The extension of the wedge is accommodated by listric normal faulting which thins the sequence. This mechanism appears to be plausible, but as yet definitive field evidence to support the model is lacking. Ernst (1988) suggested a model of uplift through collision for those blueschists which show a partial greenschist overprint. According to this model, after the collisional event the blueschist rocks should rise to the surface driven by buoyant forces. This model may contain some truth, but it is difficult to see why the blueschists should return to the surface quickly, driven only by erosion and isostatic rebound. They would probably remain trapped in the locked subduction system, and experience a temperature rise causing extensive overprinting or total obliteration.

It is apparent that further work is needed on the thermal evolution of blueschists in order to fully understand all the processes involved. However, the basic elements of all the thermal models are the same, and involve the continuous addition of cold material to the wedge to keep the temperature low in the initial stack, and either rapid

uplift, to prevent prograde "retrogression", or protracted cooling, i.e. the continued subduction of cold material, to allow the subducted rocks to be uplifted more slowly. If lateral heat conduction or advection is neglected for simplicity, then a one-dimensional approach is reasonable. Ridley, (1982) was successfully able to reproduce the characteristics of blueschist metamorphism on Syros using a simple one dimensional model, where the rate of addition of cold material at the base of the structural stack was balanced by the removal of material from the top.

From this discussion it is clear that the tectonic regimes required to produce greenschist/amphibolite facies rocks and blueschist facies rocks are very different. Fluid sources and pathways will also be different in the two facies, and some of these differences are considered below.

1) Greenschist and amphibolite facies

In the case of greenschist and amphibolite facies rocks, temperature will generally increase regularly with depth, and devolatilization reactions will provide the major source of fluid during metamorphism. If partial melting occurs at depth in the crust, any free volatiles available will participate in melting reactions, leaving the surrounding rocks dehydrated. However, during the ascent and emplacement of this magma, volatiles may exsolve and could then infiltrate the surrounding rocks.

2) Blueschist facies

In subduction zones volatiles as well as crustal material are recycled. Fyfe *et al.* (1978) calculated that the amount of water subducted is approximately $10^{15}ga^{-1}$ and this fluid must escape from the descending plate and be recycled. Otherwise, as Fyfe *et al.* (1978) point out, the subduction process would have removed the oceans long ago. Therefore fluids released by devolatilization reactions and any interstitial fluid will tend to be expelled. It appears from several studies (Cloos (1984), Moore (1987), Vrolijk *et al.* (1988) that some fluid will migrate "up-dip", parallel to the subduction thrust, with the fault zone acting as a fluid channel at shallow levels in the subduction zone, and hydrothermal vents have now been described from active fore-arc regions such as Barbados (Westbrook and Smith 1983). Vrolijk *et al.* (1988) determined fluid temperatures in the decollément zone from fluid inclusions, and found that the temperatures were higher than predicted by conductive heat flow models. They interpreted this difference to be due to the escape of warm fluids from deeper parts of the subduction zone. The movement of fluids along the decollément

zone could affect the thermal structure of the subduction zone (Oxburgh & Turcotte 1976), and fluids transporting heat from deep to shallow levels of the subduction zone, could help to keep the rocks at depth cool. The production of fluids, and fluid flow, obviously occurs in subduction zones, but much less heat is available overall, and the synsubduction increase of temperature with depth will be very much less than that experienced in medium pressure terrains. This means that the thermal structure of subduction zones will be very sensitive, both to the movement of material and fluids, and the thermal structure may be much more complicated than predicted by conductive thermal models.

Dehydration reactions occurring on subduction will be endothermic, and will thus act as energy sinks, further cooling the subducted rocks (Anderson 1977). If significant quantities of relatively unaltered igneous rocks are present in the subducting sequence, then the initial prograde reactions in these rocks will be hydrating, (exothermic), and fluid will be removed from the system. The low geothermal gradients encountered in subduction zones mean that melting will not occur at shallow levels. However, the fluids released deeper down from subducted material play an important role in associated arc magmatism (Wyllie & Sekine 1982). Wyllie and Sekine (1982) suggest that aqueous fluids derived from the dehydrating subducted crust cause melting at depths greater than 100km down the subduction zone, ultimately producing tholeiitic and calc-alkaline magmas.

Discussion

While fluids are obviously present during both greenschist/amphibolite and blueschist facies metamorphism, the fluid regime encountered in a subduction zone is significantly different and more complicated, than that for medium pressure rocks. If metamorphism occurs at the maximum depth reached, then for any subducted sediment packet this will be at the point prior to underplating. The packet will be underlain by what fails to be underplated, and whether or not fluid is available at this point in time will depend on the nature of the underlying material. If it is largely composed of oceanic crust with a thin veneer of pelagic sediments, then the fluid generating potential of the sequence will be low, regardless of temperature. However, if a continental margin with an associated thick wedge of sediments is being subducted, the fluid generating potential will be much higher. The amount of fluid produced may be enhanced further in this situation because it is intrinsically difficult to subduct continental sequences due to buoyant effects. Instead, they will tend to "stick" in the subduction zone and heat up. Alternatively, fluids travelling up-

dip from deeper levels may provide a fluid source at the time of underplating. What is not clear from the steady state models is whether enhanced fluid infiltration is to be expected during uplift. Any particular sediment packet will be uplifted through the wedge by the continued underplating of new material, and the underlying material will now be another sediment packet undergoing blueschist metamorphism. There is no reason why uplifted packets should experience an increase in the (probably quite small) amount of fluid available from below, because the potential fluid sources have remained the same. However, channellized fluids may be introduced laterally into the wedge from much deeper sources. In order to construct and maintain the wedge, a combination of underthrusting, and extensional thinning (via listric normal faulting) must occur. These processes will produce a network of structural surfaces within the wedge which could act as conduits for upward-moving fluid derived from deeper down. Thus uplifted packets could experience extensive infiltration if intersected by one of these fluid channels.

Conclusions

In conclusion, the differences in PT conditions, tectonic and fluid regimes mean that models of fluid-rock interaction formulated for greenschist and amphibolite facies rocks may not apply under blueschist conditions. The ultimate aim of this project is to develop a unified model of fluid generation and transport in a blueschist regime, using a variety of analytical techniques. There are two main main objectives. The first is to assess the role and extent of fluid infiltration under blueschist facies conditions, coupled with work to determine the composition of the syn-metamorphic fluid. The second relates to the role of fluids in the blueschist to greenschist transformation. In common with many other high-pressure, low-temperature terrains, the Syros blueschists are partly overprinted by later, lower pressure, greenschist facies assemblages. The development of the greenschist overprint involves hydration and carbonation reactions, and thus *both* fluid and heat are required to drive the alteration process. This study examines the evidence for fluid infiltration during the blueschist to greenschist transformation, and attempts to constrain the volumes of fluid required.

The work fell into five main parts, each of which forms the basis of a chapter.

Two short field seasons were spent on Syros, Greece. Most of the fieldwork involved detailed sampling of blueschist and greenschist facies rocks, with an emphasis being placed on carbonate-bearing metasediments.

The mineralogy and chemistry of the blueschist facies samples were used, together with mineral assemblage data, to construct a model system, and all possible reactions between the model phases were determined. Using available P-T-X data, and a computer program, the positions of the fluid-rock equilibria were constrained, and the fluid composition in equilibrium with the different mineral assemblages was deduced. The importance of internal versus external fluid composition control for the blueschists was determined from the spatial relationships of the different mineral assemblages.

Stable isotope analysis was carried out on whole rock and mineral separate samples from blueschist and greenschist facies rocks. Isotopic work on blueschist facies rocks confirmed the conclusions about fluid infiltration suggested by the mineral equilibria studies. Stable isotopes were also used to assess the role of infiltration in the blueschist to greenschist transformation. Various other aspects of the fluid-rock interaction history were examined, mostly dealing with questions about fluid transport, i.e do thick marbles act as fluid barriers ?, do albite porphyroblast schists delineate former zones of high fluid flux ?, etc. Work on the extent of isotopic equilibrium in both metamorphic events, and some isotopic geothermometry was also carried out.

The mineralogy and chemistry of the greenschist facies rocks have been considered, but in less detail than for the blueschist rocks, and onsiderable further work could be carried out. Preliminary fluid inclusion data was collected mainly to ascertain if the blueschist fluid compositions predicted by the mineral equilibria studies corresponded to the compositions of any fluid inclusions in the rock. Information about the salinity of the proposed primary fluid was also determined.

Terms and definitions

The term blueschist/s is used in a general way to describe the rocks which, having experienced the high pressure metamorphic event, have remained essentially unaltered.

The term greenschist/s refers to those rocks which bear some mineralogical evidence of the greenschist facies overprint, i.e samples in which the high pressure mineralogy has been partially or completely destroyed, and replaced with secondary calcite, chlorite, albite and actinolite. A number of other terms are used to refer to these rocks in the text depending on the degree of alteration, i.e (partially) altered blueschists, or retrogressed or retrograded schists/metabasites/samples.

1.2 FLUID-ROCK INTERACTIONS - INTRODUCTION

The following sections provide a brief summary of the current ideas in fluid-rock interaction studies.

Traditionally, the study of metamorphism and metamorphic rocks has been approached as an investigation into the mineralogical changes which occur in response to changing pressure and temperature conditions. However, the presence of fluid inclusions in metamorphic minerals (Crawford and Hollister 1986), the depletion of high grade rocks in volatiles (Shaw 1956), the ubiquity of hydrated and carbonated mineral phases and the common occurrence of veins, all points to the presence of a volatile phase during metamorphism. This conclusion is supported by more tangible evidence from modern geothermal fields where metamorphism is seen to be occurring in the presence of a fluid phase (Keith *et al.* 1968; Muffler and White 1969; Thomasson and Kristmannsdottir 1972). During the past three decades, fluid-rock interaction studies have shown that far from being a passive by-product, fluids play a very active role in metamorphism. As well as initiating mineral reactions, fluids can act as effective heat transfer agents, locally controlling the thermal structure of an area (Ferry 1984b, 1983c, 1980a; Ferry and Rice 1982), and thus, fluids have been proposed as one of the fundamental driving forces of crustal metamorphism.

The aims of most fluid-rock studies in metamorphic rocks are to identify and quantify the following:

-fluid sources

-fluid compositions

-fluid-rock ratios

-fluid pathways

-mechanisms of fluid transport

The following sections will briefly consider each of these topics in turn.

1.1 FLUID SOURCES

A number of different fluid sources have been put forward by various authors. Examples include CO_2 derived from the outgassing of a carbonated mantle (Newton *et al.* 1980, Wyllie 1987), degassing of hydrated oceanic crust in a subduction zone (Wyllie 1982, Wyllie and Sekine 1982), and release of fluid from crystallizing

magmas. Until recently it was assumed that surface waters (i.e. meteoric water and sea-water) were of limited importance as a fluid source in regional metamorphism. However, work by Wickham and Taylor (Wickham and Taylor 1985; Wickham and Taylor 1987) suggests that large volumes of sea-water have penetrated to depths of 8-12 kms during high T, low P metamorphism in the French Pyrenees, causing isotopic homogenisation and high-level melt phenomena. Wickham and Taylor (1985) also point out that extremely deep circulation of ground waters has been demonstrated in other areas of rifted continental crust, such as the Imperial Valley, California (Muffler and White 1969), and the east Greenland-Skaergaard dike swarm (Taylor and Forrester 1979).

The fluid sources listed above will all be important in specific instances, but the single most important fluid source in prograde metamorphism is undoubtedly devolatilisation reactions occurring in the rocks themselves (Walther and Wood 1984; Walther and Orville 1982; Wood and Walther 1986). When an argillaceous sediment is initially deposited it has a high porosity of up to 50 volume % (Fyfe *et al.* 1978). The sediment consists of hydrated phases, such as kaolinite, and mixed layer clays belonging to the montmorillonite and illite groups, with some additional quartz, carbonate, and organic material (Frey 1978). During burial, compaction occurs by collapse of the pore space, and the initial porosity decreases rapidly, causing expulsion of much of the original pore fluid. However, H_2O and CO_2 held in hydrated and carbonated mineral phases remains, and it is this structurally bound fluid which is later released during devolatilisation reactions accompanying metamorphism.

The main species released by devolatilisation reactions are H_2O and CO_2, though small amounts of other phases such as CH_4 and H_2S can also be produced. Kerrick (1974) calculated the slopes for the 5 possible types of H_2O-CO_2 devolatilization equilibria on T-X sections, and these are illustrated in figure 1.1. Walther and Orville (1982) calculated that the metamorphic devolatilisation of 1kg of "average pelite" would produce 1.44 moles of H_2O and 0.55 moles of CO_2. If all this fluid was released at 500 ^{o}C and 5 kbars, it would occupy 12% of the rock by volume. However, not all rocks have the same fluid generating potential. This depends partly on the original lithology, (a quartzite, for instance, has little potential to generate fluid), and partly on the P-T path followed by the rock.

Within any particular rock volume, fluid release by devolatilization reactions is likely to be episodic, and Walther and Orville (1982) make the point that a discrete fluid phase will only be present when devolatilization reactions are actually occurring.

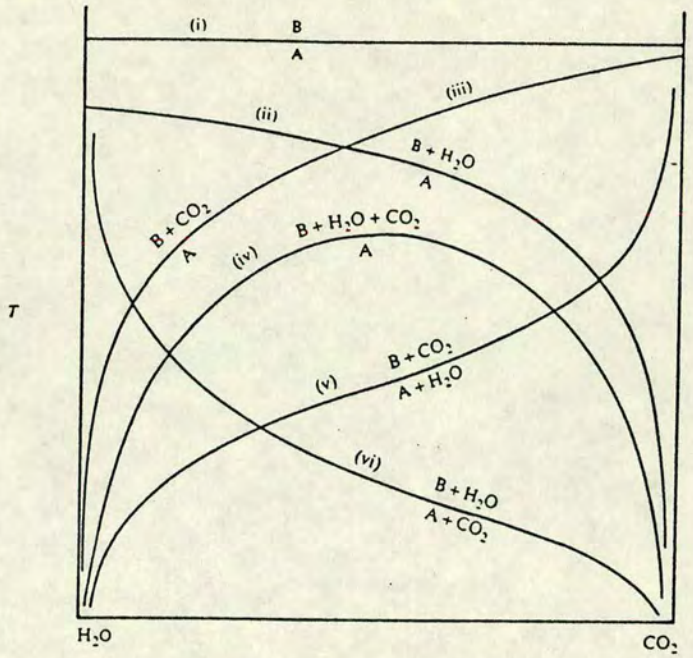

Figure 1.1 The five possible topologies of univariant mineral-fluid equilibria plotted on an isobaric T-XCO_2 diagram. (from Kerrick 1970)

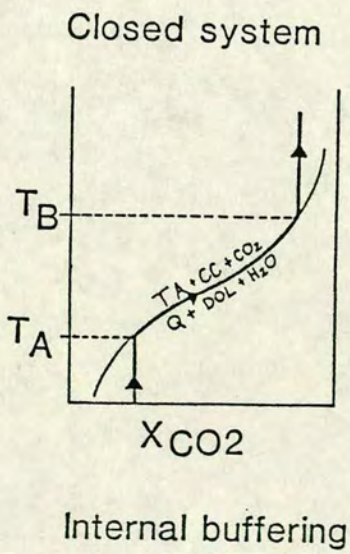

Figure 1.2a Internal control of the fluid composition, buffering. The initial fluid has a composition of $XCO_2 = 0.25$. Addition of heat raises the temperature of the rock until the reaction boundary is intersected at T_A. Further addition of heat causes the reaction to proceed, consuming quartz, dolomite and H_2O and producing talc, calcite and CO_2, thereby increasing the mole fraction of CO_2 in the fluid phase. The path of the fluid composition follows the univariant curve until one of the reactants is used up when the assemblage loses its buffering capacity, as is shown above, or when an invariant point is reached.

Consequently, Thompson (1983) and Walther and Orville (1982) suggest thatregionally metamorphosed rocks will experience time intervals when little or no fluid is present. However, in practice, the supply of fluid to any particular rock volume should be effectively continuous. As isotherms and reaction isograds move through a column of rock undergoing progressive metamorphism, so the timing of reactions will be diachronous throughout the pile.

1.2 FLUID COMPOSITIONS

The characterization of metamorphic fluid compositions can be approached in a number of different ways. In the case of a geothermal field, the coexisting fluid can be sampled and analysed directly. However, when dealing with deeply buried metamorphic rocks, fluid inclusion and mineral equilibria studies are the two techniques most commonly used to characterise the composition of the now absent fluid phase.

Fluid inclusion studies.

The study of fluid inclusions in metamorphic rocks has been slow to develop, largely because it was felt that the composition and density of fluid inclusions could be subject to post-entrapment modifications (Roedder 1981a, 1981b). However, several studies of fluid inclusions in metamorphic rocks have shown that the CO_2/H_2O ratio of fluid inclusions corresponds very well to that predicted from the observed mineral assemblages (Crawford and Hollister 1986; Crawford *et al.* 1979). Also, CO_2-bearing inclusions from granulite terrains consistently display densities appropriate to the independently-determined pressures and temperatures of metamorphism (Newton *et al.* 1980; Sisson *et al.* 1981; Touret 1977). This suggests that fluid inclusions can preserve peak metamorphic fluids. Fluid inclusions also provide important information about the fluid composition which cannot be obtained by other means. For example, fluid inclusion studies have demonstrated that most aqueous metamorphic fluids contain dissolved salts. These are mostly NaCl, but KCl, $MgCl_2$ and $CaCl_2$ have also been detected (Crawford 1981b; Roedder 1984). Such information is important in understanding the P-V-T-X relations of metamorphic fluids, for example, the increased immiscibility of H_2O-CO_2 fluids in the presence of NaCl (Bowers and Helgeson 1983a, 1983b).

Mineral equilibria studies

The composition of a fluid in equilibrium with an observed mineral assemblage can be calculated using basic thermodynamic expressions which describe the relationship between solids and a coexisting fluid. The thermodynamic expressions used to describe mineral-fluid equilibria include terms which account for impure solids, and non-ideal mixing in real fluids. The only other information required is an independent estimate of the P-T conditions of metamorphism. A fundamental aim in fluid-rock interaction studies is to determine the extent to which mineral assemblages in a rock have controlled the composition of the coexisting fluid. In his influential paper on "The buffering of pore fluids by metamorphic reactions" Greenwood (1975) compared the condition of internal buffering, where the composition of the fluid is solely controlled by local devolatilization reactions occurring within that rock volume, to the situation of external buffering, where the fluid composition is controlled by a large external fluid reservoir. These concepts are explained diagrammatically in figure 1.2. The internal control of metamorphic fluids has been cited by many authors (Ferry 1976a; Ghent *et al.* 1979; Hewitt 1973; Rice 1977b; Rumble 1978), and it is thought to be a common phenomenon in metamorphic rocks, but clear examples of fluid infiltration have also been documented. For example, the most commonly quoted paradox in fluid-rock interaction studies involves the composition of fluids in equilibrium with impure metacarbonates. The paradox arises because these rocks contain assemblages which imply an H_2O-rich equilibrium fluid, yet the fluid evolved from the rocks during prograde metamorphism must have been CO_2-rich (assuming that the carbonates were the source of the calc-silicates now present). However, when the action of an external H_2O-rich infiltrating fluid in the system is recognised, the paradox disappears, as progressive dilution and flushing of generated CO_2-rich fluids by external H_2O can be invoked. In many cases the source of this infiltrating fluid can be traced to devolatilization reactions occurring in neighbouring, and more plentiful, pelitic lithologies.

1.3 FLUID-ROCK RATIOS

Fluid-rock ratios attempt to place a limit on the amount of fluid which has interacted with a rock. The methods used to calculate these ratios fall into two main categories.

1) Reaction progress

When a fluid infiltrates a rock volume, and the two are not in chemical equilibrium, reactions will proceed between the fluid and the minerals forming the rock.

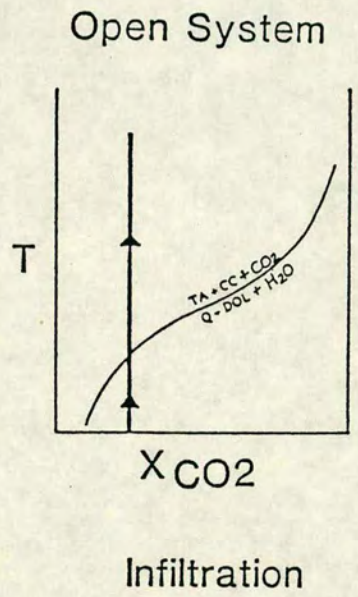

Figure 1.2b In this example the fluid composition is externally controlled by infiltration of large quantities of fluid. The path of the fluid corresponds to a vertical line on the T-XCO_2 diagram because the fluid composition is imposed on the rocks. The large volume of infiltrating fluid involved means that the small volume of fluid generated internally cannot affect the overall composition. The buffering capacity of the rocks is exceeded and the fluid composition is controlled externally.

If the pre-existing modal mineralogy of the rock is known, or can be estimated, and a net-transfer fluid-driven reaction can be identified, then the progress of this reaction will record the minimum amount of fluid with which the rock has interacted.

2) Isotopic mass balance

This method measures the isotopic shift which occurs when a rock of known initial isotopic composition is infiltrated by an external fluid, also of known isotopic composition. The magnitude of the isotopic shift is used as a quantitative measure of how much fluid has passed through the rock.

As a number of uncertainties and assumptions are involved in both these techniques, the calculated fluid-rock ratios can be subject to significant errors. With the reaction progress technique, particular problems are encountered when trying to identify which reactions actually occurred, and in estimating the initial mineralogy of the protolith. In both techniques, the final equilibrium fluid composition is taken as the composition of the fluid calculated from the observed mineral assemblage, which may or may not be the case in reality. However, probably the most difficult variable to evaluate in both methods is the initial composition of the fluid prior to infiltration. Having pointed out some areas of potential error, the estimates generated by both techniques usually agree within reasonable limits, suggesting that the calculated values do have some meaning, even if comparisons between different fluid-rock ratios can only be made in a qualitative way.

Rocks will also differ in their sensitivity to the passage of fluid. Impure carbonates undergo extensive reaction when they are infiltrated by a H_2O-rich fluid because the rock and the fluid are out of equilibrium, but fluid-rock interaction in pelitic schists will produce little or no petrographic signature because the fluid and the rock are in approximate equilibrium (Ferry 1986, 1984, 1983a,). Calculated fluid-rock ratios will always be minimum values since they only record the passage of fluid which has chemically interacted with the rock in some way, and this may not be an accurate reflection of the real fluid-rock ratio. Fluid-rock ratios are also time-integrated over the whole history of the rock, and therefore they say nothing about the timing of individual fluid pulses or the rates of fluid production.

High fluid-rock ratios have been demonstrated in reactive lithologies such as metacarbonates and metabasites (Ferry 1983a, 1986; Graham *et al.* 1983; Rumble *et al.* 1982), but it is unclear whether these are representative of the metamorphic pile as a whole, or are confined to the particular lithology studied. Until recently, only Ferry (1984), in his comprehensive study of the Waterville Formation, Maine; has

suggested the infiltration of pelitic lithologies by large volumes of fluid. He proposed that during a biotite-forming reaction the pelitic rocks were infiltrated by at least 0.9-2.2 rock volumes of H_2O. However, Wood and Walther (1986), who calculated the time-integrated fluid-rock ratios for a model pile of quartz-saturated pelites, showed that high fluid-rock ratios can be produced in normal lithologies by single-pass fluid flow, without the need to invoke deep fluid convection under lithostatic conditions (Etheridge *et al.* 1983).

1.4 FLUID PATHWAYS AND MECHANISMS OF FLUID TRANSPORT

The amount of fluid released from minerals during prograde metamorphism is too great to be accommodated by the very small porosity of metamorphic rocks, which is commonly less than 0.01 volume % (Fyfe *et al.* 1978). Walther and Orville (1982) showed that the instantaneous fluid-rock ratio in metamorphic rocks cannot exceed 0.01, and therefore the fluid produced by devolatilization reactions must leave the site of generation. At shallow depths in the crust, rocks can support a system of open fractures and pores, and fluid circulation can occur driven by gradients in temperature and density (Etheridge *et al.* 1983; Fyfe *et al.* 1978; Norris and Henley 1974). Fluid convection and circulation is a particularly important process occurring in shallow contact metamorphic aureoles, and very large fluid-rock ratios have been recorded (Taylor 1977; Taylor and Forrester 1979).

Below a certain depth, usually around 3-6 kms, a rapid decrease in rock strength means that open pores cannot be sustained. Gregory and Backus (1980) measured fluid pressure as a function of depth, and their results are shown in figure 1.3. Below 3 kms the fluid pressure increases steadily, until at a depth of 5.5 kms the fluid pressure approaches lithostatic pressure. Wickham and Taylor (1985) provide convincing evidence that circulation of sea-water did occur at depths in excess of 8 kms in the Trois Seigneurs Massif, but, in general, open pores cannot be sustained at depths greater than 6 km, and in most cases of regional metamorphism, the fluid pressure will equal lithostatic pressure. If the rate of fluid production is high, and the permeability of the rocks is low, then fluid will be produced faster than it can escape. Under these circumstances, fluid pressure will build up until the tensile strength of the rock is exceeded, when fracturing occurs. The large density contrasts between the fluid and the surrounding rocks will compel the fluid to move upwards. As fluids tend to move from hotter to colder rocks, geothermal gradients can provide a further driving mechanism for fluid transport.

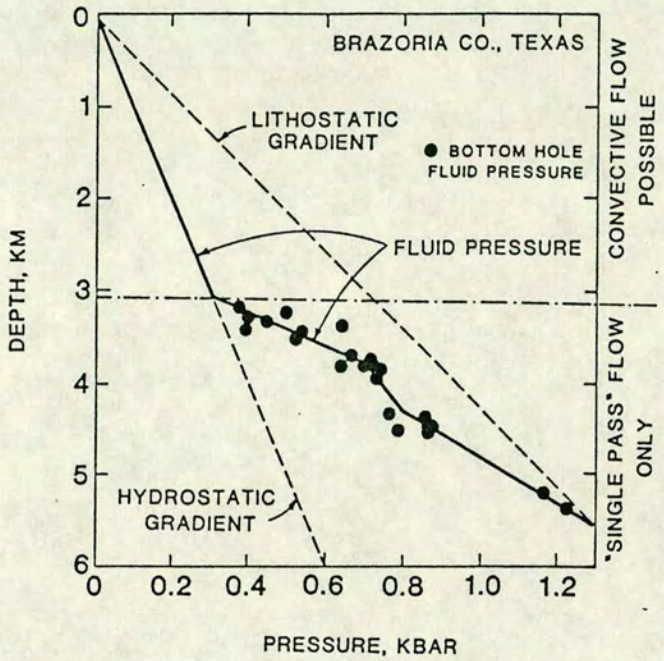

Figure 1.3 Fluid pressure as a function of depth in a sedimentary basin (from Gregory and Backus, 1980). As the depth increases so the fluid is pressurized to the lithostatic gradient. In this example the transition from hydrostatic to lithostatic conditions is complete by a depth of less than 6 km.

There are two commonly cited mechanisms used to describe fluid flow through rocks. One involves grain boundary flow, and the other, fluid channelling through a dendritic pattern of fractures (Wood and Walther 1986). Many workers believe that almost all fluid flow must occur along fractures (Norris and Henley 1976; Walther and Wood 1984; Wood and Walther 1986; Yardley 1983), and that grain boundary flow will only occur over short distances between fractures. The common occurrence of quartz veins and segregations, generally interpreted as representing the escape paths of metamorphic fluids, seems to argue for a fracture dominated transport regime, but this extreme channellizing of fluids would provide little opportunity for interaction with rocks higher in the sequence. This further implies that the potential for fluids to cause retrograde effects would be very limited, a view which does not appear to fit with field observations made on Syros and elsewhere. As is pointed out by Wood and Walther (1986), vein spacing probably gives too low an estimate for distances of grain boundary flow. Isotopic equilibration has been demonstrated over areas several hundreds of metres across (Shieh and Schwarcz 1974; Taylor *et al.* 1963), and therefore grain boundary flow must occur over similar length scales, in certain instances. The distribution of reaction progress in an outcrop is also evidence for pervasive (i.e grain boundary) fluid-rock interaction, at least through certain lithologies (Ferry 1986). Negative volume changes accompanying devolatilization reactions create an instantaneous increase in porosity and permeability. Changes in the pressure gradient accompanying this phenomenon mean that fluids will literally be sucked in, interacting pervasively with the surrounding rock (Rumble and Spear 1983). The distances over which grain boundary flow will operate are probably highly variable, and may also depend on the rheology of the rocks in question, i.e whether plastic or brittle behaviour dominates.

The extent to which fluid pathways are channellized is still an unresolved question, but there is a growing body of evidence which supports the idea that fluid channelling does occur over a range of scales, from microfractures less than a millimetre wide, to beds of reactive metacarbonate or metabasite several metres thick. It is certain that the actual geometries of fluid pathways will be very complex in detail. Although the overall impetus for fluid movement will be upwards towards the earth's surface, compositional and structural heterogenities and anisotropies could modify the fluid transport direction for considerable distances. Lithological contrasts through the metamorphic pile will provide a series of more or less permeable and impermeable horizons which will in turn control the direction of fluid flow. Structural anisotropies such as strong planar foliations and folds, particularly in aquitard lithologies, will also affect fluid transport directions.

The next chapter dicusses the regional geological setting of the field area, and reviews the geology of Syros itself.

CHAPTER 2

GEOLOGICAL SETTING OF THE CYCLADIC METAMORPHIC BELT, AND A REVIEW OF THE GEOLOGY OF SYROS.

TABLE OF CONTENTS

2.0 INTRODUCTION

This chapter will outline the geolgy of Syros and the surrounding Attico-Cycladic massif of which Syros is part.

The island of Syros was selected as the field area for this study principally because Syros displays some of the best preserved blueschists in the Cyclades. Previous work carried out on the island identified it as having a wellexposed suite of varied, but structurally coherent lithologies, all important factors when conducting detailed sampling work (Dixon 1969; Ridley 1982). Due to the subject matter of this study, the work has mostly been conducted outwith the context of the regional setting, and the regional survey presented here is mainly included for completeness. The regional information has largely been compiled from published sources in the literature, and these are referenced where appropriate.

Although the metamorphic and igneous evolution of the Cycladic area is very complicated, it is best known for the spectacular development of blueschist facies rocks, and indeed glaucophane was first described from this area by Hausmann (1845) after a trip to Syros. The Cycladic blueschist belt is part of an extended zone of high-pressure metamorphic rocks which stretchs from Attica and southern Evia to the Menderes massif in Turkey (Papanikolaou 1987). Figure 2.1 shows the regional geological setting of the Cycladic blueschist belt, while figure 2.2 shows the rocks of the Attico-Cycladic massif in more detail. The Cycladic massif itself consists of two main tectonic units which were thrust over an older Hercynian basement.

The main outcrops of the basement rocks are in central and southern Ios (Van der Maar 1980). The rocks consist largely of augen gneiss mantled by garnet-mica schists. U-Pb determinations on zircons, and Rb-Sr analyses on muscovites have dated the Hercynian amphibolite facies metamorphism, which formed the orthogneisses, as occurring between 305 and 288 Ma. (Henjes-Kunst and Kreuzer 1982). The lineation in the basement rocks parallels that in the overlying blueschists, which suggest that the overthrusting of the blueschist unit must have occurred either before or during the high-pressure metamorphic event (Van der Maar 1980). Similar basement rocks are also seen at the base of the sequences on Paros and Naxos (Jansen and Schuiling 1976; Papanikolaou 1980b).

Figure 2.1 Regional geological setting of the Cycladic blueschist belt (from Blake *et al.*, 1981)

Figure 2.2 Generalised geological map of the Attico-Cycladic massif showing the distribution of blueschist and greenschist facies rocks (from Ridley 1982)

The lower tectonic unit containing the blueschist belt is part of an allochthonous thrust sheet which was emplaced onto these basement rocks. The unit is composed of syn- and premetamorphic nappe sequences of metamorphosed Mesozoic carbonates, some of which contain metabauxite horizons, schists and a variety of metabasic and meta-acidic rocks. Petrological and geochronological studies have identified two major metamorphic events in this lower unit, known in the literature as M1 and M2.

Continental collision probably involving the underthrusting of the Apulian plate beneath the European plate resulted in the initial high pressure-low temperature metamorphic event, M1, which caused the development of blueschist and eclogite facies rocks. The metamorphic grade increases towards the S.E, from pumpellyite-lawsonite bearing rocks at Osssa, near Mount Olympus, to glaucophane-lawsonite bearing rocks in Evia, eastern Greece, (P-T conditions approximately 8 kbars and 320 °C), and finally to glaucophane-garnet-pyroxene bearing rocks on Syros and Sifnos, (see figure 2.3). The highest grade blueschist assemblages are developed in a N.E trending belt which runs through the islands of Milos, Sifnos, Syros and Tinos, the P-T conditions of metamorphism here are approximately 14kbars and 450 °C, (Dixon 1969, Komprobst *et al.* 1977, Schliestedt *et al.* 1987). The blueschists developed on the islands of Ios and Sikinos lying to the south of this high grade axis are again of lower grade (PT conditions for M1 are estimated as 9-11 kbars and 350-400 °C, Van der Maar 1980)..

A summary of the Rb-Sr and K-Ar geochronological data for this high pressure event is given in figure 2.4, (from Schliestedt *et al.* 1987). The most reliable dates are thought to be those made on coexisting paragonite and phengite, where the phengite shows the 3T high-pressure polytype (Altherr *et al.* 1979). The dates derived from these phases lie in a narrow band from 40 to 42 Ma. Values lying outwith this range tend to be dismissed, being explained either in terms of later resetting or the presence of excess argon. It is not entirely clear whether these dates truely represent the end of metamorphic recrystallisation.

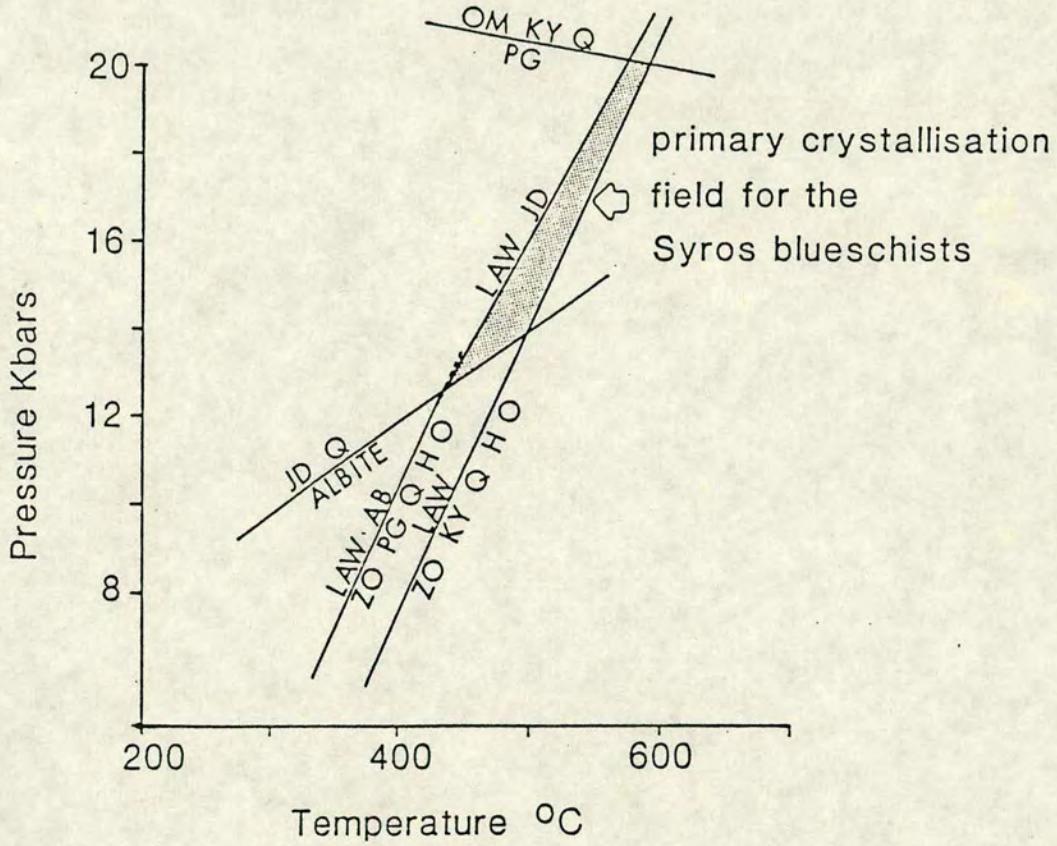

Figure 2.3 Calculated equilibria defining the peak PT conditions for the Syros blueschists. All equilibria calculated using thermocalc (Holland and Powell, 1988) and the extended data-set (Powell and Holland pers. comm., 1988).

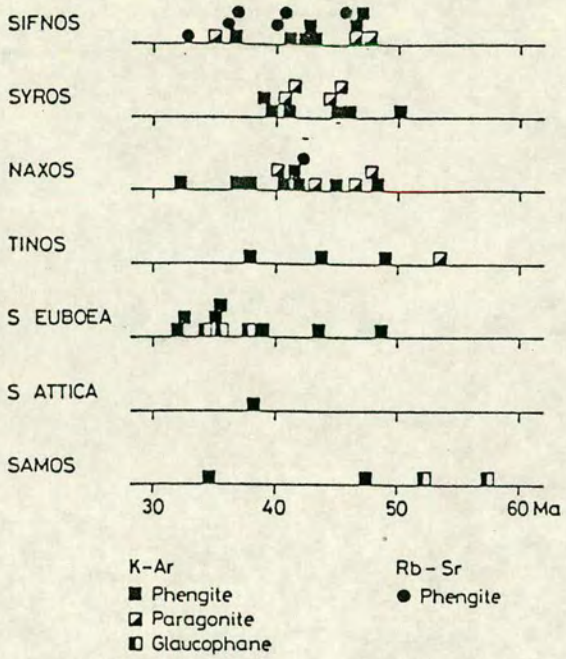

Figure 2.4 Geochronological data for the Eocene high-pressure metamorphism (from Schliestedt *et al.* 1987)

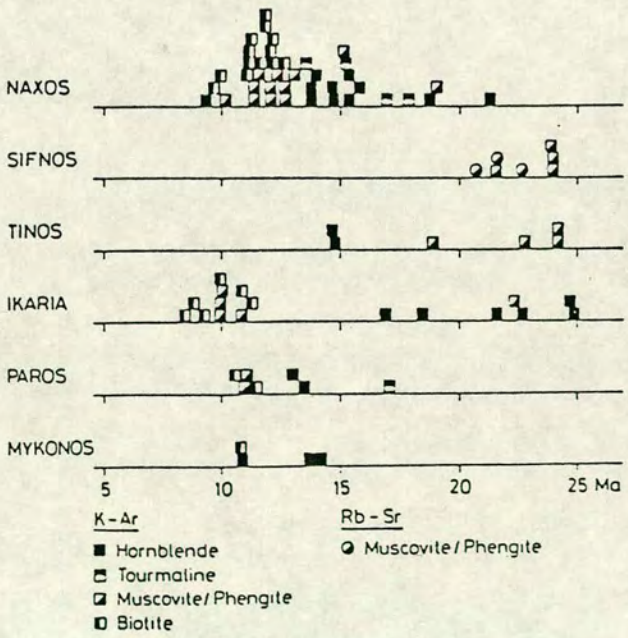

Figure 2.5 Geochronological data for the Miocene medium-pressure metamorphism. The range of dates down to 10 Ma indicates a prolonged period of cooling (from Schliestedt *et al.* 1987)

Tectonics and structure associated with M1

The whole metamorphic massif has been intensely deformed during the M1 event, with several phases of isoclinal folding causing the development of a pronounced layer-parallel foliation throughout the massif. A lineation can be seen in most outcrops, defined by the alignment of fold axes and elongate mineral phases such as glaucophane. The orientation of this lineation changes across the massif, from a north-easterly direction in the northern Cyclades to a northerly direction in the southern Cyclades. Within individual islands the trend of the lineation can also vary, in some cases by up to 90 degrees, e.g Paros (Papanikolaou 1980) and Syros (Ridley 1982). Blake *et al.* (1981) proposed the existence of two initially independent subduction zones which collided at the peak of the M1 deformational episode, to explain the variation in the lineation trend between the northern and southern segments of the Cyclades, and the progressive increase in metamorphic grade in both segments towards the Milos-Sifnos-Syros axis.

Blake *et al.* (1981) suggested that the lineation trends were perpendicular to the direction of transport of material into the subduction zones. This was challenged by Rodgers (1984) who proposed that the direction of subduction was parallel to the extensional lineation. He further suggested the existence of a single arcuate subduction zone dipping to the northeast. In the reply to this article Blake *et al.* (in Rodgers 1984) presented a map of the Cyclades showing the lineations rotated using the reconstructions of Le Pichon and Angelier (1979). On the basis of these rotated lineations Blake *et al.* (in Rodgers 1984) stated that "we no longer see any significant difference in the orientation of lineations between the two segments." They concluded that the Cycladic blueschist belt was only composed of one segment, and that the transport of material into the subduction zone paralled the direction of the observed lineations, as was suggested by Rodgers (1984).

M2 metamorphic event.

Superimposed on the high pressure assemblages of M1 is a regional greenschist to lower-amphibolite facies overprint. Accompanying this overprint is the breakdown of glaucophane bearing assemblages and the development of albite, chlorite, calcite and actinolite. This overprint is associated with the essentially isothermal uplift of the terrain and regional P-T conditions are estimated as 5-8 kbars and 450-500 °C. The greenschist overprint is most strongly developed in the island of Paros and Naxos which lie immediately to the south of the N.E.

trending belt showing the highest grade blueschists. In Naxos the overprinting assemblages reached upper amphibolite grade, with the development of a thermal dome and the initiation of anatexis, temperatures here are estimated to be in excess of 600 °C.

K-Ar and Rb-Sr dates on a variety of minerals associated with the overprint place the metamorphism in the early Miocene (20-25 Ma). A summary of the available dates is presented in figure 2.5, (page 26) taken from Schliestedt *et al.* (1987). The meaning of the geochronological dates for both the blueschist and the greenschist events is unclear. Uplift has been more or less isothermal, over a very large pressure range, 14-5 kbars, and there is no obvious reason why Ar, and the isotopic systems should not continue to exchange. For the greenschists at least, the dates may refer to a specific event, possibly the final phase of uplift, when the rocks will cool rapidly, closing the exchange systems.

Miocene magmatic activity involving the intrusion of I and S type granitoids occurred shortly after the culmination of the greenschist event. The intrusion of these granitoids also produced contact metamorphic aureoles, and the development of metasomatic skarn features on some islands, e.g. Seriphos (Salemink 1987). There is a regional variation in the composition of these intrusions from granodiorites in the south-west (Seriphos), to granites and leucogranites in the central Cycladic area (Naxos, Mykonos and Tinos) and monzonites in the north-east (Samos and Kos). Various attempts have been made to date the granitoids using a variety of methods, but the dates obtained show a wide variation from 10 to 21 Ma.

Many of the Cycladic islands contain isolated remnants of an upper allochthonous unit, composed of weakly, or non-metamorphic Permian and Triassic sediments and ophiolitic material. These rocks were interpreted as being relics of a far-travelled allochthonous nappe, but recent thinking favours the idea of extensional collapse. Ridley (1985,1982) suggests that these low-grade rocks were originally at a higher level in the pile, and were then down faulted by the action of extensional listric normal faulting (c.f. Platt 1986). There is certainly evidence for such a process on Syros, where the allochthonous units, bounded by low angle faults, (the toes of early listric faults, Ridley 1985, 1982) can be correlated with sequences towards the top of the autochthon.

2.1 OUTLINE OF THE GEOLOGY OF SYROS

Previous work

Previous work on the island has been conducted by Dixon (1969) who produced a lithologic map of the north of the island, as well as a detailed discussion of the mineralogy, petrology and metamorphism of the meta-igneous rocks there. More recently Ridley (1982) produced a 1:10,000 geological map for the whole of the island, and examined the minor structures in the blueschists to determine the nature of the deformation. He carried out a brief analysis of some metamorphic features pertinent to the theorectical heat-flow modelling which he also undertook. This modelling attempts to predict the P-T-t conditions associated with the tectono-thermal evolution of the island. Hecht (1984) produced a 1:50,000 map of the whole island, under the direction of the Greek geological survey (I.G.M.E). Syros has also been visited by a number of other workers engaged in broader studies, and it is mentioned in a number of review papers covering the Cycladic islands. Of particular note are the papers by Blake *et al.* (1981) and Schliestedt *et al.* (1987). However, nothing specifically relating to fluid evolution has previously been published about the island.

The geology of Syros

The geological map of Syros produced by Ridley (1982) is located at the back of this thesis, and it shows the main structural and lithological features of the island.

Division of the island into the main structural units.

The main structural unit is composed of a coherent lithological succession which can be traced from the southernmost peninsula of Mavra Vounakia up section to the north coast of the island. Figure 2.6, taken from Ridley (1982), shows the location of the different structural units mentioned in the text. The Galissas fault zone, which occurs in the south-west of the island, separates the peninsulas of Khirassou and Kefalos from the main unit. The succession developed to the west of the fault is largely composed of marble and schist, and the high proportion of marble suggests affinities to the sequence developed in the north of the island.

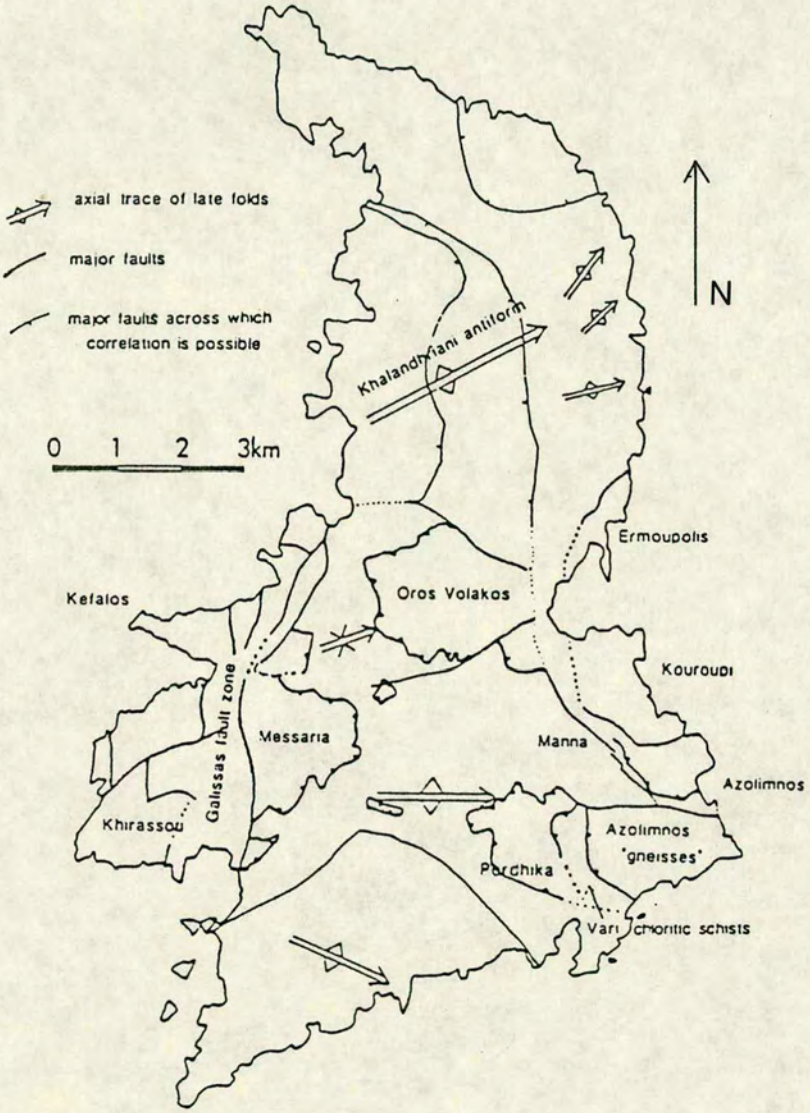

Figure 2.6 A map of Syros showing the location of the different structural units. Also shown are the traces of large-scale post-metamorphic folds in the main unit (from Ridley 1982)

The Volokos klippe is also largely composed of marble, and it forms the high ground in the centre of the island. Again the succession developed here is similar to that found in the upper part of the main unit. On the east coast, the Ermoupolis and Kouroupi gneisses, form an allochthonous sheet, overlying the main unit and the Volakos klippe. These rocks show close similarities to those found in the meta-igneous belt developed in the north of the island, and they may have been down faulted from higher levels in the pile (Ridley 1985, 1982). The Azolimnos gneisses and the underlying Vari chloritic schists also have a low angle tectonic contact with the underlying main unit. The Vari schists are very uniform in appearance and contain chlorite-epidote-quartz-albite bearing assemblages. The Azolimnos gneisses, predominantly quartzose rocks, overlie the Vari chloritic schists, and the contact between the two units is tectonic. There is no evidence that either of these units have experienced the high pressure blueschist facies metamorphism. The Azolimnos gneisses appear to have undergone an early epidote-amphibolite facies metamorphism followed by a greenschist facies event, and Ridley (1982) postulates that these allochthonous units may be down faulted higher levels of the syn-metamorphic structural pile.

Lithologies of the main unit

The following section will present a brief description of the lithogies comprising the main unit.

The peninsula of Mavra Vounakia represents the base of the structural section developed on Syros. The rock types present include schists, marbles, quartzites, quartzose schists and a number of metabasic units. The M2 greenschist metamorphic overprint is strongly developed here, but relict glaucophane confirms that these rocks did experience the earlier high pressure event. The margins of the larger metabasites and all of the smaller meta-igneous bodies are sheared, showing the development of a penetrative foliation, while the centres of the large units remain apparently undeformed. This textural development is repeated in metabasites throughout the island. The metabasites occurring in this southern tip of the island are now essentially greenstones, and consist of epidote, chlorite, albite, calcite and actinolite. Moving northward towards Nites, there are more quartzites and quartzose schists which pass upwards into predominantly chloritic and micaceous schists with some intercalated metabasites. At the ridge of Nites itself there are a large number of thick marble lenses which interleave

with the schists. The marbles are predominantly calcitic, but elongate dolomite lenses occur near the base of the larger units. Well developed mesoscopic isoclinal folding was observed in these marble units, and an example of this folding is shown in figure 2.7. The primary blueschist assemblages are less throughly overprinted in this area, and glaucophane is frequently preserved. Just to the south of Nites a large number of metabasite units occur. These spectacular blue and green rocks are predominantly composed of glaucophane and epidote, with some additional white mica, quartz, carbonate and accessory sphene. One unit, laterally continuous over 2 kms, was named the "epidote-megacryst" rock by Ridley (1982) after the huge epidote porphyroblasts developed in it which are commonly 1 cm long, and in places up to several centimetres in length.

Towards the centre of the island there are further quartzose schists with intercalated metabasites and thin marbles. Up section the schists become progressively more pelitic and these are intercalated with further marbles. Exposure in this central low-lying part of the island is generally poor, as much of the land is cultivated. Figures 2.8a and 2.8b are typical of the low-lying, poorly exposed areas of central and southern Syros. Around Ormos Kini, on the west coast of the island, thick sequences of a widespread pelitic Mg-glaucophane-w.mica-chlorite-graphite schist, named "greyschist" by Dixon (1969), are developed. These have largely escaped the effects of the greenschist overprint, but some heavily altered schists occur along the coast and near the village of Dhanakos, suggesting that this alteration may be due to the channelling of retrograde fluids along the nearby Galissas fault zone. West of Dhanakos the schists are overlayen by the Volakos klippe. Just above the contact with the Kini schists, the tectonically overlying marble is brecciated, with angular clasts of white marble held in an anastomising pinkish-brown carbonate matrix.

To the north of Ormos Kini some large metabasite bodies occur surrounded by schist. On the basis of their similar structural position, Ridley (1982) suggested a correlation between these units and the large glaucophane-epidote mass south of Talanda. North of Kini, from Stonikas to San Mikhali, the succession is dominated by marble, which makes up two-thirds of the sequence. Figure 2.9, taken from Oros Volakos looking north, shows two of the thick northern marble units. The marbles are predominantly calcitic, and they vary in colour from white to grey. Dolomitic units occur within these marbles, but these are much finer grained, and have a characteristic yellowish or pinkish-brown colour.

Figure 2.7 Repeated isoclinal folding seen in a thick marble unit near the top of the south facing side of the Nites massif.

Figure 2.8a Taken from the top of the Nites ridge looking north-west towards Kini, this view is typical of much of central Syros which tends to be low-lying and extensively cultivated.

Figure 2.8b A similar view, again taken from the Nites Ridge but this time looking south-west towards Megas Yialos. Again, the gentle topography means that exposure is poor except for coastal stretches.

Figure 2.9 Taken from Oros Volakos looking north-east towards Oros Pirgos the view shows some of the thick marble units which make up two-thirds of the sequence in the northern part of the island. The marble-schist contacts are highlighted by the absence of vegetation on the marble units.

The intervening schists are mostly typical northern greyschists, i.e fine-grained and lead-grey in colour with a graphitic lustre on foliation surfaces..

There are five thick marble units in this part of the sequence, each of which has a schist horizon developed just above the centre of the unit. This similarity between the marble units, and the rhythmic alternation of schist and marble led Ridley (1982) to interprete this sequence as a thrust stack. The tectonic duplication is presumed to have occurred either pre- or syn-M1, and microstructures imply that the thrust movement was top to south or southeast, (Ridley 1982). Tectonic contacts have not been found, but these may either have been lost during later recystallisation of the marble, or they occur in the underlying schists, where they would be very difficult to detect. Figure 2.10a and 2.10b are two views of northern Syros showing the typically good exposure found in the north.

North of San Mikhali, and forming an east-west trending belt across the top of the island is the so called "northern gneiss-serpentinite belt" (Dixon 1969). The gneiss-serpentinite belt has no coherent stratigraphy, and consists of a large number of meta-igneous blocks held in an intervening matrix of serpentinite and pelitic derivatives. The character of the included blocks is highly variable, ranging from finely striped glaucophane-epidote gneisses, to large, and relatively undeformed, metagabbroic bodies which preserve their former igneous textures. This belt has been interpreted as an ophiolitic debris-flow, or olistostrome, and as such the unit is essentially sedimentary, having formed on the seafloor and experiencing the same metamorphic and structural history as the rest of the island. Similar ophiolite derived deposits are developed near the top of the sequence on the neighbouring islands of Andros and Tinos (Blake *et al.* 1981, Dixon and Ridley 1988). The metagabbro at Kaloyeros, in the eastern part of the belt, is surrounded by concentric zones of metamorphosed conglomerate and breccia of igneous origin. The breccia is composed of angular to rounded meta-igneous blocks held in glaucophane-rich or omphacite-ankerite rich matrices, and it is interpreted as a sedimentary deposit, or debris flow of plutonic and volcanic material which was deposited on top and around the metagabbroic block (Dixon 1969).

Although the majority of the included blocks are metabasic in composition, some more leucocratic meta-acidites do occur. Acid gneisses are much paler in colour than their basic equivalents, and they are predominantly composed of quartz, jadeitic pyroxene, paragonite, garnet and glaucophane.

Figure 2.10a Taken from Oros Syringas looking south-southeast towards Oros Pingos and Ano Siros this view shows the steep terraced fields and more rugged terrain of northern Syros.

Figure 2.10b This view was taken from near Trakhilaki on the north-west coast and looks almost due east towards the village of San Mikhali just visible on the horizon. In the foreground is the huge dark meta-igneous block known as "monolith 1", see text.

Some meta-acidic blocks occur in the breccia zones surrounding the Kaloyeros metagabbro, and in the small meta-igneous body at Gria Spilia, perfectly preserved igneous net-veining of acid and basic material can be seen.

At Kastri on the east coast, structurally below the main development of the gneiss-serpentinite belt, a small melange unit occurs interbedded with a sequence of alternating thin marbles and schists (Ridley 1982). Figures 2.11a and 2.11b show two different aspects of the Kastri melange. The included metabasic blocks are generally rounded, and they are held in a talc-chlorite matrix. The blocks are usually only a metre or so in diameter, but some much larger blocks do occur, up to 10 metres in diameter. The position of this unit, sandwiched in a marble-schist sequence, makes its sedimentary origin obvious, and its small size makes it easier to identify this unit as an olistostrome. A number of the included metaigneous blocks show spectacular metasomatic rinds. The affected blocks are wrapped round by a silvery mass of fine grained chlorite and talc which is studded with large actinolite crystals, and occasionally a monomineralic layer of glaucophane is also seen, developed next to the block. The melange overlies a sequence of colourful blue and green basic schists, which probably owe their character to the reactive influence of detrital serpentinite. Isolated meta-igneous clasts are also found in the underlying normal schists (see figure 2.11a), and these blocks presumably herald the first appearance of ophiolitic debris in the sequence.

The central part of the belt is characterised by a continuous serpentinite body with included blocks. The size of these included blocks is variable, and though most tend to be a metre or so in diameter, some like "monolith 1" (Dixon 1969), a huge block of glaucophane-eclogite, are several tens of metres in diameter (see figure 2.12). Where metasomatic reactions have occurred between the serpentinite and the enclosed metabasic blocks, the serpentinite has been altered to chlorite and talc derivatives. However, unaltered serpentinite can be found near Kambos, where the density of meta-igneous blocks is lower, and here it occurs as a soft, bluish-green coloured rock, which is almost completly weathered away to produce a characteristically green coloured soil. North of Megas Lakkos, on the west coast of the island, a large body of relatively unaltered serpentinite occurs. A number of thin anastomising carbonate veins are seen cutting the serpentinite, and talc plates are found infilling fractures.

Figure 2.11a This photograph shows one of the exotic meta-igneous blocks surrounded by semi-pelitic schist. These exotic blocks begin to appear in the schists some metres below the full development of the melange unit, and they represent the first input of ophiolitic debris into the sequence.

Figure 2.11b A general view of the fully developed Kastri melange taken from the north side of Ormos Kastri Bay. Several rounded meta-igenous blocks can be seen sitting in a talc-chlorite matrix.

Figure 2.12 "Monolith 1" (Dixon 1969) a 20m high block of glaucophane-eclogite held in a matrix of serpentinite derivatives. The photograph was taken south of Kambos looking west towards Megas Lakkos.

The commonest included blocks are glaucophane-eclogites, but north of Megas Lakkos a branch of serpentinite encloses a number of very pure jadeite-quartz blocks. The pyroxenes in these blocks are very sodium rich, with up to 85 mole % of the jadeite component. As serpentinite is a very powerful desilicifier, and the fact that quartz remains in these blocks indicates that the all the serpentinite was reacted out before the quartz was used up. The other included blocks surrounded by serpentinite are essentially quartz free.

The area above the gneiss-serpentinite belt is predominantly composed of greyschists and marbles, but the stratigraphy of the sequence is somewhat jumbled, as the area is cut by a large number of syn-metamorphic tectonic breaks. Figure 2.13, taken from the ridge of high ground between Oros Syringas and Sarakiniko, shows a view of the north-western part of the island.

The island of Sifnos

At this point it is worthwhile giving a brief description of the island of Sifnos. Sifnos lies some 50 kms to the south-southwest of Syros, and it is also part of the N.E trending belt which contains the highest grade blueschists. The P-T-t histories of Syros and Sifnos have been very similar and like Syros, Sifnos has experienced a partial greenschist facies overprint. Work by Matthews and Schliestedt (Matthews and Schliestedt 1984, Schliestedt and Matthews 1987) has addressed the evolution of blueschist rocks into greenschist facies rocks, looking particularly at the role is fluid infiltration in this transformation. Figure 2.14 shows a simplified geological map of Sifnos. Sifnos has a relatively simple stratigraphy which mainly consists of metabasic and meta-acidic volcanic rocks interbedded with thinner metasedimentary layers. The island is divided into a number of units: a lower greenschist unit, a central marble complex, an upper sequence of high pressure blueschists and an upper marble unit. These units are arranged in a domal structure, with the greenschist facies rocks representing the lowest structural unit.

From their isotopic work Matthews and Schliestedt came to a number of conclusions about fluid involvement in the blueschist to greenschist transformation. Although in their 1984 paper they concluded that pervasive isotopic equilibriation had not occurred in the blueschist unit, this conclusion was reversed in their more recent paper, (Schliestedt and Matthews 1987).

Figure 2.13 Taken from near Oros Syringas looking north, this photograph shows a panoramic view of the north-western part of the island. The bays of Ormos Megas Lakkos, Marmari and Ormos Grammata are clearly visible, and the sliver of marble forming the tip of Aspro is also seen. The jumbled sequence of schists and marbles forming the sequence above the gneiss-serpentinite is well displayed.

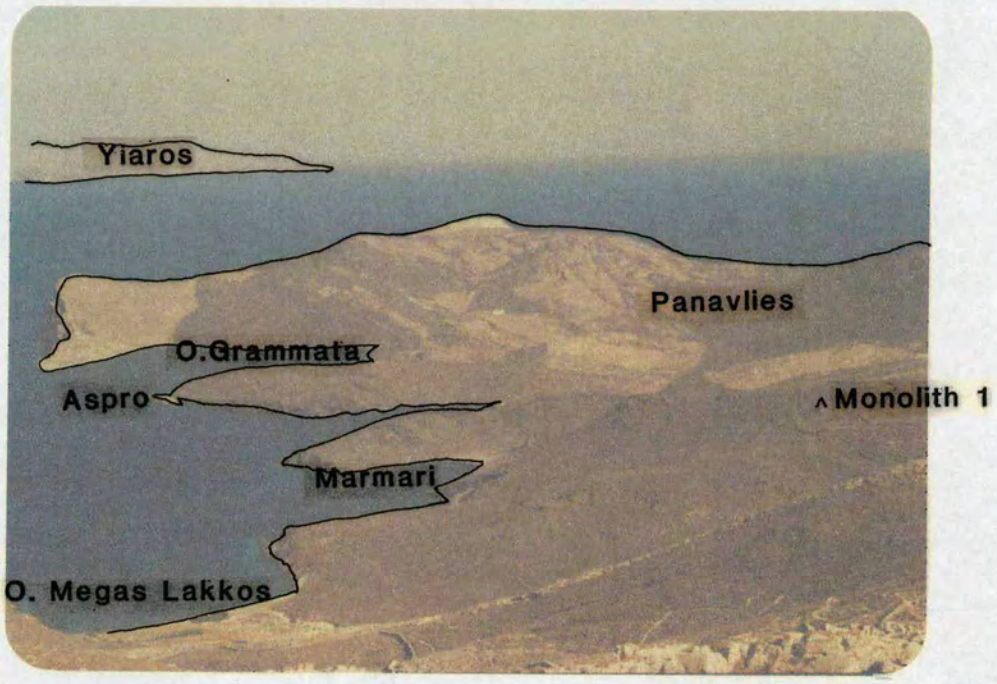

Figure 2.13 Taken from near Oros Syringas looking north, this photograph shows a panoramic view of the north-western part of the island. The bays of Ormos Megas Lakkos, Marmari and Ormos Grammata are clearly visible, and the sliver of marble forming the tip of Aspro is also seen. The jumbled sequence of schists and marbles forming the sequence above the gneiss-serpentinite is well displayed.

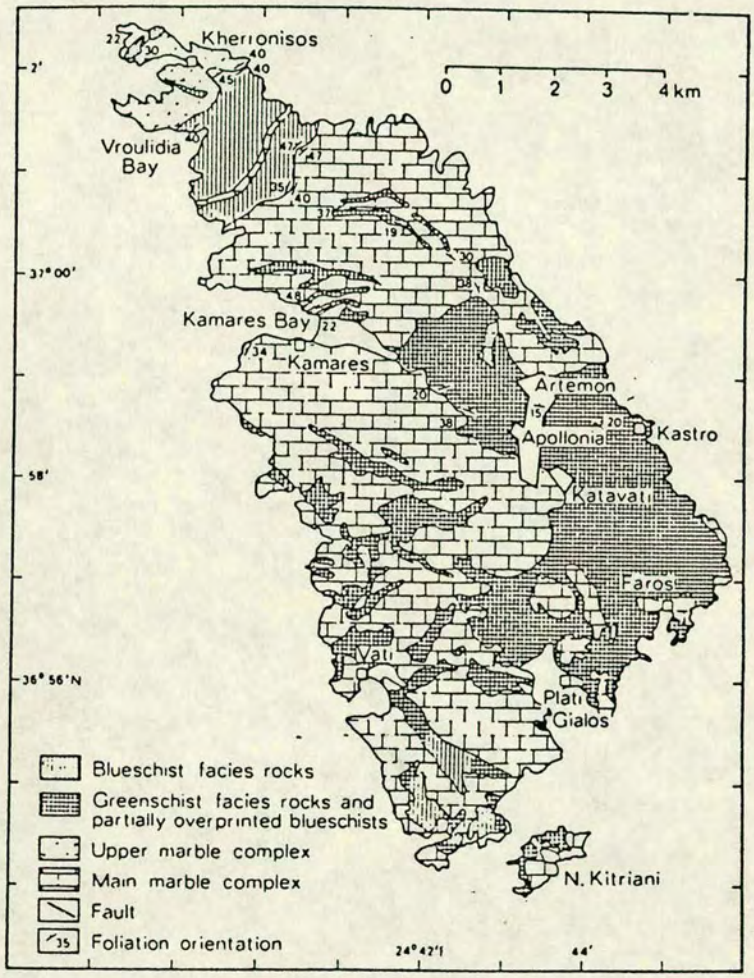

Figure 2.14 A simplified geological map of Sifnos (from Schliestedt *et al.* 1987).

More detailed sampling at two lithologically equivalent localities revealed a tendency for the interlayered rocks to approach isotopic equilibrium, both during the high pressure metamorphism and the subsequent greenschist facies overprint. They also noted that the minerals and whole rocks of the greenschist unit were enriched in $\delta^{18}O$ relative to the blueschist assemblages, and this was interpreted as indicating the involvement of an $\delta^{18}O$ enriched fluid during the greenschist event. Minimum fluid-rock ratios for the blueschist to greenschist transformation were estimated using isotopic mass balance calculations, and these showed a decrease from ≈ 0.4 in central Sifnos, where the greenschist overprint is strongly developed, to a value of zero in the unaltered northern blueschists. Matthews and Schliestedt (1984) suggested that the large thickness of marble present in the northern part of the island acted as a barrier to fluid infiltration, and thus the marbles were responsible for the preservation of the northern blueschists. In their study, (Matthews and Schliestedt 1984, Schliestedt and Matthews 1987) Matthews and Schliestedt suggest that the source of the infiltrating fluid which drove the greenschist alteration was either derived from a crystallizing magma, or from the dehydration of metamorphic rocks at depth. In either case, they suggest that this fluid is further buffered by interaction with marble at depth, a prerequisite feature in order to generate a fluid sufficiently enriched in ^{18}O to produce the isotopic shifts seen in the greenschists.

The work on Sifnos is mentioned here because it is obviously of great relevance to this study. As the titles of their papers suggests, (Matthews and Schliestedt 1984; Schliestedt and Matthews 1987) the work on Sifnos largely concentrates on the blueschist to greenschist transformation, no attempt was made to construct a petrogenetic grid for the blueschist assemblages, and the X_{CO2} content of the fluid is left unconstrained. However, the Matthews and Schliestedt study has been of great value because it permitted a number of general hypotheses about Syros to be put forward at an early stage of this project.

2.2 DESCRIPTION OF SAMPLED LOCALITIES

The following section discusses the field methodology, and gives a brief description of the twelve most important localities.

The fieldwork associated with this study was orientated towards observation and detailed sampling. The strategy was relatively simple, outcrops were selected

which showed the greatest diversity of rock types, in the hope that these would yield a varied suite of mineral assemblages. Collecting initially concentrated on carbonate-bearing metasediments, which could provide a greater control on the coexisting fluid composition. Quartz segregations were collected for fluid inclusion studies when they appeared to be of synmetamorphic origin, or were associated with the greenschist alteration. The procedure followed at each locality was more or less the same. Initially a detailed sketch was made, recording the main features of the different lithological units, their contacts with neighbouring rock types, the occurrence and distribution of veins etc. The site would then be photographed, and in some instances polaroid photographs were used as an instant "map" to record the exact position of the collected samples.

Sampling was always carried out perpendicular to the perceived strike and, as far as possible, samples were collected at true measured distances away from a particular contact or marker horizon.

Description of localities

Locality name: **Agkathopes**

Location: Agkathopes forms a narrow peninsula on the south-west coast of the island, lying to the south of Ormos Finikos

Samples: 87/136 - 87/156

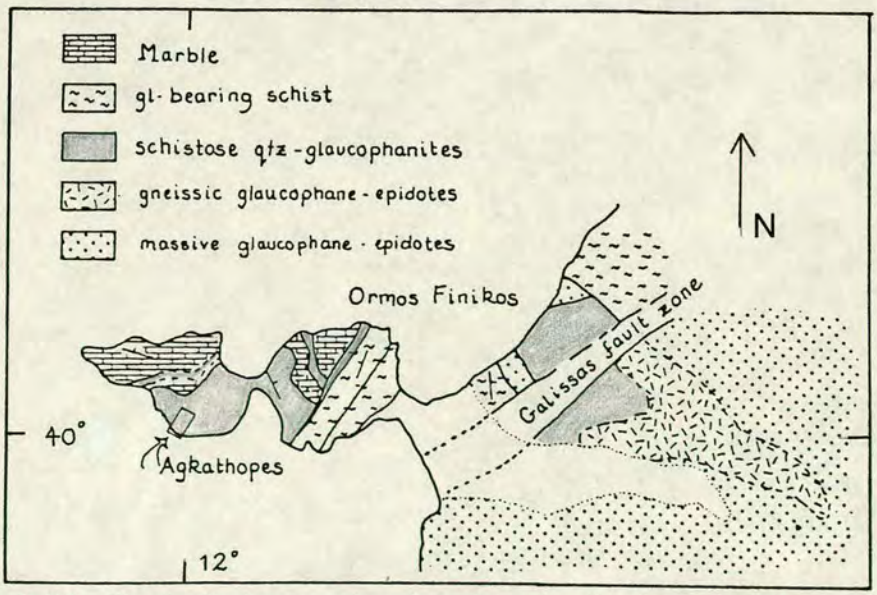

Figure 2.14 Geological map showing the distribution of rock types around Agkathopes. The box indicates the area where the majority of the samples were collected.

Description:

A series of foliated and folded metabasic and meta-acidic gneisses form most of the peninsula, with an overlying marble unit forming the seaward tip. Agkathopes is isolated from the main structural unit of the island by a series of faults which occur on the coastward side of the peninsula. Ridley (1982) suggested that these faults are a continuation of the Galissas fault zone, which occurs further north.

Mesoscopic folding is well developed, and a pronounced strain-slip cleavage is associated with this. Extensive veining is present at this locality, and the vein material is invariably brown carbonate. Greenschist alteration is associated with the veining, and an alteration "halo" commonly develops around the vein. In the altered zones glaucophane and garnet are replaced by chlorite and albite, causing a marked colour change in the rocks from blue to green. Samples were collected from the vein material, the surrounding altered rocks and from unaltered blueschists.

Locality name:	Aspro
Location:	north-west coast, the tip of the peninsula lying to the south of Ormos Grammata
Samples:	86/49 - 86/69

Description

A small sequence, 12 metres thick, of thinly bedded metasomatic schists overlain by normal greyschists. The contact between the two units is apparently conformable, but the greyschists and the underlying metasomatic schists develop a very fine sheared fabric over a distance of 5-8 centimetres, which may indicate a thrust contact. A marked colour change occurs in the contact zone. The schists change from grey to pale blues and greens, brown carbonate and green fuchsite mica appear and the lawsonite pseudomorphs change colour from grey to green. This colour change is thought to be due to compositional differences caused by the incoming of detrital serpentinite material. A variety of rock types occur within the metasomatic unit, and these are listed below.

Samples were collected from all the different rock types.

- pure marbles
- sheared pale-blue rock, fine glaucophanic matrix studded with ankerite nodules and green lawsonite pseudomorphs
- banded sequences of alternating glaucophanic and chlorite-actinolite layers.
- exotic glaucophane-rich meta-igneous blocks
- layer parallel lenses of ankerite, fuchsite and quartz.

Figure 2.15 Photograph of the sequence at Aspro. The colour change between the metasomatic and the normal schists is marked. The thin, folded, marble ribs are well displayed, as are the brown qtz-carbonate segregations. The intervening material is a mixture of fine-grained glaucophanic, and chlorite-actinolite layers.

Locality name: **Ermoupolis**

Location: A small cove on the east coast, reached by walking through the town along the coast road, headed north, and descending into the small bay by the steps opposite the Hotel Voulis.

Samples: 86/122 - 86/125

Description

In the bay a series of meta-igneous blocks are held in chlorite-talc schist. Moving northwards along the coast a much larger block tens of metres in diameter, occurs and this is extensively veined by carbonate material. This locality is a good example of vein-driven retrogression. The glaucophane-omphacite bearing metabasite is altered to a chlorite-albite-calcite rock, which forms a symetrically arranged zone on either side of the vein. The visible alteration zone is 70cm wide in total.

Locality name: **Gria Spilia**

Location: North-west coast, off the bay of Ormes Grammata.

Samples: 86/127 - 86-144

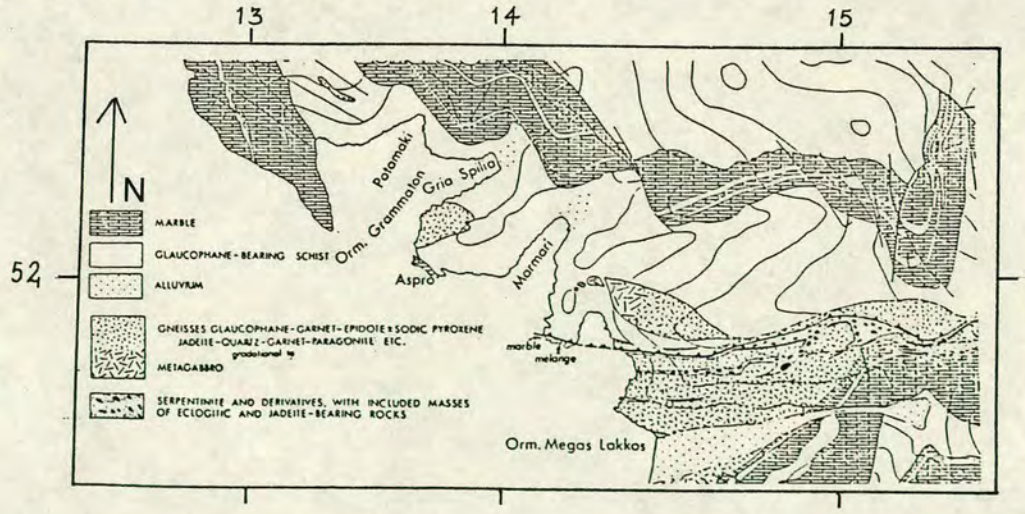

Figure 2.16 Geological map showing the area around the Gria Spilia metabasite.Aspro is also shown, (from Dixon 1969).

Description

The Gria Spilia gneiss body is a small area of meta-igneous rock, 20 metres across, completely surrounded by schists. It was selected as a good locality to study the extent of fluid infiltration from the matrix, which is carbonate bearing, to the gneiss which is carbonate free. It was also selected as a study area because of the variety of rock types present within the gneiss. The different types of gneiss were sampled both close to the contacts and within the body itself, and sequences were collected across several schist-gneiss contacts.

The gneisses consist of three main rock types: a mafic unit (glaucophane, garnet) an acid unit, (jadeite, quartz, w mica) and a "mixed" unit, intermediate between the first two types. The relationships between the different rocks types are largely igneous in character. Examples of net-veining, assimilation and hybridisation were all seen. At schist contacts the metabasite becomes studded with pale lawsonite pseudomorphs, and the proportion of glaucophane seemingly increases. The effects seen in the schists are variable. In some places they are negligible, while at other more sheared contacts the schists contain more carbonate, fuchsite mica and glaucophane. At the inland contact a spectacular metasomatic mineral sequence is seen. The gneiss here is of the hybrid type and close to the contact it becomes packed with pale lawsonite pseudomorphs and garnets set in a glaucophanic matrix. This zone passes outwards to a glaucophane-garnet rock, then into a 3cm thick monomineralic glaucophane layer, which merges into a soft, pale blue glaucophane-rich schist. Such contact effects must be interpreted with care as the gneiss body is probably a huge olistolith, and contact effects could be due to isochemical metamorphism of original alteration zones around the olistolith, formed at the time it was deposited (i.e. prior to blueschist facies metamorphism)

Locality name: **Kaloyeros metagabbro**

Location: northern coast to the east of Ormos Griza
Samples: 87/187 - 87/193

Description

The schists next to the metabasite are typical northern lawsonite-bearing greyschists. The metabasite is sheared at its contact with the schists, and a layer of pale-blue glaucophanic material approximately 50cm wide is developed, which encloses occasional resistant pods of coarser material. A few metres in from the contact, the metabasite becomes much coarser and glaucophane-garnet bearing. Samples were collected from the interior of the metabasite, and here the rock is very much coarser, meriting the field-name metagabbro. The metagabbro is unfoliated with dark-green amphibole patches (actinolite) set in a pale clinozoisite matrix. In places the green actinolite can be seen rimmed and altered to patches of dark blue glaucophane.

Locality name: **Kini**

Location: Bay on the central-western coast, Ormos Kini
Samples: 87/201 - 87/209

Description

On the southern side of Kini bay a sequence of variably regressed basic schists is developed. The schists appear green in colour, and are predominantly composed of chlorite, albite and epidote. Alteration becomes more pervasive to the west, as the Galissas fault zone is approached. At the sampled locality a set of carbonate veins cut through the sequence (general trend 174/80W), but these did not appear to be related to the greenschist alteration.

Locality name: **Kouroupi gneisses**

Location: east coast, between Ermoupolis and Azolimnos
Samples: 87/157 - 87/175

Description

Near Kalamista glaucophane-omphacite bearing gneisses are transformed to albite-chlorite bearing rocks. Several carbonate veins are present, (average trend 122/ vertical) but these do not seem to be related to the alteration, and there is no obvious vein-retrogression relationship such as was seen at Agkathopes. The unaltered gneisses are strongly foliated and dark blue in colour, with obvious pink garnets. In rocks where omphacite is abundant, the pyroxene forms dark-green bands and pods in the rock. The altered gneisses are very obviously green in colour, with pale albite porphyroblasts standing proud of the rock surface. Areas of serpentinite and serpentinite derivatives (chlorite and talc) with included meta-igneous blocks are seen in the gneisses, an association highly reminiscent of the northern meta-igneous belt.

Locality name: Nites (massif)

Location: central-southern area of the island. Nites forms a central area of high ground and can be approached from the village of Khrousa in the north or from the southern coast road.

Samples: 87/43 - 87/85

Figure 2.17 Taken from the coast road, near Megas Yialos, looking north, this photograph shows a number of the marble units making up the Nites ridge. The lenticular shape of many of the units can be clearly seen.

Description

The sequence comprises numerous thin (usually less than 5 metres), but continous marbles interleaved with variably altered schists. A number of metabasite units are also present, some of which are laterally continuous over hundreds of metres. The marbles near the top of the sequence are much thicker (30 metres), and tend to be lens shaped. Fine grained dolomitic horizons were seen near the base of these large marbles. Samples were collected through the main marble and several of the smaller marble lenses. The samples were primarily collected for stable isotope work, but thin sections were also made from a number of the marbles in order to determine the percentage of silicates present.

Locality name: **North of Aspro**

Location: north-west coast in between Aspro and the metabasic body at Gria Spilia

Samples: 86/70 - 86/84

Description

A lithologically diverse sequence of thinly bedded greyschists. Thirteen samples were collected over a distance of three metres. These samples are the best examples of unaltered blueschists collected anywhere on the island.

Locality name: **Ormos Akhladhi**

Location: A small bay on the south coast lying just to the west of Vari.

Samples: 87/14 - 87/26
87/110 - 87/135
87/173 - 87/175

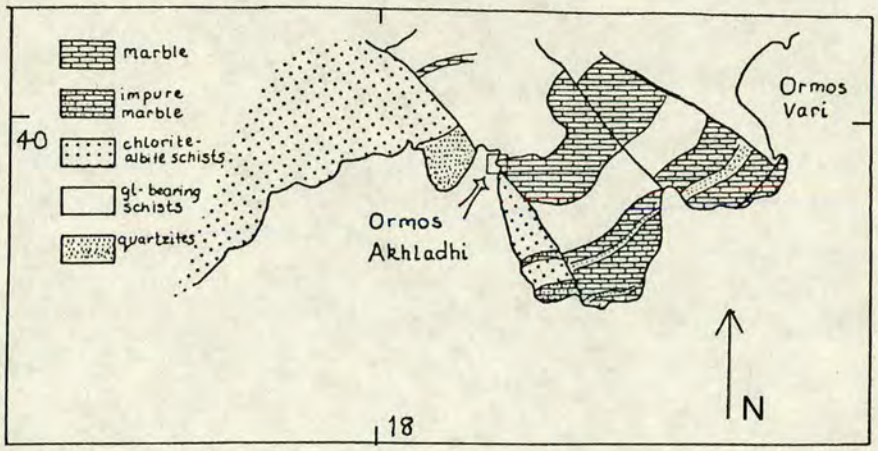

Figure 2.18 Geological map of the area aound Ormos Akhladhi

Description:

The small bay is formed of three faulted units, (see figure 2.18). On the left hand side, close to the shore, are some variably altered metatuffs, with thin interbedded chert layers. The metatuff comes to an abrupt end next to quartz-rich sediments, suggesting that, either the metatuff unit is an exotic block, or the field relations have been produced by faulting. On the right hand side of the cove, a sequence of impure carbonates, with calcic pebbles, is developed at the base of the sequence. This grades upwards into micaceous schists, with thin marble ribs. Above this, metatuffs are present, partially altered to chl-alb-cc greenstones. The tuffaceous bands are intercalated with sedimentary layers, most of which are impure marble. Extensive faulting occurs at the top of metatuff sequence. Nearest to the shore, there is an interlayered sequence of marbles and schists. The schists show varying degrees of alteration, some preserving glaucophane, while in others, little trace of the original blueschist mineralogy remains. There are no obvious structural features controlling the retrogression, which is widespread, and quite pervasive in this area. Samples were collected from all the rock types, to assess the degree of alteration. Collecting concentrated on the interlayered marble-schist sequence, where samples were collected at spaced intervals for isotopic analysis.

Locality name: **Ormos Kastri**

Location: small peninsula on the north east coast, south of Kaloyeros

Samples: sequence 1 (above marble) 86/2 - 86/46
sequence 2 (below marble) 86/93 - 86-105.
melange unit 86/85 - 86/92

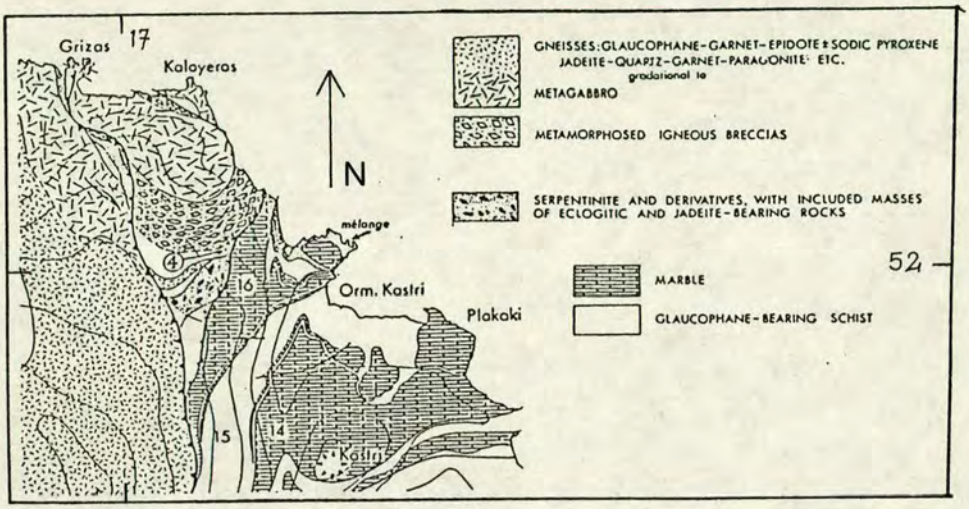

Figure 2.19 Geological map of the area around Ormos Kastri. The position of the melange unit is shown, and the boxes indicate the location of the two sampled sequences.

Description

Three traverses were made at this locality close to the shore where the exposure is good. An alternating sequence of thin marbles and schists is divided by a thick (~10m) marble, and traverses were made through the metasediments both above the marble unit and below it. The upper sequence of schists grades into a melange unit. Blocks of exotic meta-igneous material occur in the schists, and rapidly increase in size and number until the full development of the melange unit in the space of a few metres. The metasediments consist of semi-pelitic and pelitic schists interspersed with thin, and often impure, marble ribs. Lawsonite pseudomorphs are abundant. A number of the schists have been altered, and glaucophane is no longer present. The greenschist alteration is concentrated in the schists immediately above and below the thick dividing marble. Towards the top of the first sampled sequence there are a number of soft, green chloritic schists, in which the first exotic blocks appear. These blocks are rounded in shape, and

largely composed of glaucophane and garnet. The margins of the blocks have rims of coarse white mica, in places followed by an outer rim of coarse actinolite needles set in talc. The colour and mineralogy of these schists suggest that there has been input of detrital serpentinite with a few blocks of ophiolitic debris. "Normal" schists occur above the block horizon, but these are only developed over 1 metre before the schists become very green in colour again and the included meta-igneous blocks become larger and more numerous. On the promontory on the north side of Ormos Kastri, the melange unit is fully developed with huge meta-igneous blocks, showing well developed metasomatic reaction rims, sitting in an actinolite-talc matrix.

The melange unit is conformable with the rest of the sequence and it is considered to be sedimentary in origin. The melange unit, and the block-rich horizons, represent layers richer in detrital serpentinite and basic debris, presumably derived from an uplifted (fault-scarp?) section of ocean floor.

Locality name:	**Oros Syringas**
Location:	central northern Syros
Samples:	sequence 1 86/168 - 86/189
	sequence 2 86/190 - 86/198
	schists below marble 86/209 - 86/216 and 87/224 - 87/243

Description

This thick sequence of marbles interbedded with thinner schist horizons forms a roughly east-west trending ridge. The marble is largely calcitic, but dolomitic units do occur, distinguishable by their finer grain size and pale yellow colour. At this locality collecting was directed towards gathering material for stable isotope work, with the aim being to determine the stable isotope geochemistry of the marble units. Two spaced traverses were made through the marble-schist sequence, 0.5km apart. Samples were collected from the upper and lower contacts of each marble unit, and also from the centres of the units.

The intercalated schists were also sampled, although the poor exposure made systematic collecting difficult.

Samples were collected from the schists outcropping beneath the structurally lowest marble unit. These schists often showed signs of greenschist alteration, and albite porphyroblast schists were developed in the units directly beneath the marble unit.

Figure 2.20 Panorama looking north-west towards Oros Syringas. The marble and schist units making up the sequence can be clearly seen.

CHAPTER 3

MINERALOGY AND PETROLOGY OF THE BLUESCHISTS

3.0 INTRODUCTION

In this chapter the mineralogy of the blueschists is considered in detail. The overall aim of the chapter is to establish the credentials of the primary mineral phases, so that mineral assemblage lists for the blueschists can established, and used to calculate the composition of the coexisting synmetamorphic fluid (see chapter 4). The chapter is sub-divided into sections, each of which looks at a different mineral phase. The typical habit of the mineral is described, and the mineral chemistry is discussed. Representative probe analyses are listed for most phases.

3.1 AMPHIBOLES

Under the primary conditions of metamorphism, approximately 14kbars and 450 ^{o}C, glaucophane is the predominant amphibole phase, and it is a common constituent of all the rock types.

Crystal habit

In the schists and impure marbles, glaucophane either occurs as small prismatic crystals, with a diamond shaped cross section, or as acicular crystals aligned parallel to the foliation. The glaucophane crystals are generally comparable in size to the other mineral phases, only attaining porphyroblastic status in a few cases, (see figure 3.1). In the metabasites, glaucophane has two distinct habits depending on the degree of deformation which the metabasite has experienced. In the larger, relatively undeformed metabasite bodies, a gabbroic texture is preserved, and glaucophane commonly forms porphyroblasts along with epidote and garnet. The margins of the large units, and smaller metabasite bodies, have experienced more intense shear strain, and as a result, glaucophane occurs as very fine grained acicular crystals. A penetrative foliation is often developed, giving rise to a marked banded appearance in the rocks, which is reflected in their field name, "metabasic gneisses" (Dixon 1969). The significance of these observations is discussed in more detail later in the chapter (see section on coexisting glaucophane and actinolite).

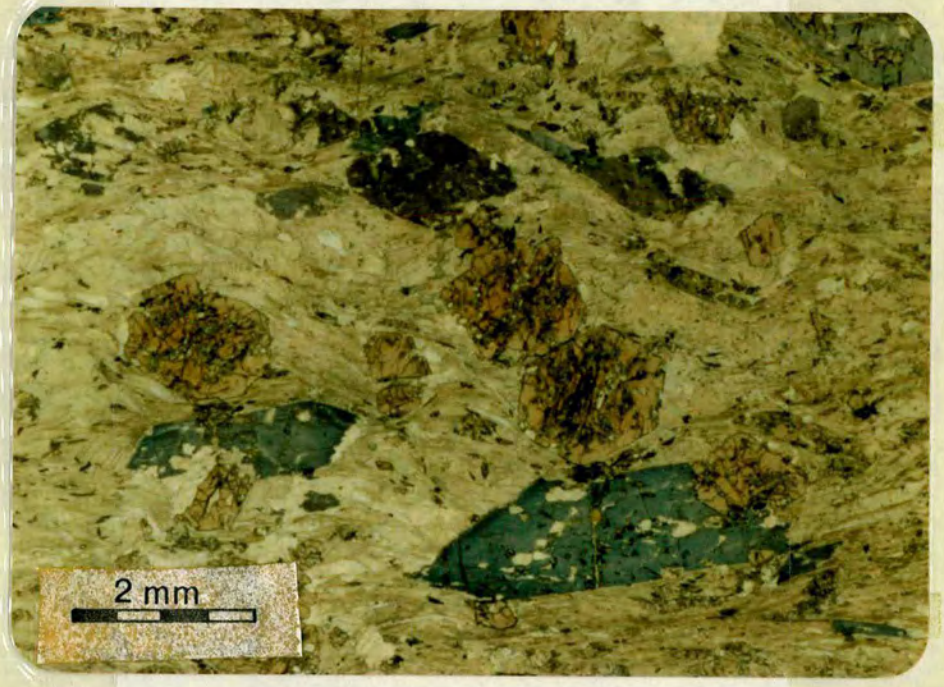

Figure 3.1 Glaucophane-garnet porphyroblast schist from near Kini, (87/222). Although this porphyroblastic habit is atypical for the schists, this slide was chosen because, both diamond-shaped cross-sections, and prismatic length sections can be seen, and glaucophane displays the characteristic blue-purple colours. Assemblage : glaucophane-garnet-phengite-calcite-epidote-chlorite-sphene (x 8, PPL).

Colour

Glaucophane is commonly identified on the basis of its distinctive colour in PPL. The intensity of this colour is determined by the ferric-iron content. In general, glaucophane crystals from Syros show the expected purple colour, with pleochroism ranging from blue to colourless to purple, but in the very magnesian schists it is almost colourless. In this case, glaucophane cannot be distinguished from tremolite/actinolite on the basis of colour alone, and other optical properties must be used, (glaucophane has a smaller 2V, and extinction angle than the calcic amphiboles). Glaucophane occasionally shows optical zoning, though generally this is rare. The zoning is always in the same sense, with pale coloured cores and deeper coloured rims.

Recalculation of Fe^{3+}

The electron microprobe cannot distinguish between Fe^{3+} and Fe^{2+}, and therefore only total iron contents can be determined using this technique, quoted as a wt% FeO. However, on the basis of colour alone, it is obvious that most glaucophane crystals will contain both Fe^{2+} and Fe^{3+}. Fe^{2+} and Fe^{3+} play different roles in amphibole crystal chemistry, and in particular, the amount of Fe^{3+} is critical in determining the occupancy of the A-site (Robinson et al 1981). Wet chemical analysis, combined with electron microprobe data, undoubtedly provides that most accurate way of determining the Fe^{2+}/Fe^{3+} ratio, but an acceptable alternative involves estimating Fe^{3+} from the stoichiometric constraints of amphibole crystal chemistry. The Fe^{3+} contents of glaucophane were estimated using the RECAMP program of Spear and Kimball (1974). RECAMP uses nine recalculation procedures, which should span the range of possible Fe^{3+} contents in a given amphibole. The recalculation options available are:

1) All iron as Fe^{2+}
2) All iron as Fe^{3+}
3) Si = 8, assumes no tetrahedral Al^{3+}
4) Si+Al = 8, allows tetrahedral Al^{3+}
5) SUM FM=13, only Ca and Na permitted in the M4 site
6) SUM CA=15, all Ca assigned to the M4 site
7) SUM NA=15, all Na assigned to the M4 site

8) SUM K=16, A site is filled

9) Average Fe^{3+}, in this recalculation the amphibole formula is calculated using the average of the highest and lowest values of Fe^{3+} contained in the other stoichiometrically acceptable recalculations.

For each analysis the program outputs every stoichiometrically acceptable recalculation, and in the case of the Syros amphiboles the recalculations given are usually 1), 9), and either 7) or 5). Recalculation 1) assumes that all iron is Fe^{2+}, which is obviously unacceptable, 5) minimises Na in the A-site and maximises Fe^{3+}, while 7) excludes Na from the A-site altogether, which is unlikely to be true. As each of the recalculations, 1),5) and 7) have disadvantages, or obvious flaws, recalculation 9), using the average value of Fe^{3+} was chosen in all cases.

The compositions of the glaucophanic amphiboles from the schists, marbles and metabasites are plotted in a Miyashiro diagram (Miyashiro 1957), figure 3.2a, in terms of Mg/Fe glaucophane and Mg/Fe riebeckite. Most analyses plot as glaucophane, with only a few ferric-iron rich amphiboles plotting in the crossite field. Table 3.1 lists some representative amphiboles analyses. Figure 3.2b shows core and rim analyses of glaucophane from the schists again plotted on a Miyashiro diagram. Although optically the zoning is always in the same sense (see section on colour), chemically it is more erratic. There is no consistent trend showing an increase in Fe^{3+} coupled with a decrease in Mg and Al such as might be expected if crystallisation continued under conditions of falling pressure.

Coexisting glaucophane and actinolite

There are two distinct situations where coexisting glaucophane and actinolite form part of the primary assemblage.

Kaloyeros metagabbro

Glaucophane and actinolite occur together in the interior of a large gabbroic body on the northern coast of the island. It is inferred that the original pyroxene was replaced by actinolite, and the original plagioclase by a mixture of clinozoisite and albite, probably as a result of sub-seafloor epidote-amphibolite facies metamorphism.

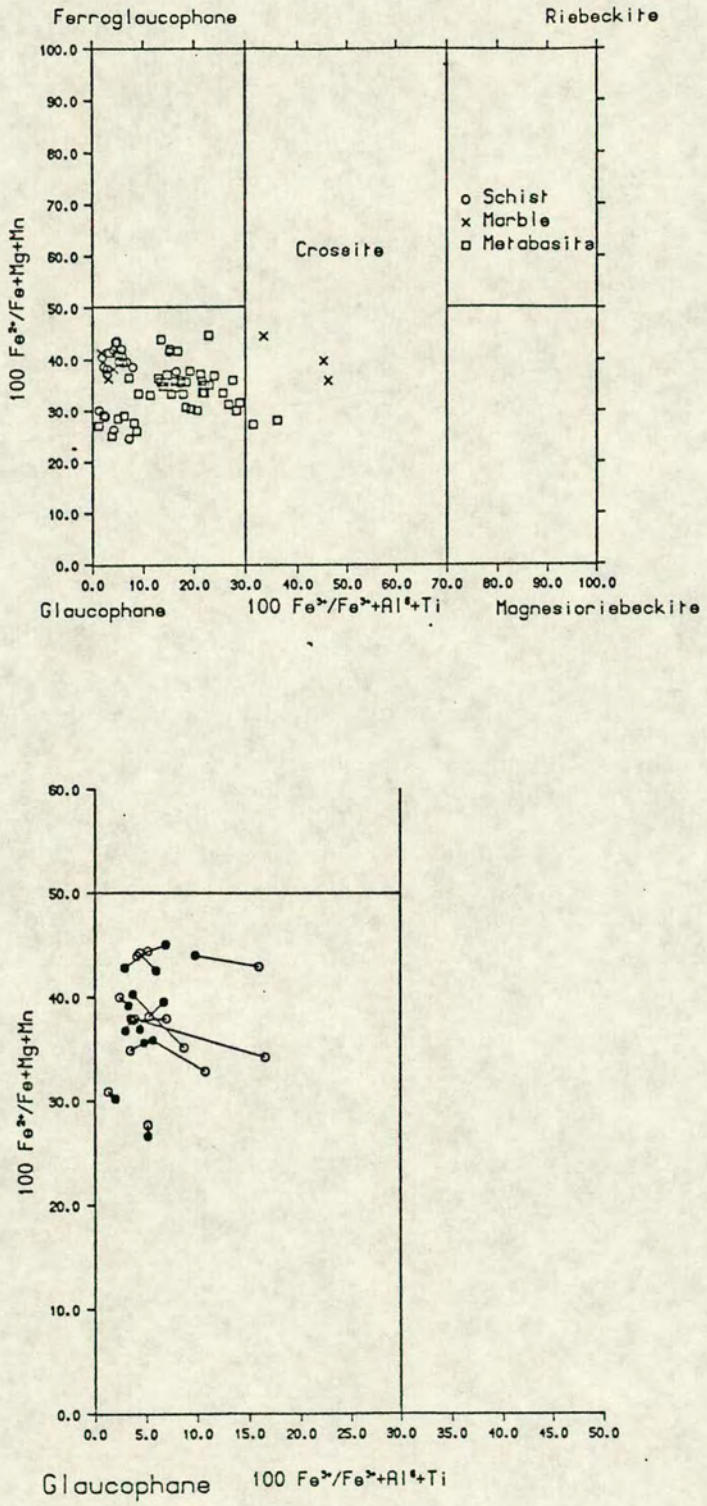

Figure 3.2 a) Classification of sodic amphiboles in a Miyashiro diagram (Miyashiro 1957). Analyses from different rock types are identified in the key. b) Core and rim analyses of glaucophane from schists. Lines connect analyses from the same crystal. Filled circles = rims; open circles = cores.

Table 3.1 Representative analyses, and structural formulae of glaucophane. See text for comments on Fe3+ recalculation.

	1	2	3	4	5	6	7	8	9	10
SiO2	56.76	56.43	56.69	57.73	56.36	56.98	57.14	55.37	57.02	57.78
Al_2O_3	10.68	10.10	10.64	11.82	11.66	10.90	10.93	11.43	12.06	11.45
TiO_2	0.00	0.02	0.01	0.05	0.00	0.01	0.02	0.05	0.03	0.02
Cr_2O_3	0.00	0.01	0.02	0.02	0.00	0.02	0.00	0.02	0.04	0.01
MgO	9.66	9.86	9.96	11.11	11.52	8.66	8.79	8.50	8.54	9.17
FeO	11.04	11.88	10.59	8.52	7.82	12.46	11.97	12.98	12.40	11.10
MnO	0.04	0.04	0.07	0.10	0.03	0.09	0.05	0.09	0.02	0.11
CaO	1.11	1.00	1.06	1.24	0.85	0.20	0.50	1.31	0.47	0.16
Na_2O	7.16	7.11	7.01	7.30	7.29	7.51	7.22	7.13	7.54	7.71
K_2O	0.01	0.02	0.04	0.03	0.01	0.03	0.01	0.04	0.02	0.01
Total	96.46	96.47	96.09	97.92	95.54	96.86	96.63	96.92	98.14	97.52
Si	7.94	7.91	7.94	7.87	7.83	7.96	7.98	7.80	7.87	7.97
Al^{iv}	0.06	0.09	0.06	0.13	0.17	0.04	0.02	0.20	0.13	0.03
Al^{vi}	1.70	1.58	1.69	1.76	1.74	1.76	1.78	1.70	1.83	1.83
Ti	0.00	0.00	0.00	0.01	0.00	0.00	0.00	0.01	0.00	0.00
Fe^{3+}	0.05	0.16	0.09	0.04	0.13	0.11	0.08	0.09	0.09	0.05
Mg	2.01	2.06	2.08	2.26	2.38	1.80	1.83	1.78	1.76	1.88
Fe^{2+}	1.24	1.23	1.15	0.93	0.77	1.34	1.32	1.44	1.34	1.23
Mn	0.01	0.01	0.01	0.01	0.00	0.01	0.01	0.01	0.00	0.01
Ca	0.17	0.15	0.16	0.18	0.13	0.03	0.08	0.19	0.07	0.02
Na	1.82	1.80	1.82	1.81	1.84	1.94	1.90	1.78	1.91	1.96
Na	0.12	0.13	0.09	0.12	0.13	0.10	0.05	0.17	0.11	0.10
K	0.00	0.00	0.01	0.01	0.00	0.01	0.00	0.01	0.00	0.00

Under the peak metamorphic conditions glaucophane was stabilised relative to actinolite, but, the bulk chemical equilibration of individual samples was dependent on the degree and intensity of local deformation, (Ridley and Dixon 1984). This agrees with the observation that actinolite, albeit largely replaced by glaucophane, is only preserved in the relatively undeformed centre of the metabasite, where equilibrium has been established on a very small scale. Towards the margins of the metagabbro where the rock is more intensely sheared and deformed, actinolite is absent, having been entirely replaced by glaucophane, the equilibrium situation. Figure 3.3 shows an example of the partial replacement of actinolite.

Aspro

On the north-west coast, at Aspro, glaucophane and actinolite again coexist, but here there is no suggestion of a reaction relationship. Individual crystals are composed partly of glaucophane and partly of actinolite, but importantly, there is no consistent core/rim relationship between the two phases such as would be expected if one phase were replacing another. The intracrystalline contacts between the two amphiboles are optically and chemically sharp, (see figure 3.4). Examples of these "mixed crystals" are rare on Syros. Although Dixon (1969) records their occurrence in metabasites at Kastri, in this study they have only been found at Aspro, in Ca-rich schists. However, examples of coexisting glaucophane and actinolite have been reported from many other blueschist terrains, (Banno 1958, Black 1973,Maresch 1982, McBirney *et al* 1967), and the homoaxial intergrowths seen on Syros are particularly similar to those described by Himmelberg and Papike (1969). The equilibrium coexistence of primary glaucophane and actinolite is due to the presence of a miscibility gap between sodic and calcic amphiboles under these PT conditions.

Figure 3.5 shows the compositional range of the calcic amphiboles and their coexisting sodic counterparts. A significant feature of the plot is the large compositional range seen in the calcic amphiboles compared to the restricted range of the coexisting glaucophane compositions. This suggests that the solvus is asymmetrical, with a steep limb towards the glaucophane endmember, and a more gentle limb towards the actinolite end.

Recent work by Reynard and Ballevre (1988) tried to constrain the shape of this miscibility gap using natural examples. They selected examples of coexisting glaucophane and actinolite from the available literature, including data from Sifnos (Schliestedt 1980, 1986).

Figure 3.3 Photomicrograph of the Kaloyeros metagabbro (87/194). The centre of the photograph shows a large relic of unrecrystallized actinolite, partially replaced by pale purple glaucophane (magnification x 8, PPL).

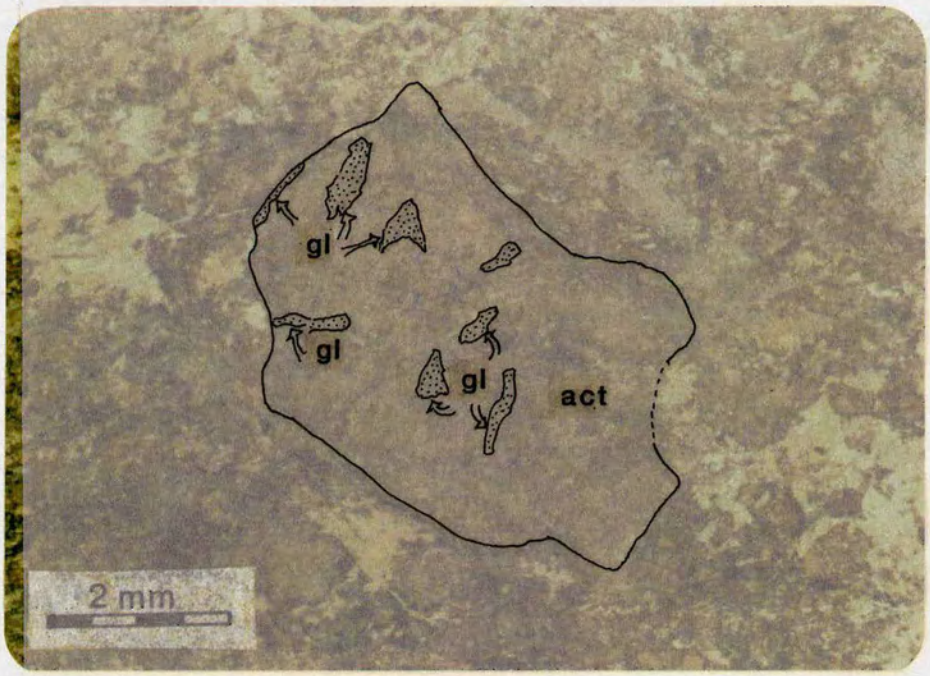

Figure 3.3 Photomicrograph of the Kaloyeros metagabbro (87/194). The centre of the photograph shows a large relic of unrecrystallized actinolite, partially replaced by pale purple glaucophane (magnification x 8, PPL).

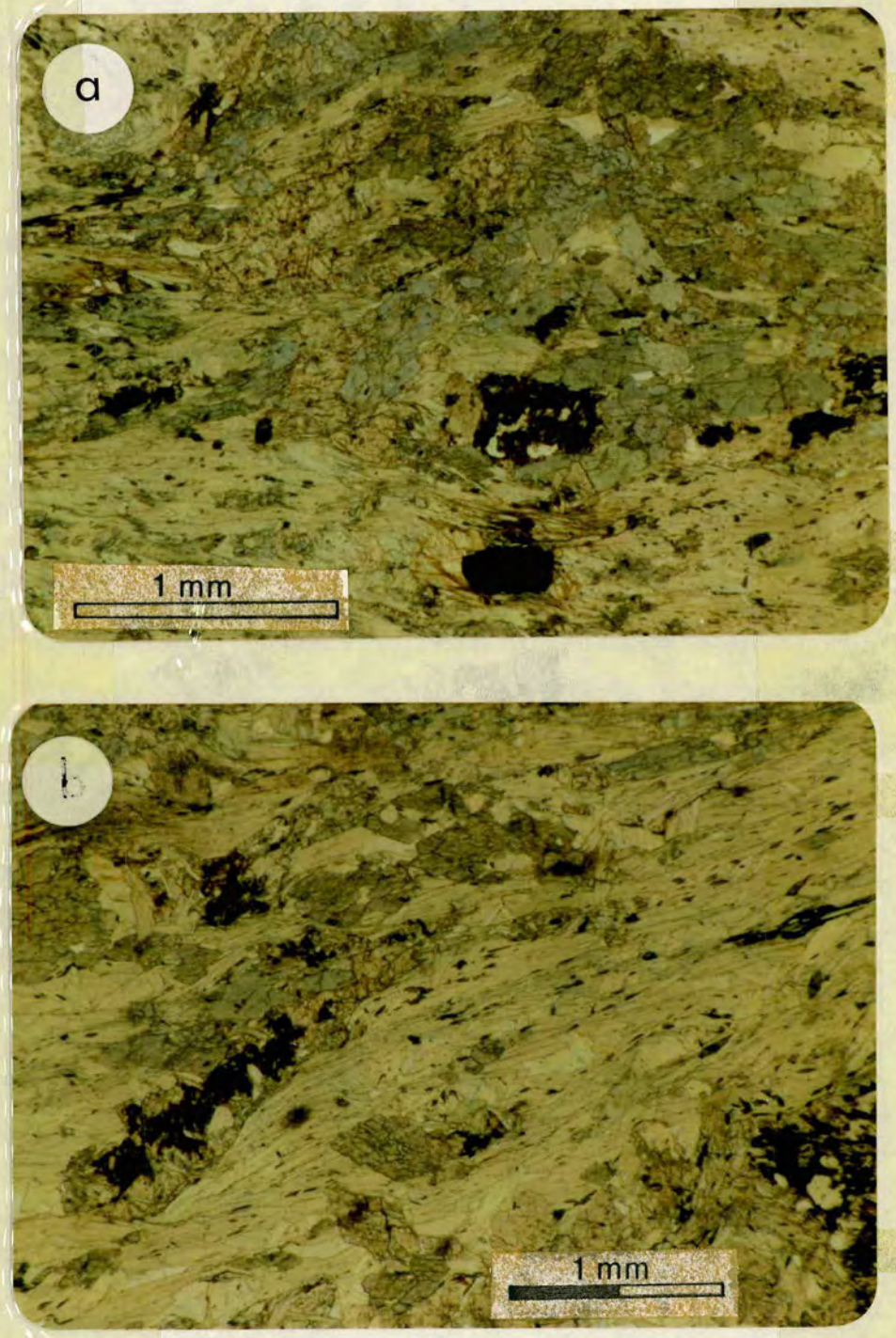

Figure 3.4 a) and b) show a number of single amphibole grains composed of intergrown sodic (blue, purple) and calcic (green) amphibole. In both examples the matrix is composed of interleaved chlorite and phengite, quartz and calcite, with accessory sphene. The dark patches are former dolomite-ankerite rhombs, now replaced by calcite. (see section on carbonates for discussion).
a) 86/53A x25, PPL; b) 86/53H x 20, PPL)

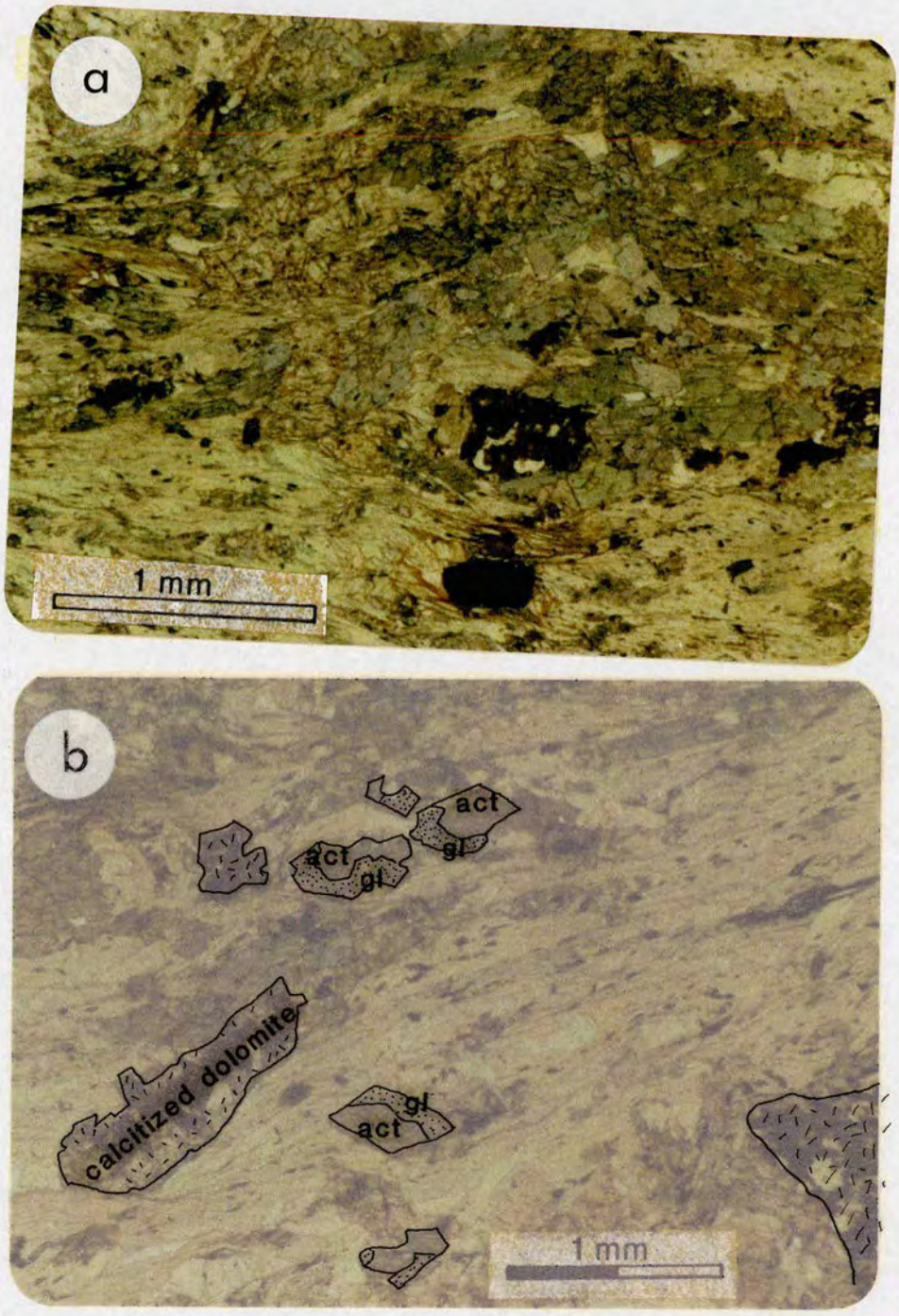

Figure 3.4 a) and b) show a number of single amphibole grains composed of intergrown sodic (blue, purple) and calcic (green) amphibole. In both examples the matrix is composed of interleaved chlorite and phengite, quartz and calcite, with accessory sphene. The dark patches are former dolomite-ankerite rhombs, now replaced by calcite. (see section on carbonates for discussion).
a) 86/53A x25, PPL; b) 86/53H x 20, PPL)

Table 3.2 Representative analyses and structural formulae of coexisting actinolites and glaucophanes. Pair analyses have the same number.

	1A	1G	2A	2G	3A	3G	4A	4G	5A	5G
SiO_2	54.34	56.90	54.62	57.20	54.51	57.08	54.90	56.93	53.99	57.32
Al_2O_3	3.37	10.25	3.09	10.23	2.99	10.64	1.20	10.21	3.47	10.23
TiO_2	0.03	0.02	0.05	0.04	0.02	0.04	0.02	0.05	0.06	0.03
Cr_2O_3	0.07	0.03	0.16	0.17	0.10	0.10	0.00	0.00	0.00	0.00
MgO	16.44	10.09	16.74	10.26	16.84	10.39	17.18	9.80	16.00	9.75
FeO	9.66	10.51	9.70	10.25	9.73	10.00	10.08	10.93	10.80	11.31
MnO	0.11	0.07	0.05	0.02	0.07	0.06	0.12	0.03	0.08	0.06
CaO	10.30	0.92	10.48	0.82	10.84	1.09	11.54	6.86	10.36	0.95
Na_2O	1.77	7.04	1.63	7.13	1.52	6.96	0.85	7.13	1.73	7.19
K_2O	1.10	0.00	0.08	0.03	0.08	0.03	0.06	0.03	0.17	0.02
Total	96.19	95.83	96.60	96.15	96.70	96.39	95.95	95.97	96.60	96.86
Si	7.78	7.98	7.78	7.98	7.77	7.94	7.91	7.99	7.73	7.99
Al^{iv}	0.22	0.02	0.22	0.02	0.23	0.06	0.09	0.01	0.27	0.01
Al^{iv}	0.35	1.67	0.30	1.67	0.27	1.69	0.11	1.68	0.32	1.67
Ti	0.00	0.00	0.00	0.00	0.00	0.00	0.00	0.00	0.01	0.00
Fe^3	0.12	0.10	0.14	0.09	0.12	0.09	0.11	0.08	0.016	0.07
Mg	3.51	2.11	3.55	2.14	3.58	2.15	3.69	2.05	3.42	2.02
Fe^{2+}	1.03	1.14	1.01	1.11	1.04	1.07	1.11	1.20	1.13	1.25
Mn	0.01	0.01	0.01	0.00	0.01	0.01	0.00	0.00	0.01	0.01
Cr^{3+}	0.00	0.00	0.02	0.02	0.01	0.01	0.00	0.00	0.00	0.00
Ca	1.58	0.14	1.60	0.12	1.66	0.16	1.78	0.13	1.59	0.14
Na	0.39	1.83	0.36	1.85	0.31	1.81	0.19	1.85	0.36	1.84
Na	0.11	0.08	0.10	0.08	0.11	0.07	0.05	0.09	0.12	0.10
K	0.02	0.00	0.02	0.01	0.02	0.00	0.01	0.00	0.02	0.00

The shape of the solvus is essentially temperature dependent but, as pointed out by Reynard and Ballevre (1988), the solvus is multidimensional, and they therefore suggest that any representation in two dimensional space can only be valid if the chemistry of the amphiboles is governed by a single substitution, in this case the glaucophane substitution. In fact this is not strictly true, since a two dimensional section of a three dimensional solvus can hold one substitution at a fixed value while showing the effect of another. In any case, due to the complex nature of amphibole chemistry, several substitution vectors are likely to be involved. Figure 3.6a is a plot of Na_{M4} versus $R^{3+}=Al^{VI}+2Ti+Cr+Fe^{3+}$. This plot was used by Reynard and Ballevre (1988) to determine how closely the coexisting amphiboles conformed to the endmember glaucophane and actinolite compositions. The fit using Syros amphiboles is very good. However, the diagram only measures variations in two parameters, and other important substitution vectors, such as the edenite vector, will be ignored. Analyses of coexisting glaucophane and actinolite from Syros have been plotted on the solvus diagram of Reynard and Ballevre (1988), figure 3.6b, and some of the corresponding probe analyses are given in table 3.2. The Syros data, plotted over the temperature range 450-500°C, lies quite a distance off the proposed solvus. When estimating the Fe^{2+}/Fe^{3+} ratio, Reynard and Ballevre (1988) opted for a recalculation scheme which maximised the Fe^{3+} content, and this is in contrast to the scheme used for the Syros amphiboles, (average Fe^{3+}). This obviously affects the structural formulae of the amphibole, and consequently the $NaAlCa_{-1}Mg_{-1}$ vector. In order to quantify the magnitude of this effect the Syros amphiboles analyses were recalculated adopting the Reynard and Ballevre (1988) scheme. The position of the amphiboles does change slightly, but not enough to move them onto the solvus, (see figure 3.6b). This discrepancy indicates a failure to take into account some other important factor or factors, such as f_{O2}, which influence the natural solvus.

Other examples of coexisting amphiboles

In the South of the island where the greenschist overprint is strongly developed, glaucophane often occurs rimmed by a strongly coloured blue-green amphibole. In this case the two amphiboles are not in stable equilibrium. The calcic amphibole displays a consistent rimming relationship to the glaucophane, suggesting it is a later overgrowth. Such textures are related to changing P-T-a_{H2O} conditions through the metamorphic pile. Ridley (1982) produced PTt paths for a simple vertical stack accumulated from the base. Applying the results of this modelling to Syros, the south of the island should have experienced its maximum temperature ($\approx$ 550 °C) at lower pressures, (see figure 3.7).

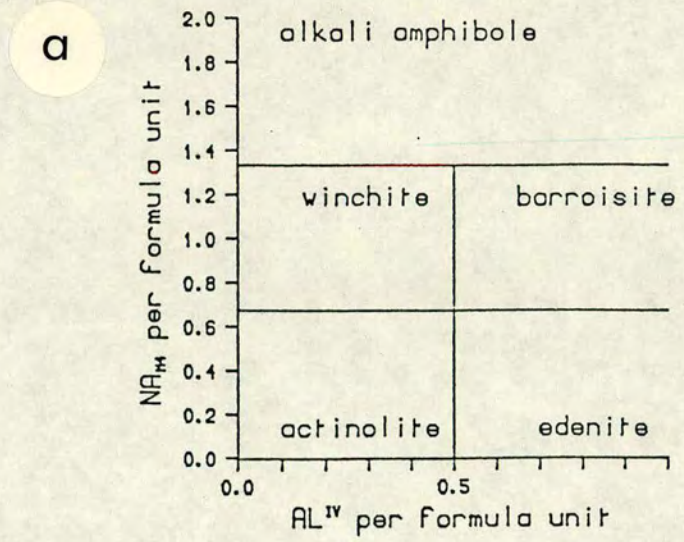

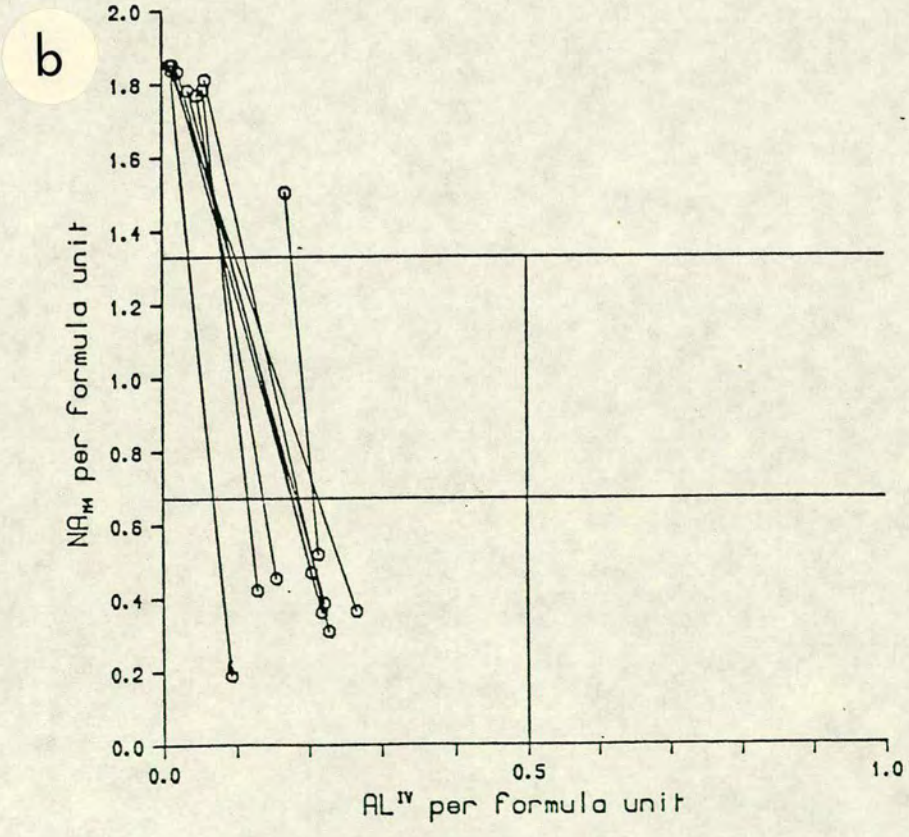

Figure 3.5 Na^{m4} versus Al^{IV} for coexisting calcic and sodic amphiboles. Tie-lines connect analyses from the same crystal.

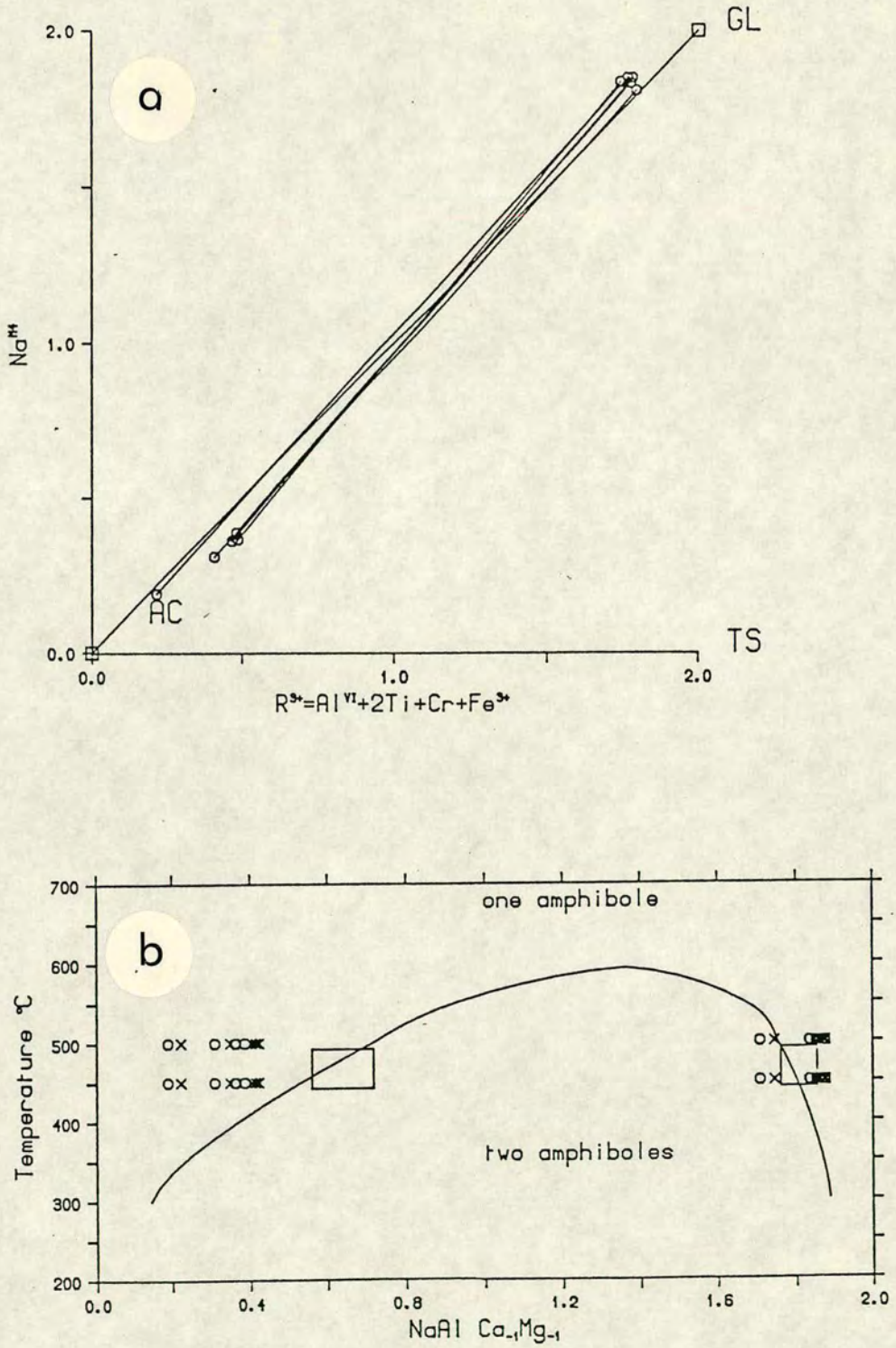

Figure 3.6 a) Na^{M4} versus $R^{3+} = Al^{VI} + 2Ti + Cr + Fe^{3+}$ content of coexisting actinolite-glaucophane pairs. Tie-lines connect analyses from the same crystal. b) Proposed solvus between calcic and sodic amphiboles (after Reynard and Ballèvre 1988). Circles = coexisting calcic and sodic amphiboles from Syros, calculated for average Fe^{3+}, crosses = Syros data, amphiboles recalculated to maximise Fe^{3+}, boxes = range of data from Sifnos.

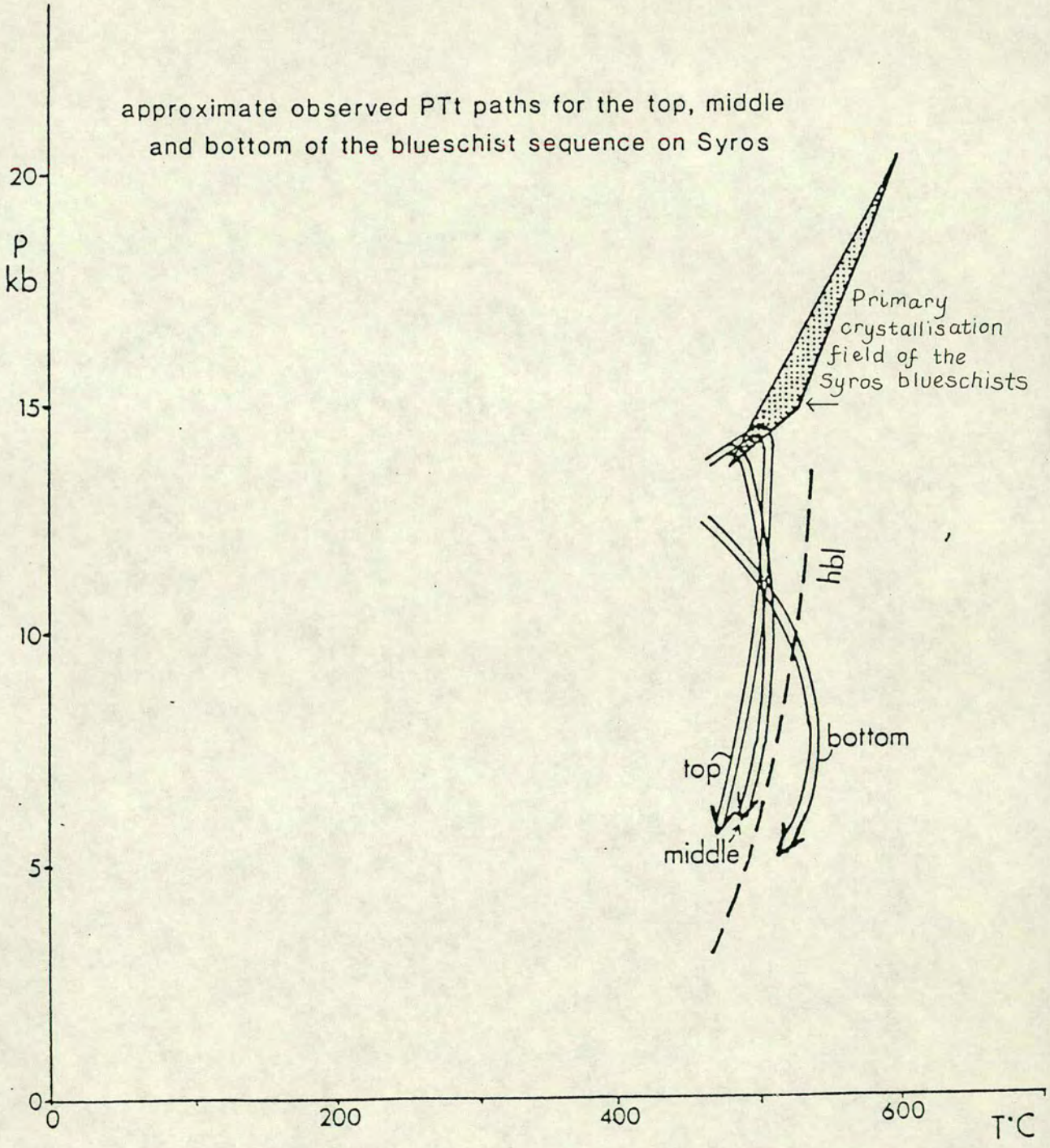

Figure 3.7 Summary of the inferable segments of the PTt paths for the top, bottom and middle of the sequence in the main unit on Syros (from Ridley 1982).

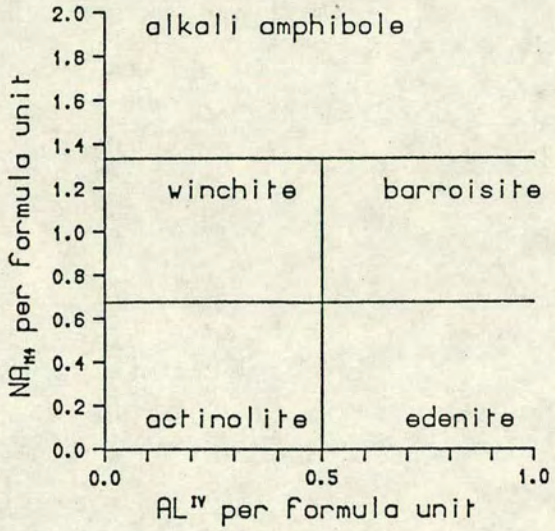

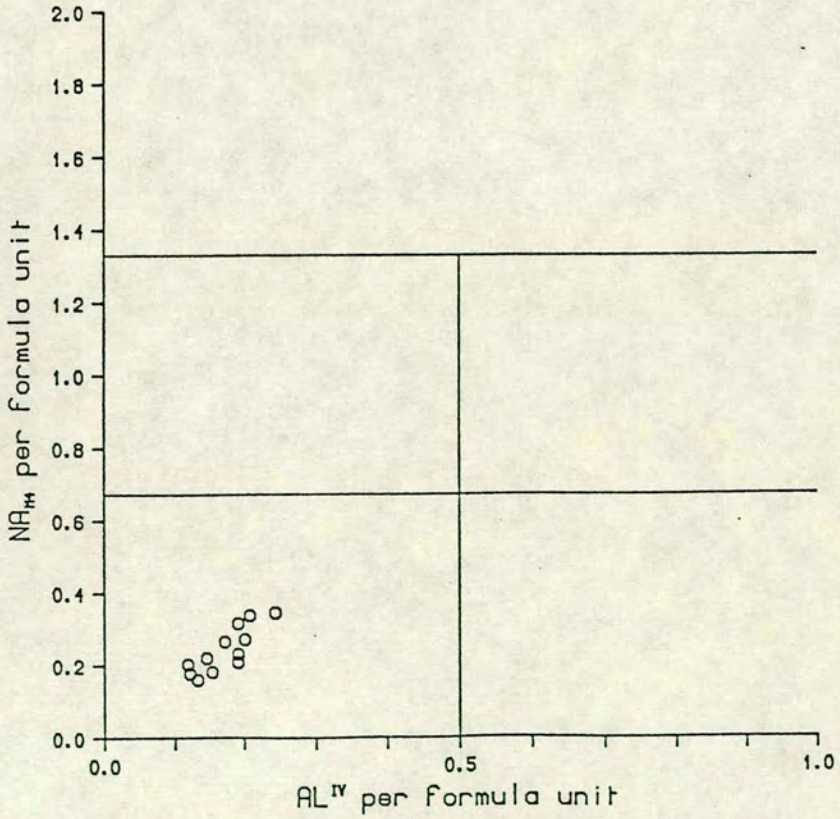

Figure 3.8 Plot of Na^{M4} versus Al^{IV}, showing the range of compositions in primary actinolites.

This may explain why these calcic amphibole overgrowths are restricted to rocks from the south of the island.

Actinolite

Primary actinolite is present on its own in some impure marbles and chloritic schists. These rocks typically have a low Na content, and a high Mg or Ca content, and the actinolite occurs as small prismatic crystals with a faint green colour. The compositions of the primary actinolites are plotted in figure 3.8 in terms of Al^{VI} versus Na^{M4}. The points define a linear trend of increasing Na with increasing Al, indicating a regular substitution of Na and Al for Ca, ($Na^{M4}Al^{M13} = Ca^{M4}Mg^{M13}$) in these amphiboles.

3.2 WHITE MICAS

White micas are ubiquitous in the metasediments, and occur widely in the metabasites, though they are not as abundant. In the metasediments they occur largely as laths outlining the foliation, and are an important matrix phase. Occasionally the mica occurs as large plates, which have overgrown an earlier fabric, but this habit is largely restricted to the metabasic rocks. No pyrophyllite or margarite was detected, and the Ca content of all the micas is low.

K-mica - phengite

All the K-bearing micas analysed are phengitic, with 3.2 to 3.5 Si^{VI} ions per formula unit. In all assemblages K-mica is the only K-bearing phase. Figure 3.9a shows a plot of Al_{total} versus Si^{VI}, and the marked negative correlation between the Si and Al contents shows the importance of Tschermak exchange, $(Mg,Fe)^{VI},Si^{IV}$ -- Al^{VI},Al^{IV}, in these micas.

There has been much discussion and dispute in the literature as to whether the Si content of phengites is controlled by metamorphic grade (Velde 1967), or host rock composition (Brown 1968, Hock 1974). Although there are examples which suggest that the maximum amount of Si stable in phengites decreases with increasing metamorphic grade (Black 1975, Frey 1983), it appears that under any particular set of PT conditions the Si content can vary quite considerably and closely reflects the parent rock chemistry (Brown 1968). Most of the phengites on Syros show remarkably small variations in Si^{VI}, despite a range of parent rock compositions, and this implies that the rock compositions are buffering the phengite content to some

extent, though exactly how is not clear. Figure 3.9b is an AKF plot of the phengites, with some paragonite analyses plotted for comparison.

Some of the phengites, and particularly those from Aspro on the north-west coast, have a distinct greenish colouration in PPL. Although highly celadonitic phengites can appear green in colour even when Cr contents are low, the phengites at Aspro contain up to 0.8 wt% chrome, and this is thought to cause the colouration at this locality.

Na-mica - paragonite

Phengite is the dominant sheet silicate in the metasediments, but paragonite can also be present. Although the metabasites have not been studied as extensively as the schists in this study, work by Ridley (1982) and Dixon (1969) suggests that paragonite is common in the metabasic rocks. Paragonite has not been detected in any of the marbles.

Paragonite often occurs interleaved with phengite, and in such cases it is not possible to optically distinguish between the two micas in thin section. However, paragonite produces a distinctive X.R.D trace (paragonite has distinctive peaks at 2Θ = 9.14, 18.39 and 27.77, compared to muscovite peaks at 8.89, 26.85 and 29.91). Approximately 120 samples were examined for paragonite, using the electron microprobe and X-ray diffraction analysis. When paragonite is abundant, and occurs as a distinctly separate phase from phengite, it is much finer grained than the K-mica, often occurring as silky bundles within the foliation.

Coexisting phengite and paragonite are separated by a solvus (Thompson 1974). As temperature increases, muscovite and paragonite approach each other compositionally, but the solvus never closes, (Eugster *et al.* 1972, Zen and Albee 1964). Pressure also influences the solvus, with increasing pressure acting in the opposite sense to temperature, causing the limbs of the solvus to move apart. Figure 3.10a shows a plot of K versus Na per formula unit for coexisting phengites and paragonites. The two micas show a very limited degree of solid solution with each other, indicating that the misciblity gap reaches close to its maximum width under low T, high P conditions. Figure 3.10b again shows a plot of K versus Na per formula unit, for white micas forming lawsonite pseudomorphs.

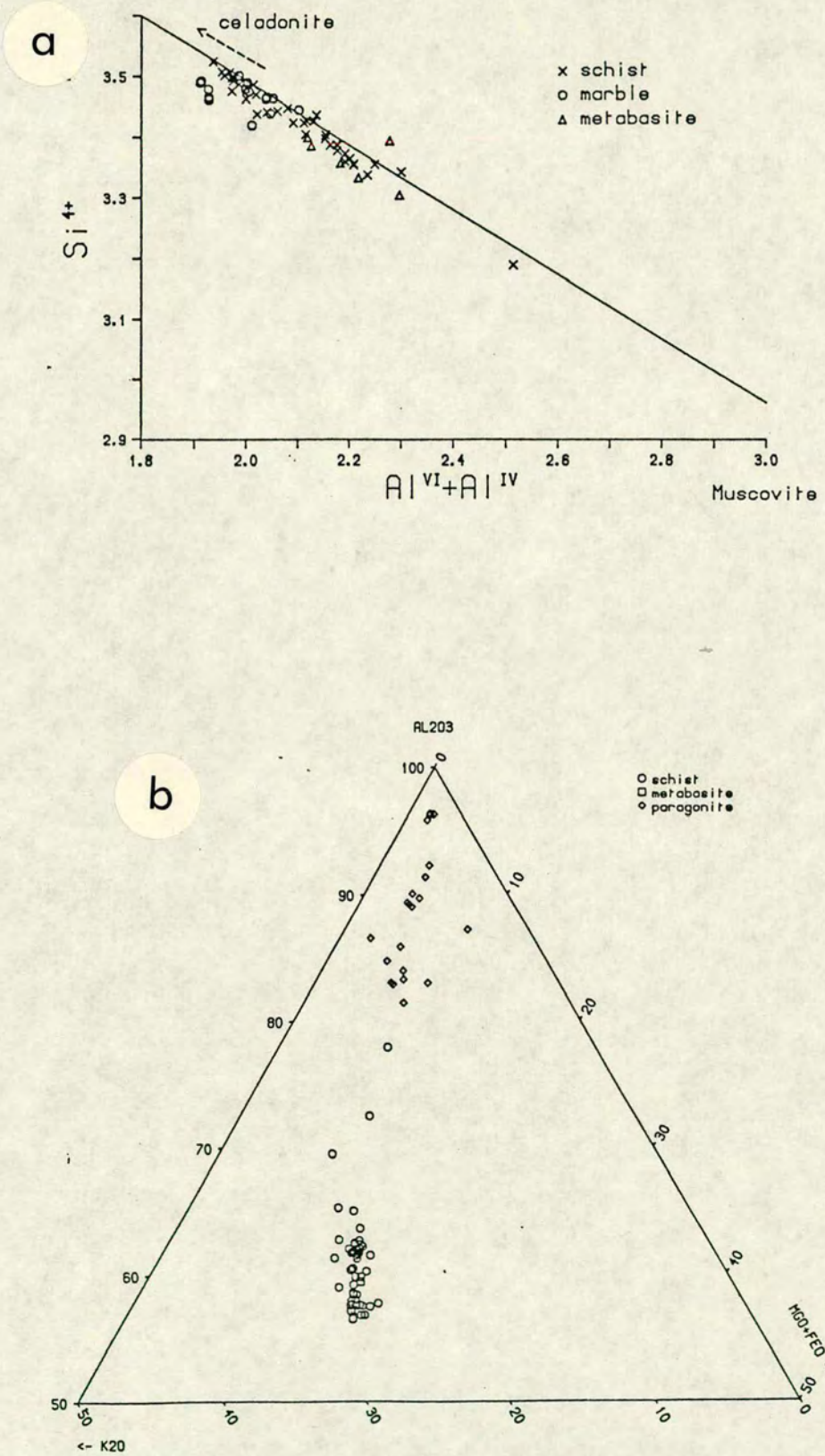

Figure 3.9 a) Si^4 versus Al total for phengites from a variety of rock types (see key). The line indicates the muscovite-celadonite join. b) Phengite compositions from the schists and metabasites plotted on an AKF diagram. Open circles = schists; filled circles = metabasites, diamonds = paragonite.

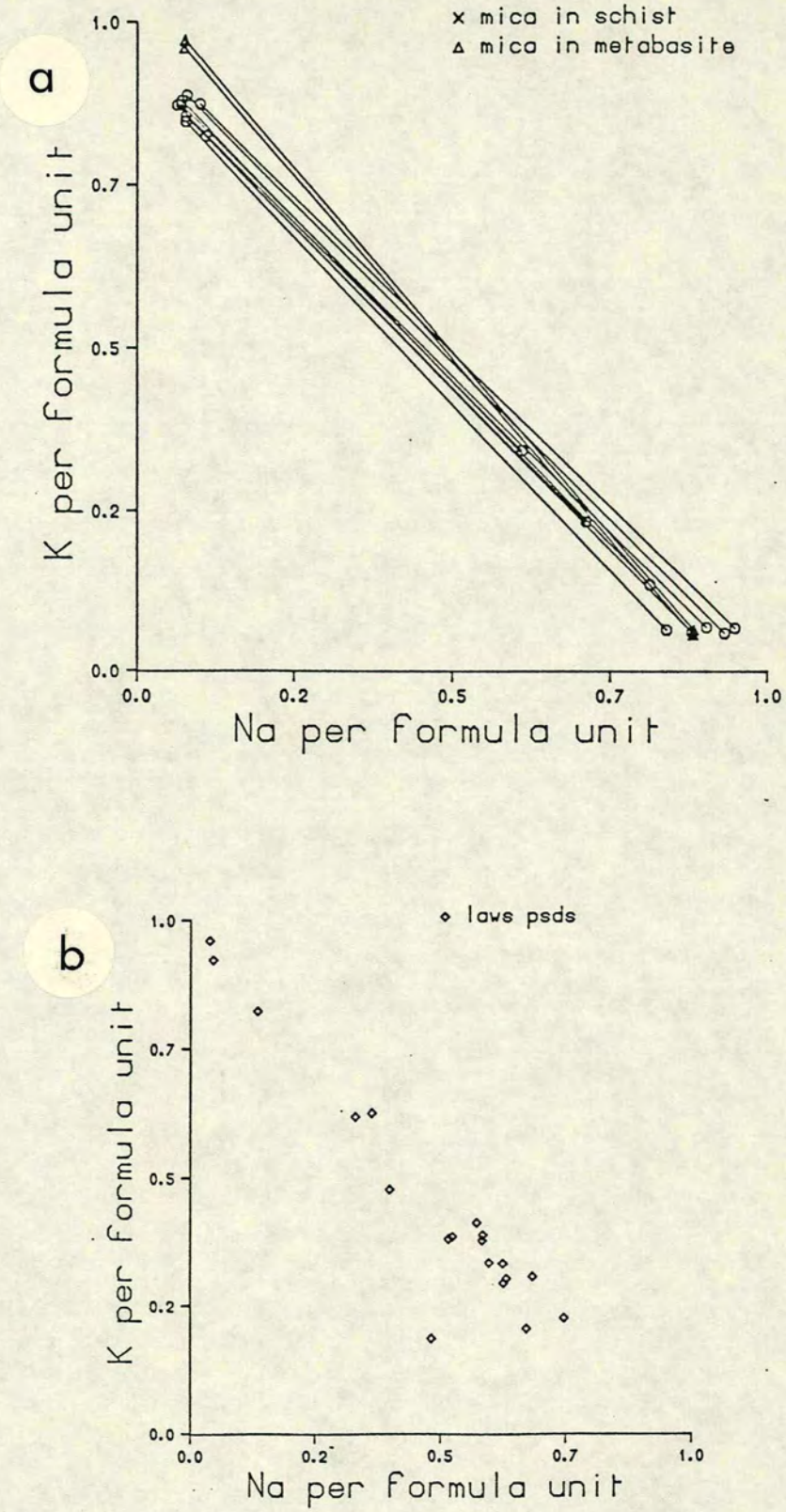

Figure 3.10 a) K versus Na for coexisting phengite-paragonite pairs in schists (open circles) and metabasites (triangles). b) K versus Na for white micas forming lawsonite pseudomorphs. These micas *apparently* show a wide range of Na-K solid-solution, with Na contents in the micas ranging from 0.1 to 0.8.

Table 3.3 Representative analyses and structural formulae of white micas.

	Phen.					Parag.					- Talc		
	49	53	67	69	123	72	98	PH 83	PG 83	PH 94	PG 94	B288	40
SiO2	51.39	51.01	51.07	51.15	49.34	47.71	47.02	50.02	46.81	48.50	46.29	59.68	62.33
TiO2	0.15	0.14	0.15	0.13	0.12	0.03	0.05	0.23	0.06	0.19	0.05	0.04	0.02
Al2O3	25.19	24.99	24.88	23.76	26.29	39.72	39.46	27.10	37.70	27.10	39.04	0.11	0.09
Cr2O3	0.00	0.28	0.00	0.00	0.04	0.04	0.03	0.02	0.04	0.04	0.00	0.02	0.02
FeO	2.50	2.28	2.55	4.46	3.29	0.82	0.67	2.97	0.78	3.56	0.53	6.15	5.01
MnO	0.01	0.03	0.00	0.02	0.02	0.00	0.02	0.01	0.00	0.01	0.00	0.06	0.06
MgO	3.76	4.07	3.86	3.68	3.37	0.05	0.01	3.14	0.68	2.60	0.13	26.13	28.20
CaO	0.00	0.00	0.00	0.14	0.01	0.22	0.08	0.00	0.08	0.02	0.15	0.15	0.03
Na2O	0.27	0.23	0.27	0.23	0.49	7.88	7.10	0.53	6.46	0.58	7.38	0.04	0.01
K2O	10.52	11.12	10.98	11.04	10.47	0.99	0.68	10.18	1.60	10.06	0.82	0.02	0.01
TOTAL	93.79	94.15	93.76	94.61	93.44	97.46	95.12	94.20	94.21	92.66	94.66	92.42	95.83
	Cations per 11 oxygens							Cations per 11 oxygens					
Si	3.48	3.46	3.47	3.49	3.38	2.99	3.00	3.38	3.03	3.35	2.99	4.00	4.00
Al	2.01	2.00	1.99	1.91	2.12	2.94	2.97	2.16	2.88	2.20	2.97	0.00	0.00
Ti	0.00	0.00	0.00	0.00	0.00	0.00	0.00	0.01	0.00	0.01	0.00	0.00	0.00
Cr3+	0.00	0.01	0.00	0.00	0.00	0.00	0.00	0.00	0.00	0.00	0.00	0.00	0.00
Fe2+	0.14	0.12	0.14	0.25	0.18	0.04	0.03	0.16	0.04	0.20	0.03	0.34	0.26
Mn	0.00	0.00	0.00	0.00	0.00	0.00	0.00	0.00	0.00	0.00	0.00	0.00	0.00
Mg	0.38	0.41	0.39	0.37	0.34	0.00	0.00	0.31	0.06	0.26	0.01	2.61	2.69
Ca	0.00	0.00	0.00	0.01	0.00	0.01	0.00	0.00	0.00	0.00	0.01	0.01	0.00
Na	0.03	0.03	0.03	0.03	0.06	0.96	0.88	0.07	0.81	0.07	0.92	0.00	0.00
K	0.91	0.96	0.95	0.96	0.91	0.07	0.05	0.87	0.13	0.88	0.06	0.00	0.00
TOTAL	6.97	7.02	7.01	7.01	7.03	7.04	6.96	6.99	6.98	7.01	7.01	6.99	6.99

In view of the miscibility gap, the apparent intermediate compositions cannot represent true variations in the mica composition.

The most likely explanation for this phenomenon is that finely intergrown phengite and paragonite, forming the pseudomorphs, have been analysed together by the microprobe, resulting in an averaged composition.

Talc

Talc is relatively rare, being restricted to rocks with extremely low Fe/Mg ratios. It was detected in two, highly magnesian, chloritic schists, and in one basic metasomatic schist close to the ultrabasic melange at Kastri. The talc analyses are close to the ideal formula, $(Mg,Fe^{2+})_3Si_4O_{10}(OH)_2$, and contain quite a high percentage of the iron end-member, minnesotaite, (see table 3.3).

In the metasediments, talc coexists with chlorite and phengite. The coexistence of talc and phengite is a characteristic association of high pressure, low temperature rocks (Abraham and Schreyer 1976; Chopin 1981). Experimental work by Schreyer and Baller (1977) found that talc could coexist with phengitic mica at water pressures between 15 and 25 kbars, with the high temperature breakdown of the assemblage occurring at about 650 °C. This assemblage therefore requires a high P_{H2O}, a fact which imposes a large degree of compositional constraint on a coexisting fluid phase. The consequences of this constraint on the blueschist fluid will be discussed more fully in the next chapter.

3.3 CHLORITE

Primary chlorite mainly occurs in the schists, where it can be quite abundant. It is seen occasionally in impure marble units, and never, as a primary phase, in the unmetasomatised metabasites. The chlorite is pale silvery green in colour, weakly pleochroic, and forms lath-shaped crystals aligned in the foliation. The interference colours of these chlorites are normal, first order greys, and this is in contrast to the secondary chlorites which show anomalous blues, purples and browns. The differences between primary and secondary chlorites are discussed in more detail in Chapter 5. Probe analyses of some typical primary chlorites are given in table 3.4. Two methods of chemical classification are commonly used, that of Hey (1954), and Foster (1962).

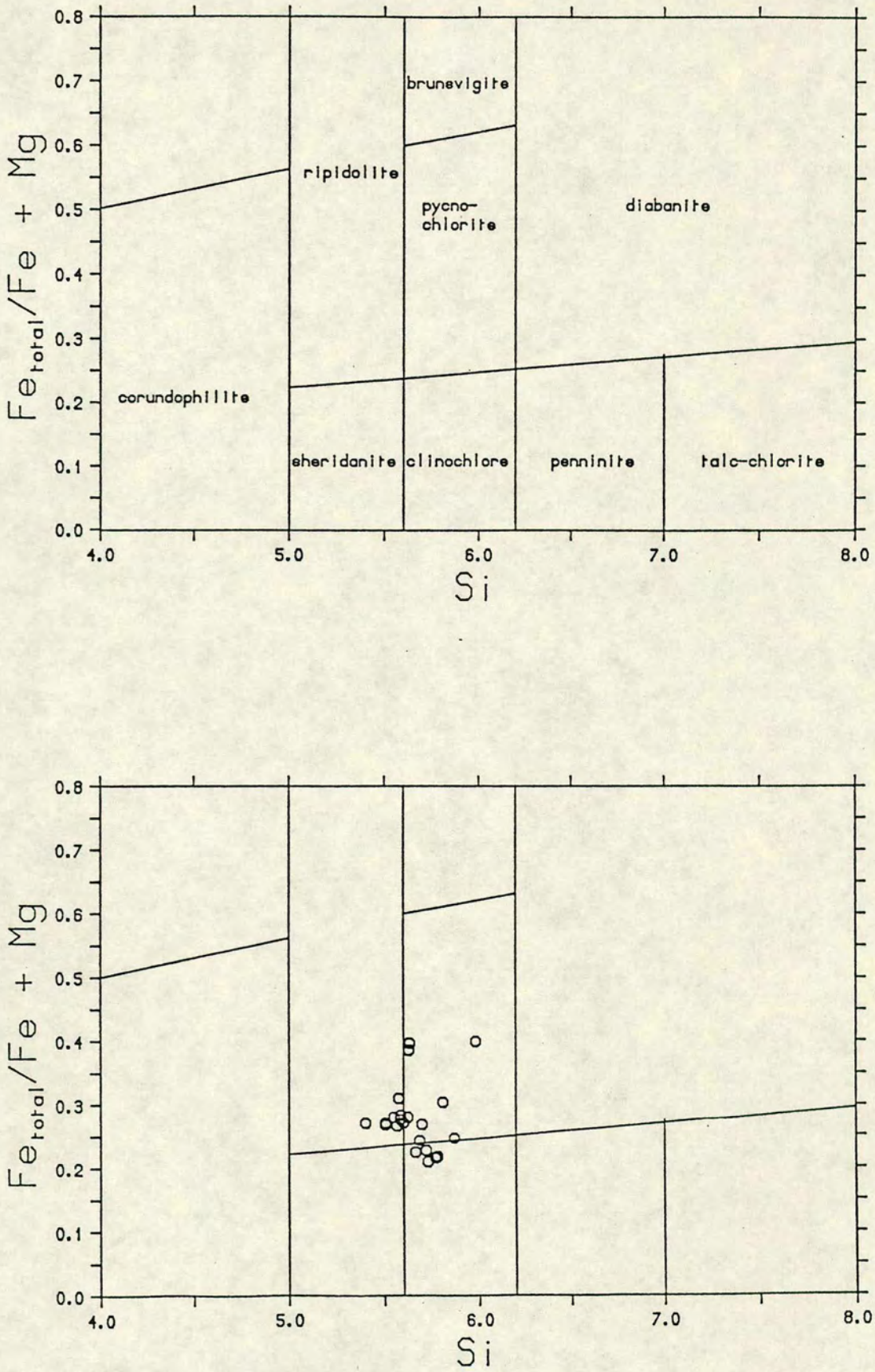

Figure 3.11 Classification of primary chlorites (after Hey 1954).

Table 3.4 Representative analyses and structural formulae of primary chlorites.

	40	31	53	53	63	71	71	40
SiO2	28.68	28.75	28.26	27.28	27.93	27.15	27.20	27.94
TiO2	0.04	0.03	0.04	0.03	0.03	0.04	0.06	0.03
Al2O3	19.18	18.53	18.82	19.52	19.01	20.38	19.91	19.00
Cr2O3	0.47	0.17	0.23	0.11	0.11	0.43	0.49	0.70
FeO	12.03	12.61	13.04	16.38	15.28	15.08	14.83	12.74
MnO	0.14	0.13	0.13	0.15	0.14	0.10	0.08	0.14
MgO	25.59	25.80	24.97	22.09	23.34	23.12	22.90	24.82
CaO	0.03	0.03	0.02	0.03	0.02	0.02	0.05	0.04
Na2O	0.01	0.02	0.02	0.02	0.01	0.00	0.00	0.03
K2O	0.01	0.01	0.04	0.01	0.01	0.01	0.00	0.02
TOTAL	86.18	86.08	85.57	85.62	85.88	86.33	85.47	85.46
			cations	per	28 (O)			
Si	5.72	5.76	5.71	5.61	5.69	5.50	5.56	5.66
Al4	2.27	2.23	2.28	2.38	2.30	2.49	2.43	2.34
Al6	2.24	2.14	2.20	2.35	2.26	2.37	2.36	2.19
Ti	0.00	0.00	0.00	0.00	0.00	0.00	0.00	0.00
Cr3+	0.07	0.02	0.03	0.01	0.01	0.06	0.08	0.11
Fe2+	2.00	2.11	2.20	2.82	2.60	2.55	2.53	2.15
Mn	0.02	0.02	0.02	0.02	0.02	0.01	0.01	0.02
Mg	7.61	7.70	7.52	6.77	7.09	6.98	6.98	7.49
Ca	0.00	0.00	0.00	0.00	0.00	0.00	0.01	0.00
Na	0.00	0.00	0.00	0.00	0.00	0.00	0.00	0.01
K	0.00	0.00	0.01	0.00	0.00	0.00	0.00	0.00
TOTAL	19.97	20.02	20.02	20.00	20.00	20.02	19.99	20.01

Foster's classification involves plotting Fe^{2+}/R^{2+} against silica, and as there is no accurate way of distinguishing between Fe^{3+} and Fe^{2+} in chlorites, (except for wet chemical analysis), Hey's classification is preferred, since only a knowledge of the total iron content is required. Primary chlorite compositions are plotted in figure 3.11. The chlorites show a range of Fe/Mg ratios, largely determined by the bulk rock Fe/Mg ratio. Fe/Fe+Mg ratios range from 0.15 to 0.4, whereas the silica content of the chlorites is more restricted. On the Hey diagram, the chlorites plot as clinochlore or ripidolite with a few pycnochlorites. Several of the chlorites contain quite high amounts (0.5-0.7 wt%) of chrome, (see table 3.4), probably indicating a significant detrital ultramafic component in the host sediment.

3.4 CARBONATES

The majority of the carbonate present on Syros occurs in marble. These are usually calcitic, but dolomite-rich bands are quite common, and dolomite lenses often occur near the base of the larger marble units. The dolomitic lenses can be quite large, as at Oros Syringas, northern Syros, where they are tens of metres long. Carbonate is also found in the metasediments and metabasites. In the metabasites, carbonate often occurs as irregular shaped patches which cut across, or overprint, the rock fabric. Sometimes calcite is replacing a phase, such as epidote or glaucophane, or it occurs associated with other retrograde effects such as chloritization and the development of albite porphyroblasts. The textural habits of carbonate in the metabasites suggest that, in most cases, it is of secondary origin, relative to the blueschist metamorphism. Carbonate in the metasediments can be primary or secondary. The secondary textures are similar to those described in the metabasites, with the development of irregular patches overprinting the fabric, and the replacement of primary blueschist phases. Primary calcite has a grain size comparable to that of other phases in the rock, and carbonate rich layers appear to have deformed with the rock. As deformation is only associated with the blueschist event, the occurrence of folded, carbonate-rich, layers in the schists attests to the fact that this carbonate was present during the peak metamorphic event, (see figure 3.12). Further evidence for this, is the occurrence of carbonate pressure shadows round garnets and ex-lawsonites.

The occurrence of dolomite

As mentioned above, dolomite occurs in the marbles, where it often forms as bands or lenses. Optically, dolomite can be distinguished from coexisting calcite, because it occurs as small rounded grains, which stand out from the surrounding plates of coarsely crystalline calcite, (see figure 3.13a).

In the metasediments the situation is more complicated, because the original dolomite has been replaced by calcite, a process known as dedolomitization. Although dedolomitization has been described by many sedimentary workers (Adams *et al.* 1984; Evamy 1967; Shearman 1959; Saunders 1951; Tucker 1981), it is a rarely described phenomenon in metamorphic rocks. In hand specimen and thin section two types of carbonate can be distinguished, a rusty-brown carbonate, and a clear, 'calcite-like' carbonate. The rusty carbonate was therefore inferred to be ankeritic in composition. However, an extensive study of the carbonate using X-ray diffraction and the electron microprobe, shows that it is in fact calcite. Detailed examination of thin sections provided further textural evidence for dedolomitization. Dolomite is strongly crystalloblastic (Shearman 1959), and tends to develop good rhombohedral outlines. The boundaries of the rhombs in the Syros rocks are still sharply defined, but the dolomite is now pseudomorphed by a fine mosaic of calcite crystals. A characteristic feature of the replacement process is the presence of abundant ferric oxides within the altered rhombs. Holland (1979), described similar textures in ankerites occurring in kyanite eclogites. Although ankerite is still present in this case, he comments, "hematite exsolved as blebs testifies to an earlier higher iron content of these carbonates". The iron oxides occurring in the Syros carbonates were examined under reflected light, where they were identified as being hydrated iron oxides, probably goethite and/or lepidocrocite, rather than hematite. In some cases the oxide inclusions are apparently randomly orientated within the calcite, but in others distinct rhombic zones of ferric oxides are present, picking out "ghost" growth zones in the earlier dolomite crystals.

Use of cathodoluminescence

Further convincing evidence for dedolomitization is the occurrence of small relics of dolomite within pseudomorphed rhombohedra. These relics were first detected by chance, using the electron microprobe, however a more visual and complete picture of the calcite-dolomite distribution was obtained using cathodoluminescence microscopy.

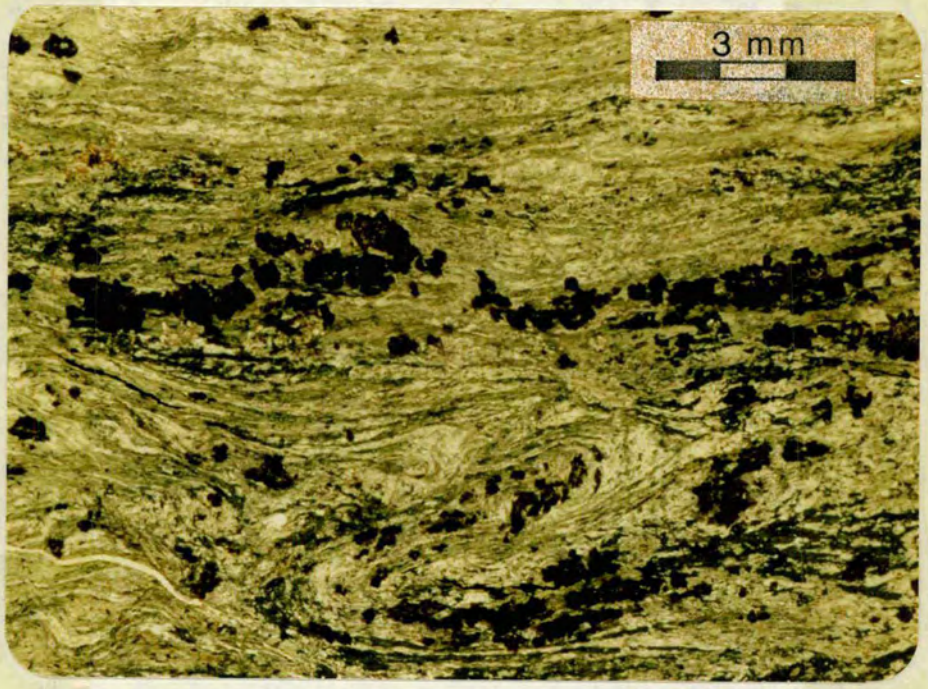

Figure 3.12 Magnesian schist from north of Aspro (86/71). The dark areas are calcitized dolomite-ankerite, note the extent of iron exsolution. In the bottom portion of the photograph a dolomite-rich layer is clearly seen to be folded with the surrounding matrix. This rock contains a large amount of primary chlorite in addition to glaucophane (colourless), quartz, dolomite (psd) and lawsonite (psd) (x 6.3, PPL).

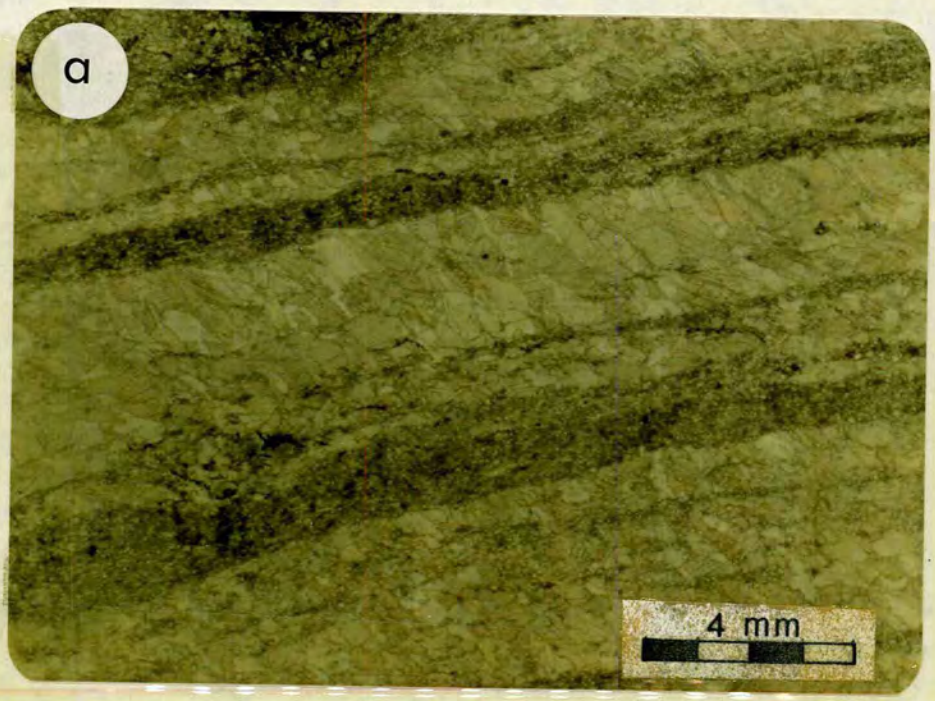

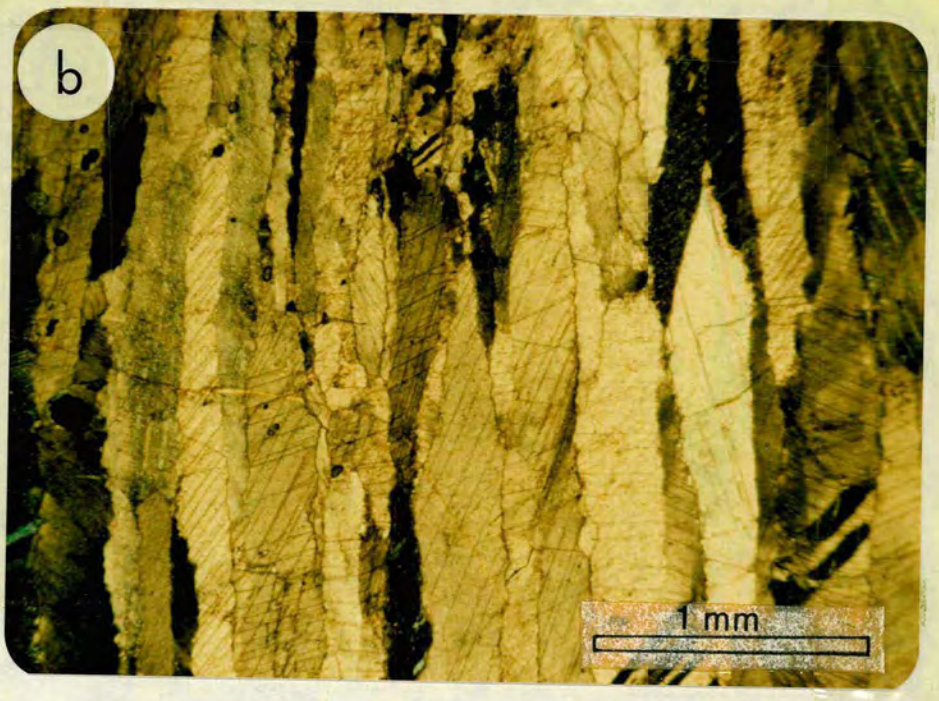

Figure 3.13 a) Dolomite-bearing marble from Kastri (86/104). The dolomite occurs in bands, and is clearly distinguished from the coexisting calcite by its smaller grain size. Note the columnar habit of the intervening calcite. b) Close-up photograph showing the columnar habit of calcite found in the northern marbles (86/6). This habit is interpreted as being pseudomorphic after aragonite. a) = x 5, PPL; b) = x 25 PPL.

Cathodoluminescence is a very useful petrographic tool, it can highlight fabric and textural characteristics which are not obvious in transmitted light, and it allows rapid identification of mineral distributions when the minerals have similar optical properties. Samples do not require sophisticated preparation, uncovered thin sections work well, but most of the samples studied here were simply prepared as cut chips. The sample is placed under vacuum, and bombarded by electrons. The resulting cathodoluminescence is due to electronic transitions within excited atoms or molecules. Mn^{2+} in the calcite lattice activates luminescence, whereas Fe^{2+} quenches luminescence, thus the intensity of the luminescence observed is critically dependent on the Fe/Mn ratio. Examining the Syros samples, the boundaries of the dolomite rhombs could be clearly seen, the calcite luminesed a dull-blue, both within the rhombs, and in the rock matrix, while the small relic patches of dolomite luminesed red, indicating a high Mn content.

Sedimentary examples of dedolomitization (see earlier references) are thought to result from late stage, low temperature processes, probably involving the action of oxidising meteoric water. Replacement under these conditions causes any ferrous iron in the dolomite/ankerite to be oxidised, and thus the altered dolomite contains inclusions of iron oxides (note: calcite can only accommodate very limited amounts of iron into its structure under any conditions). The replacement of dolomite by calcite on Syros probably also occurred at a relatively late stage, and therefore dolomite-ankerite is included as a primary blueschist phase.

Aragonite

The conditions of blueschist metamorphism, 450°C and 14 kbars, mean that the primary carbonate must have lain on the high pressure side of the experimentally derived calcite-aragonite equilibrium (Johannes and Puhan 1971). However, although aragonite has been documented from other blueschist terrains, such as the Franciscan formation, northern California (Coleman and Lee 1962), and New Caledonia (Brothers1970), it has never been found on Syros, despite a comprehensive X.R.D study by Dixon (1969). Calcite crystals in the northern marbles often occur as aligned, elongate grains, a texture which produces a distinctive lineation in the rock, clearly visible in hand specimen, (see figure 3.13b). This texture has been observed by several other workers in the Cyclades (Ridley 1982; Van der Maar 1974), and the texture is interpreted as being a pseudomorphic form after aragonite.

Preservation of aragonite

As was mentioned above, aragonite occurs widely in some blueschist terrains, and is absent from others. The PT conditions experienced by many of these terrains demands that aragonite was the stable polymorph of $CaCO_3$ under the peak metamorphic conditions, so what factors lead to the preservation of aragonite in some areas, and not in others? Carlson and Rosenfeld (1981), examined the preservation of aragonite in the Franciscan blueschists. From a kinetic study of the transition, they inferred that the extent of the aragonite/calcite transformation was dependent on the temperatures encountered by the rocks during their upward transport. For aragonite to be preserved during uplift the temperature cannot exceed 200-250 °C, within the calcite stability field, unless unreasonably high rates of uplift are involved. They concluded that in order to preserve aragonite, uplift must occur under PT conditions similar to those of the prograde blueschist metamorphism. In a similar study, Brown (1962), postulated that the critical maximum temperature for the preservation of aragonite was 300°C, though he concluded that aragonite was unlikely to survive, even at these low temperatures, if a fluid phase was present.

Thermal modelling, carried out by Ridley (1982), suggests that uplift was more or less isothermal for the Syros blueschists, with slightly higher uplift temperatures (≈50 to 100 °C) being experienced down the structural pile. Thus, at the pressure of the calcite-aragonite inversion, the retrograde temperatures would still be above 400 °C, causing aragonite to undergo complete inversion within the calcite field, as would be expected, (Carlson and Rosenfeld 1981). The results of the thermal modelling (Ridley 1982) may also explain the lack of the aragonite pseudomorphic texture in the southern marbles. As the south of the island (bottom of the structural pile) experienced higher uplift temperatures, (see figure 3.7), this may have enabled the southern marbles to recrystallise, obliterating the columnar texture still preserved in marbles from the north.

3.5 LAWSONITE

Lawsonite is found in abundance in the north of the Syros, where it occurs in the graphite-bearing schists, and to a lesser extent in the impure marbles and metabasites. In hand specimen the lawsonite crystals have a distinctive rhombohedral shape, and the rhombs vary in size from a few millimetres up to a centimetre or more, (see figure 3.14a).

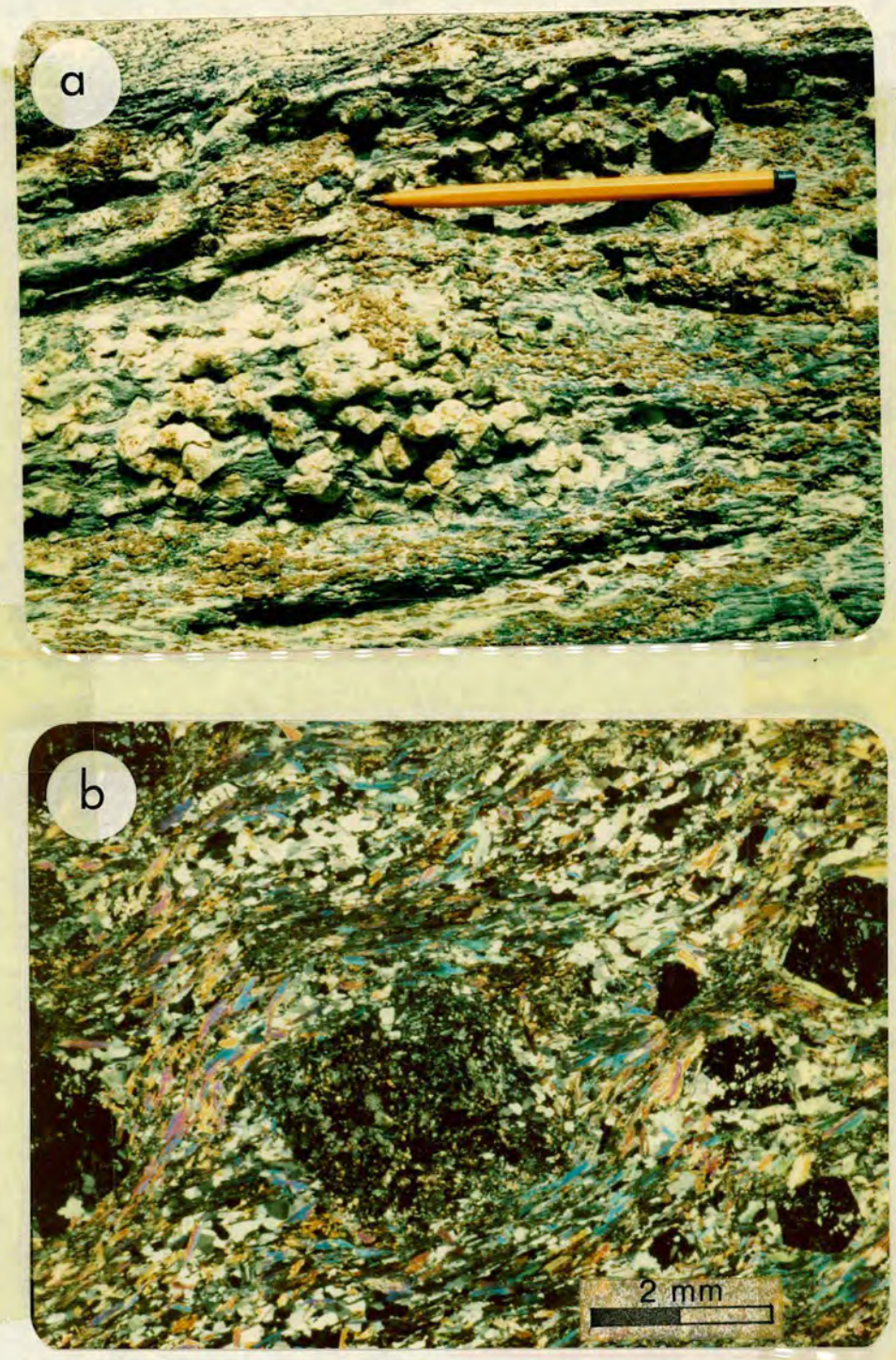

Figure 3.14 a) Distinctive lawsonite rhombs in a matrix of fine grained glaucophane, white mica, and carbonate, Aspro, north-west coast. The colour of the lawsonite pseudomorphs are variable at this locality. Where the matrix is predominantly glaucophane without ankerite, the pseudomorphs are pale, but when ankerite is present (e.g. top right) the pseudomorphs are green. This must be due to a reaction between ankerite, and either the original lawsonite, or, possibly, the later pseudomorphing phases b) Lawsonite pseudomorph in metabasite, showing the characteristic squarish cross section, Gria Spilia (86/141). In this instance the pseudomorph is largely composed of clinozoisite. Note, 1) matrix fabric bends round the porphyroblast; 2) small size of qtz inclusions in garnet compared to matrix quartz. (x 9, PPL).

Table 3.5 Representative analyses and structural formulae of minerals forming lawsonite pseudomorphs.

	cz			mica				
	67	52		52	71	71	10	57
SiO2	38.64	38.30	SiO2	45.59	47.21	48.31	47.64	47.54
TiO2	0.22	0.08	TiO2	0.07	0.14	0.13	0.12	0.07
Al2O3	32.01	32.17	Al2O3	34.71	36.14	28.45	36.07	35.55
Cr2O3	0.00	0.01	Cr2O3	0.07	0.00	0.00	0.04	0.38
FeO	1.08	0.37	FeO	1.42	0.65	2.07	0.71	1.09
MnO	0.02	0.02	MnO	0.00	0.00	0.03	0.03	0.02
MgO	0.05	0.00	MgO	1.58	0.79	2.86	1.14	1.32
CaO	23.85	24.46	CaO	0.07	0.05	0.03	0.03	0.04
Na2O	0.02	0.02	Na2O	4.49	4.96	1.02	5.43	4.73
K2O	0.00	0.00	K2O	4.54	3.63	9.40	3.71	4.03
TOTAL	95.89	95.43		92.51	93.57	92.30	94.92	94.77
	12.5 oxygens			cations per 22 O				
Si	2.99	2.98	Si	3.06	3.10	3.31	3.09	3.10
Al4	0.00	0.01	Al	2.75	2.79	2.30	2.76	2.73
			Ti	0.00	0.00	0.00	0.00	0.00
Al6	1.94	1.94	Cr	0.00	0.00	0.00	0.00	0.02
Ti	0.01	0.00	Fe2+	0.08	0.03	0.11	0.03	0.05
Cr	0.00	0.00	Mn	0.00	0.00	0.00	0.00	0.00
Fe3+	0.07	0.02	Mg	0.15	0.07	0.29	0.11	0.12
Mn	0.00	0.00	Ca	0.00	0.00	0.00	0.00	0.00
Mg	0.00	0.00	Na	0.58	0.63	0.13	0.68	0.59
Ca	1.98	2.04	K	0.38	0.30	0.82	0.30	0.33
Na	0.00	0.00		7.04	6.96	7.00	7.01	6.98
K	0.00	0.00						
TOTAL	6.99	6.99						

In some schists the rhombic shape is less well developed, and lawsonite appears as knobbly lumps on the foliation surfaces. The different colours of the rhombs seen in the field largely depends on the dominant pseudomorphing phases present. Pseudomorphs largely composed of micas tend to be green, while those composed of clinozoisite are whitish-grey in colour.

Thin section examination of these rocks shows that, in every case, lawsonite has been pseudomorphed by mineral aggregates. The pseudomorphing phases show some variation according to the host rock type. In the metabasites the dominant pseudomorphing phase is clinozoisite. Several clinozoisite crystals, in no particular crystallographic orientation, form the pseudomorph, and the skeletal appearance of the original lawsonite is faithfully retained, (see figure 3.14b). In the schists the pseudomorphing phases are more variable. The pseudomorphs tend to be mica-rich, often with a narrow clinozoisite rim. The mica is usually very fine grained, almost sericitic in appearance, and, compositionally, a mixture of finely interleaved phengite and paragonite. Electron microprobe analyses of the mica phase produce composite results, giving an averaged composition between phengite and paragonite. Other pseudomorphs can contain large amounts of chlorite, albite and/or calcite, and in a few cases small lawsonites were replaced by single crystals of calcite or albite. The pseudomorphs in marbles are largely mica or calcite, but Ca-Al silicates also play an important role. Microprobe analyses of some pseudomorphing phases are given in table 3.5.

No fresh lawsonite was found in this study, but Dixon (1969) reports finding four rocks from Northern Syros which contained fresh lawsonite. The habit of the fresh lawsonite is identical to that of the pseudomorphs, both show sharp crystal outlines, and 'spongy', inclusion rich, interiors. The lawsonite was analysed using the electron microprobe (Dixon 1969), and its composition did not depart significantly from the ideal formula, $CaAl_2(OH)_2[Si_2O_7]H_2O$.

Textural status of Lawsonite

The textural evidence suggests that lawsonite grew under the peak metamorphic conditions. In the schists, aligned crystals of glaucophane and mica are the main matrix forming phases, and, although the rock fabric abuts against the edge of a lawsonite pseudomorph in some cases, other examples clearly show a deviation of the fabric around the lawsonite porphyroblasts. This suggests that lawsonite overgrew an existing fabric, but was present during the deformation event which accompanied the blueschist metamorphism.

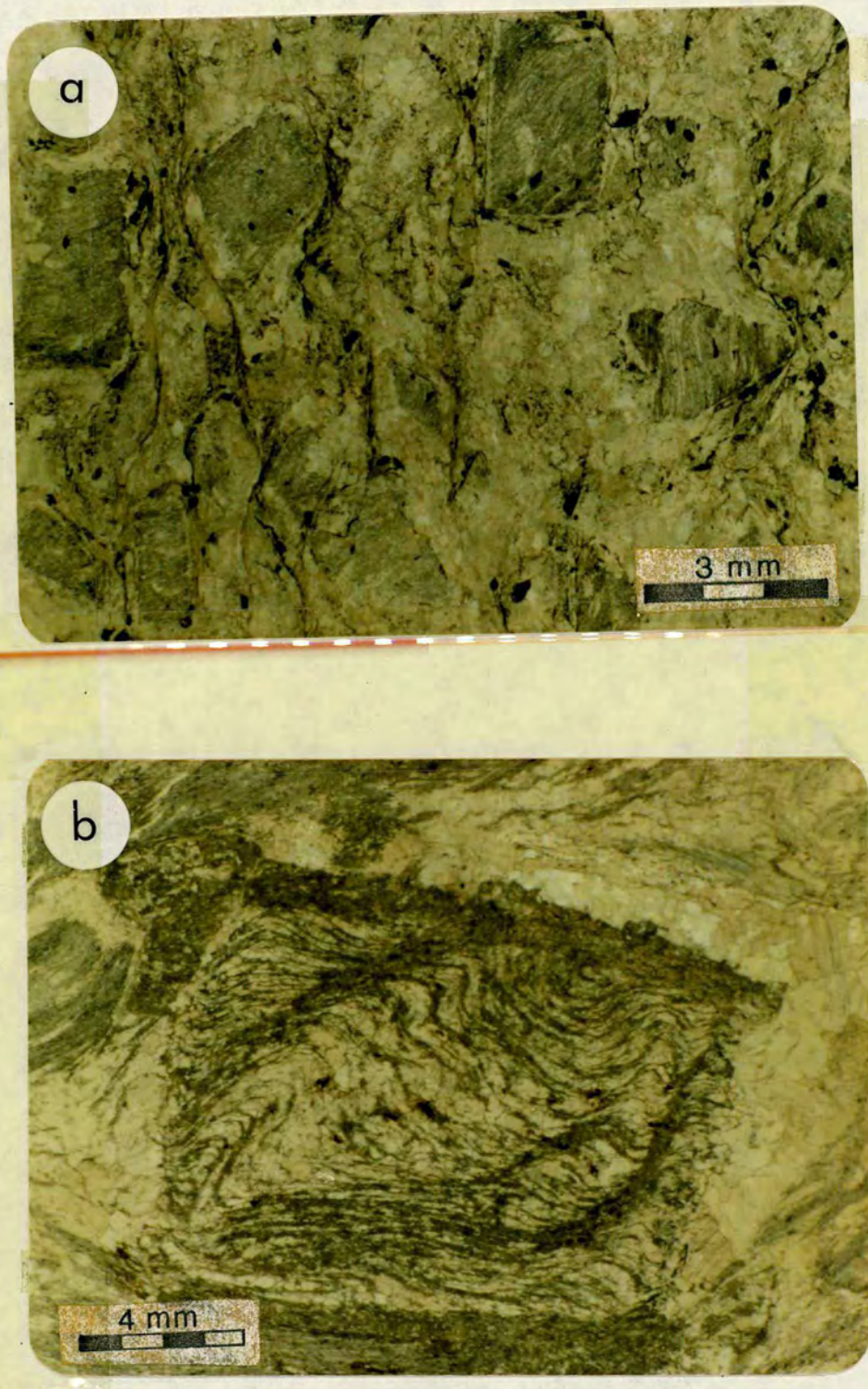

Figure 3.15 a) Lawsonite pseudomorphs with graphite trails, note the slight crenulations. b) Complex inclusion trails in a lawsonite pseudomorph in impure marble. The lawsonite has been replaced by calcite, the trails appear to be composed of calc-silicate material. a) 86/167 x 6.3, PPL; b) 86/67 x 4, PPL.

Some of the lawsonite pseudomorphs contain fine, crenulated trails of graphite within them. These trails were originally preserved within lawsonite, and they now persist as "ghosts" in the later pseudomorphs. The trails represent an early stage in the fabric development of the rock, and in the outside matrix development of the fabric has continued, transposing the crenulations, and coarsening the graphite. Growth zoning within the lawsonite has been preserved in the pseudomorphs, and graphite trails outline the rhombohedral shape of the original lawsonite at several successive stages of the crystal growth, (see figure 3.15).

Lawsonite is pseudomorphed in rocks which are otherwise unaltered, pristine blueschists, indicating that the breakdown of lawsonite is unconnected to the development of the greenschist overprint. The preservation of lawsonite outlines suggests that the original crystals existed at least until the cessation of the blueschist deformation. If lawsonite had been pseudomorphed prior to this, it is very doubtful that the pseudomorphing phases would have been mechanically strong enough to preserve the rhombohedral outlines of the lawsonite crystals so perfectly (Dixon 1969; Ridley 1982).

Both Dixon (1969), and Ridley (1982,) discuss possible reactions governing the breakdown of lawsonite. The experimentally determined breakdown of lawsonite in the presence of excess quartz, produces zoisite, kyanite and H_2O (Newton and Kennedy 1972). However, as was pointed out by Ridley (1982), kyanite will be unstable with respect to pyrophyllite under the high P_{H2O} conditions inferred for Syros (Nitsch 1972). In the absence of pyrophyllite (it has never been identified on Syros), the aluminous phase replacing lawsonite is either muscovite or albite, which suggests the involvement of coupled reactions in the replacement of lawsonite, such as;

$$\text{lawsonite} + \text{qtz} = \text{zoisite} + \text{pyrophyllite} + H_2O$$

$$\text{and pyrophyllite} + K^+ = SiO_2 + \text{muscovite} + H_2O \quad \text{(Ridley 1982)}$$

Distribution of Lawsonite

Lawsonite pseudomorphs occur extensively throughout the north of the island, but they are rare in rocks from the south. Lithologically equivalent rock types, with comparable chemical compositions, occur in the south and the north of the island, so some other factor, or factors, must control lawsonite distribution. Experimental work by Nitsch (1972,1974,) showed that the stability of lawsonite is dependent on the X_{CO2} of the coexisting fluid. Nitsch (1972) showed that lawsonite+quartz is unstable, with respect to calcite+pyrophillite, at values of X_{CO2} greater than 3 mol%.

$$\text{Calcite} + \text{pyrophyllite} + H_2O = \text{lawsonite} + CO_2$$

The reaction has an "S" shape on a T-X_{CO2} diagram (Kerrick 1974), and as X_{CO2} tends to zero, the equilibrium becomes asymptotic towards the H_2O axis. Nitsch's experiments were undertaken over the pressure range 3 to 7 kbars, however at 14 kbars, the pressure experienced by the Syros rocks, the increased non-ideality of H_2O-CO_2 mixtures will cause the equilibrium to be displaced to the right, towards the H_2O axis, decreasing the stability field of lawsonite further. With Nitsch's conclusions in mind, Ridley (1982) linked lawsonite growth to the presence of a large serpentinite body in the north.

The serpentinite forms a sill-like body, and is an important part of the northern gneiss belt (see map, back pocket). Its main outcrop is from San Mikhalis westwards towards Megas Lakkos. The thickness of the serpentinite is highly variable, ranging from several metres down to centimetres. Included within the serpentinite are numerous blocks of igneous origin. Where a large number of blocks are concentrated, or the serpentinite is thin, it is largely transformed to talc and chlorite.

$$2Mg_3Si_2O_5(OH)_4 + 3CO_2 = Mg_3Si_4O_{10}(OH)_2 + 3MgCO_3 + 3H_2O$$

The talc and chlorite producing reactions liberate H_2O, by inference diluting the X_{CO2} content of the fluid in the neighbouring rocks. Ridley (1982), suggested that these H_2O-producing reactions, occurring within the serpentinite masses, controlled the composition of the fluid phase, and hence the growth of lawsonite.

If the serpentinite reactions occurred essentially at one point in time, then the release of a large packet of H_2O-rich fluid could trigger lawsonite formation, e.g:

$$3 \text{ calcite} + \text{muscovite} + 2H^+ = 3 \text{ lawsonite} + 3\ CO_2 + 2\ K^+ \quad \text{(Ridley 1982)}$$

Ridley (1982) calculated ΔV_s for the comparable reaction involving pyrophyllite.

$$\text{Pyrophyllite} + \text{calcite} + H_2O = \text{lawsonite} + 2\text{qtz} + CO_2 \quad \Delta V_s = -15.2\ cm^3$$

The volume reduction will produce a significant, if transitory, increase in the rock porosity, aiding the infiltration of further fluid, (Rumble and Spear 1983). This seems a plausible mechanism for lawsonite growth, though it is doubtful whether reactions occurring in the serpentinite alone could liberate sufficient quantities of H_2O to generate all the lawsonite seen, another external fluid source is probably involved as well. If the growth of lawsonite is controlled by the infiltration of a H_2O-rich fluid, then pervasive infiltration must have occurred throughout much of northern Syros

during the blueschist event. This conclusion raises several apparent problems, because the mineralogical and isotopic evidence (discussed in chapters 4 and 6), suggests that the blueschist metamorphism occurred under closed system conditions, with little or no fluid communication between rock layers. The question of lawsonite growth and fluid infiltration is discussed fully in chapter 7, after the mineralogical and isotopic evidence has been considered.

However, whatever the mechanism of formation there is no obvious reason why lawsonite should be absent in the south of the island. In the north, the assemblage lawsonite+jadeite was near its high temperature stability limit during the blueschist event, and a small increase in temperature during uplift, replaced this assemblage with the equivalent zoisite+paragonite+quartz. Further down the structural pile, the temperatures during the primary event may have been slightly higher again, causing the majority of the rocks to recrystallise outwith the lawsonite stability field.

3.6 GARNET

Garnets occur as porphyroblasts in the schists, metabasites and marbles. They often contain numerous inclusions, the commonest being, rutile, epidote, glaucophane and quartz. Although in most cases, the inclusions are randomly orientated, distinct trails are seen in some at high angles to the outside matrix, indicating that the fabric continued to evolve after the period of garnet growth. The garnets appear to have grown early in the prograde event, as the grain size of included phases is much finer than that of the recrystallised matrix. There is a tendency towards skeletal, or sieve textured, growth in the garnets, which is most spectacularly developed in the impure marbles, (see figure 3.16).

Some representative garnet microprobe analyses are listed in table 3.6. The Fe^{2+}/Fe^{3+} ratio has been estimated from charge balance constraints, assuming a close approach to the theoretical structure, $(R^{2+})_6(R^{3+})_4[R_6^{4+}O_{24}]$, in natural samples. Normative molecules were calculated in the order andradite, grossular, spessartine, pyrope and almandine, following the method of Dixon (1969), (see also Rickwood 1968). The compositional field of the garnets is shown in the system (Alm+Pyr)-(Gross+And)-Spess, (figure 3.17).

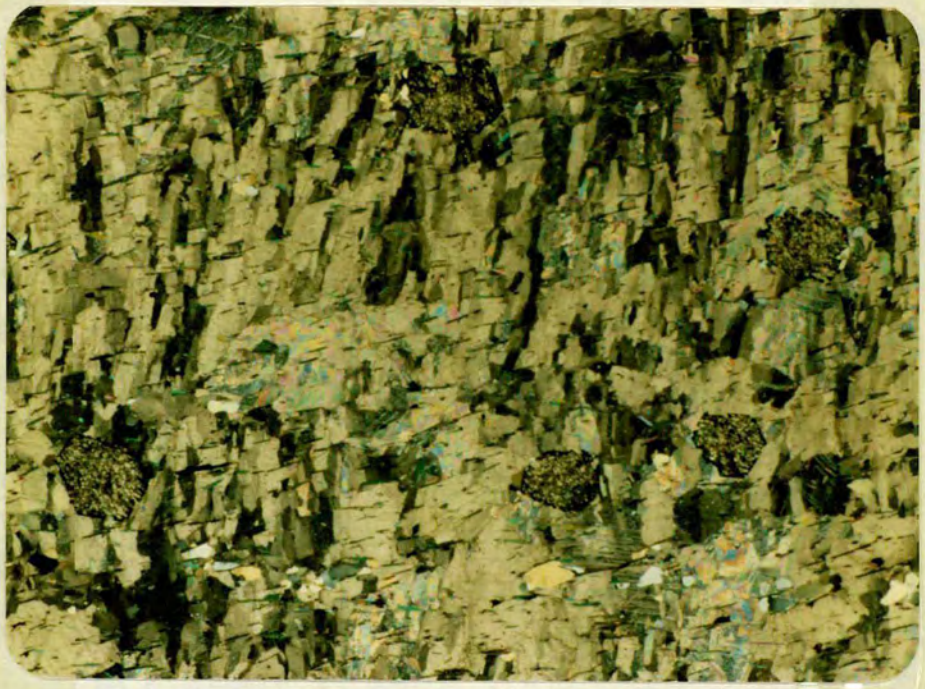

Figure 3.16 Skeletal garnets in an impure marble, Aspro (86/ 7). Note: 1) the grain size of the included calcite grains compared to those in the matrix; 2) the inclusion trails at a high angle to the matrix foliation; 3) columnar texture in matrix calcite. (x 7, PPL).

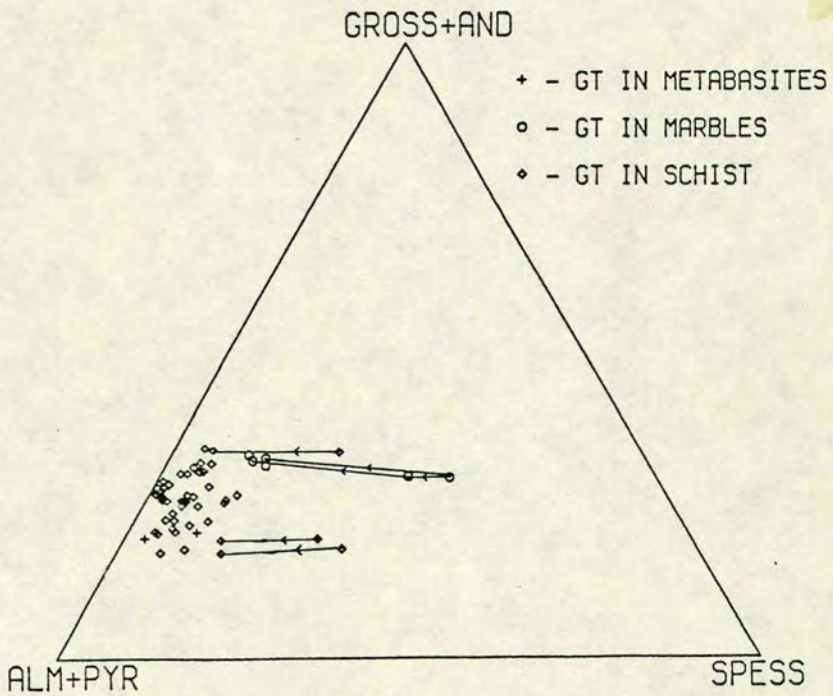

Figure 3.17 Compositions of the Syros garnets, plotted in terms of mole percentage of grossular+andradite-almandine+pyrope-spessartine. Tie-lines connect analyses from the same garnet, the arrows point from core to rim.

Table 3.6 Representative analyses and structural formulae of garnets. r = rim, c = core.

	40	r 67	c 67	49	r 72	c 72	r 78	c 78
SiO2	37.98	37.07	36.41	37.95	38.60	38.18	37.35	37.41
TiO2	0.20	0.07	0.24	0.12	0.11	0.17	0.10	0.19
Al2O3	21.07	20.85	20.40	20.66	21.20	21.13	20.21	20.34
Cr2O3	0.02	0.02	0.03	0.08	0.06	0.04	0.20	0.04
Fe2O3	0.00	1.05	2.27	0.85	0.09	0.31	0.85	1.06
FeO	28.39	22.96	11.78	26.99	29.46	26.18	26.90	21.54
MnO	4.24	5.28	17.95	1.65	0.34	5.07	6.06	12.17
MgO	1.63	0.95	0.50	1.82	2.40	1.56	1.83	1.34
CaO	7.16	11.24	10.09	10.60	9.50	9.14	6.60	6.75
TOTAL	100.69	99.48	99.67	100.72	101.75	101.78	99.84	100.74
			cations	per	24	oxygens		
Si	6.03	5.95	5.88	6.00	6.02	6.00	6.01	5.99
Al4	----	0.04	0.01	----	----	----	----	0.01
Al6	3.94	3.90	3.87	3.85	3.90	3.91	3.83	3.83
Ti	0.02	0.00	0.02	0.01	0.01	0.02	0.01	0.02
Cr	0.00	0.00	0.00	0.01	0.00	0.00	0.00	0.00
Fe3+	0.00	0.12	0.27	0.10	0.01	0.03	0.10	0.12
Fe2+	3.77	3.09	1.60	3.57	3.84	3.44	3.63	2.89
Mn	0.57	0.71	2.45	0.22	0.04	0.67	0.82	1.65
Mg	0.38	0.22	0.12	0.42	0.55	0.36	0.42	0.32
Ca	1.21	1.93	1.74	1.79	1.58	1.53	1.13	1.15
TOTAL	15.96	16.00	16.01	16.00	16.00	16.00	16.00	16.00
And	0.60	3.41	7.77	2.92	0.59	1.43	2.94	3.79
Gross	19.89	28.95	21.71	27.26	26.40	24.40	16.26	15.56
Spess	9.59	12.03	41.47	3.71	0.76	11.33	13.94	27.57
Pyr	6.49	3.81	2.03	7.21	9.48	6.13	7.41	5.34
Alm	63.42	51.80	27.02	58.90	62.76	56.70	59.45	47.74

The garnets are essentially grossular-almandine solid-solutions, with a fairly constant mole fraction of the grossular component, usually between 15 and 30 percent. The pyrope and andradite contents are low, and relatively uniform, varying between 4-10% and 0-3% respectively. The spessartine content is low in most garnet rims (<10%), but rises to values of 30% and more in the Mn-enriched cores. In general the zoning involves an increase in almandine and pyrope (and possibly grossular too) at the expense of spessartine moving from core to rim.

3.7 SODIC PYROXENES

Sodic pyroxene occurs as apple-green to pale-green pleochroic crystals, often associated with more riebeckitic glaucophanes. The pyroxene can be distinguished from coexisting epidote on the basis of its colour, shape, lower birefringence and the occurrence of two cleavages intersecting at 90°. Sodic pyroxene occurs most frequently in the metabasites, where it forms solid bands composed of interlocking crystals, but is has also been found in some impure marble units as small discrete crystals, (see figure 3.18).

The few analyses made of this phase come from metabasic gneisses at Kastri, and an impure ferric iron-rich marble from Aspro on the north west coast. Dixon (1969) produced a number of probe analyses of pyroxenes, and some of these have been included, in order to represent the compositional range of the group more accurately, (see table 3.7). Analyses were recalculated into atomic proportions on the basis of 6 oxygens, and the estimation of Fe^{3+} assumed that Fe^{3+}=Na-Al, and Fe^{2+}=Fe_{total}-Fe^{3+}. End-member components were calculated assuming jd=Al, ac=Fe^{3+} and "en"=(Ca+Mg+Fe^{2+})/2 (Dixon 1969). The analyses, normalised in terms of the these three endmember components, are plotted in figure 3.19.

The compositions of sodic pyroxene are largely dependent on the parent rock chemistry, i.e jadeitic pyroxenes are common in metagreywackes, acmitic pyroxene in metacherts, and omphacites in basic rocks. On Syros, the pyroxenes in metabasites tend to be omphacite, whereas those from marbles are chloromelanite, richer in Fe^{3+}. The pyroxenes on Syros show a comparable range in composition to pyroxenes analysed from other blueschist terrains, e.g Ouega district, New Caledonia (Black 1974), Franciscan, northern California (Essene and Fyfe 1967), and the Fairbanks district, Alaska (Brown and Forbes 1986).

Figure 3.18 gnt-omphacite metabasite from Kouroupi gneisses, near Azolimnos, (87/168A). The omphacite is present throughout the matrix, and is recognised by its light apple-green colour. Assemblage: omphacite-garnet-glaucophane-paragonite-phengite-quartz-sphene.

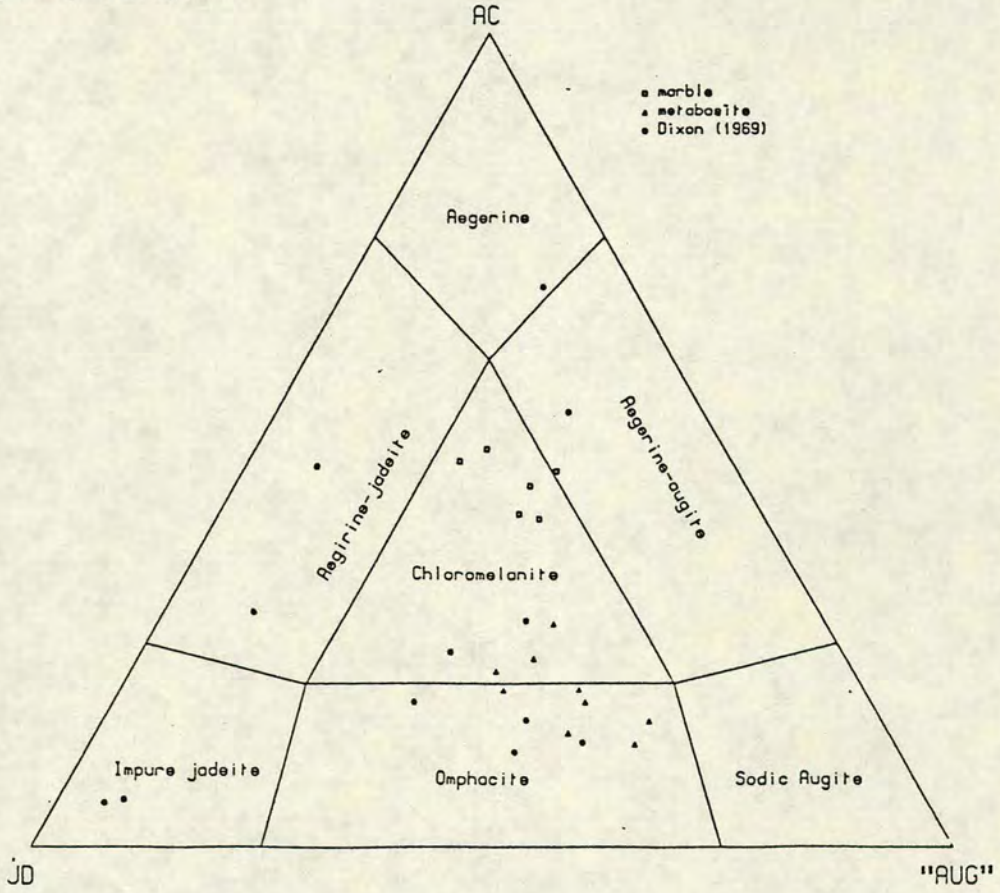

Figure 3.19 a) Classification of sodic pyroxenes (after Essene and Fyfe, 1967). Open square = marble, triangle = metabasite, circle = Dixon (1969).

Table 3.7 Representative analyses and structural formulae of sodic pyroxenes. r = rim, c = core, d = Dixon (1969).

	r 88	c 88	88	69	D918	D926
SiO2	55.90	55.15	54.50	53.80	59.09	56.08
TiO2	0.05	0.08	0.07	0.04	0.02	0.00
Al2O3	8.89	7.68	8.01	6.51	20.62	14.94
Cr2O3	0.05	0.04	0.07	0.04	0.00	0.00
Fe2O3	7.20	10.03	8.52	17.70	2.10	12.80
FeO	1.24	0.42	0.55	1.24	1.00	0.00
MnO	0.06	0.09	0.04	0.16	0.00	0.00
MgO	7.70	7.50	7.62	3.47	0.74	0.89
CaO	12.79	12.03	13.14	6.31	1.97	2.57
Na2O	7.49	8.01	7.45	10.83	14.57	12.47
TOTAL	100.56	101.02	99.96	100.12	100.12	99.75
	Cations	per	6	oxygens		
Si	1.97	1.97	1.96	1.97	2.02	1.99
Al4	0.03	0.02	0.00	0.02	----	0.00
Al6	0.34	0.29	0.30	0.25	0.83	0.62
Ti	0.00	0.00	0.00	0.00	0.00	0.00
Cr	0.00	0.00	0.00	0.00	0.00	0.00
Fe3+	0.19	0.27	0.23	0.51	0.05	0.29
Fe2+	0.03	0.01	0.01	0.04	0.02	0.00
Mn	0.00	0.00	0.00	0.00	0.00	0.05
Mg	0.41	0.40	0.41	0.19	0.03	0.04
Ca	0.49	0.46	0.50	0.24	0.07	0.09
Na	0.51	0.55	0.52	0.77	0.96	0.86
TOTAL	4.00	4.00	4.00	4.02	4.01	3.97
JD	34.03	29.23	30.36	25.39	87.30	61.40
AC	19.45	27.34	23.28	50.62	5.70	28.80
UR	0.14	0.11	0.20	0.11	0.00	0.00
DI	40.50	39.53	40.43	18.77	4.00	4.60
HED	3.72	1.26	1.66	3.95	3.00	5.00
'EN'	2.16	2.53	4.08	1.16	0.00	0.00

3.8. EPIDOTE GROUP

In the majority of the schists epidote is a minor phase. It forms small rounded grains which can be quite difficult to distinguish from sphene. In the greyschists the phase combination lawsonite+calcite+graphite is very common, and it always occurs without epidote. If lawsonite is absent, then epidote and calcite may occur together (as in the impure marbles), or epidote and graphite, a rare combination in the schists. The significance of this apparent mutual exclusion between epidote and lawsonite+graphite is discussed in the light of fluid infiltration in chapter 7.

Epidote is a major component in the metabasic rocks, where it can form up to 40 vol% of the rock. The epidotes occur as stubby prismatic porphyroblasts, or as granular crystal aggregates. The crystals are yellow-green in colour, and weakly pleochroic. Optical zoning of individual crystals is commonly observed due to a slight decrease in the $Fe^{3+}/(Fe^{3+}Al^{VI})$ ratio moving form core to rim.

Figure 3.20 shows the proportions of octahedrally co-ordinated aluminium and ferric iron in epidotes from the schists, metabasites and marbles. As practically all the iron in epidotes is in the Fe^{3+} state, the formulae were calculated based on this assumption. The epidotes show quite a range of compositions, but there is no obvious systematic difference in relation to host rock chemistry. An apparent gap exists in the range Fe3+=0.25 to 0.40, however this is probably a "lithological" gap as oppose to a true compositional gap. Although the Fe3+/Al partitioning in coexisting phases is an important factor in determining the epidote composition, the maximum Fe^{3+} content also varies as a function of f_{O2}, and epidote is at its most iron rich at high oxygen buffers, (Liou 1974). Most of the analyses from Syros are some way off the one Fe^{3+} atom per formula unit that is the practical limit for replacement of Al, thus it is unlikely that f_{O2} was high enough to influence the epidote composition significantly. This conclusion is reinforced by the common occurrence of graphite as an accessory phase in the schists, which indicates moderate to low oxygen fugacities during metamorphism.

Table 3.8 lists some representative epidote analyses. The epidotes in sample 86/94 contain almost 4wt% chrome in the cores. This sample was collected close to the melange unit at Kastri, on the north-west coast, and the high chrome content of the epidotes at this locality probably reflects the influx of detrital ultramafic material. The marble analyses come from a ferric iron rich impure marble, where the epidote is in equilibrium with crossitic amphibole and chloromelanite pyroxene.

Table 3.8 Representative analyses and structural formulae of epidote. r = rim, c = core.

	69	c 94	r 94	21	204	88	36	83
SiO2	36.78	38.01	38.44	37.84	39.18	38.46	39.01	37.67
TiO2	0.03	0.12	0.12	0.07	0.06	0.14	0.10	0.13
Al2O3	22.53	24.69	26.51	23.47	30.92	26.94	32.18	24.10
Cr2O3	0.00	4.00	0.06	0.06	0.00	0.02	0.05	0.00
FeO	12.70	10.57	8.20	11.76	3.52	8.10	1.77	11.11
MnO	0.57	0.13	0.09	0.25	0.09	0.06	0.03	1.09
MgO	0.04	0.05	0.05	0.06	0.00	0.07	0.03	0.06
CaO	22.83	22.97	23.52	23.33	24.31	23.46	24.32	21.74
TOTAL	95.49	100.56	96.99	96.84	98.08	97.25	97.53	95.90
			cations per		28 oxygens			
Si	2.97	2.91	3.00	3.00	2.99	3.00	2.89	3.00
Al4	0.02	0.08	----	----	0.00	----	0.01	----
Al6	2.12	2.14	2.44	2.19	2.77	2.50	2.88	2.26
Ti	0.00	0.00	0.00	0.00	0.00	0.00	0.00	0.01
Cr	0.00	0.23	0.00	0.00	0.00	0.00	0.00	0.00
Fe3+	0.86	0.68	0.53	0.78	0.22	0.48	0.11	0.73
Mn	0.03	0.01	0.00	0.01	0.00	0.00	0.00	0.07
Mg	0.00	0.00	0.00	0.00	0.00	0.00	0.00	0.00
Ca	1.98	1.89	1.96	1.98	1.98	1.97	1.99	1.86
TOTAL	8.01	7.98	7.98	8.00	7.99	7.99	8.09	7.96

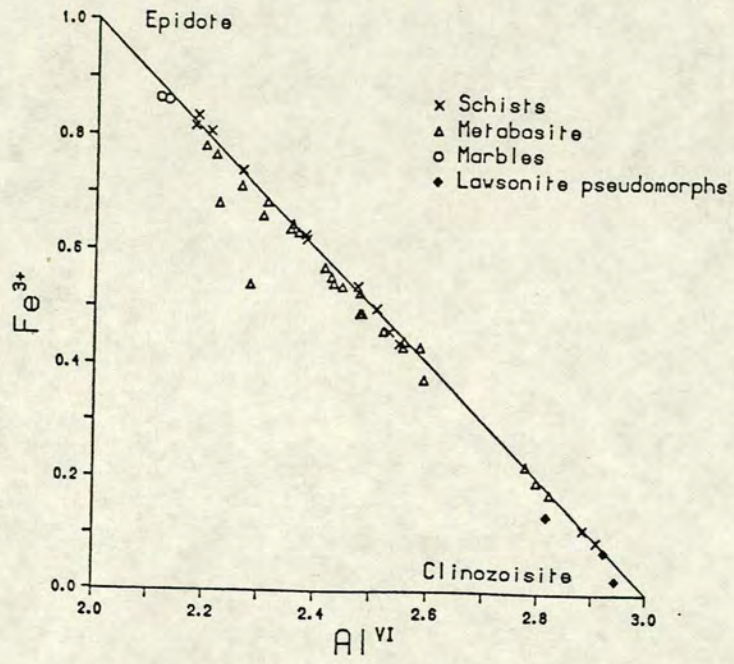

Figure 3.20 Plot of Fe^{3+} versus Al^{VI} for epidotes from the metabasites and metasediments. The line is the ideal octahedral substitution of Fe^{3+} for Al.

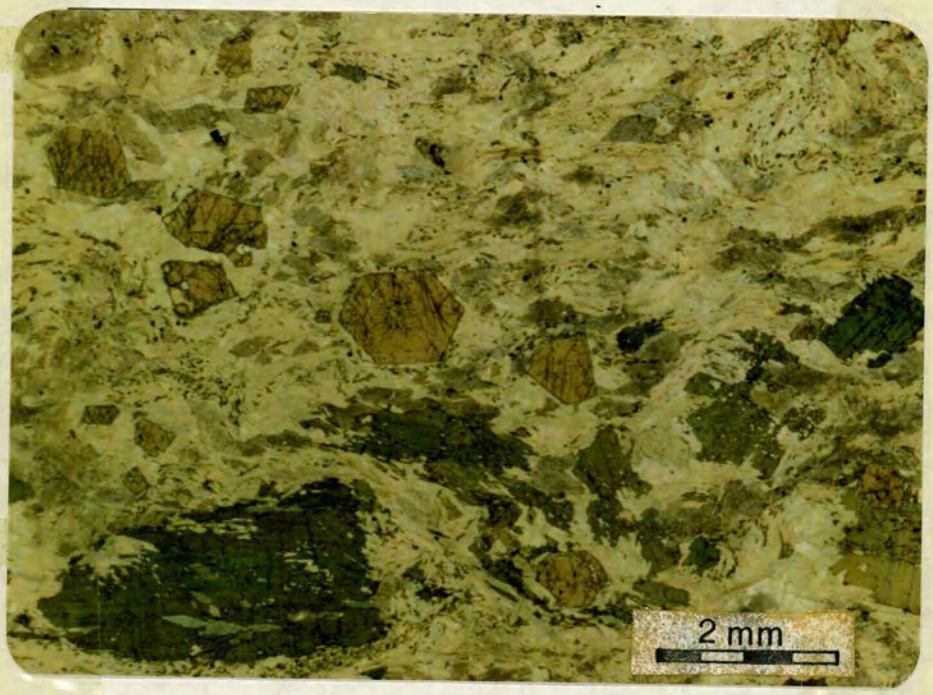

Figure 3.21 Chloritoid-bearing blueschist from north of Aspro (86/78). Note the ragged edges of the porphyroblasts,where chloritoid is being replaced by paragonite and chlorite. Assemblage chloritoid-glaucophane-phengite-paragonite-quartz-garnet-rutile. (x 8, PPL).

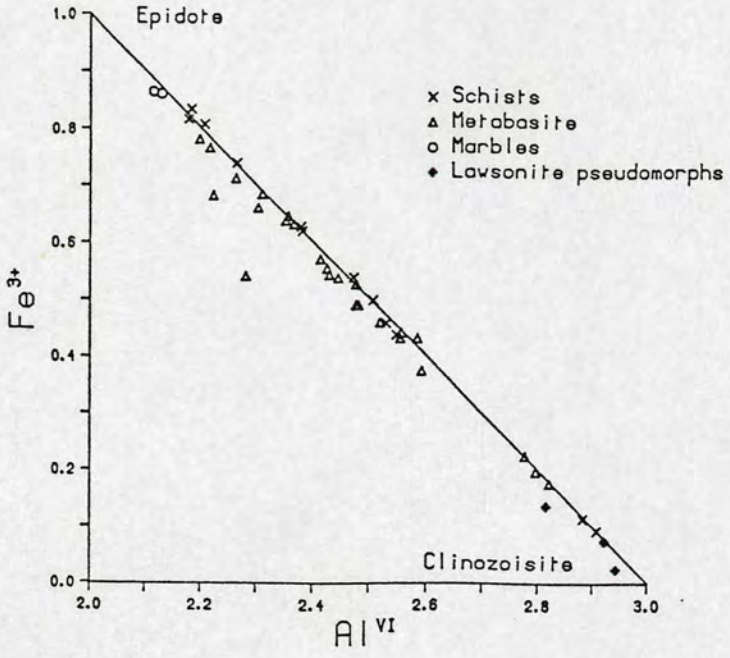

Figure 3.20 Plot of Fe^{3+} versus Al^{VI} for epidotes from the metabasites and metasediments. The line is the ideal octahedral substitution of Fe^{3+} for Al.

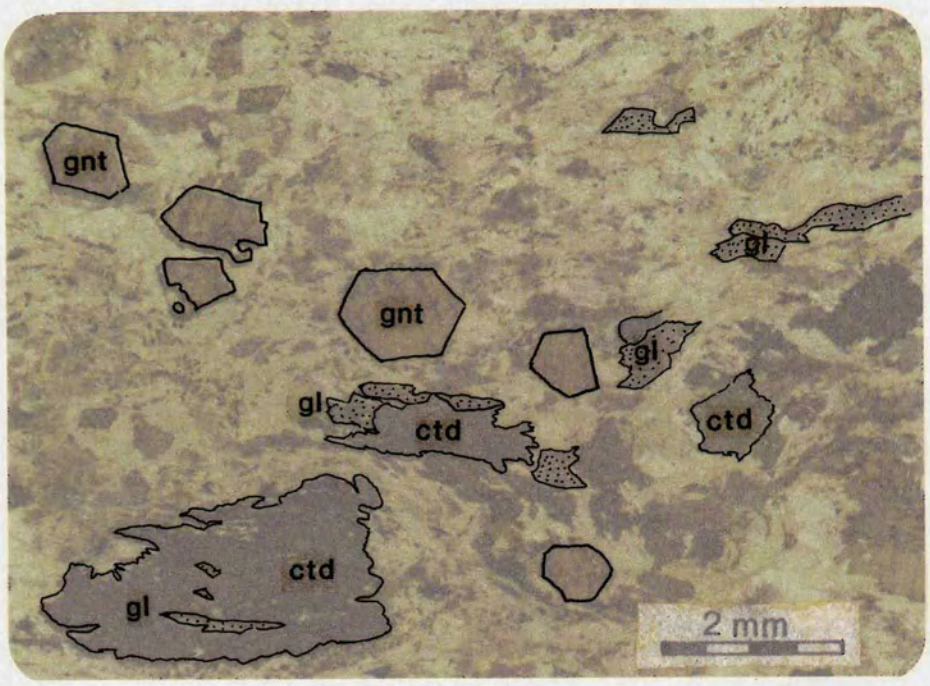

Figure 3.21 Chloritoid-bearing blueschist from north of Aspro (86/78). Note the ragged edges of the porphyroblasts,where chloritoid is being replaced by paragonite and chlorite. Assemblage chloritoid-glaucophane-phengite-paragonite-quartz-garnet-rutile. (x 8, PPL).

3.9 CHLORITOID

Chloritoid is quite rare, occurring in only a few Al,Fe^{3+}-rich schists from northern Syros.

It forms large tabular porphyroblasts, which have a characteristic greyish-blue colour, (see figure 3.21). The crystals are pleochroic from pale-yellow to grey-green to slaty-blue. They have greyish green interference colours and commonly show lamellar twinning. The porphyroblasts often contain numerous inclusions of quartz, epidote, glaucophane and opaques. Despite the small grain size of the included quartz and epidote, all other features point to relatively late stage growth of the chloritoid. The mica fabric abuts against the porphyroblasts, instead of bending round them, and the porphyroblasts themselves are not aligned in the foliation, but appear to be scattered randomly. However, the inclusion trails are at variance with the external foliation, suggesting a late, but not post tectonic origin. Representative microprobe analyses are given in table 3.9. The presence of more than 3.9Al atoms per formula unit in all but one of the analyses suggests that there is very little ferric iron in the octahedral site, therefore total iron has been left as Fe^{2+}.

Glaucophane appears to coexist stably with chloritoid, and it is present in all the chloritoid-bearing rocks, in contrast to the situation in New Caledonia, described by Ghent *et al.* (1987). Here, rocks of comparable bulk composition develop the assemblage qtz-chl-mu-gnt-ctd, and glaucophane-chloritoid is not a common assemblage. Brown and Forbes (1986) have constructed a P-T petrogenetic grid for blueschists and eclogites, and they suggest that the equilibrium:

$$\text{chloritoid} + \text{glaucophane} + H_2O = \text{chlorite} + \text{paragonite} + \text{quartz}$$

has P,T points near 450°C at 13 kbars and 550°C at 10 kbars, with glaucophane+chloritoid stable on the high pressure side of the curve. The rarity of glaucophane-chloritoid in New Caledonia suggests that the blueschists crystallized outside the stability field of chloritoid-glaucophane. The P-T conditions, during the primary metamorphic event on Syros, mean that glaucophane-chloritoid was stable. However, the chloritoid porphyroblasts often have ragged crystal outlines, and textural evidence suggests that the reaction given above proceeded to the left during uplift, generating paragonite and chlorite.

Table 3.9 Representative analyses and structural formulae of chloritoid.

	core 78	rim 78	78	94
SiO2	24.49	24.59	24.81	24.24
TiO2	0.04	0.02	0.02	0.02
Al2O3	40.68	40.42	39.20	40.87
Cr2O3	0.05	0.05	0.00	0.01
FeO	20.77	21.05	21.56	23.44
MnO	0.19	0.25	0.22	0.07
MgO	3.85	5.04	5.43	3.13
CaO	0.01	0.00	0.00	0.01
Na2O	0.02	0.02	0.00	0.02
K2O	0.01	0.01	0.00	0.00
TOTAL	90.11	91.45	91.24	91.81

	cations	per	12	oxygens
Si	2.03	2.02	2.04	2.00
Al4	3.00	3.00	3.00	3.00
Al6	0.98	0.91	0.81	0.98
Ti	0.00	0.00	0.00	0.00
Cr	0.00	0.00	0.00	0.00
Fe2+	1.44	1.44	1.48	1.62
Mn	0.01	0.01	0.01	0.00
Mg	0.47	0.61	0.66	0.38
Ca	0.00	0.00	0.00	0.00
Na	0.00	0.00	0.00	0.00
K	0.00	0.00	0.00	0.00
TOTAL	7.96	8.02	8.03	8.00

The chloritoid on Syros is generally more magnesium-rich than those described from glaucophanic greenschist terrains, or lower grade blueschists (Liou and Chen 1978; Katagas 1980; Seidel *et al.* 1975), but they are not as magnesian as those reported by Chopin (1981,1982) from the Western Alps. In the Alps, the magnesium content of the chloritoid is exceptionally high, ranging from 25 up to 71 mol% of the Mg-endmember. This magnesium chloritoid has been cited as indicative of extremely high metamorphic pressures. However, the occurrence of Mg-rich chloritoid is a function of bulk rock composition, and the Fe/Mg partitioning between chloritoid and other coexisting ferromagnesian phases, as well as metamorphic grade. The Syros chloritoid does not belong to a very high magnesian group, but this does not mean that it formed at low pressure. The reaction limiting the stability of Mg/Fe chloritoid on Syros is likely to be:

chloritoid + chlorite = almandine garnet

3.10 SPHENE AND RUTILE

Both sphene and rutile are common accessory phases in the Syros rocks, although sphene is without question the dominant Ti-bearing phase, occurring in about 95% of the rocks. Sphene commonly forms euhedral diamond shaped grains, which have a whitish-yellow colour, while rutile varies in colour from honey-brown to dark reddy-brown, and occurs as lozenge shaped crystals, or rounded crystals aggregates.

The distribution of sphene and rutile in the rocks can provide valuable information about the fluid composition (see chapter 4), and thus the occurrence, and relationship between the two phases was studied in detail. Sphene is present on its own in the majority of the schists, and a large proportion of the metabasites. It is the only Ti-bearing phase present in the impure marbles. The sphene contains some Al_2O_3, up to 2.5 wt%, and minor FeO, analyses are listed in table 3.10. Sphene is found as inclusions in garnet and glaucophane, both of which are primary blueschist phases. In the matrix, sphene occurs with mica, and the crystals are aligned parallel to the foliation of the rock. In some of the schists it appears that sphene has been pseudomorphed by calcite and rutile, though the texture is poorly developed. The outlines of the sphene crystals are preserved, and small rhombs of carbonate are present in the interior of the crystal. This texture was seen in only 15 schists out of more than 200 examined.

Table 3.10 Representative analyses of sphene and rutile.

	Sphene			
	41	70	80	83
SiO2	31.85	30.80	30.37	30.85
TiO2	36.60	38.80	37.10	36.84
Al2O3	1.92	1.24	1.89	2.54
FeO	1.28	0.68	----	0.41
CaO	27.31	28.49	28.33	28.57
TOTAL	98.96	100.01	97.69	99.21

	Rutile			
	88	78	83	98
SiO2	30.25	----	----	----
TiO2	36.64	99.95	99.62	99.87
Al2O3	2.00	----	----	----
Cr2O3	----	0.11	----	----
FeO	0.44	0.58	0.65	0.72
CaO	28.06	----	----	----
TOTAL	97.39	100.64	100.27	100.59

Rutile is the sole Ti-bearing phase in some schists, and more commonly in metabasites. It is found both in the matrix of the rock, and included within other phases, commonly garnet. Rutile has a constant composition in all rock types, and it is pure TiO2 except for a small amount of FeO. Rutile analyses are given in table 3.10. A number of samples were examined in reflected light, and this revealed the presence of inclusions in rutile. These inclusions, probably of quartz, have a much smaller grain size than any phase now present in the matrix, and they are often aligned. The inclusions trails are at a high angle to the external fabric, and they are clearly "remembering" an earlier stage in the fabric development. Rutile is commonly seen in garnet porphyroblasts, where it has a smaller grain size than matrix rutile, and is parallel to the garnet growth zones. These textures indicate that rutile was present during the primary metamorphic event.

Sphene and rutile coexist in a number of the schists, and the textural relationships between the two phases are of particular importance. Rutile and sphene commonly form composite aggregates, and in almost every example, these consist of a rutile core surrounded by sphene, indicating that sphene post-dates rutile. Sphene appears to be replacing rutile, but it is not clear whether this occurred during the blueschist metamorphism, or during later regression. A few examples show the opposite relationship, and here sphene shows signs of alteration to rutile along the grain margins. Similar textures are reported from New Caledonia (Itaya *et al.* 1985) where rutile has formed at the expense of sphene. Itaya *et al.* (1985) suggest the following reaction to explain this texture:

$$\text{sphene} + \text{cz (or laws)} = \text{gross} + \text{rutile} + \text{qtz} + H_2O$$

This reaction obviously has the potential to buffer the grossular component of the garnet, and this is pointed out by Itaya *et al.* (1985). If such a reaction were occurring commonly in the schists, it could explain why zoned garnets on Syros have an almost constant grossular component, but because of the rarity of the sphene⇒rutile texture described, this cannot be the dominant process controlling the garnet compositions.

3.11 GRAPHITE, OXIDES AND SULPHIDES

Graphite is common in the metasediments, but oxide phases such as magnetite, hematite and ilmenite are comparatively rare.

Graphite

Fine trails of graphite, occurring between mica grains, and as inclusions in most other phases, are a characteristic feature of many of the northern schists. In thin section the graphite appears as fine dusty material within lawsonite pseudomorphs, and as slightly coarser laths in the rock matrix. It is the presence of graphite which gives the northern schists their characteristic lead grey lustre and leads to their field name, greyschists. Polished blocks of graphite-rich schist were examined in reflected light, using oil immersion objectives. The graphite occurs as small laths, which are strong anisotropic, from yellow to bluish-brown.

Fifty samples, standards and blanks were analysed on the LECO carbon analyser to determine the amount of graphite present in the schists. Approximately 0.7 grams of decarbonated sample was placed in a LECO crucible, with 1.5 scoops of tin accelerator and 1 steel ring. The crucible was then placed in the LECO furnace and ignited. The results are given in table 3.11. Five samples were analysed in duplicate or triplicate to check the reproducibility of results.

Table 3.11 Percentages of graphite present in the schists determined by LECO analysis. Errors are given for samples analysed in triplicate.

Sample #	wt% carbon
86/14	0.11
86/25	0.27
86/34	0.23 $\pm$ 0.005
86/49	0.37
86/70	0.24 $\pm$ 0.004
86/72	0.27 $\pm$ 0.010
86/74	0.24 $\pm$ 0.002
86/103b	0.21
86/142	0.06
86/144	0.30
86/167	0.16
87/217	0.31 $\pm$ 0.004

The presence of graphite in many of the northern schists both constrains and complicates the fluid chemistry, and the implications of this are discused in chapter 4

Sulphides

A number of the schists contain opaques which are characteristically square or triangular in outline, and these were interpreted as being pyrite. Some of these sulphide grains contain inclusions of glaucophane, and were therefore part of the primary assemblage. In reflected light, the sulphide phase is seen to be altered, and replaced by hydrated iron oxides. This replacement has been a two stage process, as the pseudomorphed sulphides have a white core, probably lepidocroite (γ-FeO.OH), and an outer blue margin thought to be goethite (FeO.OH). In one or two cases a few grains of sulphide remain, and these were identified as being pyrrhotite, $Fe_{1-X}S$. It appears that the pyrrhotite has replaced the primary pyrite, possibly by a simple desulphurization during heating.

3.12 SUMMARY

The different minerals occurring in the blueschist facies rocks have been examined petrographically, and chemically, and the following phases are considered to be primary with respect to the blueschist metamorphism.

glaucophane
actinolite (only present in Ca-Mg rich rocks)
phengite
paragonite
talc (restricted to rocks with low Fe/Mg ratios)
chlorite
aragonite (now calcite)
dolomite (now calcite)
lawsonite (pseudomorphed by a variety of phases)
grossular-almandine garnet
Na-pyroxene
clinozoisite/epidote
chloritoid
sphene
rutile
graphite
pyrite

Various combinations of these minerals form all the blueschist assemblages. The next chapter begins by considering the assemblages found in each of the three main rock types. A subset of the primary mineral phases is chosen, and modelled in the system, Al_2O_3-MgO-CaO-Na_2O. Mineral-fluid equilibria are determined, and a T-X_{CO2} grid is produced, from which conclusions about the X_{CO2} of the fluid, and the roles of buffering and infiltration, are made.

CHAPTER 4:

FLUID-ROCK INTERACTIONS IN THE BLUESCHIST METASEDIMENTS

TABLE OF CONTENTS

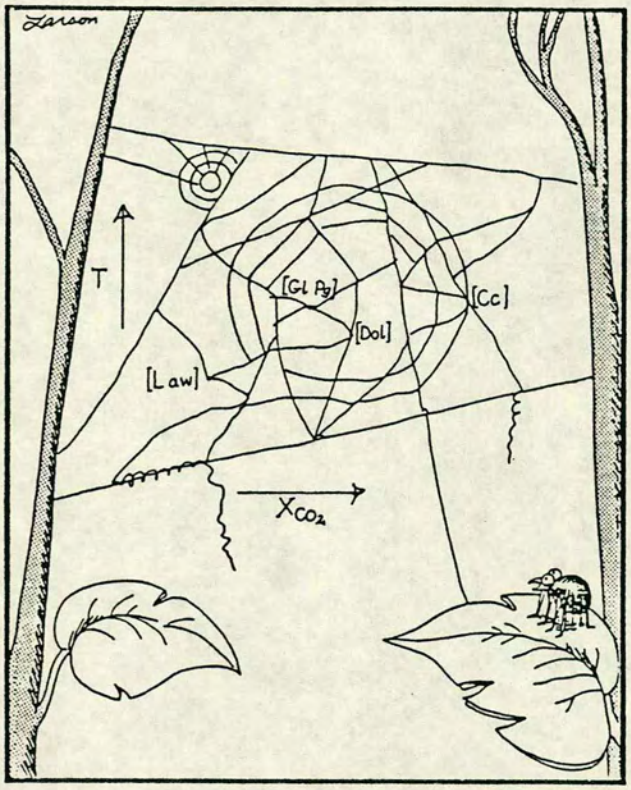

"Whoa! . . . That CAN'T be right!"

4.0 INTRODUCTION

In this chapter the blueschist facies mineral assemblages will be considered in detail, with the ultimate aim being the construction of a T-X_{CO2} petrogenetic grid. This grid will allow variations in the equilibrium fluid composition between different rock layers, collected on an outcrop scale, to be detected. The variation (or uniformity) in fluid compositions across several layers will provide information about the relative roles of fluid buffering and infiltration during the blueschist facies event.

Previously constructed petrogenetic grids (Albee 1965a; Pattison & Harte 1985) have concentrated on the P-T relationships between assemblages. Existing T-X_{CO2} grids have examined the mineral-fluid phase relationships in greenschist, epidote-amphibolite and amphibolite facies rocks, (Ferry 1983, 1976a; Graham *et al.* 1983; Hoscheck 1980 a,b; Rumble *et al.* 1982) but very few detailed studies exist of fluid composition and transport in blueschist terrains, and consequently little is known about the behaviour of metamorphic fluids in crust undergoing high pressure, low temperature metamorphism. The studies undertaken on the neighbouring Cycladic islands of Naxos and Sifnos (Kreulen 1980; Matthews and Schliestedt 1984, 1987; Rye *et al.* 1976) are strongly biased towards isotopic work, and in general these studies have not examined mineral-fluid relationships in any great detail. One of the few T-X_{CO2} reaction grids dealing with blueschist assemblages was published by Chatterjee in 1971, following his work in the Dora-Maira Massif, Italy. In Chatterjee's grid, albite and tremolite are important phases which appear in a large number of the reaction equilibria. However, on Syros, the higher pressure attained during metamorphism means that the high pressure stability limit of albite has been exceeded, and tremolite is restricted to very magnesian rock compositions. These major mineralogical differences mean that Chatterjee's grid cannot be used to model the Syros assemblages.

4.1 AIMS

In order to detect buffering and infiltration processes it is necessary to establish whether relative differences in the X_{CO2} of the fluid exist between assemblages. When trying to establish the composition of the coexisting fluid, an initial starting point may be to assume that the mineral assemblages controlled the composition of the fluid, i.e. the fluid composition was internally buffered. In such cases changes in the equilibrium fluid composition would be expected across different lithologies, possibly on an outcrop scale. However, if in reality the rocks were flushed through by large volumes of externally derived fluid, then the mineral assemblages would have little or no control on the composition of the fluid, and the mineral equilibria in such affected rocks would record the presence of a common fluid composition. The scale over which infiltration is important will obviously vary, but examples from Shieh and Taylor (1969) and Rye (1978) suggest that pervasive fluid infiltration can operate over distances of hundreds of kilometres. With time the mineralogy of infiltrated rocks may adjust so as to be in equilibrium with this external fluid. The mineral equilibria in such rocks will record the presence of a common fluid composition throughout a large volume of rock, and it is unlikely that assemblages containing both reactants and products of reaction equilibria will be common. Thus, far from being a purely academic exercise the construction of a T-X_{CO2} grid for the Syros blueschists will enable differences in the fluid composition between assemblages to be detected.

4.2 MINERAL ASSEMBLAGES - SCHISTS, MARBLES AND METABASITES

The mineral assemblages have been deduced on the basis of thin section, X-ray diffraction and electron microprobe studies. Two main criteria were applied to determine the primary assemblages:

1) All the mineral phases in an assemblage must have coexisted together at one point in time, and have experienced the same P-T conditions.

2) Each mineral phase must have a contact with every other phase in the assemblage, and these contacts should show no evidence for reaction.

Another obvious criterion is that each mineral phase in the assemblage must be present in the thin section. However, in the case of the Syros blueschists, some primary mineral phases have broken down or been pseudomorphed during uplift. Examples of this are the pervasive pseudomorphing of lawsonite, the inversion of aragonite to calcite and the calcitization of dolomite. In such cases, where a phase is

now absent, its former presence has not been neglected. Bearing these difficulties in mind, assemblage lists have been prepared for the three main rock-types, schists, marbles and metabasites, and these are listed in the following pages. For each rock-type the assemblage lists have been grouped together according to the presence or absence of a certain important phase or phases, after the manner of Dixon (1969). The selected phases are listed first, followed by the other minerals forming the assemblage, listed, as far as possible, in order of abundance.

TABLE 4.1

List of the mineral abbreviations used:

act = actinolite
cc = Ca carbonate (calcite or aragonite)
chl = clinochlore
ctd = chloritoid
cz = clinozoisite
dol = dolomite
ep = epidote
gl = glaucophane
gnt = garnet
hm = haematite
ilm = ilmenite
jd = jadeite
law = lawsonite
mu = white mica (phengite)
mg = magnetite
omph = omphacite
pg = paragonite
px = pyroxene
qtz = quartz
rut = rutile
sph = sphene
zoi = zoisite

Schist assemblages

Assemblages containing:

1. calcite

cc+gl+mu+qtz+law±gnt±ep±pg±sph

Note: the primary carbonate present in the blueschists was the high pressure polymorph of calcite, aragonite. However, for ease of recognition, the abbreviation, cc (Ca-carbonate) has been used.

2. dolomite

dol+gl+mu+qtz+law±gnt±chl±pg±sph±rut
dol+gl+mu+qtz+law+act±chl±ep±pg±sph
dol+gl+mu+qtz+ep±gnt±pg±sph±rut

dol+gl+mu+qtz+law+gnt+chl is a common combination in the carbonate bearing schists

3. dolomite and calcite

cc+dol+gl+mu+qtz+law±gnt±chl±sph
cc+dol+gl+mu+qtz+ep±gnt±pg±sph
cc+dol+gl+mu+qtz+law+ep+act+chl+sph (rock 86/53A)

4. carbonate free

gl+mu+qtz+law+pg±gnt±ep±rut
gl+mu+qtz+pg+gnt+sph±ep
gl+mu+qtz+gnt+cz±law±chl±sph
gl+mu+qtz+gnt+sph

5. chloritoid

ctd+gl+mu+qtz+gnt+ep±law±dol±pg±sph±rut

6. talc

talc+mu+act+chl+sph

Marble Assemblages

'Pure' Marbles

cc+qtz+mu
cc+dol+qtz±mu

Impure Marbles

Assemblages containing:

1. glaucophane

gl+cc+mu+qtz+sph±ep±gnt±law
gl+cc+dol+mu+qtz+ep±gnt±chl±sph

2. pyroxene

omph+cc+dol+mu+gl+qtz+ep±gnt

3. others

cc+mu+qtz+ep±gnt±chl
cc+dol+mu+qtz±ep±gnt±law±sph

Metabasite Assemblages

Assemblages containing:

1. pyroxene

omph+gl+ep+sph±qtz±gnt±mu±pg
omph+gl+cz+qtz+act+pg±gnt±mu
jd+gl+ep+qtz+pg+sph±gnt±mu

2. lawsonite

law+gl+mu+qtz+gnt+sph±ep±pg

3. others

gl+ep+qtz±gnt±mu±pg±sph

The assemblage lists are most complete for the schists and marbles as the majority of the rocks studied come from these two groups. A fuller listing of the metabasite assemblages was compiled by Dixon (1969, Chapter 8, pp 195 - 209), and these are listed below for completeness. Again the "+" and "-" signs are used rigourously, and the mineral phases are listed in order of abundance.

Metabasite assemblages

Assemblages containing:

1. pyroxene

px±gl+gt±ep±mica±qtz
px+gl±ep±qtz+hm
A. px+gl+act±gnt+zoi+qtz (metagabbro)
B. px+gl+gt+law+sph

2. lawsonite

law+omph+gl+gnt+sph
law+gt+pg+qtz+sph
law+gl+gnt+ep+mica+qtz+sph
law+gl+gnt+sph

3. chloritoid

ctd+gl+gnt+ep+mica+qtz+rut±ilm
ctd+gt+ep+mica+qtz+sph

4. actinolite

act+gl+gnt+ep+mica±qtz
act+gl+ep+mica+chl+qtz
act+omph+gl±gnt+zoi+pg+qtz

5. none of act, law, px, or ctd

gl+gnt+ep+mica+qtz
gl+ep+chl+qtz
gl+qtz
gl+ep+qtz+ilm+rut
crossite+ep+qtz+mt+hm (rock X1025)

The rest of the chapter catalogues the development of the T-X_{CO2} grid.

4.3 THE MODEL SYSTEM

In order to construct a grid a suitable model system must first be selected which will allow a satisfactory representation of the natural mineral assemblages. It is important to select a useful set of components, as graphically representable chemographic analysis is limited to 4 components in 3 dimensional space. If key mineral assemblages cannot be represented then a different combination of components is required. Disregarding accessory phases, the mineral assemblages in the metasediments can be represented by the multicomponent system SiO_2-Al_2O_3-Fe_2O_3-MgO-FeO-CaO-Na_2O-K_2O-CO_2-H_2O. As the majority of the metasediments (schists and marbles) and metabasites contain free quartz, and phengitic mica, only assemblages containing these phases have been considered, and SiO_2 and K_2O can be treated as excess components. It was assumed that a fluid phase was present at all times, and H_2O and CO_2 were regarded as "perfectly mobile" components (Korzhinskii 1959). The solid phases were modelled as magnesium-aluminium end-members, which allows the effects of Fe/Mg and Fe^{3+}/Al solid-solution to be neglected in the first instance.

This reduces the number of non-mobile components to four, Al_2O_3-MgO-CaO-Na_2O, and within this framework all the principal phases can be represented. These four components are also the corners of the phase compatibility tetrahedron, shown in figure 4.1.

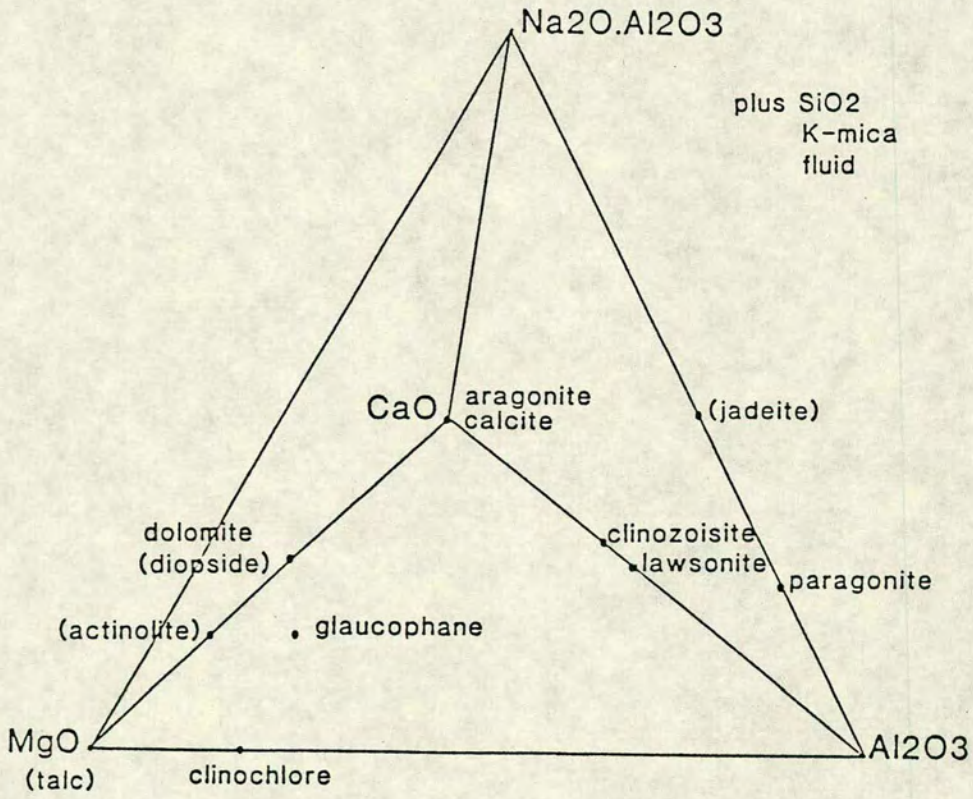

Figure 4.1 Phase compatibility tetrahedron for the system Al_2O_3-MgO-CaO-Na_2O (+ excess SiO_2, K_2O and fluid). The phases in parenthesis are not considered in the T-X grid.

This tetrahedron is basically a slightly simplified version of the Na_2O-R_2O_3-CaO-MgO,FeO tetrahedron used by Dixon (1969), Ernst (1963) and Seki (1960) for blueschist assemblages.

Seven commonly occurring phases have been considered in this study. They are glaucophane, paragonite, lawsonite, clinochlore, clinozoisite, Ca-carbonate and dolomite. Table 4.2 lists the idealised mineral formulae and abbreviations for each of these phases.

Table 4.2 List of the mineral phases considered in the chemographic analysis

phase name	**abbrev.**	**formula**
Ca carbonate	cc	$CaCO_3$
clinochlore	chl	$Mg_5Al_2Si_3O_{10}(OH)_8$
clinozoisite	cz	$Ca_2Al_3Si_3O_{12}(OH)$
dolomite	dol	$CaMg(CO_3)_2$
glaucophane	gl	$Na_2Mg_3Al_2Si_8O_{22}(OH)_2$
lawsonite	law	$CaAl_2Si_2O_7(OH)_2H_2O$
paragonite	pg	$NaAl_3Si_3O_{10}(OH)_2$
quartz	qtz	SiO_2
water	H2O	H_2O
carbon dioxide	CO2	CO_2

Certain phases listed in table 4.1, such as garnet, Na-pyroxene, talc, chloritoid, actinolite and epidote have not been included in the initial analysis. A major reason for pruning the number of phases considered was simply to reduce the number of reaction equilibria to a manageable size. Phases such as talc, actinolite, sodic pyroxene and chloritoid tend to be restricted to rocks of extreme bulk composition, and thus these phases are only developed in a handful of the samples considered. Furthermore, Na-pyroxene and epidote both contain significant amounts of FeO and Fe_2O_3 which cannot be represented in the model tetrahedron. As garnets are anhydrous, the presence or absence of this phase is largely dependent on the Fe/Mg ratio of the host rock not the fluid composition, and thus it was not felt to be a significant phase.

A textural approach is unhelpful when trying to identify possible fluid-controlled reactions in the blueschists, largely because the blueschist metamorphism did not develop over a range of metamorphic grades. There are very few examples of 'frozen-in' reactions in the metasediments, and those that are present are mainly due to later alteration processes. In general, the rocks are well crystallized, and the

minerals appear to be in equilibrium with one another. This is probably due to continuing textural equilibration during deformation, once the equilibrium assemblage had been created. Such apparent harmony means that reactions must be determined theoretically, and therefore the above-mentioned phases were entered into the 'REACTION' program (Finger and Burt 1972) in terms of moles of components. The program uses the ideal mineral compositions to identify all the possible reactions between the phases, and lists the stoichiometric coefficients.

4.4 SCHREINEMAKERS' ANALYSIS AND THE PHASE RULE

Any attempt to use mineral assemblages to estimate metamorphic parameters presupposes that equilibrium has been attained in the rocks. One test of equilibrium is to determine whether or not the Gibbs Phase Rule is obeyed. However, some care must be exercised when applying this criteria, since adherence to the phase rule, though a necessary condition for equilibrium, does not guarantee its attainment.

The Gibbs phase rule can be expressed as below:

$$F + P = C + 2$$

where F = degrees of freedom, P = no. of phases and C = no. of components. For the Syros metasediments, P = 7 (not including quartz and the fluid phase which are always present) and C = 4 (non-mobile components). When F = 0 the system is invariant with P = 6, i.e. 6 phases (plus quartz and fluid) may coexist in stable equilibrium. However, the model system contains 7 phases, and it must therefore contain several invariant points, because the total number of phases exceeds that which is possible at a single invariant point. The number of invariant points is equal to the number of combinations of 7 phases taken 6 at a time, i.e 7 possible omissions.

$$_6C_7 = \frac{7!}{6!(7-6)!} = 7$$

6 univariant curves will radiate from each of the invariant points, and along these univariant curves a maximum of 5 phases, plus quartz and fluid, can coexist.

Having generated the reaction equilibria, Schreinemakers' theorems were used to find the relative positioning of the univariant curves around the appropriate invariant points. Figure 4.2 illustrates the Schreinemakers' bundles determined for each of the invariant points. Obviously the mirror image of each bundle of curves would be equally correct at this stage.

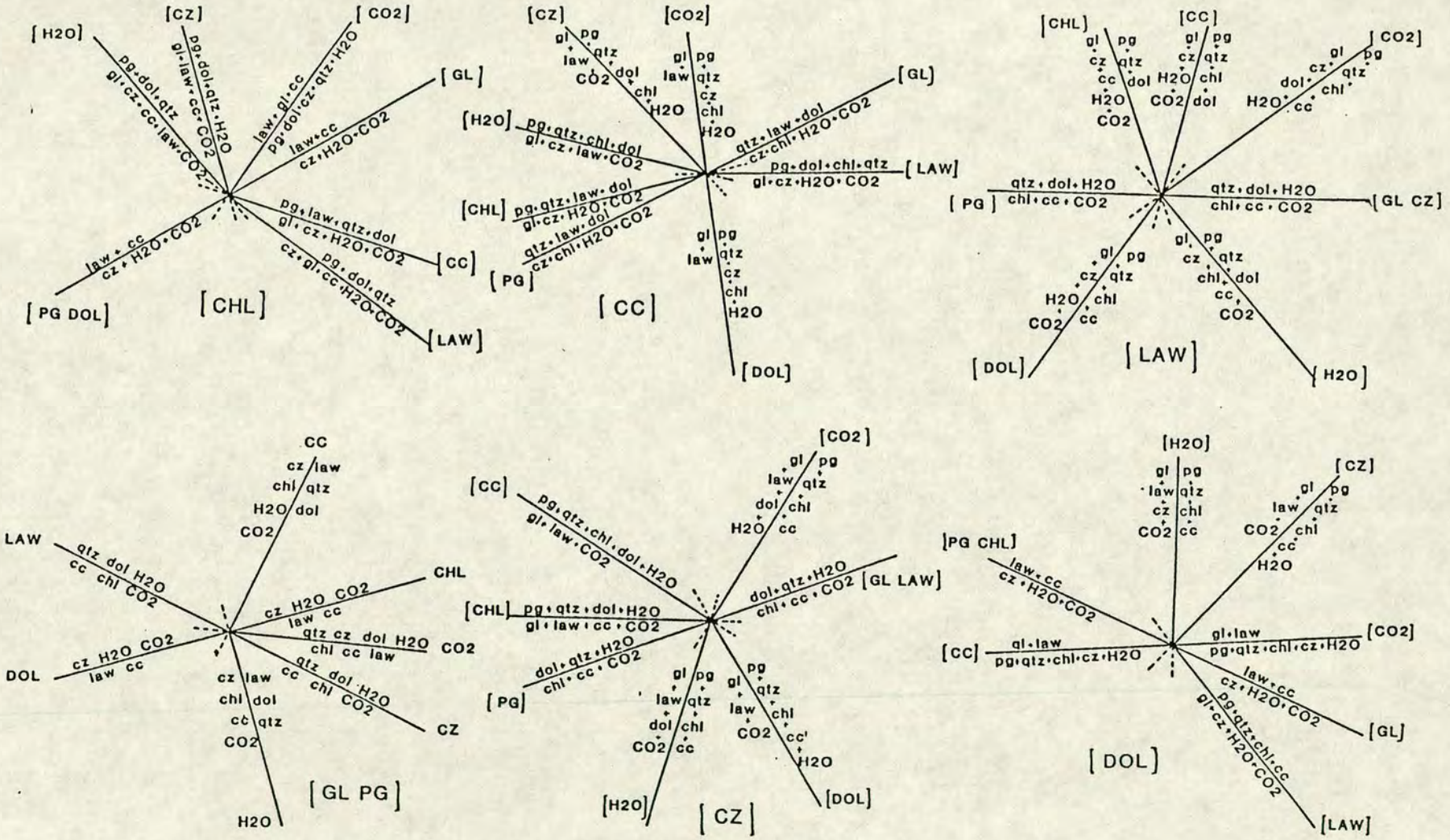

Figure 4.2 Six of the nine possible invariant points are shown above. [Qtz], [H_2O] and [CO_2] have been omitted. The univariant equilibria are labelled with the absent phase (s) in parenthesis. The stoichiometric coefficients of the reactions are not given.

An illustrated example showing the construction of a Schreinemakers' bundle is given in Appendix 1.

As each univariant curve must pass through at least two invariant points, it is possible to link up reaction curves and invariant points to form a network of reactions in T-X space. For example, the phases clinozoisite and dolomite are absent from the reaction given below:

$$5gl+13law+13CO_2 = 9H_2O+27qz+10pg+3chl+13arag\ [CZ,DOL]$$

and therefore this univariant curve must belong to both the [CZ] and the [DOL] invariant points, and will of necessity pass through both. This approach, though helpful when determining the basic phase relations, becomes cumbersome when more than two or three invariant points are present. It was not possible to determine a unique solution for the topology of the grid using this approach, largely because criteria were lacking to decide which subset of invariant points would be stable or metastable from a petrological and textural examination of the blueschist assemblages. Instead, it was decided that a more rigourous, quantitative approach, using internally consistent thermodynamic data for the phases of interest, would provide a ready means of determining both the topology, and the 'absolute' location of the mineral-fluid equilibria of interest in T-X_{CO2} space.

4.5 THERMODYNAMIC MODELLING

For an equilibrium relation between several solid mineral phases (s), and a mixed H_2O-CO_2 fluid, the equation describing mineral-fluid equilibria is:

$$(\Delta G^o)^{P,T} + RTlnK_s + nRTln(f^o_{H2O}.X_{H2O}.\gamma_{H2O})+mRTln(f^o_{CO2}.X_{CO2}.\gamma_{CO2}) = 0$$

$(\Delta G^o)^{P,T}$ — Gibbs energy for a reaction among pure end-members at the temperature and pressure of interest.

$$(\Delta G^o)^{P,T} = \Delta H_{1,298} + \int \Delta Cp dT - T(\Delta S_{298} + \int \Delta Cp/T\ dT) + \Delta VsP$$

V_s — volume of solid phases at 1 bar, 298K

Cp — heat capacity, $Cp = a+bT+cT^{-2}+dT^{-1/2}$ after Holland and Powell (1985)

K_s — equilibrium constant

f^o — fugacity of pure H_2O and CO_2

γ	activity coefficient, modifies the activity term when mixing is non-ideal
X_{H2O}, X_{CO2}	mole fraction of H_2O and CO_2
m,n	stoichiometric coefficients

This expression is true for any P or T, and it allows for the existence of impure multicomponent phases, and for non-ideal mixing of real H_2O-CO_2 fluids. The information required to quantitatively evaluate this equation for the reactions in the grid can be obtained from existing internally consistent thermodynamic data-sets (Berman *et al.* 1985; Helgeson *et al.* 1978; Holland and Powell 1985; Holland and Powell pers. comm., 1988), which include data for a large variety of mineral and fluid species over a wide range of P-T conditions.

The principal uncertainty when attempting calculations of this sort is the reliability of the mineral and fluid thermodynamic data, and, at best, the results can only be as good as the original data on which they are based. Fortunately, with the exception of the enthalpy of formation, ΔH_f, the other data required, heat capacity, molar volume and entropy, are reasonably well known, and sufficiently precise for the phases of interest in this study (but see discussion of glaucophane below).

Glaucophane - Thermodynamic data

The principal reason why a thermodynamic approach to the reaction grid was not adopted from the beginning of this study was the complete lack of thermodynamic data for glaucophane. Attempts to synthesize pure glaucophane have been largely unsuccessful (Ernst 1961; Koons 1982; Maresch 1977), and thus it has been impossible to determine reliable thermodynamic data for the phase. However, in a recent paper published by Holland (1988), new heat capacity measurements, and cell volume data were presented for a magnesian glaucophane from the Eastern Alps, and this was combined with estimates of the other parameters to produce a complete set of thermodynamic properties for the phase. As usual, the major uncertainty lay in estimating the heat of formation. Holland used estimated data for entropy, thermal expansion and compressibility, in order to generate an enthalpy of formation for glaucophane using the experimental brackets of Carman and Gilbert (1983) for the reaction glaucophane = 2 jadeite + talc.

Although Holland uses the Carman and Gilbert data with some reservations, his concern should perhaps have been greater. In their paper, Carman and Gilbert claim to have synthesized pure end-member glaucophane. The validity of that claim will be

examined through the following discussion which is based on the work of Koons (1987), on OH-glaucophane, and Welch (1987,1989), on fluor-glaucophane, both of whom come to a different conclusion from Carman and Gilbert (1983).

No probe analyses are given in the Carman and Gilbert (1983) paper to justify their claim to have synthesized pure end-member glaucophane. Instead the synthesized amphibole compositions are displayed on a plot of Na-Mg-Al, reproduced here as figure 4.3, where they appear to cluster around the end-member glaucophane composition. Figure 4.4 is a comparable Na-Mg-Al plot produced by M.Welch (1987,1989), displaying the compositions of amphiboles generated in the fluor-glaucophane system. The circled region labelled CG encloses the Carman and Gilbert data, and, as can be seen, the Carman and Gilbert amphiboles are at least binary in composition, having a significant katophorite component. The fluor-amphibole compositions show a similar spread to those of Carman and Gilbert, and some of the fluor-amphiboles apparently plot closer to the end-member glaucophane composition point. However, this Na-Mg-Al plot is projected from SiO_2, and does not give a true picture of the deviations that can occur from ideal glaucophane. Figure 4.5 shows the 3rd dimension of the previous plot, along the katophorite-nyboite join, and provides a more representative and informative picture. When the fluor-amphiboles are considered in this way they are seen to be displaced from end-member glaucophane by a significant edenite ($NaAlSi_{-1}$) vector. It seems likely that if the information was available to plot the Carman and Gilbert data in this manner, their amphibole compositions would show a similar edenite vector. Since no probe analyses are given to disprove this, their data must be treated with caution.

The effect of this compositional displacement on the activity of glaucophane can be shown in a simple example. The fluor-amphibole, AJC-1, was in equilibrium with jadeite and coesite at 31 kbars and 803°C (M.Welch pers comm. 1989). This amphibole is identified in figures 4.4 and 4.5, and in the former it appears to plot on top of end-member glaucophane. A probe analysis of this amphibole is reproduced below in table 4.3, courtesy of Dr. M. Welch.

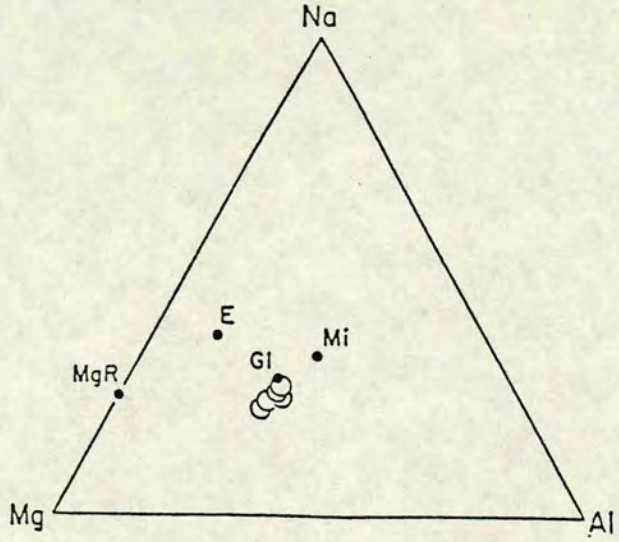

Figure 4.3 Shown on the Na-Mg-Al plot are electron microprobe analyses of amphiboles synthesized at 750°C and 25 kb by Carman and Gilbert (1983 (open circle symbol). The solid dots represent endmember compositions gl = glaucophane; Mi = miyashiroite, $Na_3Mg_3Al_3$; E = eckermannite, (Na_3Mg_4Al) and MgR = magnesiorichterite, (Na_2Mg_6) (from Carman and Gilbert 1983, fig. 3).

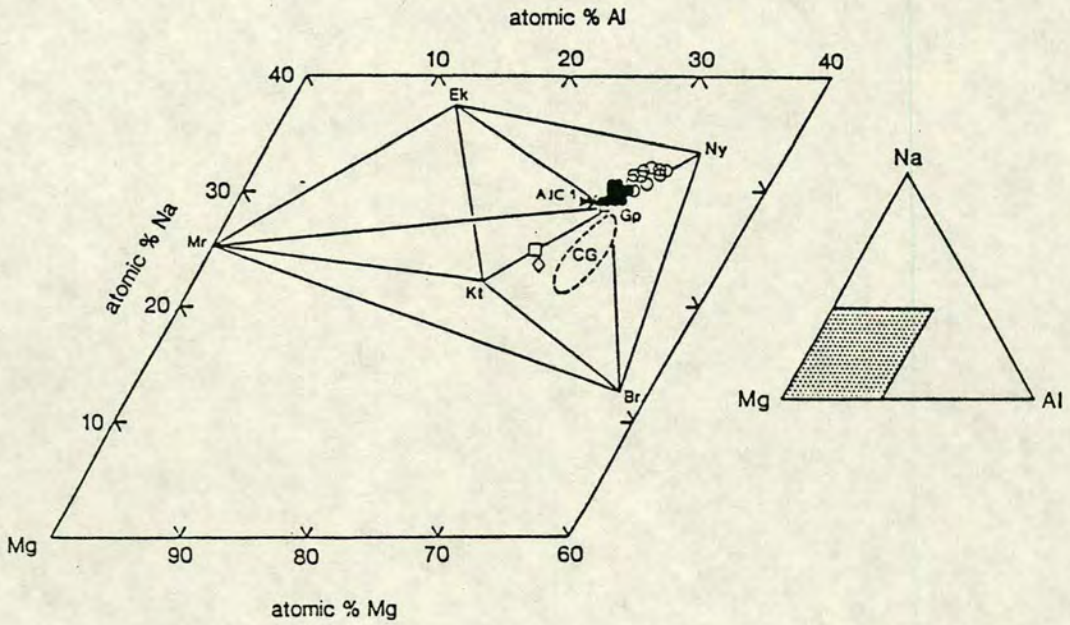

Figure 4.4 Electron microprobe analyses of fluor-amphiboles from Welch (1987) are shown as a Na-Mg-Al atomic % plot projected from Si. Δ = Am + Jd + Co, • Am + qtz/co, o Am + sphl + qtz. Also shown are the data of Carman and Gilbert (1983) labelled as CG, and Koons' average amphibole (◊) (1982), and z - 52 (□). Amphibole AJC-1 is discussed in the text. Gp = glaucophane, Ny = Nyböit, Kt = Mg - katophorite, Br = Mg - Barröisite, Ek = Eckermannite, Mr = Mg - richterite, Sphl = Sodic Phlogopite, Co = coesite, (from Welch 1987, fig. 5)

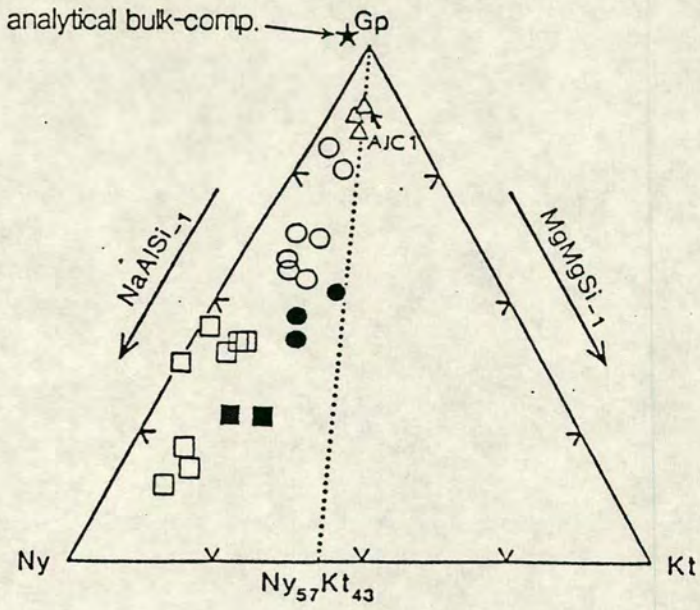

Figure.4.5 Here the fluor-amphibole data (Welch 1987) is projected from eckermannite onto the Gp-Ny-Kt plane. This projection gives a much more representative picture of the deviations from the ideal glaucophane composition. The symbols are the same as those in the previous figure. Filled symbols - runs at 850°C, open symbols - runs at 800°C (from Welch 1987, fig. 6).

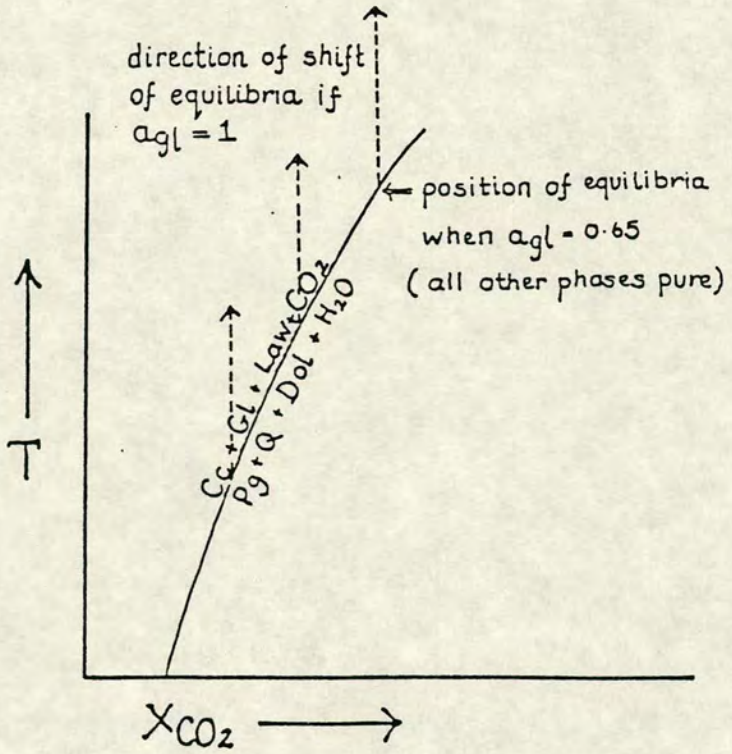

Figure 4.6 Sketch T-X_{CO2} section showing the effect of changing glaucophane activity on the position of a reaction equilibria, see text for discussion.

Table 4.3 Electron microprobe analysis of the amphibole AJC-1.

AJC-1 (run conditions - 31kbars 803°C)

Na20	8.07
MgO	15.65
Al2O3	12.99
SiO2	58.58
	95.29

Cations per formula unit	
Na	2.10
Mg	3.13
Al	2.06
Si	7.86
Total	15.15

Formula		
T1	Si	4.000
T2	Si	3.860
	Al	0.140
M2	Al	1.920
	Mg	0.080
M1	Mg	3.000
M3		
M4	Mg	0.050
	Na	1.950
A	Na	0.150
		0.850

If the activity of glaucophane is calculated for this amphibole using the standard ideal mixing on sites model(Powell 1978), it is seen to be significantly less than 1.

$$X_{\square A}.(X_{NaM4})^2.(X_{MgM1,3})^3.(X_{AlM2})^2.(X_{SiT1})^4$$

$$(0.85).(0.975)^2.(1)^3.(0.96)^2.(0.965)^4 = 0.645$$

Bearing the preceding discussion in mind, it seems likely that the amphiboles generated by Carman and Gilbert (1983) will have a activities. It is worrying that the experiments by Carman and Gilbert (1983) form the basis from which Holland (1988) derived the enthalpy of formation for supposedly pure end-member glaucophane. The enthalpy data is almost certainly not for pure glaucophane, a fact which has important implications when considering the positions of glaucophane bearing reaction curves. If the activity of the supposedly pure glaucophane, used to construct the data-set, was actually 0.65 instead of 1.0, then an error will occur in the positioning of glaucophane-bearing equilibria. Consider the equilibria,

$$qtz+2pg+3dol+3H_2O = cc+gl+2law+5CO_2$$

If the initially pure glaucophane is diluted by an impurity, then its free energy, and that for the products side of the reaction, will be lowered, favouring the products, and increasing their stability field. For the Carman and Gilbert data (1983) discussed here the situation is the reverse of that described above. Here the supposedly pure glaucophane may be impure, and the true position of the curve for pure glaucophane will be displaced from that calculated using the Carman and Gilbert data (1983). The actual degree and direction of shift will depend on a number of factors such as the stoichiometric coefficient of glaucophane, whether glaucophane appears as a product or a reactant, and the entropy of the reaction. The entropy term is of great importance since:

$$\frac{(\partial G)}{(\partial T)_p} = -S$$

The amount of temperature shift for a particular gl-bearing equilibria will be largely dependent on the entropy of the reaction. The larger the entropy the smaller the change in temperature, for any specified change in ΔG. The most susceptible reactions will be those with a small entropy change, i.e solid-solid reactions. (This means that reactions like gl=jd+talc used by Carman and Gilbert (1983) will be very sensitive to changes in G). Figure 4.6 (page 126), is a sketched T-X_{CO2} section showing the glaucophane-bearing equilibria given above. If it was assumed that the position of this equilibria was calculated for pure phases, when in fact the activity of glaucophane was only 0.65, then the position of the equilibria when a_{gl} actually equals 1.0 will lie up temperature as indicated on the figure. As the Holland and Powell data-set (pers. comm., July 1988) assumes that the thermodynamic properties of glaucophane refer to the pure phase, there is no way of quantitatively correcting for a lowered glaucophane activity, except by entering an activity greater than one for glaucophane into the program, which of course is not allowed. The main point of this discussion is that because this study has used the Holland and Powell dataset (pers. comm., July 1988) the positioning of glaucophane-bearing equilibria may be in error, causing a degree of "slop" in the T-X grid.

Having pointed out the possible weaknesses in the glaucophane data, it must be said that this is still a great improvement on the previous absence of data. The thermodynamic data for glaucophane is internally consistent with the extended Holland and Powell data-set (pers comm., July 1988), which now covers all the Syros model phases. The extended data-set now allows at least preliminary T-X_{CO2} phase-relation calculations to be made on the Syros blueschists, and other glaucophane bearing rocks, something which was previously impossible.

4.6 THE POSSIBILTY OF METHANE IN THE BLUESCHIST FLUID

Metamorphic fluids are commonly modelled in terms of just two components, H_2O and CO_2. However, the presence of graphite as a common accessory phase in the blueschist metasediments challenges the assumption of a simple binary fluid, and the possibility of additional species, such as methane CH_4, must be investigated. Figure 4.7 shows the generalised fluid composition regions in the system C-O-H-S projected onto the C-O-H plane (after Holloway 1981). When graphite is present the fluid composition must lie along the graphite boundary, and at low oxygen fugacities additional reduced fluid species such as CH_4, CO and H_2 could be present (Ferry and Burt 1982, Frost 1979). However, as X_{H2} and X_{CO} will only exceed 0.1 at low pressures and high temperatures (T>800 ^oC), under blueschist facies conditions the main constituents of a fluid in equilibrium with graphite will be CH_4, CO_2 and H_2O (Ohmoto and Kerrick 1977).

It is important to consider what effect the presence of methane in the fluid will have, since its presence will effect the stability fields of mineral assemblages relative to their positions in a binary H_2O-CO_2 system. Jacobs and Kerrick (1981) suggest that even small amounts of CH_4 in H_2O-CO_2-CH_4 fluids may affect the activity of H_2O and CO_2 significantly. CH_4 will act as a dilutent of CO_2, and this will reduce its activity relative to its value in a binary H_2O-CO_2 fluid, whereas the activity of H_2O will show a slight increase. If a methane-bearing fluid is modelled as being a simple H_2O-CO_2 mixture the reduction in the activity of CO_2 will make the fluid appear more water-rich than it actually is, and in reality the assemblages will coexist with fluids having higher CO_2 contents than those suggested by the T-X_{CO2} section.

The relative proportions of CH_4, H_2O and CO_2 in the fluid are controlled by a number of factors, including the PT conditions of metamorphism. Figure 4.8 is taken from Ohmoto and Kerrick (1977), and shows the isopleths of maximum X_{H2O} for fluids in equilibrium with graphite, pyrite and pyrrhotite. The maximum X_{H2O} content of the fluid is greatest under low temperature, high pressure conditions. The proportions of CO_2 and CH_4 increase with increasing temperature, or decreasing pressure, because the reaction:

$$2C + 2H_2O = CO_2 + CH_4$$

is favoured by increasing temperature. Under the pressures and temperatures experienced during blueschist metamorphism, graphite can coexist with a fluid which is almost pure water, (see figure 4.8).

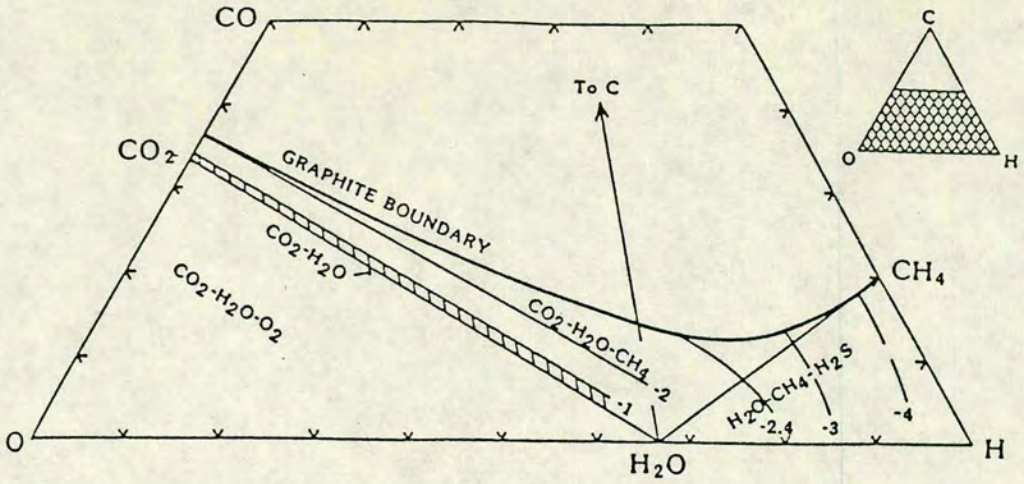

Figure 4.7 Generalized fluid composition regions in the C-O-H-S system projected onto the C-O-H join. The diagram refers to T = 1100°C and P = 5000 bars, but the general characteristics are independent at P and T. The numbered lines are fO_2 isobars relative to the QMF buffer (from Holloway 1981).

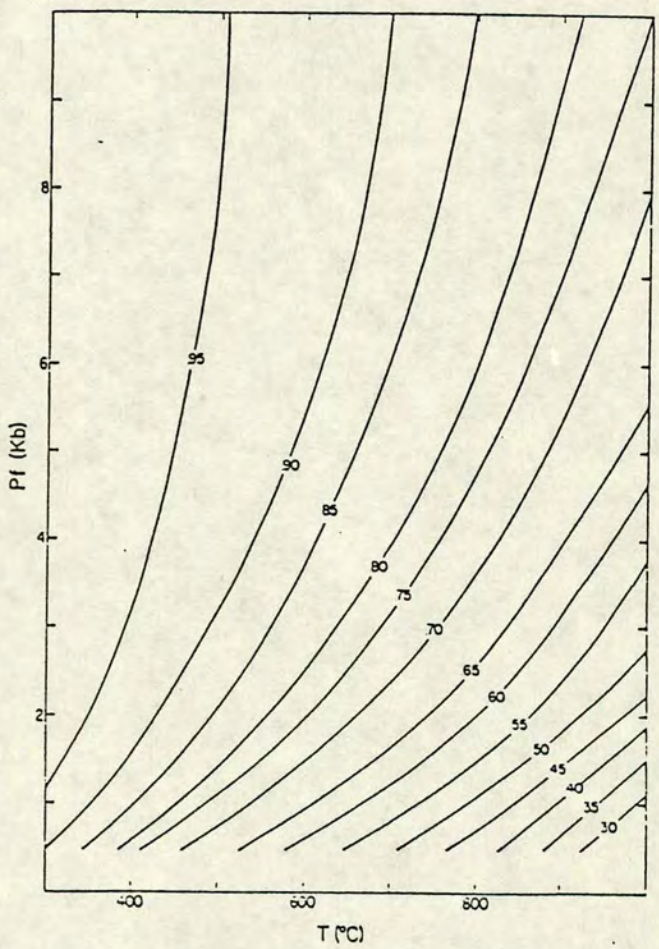

Figure 4.8 Isopleth of maximum XH_2O for fluids in equilibrium with graphite, pyrite and pyrrhotite (after Ohmoto and Kerrick 1977).

The compositional variation of the fluid will also be critically dependent on the prevailing oxygen fugacity, a parameter which is much harder to constrain in the Syros blueschists. As is discussed in chapter 3, oxide minerals are rare in the metasediments, and no oxide assemblages were found which could buffer the oxygen content of the fluid. Figure 4.9 shows five plots of log f_{O2} versus the the proportions of CH_4, CO_2 and H_2O in the fluid. The plots are calculated for a fluid in equilibrium with graphite at pressures of 14, 6 and 2 kbars, and temperatures in the range 350 to 450 °C. These plots show the important effect of pressure on the graphite-fluid equilibria. As pressure increases the X_{H2O} curve broadens out, and the range of f_{O2} values where more than one fluid species is important becomes very narrow. At high pressures, CO_2 is dominant at high f_{O2}, CH_4 at low f_{O2}, and H_2O is the major constituent at intermediate f_{O2}. Using a program developed by Jacobs and Kerrick (1981), the compositions of fluids in equilibrium with graphite were calculated using the methods of Ohmoto and Kerrick (1977) and the MHSRK of Jacobs and Kerrick (1981). The positions of these reaction curves were then compared to their positions when in equilibrium with a binary H_2O-CO_2 fluid. Because of certain restrictions in the Jacobs and Kerrick program, the data-set used had to be that of Holland and Powell (1985), rather than the extended data-set (Holland and Powell pers. comm., July 1988), which means that glaucophane-bearing equilibria could not be considered. Table 4.4 compares the temperatures calculated for two equilibria at fixed values of X_{CO2} for the two different cases, 1) for a fluid in equilibrium with graphite, and 2) for a binary H2O-CO2 fluid. Even at low values of X_{CO2}, where the presence of CH_4 should have the greatest effect, the positions of the two curves are almost identical. However this is not altogether surprising. The Jacobs and Kerrick program (1981) calculates the mole fractions of C-O-H fluid species in equilibrium with graphite at given values of X_{CO2}, P and T and, as was noted in figure 4.9, because there is virtually no overlap between the fluid species at high pressure, when the values of X_{CO2} are low, the remaining fluid will be composed of H_2O, and X_{CH4} will be negligiable.

In conclusion, under the peak PT conditions experienced by the Syros blueschists, it appears that the assumption of a binary H_2O-CO_2 fluid is justified, despite the presence of graphite in the metasediments.

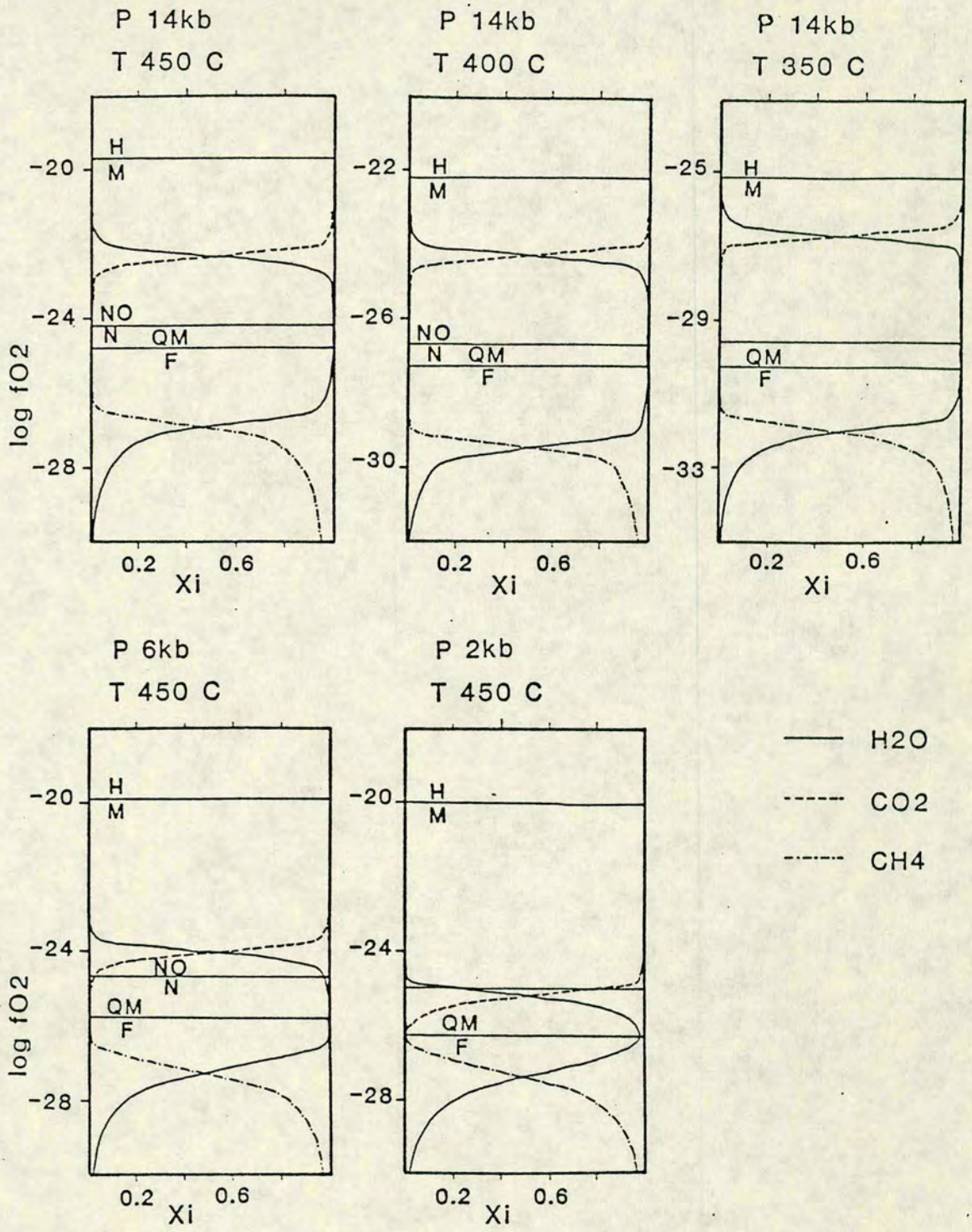

Figure 4.9 The five plots above were calculated using a program developed by Jacobs and Kerrrick (1981), and show the compostional variation in fluids coexisting with graphite over a range of P and T. See text for discussion. The positions of the oxygen buffers were calculated from the equations given in Ohmoto and Kerrick (1977, table 1). (Note the expression given for the magnetite/hematite equilibria is out by a factor of 2, see Huebner 1971).

ble 4.4

uilibrium considered:

$$6\ cc + chl + 4\ CO_2 = qtz + law + 5\ dol + 2\ H_2O.$$

CO_2)	T°C for a binary H_2O-CO_2 fluid	corresponding temperature °C for a fluid in equilibrium with graphite
5	665.3	666.3
0	714.9	715.8
5	742.9	743.6
0	763.1	764.4
5	780.0	782.9

uilibrium considered:

$$cc + 3\ law = 2\ cz + 5\ H_2O + CO_2.$$

CO_2)	corresponding temperature (°C) for a binary H_2O-CO_2 fluid	corresponding temperature °C for a fluid in equilibrium with graphite
5	496.2	
0	501.0	
5	502.1	
0	502.0	
5	501.4	

4.7 COMPUTER PROGRAMS AVAILABLE FOR THERMODYNAMIC CALCULATIONS

There are two computer programs available at Edinburgh which can perform thermodynamic calculations of phase relation using an internally consistent data-set. They are THERMOCALC (Powell and Holland 1988), and 3 interlinked programs by Perkins, Brown and Berman (1986), PT-SYSTEM, TX-SYSTEM and PX-SYSTEM. Table 4.5 provides a comparison of the two programs, listing positive and negative features from the point of view of modelling the Syros blueschist assemblages. Some of these comments will only apply to the Edinburgh computing system.

Table 4.5

	THERMOCALC	PT,TX,PX - SYSTEM
Authors	Powell and Holland (1988)	Perkins, Brown and Berman (1986)
Language	Turbo-Pascal	Fortran 77
Availabilty	Micro	Mainframe and micro
Documentation	Fair	Good
Thermodynamic data base	Holland & Powell (1985), extended dataset Holland & Powell pers comm., July (1988).	Berman *et al.* (1985)
Glaucophane data ?	Yes	No
Flexibility	Difficult to alter anything	User customisation is easy to achieve
T-X sections	Not directly, to generate a T-X section multiple PT sections must be generated at different values of X_{CO2}. Not very satisfactory.	Yes, use TX-SYSTEM program

Graphical display and output	Graphics not yet implemented. Output is not in a suitable form for use with EASYGRAPH (ERCC, Edinburgh)	Graphics available. Plot file can be modified for use with EASYGRAPH, or used directly with GR.TXBOBJ (A.Baker pers comm. 1988)

From the point of view of producing TX sections, and generating hard copy graphical output, the program by Perkins *et al.* (1986) is superior, however the Berman *et al.* dataset (1985) does not contain thermodynamic data for glaucophane. The flexibility of the Perkins program allows a new input data file to be created using the extended Holland and Powell data-set (pers comm., July 1988) which is compatible with the TX-SYSTEM program. All the thermodynamic variables are comparable except for the heat capacity coefficients, and Table 4.6 below illustrates how the heat capacity coefficients used in the Berman *et al* dataset (1985) relate to those used by Holland and Powell (1985,1988).

Table 4.6 Comparison of Cp terms

Source of equations	Terms in Cp equation						
	T^2	T^1	T^o	$T^{-0.5}$	T^{-1}	T^{-2}	T^{-3}
Holland & Powell 1985		b	a	d		c	
Berman *et al.* 1985	k_6	k_5	k_o	k_1	K_4	K_5	K_3

The extra coefficients in the Berman *et al.* (1985) formulation of the heat capacity equation were set to zero

H_2O - CO_2 Mixing

One further discrepancy between the two programs which must be considered is the routine used to model H_2O-CO_2 mixing. The Perkins program offers two options for this:

1. Ideal Mixing

2. Kerrick and Jacobs Redlich-Kwong
   325 <T< 1050 °C P> 0.5 Kbars

It is clear that the low temperature, high pressure conditions attending metamorphism on Syros mean that non-ideal behaviour will prevail in the fluid phase, and thus the Kerrick and Jacobs model (1981) was selected. THERMOCALC also bases its estimate of the mixing properties of H_2O-CO_2 fluids on the Kerrick and Jacobs Redlich-Kwong equation. However, the calculated activities are then fitted to a pressure-temperature dependent sub-regular solution model, and values for the interaction parameter, ω, are calculated for H_2O and CO_2. The modified activities are then used in the program. Combining the Holland and Powell data-set (pers. comm., July 1988) with the Kerrick and Jacobs mixing routine in the Perkins program means that the thermodynamic dataset is no longer strictly internally consistent, and this will affect the positioning of the reaction curves in T-X space. The effect of this inconsistency was tested by comparing the temperature values calculated for non-glaucophane bearing reactions using the two programs, THERMOCALC and the modified Perkins program. The temperature agreement between the two programs is generally good, and where both H_2O and CO_2 occur on the same side of a reaction temperature differences are generally less than 2 °C, (see table 4.7). In cases where H_2O and CO_2 appear on opposing sides of a reaction the temperature differences are larger, up to 17 °C.

In the ideal situation it should be possible to use a totally internally consistent dataset. Such a dataset does exist in THERMOCALC, but because of the time-consuming difficulties to be overcome at present when trying to generate and output complicated T-X sections it was decided to use the Perkins program, TX-SYSTEM, with the Holland and Powell dataset, despite the slight inconsistencies generated because of the different H_2O-CO_2 mixing models. It was felt that the errors introduced by doing this are comparatively small in comparison to the errors inherent in the thermodynamic data itself, and the enthalpy of formation data for glaucophane in particular (see previous discussion).

Table 4.7

P = Perkins et al. (1986) program + MHSRK (Kerrick and Jacobs 1981); + Holland and Powell (1988) data-set; HP = Internally consistent arrangement. THERMOCALC program (Powell and Holland 1988) + modified Kerrick and Jacobs (1981) H_2O-CO_2 mixing routine + Holland and Powell (1988) data-set.

See text for discussion. Equilibria calculated at P = 14 Kbars.

1) CC+3 law = 2 CZ+5 H_2O+CO_2

$X(CO_2)$	T°C-P	T°C-HP
0.39	514.7	515
0.20	519.4	518
0.005	478	477
0.004	473	474
0.002	468	466

2) 5 dol+19 law+3 qtz = 12 CZ+chl+28 H_2O+10 CO_2

$X(CO_2)$	T°C-P	T°O-HP
0.50	541.8	540
0.39	546	543
0.14	545	547
0.005	480	477
0.004	475	473

3) 5 dol+law+qtz+2 H_2O = 4 CO_2 + chl + 6cc

$X(CO_2)$	T°C-P	T°C-HP
0.005	-	476
0.004	475	465
0.0025	449	438
0.001	419	405
0.0008	404	<400

4) 19 cc+3 chl+11 CO_2 = 11 H_2O+2 CZ+3 qtz+15 dol

$X(CO_2)$	T°C-P	T°C-HP
0.016	600	572
0.010	549	529
0.0068	514	499
0.0060	504	489
0.0050	489	475
0.0041	475	462

4.8 THE T-X_{CO2} GRID

Having decided on the program, the model phases were input into TX-SYSTEM, all possible reactions between the phases were generated, and these were plotted up to form a T-X_{CO2} grid. As the system was modelled as being silica saturated, any quartz absent reactions generated were removed. Fluid absent (or fluid conserving) reactions, i.e [H_2O, CO_2], were also removed as these could not provide any information about the fluid phase. Where a single fluid species was absent, i.e [H_2O] or [CO_2], the number of solid phases present in a non-degenerate univariant reaction exceeded that possible under the phase rule, for example;

$$pg+qtz+chl+dol = gl+cz+law+CO_2\ [CC,H_2O]$$

The phase rule states that for a univariant curve in the system described (see section 4.4) the maximum number of solid phases is 5+qtz+fluid, and therefore reactions of this type were also removed.

Figure 4.10 shows the grid generated for the pure Mg,Al end-member phases (activity of all phases = 1), at a total pressure of 14 kbars over the temperature range 350 - 520 ^oC, (loose copy out of text). Examining the plot a number of important points can be made. The first point to note is that most of the univariant equilibria occur close to the water-rich side of the T-X_{CO2} diagram. This is largely because CO_2-H_2O mixtures show strongly non-ideal mixing under high pressure, low temperature conditions.

The activity of a fluid species is essentially the effective concentration, and it can be expressed as;

$$a_{ifluid} = \gamma_i . X_{ifluid}$$

where γ_i is the activity coefficient, and X_i is the mole fraction of species i in the fluid. When a fluid is considered to mix ideally then the activity coefficient is equal to one and $a_i = X_i$. Although ideal mixing has served as an adequate model of mineral-fluid equilibria in many studies of greenschist and amphibolite facies rocks (Ohmoto and Kerrick 1977; Ferry 1976b; Valley and Essene 1980), under blueschist facies conditions large deviations from ideal mixing occur, and values of the activity coefficient, γ, are large. The effects of non-ideal mixing can be shown using simple activity-composition plots, (see figure 4.11). Non-ideality increases with increasing pressure and decreasing temperature for a particular mixture, and thus accounting for non-ideal mixing will be of critical importance when trying to model blueschist phase relations.

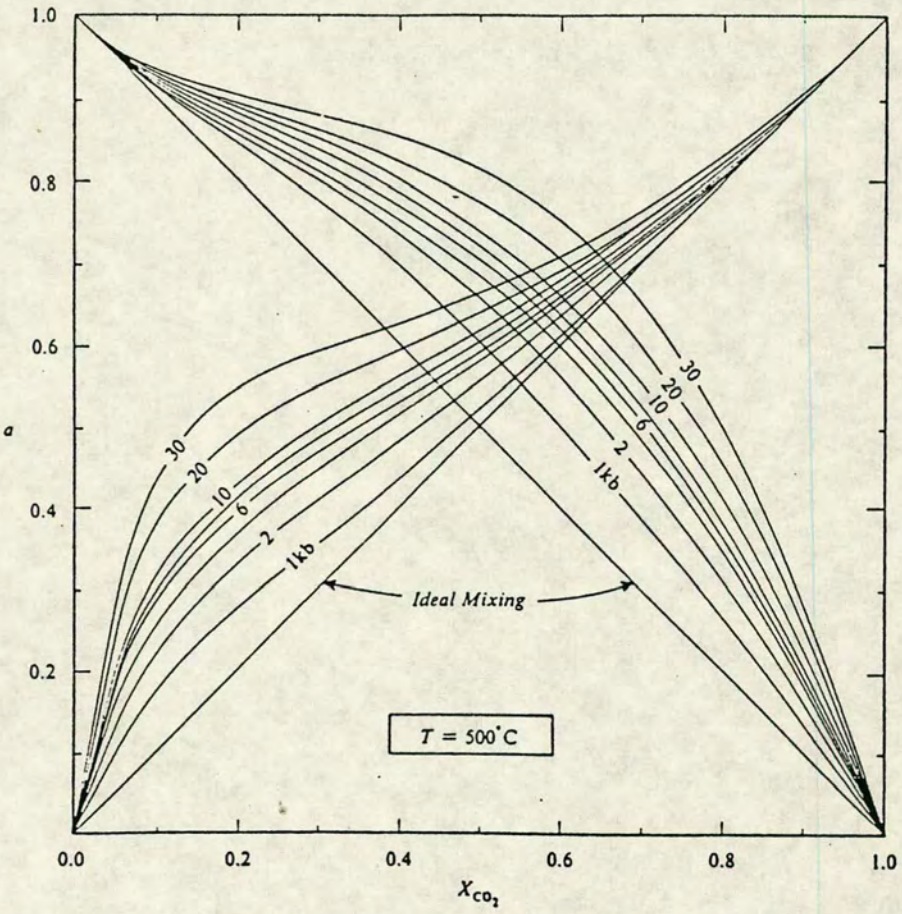

Figure 4.11 An activity-composition diagram for H_2O-CO_2 mixtures at 500°C. The contours show total pressure (P_{total} = $P(H_2O)$ + $P(CO_2)$ in kbars. The contours were calculated using the modified Redlich-Kwong equation (from Kerrick and Jacobs 1981, fig. 12).

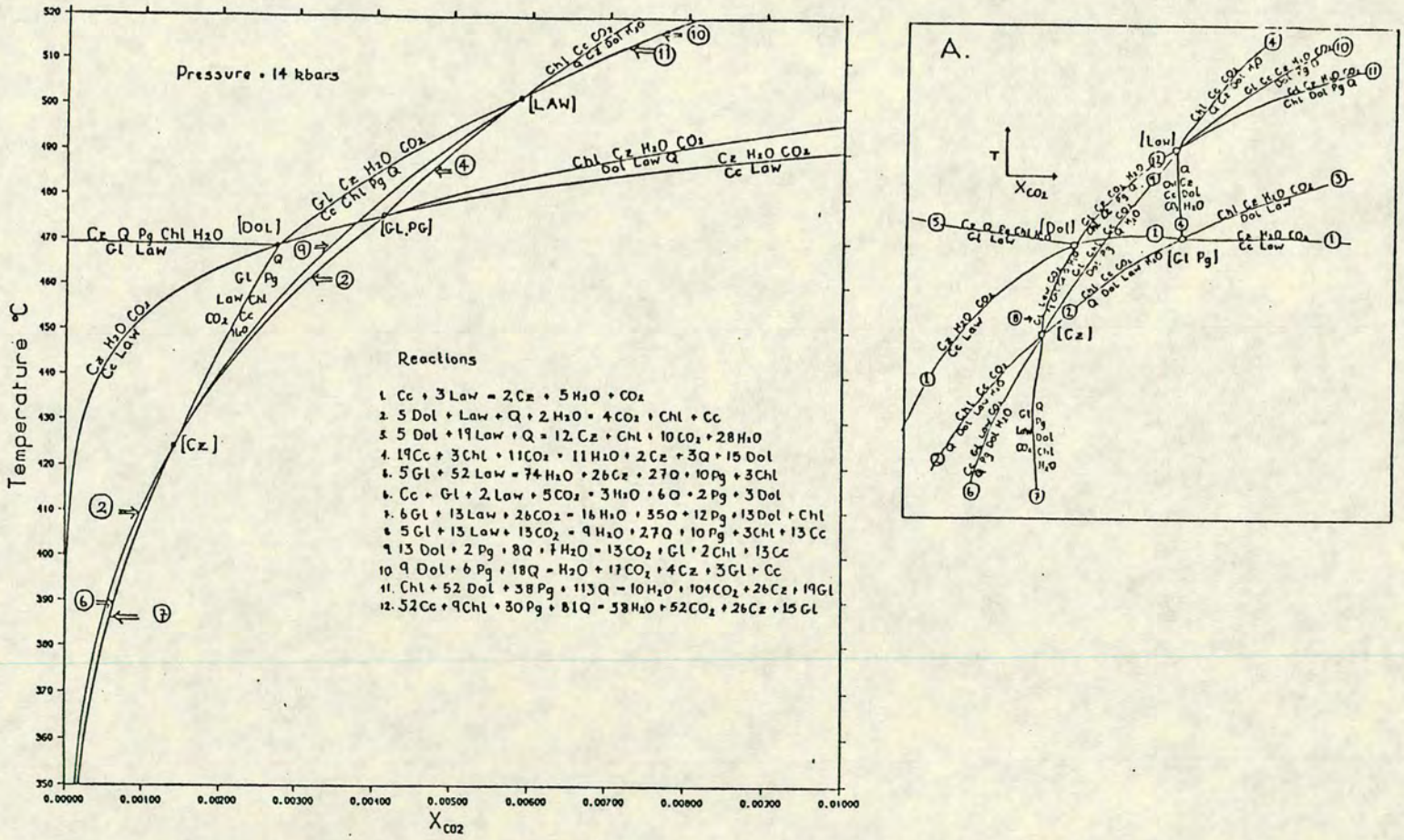

Figure 4.10 T-XCO_2 section showing reactions with excess quartz amongst pure phases in the system NCMASH-CO_2 at P(fluid) = 14 kbars. Equilibria were calculated using the thermodynamic data-set of Holland and Powell (pers. comm., July 1988) and the program TX-SYSTEM (Perkins *et al.* 1986). Invariant points are labelled according to the phases absent. For clarity diagram A is a schematic sketch of the area around the invariant points.

The large positive deviations of CO_2 from ideality at small mole fractions tends to shift the position of reaction equilibria towards the water-rich axis. As can be seen in figure 4.10, the X_{CO2} of the fluid involved is considerably less than 1 mol%. Thus, even before considering specific assemblages in detail it appears that the blueschist fluid was extremely water rich.

4.9 INTRODUCTION OF OBSERVED ASSEMBLAGES

Table 4.8 is a list of selected mineral assemblages which span the range of those so far observed in the Syros blueschist metasediments, (loose copy out of text). A number of inconsistencies are observed when the assemblage lists in table 4.8 are compared to the allowed assemblages determined from the phase compatibility tetrahedra. A number of extra phases not considered by the grid occur quite frequently, the commonest of which are garnet, actinolite and omphacite. Discrepancies between the theoretically determined phase relations and the observed mineral assemblages are mostly caused by the presence of additional components, such as FeO and Fe_2O_3, and the effects of solid solution. Probe analyses given in the previous chapter for glaucophane, chlorite and epidote indicate that in reality these minerals cannot be represented accurately in the simple system Na_2O-CaO-MgO-Al_2O_3, and the same must also be true for "real" mineral equilibria in the grid. Dolomite, chlorite and glaucophane will contain significant amounts of FeO, and clinozoisite and glaucophane will contain some Fe_2O_3. These solid solution effects must be taken into account when dealing with the natural assemblages, as critical changes in the mineral tie lines can occur with Fe^{3+}:Al and Mg:Fe variations. Introducing further components into the system will increase the number of degrees of freedom. Apparently invariant assemblages may become univariant, or divariant, and univariant assemblages may become divariant in T-X_{CO2}-$X_{Fe/Mg,Fe3+/Al}$ space.

The departure of real mineral compositions from their ideal pure end-members is expressed by the activity term, a. If a mineral consists only of the pure end-member then its activity is equal to 1, otherwise the activity is generally less than 1. Activities are a complex function of composition, and when applying equilibrium thermodynamics to real phases it is important to ensure that the activity-composition relationships have been carefully considered. In the case of the Syros phases, with the exception of glaucophane, chlorite, dolomite and epidote, all other minerals are treated as being of approximately end-member composition.

Electron microprobe data can be used to determine the activities of phases showing solid-solution effects using the formulations given in Table 4.9 above.

Table 4.8 Selected mineral assemblages from the schists and impure marbles (marbles are marked with an asterisk). All assemblages contain quartz and phengitic mica in addition to the phases listed.

sample #	gl	pg	law	chl	cc	dol	ep	gnt	om	act	sph	rut
86/14	X		X	X		X		X			X	X
86/40	X			X						X	X	
86/47	X		X	X		X		X			X	
86/49	X		X	X	X	X		X			X	
86/52	X	X	X	X	X		X				X	
86/53B	X		X	X		X				X	X	
86/53H	X		X	X	X	X				X	X	
86/59	X		X	X			X				X	
86/67*	X		X		X		X	X			X	
86/68	X			X	X	X	X	X				
86/69*	X				X	X	X		X			
86/71	X		X	X	X						X	
86/72	X	X	X	X				X			X	X
86/75*	X				X	X	X	X			X	
86/77	X		X	X		X	X				X	X
86/78	X	X					X	X				X
86/80	X	X				X	X	X			X	
86/81*	X				X	X	X	X	X			
86/83	X	X				X	X	X			X	X
86/84	X					X	X	X			X	
86/145	X			X	X	X	X					
86/149	X				X	X	X		X		X	
86/155	X				X	X	X					

X = present. gl = glaucophane, pg = paragonite, law = lawsonite, chl = chlorite, cc = calcite, dol = dolomite, ep = epidote, gnt = garnet, om = omphacite, act = actinolite, sph = sphene, rut = rutile.

Table 4.9 Formulation of activity-composition relationships.

END-MEMBER PHASE	COMPOSITION	ACTIVITY FORMULATION
glaucophane	$Na_2{}^{2}Mg_3Al_2[Si_8O_{22}](OH)_2$	$a_{gl}^{am} = X^{A}(X_{Na}^{M4})^2 (X_{Mg}^{M1\text{-}M3}) (X_{Al}^{M2})^2 (X_{Si}^{Ti})^4$ a
paragonite	$NaAl_2[Si_3AlO_{10}](OH)_2$	$a_{pg}^{mica} = 9.48 (X_{Na}^{A}) (X_{Al}^{M1}) (X_{Al}^{M2})^2 (X_{Al}^{iv}) \cdot (X_{Si}^{iv})^3$ b
clinochlore	$Mg_5Al[Si,Al)_4O_{10}](OH)_8$	$a_{clin}^{chlorite} = 64 (X_{Mg}^{M2})^3 (X_{Mg}^{M1})^2 (X_{Al}^{M1}) (X_{Al}^{iv}) (X_{Si}^{iv})^3$ c
clinozoisite	$Ca_2Al_3Si_3O_{12}(OH)$	$a_{cz}^{epidote} = X_{Al}^{M3}$ b
dolomite	$CaMg(CO_3)_2$	$a_{dol}^{dol\text{-}ank} = X_{Ca}^{H2} X_{Mg}^{M1}$ d
Calcite	$CaCO_3$	$a_{cc}^{cc} = X_{Ca}^{cc}$ d
Lawsonite	$CaAl_2[Si_2O_7](OH)_2 H_2O$	$a_{law}^{law} = (X_{Ca}) (X_{Al}^{vi})^2 (X_{Si}^{iv})^2$ a
sphene	$CaTiSiO_5$	$a_{sph}^{sph} = (X_{Ca}) (X_{Ti})$ a

Source of activity formulations; a = ideal mixing on sites; b = Powell (1978); c = Powell and Evans (1983); d = Bickle and Powell (1977).

The phases, calcite, lawsonite, paragonite and sphene maintain a fairly uniform composition throughout the metasediments, which only differs slightly from their ideal formulae. Averaged probe data was used to calculate the activities of these phases, and the same value was used in each of the three T-X section.

However, unless an average mineral composition is used, the activities will refer to the phases present in one particular rock. When a group of rocks, like the Syros metasediments, are examined the range of bulk compositions, and hence the variation in individual mineral activity, must be taken into account. It was decided that the best way to study the shifts in the phase equilibria caused both by the introduction of real mineral compositions, and by the range of bulk rock compositions, would be to generate 3 T-X sections which would span the range of bulk compositions. In order to generate T-X sections for real rocks, activity-composition data must be available for every phase which shows solid-solution effects. In practice this means that for each T-X section activity data for glaucophane, chlorite, dolomite and epidote is required. Although it appears to be the most obvious and direct approach, it is not possible to select individual rocks at the approximate limits of the bulk compositional range to determine the required activity data because such rocks, by virtue of their extreme bulk composition, will often not develop all the phases present in the grid.

For example, the very magnesian schists which occur at Kastri appear to be suitable candidates to constrain the "Mg" T-X section. These schists contain the assemblage chlorite-tremolite-dolomite-quartz-phengite. Neither glaucophane nor clinozoisite is present. In order to estimate suitable compositions, and hence activities, for these absent phases K_D plots are required which examine the distribution of Fe/Mg and Fe^{3+}/Al between different mineral phases from a variety of rock compositions. If a suitable K_D plot is available, then, for example, the Fe/Mg ratio of chlorites in the magnesian schists can be used to predict a suitable Fe/Mg ratio for an imaginary coexisting glaucophane. Electron microprobe analyses of coexisting glaucophane-chlorite and glaucophane-epidote were used to determine the distribution coefficients, K_D. The Fe/Mg partitioning between glaucophane and chlorite is presented in Figure 4.12a, and the Fe^{3+}/Al partitioning between glaucophane and epidote in Figure 4.12b. In all cases rim analyses of the mineral phases were used, to try to eliminate growth zoning effects.

Fe/Mg distribution between dolomite-ankerite and chlorite

Fe^{2+} and Mg will also be distributed between coexisting dolomite and chlorite, but in this case it is not possible to determine the K_D directly. As discussed in the introductory remarks to this chapter, dolomite, although originally part of the primary assemblage, has been calcitized, with the loss of its original composition. Judging by the amount of iron exsolved during this calcitising event it would be inappropriate to assume that the original dolomite had a composition close to the $CaMg(CO3)_2$ end-member.

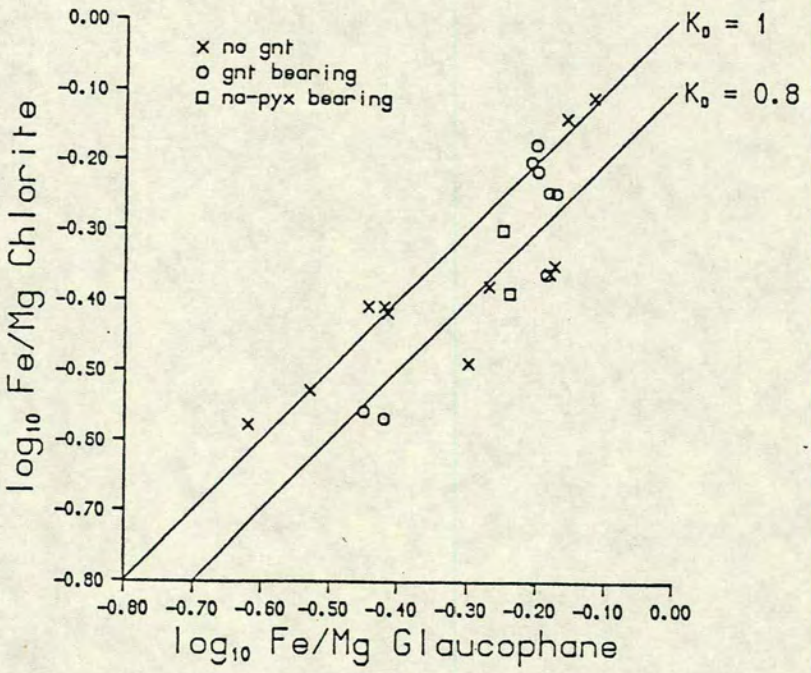

Figure 4.12a Log Fe/Mg in glaucophane versus log Fe/Mg in chlorite. Different assemblages in the metasediments are indicated by the key. Lines of constant K_D are shown for reference.

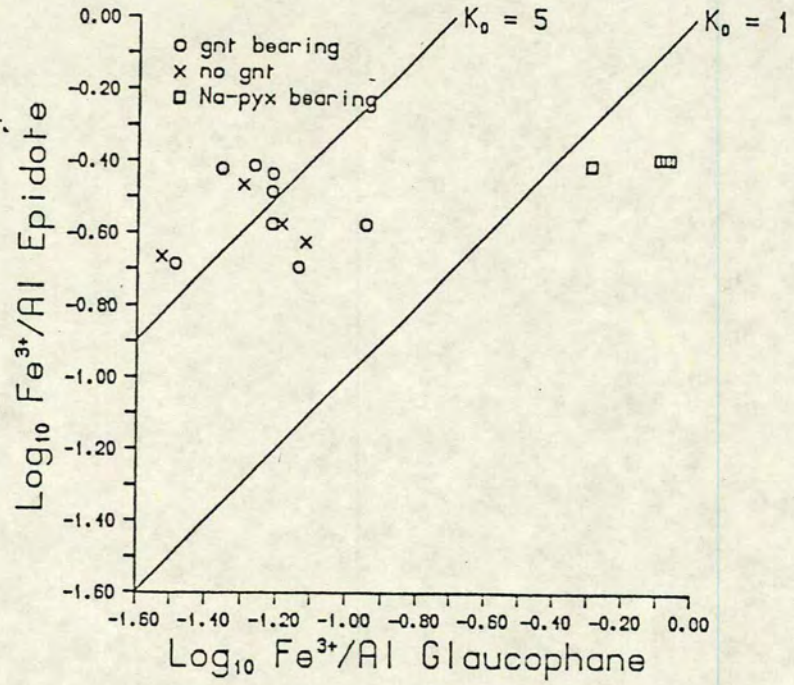

Figure 4.12b Log Fe^{3+}/Al in glaucophane versus log Fe^{3+}/Al in epidote, again lines of constan K_D are shown for reference.

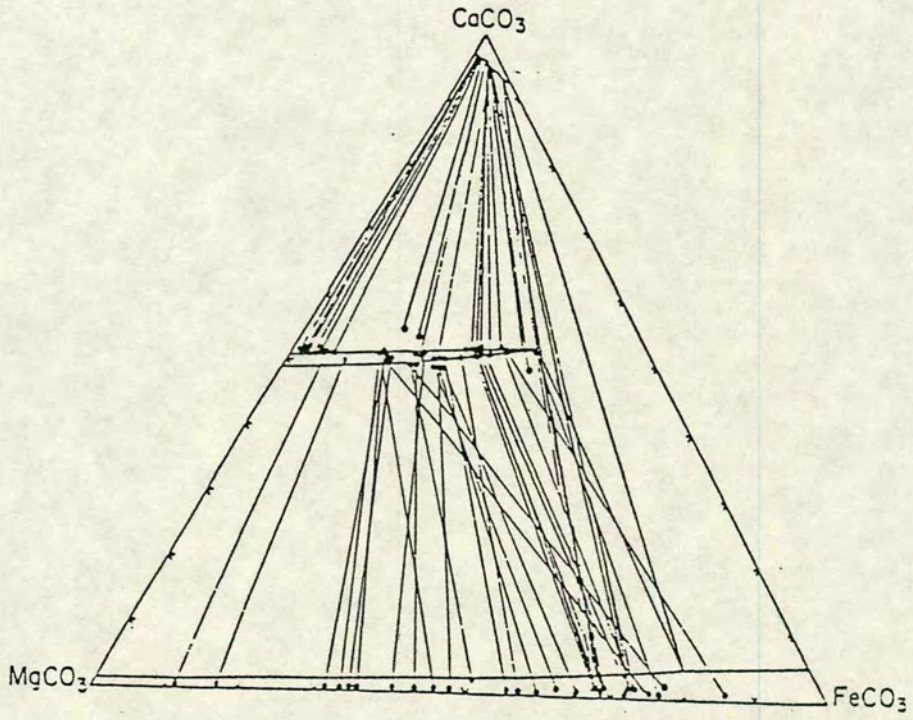

Figure 4.13 Carbonates in the system $CaCO_3$-$MgCO_3$-$FeCO_3$ with T≈ 400°C (from Anovitz + Essene 1987, fig. 7).

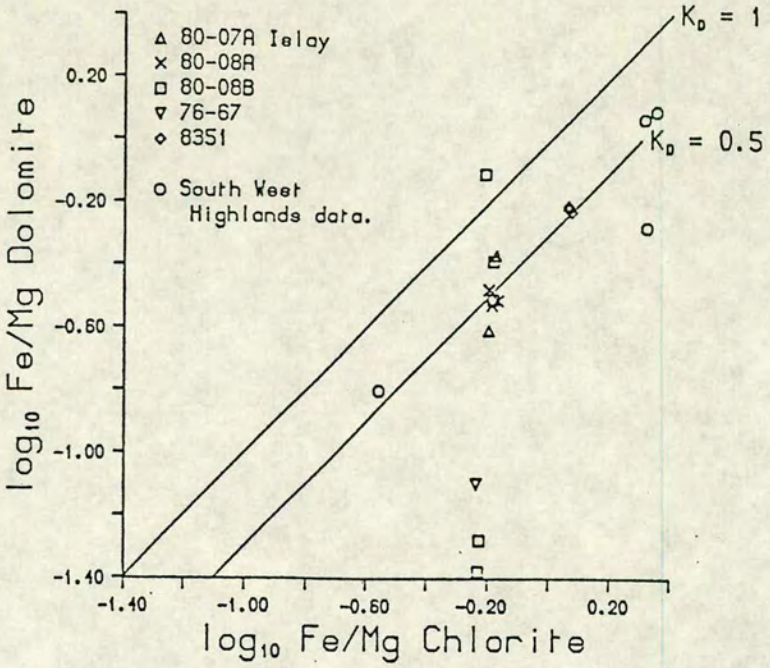

Figure 4.14 Log Fe/Mg chlorite versus log Fe/Mg dolomite. The data used to produce this plot comes from Dalradian rocks in the south-west Highlands, see text for discussion.

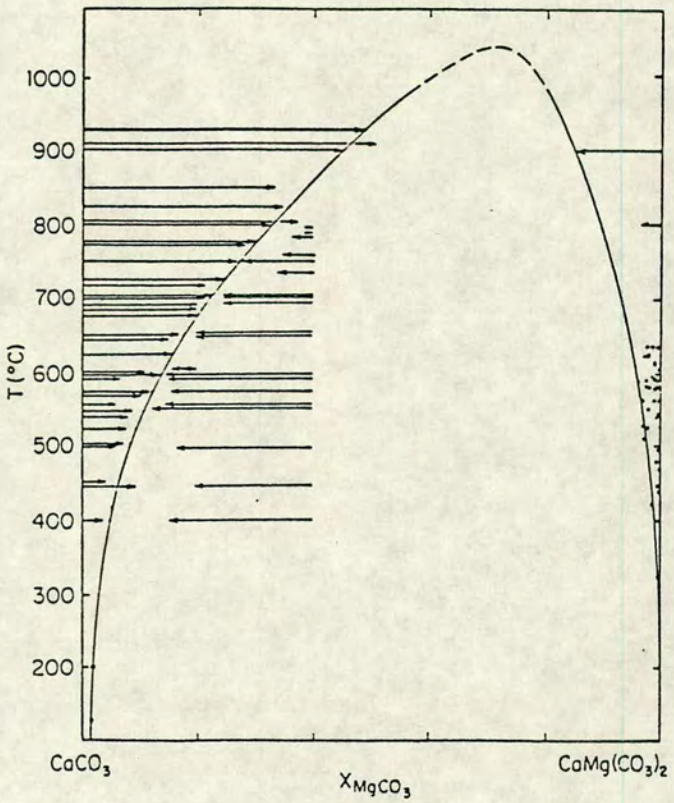

Figure 4.15 The proposed calcite-dolomite solvus. The position of the solvus was constrained by several experimental reversals (see Anovitz and Essene 1987).

The original carbonate would be part of the ternary system $CaCO_3$-$MgCO_3$-$FeCO_3$, with the composition presumably lying close to the binary dolomite-ankerite join. Phase equilibria for this system have recently been re-evaluated by Anovitz and Essene (1987). Figure 4.13 is taken from this paper, and shows the calculated phase diagram for the system $CaCO_3$-$MgCO_3$-$FeCO_3$ at a temperature of 400 °C.

The effect of pressure on the carbonate phase relations is very small compared to that of temperature, and so it was decided to use electron microprobe data for coexisting dolomite and chlorite from an equivalent temperature terrain in order to generate a K_D plot. The data used to produce the K_D plot comes from work performed by Dr. C. M. Graham on Dalradian rocks from Islay and elsewhere in the South-West Highlands, Scotland. Figure 4.14 is a plot of the Fe/Mg distribution between these coexisting dolomites and chlorites. Using this K_D plot the Fe/Mg ratios of the Syros chlorites were used to determine the Fe/Mg ratios of the original coexisting ankeritic carbonates.

Activity of dolomite

A solvus exists between calcite and dolomite up to temperatures in excess of 1000 °C, and the effect of this must be considered before an activity value for dolomite can be calculated. The activity of dolomite is expressed as $[X_{Ca}^{M2}].[X_{Mg}^{M1}]$ (see table 4.9), and, from figure 4.13, it is apparent that the activity of dolomite will be highest when the composition of the carbonate lies exactly along the dolomite-ankerite join. In cases where dolomite coexists with siderite, Ca in the M2 site will be slightly deficient, and as a result the activity of dolomite will be reduced. Similarly, if dolomite and calcite coexist, as is the case for a large number of Syros metasediments, then the amount of calcium present may exceed 1, and Ca will be present in the M1 as well as the M2 site, again reducing the activity of dolomite. The amount of excess calcium which could be expected in the Syros dolomites was estimated from Anovitz and Essene (1986, figure 3), see figure 4.15. Taking a temperature of 450 °C as being a reasonable estimate for Syros the amount of calcite dissolved in dolomite is approximately 4 mol%, and this figure has been used to model the excess calcium present in dolomites coexisting with calcite. Thus, although the activity-composition relationship used is the simple one given in Table 4.9, which assumes ideal mixing, an empirical correction has been made to take account of the solvus, the presence of which is an obvious indication that mixing is strongly non-ideal.

4.10 APPLICATION OF THE T-X GRID TO REAL MINERAL ASSEMBLAGES

Using the KD plots, and existing microprobe data it was possible to generate activity data for 3 T-X_{CO2} sections, one representing the magnesium end of the metasediment compositions, one the iron end, and one approximately half way between. These sections labelled, S1 (Mg end), S2 (intermediate), and S3 (Fe end) are shown in figures 4.16 a-c, (loose copies of these diagrams can be found in the back pocket). The activities of the phases used to construct a particular section are listed on the appropriate grid. One immediately noticeable feature is the change in grid topology moving from S2 to S3. In S1 and S2 the invariant points [Gl,Pg], [Law], [Cz] and [Dol] are stable, but in S3 the shift in the phase equilibria due to the presence of iron means that a new set of invariant points are stabilised, [Gl,Pg], [Cc] and [Chl]. The acute angle of intersection between many of the reaction curves means that the locations of the invariant points, and hence their relative stable/metastable relationships, are very sensitive to relatively small shifts in phase activities. Somewhere between S2 and S3 the invariant points must slide towards each other, meet, then diverge with a new set of stable invariant points appearing. The divariant areas on the T-X sections have been labelled according to the relevant invariant point, and this coding is explained in figure 4.17.

The principal remaining task is to relate the observed mineral assemblages listed in table 4.8 to the theoretically determined assemblages, and then "place" the observed assemblages within the framework of the T-X grid. Mutual agreement between the phase assemblages derived theoretically and those determined from observed assemblages will support the validity of the grid, and the conclusion that in general chemical equilibrium has been established in the metasediments. The possible assemblages stable in each portion of the T-XCO2 grids were determined and figures 4.18a-h illustrate some of the important compatibility tetrahedra from the S1/S2 and S3 grids (loose copies out of text). The "exploded" versions of the tetrahedra are given to allow easier identification of the 4-phase volumes. Through a consideration of these tetrahedra, and the changes in assemblage which occur as various reaction equilibria are crossed, the observed assemblages could be assigned to particular regions of space in the T-X_{CO2} sections. Only occasionally would an assemblage be uniquely defined by one region of divariant space, and more frequently an assemblage would be stable in several adjacent volumes. (Loose copies of these tetrahedra are provided in the back pocket.)

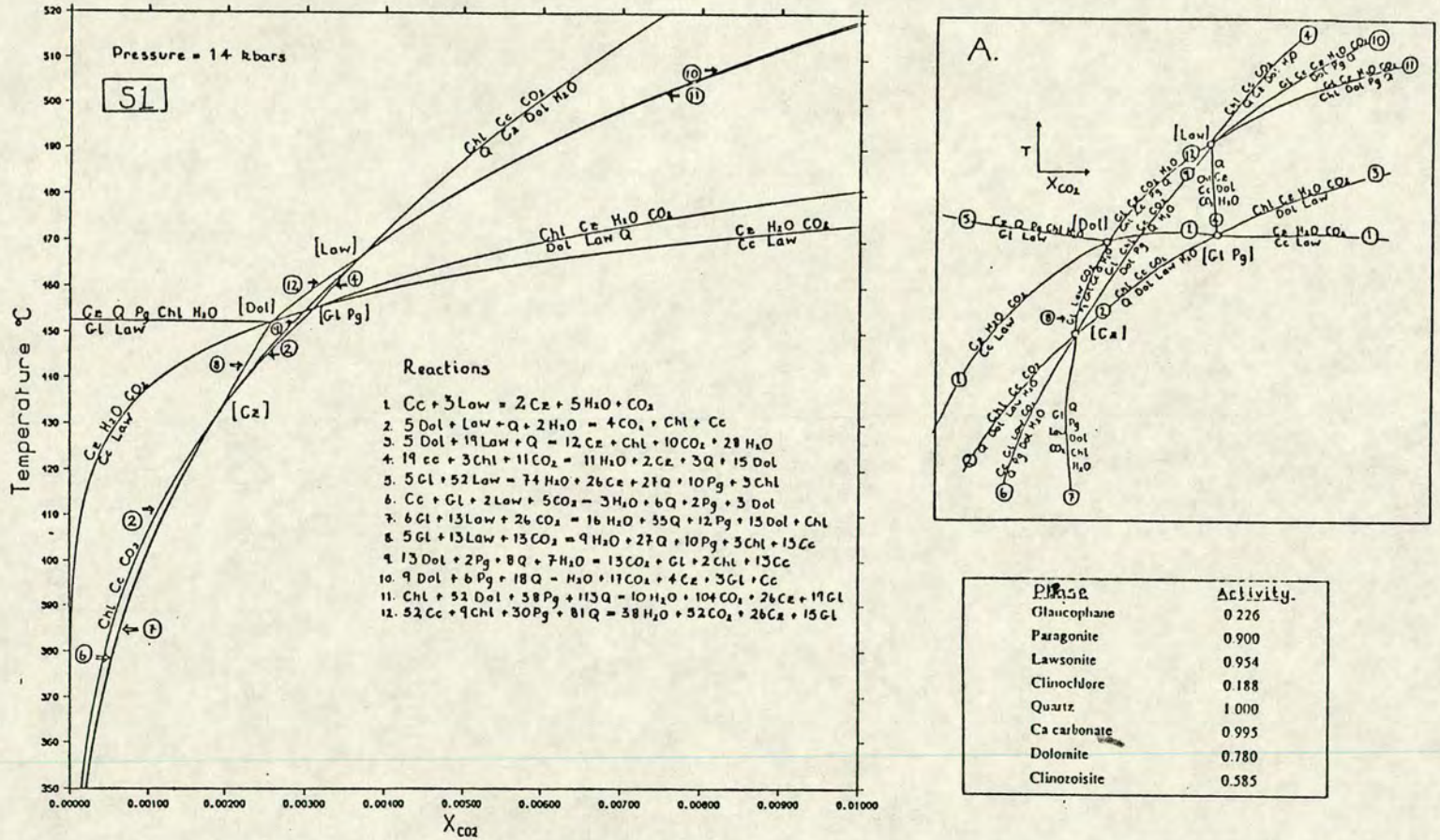

Phase	Activity.
Glaucophane	0.226
Paragonite	0.900
Lawsonite	0.954
Clinochlore	0.188
Quartz	1.000
Ca carbonate	0.995
Dolomite	0.780
Clinozoisite	0.585

Figure 4.16a T-X(CO_2) section showing the equilibria from fig. 4.10 recalculated to take account of real mineral compositions. The activities of the solids were calculated using the formulations in table 4.9, and these are shown above. This T-X(CO_2) section relates to the "magnesian-end" of the metasedimentary compositions, and is referred to as S1 in the text. Invariant points are labelled according to the phases absent.

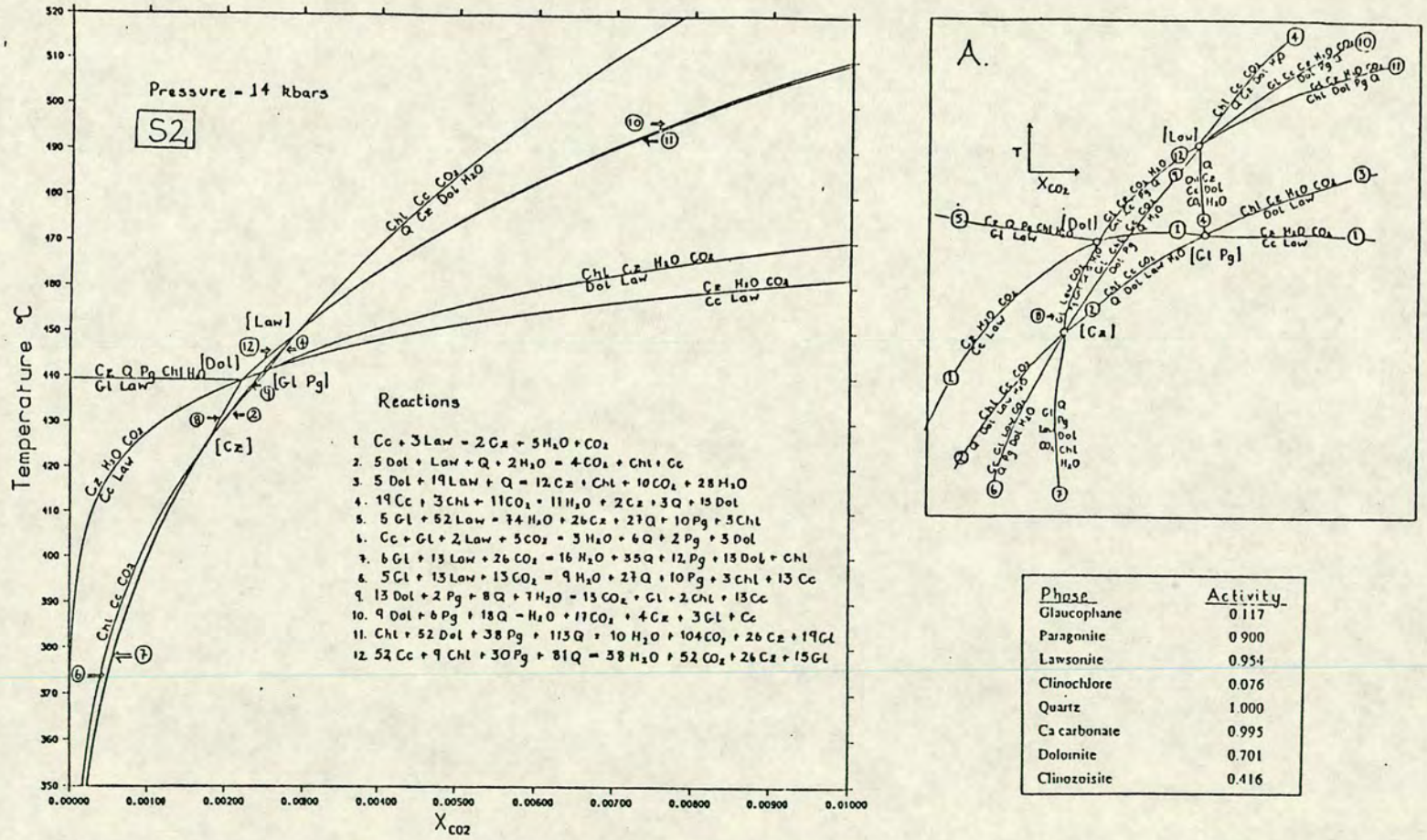

Phase	Activity
Glaucophane	0.117
Paragonite	0.900
Lawsonite	0.954
Clinochlore	0.076
Quartz	1.000
Ca carbonate	0.995
Dolomite	0.701
Clinozoisite	0.416

Figure 4.16b T-X(CO_2) section for rocks of intermediate composition, approximately midway between the Mg and Fe end-sections. The equilibria have been recalculated using the appropriate mineral activities (given above). This section is referred to as S2.

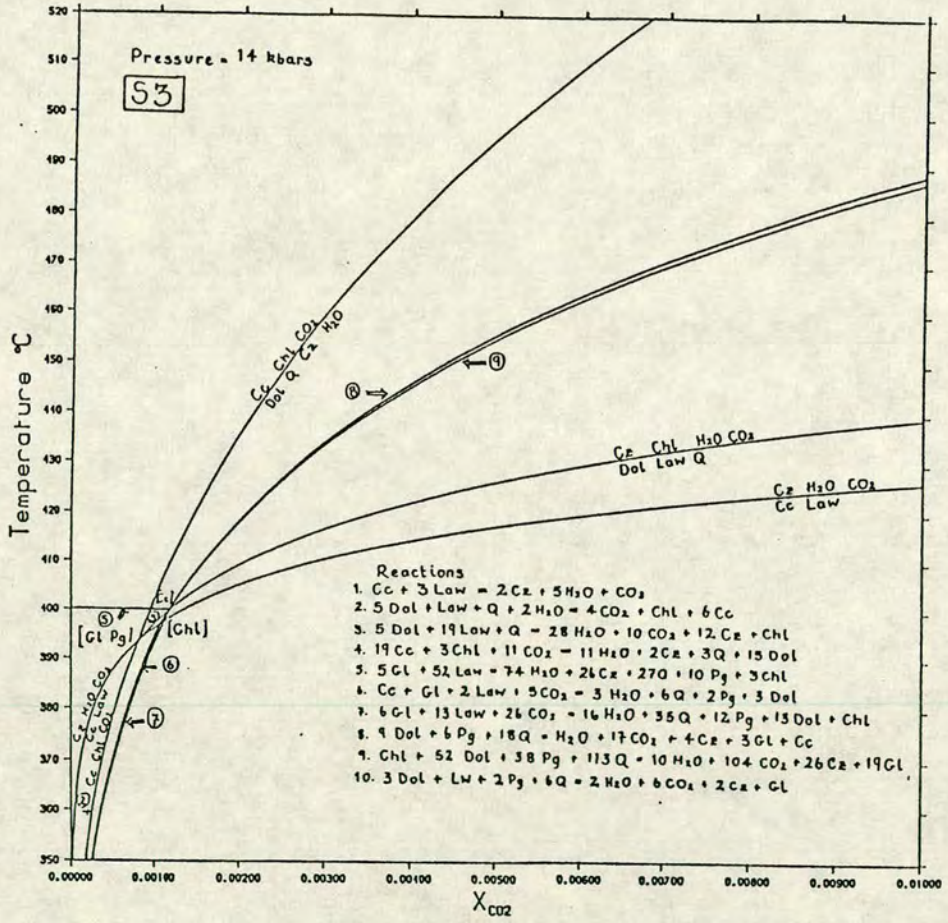

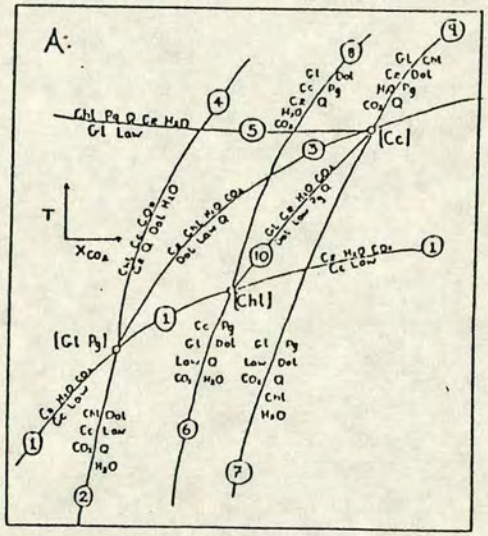

Phase	Activity
Glaucophane	0.055
Paragonite	0.900
Lawsonite	0.954
Clinochlore	0.051
Quartz	1.000
Ca carbonate	0.995
Dolomite	0.678
Clinozoisite	0.136

Figure 4.16c T-X(CO_2) section for Fe-rich rocks, referred to as S3. Again the equilibria have been recalculated to take account of the changing mineral activities, and a different set of invariant points are stabilised. See text for discussion.

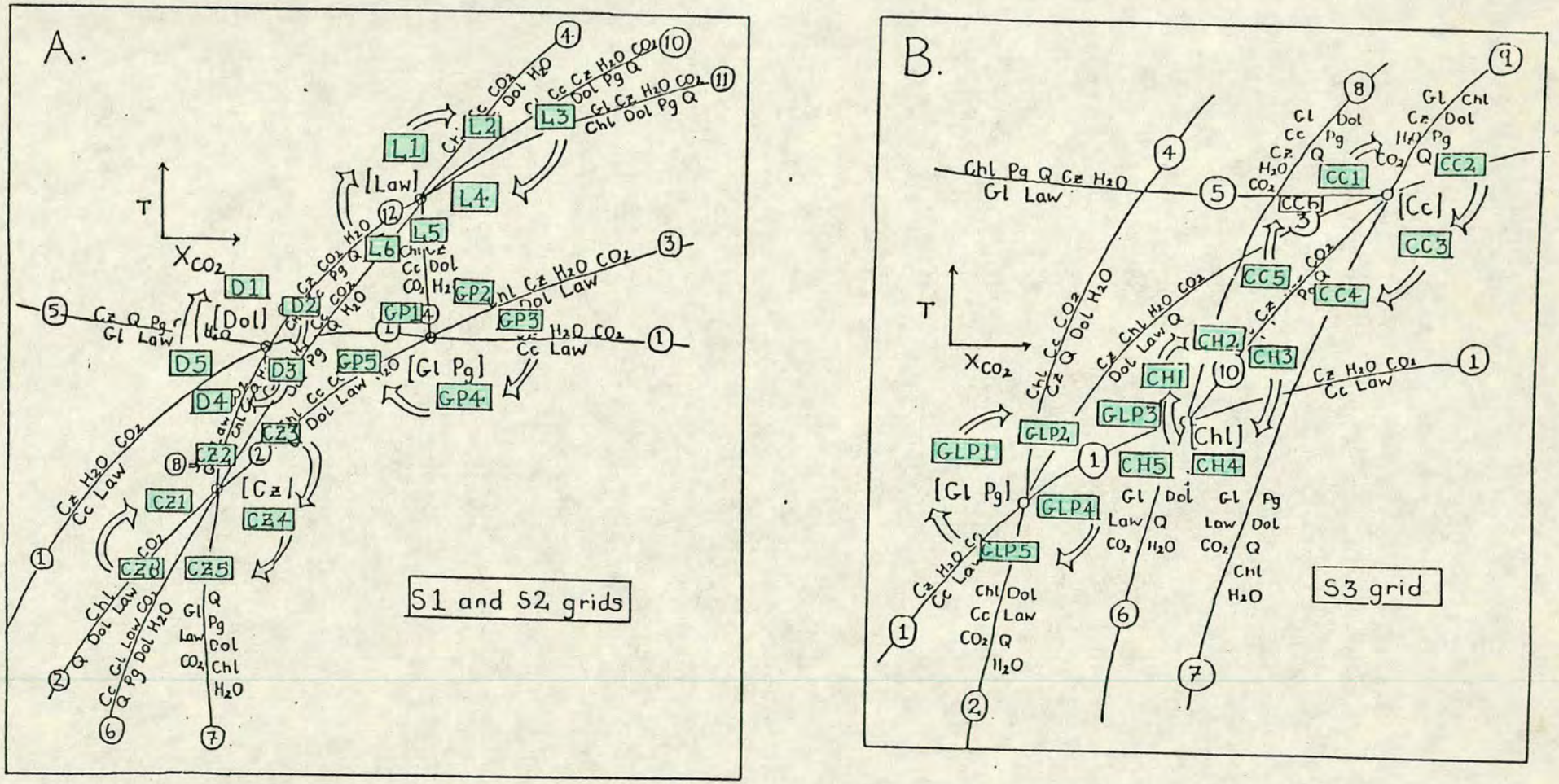

Figure 4.17a,b Divariant areas on the T-X(CO_2) section are labelled after the relevent invariant points. A number of equivalents exist as some areas have more than one label, i.e. in S1/S2, CZ1=D4, CZ2=D3, and in S3 GLP3 = CI, CLP4 = CH5 etc.

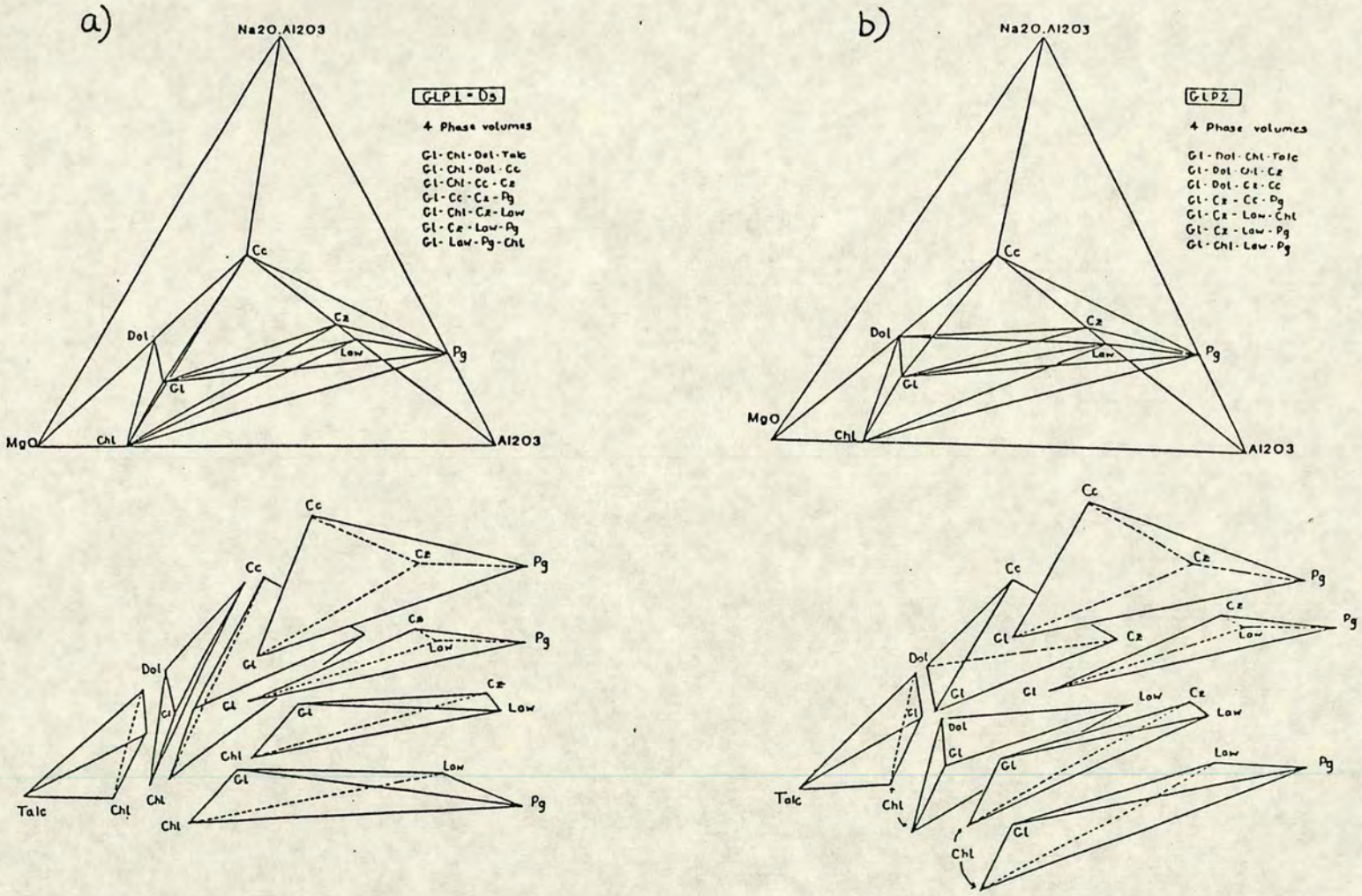

Figure 4.18a-h Phase compatibility tetrahedra for important divariant areas in the S1/S2, and S3 T-X(CO_2) sections. The tetrahedra emphasise the progressive change in assemblage which occurs as reaction equilibria are crossed. The area coding is explained in fig. 4.17.

c)

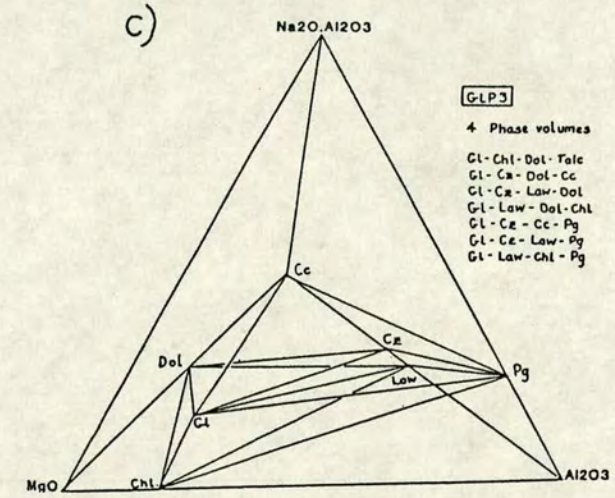

GLP3

4 Phase volumes

Gl - Chl - Dol - Talc
Gl - Cz - Dol - Cc
Gl - Cz - Law - Dol
Gl - Law - Dol - Chl
Gl - Cz - Cc - Pg
Gl - Cz - Law - Pg
Gl - Law - Chl - Pg

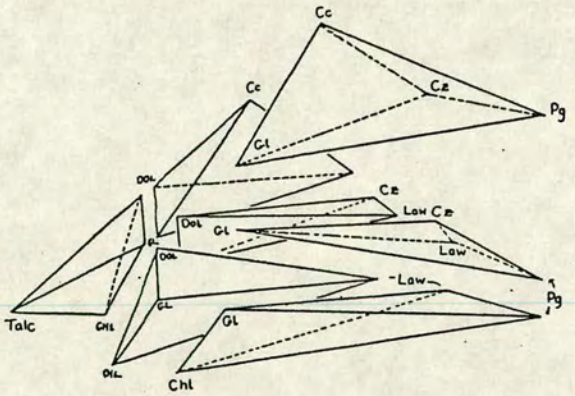

d)

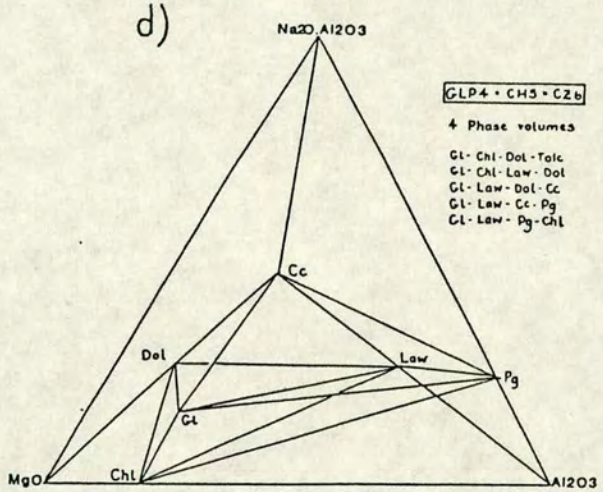

GLP4 + CH3 + CZb

4 Phase volumes

Gl - Chl - Dol - Talc
Gl - Chl - Law - Dol
Gl - Law - Dol - Cc
Gl - Law - Cc - Pg
Gl - Law - Pg - Chl

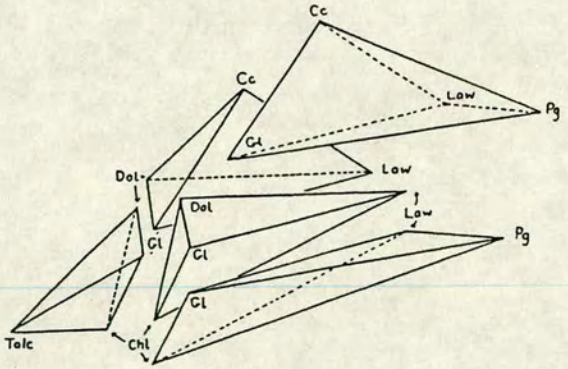

e)

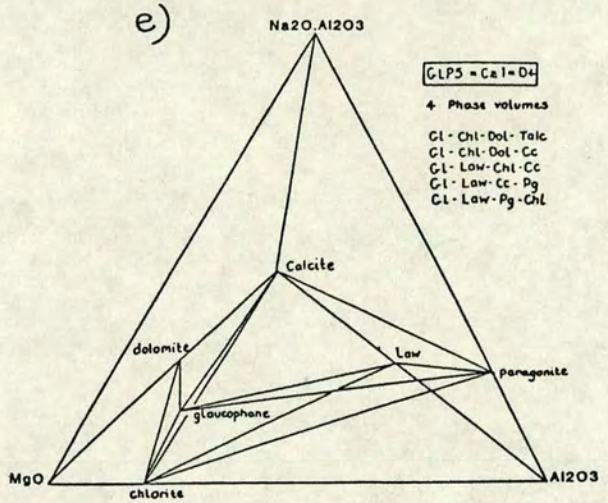
Na2O.Al2O3
GLP5 = Ca1 = D4
4 Phase volumes
Gl - Chl - Dol - Talc
Gl - Chl - Dol - Cc
Gl - Law - Chl - Cc
Gl - Law - Cc - Pg
Gl - Law - Pg - Chl
Calcite
dolomite
Law
paragonite
glaucophane
MgO
chlorite
Al2O3

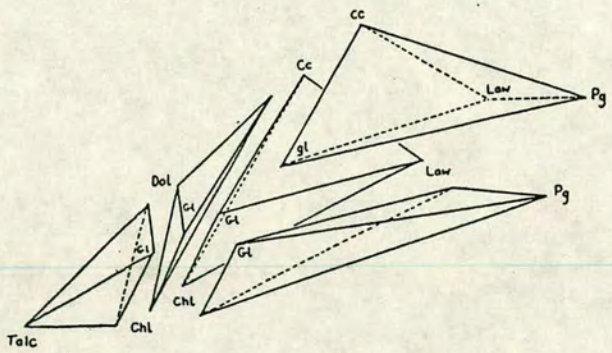
cc
Cc
Law
Pg
gl
Dol
Gl
Law
Pg
Gl
Gl
Chl
Talc
Chl

f)

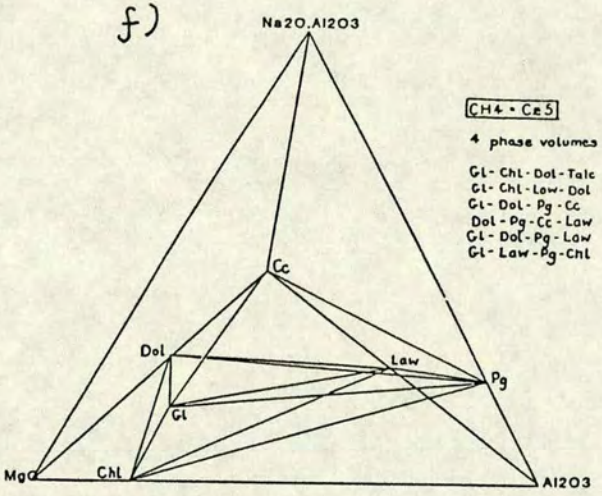
Na2O.Al2O3
CH4 = Ce5
4 phase volumes
Gl - Chl - Dol - Talc
Gl - Chl - Law - Dol
Gl - Dol - Pg - Cc
Dol - Pg - Cc - Law
Gl - Dol - Pg - Law
Gl - Law - Pg - Chl
Cc
Dol
Law
Pg
Gl
MgO
Chl
Al2O3

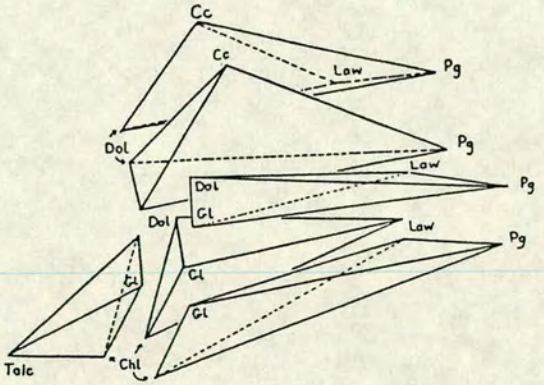
Cc
Cc
Law
Pg
Dol
Pg
Law
Dol
Pg
Dol
Gl
Law
Pg
Gl
Gl
Talc
Chl

g)

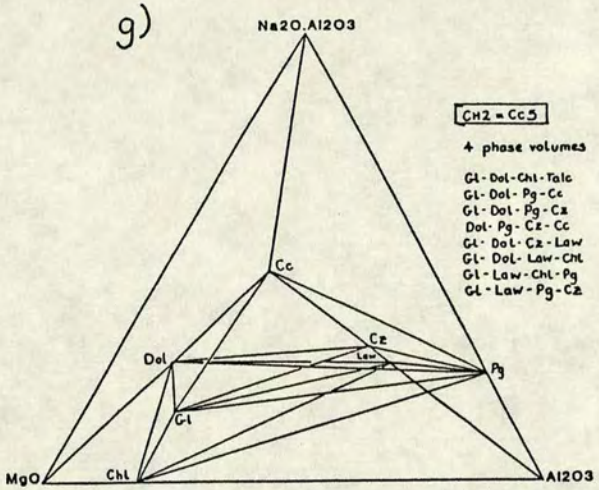

CH2 = CC5

4 phase volumes

Gl - Dol - Chl - Talc
Gl - Dol - Pg - Cc
Gl - Dol - Pg - Cz
Dol - Pg - Cz - Cc
Gl - Dol - Cz - Law
Gl - Dol - Law - Chl
Gl - Law - Chl - Pg
Gl - Law - Pg - Cz

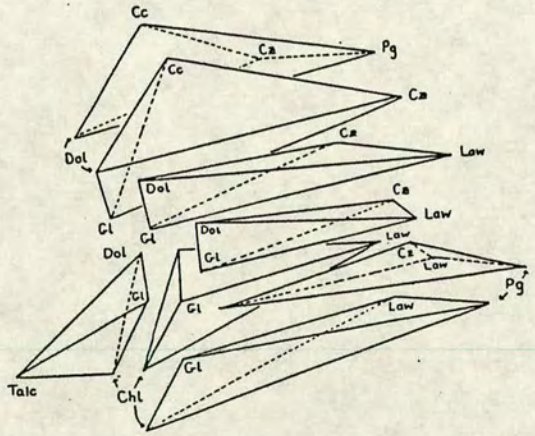

h)

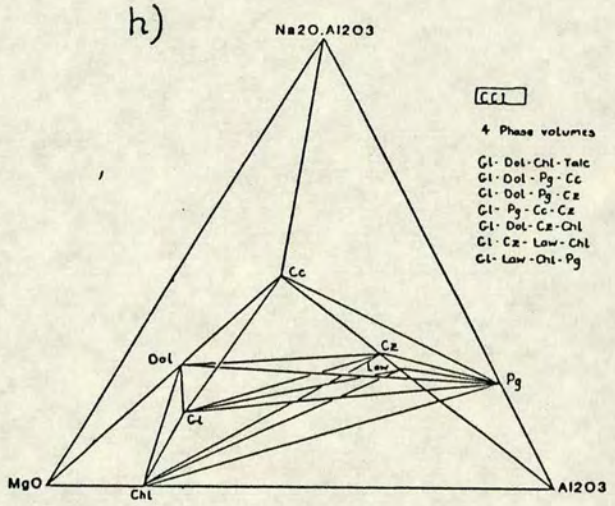

CC1

4 Phase volumes

Gl - Dol - Chl - Talc
Gl - Dol - Pg - Cc
Gl - Dol - Pg - Cz
Gl - Pg - Cc - Cz
Gl - Dol - Cz - Chl
Gl - Cz - Law - Chl
Gl - Law - Chl - Pg

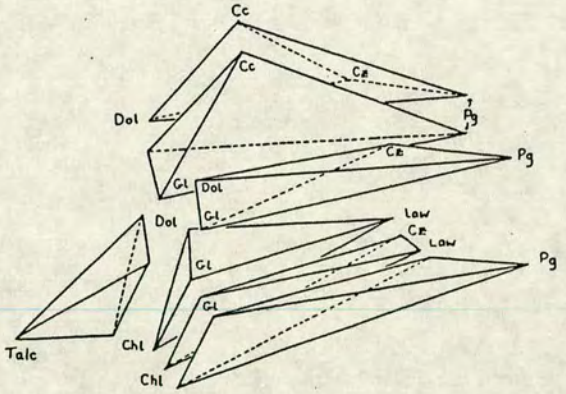

Bounding reactions

All but one of the assemblages contain a glaucophane-lawsonite or a glaucophane-epidote tie-line, or both. Thus, the critical bounding reactions for the Syros blueschists concern the breakdown of these tie-lines. This point is illustrated in figure 4.19a-b, by enlarged sketches of the S1/S2 and S3 T-X sections, which show how the bounding reactions restrict the X_{CO2} range of the coexisting fluid to very low values for the majority of the assemblages. The bounding reactions involved in the S1/S2 grid are:

1)5gl+52law = 74H2O+26cz+27qtz+10pg+3chl
2)6gl+13law+26CO2 = 16H2O+35qtz+12pg+13dol+chl
3)5gl+13law+13CO2 = 9H2O+27qtz+10pg+3chl+13cc
4)19gl+26cz+104CO2+10H2O = chl+52dol+38pg+113qtz
5)15gl+26cz+52CO2+38H2O = 52cc+9chl+30pg+81qtz

The bounding reactions in S3 are 1), 2), 4) and,

6)gl+2cz+6CO2+2H2O = 3dol+law+2pg+6qtz

Temperature Constraints

The positions of the reaction equilibria cannot be located precisely in T-X_{CO2} space due to inherent errors in the thermodynamic data, and the possible presence of additional species such as Ti^{4+}, Cr^{3+} and Mn, which will cause changes in the positions of the equilibria. However, the exact positioning of the curves in T-X space is of secondary importance relative to the positioning of the assemblages. The many different observed assemblages are evidence that the rocks were "aware" of the reaction curves, but ideally all the samples from one outcrop should plot along the same isotherm (regardless of the absolute location of the curves in the T-X_{CO2} grid). There is no evidence that any large temperature gradient existed on Syros during the blueschist metamorphism, and assuming a geothermal gradient of around 10°C/km the T-gradient over a 10 metre outcrop should be negligible. However, in order to place the observed assemblages in the T-X sections real temperature differences appear to exist over a single outcrop. Although this may just be an artifact of the grid, it is worth considering possible situations where temperature differences of around 10-15 °C could exist on a scale of metres.

1) Final crystallisation of all the assemblages in an outcrop may not occur synchronously, a phenomenon which may be related to cessation of deformation. As a phase of deformation can be diachronous through an area so the final crystallisation of assemblages in a sequence may occur over some finite time period, with the different layers recording different "closure" temperatures.

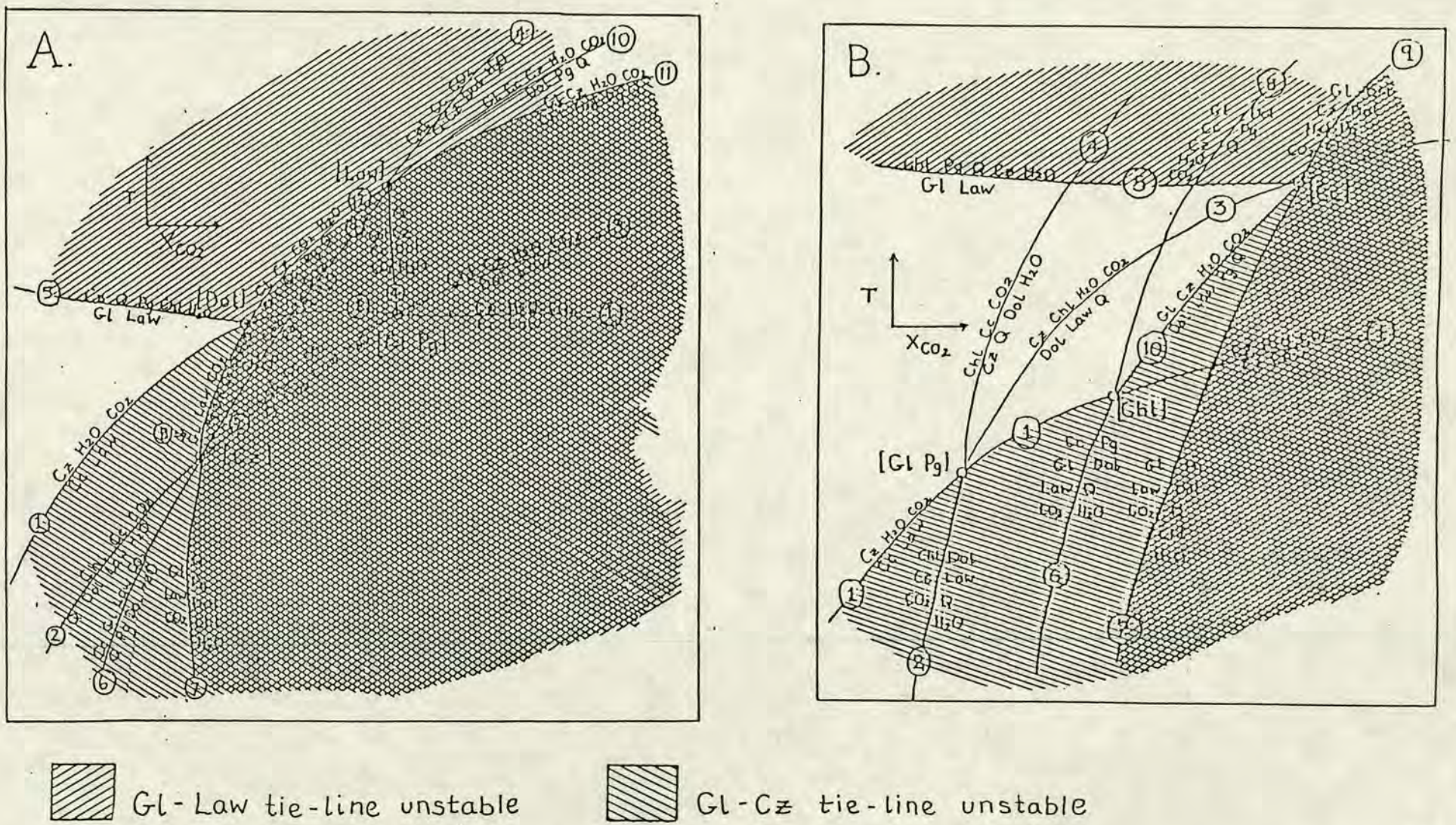

Figure 4.19a,b Sketches of the bounding T-X(CO_2) conditions for the S1/S2 and S3 grids. The two diagrams, a and b, are enlarged sketches of the area around the invariant points in the S1/S2 and S3 grids (see fig. 4.16a-c). The majority of the assemblages contain a gl-law or gl-cz tie-line (or both), and the stability of these tie-lines restricts the X(CO_2) of the coexisting fluid to very H_2O-rich compositions.

2) Reactions in adjacent layers may occur at different times. One layer may be undergoing exothermic hydration reactions while an adjacent layer is inert, and a 'staggered reaction' situation could cause temperature gradients on the scale of metres.

3) In a sequence of interlayered rocks some units will act as metamorphic aquifers and some as aquitards. If a large amount of infiltrating fluid is available then the focussing of fluid flow through reactive, permeable units could raise the temperature of the surrounding rock, causing local temperature gradients (Ferry 1980a). This mechanism of fluid-channelling is unlikely to be of any importance for Syros as the volume of external fluid present during the blueschist event appears to be very low. This problem has not really been resolved. When fitting the assemblages into the grid a "best-fit" temperature window accommodating all the assemblages occurs between 385 and 400 ^{o}C approximately. While this temperature band is lower than that deduced by experimentally derived phase relations, given the uncertainties involved in constructing the grid, the correlation is still reasonably good.

One of the most useful ways to consider the assemblage list is to divide it up into those assemblages which contain a gl-law tie-line and those which have a gl-ep tie-line, as such a division also separates the rocks compositionally. Rocks with a gl-law tie-line tend to be more Mg-rich, and plot in the S1 or S2 diagram, whereas those with a gl-ep tie-line are more iron-rich and plot in the S3 diagram. Table 4.10 lists the samples divided up into groups on the basis given above. Also listed are the areas on the grids where these different rocks are located. The areas, GP1, D2 etc, are named after the relevant invariant points, and are labelled consecutively from the top left-hand quadrant (i.e GP = [gl pg], D = [dol] etc).

As was mentioned in section 4.9 a number of apparent phase incompatibilities appear in the assemblages due to the presence of extra phases. Table 4.10 will be used as a starting point to examine these discrepancies. Rocks containing a gl-law tie-line will be examined before those with a gl-ep tie-line, so that a general progression will be followed from less iron-rich rocks to more iron-rich rocks.

Rock 86/40 contains the assemblage gl-chl-act-talc. The chl-act tie-line means that talc bearing assemblages are restricted to very magnesian rocks and as such rock 86/40 represents the most magnesian bulk rock composition encountered on Syros.

Rock 53B and 53H also contain actinolite, and theoretically the chl-dol tie-line should restrict actinolite to very magnesian assemblages. However, lawsonite is also present in these rocks, and an apparent incompatibility arises.

Table 4.10 Division of assemblages on the presence (or absence) of gl-lawsonite and gl-epidote tie-lines. Also given are the suggested area(s) on the T-X grids where each assemblage is located.

Sample No.	Critical phases in assemblage	Suggested Grid	Suggested area(s)
A. 86/14	gl-law-dol-chl-(gnt)	s2 or s1	CZ5(=CH_4 in S3) or CZ (=GLP4)
86/40	gl-chl-act	s1	area cannot be defined
86/47	gl-law-dol-chl-(gnt)	s2/s1	CZ5 or CZ6
86/49	gl-law-dol-chl-(gnt)	s2/s1	CZ5 or CZ6
86/53B	gl-law-dol-chl-act	s1	CZ5 or CZ6
86/53H	gl-law-cc-dol-chl	s1	CZ1 (= D4=GLP5)
86/57	gl-law-dol-cc-chl-(gnt)	s2	CZ1
86/71	gl-law-chl-cc	s1	CZ1 (= D4=GLP5)
86/72	gl-pg-law-chl-(gnt)	s2 or s1	area cannot be defined
86/77	gl-law-chl-dol-(gnt)	s2 or s1	CZ5 or CZ6
B. 85/52	gl-pg-law-chl-cc-ep	s1/s2	[Dol] invariant point
86/59	gl-law-chl-ep-(gnt)	s2	D5
86/67	gl-law-cc-ep-(gnt)	s2	D5
C. 86/68	gl-chl-cc-dol-ep-(gnt)	s3	GLP1
86/69	gl-cc-dol-ep-Na-pyroxene	s3	GLP2
86/75	gl-cc-dol-ep-gnt	s3	GLP2 or GLP3
86/78	gl-pg-ep-gnt-dol	s3	CC1 or CC6
86/80	gl-pg-ep-dol	s3	CC6 or CC1
86/81	gl-cc-dol-ep-Na-pyroxene	s3	CC6 or CC1 or CC5
86/83	gl-ep-pg-dol	s3	CC6 or CC1 or CC5
86/84	gl-dol-ep-gnt	s3	GLP2 or CC6 or CC1
86/149	gl-cc-dol-ep-Na pyroxene	s3	CC6 or CC1
86/155	gl-cc-dol-ep	s3	GLP2 or GLP3

Group A. = those rocks containing only a gl-law tie-line; B. = those rocks containing both a gl-law and a gl-ep tie-line; C. = those rocks containing a gl-ep tieline. Some assemblage equivalence exists between the s1/s2 T-X grid and the s3 grid, D5 (s1/s2) = GLP1, CZ5 (s1/s2) = ch4 AND CZ6 (s1/s2) = GLP4. Also, because of the way volumes were labelled in the T-X grids, areas common to more than one invariant point have more than one identifying label, ie. D4 = CZ1 in the s1/s2 grid while GLP3 = CH1, GLP4 = CH5, CH2 = CC5 and CH3 = CC4 in the s3 grid.

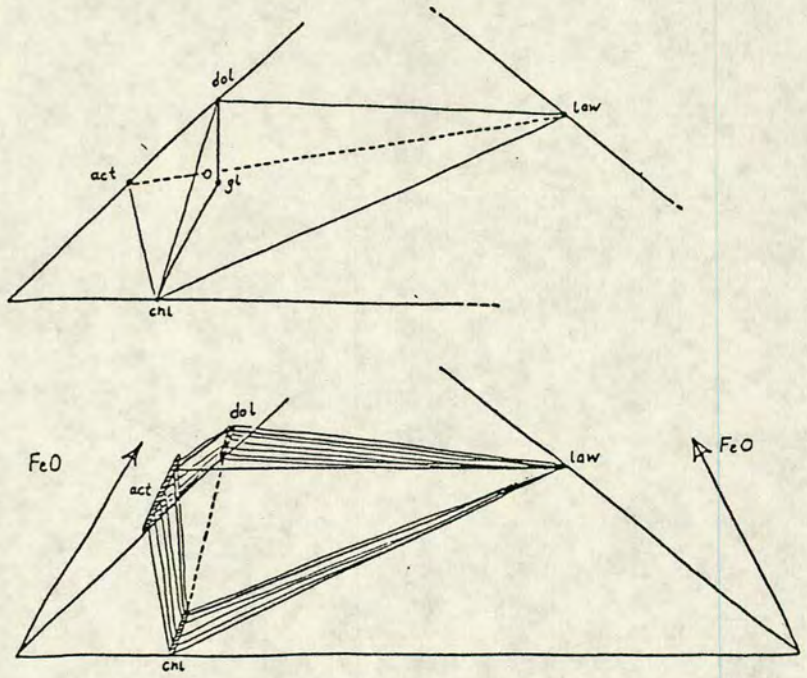

Figure 4.20 The apparently incompatible assemblage chl-dol-act-law is stabilised when the effect of FeO on the pure NCMASH-CO_2 system is considered.

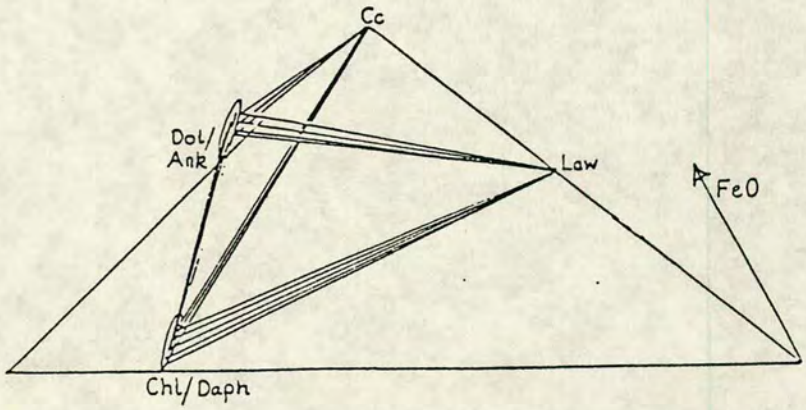

Figure 4.21 Again, when the effect of FeO in the system NCMASH-CO_2 is considered differences in the Mg/Fe distribution between chlorite and dolomite allow the existence of an apparently incompatible assemblage. For FeO-poor rocks the assemblage chl-cc-dol or chl-cc-law will exist. At a specific value of FeO a four-phase volume exists, and bulk rock compositions occurring within this volume will develop the assemblage chl-dol-cl-law. FeO-rich rocks will contain either ank-cc-law or ank-Fe-chl-law.

Theoretically, only the assemblages dol-act-chl-gl or dol-chl-gl-law are permitted, as a lawsonite-actinolite join precludes a dolomite-chlorite join and vice versa. However, when Fe/Mg and Fe^{3+}/Al variation is taken into account, changes in tie-lines occur which cannot be depicted on the original "theoretical" tetrahedron. Figure 4.20 illustrates the effect of adding FeO to the system. Examining this figure it can be seen that for low FeO rocks either the assemblage dol-chl-act or dol-chl-law can exist. At a specific fixed value of FeO the four phase assemblage law-act-dol-chl will be stable, while at higher values of FeO the permitted assemblages are law-dol-act or law-chl-act. An important point to note is that when all 4 phases coexist the number of degrees of freedom is reduced by 1, and thus the compositions of the four phases must be fixed.

Similar reasoning may be applied to explain the assemblage in rock 71, which again contains an apparent incompatibility, with both the lawsonite-dolomite and the chlorite-calcite joins stable. Figure 4.21 explains how this situation can be resolved when the effect of solid solution in chlorite and dolomite is considered. Rocks 47,49 and 14 may all be considered together. In these rocks garnet appears as an extra phase. Ignoring the spessartine component, the garnets in the metasediments have compositions approximating to Alm_{60}-$Gross_{30}$-Pyr_{10}. Figure 4.22 shows an Al_2O_3-CaO-MgO-FeO tetrahedron on which the garnet compositional plane is indicated. The approximate compositional range of the Syros garnets is shown as the shaded area. For ease of drawing this composition has been further simplified by projecting it onto the almandine-pyrope join. The assemblage found in rock 14 is also illustrated in this tetrahedron (figure 4.22), and it can be seen that differences in X_{Mg} between the coexisting phases mean that there is a large area of compositional space where rocks of an appropriate bulk composition will develop garnet as an extra phase.

In those rocks containing a gl-ep tie-line the effect of Fe_2O_3 needs to be considered. For example rock, 86/145 contains the assemblage gl-chl-cc-dol-ep, theoretically the only permitted assemblages are gl-chl-cc-cz or gl-cc-dol-chl, but if the effect of dissolving Fe^{3+} in clinozoisite is considered, it is possible to generate a finite four-phase volume where the assemblage chl-cc-dol-ep is stable. This situation is illustrated in figure 4.23, and explained in table 4.11.

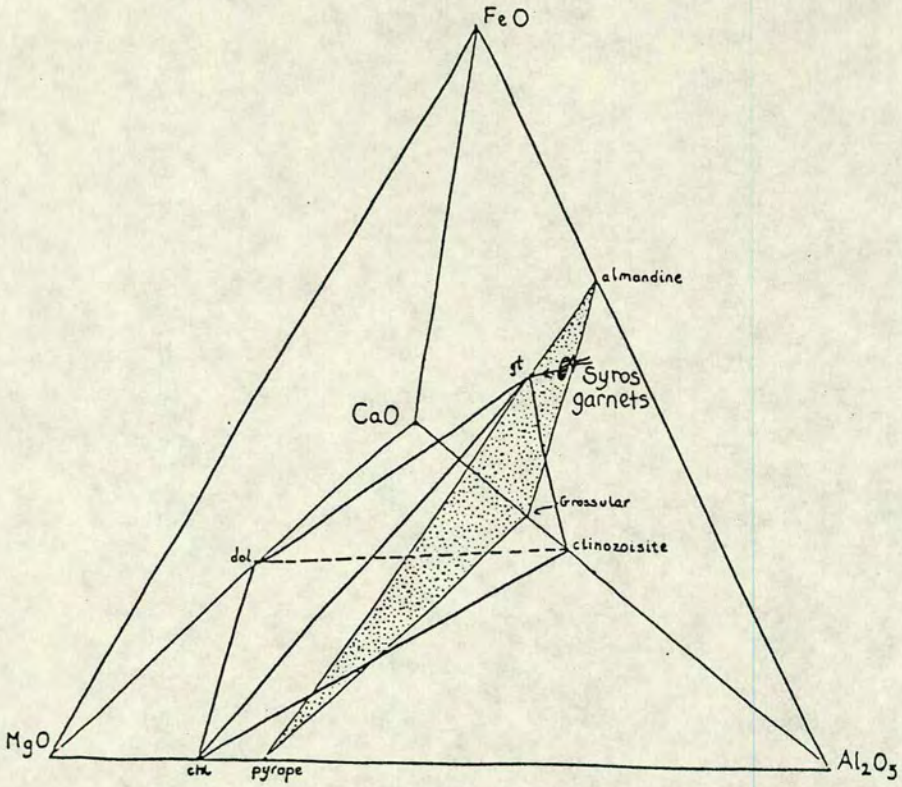

Figure 4.22 Bulk rock compositions occurring within the large 4-phase volume will develop garnet as an extra phase. Glaucophane is assumed to be stable with each of the phases, chl, dol, cz and gnt.

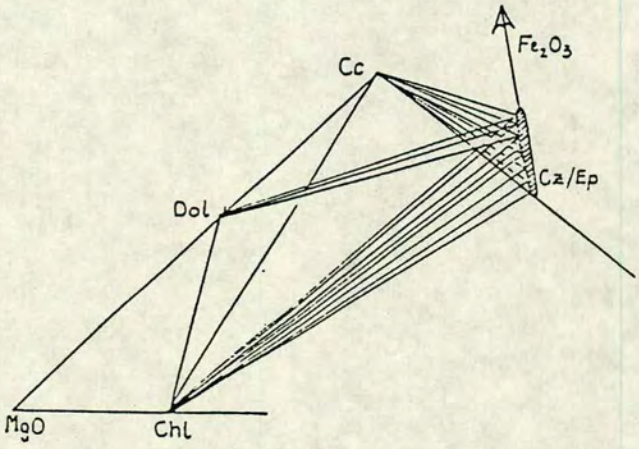

Figure 4.23 Fe_2O_3 substitution in clinozoisite stabilizes the cz/ep-dol join and allows the existance of the 4 phase volume chl-dol-cc-ep. The compositions of the 4 phases in this volume are fixed.

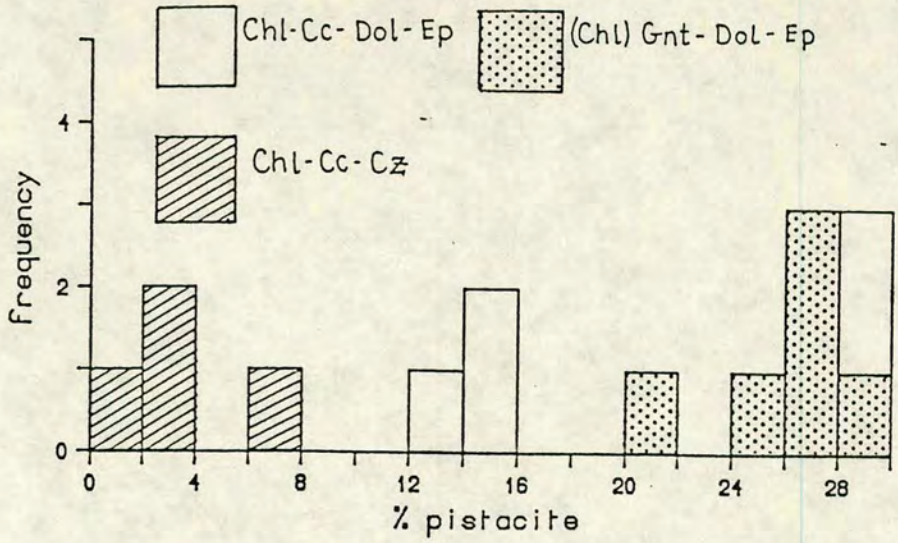

Figure 4.24 Histogram plot comparing the % pistacite in epidote from rocks containing the assemblages a) chl-cc-ep, b) cc-dol-chl-ep and c) gnt-dol-ep, see text for discussion. It is not clear why the epidote compositions of group B show a wide variation, possibly the assemblages in some of the samples are not in equilibrium. As no rocks with the assemblage ep-dol-chl were available, group C comprises rocks with the assemblage ep-dol-gnt.

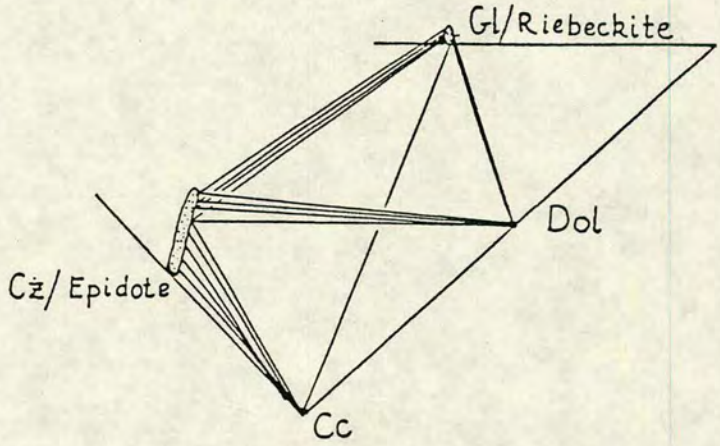

Figure 4.25 Na-pyroxene is assumed to be stable with each of the phases gl, cc, dol and epidote. Fe_2O_3 substitution will affect glaucophane and clinozoisite, and the greater degree of Fe_2O_3 substitution in cz/ep stabilizes the ep-dol tie-line and allows the existence of the 4-phase volume, ep-cc-dol-riebeckitic-gl.

Table 4.11

low Fe_2O_3 rocks	"fixed" Fe_2O_3 rocks	high Fe_2O_3 rocks
allowed phase assemblages	allowed phase assemblages	allowed phase assemblages
chl-cc-dol	4 phase volume	**chl-dol-high pistacite epidote**
or	**chl-cc-dol-ep** all compositions	or
chl-cc-ep	fixed.	**dol-cc-high pistacite epidote**

In an ideal situation it should be possible to prove these conclusions using probe data. A plot of Fe^{3+}:Al substitution in epidotes should reveal a grouping dependent on assemblage, and all epidotes from 4 phase assemblages should plot approximately in the same place. Figure 4.24 shows such a plot. Unfortunately, in practice, the compositional groupings which should occur are not as clear cut as would be wished. This spread of compositions may either be due to compositional zoning within the epidote crystals, or the presence of non-equilibrium assemblages.

In rocks containing larger amounts of iron, the development of garnet is favoured over that of chlorite, and in some cases chlorite is entirely replaced by garnet in the assemblage. This occurs, for example, in the rocks 75, 78, 83 and 84, which all contain garnet but no chlorite, and it is possible to suggest a number of likely garnet forming reactions:

1) 2cc + chl + 2 CO2 = gnt + 2dol + 4H2O
2) 9dol + 3qtz + 2cz = H2O + 5CO2 + 3gnt + 13cc
3) 9chl + 6qtz + 4cz + 8CO2 = 8cc + 15gnt + 38H2O
4) 13gl + 18cz + 72CO2 + 4H2O = 36dol + 26pg + gnt + 77qz

Pyroxene bearing assemblages

In general sodic pyroxene is absent from the metasediments because the bulk compositions of the schists plot close to the base of the tetrahedron, and possible tie-lines with jadeite are cut out by the plane gl-cc-pg. However, some sodium rich rocks do contain a Na-pyroxene, and in these cases the jadeite-epidote, or jadeite-lawsonite tie-line is preferred to the paragonite-calcite join. The composition of the

pyroxenes in the schists is displaced from the jadeite endmember towards diopside (diopside plots on the same compositional point as dolomite in the tetrahedron). Figure 4.25 illustrates one of the pyroxene bearing assemblages, rock 69, which contains the assemblage gl-ep-cc-dol-Na-pyroxene

4.11 THE RELATIVE ROLES OF BUFFERING AND INFILTRATION IN THE BLUESCHIST FLUIDS

As well as constraining the X_{CO2} content of the blueschist fluid, the T-X grid can also elucidate the relative roles of fluid buffering and infiltration in the metasediments. As was explained in the introductory chapter, two extremes of fluid behaviour exist. The first, termed buffering, is where the fluid composition is controlled by dehydration (and in cases hydration) reactions within the rocks themselves. The second type of behaviour, termed infiltration, is where the fluid composition is imposed on the rocks from outside by the pervasive infiltration of large amounts of external fluid. Whether buffering of infiltration was the dominant process in the blueschists can be established by examining the assemblages present in different rock layers on a variety of scales, from single outcrops, to samples collected several kilometres apart. Figure 4.27a,b illustrates how the assemblages from two localities on the north-west coast, Aspro and north of Aspro, (see chapter 2) are distributed on the T-X_{CO2} sections Although some of the rocks plot in a the same divariant volume this probably reflects an initial similarity in bulk composition rather than the presence of a common fluid. Within one outcrop assemblages are still spread across a range of possible divariant volumes, indicating that each layer has equilibrated with a fluid of slightly different composition. This observation is of great importance since it implies that each rock layer has evolved as a closed buffered system during the blueschist event, and the input of external fluid must have been low or non-existent.

One of the fundamental aims of this study was to assess the extent to which mineral assemblages in individual rock layers had controlled the composition of the coexisting fluid. The two examples documented above clearly suggest that the blueschist mineral assemblages have indeed controlled or buffered the composition of the fluid. There is no evidence to suggest that these rocks have been in communication with an external fluid reservoir. However, between the two extremes of internal buffering and pervasive infiltration a whole range of possible combinations involving the two processes exists, and it is possible that the blueschists did receive some external fluid. The volume of this external fluid must have been quite low as the buffering capacity of the rocks has not been exceeded.

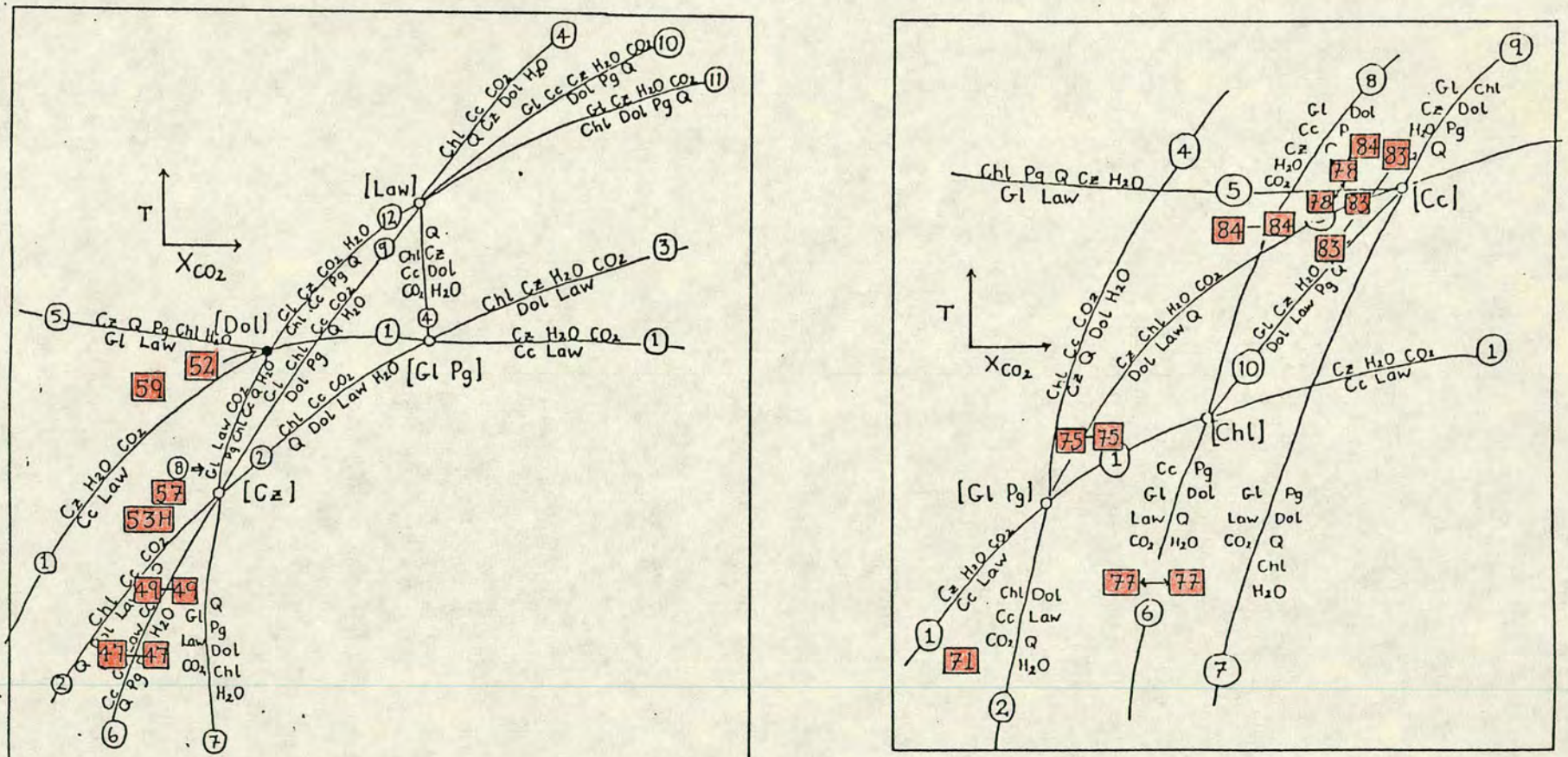

Figure 4.26a-b Schematic T-X(CO_2) sections of the S1/S2 and S3 grid (see fig. 1.16) showing the distribution of assemblages from two localities, A - Aspro, B - north of Aspro. The numbers outlined refer to sample numbers (see tables 4.8 and 4.10).

4.12 DISCUSSION AND CONCLUSIONS

Two major conclusions about the fluid phase have arisen from considering the blueschist assemblages in terms of the T-X_{CO2} sections.

1) Buffering of the fluid composition. As was discussed in section 4.11 a major conclusion to emerge from this study is that individual rock layers have acted as closed systems during the blueschist metamorphism, and the composition of the coexisting fluid was buffered by the mineral assemblages present.

2) Secondly, regarding the fluid composition, it can be seen from each of the T-X_{CO2} sections, S1, S2 and S3, that the compositions of the coexisting blueschist fluids are constrained to very H_2O-rich values by the bounding reactions defining the stability of the glaucophane-epidote and the glaucophane-lawsonite tie-lines. Indeed the fluid in equilibrium with the blueschist assemblages must have had an X_{CO2} of less than 1 mol%. On Syros there is also further mineralogical evidence to support the conclusion of an extremely H_2O-rich fluid during the blueschist event.

1) Lawsonite

The occurrence of lawsonite in the metasediments places some constraints on the fluid composition. Experimental work by Nitsch (1972, 1974) showed that the stability of lawsonite is critically controlled by X_{CO2}, and he found that lawsonite and quartz are unstable with respect to calcite and pyrophyllite at values of X_{CO2} greater than 3 mol%. These experiments were undertaken over the pressure range 3-7 kbars, and the stability field of lawsonite decreased with increasing pressure. Thus the occurrence of lawsonite and quartz at total pressures of around 14 kbars again suggests that the fluid in equilibrium with these rocks was very water rich.

2) Distribution of sphene and rutile

The relationship between sphene and rutile is a very important one when considering constraints on the fluid composition. The distribution of sphene and rutile in the metasediments has been described in Chapter 3 and, as was is pointed out there, sphene often occurs as the only Ti bearing phase in an assemblage.

The two titanium bearing phases are related via the reaction:

$$\text{sphene} + CO_2 = \text{rutile} + \text{calcite} + \text{quartz}$$

This reaction was examined by Schuiling and Vink (1967), and more recently by Hunt and Kerrick (1977). Although their two studies vary in detail the overall

conclusions are the same, and under the P-T conditions relevant for the Syros blueschists sphene can only be stabilised in the presence of a very water rich fluid. The presence of abundant sphene in the blueschist metasediments would appear to be consistent with the presence of a very water rich fluid. Where rutile is seen mantled by sphene this may indicate a change in the X_{CO2} of the fluid towards more water rich compositions during metamorphism. Alternatively rutile may have been present as detrital grains in the original sediment, and, being a source of TiO_2, these grains make an obvious site for sphene growth during metamorphism. If rutile occurs as the only Ti bearing phase in a rock, with quartz but no carbonate, as is the case for several of the metabasites the fluid composition is not constrained. Indeed the assemblage rutile+epidote+quartz is indicative of low X_{CO2} conditions (Hunt and Kerrick 1977)

In figures 4.27 a-c the reaction sphene $\Rightarrow$ rutile has been superimposed on the three T-X sections. As sphene is without doubt the dominant Ti-bearing phase in the majority of the rocks, those rock containing only sphene should lie to the left hand side, ie the water-rich side, of the sphene $\Rightarrow$ rutile curve. As can be seen from figure 4.27 the additional constraint of the sphene-rutile equilibria is not entirely consistent with the positions of the assemblages within the framework of the T-X_{CO2} grid. The sphene-rutile equilibria would have to lie further to the right, towards more CO_2-rich compositions, in order to be consistent with the T-X grid. The discrepancy between the position of the sphene-rutile equilibria and the rest of the grid is almost undoubtedly due to a degree of slop in the position of the reaction equilibria forming the grid. This slop is probably due to inaccuracies in the thermodynamic data for individual phases and, inaccuracies in the thermodynamic data for glaucophane in particular.

Metabasites

This discussion has centred around blueschist metasediments, schists and marbles, and metabasites have not been considered. This omission is partly because sampling concentrated on the carbonate-bearing metasediments, and because some of the dominant phases present in the metabasites, i.e sodic pyroxene and garnet were not considered in the analysis. However some constraint can be placed on the composition of the fluid coexisting with the metabasites. Sphene is the dominant Ti-bearing phase in the metabasites, and as was discussed in the previous section this places tight constraints on the X_{CO2} content of the coexisting fluid.

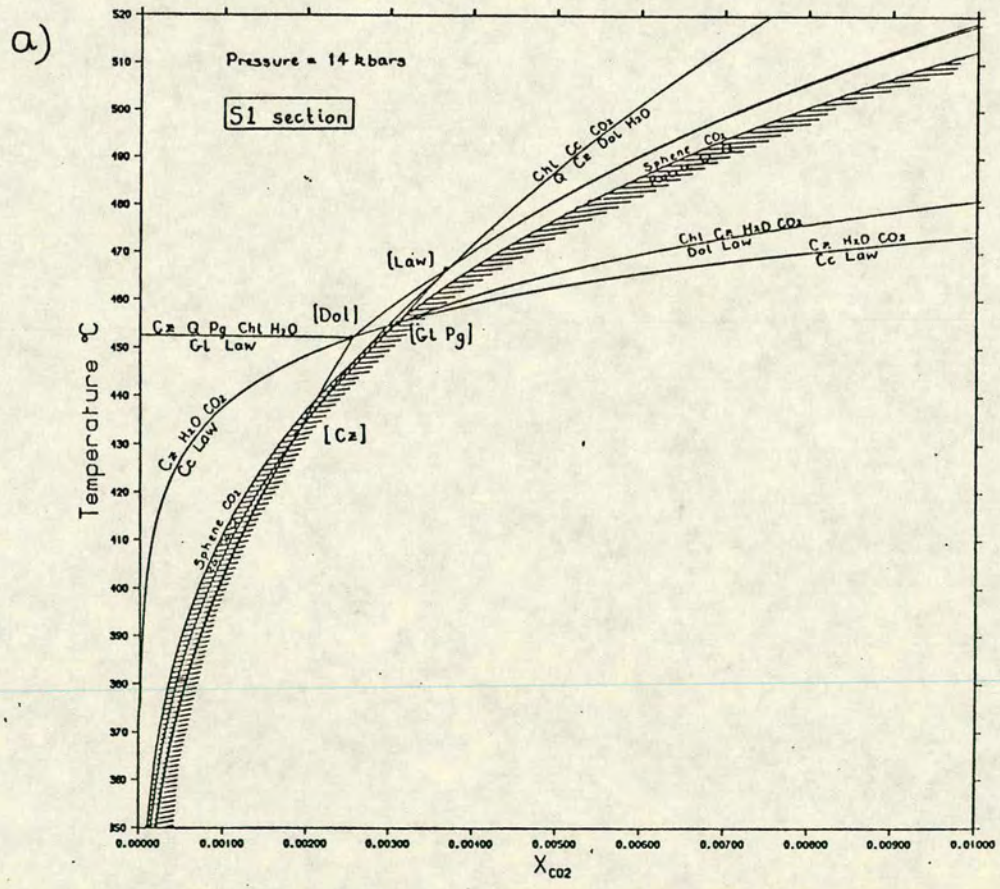

Figure 4.27a-c The equilibria sphene + CO_2 = rutile + CO + qtz is superimposed on the 3 T-X(CO_2) sections, S1, S2 and S3. The sphene equilibria was calculated using the thermodynamic data of Holland and Powell (pers. comm., July 1988), the activity of sphene = 0.948 (see table 4.9). See text for discussion.

b)

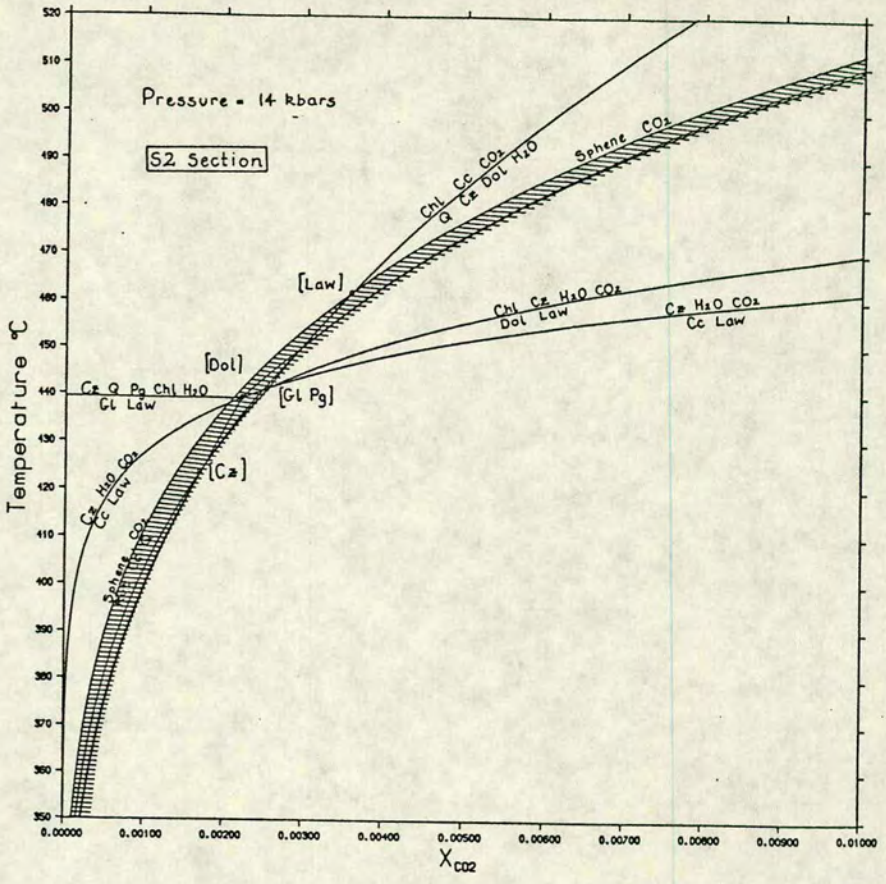
Pressure = 14 kbars
S2 Section
Chl Cc CO2
Q Cz Dol H2O
Sphene CO2
[Law]
Chl Cz H2O CO2
Dol Law
Cz H2O CO2
Cc Law
[Dol]
Cz Q Pg Chl H2O
Cl Law
[Gl Pg]
Cz H2O CO2
Cc Law
[Cz]
Sphene CO2
Temperature °C
XCO2

c)

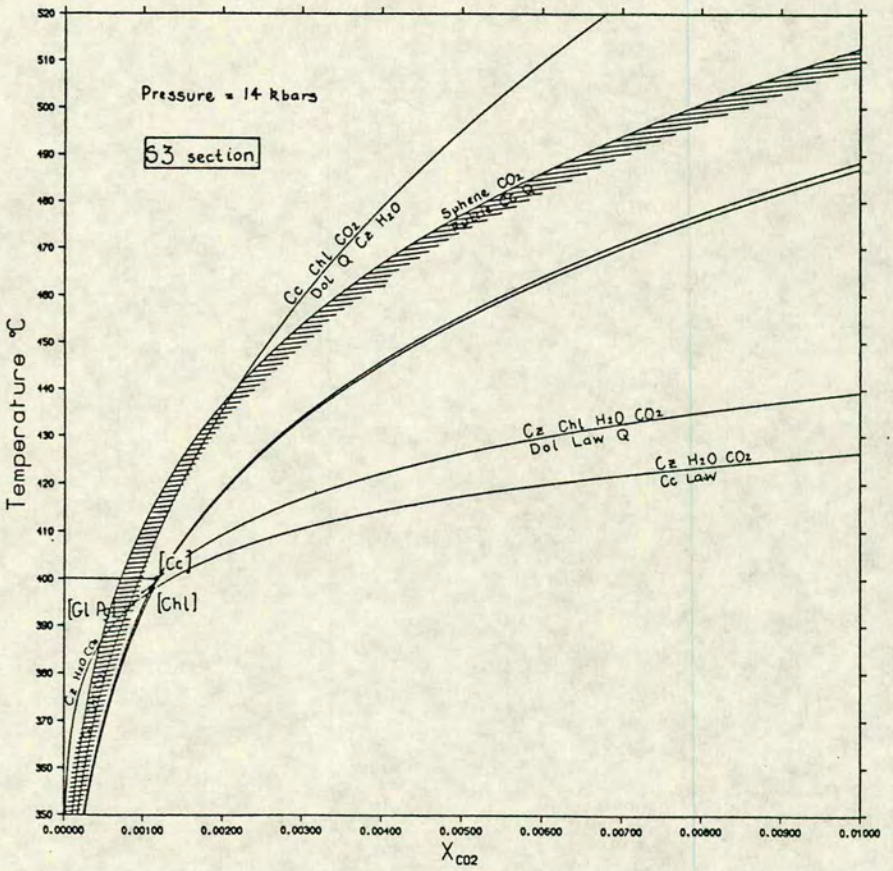
Pressure = 14 kbars
S3 section
Cc Chl CO2
Dol Q Cz H2O
Sphene CO2
Cz Chl H2O CO2
Dol Law Q
Cz H2O CO2
Cc Law
[Cc]
[Gl Pg]
[Chl]
Cz H2O CO2
Temperature °C
XCO2

In almost all the metabasites examined the glaucophane-epidote tie-line is stable, a fact which also limits the composition of coexisting fluids to very water-rich values, (see figure 4.19).

4.13 SUMMARY

The main conclusions arising from this chapter can be briefly summarized:.

1) The fluid in equilibrium with the blueschist assemblages is almost pure H_2O. This conclusion is supported by other mineralogical evidence, i.e the abundance of sphene and the presence of lawsonite.

2) Differences in the equilibrium fluid composition exist between samples collected on an outcrop scale. These differences suggest that the mineral assemblages have controlled the composition of the coexisting fluid during the blueschist metamorphic event. By implication the volume of external fluid involved is negliable.

Having discussed the blueschist rocks at some length, the following chapter will consider the greenschist rocks on Syros. The petrographic characteristics of the rocks are described, and possible mechanisms for the blueschist to greenschist transformation are examined.

CHAPTER 5

THE GREENSCHISTS

TABLE OF CONTENTS

5.0 INTRODUCTION

As was discussed in chapter 2, the metamorphic evolution of Syros is dominated by an initial blueschist facies event in the Eocene, and a subsequent lower to medium pressure greenschist overprint, which presumably occurred in the early Miocene. The greenschist overprint is of regional extent, and has affected many of the other islands in the Cycladic massif, e.g Sifnos, Tinos, Sikinos, Serifos, Milos and Andros. The transformation of the high pressure blueschist minerals to greenschist facies assemblages has occurred to varying degrees, and in places the blueschist facies assemblages are completely obliterated, e.g Kea.

Most blueschist terrains show at least a partially developed greenschist overprint (an exception being the Franciscan formation, California, Ernst, 1963). Traditional thermal models essentially regard the overprinting of blueschist rocks during uplift as a thermal problem. The uplift models are concerned with unloading the blueschists rapidly, so that there will be no time for any significant temperature rise, via thermal relaxation or internal heat generation (Draper and Bone 1981; England and Thompson 1984; Ridley 1982). The role of fluids in this transformation has commonly been ignored, yet they must play an important part. This is because the transformation to greenschist rocks involves the hydration and carbonation of the blueschist assemblages, and therefore *both* heat and fluid are required.

This chapter will consider the blueschist to greenschist transformation on Syros, which is recognised by the development of Barrovian mineral assemblages. The textures accompanying this transformation will be described, and used to deduce possible mineral reactions. The selected reactions will then be used to constrain the P-T-X_{CO2} conditions accompanying the greenschist event as far as possible. The geographical distribution of the greenschist facies rocks will also be considered, and the implications of this distribution will be discussed in the light of fluid infiltration and transport mechanisms.

5.1 PETROGRAPHY OF THE GREENSCHISTS

The greenschist overprint causes glaucophane-bearing assemblages to be replaced by albite-chlorite-epidote-calcite$\pm$actinolite-bearing assemblages, characteristic of the greenschist facies. This section presents the petrographic observations made on the secondary assemblages, itemising the various replacement textures seen, and proposing possible reactions to explain their growth.

Albitization

The development of albite is one of the main mineralogical features associated with the greenschist overprint. Secondary albite is found in all the rock types, though it is particularly common in the schists and metabasites. The albite formed is almost pure, having a composition $Ab_{99}An_{01}$, even when in equilibrium with calcite or epidote.

There is a progressive development of albite related to the degree of overprinting experienced by the primary assemblage. Albite first appears as a pseudomorphing phase, replacing glaucophane and chlorite, and then, with increasing degrees of alteration, it becomes abundant in the rock matrix. Although the size of individual albite grains is usually comparable with that of the other phases, they often cluster together forming small rosettes, which are invariably surrounded by secondary chlorite. Figure 5.1 is a photomicrograph showing matrix albite in a partially altered blueschist. In most examples the albite grains have a turbid appearance due to the presence of numerous inclusions. Commonly included phases are graphite, epidote, white mica and glaucophane. In rocks where the greenschist overprint is strongly developed and albitisation is more intense, so the preferred orientation of the matrix is lost, and a "randomization" of the fabric occurs.

Albite porphyroblast schists

There are localities on Syros, mostly in the south, where zones of true albite porphyroblast schists are developed. Albite porphyroblast schists are found in many metamorphic terrains around the world, where they are consistently associated with high fluid-rock ratios during metamorphism, e.g the S.W Highlands of Scotland (Dymoke 1988; Graham et al 1983; Watkins 1983), the Pelona Schist, southern California, U.S.A, (Graham pers. comm., 1989), and the Siviez-Mischabel nappe, Switzerland (Thelin and Sartori 1987).

On Syros their presence can be detected in the field by the occurrence of white spots in the rock. In thin section these spots are seen to be single albite crystals, which have a rounded shape and lobate crystal margins. Twinning of these crystals is quite common. The porphyroblasts tend to form in the mica-rich portions of the rock, surrounded by thick bands of secondary chlorite. The matrix foliation has not been pushed aside to accommodate the porphyroblasts; rather it has been neatly overprinted, and the external fabric abuts against the porphyroblasts without showing any deflection. Figures 5.2a and 5.2b are photomicrographs of albite porphyroblast schists, showing some of the features described above.

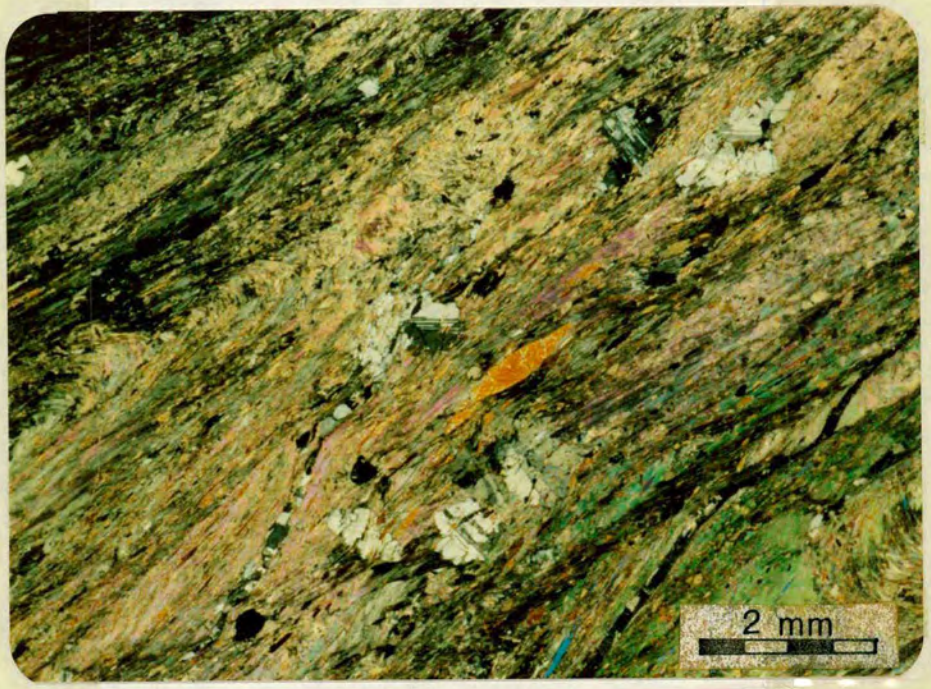

Figure 5.1 Albite porphyroblasts developed in a chl-talc-actinolite schist, Kastri (86/40). (Magnification x 8, XPL).

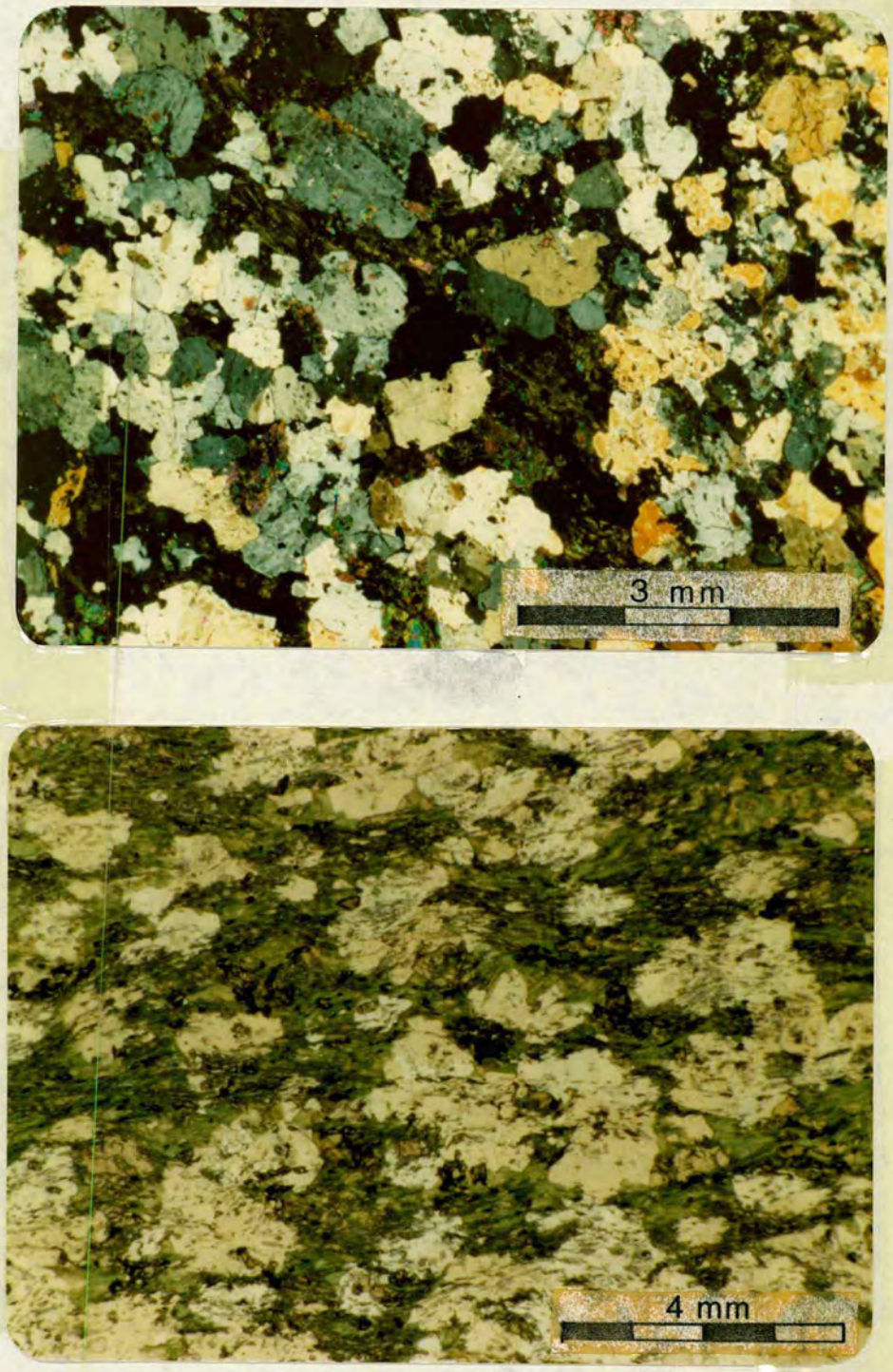

Figure 5.2 a) Albite porphyroblast schist from Kini, (87/205). Albite is abundant, and composes 60% of the rock. Also present are chlorite, epidote, quartz, actinolite and sphene (x 10, XPL). b) In this photomicrograph of a basic schist (87/231), the overprinting nature of the albite porphyroblasts is seen. The inclusion trails present in the albites are continuous with the external foliation. Indicated on the overlay are glaucophane crystals, preserved within the albite. The high relief material in the chlorite is a mixture of sphene and epidote (x 7, PPL).

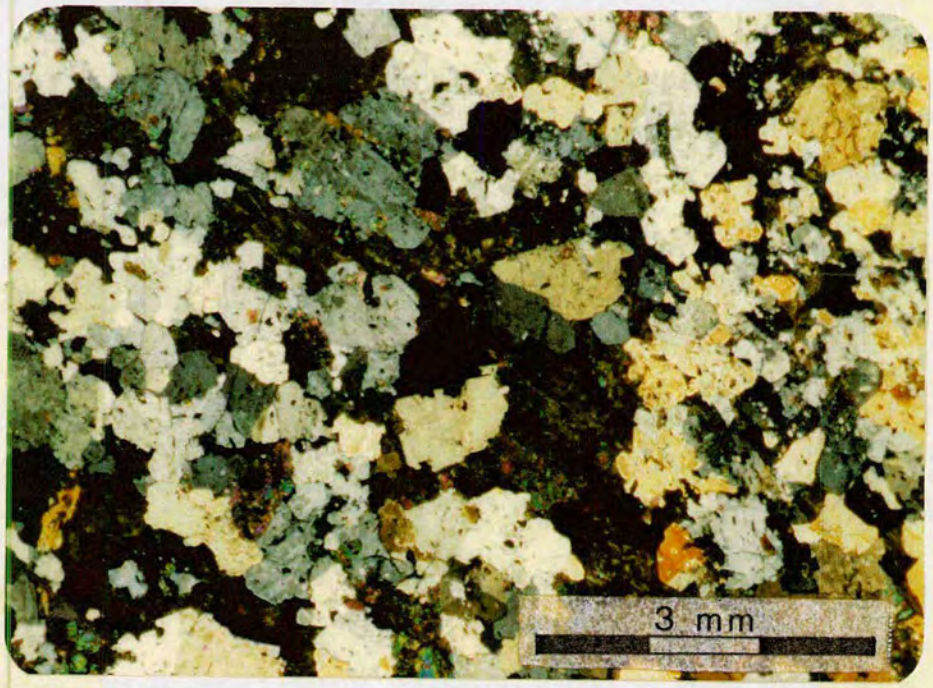

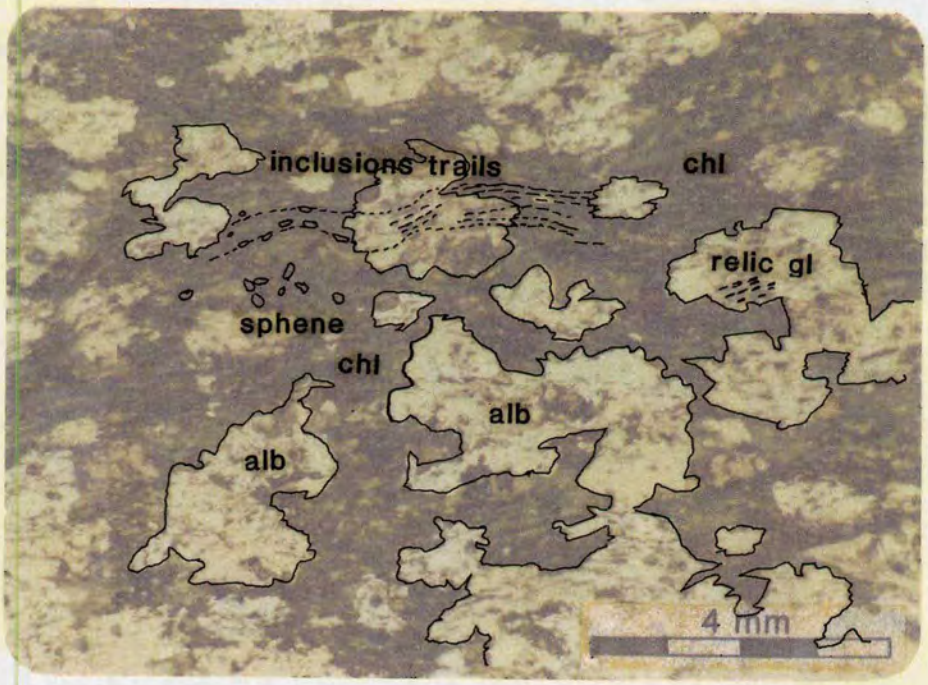

Figure 5.2 a) Albite porphyroblast schist from Kini, (87/205). Albite is abundant, and composes 60% of the rock. Also present are chlorite, epidote, quartz, actinolite and sphene (x 10, XPL). b) In this photomicrograph of a basic schist (87/231), the overprinting nature of the albite porphyroblasts is seen. The inclusion trails present in the albites are continuous with the external foliation. Indicated on the overlay are glaucophane crystals, preserved within the albite. The high relief material in the chlorite is a mixture of sphene and epidote (x 7, PPL).

Inclusion trails in albite porphyroblasts

Inclusion trails in porphyroblasts have always been of interest to petrologists, and many studies have tried to relate the geometry of inclusion trails to the external matrix fabric, in the hope of relating the growth of a porphyroblast to a specific deformational event in the regions history. Various models have been proposed to explain the geometry of inclusion trails. The early model of Zwart (1962), which allowed rotation of the porphyroblast relative to the matrix, has now been largely superceded by the work of Bell and others (Bell 1985, 1986; Bell and Rubenbach 1983; Bell *et al.* 1986). The albite porphyroblasts seen on Syros contain numerous inclusions, often of graphite, white mica, sphene and glaucophane. Where distinct inclusion trails are present in the porphyroblasts they are invariably continuous with the external foliation. In particular, continuous trails of sphene and graphite can often be followed through several albite crystals, and the intervening matrix, with no apparent deflection. Interestingly, in samples where glaucophane has broken down, and is now absent from the rock matrix, it is often preserved as armoured inclusions in albite. The undeformed nature of the inclusion trails in the porphyroblasts is interpreted as implying that deformation was absent during the greenschist event in the rock volumes concerned. In fact, throughout the island the greenschist overprint appears to have occurred in the absence of penetrative deformation, although the presence of cross-cutting veins associated with the greenschist event implies an overall extensional regime (Ridley 1982). Later deformation is of a low-strain type, producing open upright folding and high level brittle faulting (Ridley 1982).

Distribution of albite porphyroblast schists

Albite porphyroblast schists are associated with the most intense areas of greenschist retrogression. They tend to occur in zones, which vary in width from a metre or more down to a few centimetres. Watkins (1983) studied the albite porphyroblast schists occurring in the Balquhidder-Crianlarich region of the central Scottish Dalradian. These albite porphyroblasts schists developed during epidote-amphibolite facies metamorphism, (Dymoke 1988). Watkins analysed 18 samples of the albite porphyroblast schists, and a similar number of lithologically equivalent "normal" schists. He found no evidence of regional sodium metasomatism to account for the formation of the albite schists. Instead it appeared that the albite porphyroblasts had formed under closed system conditions. In the absence of metasomatism, Watkins (1983) proposed the influx of an H^+-bearing fluid, i.e H_2O, which, he suggested, caused both the redistribution of Na^+, and the crystallisation of albite porphyroblasts.

Table 5.1 Bulk rock analyses of albite-bearing greenschists and albite free blueschists.

% albite	0	0	0	0	0	0
	86/14	86/70	86/72	86/78	86/124	87/157
SIO2	53.59	56.59	61.17	53.40	50.60	50.29
AL2O3	14.91	16.18	14.65	19.59	15.73	15.46
FE2O3	0.95	1.04	0.42	2.39	3.06	4.09
FEO	5.31	6.38	6.83	5.89	6.08	6.55
MGO	4.44	6.88	6.15	4.98	6.11	5.27
CAO	6.50	2.01	1.39	1.58	10.39	8.57
NA2O	1.46	3.45	1.85	2.69	4.53	4.56
K2O	2.86	3.29	2.58	4.56	0.02	0.95
TIO2	0.73	0.88	0.79	0.89	1.78	2.21
MNO	0.11	0.11	0.09	0.32	0.19	0.18
P2O5	0.10	0.10	0.12	0.20	0.26	0.32
TOTAL	90.97	96.91	96.04	96.48	98.76	98.45

% albite	8	5	25	30	60	20
	86/19A	86/25	86/34	87/21A	87/205	87/160
SIO2	48.16	52.14	53.74	42.57	49.18	46.82
AL2O3	17.42	14.40	17.40	13.48	15.08	17.32
FE2O3	0.24	1.24	0.98	5.31	3.26	3.33
FEO	7.68	5.13	5.45	3.52	7.47	6.02
MGO	5.40	4.49	5.24	6.86	5.74	8.43
CAO	5.95	7.32	3.19	13.08	6.74	9.09
NA2O	2.55	1.56	2.64	3.97	4.44	3.38
K2O	2.90	2.70	3.41	0.53	0.08	0.19
TIO2	0.87	0.71	0.88	0.77	1.08	1.47
MNO	0.12	0.13	0.12	0.17	0.22	0.16
P2O5	0.08	0.11	0.13	0.07	0.16	0.15
TOTAL	91.37	89.93	93.18	90.33	93.45	96.35

Some bulk rocks analyses have been performed on albite-bearing greenschists and unaltered blueschists from Syros, and there appears to be no significant difference in Na_2O content between the two groups, (see table 5.1). If Watkins'(1983) mechanism is correct, then zones of albite porphyroblast schists should denote former channelways of high fluid flux, and mapping these zones may provide information about fluid pathways during metamorphism. Evidence on Syros supporting the connection between the occurrence of albite porphyroblast schists and former fluid channelways, is found at localities where alternating sequences of marble and schist are present, e.g Oros Syringas, Ormos Akhladhi and Varvarousa. At these localities there is a correlation between the position of the structurally lowest marble-schist contact, the development of pronounced greenschist alteration, and zones of albite porphyroblast schists. It appears that the marbles have acted as fluid barriers, causing a "ponding" of upward-moving fluid, and encouraging lateral fluid-flow along the marble-schist contact. Such fluid channelling could produce sufficiently high fluid-rock ratios to redistribute sodium in the rock, and form porphyroblasts. Further work is required to map out the zones of albite porphyroblast schists in relation to such features as marble bands to confirm this correlation. Pursuing the idea that albite porphyroblast schists act as markers for former zones of high fluid flow, four albite separates were analysed for $\delta^{18}O$, and the results are given in chapter 6.

Development of secondary chlorite

The replacement of AFM phases by chlorite occurs to some degree in almost all the rocks on the island, and consequently secondary chlorite is a widely developed mineral phase.

Figure 5.3 shows chlorite+albite pseudomorphs after glaucophane. It is petrographically evident that glaucophane has been replaced by albite and chlorite, and a suggested reaction to explain this texture is:

$$gl + pg + 4H_2O = 13alb + 3clin + qtz$$

Chlorite also commonly replaces garnet, and it is usually the dominant phase in such a pseudomorph, although albite can also be present. The volume of the original phase is preserved, and the chlorite grains mimic the outline of the former garnet. In the metabasites chlorite also replaces epidote to a minor degree. Lacy porphyroblasts of epidote are seen which have chlorite in the interstices. In general though, epidote appears to have remained inert during the blueschist to greenschist transformation.

Many rocks contain textural evidence to suggest the presence of two types of chlorite.

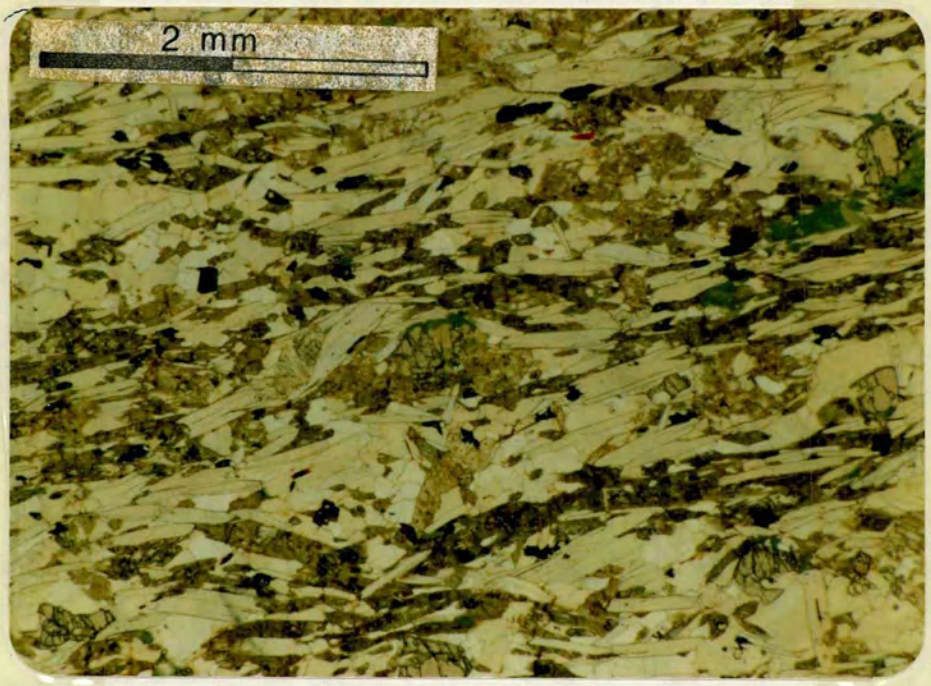

Figure 5.3 This photomicrograph shows a former qtz-glaucophanite from Agkathopes, (87/138), containing abundant chlorite + albite pseudomorphs after glaucophane. The outlines of former glaucophane crystals can be clearly seen, indicating perfect volume for volume replacement. A few relics of garnet are present, partly altered to chlorite. (x 18, PPL).

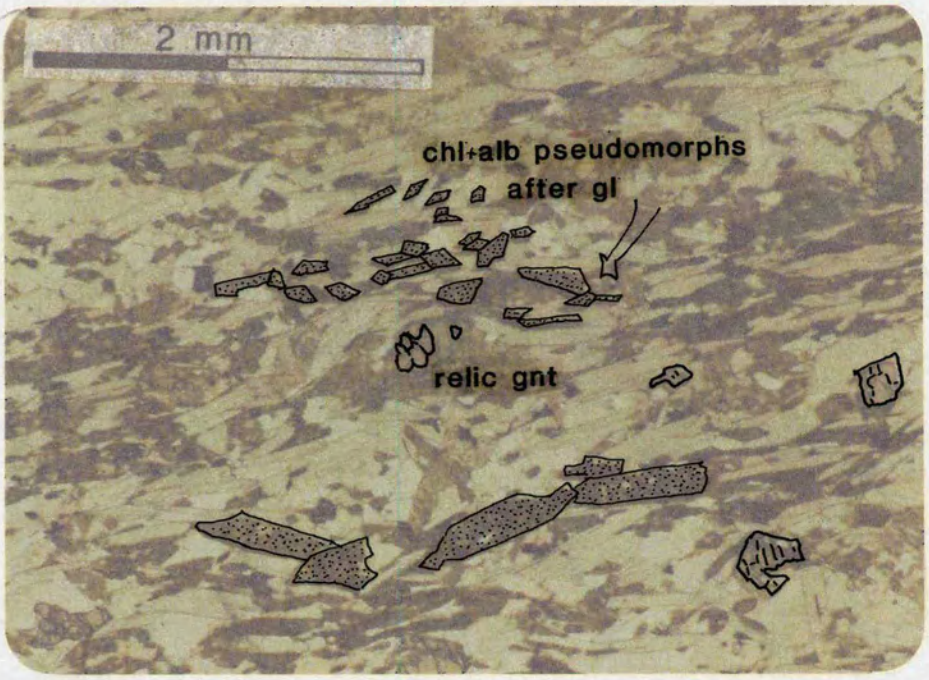

Figure 5.3 This photomicrograph shows a former qtz-glaucophanite from Agkathopes, (87/138), containing abundant chlorite + albite pseudomorphs after glaucophane. The outlines of former glaucophane crystals can be clearly seen, indicating perfect volume for volume replacement. A few relics of garnet are present, partly altered to chlorite. (x 18, PPL).

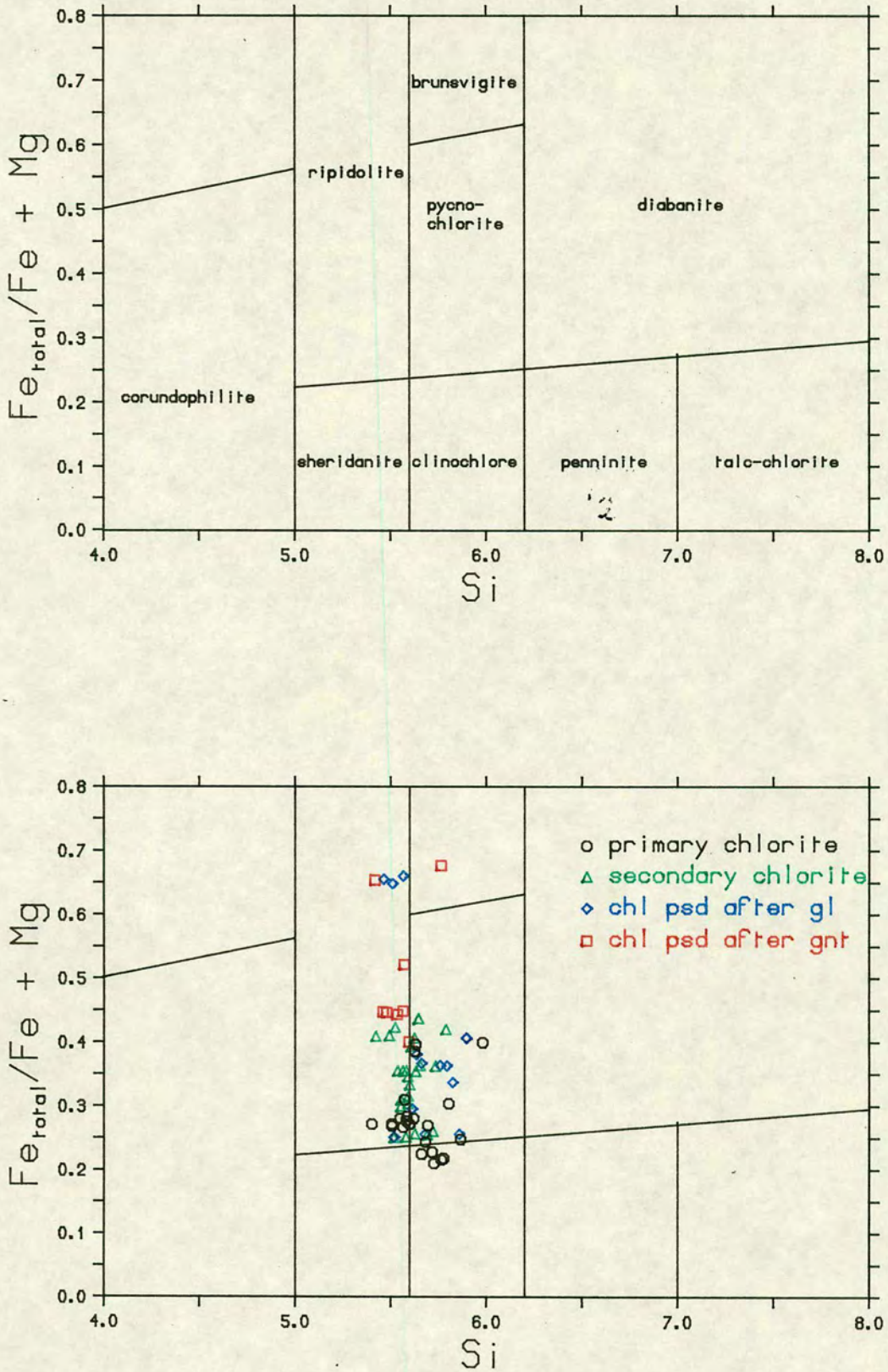

Figure 5.4 Primary and secondary chlorite compositions plotted in a Hey diagram, (Hey 1954). Primary chlorites tend to cluster near the sheridanite-clinochlore boundary, while some of the secondary chlorites are distinctly more iron-rich.

Primary chlorite is present in a number of the blueschists, where it has a pale silvery-green colour and shows normal first order interference colours. In contrast the secondary chlorite is invariably quite strongly coloured and pleochroic, and shows anomalous blue, purple and brown interference colours. Chemical analysis of the secondary chlorites may also distinguish them from the primary chlorite. Figure 5.4 shows primary and secondary chlorites plotted on a Hey diagram (Hey 1954). The two chlorites show approximately the same Si-content, but the extent of $FeMg_{-1}$ substitution is quite different in the two cases. The composition, and the Fe/Mg content in particular, of the secondary chlorite will largely depend on the Fe/Mg content of the phase it is replacing, and chlorites replacing garnet consistently show the highest Fe/Fe+Mg ratio.

Brown oxy-chlorite also occurs in a number of schists and metabasites, particularly those from the south of the island, where it was initially misidentified as biotite.

Biotite

Biotite is rare on Syros, and it was not positively identified in any rocks during this study. Ridley (1982) records the occurrence of secondary biotite in metabasites from the southern-most peninsula of Mavra Vounakia. Here biotite coexists with epidote, chlorite, albite, actinolite and calcite. It is not clear why biotite is so rare, since the P-T conditions experienced during uplift should have been conducive to its formation.

Secondary amphibole

Secondary amphibole is largely restricted to metabasites and metacherts from the south of the island, from the peninsula of Mavra Vounakia, northwards to the Nites massif. Other recorded examples were collected at Ormos Akhladhi on the south-east coast, and Komito on the west coast. No secondary amphibole has been detected north of the Nites massif; exceptions to this are the occurrence of actinolitic amphibole in heavily overprinted basic schists at Kini on the central west coast of the island, and the development of barroisitic amphibole in a narrow shear zone north of the Grizas metagabbro (Ridley 1982).

In overprinted metabasites small prismatic crystals of green secondary amphibole are associated with matrix albite, epidote and chlorite (see figure 5.5). Figures 5.6a and 5.6b are photomicrographs showing the development of the zoned sodic-calcic amphibole crystals. The consistent rimming relationship with coexisting

glaucophane, and the strong blue-green colour of the calcic amphibole, distinguish these occurrences of coexisting sodic and calcic amphibole from the mixed sodic-calcic amphibole crystals seen at Aspro on the north-west coast (see chapter 3). Optically the amphibole zoning is abrupt, and figure 5.7, which shows some 100-point element qualitative profiles made through these zoned amphibole crystals using the electron microprobe, provides supporting chemical evidence.

Figure 5.8 is a plot of Al^{iv} versus Na_{M4} per formula unit, and a number of traverses through zoned amphibole crystals are plotted, together with core and rim analyses from some matrix calcic amphiboles. The sodic amphibole cores are no different in composition to glaucophanes examined elsewhere, and the secondary amphibole formed is essentially actinolitic, with only one amphibole rim plotting in the edenite field. Among the calcic amphiboles examined, the extreme rims show an indistinct zoning towards more actinolitic compositions. Calcic amphibole also occurs in altered schists at Kini, and here the transformation to a greenschist facies assemblage has been complete. Calcic amphibole and epidote occur in a matrix of chlorite, calcite and quartz with sphene present as a common accessory. Optically the calcic amphibole appears unzoned, and there is no evidence for a former sodic phase. Figure 5.9 shows the composition of these amphiboles in an Al^{iv}-Na_{M4} plot, and as before, they are actinolitic in composition. Figure 5.10 shows the A-site occupancy of the different amphiboles. The occupancy of the A-site tends to be low in the sodic, and more actinolitic amphiboles, but as the calcic amphiboles grade towards edenitic compositions, the A-site is progressively filled.

Holland and Richardson (1979) showed that zonation and overgrowths observed in amphiboles could record the evolution of metamorphic conditions. Ridley (1982) applied the method of Holland and Richardson (1979) to examine the relative P-T differences between the primary metamorphism in the south and the north of the island, and estimate changing P-T conditions with time. He examined one sample of overprinted metabasite from the south of the island in detail, which contained calcic amphibole overgrowths on sodic cores. As in Holland and Richardson (1979), he drew up a set of exchange reactions relating the amphibole zonation to the addition and subtraction of components from the coexisting phases, in this case sodic-pyroxene, garnet and quartz. The six exchange reactions devised by Ridley (1982) are reproduced below:

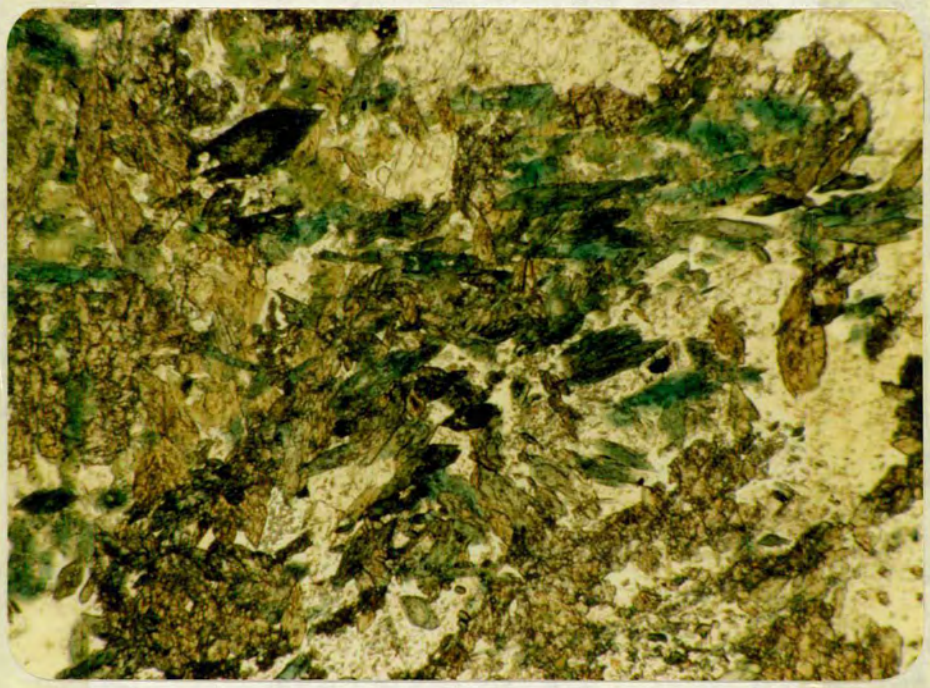

Figure 5.5 Photomicrograph of calcic amphibole in a heavily overprinted metabasite, Ormos Akhladi (87/134b). Nearly all the amphibole in this rock is calcic, and strongly pleochroic from dark bluish-green, to green, to pale yellow. The large crystal in the top left hand corner preserves a relic sodic core. Epidote, chlorite, quartz and albite form the matrix (x 40 PPL).

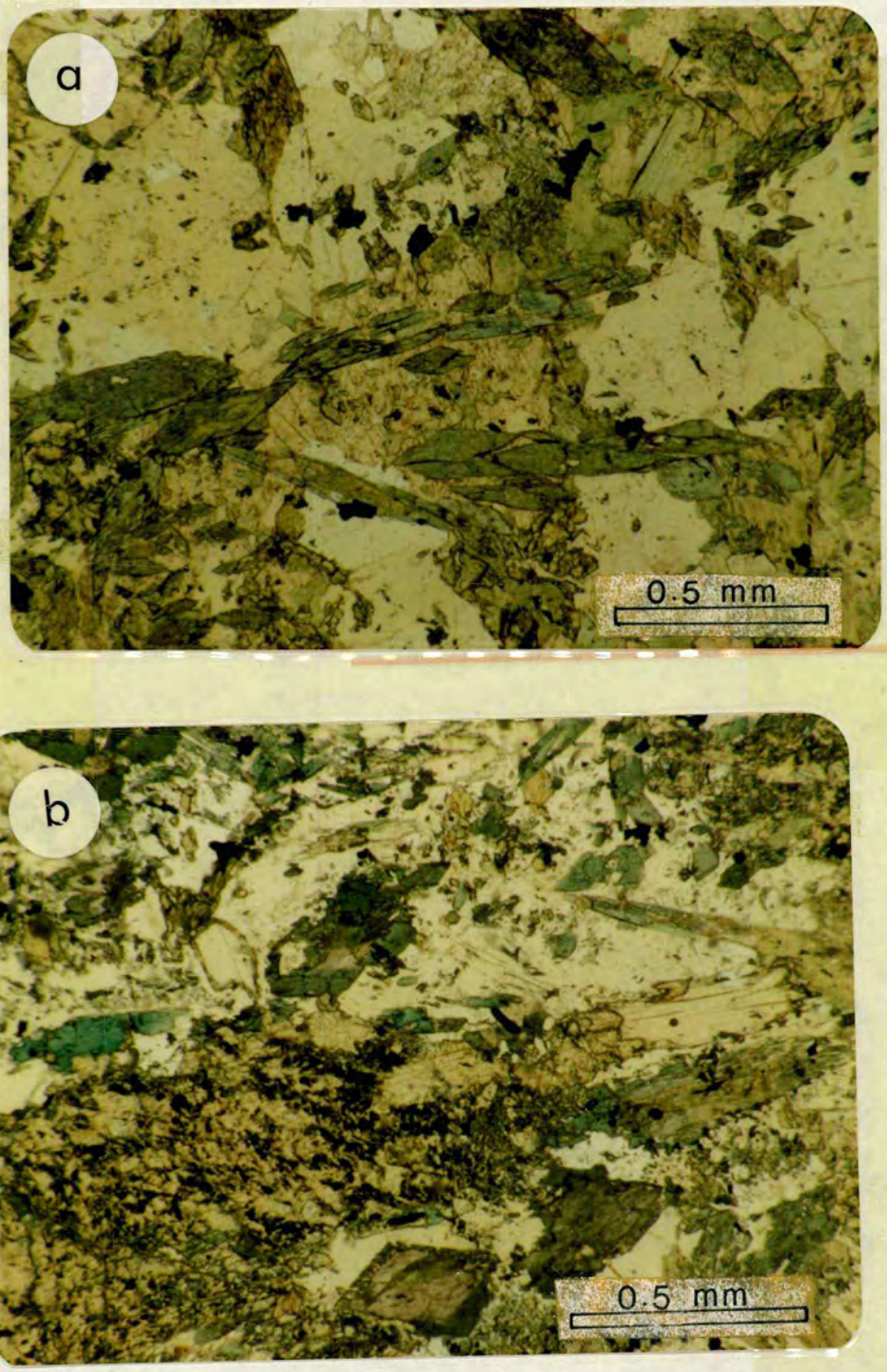

Figure 5.6 a), b) These two photomicrographs, again from metabasites (a = 87/134a, b = 87/213), show zoned sodic-calcic amphibole crystals, where glaucophane is rimmed and replaced by calcic amphibole. The blue-green calcic amphibole is increasing at the expense of sodic amphibole, which ultimately disappears in completely altered rocks (a = x 40, PPL; b = x 45 PPL).

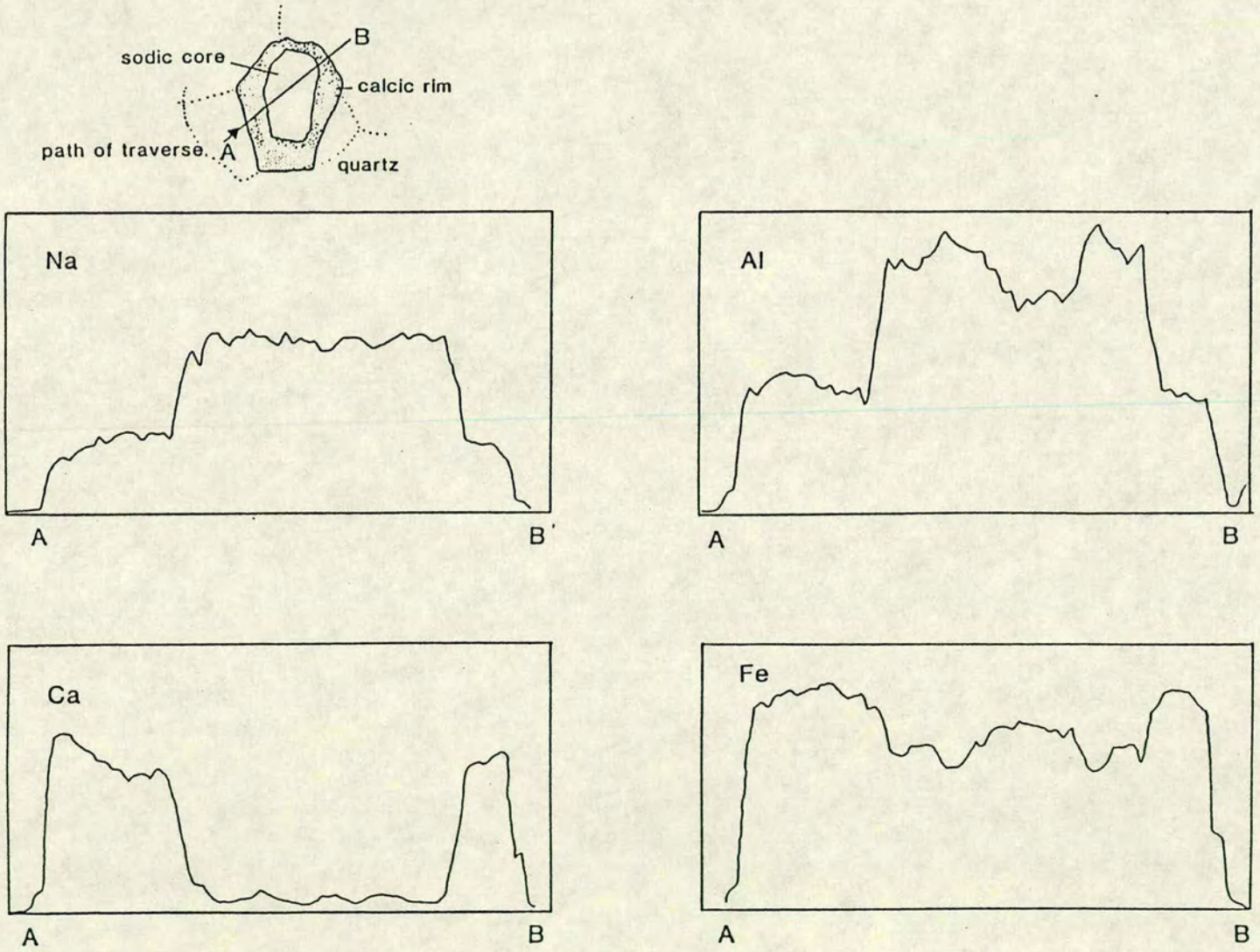

Figure 5.7 Element zonation profiles through a zoned sodic-calcic amphibole. The traverse length (A to B) is 100 microns. Changes in the amphibole chemistry are abrupt, particularly Na and Ca distribution.

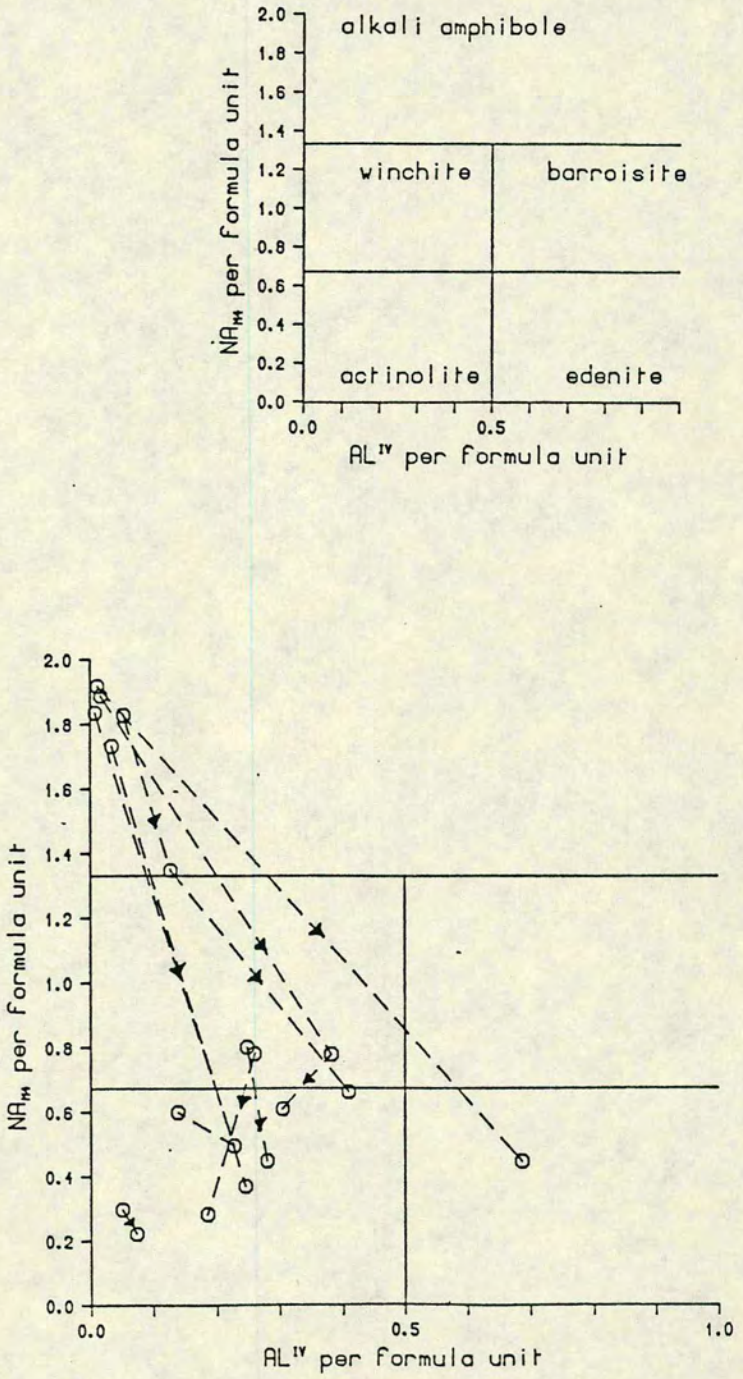

Figure 5.8 Zoning in sodic-calcic amphiboles. Lines connect analyses from the same crystal, and arrows point from cores to rims. Zoning is generally towards more edenitic compositions, with the calcic overgrowths showing an increased Al^{IV} content.

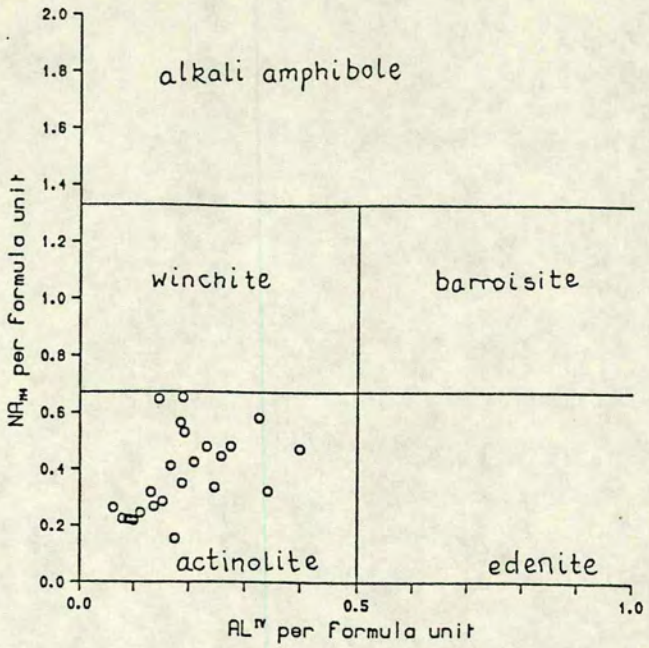

Figure 5.9 Plot of Al^{IV} versus Na M4 for secondary amphiboles in greenschists, Kini.

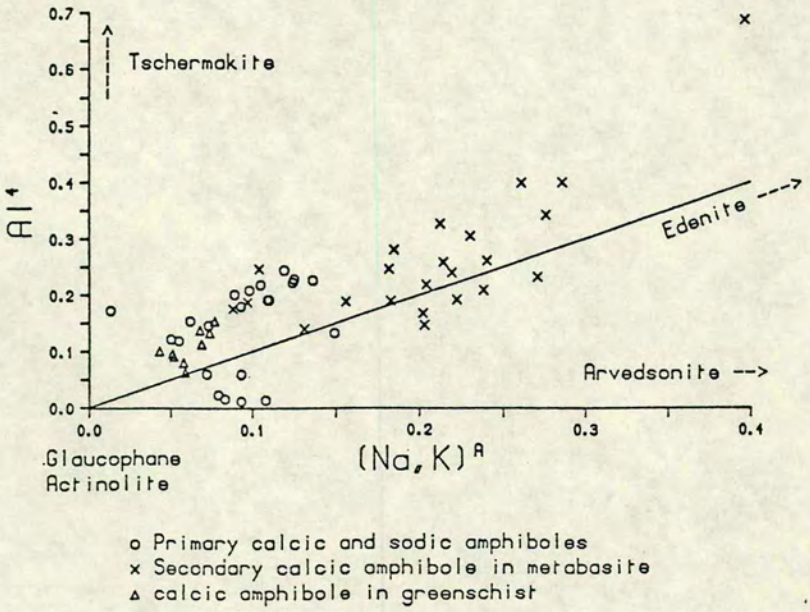

Figure 5.10 Plot showing the A-site occupancy of some primary and secondary amphiboles. As the calcic amphibole becomes more edenitic, so the A-site is progressively filled. Note that, even for relatively pure glaucophane, the A-site is not empty.

5ed + 3gr + 16qtz = 3 tsch + 13di + 5jd + 2H2O [tr,gl]
5gl + 3gr + qtz = 3tsch + 10jd + 3di + 2H2O [tr,ed]
gl + 2di = ed + jd + 3qtz [tr,tsch]
5tr + 3gr + qtz = 3tsch + 13di + 2H2O [gl,ed]
tr + jd = ed + 3qtz [gl,tsch]
gl + 2di = tr + 2jd [ed,tsch]

Table 5.2 lists some probe analyses on zoned amphiboles in metabasites, made during this study, together with the activities of the different amphibole components. The main chemical difference between the cores and rims of the zoned amphiboles is the high glaucophane activity of the cores, and the high edenite activity of the rims. The two exchange reactions used to delineate the changes in composition occurring from core to rim are [ed,tsch], relating glaucophane to tremolite, and [gl,tsch], relating tremolite to edenite. Ridley (1982) determined the equilibrium constants for these two exchange reactions for the Syros metabasites.

$$K(ed,tsch) = \frac{a_{tr}^{amph} (a_{jd}^{px})^2}{a_{gl}^{amph} (a_{di}^{px})^2}$$

$$K(gl,tsch) = \frac{a_{ed}^{amph}}{a_{tr}^{amph}.a_{jd}^{px}}$$

Figure 5.11 shows lnK(ed,tsch) versus lnK(gl,tsch) for the zoned amphiboles. Thermodynamic data for the phases involved in the exchange reactions allowed construction of the isobars and isotherms for the reaction space, (Ridley 1982). The looped form of the amphibole zonation suggests a possible qualitative P-T-t path for the rock involved. Also plotted on figure 5.11 is a glaucophanic amphibole from a glaucophane-eclogite, northern Syros. Comparing the positions for this amphibole, and those for the southern sodic cores, Ridley (1982) suggested that the maximum recorded metamorphic pressures for the rocks at the base of the sequence had been lower, and the uplift temperatures experienced, higher, than for rocks in the north.

Calcitization

Secondary calcite is present in a large proportion of the schists and metabasites, where it commonly occurs as irregularly shaped patches which overprint the primary foliation. Secondary calcite also replaces a wide variety of phases, e.g. glaucophane, garnet, white mica and epidote, and in many cases it is very difficult to balance these reactions given the phases present.

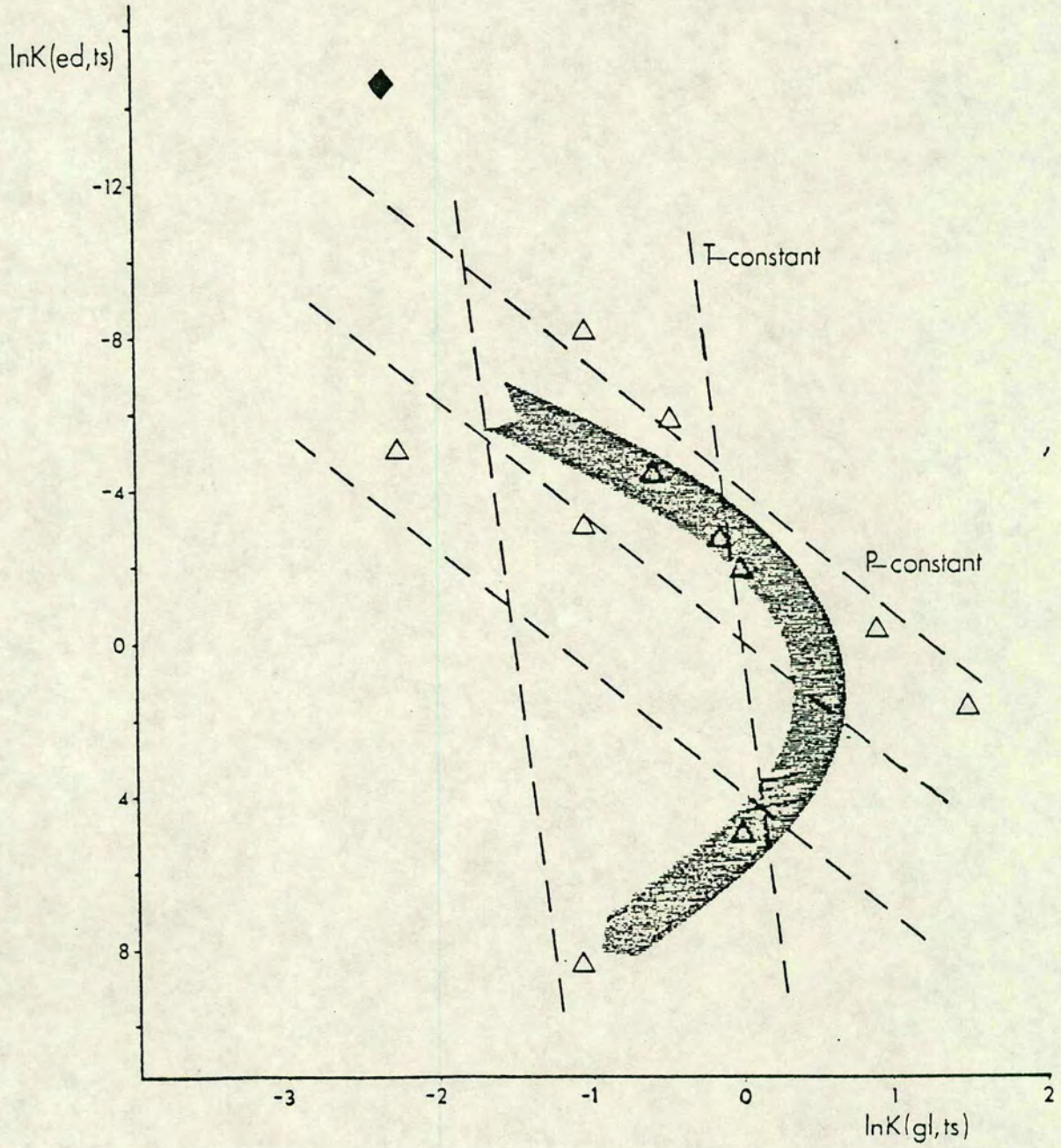

Figure 5.11 Mutual variation of (gl,ts) and (ed,ts) equilibria in the system amphibole-diopside-jadeite-garnet-qtz-H_2O for a zoned amphibole, compared against a sample of glaucophane-eclogite from northern Syros. The shaded arrow gives the direction of zoning (from Ridley 1982, figure 9.15)

Table 5.2

Zoned amphibole analyses from a southern metabasite, 87/21a,

Fe^{3+} was recalculated using RECAMP

		AM8-C	AM8-R	AM11-C	AM11-R	AM17-C	AM17-R	AM20-C	AM20-R
T2	Si	4.000	4.000	4.000	4.000	4.000	4.000	4.000	4.000
T1	Si	3.952	3.845	3.994	3.780	3.964	3.796	3.821	3.812
	Al	0.048	0.155	0.056	0.220	0.036	0.204	0.179	0.188
	Al	1.099	0.153	1.290	0.140	1.060	0.168	1.063	0.152
	Ti	0.004	0.004	0.009	0.007	0.005	0.005	0.001	0.003
M2	Fe^{3+}	0.509	0.274	0.338	0.273	0.603	0.276	0.412	0.291
	Cr	0.000	0.001	0.007	0.000	0.003	0.020	0.008	0.001
	Mg	0.280	1.214	0.247	1.258	0.236	1.182	0.353	1.208
	Fe^{2+}	0.106	0.345	0.107	0.316	0.092	0.343	0.152	0.337
	Mn	0.002	0.009	0.002	0.006	0.001	0.006	0.002	0.008
M1	Mg	2.169	2.332	2.085	2.388	2.148	2.316	2.088	2.334
M3	Fe^{2+}	0.819	0.660	0.903	0.600	0.843	0.672	0.897	0.651
	Mn	0.012	0.016	0.011	0.010	0.009	0.012	0.015	0.015
	Mg	0.056	0.061	0.065	0.063	0.044	0.060	0.082	0.066
M4	Fe^{2+}	0.021	0.019	0.027	0.016	0.016	0.015	0.037	0.016
	Ca	0.152	1.469	0.124	1.525	0.158	1.454	0.301	1.472
	Na	1.771	0.451	1.784	0.396	1.782	0.471	1.580	0.446
A	Na	0.200	0.159	0.130	0.171	0.140	0.175	0.265	0.167
	K	0.000	0.014	0.059	0.022	0.004	0.018	0.000	0.016
	□	0.800	0.826	0.811	0.808	0.856	0.807	0.735	0.817
		a_{gl}=6.82.E-1	a_{gl}=9.76.E-4	a_{gl}=8.53.E-1	a_{gl}=6.20.E-4	a_{gl}=6.76.E-1	a_{gl}=1.17.E-3	a_{gl}=3.63.E-1	a_{gl}=8.97.E-4
		a_{ed}=9.09.E-6	a_{ed}=4.80.E-2	a_{ed}=3.20.E-6	a_{ed}=8.74.E-2	a_{ed}=3.70.E-6	a_{ed}=6.13.E-2	a_{ed}=2.37.E-4	a_{ed}=5.99.E-2
		a_{tr}=3.16.E-4	a_{tr}=6.49.E-1	a_{tr}=1.48.E-4	a_{tr}=7.47.E-1	a_{tr}=2.63.E-4	a_{tr}=5.55.E-1	a_{tr}=1.47.E-3	a_{tr}=6.28.E-1

Figure 5.12 Example of vein controlled regression, from the Ermoupolis metabasite. The vein is predominantly composed of calcite, with some additional chlorite, albite and quartz. Within the pronounced retrogression halo the gl-gnt metabasite is altered to a chl-alb-cc-epid greenstone.

A number of rocks containing secondary calcite also contain a primary carbonate phase, and the textural differences between these two generations of carbonate were discussed in chapter 3. Compositionally, the secondary carbonate is invariably almost pure $CaCO_3$, with only small amounts of Fe, Mg and Mn impurities present. Oxidation of graphite provides a possible source of CO_2 for the secondary calcite. Although graphite is present as inclusion trails in some albite porphyroblasts, it is much less abundant, or absent, from the majority of the greenschists. Also the $\delta^{13}C$ values of carbonate in the greenschists are depleted relative to normal sedimentary values (see chapter 6), supporting such an oxidation process. It should be re-iterated that the presence of calcite does not require a CO_2-rich fluid. Even under moderate pressure conditions (7 kbars), the effect of non-ideal mixing in H_2O-CO_2 fluids is to give high a_{CO2} at low values of X_{CO2}, thus stabilizing carbonate under water-rich conditions.

Carbonate in veins

Calcium carbonate is also an important vein forming mineral. The veins can vary in thickness from a few tens of centimetres down to less than 1mm. Several, though by no means all, of these veins are outlined by a halo of greenschist alteration, a feature which is most commonly observed in metabasites (see figure 5.12). Albite porphyroblasts commonly occur with calcite in these veins. The albite crystals often occur along the vein margin, with the long axis of the albite crystal perpendicular to the vein wall. These greenschist veins cross-cut the rock fabric, but although orientation measurements were made on all the mesoscopic veins observed, no particular preferred orientation was apparent.

Breakdown of jadeitic pyroxene

One of the few reaction textures "frozen-in" in the Syros rocks involves the breakdown of jadeite-acmite pyroxene, and this reaction is expressed below:

Jadeite + 10% acmite + diopside + quartz = albite + aegirine-augite (Dixon 1969)

Where jadeite is preserved it forms porphyroblasts, which are colourless in PPL, and show anomalous blue and brown interference colours. A fringe of albite surrounds the jadeite crystal, and developed along the line of the original pyroxene-quartz boundary are numerous crystals of green aegirine-augite. Figures 5.13a,b show examples of the textures associated with the breakdown of jadeitic pyroxene.

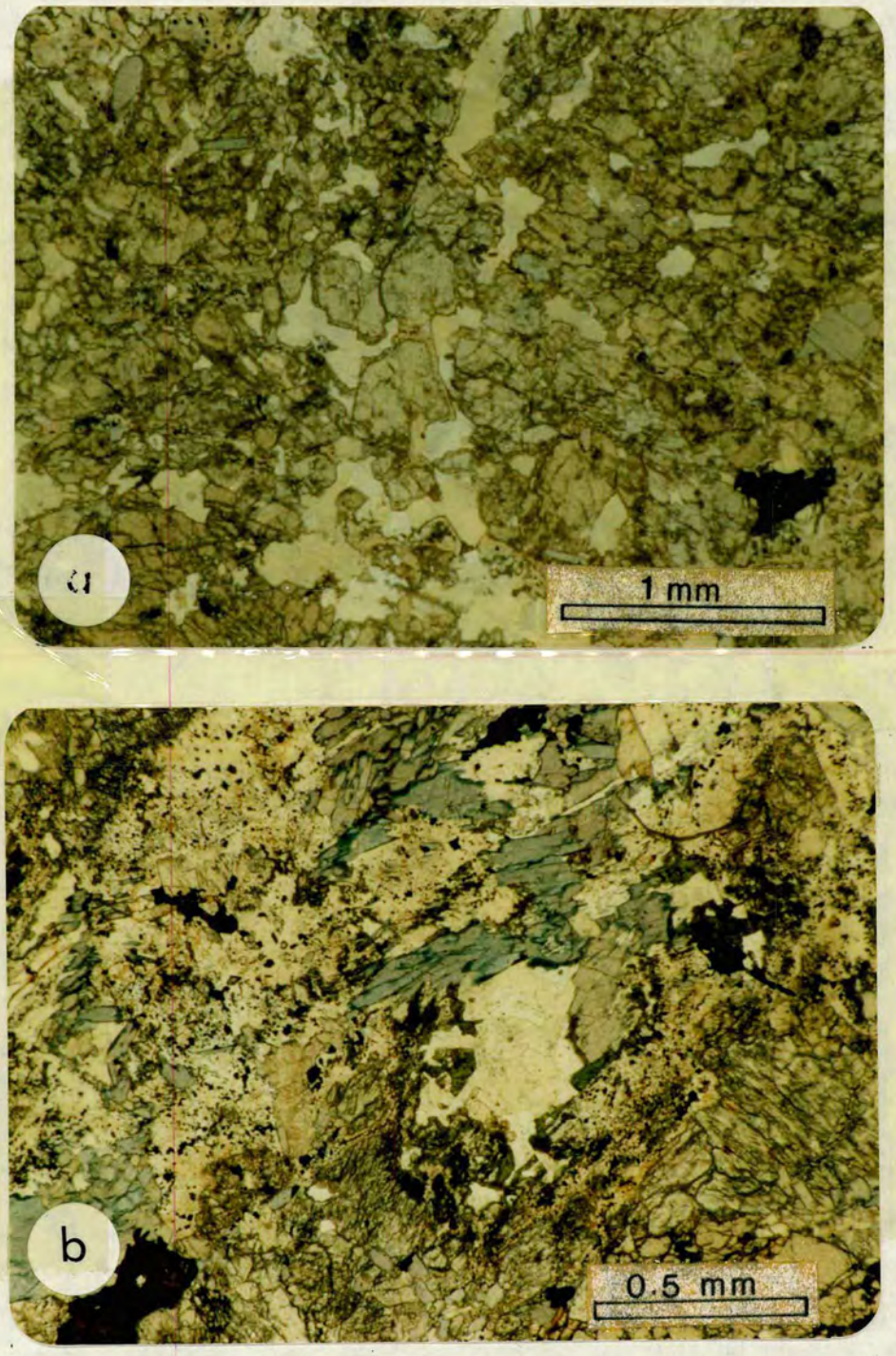

Figure 5.13 a) The jadeite in this rock (86/129) is relatively unaltered. A thin albite rim has developed along jadeite-quartz boundaries. Aegirine-augite is developed at the outer edge of the albite fringe, though it is barely visible in this picture. (x 40, PPL). b) In this example (86/134) the breakdown of jadeite is more advanced. In places jadeite is completely replaced by a symplectic of albite, w. mica and hematite (top left hand corner). Dark green aegirine-augite can be seen in the centre of the photograph, where it has used glaucophane crystals as a nucleation site. Some of the glaucophane has developed strongly coloured riebeckitic rims (x 25, PPL).

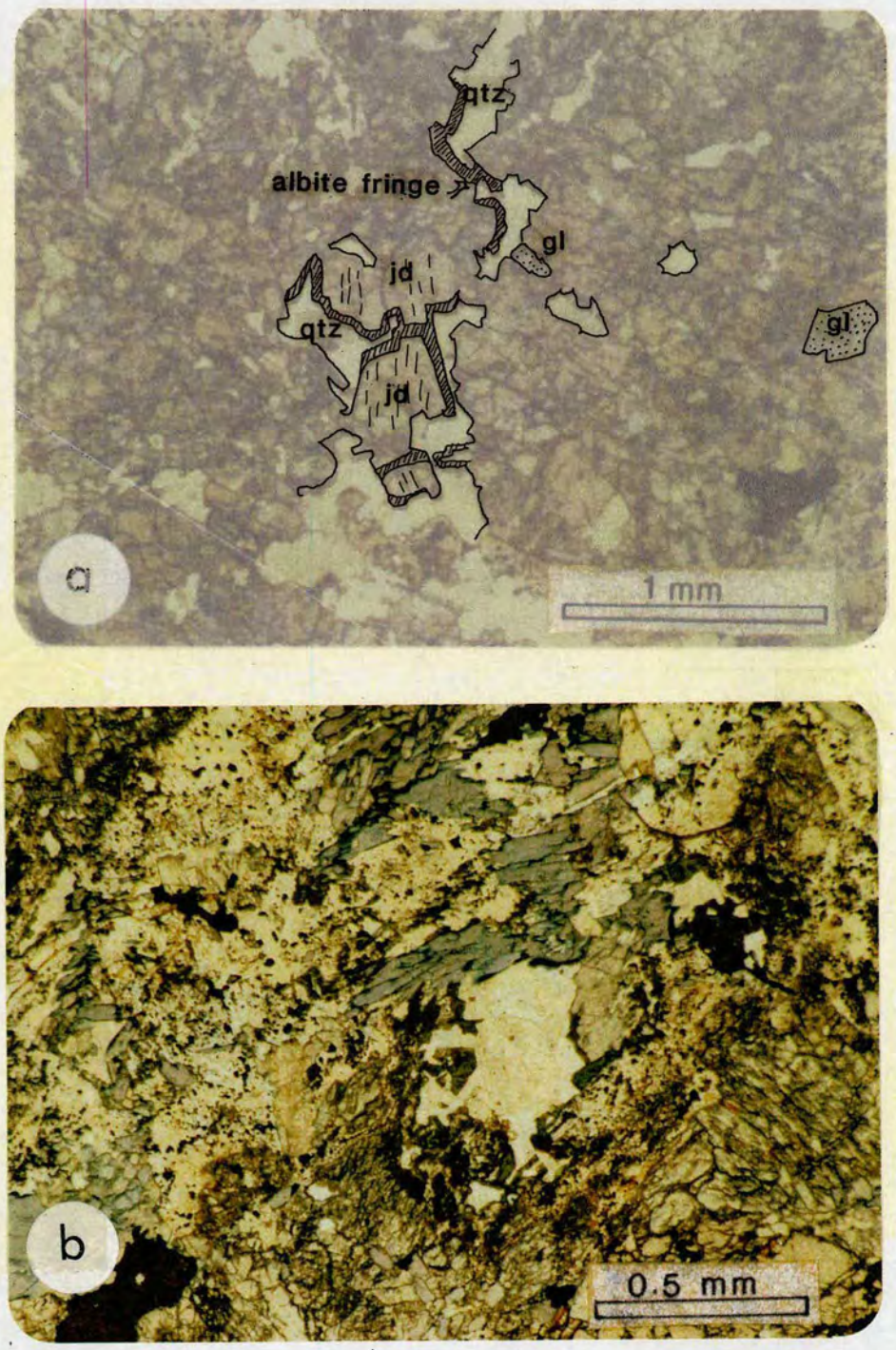

Figure 5.13 a) The jadeite in this rock (86/129) is relatively unaltered. A thin albite rim has developed along jadeite-quartz boundaries. Aegirine-augite is developed at the outer edge of the albite fringe, though it is barely visible in this picture. (x 40, PPL). b) In this example (86/134) the breakdown of jadeite is more advanced. In places jadeite is completely replaced by a symplectic of albite, w. mica and hematite (top left hand corner). Dark green aegirine-augite can be seen in the centre of the photograph, where it has used glaucophane crystals as a nucleation site. Some of the glaucophane has developed strongly coloured riebeckitic rims (x 25, PPL).

Although no probe analyses of the aegirine-augite were made in this study, work by Dixon (1969), showed that this secondary pyroxene has a low jd content, suggesting that the breakdown-reaction occurred at relatively low pressures, probably less than 6 kbars. Where breakdown of the pyroxene has gone to completion, a symplectite of albite, very fine white mica, and hematite often develops in large patches. This texture was only seen in the metabasite at Gria Spilia on the north-west coast of the island. Other phases present in the rock are glaucophane, quartz, garnet, w.mica, epidote and sphene. Dixon (1969) points out that variations in the alteration process, i.e the contemporary albitization of mica, and the substitution of hematite for aegirine-augite, will largely depend on the local activities of particular components in the fluid phase, i.e a_{SiO2}, a_{H2O} and f_{O2}.

Occurrence of sphene

Sphene is a common accessory phase in many of the overprinted rocks, a fact which has important implications for retrograde fluid composition, since it means that the fluid involved was not sufficiently CO_2-rich to cause the breakdown of sphene to rutile + calcite + quartz, (see figure 5.17). Fluid inclusion studies on greenschist samples also suggest that the X_{CO2} of the retrograde fluid was very low. No CO_2 was detected thermometrically, the inclusions examined all being of a two phase aqueous type (see chapter 8).

5.2 CHANGES IN BULK ROCK COMPOSITION ACCOMPANYING THE BLUESCHIST TO GREENSCHIST TRANSFORMATION

Matthews and Schliestedt (1984) examined the blueschist to greenschist transformation on the Cycladic island of Sifnos, some 50 kms south-west of Syros. They performed whole-rock chemical analyses on blueschists and greenschists, and concluded that the greenschist metabasites were significantly enriched in calcium relative to all other rock types. This they suggested indicated the involvement of a CO_2-rich fluid phase in the blueschist to greenschist transformation, and the concomitant development of calcium carbonate in the altered rocks.

Figure 5.14 is reproduced from this paper (Matthews and Schliestedt 1984, fig. 7) and shows the bulk rock compositions of various rock types from Sifnos plotted in an $(Al_2O_3+Fe_2O_3)$-CaO-(FeO+MgO) diagram. It should be noted that the chemical range of the greenschist unit is greatly extended by one analysis, #37, and in fact the majority of the greenschist have bulk chemical compositions not unlike their

blueschist equivalents. Although the greenschists appear to be richer in calcium, this compositional grouping may well have existed prior to alteration. The fact that these Ca-rich metabasites are now greenschists may simply be reflecting the susceptibility of these rocks to alteration. Figure 5.15 is an $(Al_2O_3+Fe_2O_3)$-CaO-(FeO+MgO) diagram illustrating the bulk chemical compositions of blueschist and greenschist rocks from Syros. The plot clearly shows that there is no significant compositional difference between equivalent greenschist and blueschist rocks, and it appears that the development of greenschist facies assemblages has occurred largely without noticeable chemical changes. X.R.F. analyses for all the rocks analysed are presented in Appendix 3.

5.3 P-T-X_{CO2} CONDITIONS ACCOMPANYING THE DEVELOPMENT OF THE GREENSCHIST FACIES ASSEMBLAGES.

The P-T conditions of the greenschist facies event are much harder to characterise than those for the blueschist facies metamorphism. This is largely because the secondary assemblages overprint existing assemblages and truly re-equilibrated greenschist facies rocks are seldom found.

Figure 5.16a is a P-T diagram showing the inferred conditions for the greenschist overprint. The pressure conditions, for this event can vary widely, but there are two definite constraints. The secondary carbonate is calcite not aragonite, and therefore the greenschist overprint must have occurred to the low pressure side of this reaction curve. Similarly, albite is a common phase in the greenschist assemblages and therefore the pressure conditions must lie to the low P side of the albite = jd + qtz curve. Some further P-T constraints can be made by considering the reactions involved in the blueschist to greenschist transformation. In particular the jd contents of the secondary aegirine pyroxenes are consistent with final equilibration pressures of 6 kbars of less. Some degree of temperature constraint is given by isotopic geothermometry. Isotopic temperatures were calculated for three greenschist facies rocks using the method of Javoy *et al.* (1970). The three rocks yielded T estimates of 456 °C, 463 °C and 485 °C. Although the validity of isotope geothermometry as a technique is clouded by some questionable assumptions (see chapter 6), these temperatures provide some constraint.

The sum total of evidence for the P-T conditions of the greenschist overprint is rather underwhelming. However, temperatures of 400-500 °C, and pressures of 5-8 kbars, appear to be the most reasonable estimates for the greenschist facies overprint. Based on the P-T-t modelling of Ridley (1982), the rocks would experience these P-T conditions for some 10 to 15 Ma.

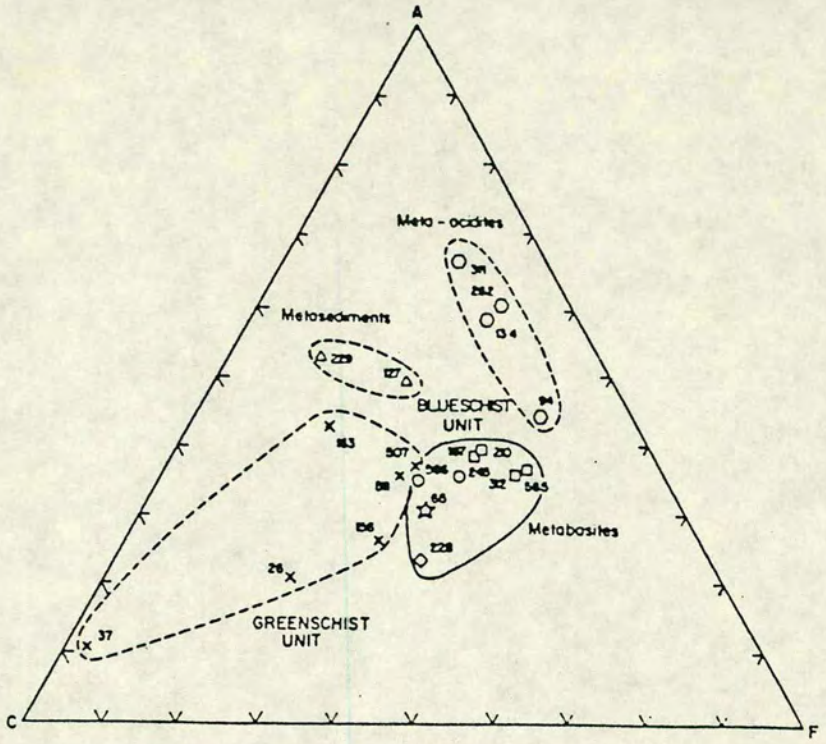

Figure 5.14 ACF plot of greenschist and blueschist rocks from Sifnos (from Matthews and Schliestedt 1984).

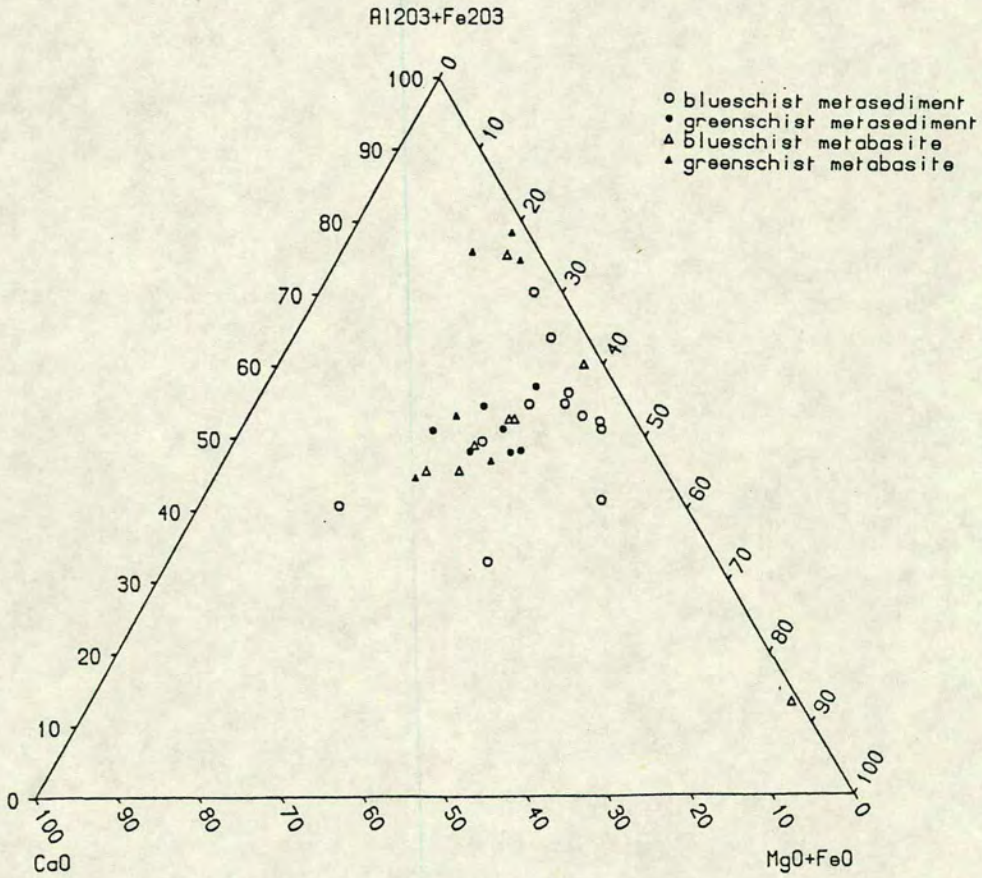

Figure 5.15 ACF plot of blueschist and greenschist rocks from Syros. There is no apparent compositional difference between the two groups.

This raises an important point, as it means the rocks were in the greenschist field for most of their uplift history. It is likely that the rocks have undergone a complex retrogression history, rather than a single event. Recrystallization of the blueschist assemblages may simply have depended on the timing of fluid infiltration.

The stability of sphene in the majority of the greenschists places quite tight constraints on the CO_2 content of the retrograde fluid. Figure 5.17, a T-X_{CO2} section calculated for a pressure of 7 kbars, shows that the maximum CO_2 content of the fluid can only be 2 mol%, a value which is compatible with the results of fluid inclusion work carried out on the greenschists.

Geographical distribution of the greenschist facies rocks

Figure 5.18 shows a simplified geological map of Syros, and the distribution of the greenschist alteration is overlayed on top of this. The data on the distribution of the greenschist facies rocks has been collated from this study and the previous work of Ridley (1982). The overprinting of blueschist assemblages becomes increasingly prominent moving down section towards the south. South of the prominent metabasite unit near Pagos, some overprinting of the blueschist assemblages is the norm, and south of the Nites massif glaucophane is rarely preserved. Almost complete overprinting of the blueschist assemblages was observed along the southern coast at Ormos Akhladhi, Megas Yialos and Komito, though Ridley (1982) reports only weak overprinting further to the east at Vari. In the southern-most peninsula, Mavra Vounakia, recognisably blueschist-facies phases are only preserved as relics, and the greenschist overprint is very strongly developed. The metabasites here are essentially greenstones, consisting largely of epidote, chlorite, albite, actinolite and calcite. However, strongly overprinted pockets do occur much higher in the sequence, at Kastri, Oros Syringas and Sarakinito. At Kini, thick sequences of greyschists are developed, which are largely unaltered, except for the area around the village of Dhanakos, and some thoroughly regressed basic schists along the coast. In places where the greenschist alteration is vein controlled, such as at Ermoupolis and Agkathopes, there are very abrupt contacts between altered greenschist facies rocks and virtually unaltered blueschists.

The role of infiltration in the blueschist to greenschist transformation

The development of the greenschist facies assemblages appears to have occurred in response to the introduction of fluid, i.e fluid infiltration, into the system.

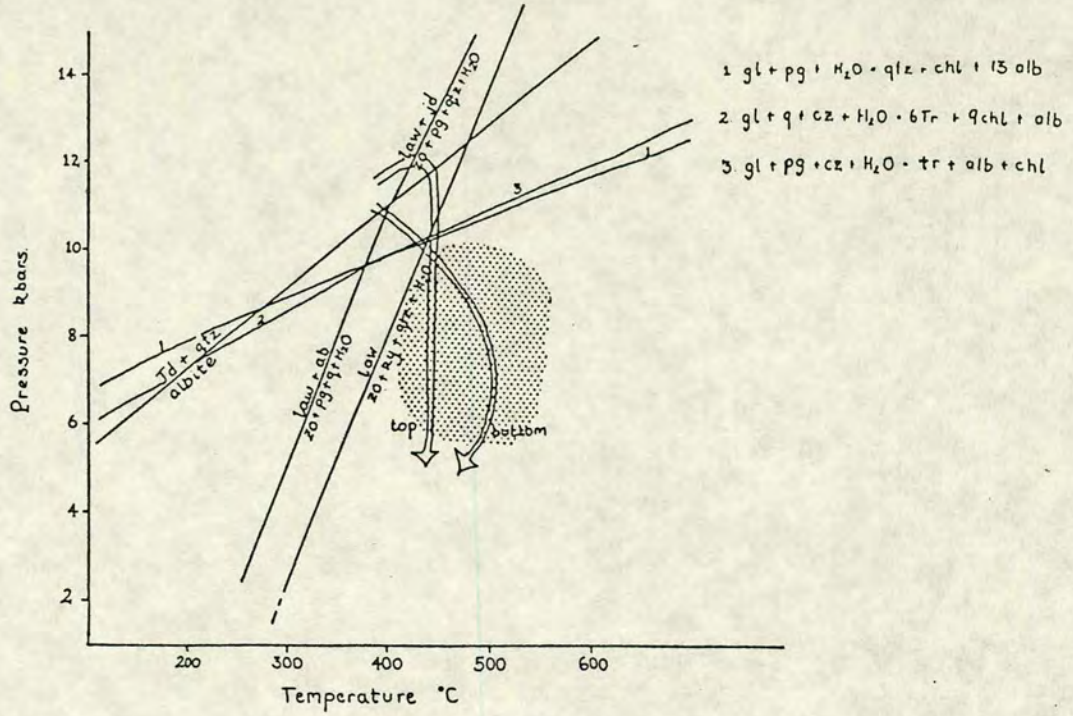

Figure 5.16 P-T plot showing some relevant equilibria for the blueschist to greenschist transformation. The arrows are the P-T-t paths for the top and bottom of the structural section, deduced by Ridley (1982). The shaded area covers the (probable) range P-T conditions associated with the overprint.

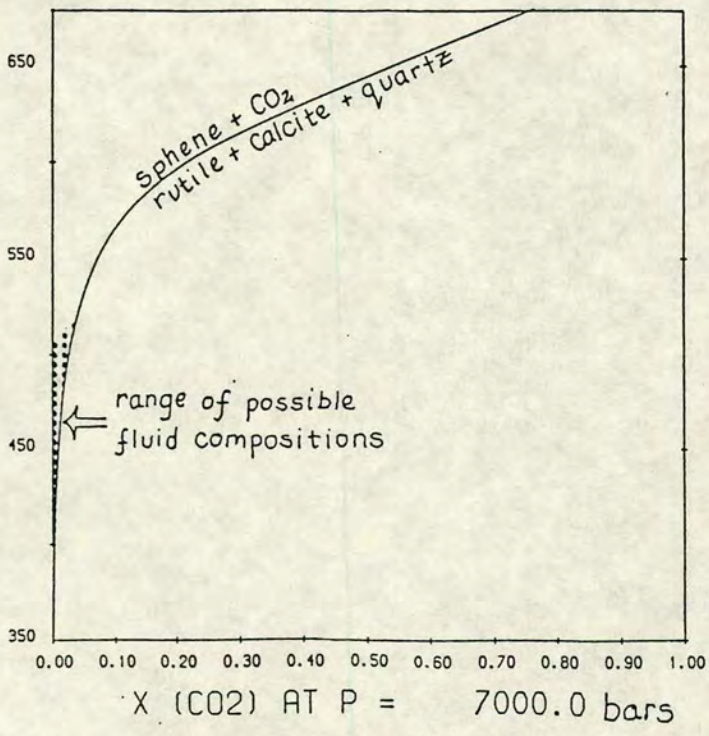

Figure 5.17 T-X(COP_2) plot showing the equilibria sphene + CO_2 = rutile + cc+Q. The shaded region outlines the area of possible fluid compositions for greenschists in equilibrium with sphene, over an assumed T range of 400-500°C. The curve was calculated using the thermodynamic data base of Holland and Powell (pers. comm., July 1988), and a sphene activity of 0.948.

Figure 5.18 Simplified geological map of Syros. The overlay shows the distribution of greenschist facies rocks.

The correlation between fluid infiltration and the occurrence of retrograde alteration is particularly marked in areas where a greenschist "halo" is developed around veins which cut through otherwise unaltered blueschists.

Intuitively it seems logical that the altered rocks should be more hydrated, even if they are stable under approximately the same temperature conditions. The reactions which express the transformation from blueschist to greenschist facies assemblages invariably involve hydration, carbonation or a combination of the two, e.g

$$gl+pg+H_2O = qtz+chl+alb$$

$$gl+qtz+cz+H_2O = trem+chl+alb$$

$$gl+pg+cz+H_2O = trem+alb+chl$$

Thus, the progress of these reactions will be critically dependent on the availability of a fluid phase. X.R.F analyses of the rocks also suggests that the volatile content of the rocks has increased during the greenschist transformation.

The petrographic and chemical evidence suggests that the blueschist to greenschist transformation has occurred as a consequence of fluid infiltration, a conclusion which mirrors the results of Schliestedt and Matthews (1987), examining a similar transformation on the island of Sifnos. Even if the general idea of fluid infiltration is accepted, it is obvious, from the distribution, and variation in intensity of the greenschist overprint alone, that the details of the fluid pathways involved must be very complicated. Walther and Orville (1982) argued that under the conditions of regional metamorphism (P > 3 kbars) fluid flow can only occur in a single-pass manner, upwards towards the surface. However, the occurrence of linear belts of greenschist alteration beneath impermeable marble units suggests that lateral fluid flow can also occur, and structural complications such as folds and faults will also tend to channellize flow. In the thoroughly overprinted areas, such as Mavra Vounakia, fluid flow must have been more or less pervasive, while in others it is definitely channellized along veins and zones of structural weakness.

A question posed by Matthews and Schliestedt (1984), which is also relevant for Syros, is why are the high-pressure blueschist assemblages preserved at all ? In both Syros and Sifnos the most heavily overprinted rocks occur at the bottom of structural section. So, if the infiltrating fluid is moving upwards through the sequence, these rocks will "see" the fluid first. There are two possible reasons which may explain why this fluid did not penetrate the upper levels of the sequence on Syros to the same extent. Firstly, assuming the volume of infiltrating fluid was not greatly in excess of that required to drive hydration and decarbonation reactions, (isotopic evidence suggests that this is the case, see chapter 6), then as the retrograde reactions proceed

so fluid will be absorbed, reducing the volume of potential fluid available for interaction higher in the sequence. Secondly, in the north of Syros two-thirds of the sequence is marble, and it is known from isotopic work undertaken during this and other studies, that pure marbles act as fluid barriers (Rye *et al.* 1976, Valley 1986). Fluid migration may have occurred laterally, along marble-schist contacts, until an upward escape route, such as a fault or fracture, presented itself. Fluid channelling in this manner could allow large volumes of fluid to escape, while incurring minimal alteration to the surrounding rocks. Thus, a combination of diminishing amounts of fluid, and the presence of marble aquitards, probably protected the overlying blueschists from alteration. A similar conclusion was reached by Matthews and Schliestedt (1984).

5.5 SUMMARY

The main points arising from this chapter are summarized below:

1) The blueschist to greenschist transformation occurred in response to the addition of both heat and fluid.

2) Glaucophane-bearing assemblages are replaced by albite, calcite, chlorite, actinolitic amphibole assemblages, stabilized under the greenschist facies conditions.

3) P-T estimates for the greenschist overprint suggest conditions of, T = 400-500 °C, and P = 5-8 kbars.

4) The greenschist retrogression was protracted, consisting of many events, developed over a long period of time, 10-15 Ma.

5) The composition of the retrograde fluid is constrained to water-rich values by the continued stability of sphene in the greenschist rocks.

Isotopic evidence for the involvement of fluid infiltration in the blueschist to greenschist transformation is presented in the following chapter, which discusses the results of the stable isotope study. $\delta^{18}O$ values for greenschist whole-rock, and mineral separates are compared to those for blueschist facies rocks, and an isotopic study of several marble units reinforces the conclusion that these units are relatively impermeable to fluid flow.

CHAPTER 6

STABLE ISOTOPE GEOCHEMISTRY

TABLE OF CONTENTS

6.0 INTRODUCTION

The study of stable isotope geochemistry began in 1947, when Urey suggested that the partitioning of stable isotopes between phases could be used to determine the temperature at which an assemblage of phases had equilibrated. Since then stable isotopes have slowly become an invaluable tool for the metamorphic petrologist. In the context of fluid-rock interaction studies stable isotopes can be used to:

-Evaluate the degree and scale of isotopic equilibrium at the peak of metamorphism, and during retrograde events.

-Examine the scale and mechanisms of fluid flow through rocks.

-Identify potential fluid sources, e.g seawater, meteoric water, magmatic water etc.

-Estimate the amounts of fluid involved, i.e fluid-rock ratios

However it should be emphasized that stable isotope data alone cannot provide a unique interpretation of fluid-rock interactions, and the most definitive studies are those which combine mineralogical, petrological and/or fluid inclusion data with stable isotope work (Garlick and Epstein 1967; Graham *et al.* 1983; Matthews and Schliestedt 1984; Rumble *et al.* 1982; Tracy *et al.* 1983; Wickham and Taylor 1985)

Stable isotope studies of fluid-rock interaction have tended to concentrate on contact metamorphism, and on hydrothermal effects occurring after the emplacement of igneous intrusions. These situations provide tighter geological controls than regional metamorphism, since, in some situations, the same lithologies can be studied both within and outside the limits of the resultant aureole (Bowman and Essene 1982; Rice 1977b; Taylor 1977). Studies on regional metamorphic terrains have concentrated on metacarbonate rocks, largely because the mineral assemblages and the isotopic compositions of these rocks are very sensitive to changing fluid conditions (Ferry 1986, 1983, 1976a; Crawford *et al.* 1979b; Ghent *et al.* 1979; Valley and Essene 1980). The amount of fluid infiltrating the metacarbonates has been estimated using both isotopic and mineralogical evidence, and the apparent fluid-rock ratios are invariably high, up to several rock volumes (Rumble *et al.* 1982; Nabelek *et al.* 1984; Ferry 1984b, 1983b).

Fluid producing reactions occurring within metasediments probably generate a large proportion of any infiltrating fluid, and therefore the interaction of such a fluid with pelitic schists higher in the sequence will not produce dramatic mineralogical changes in the rock. This is because the internal and the external fluid are in approximate equilibrium, both compositionally and isotopically, and evidence for the fluid-rock

interaction may be difficult, or impossible, to detect. In some cases this problem may be resolved by using stable isotopes. For example, it may be possible to detect isotopic homogenisation of a mineral phase across rock layers in a heterogeneous sequence, indicating the interaction of a common, pervasive fluid of fixed isotopic composition. The areas best suited to fluid-rock interaction studies are those with a largely coherent structure, and a range of lithologies, e.g.Maine U.S.A. (Ferry 1976a, 1983a) and the Scottish Dalradian (Graham *et al.* 1983). The island of Syros also meets both these criteria.

The main aims of the isotopic study on Syros are to assess:

-the role of infiltration during blueschist metamorphism.

-the importance of infiltration in the blueschist to greenschist transformation, possible sources for this fluid, and the volume of infiltrating fluid involved.

-the extent and scale of isotopic equilibration and homogenisation in the both the blueschists and the greenschists facies rocks.

-extent to which the marbles have acted as barriers to fluid flow.

Before presenting the results of this study, the general theory behind stable isotope geochemistry will be briefly discussed.

6.1 THEORY AND DEFINITIONS

The following section presents a brief review of the theory behind isotope geochemistry. For a more detailed account, see Fauré (1977), Hoefs (1973) or O'Neil (1977, 1980).

Stable isotope analyses are quoted in terms of a δ value, where δ is defined as;

$$\delta = (R_{sample}/R_{standard} - 1) \times 1000 \quad (‰)$$

In each case, R is the ratio of the heavy to the light isotope.

$$\text{e.g. } R_{sample} = {}^{18}O_{sample}/{}^{16}O_{sample}$$

Sample values are always compared to a standard because differences can be measured more precisely than absolute abundances, and the δ value is a measure of the relative enrichment or depletion of ^{18}O in the sample relative to a standard. There are two internationally accepted reference standards. One is SMOW (Standard Mean Ocean Water) used to report analyses of ^{18}O, and the other is PDB (Pee Dee

Belemnite) used to report ^{13}C analyses. The partitioning of isotopes between pairs of minerals, or between a mineral and a fluid species, is measured by the fractionation factor α, which is expressed as;

$$\alpha_{AB} = R_A/R_B$$

This expression can be rewritten in terms of the δ notation:

$$\alpha_{AB} = \frac{1 + \delta_A/1000}{1 + \delta_B/1000}$$

Taking the natural logarithm of both sides,

$$\ln\alpha_{AB} = \ln(1 + \delta_A/1000) - \ln(1 + \delta_B/1000)$$

As $\delta_A/1000$ is usually less than 1, the following approximation can be used:

$$\ln(1 + \delta_A/1000) \approx \delta_A/1000$$

$$\ln\alpha_{AB} = \delta_A/1000 - \delta_B/1000$$

$$\Rightarrow 1000 \ln\alpha_{AB} = \delta_A - \delta_B$$

$\delta_A - \delta_B$ is termed the per mil fractionation, and can also be written as Δ_{AB}. The last expression can be rewritten as:

$$10^3 \ln\alpha_{AB} \approx \delta_A - \delta_B = \Delta_{AB}$$

Theoretical studies have shown that the isotopic fractionation between mineral pairs is temperature dependent. This conclusion has been borne out by experimental studies and investigations of natural rocks (Friedman and O'Neil 1977). $\ln\alpha$ varies as $1/T^2$ at high temperature, and as $1/T$ at low T. Work by Clayton *et al.* (1975) suggests that this relationship is independent of pressure. The relationship between α and T can be written:

$$1000 \ln\alpha = A(10^6 T^{-2}) + B \quad \text{where A and B are constants}$$

Another consequence of the relationship between $1000 \ln\alpha$ and T is that the isotopic fractionation between minerals should decrease with increasing T. As T increases $1/T^2 \rightarrow 0$, and $10^3 \ln\alpha \rightarrow B$. Many studies of regional metamorphism have been able to show quite convincingly that isotopic fractionation decreases more or less in step with increasing metamorphic grade (Black 1974a; O'Neil & Ghent 1975; Rye *et al.* 1976).

6.2 MODELS OF FLUID-ROCK INTERACTION

This section will consider several different models of fluid-rock interaction, assessing their potential to change the isotopic composition of a rock and its constituent minerals.

Prograde metamorphism is usually accompanied by devolatilisation. Walther and Orville (1982) estimate that 2 moles of H_2O-CO_2 fluid are lost during the progressive metamorphism of one kilogram of pelite. This fluid must leave the rock, partly because it is considerably less dense than the surrounding rock, and partly because the porosity of metamorphic rocks at depth is so small that instantaneous fluid rock ratios cannot exceed $\approx$ 0.01(Wood and Walther 1986). The loss of fluid from the system will affect the isotopic composition of the residual rock because ^{18}O is preferentially partitioned into the fluid, leaving the rock depleted in the heavy isotope (Valley 1986). However, several studies have shown that the potential of internal devolatilisation reactions to produce shifts in the $\delta^{18}O$ values of minerals and whole rocks is very small (Früh-Green 1987; Rumble 1982; Valley 1986). Rocks can also undergo isotopic exchange with an infiltrating fluid derived from an external reservoir. The ability of an infiltrating fluid to change the $\delta^{18}O$ values of the minerals, and hence the rock, is dependent on several factors;

1)The difference between the initial $\delta^{18}O$ of the rock and the $\delta^{18}O$ of the fluid

If $\delta^{18}O_r$ is very different from $\delta^{18}O_f$, then a small amount of fluid can have a dramatic effect on the isotopic compostion of the rock, whereas if the two are initially very similar in composition, $\delta^{18}O_r \approx \delta^{18}O_f$, then a large volume of fluid would be required to produce any measurable change in the isotopic compostion of the rock.

2) The volume of infiltrating fluid available, i.e the fluid-rock ratio.

3) The nature of fluid-flow, i.e whether the flow is channellized or pervasive through the rock.

Given suitable conditions, an infiltrating fluid can produce dramatic shifts in the $\delta^{18}O$ values of rocks and minerals.

In practice infiltration will often occur concurrently with devolatilization. A volume decrease commonly accompanies devolatilization reactions, and this increases the rock permeability, opening it up to infiltrating fluids (Rumble and Spear 1983).

6.3 STABLE ISOTOPE DATA - CARBONATES

In this section oxygen and carbon isotope analyses are presented for carbonates present in the marble units, schists and metabasites.

Analytical techniques

All weathered surfaces were removed, and the cleaned samples were ground in a TEMA mill for between 30-60 seconds. X-ray diffraction analysis (X.R.D) was carried out to establish the compostions of the carbonate. If the subordinate phase (usually dolomite) comprised more than 10% of the total carbonate then both calcite, and dolomite were analysed using the chemical separation technique outlined in Walters *et al.* (1972). The CO_2 was liberated under vacuum by reaction with concentrated H_3PO_4 at 25°C (McCrea 1950; Sharma and Clayton 1965). The purified gas was then analysed on a V.G. Isogas SIRA 10 mass spectrometer at the Scottish Universities Reasearch and Reactor centre (SURRC) East KIlbride. The mass spectrometer working standard was calibrated regularly using NBS 20, (Solenhofen limestone), and one duplicate analysis was made with each batch of six samples. The results are presented in the δ notation relative to SMOW and PDB. The analytical precision is $\pm$ 0.2‰.

6.4 THE MARBLES

Tables 6.1 and 6.2 present the $\delta^{18}O$ and $\delta^{13}C$ values for the pure and impure marbles collected from various localites around the island. The results are represented graphically in figures 6.1 and 6.2. The samples have been divided into two geographical groups, northern and southern Syros, and this division is more or less in agreement with a split of the island into blueschist and greenschist facies rocks. The dividing line is taken from Kini on the west coast to Ermoupolis on the east.

It is important to establish a possible premetamorphic range of isotopic compositions for the marbles, before considering whether these values have been preserved or not. The $\delta^{18}O$ values of marine limestones have varied through time, with $\delta^{18}O$ contents generally increasing with decreasing age (Hoefs 1973). $\delta^{18}O$ values for the majority of Tertiary carbonates fall within the range 25-30‰, while the $\delta^{13}C$ of marine limestones has fluctuated between -1 and +4‰ during Phanerozoic time (Keith and Weber 1964). Examining figures 6.1 and 6.2, the majority of pure marbles from northern Syros appear to retain their pre-metamorphic compositions. $\delta^{18}O$ ranges from 23.8-29.1‰, and δ13C from 1.2 to 3.4‰.

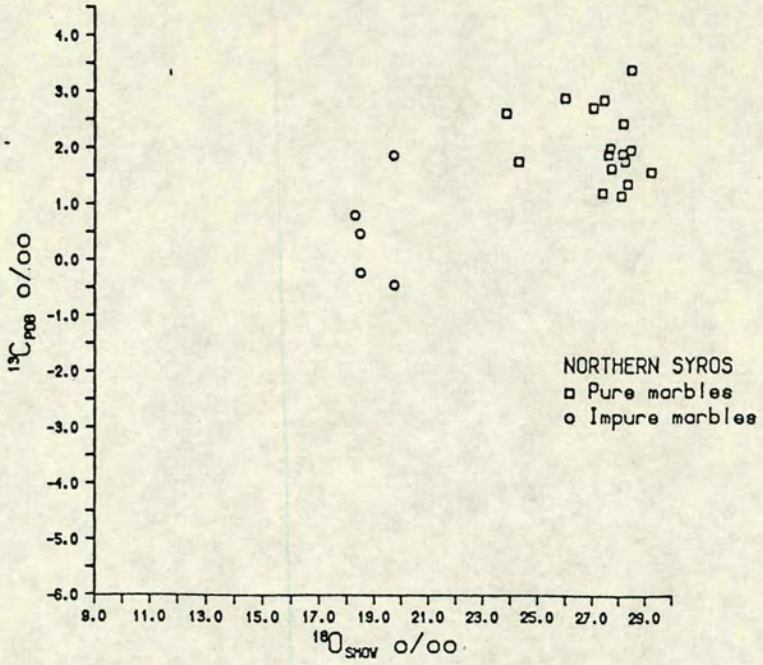

Figure 6.1 Plot of $\delta^{18}O$ versus $\delta^{13}C$ for calcite in marbles from northern Syros. The range of $\delta^{18}O$ and $\delta^{13}C$ values for the pure marbles is the same as that for unmetamorphosed limestones of approximately the same age (Hoefs 1973). The impure marbles are depleted in ^{18}O and ^{13}C, probably due to loss of isotopically enriched CO_2 via decarbonation reactions.

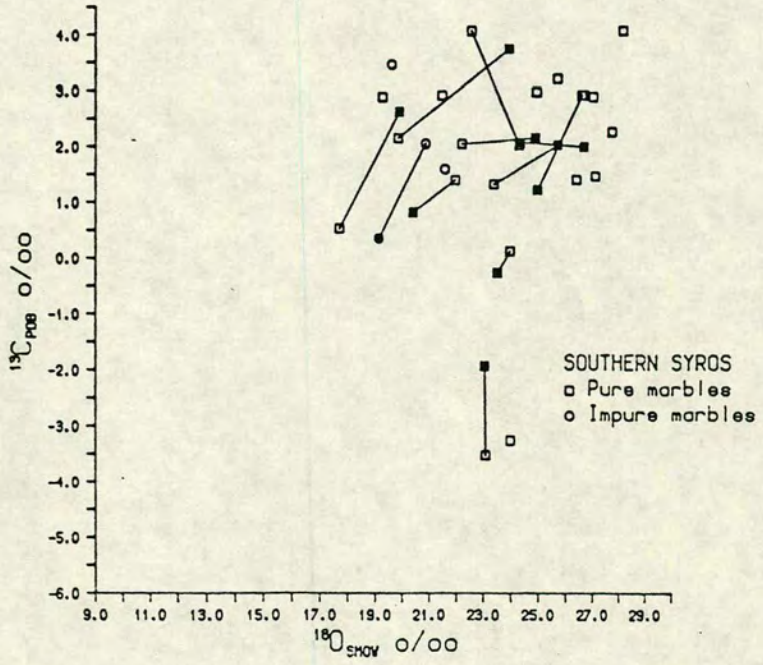

Figure 6.2 Plot of $\delta^{18}O$ versus $\delta^{13}C$ for calcite and dolomite in marbles from southern Syros. Shaded symbols refer to dolomite, and tie-lines connect analyses from the same sample.

Table 6.1 Oxygen and carbon isotope analyses of carbonate from pure and impure marbles northern Syros.

Sample No	Location	$\delta^{18}O_{SMOW}$	$\delta^{13}C_{PDB}$
Pure marbles	Oros Syringas		
86/179	centre of marble	28.31	1.39
86/180	marble/schist contact	27.42	2.89
86/182	marble/schist contact	27.00	2.75
86/183	centre of marble	27.66	2.02
86/184	marble/schist contact	27.36	1.22
86/185	marble lense in schist	27.58	1.91
86/186	marble/schist contact	28.15	2.47
86/187	centre of marble	29.20	1.60
86/188	marble/schist contact	28.21	1.79
	Traverse 2, 500m spacing		
86/190	marble/schist contact	27.69	1.66
86/192	marble lense in schist	25.96	2.92
86/194	marble/schist contact	28.47	3.42
86/195	centre of marble	28.11	1.92
86/196	marble/schist contact	28.07	1.17
86/198	centre of marble	28.43	1.99
	Kastri, N W coast		
86/4	6m from contact	24.28	1.78
86/5	marble/schist contact	23.83	2.64
Impure marbles			
86/6	Kastri	18.26	0.81
86/75	Aspro	19.68	1.89
87/253IP	O. Grammata	19.71	-0.44
87/253P	O. Grammata	19.68	1.89
86/67	Aspro	18.44	0.48

Table 6.2 Oxygen and carbon isotope analyses of carbonate from pure and impure marbles, southern Syros. Dolomite values have been corrected using the acid fractionation factor of Sharma and Clayton (1965).

Sample No.	Location	$\delta^{18}O_{smow}$	$\delta^{13}C_{pdb}$
Pure Marbles	Nites		
87/48	marble/schist contact	24.95	2.99
87/49	centre of marble	28.16	4.10
87/50	marble/schist contact	26.40	1.40
87/15	O. Akhladhi	19.28	2.89
87/153	Agkathopes-contact	27.71	3.23

Pure marbles, some with Cc. and dol.

Sample No.	Location	$\delta^{18}O$ calcite	$\delta^{18}O$ dolomite	$\delta^{13}C$ calcite	$\delta^{13}C$ dolomite	calcite %
	Nites					
87/68	centre	27.04		2.91		100
67/69	marble/schist contact	26.69		2.94		100
87/70	"	26.60	24.97	2.94	1.22	85
87/71	"	24.36	26.68	2.09	2.00	80
87/74	4m from marble base	27.11	-	1.47		100
87/75	10 from m/s contact	27·76	[illegible]	2.28		100
87.73	marble base	-	23.18	-	-6.67	6
87/118	O. Akhladhi	22.22	24.90	2.06	2.16	64
87/119	"	22.56	24.32	4.09	2.03	61
87/120	"	23.38	25.72	1.32	2.04	72
87/121	"	20.42	21.97	0.82	1.40	76
87/124	"	19.36	23.93	0.76	3.46	85
87/125	"	19.86	23.94	2.15	3.76	85
87/126	brecciated layer	21.47	-	2.93		100
87/127	"	23.08	23.05	-3.5	-1.93	68
87/128	marble/schist contact	17.70	19.92	0.54	2.64	22
Impure Marbles						
87/116	marble/schist contact	20.87	19.14	2.06	0.35	85
87/20	O. Akhladhi	19.62	-	3.47	-	100
HQ1	Vari	21.58	-	1.60	-	100

With the exception of samples 86/4 ($\delta^{18}O$=24.3) and 86/5 ($\delta^{18}O$=23.8) the pure marbles all lie within the given range for Tertiary marine limestones. In contrast the $\delta^{18}O$ values for the southern pure marbles show a much greater spread, from 17.7 to 28.1‰. Although the plot is complicated by coexisting cc-dol pairs in some of the marble units, it is apparent that a number of the southern marble units are depleted in ^{18}O relative to their unmetamorphosed counterparts and the majority of the northern marbles. $\delta^{13}C$ analyses also show more scatter (4.0-0.1‰) and two samples, 87/73 and 87/127, have negative values of $\delta^{13}C$.

$\delta^{18}O$ variations in the marbles - evidence for the mechanisms of oxygen isotope exchange.

Although figures 6.1 and 6.2 indicate the general $^{18}O/^{13}C$ field in which the marbles plot, a more informative way to display this data is to examine variations in $\delta^{18}O$ and $\delta^{13}C$ as a function of distance through the marble units. On Syros the marble bands were sampled perpendicular to the strike, at true measured distances away from the nearest marble-schist contact. Each band was sampled in three places, at the upper and lower contacts, next to the schist units, and in the centre of the marble. Figures 6.3 and 6.4 show a number of these traverses made through units of differing thickness in both northern and southern Syros. A number of the traverses, particularly those from southern Syros, show a hump-shaped isotopic profile. The margins of the marble are depleted in ^{18}O, while the interiors of the marbles retain $\delta^{18}O$ values close to those for unmetamorphosed limestones. Similar profiles were produced by Rye *et al.* (1976) for marbles on Naxos.

The simplest way to explain these profiles is to suggest that the $\delta^{18}O$ variations were produced during diagenesis, and have been preserved during metamorphism. However, isotope studies on modern carbonates do not reveal similar profiles (Dr. J. Andrews pers comm 1988) and therefore some other process, or processes, must be involved. It can be assumed that prior to metamorphism the marbles were isotopically homogeneous, with $\delta^{18}O$ values somewhere in the range for Mesozoic carbonates. The interiors of the northern marble units on Syros suggest values of around 27‰. The ^{18}O depletions in the marble margins could have occurred by two main mechanisms:

1) Decarbonation reactions.

2) O isotope exchange.

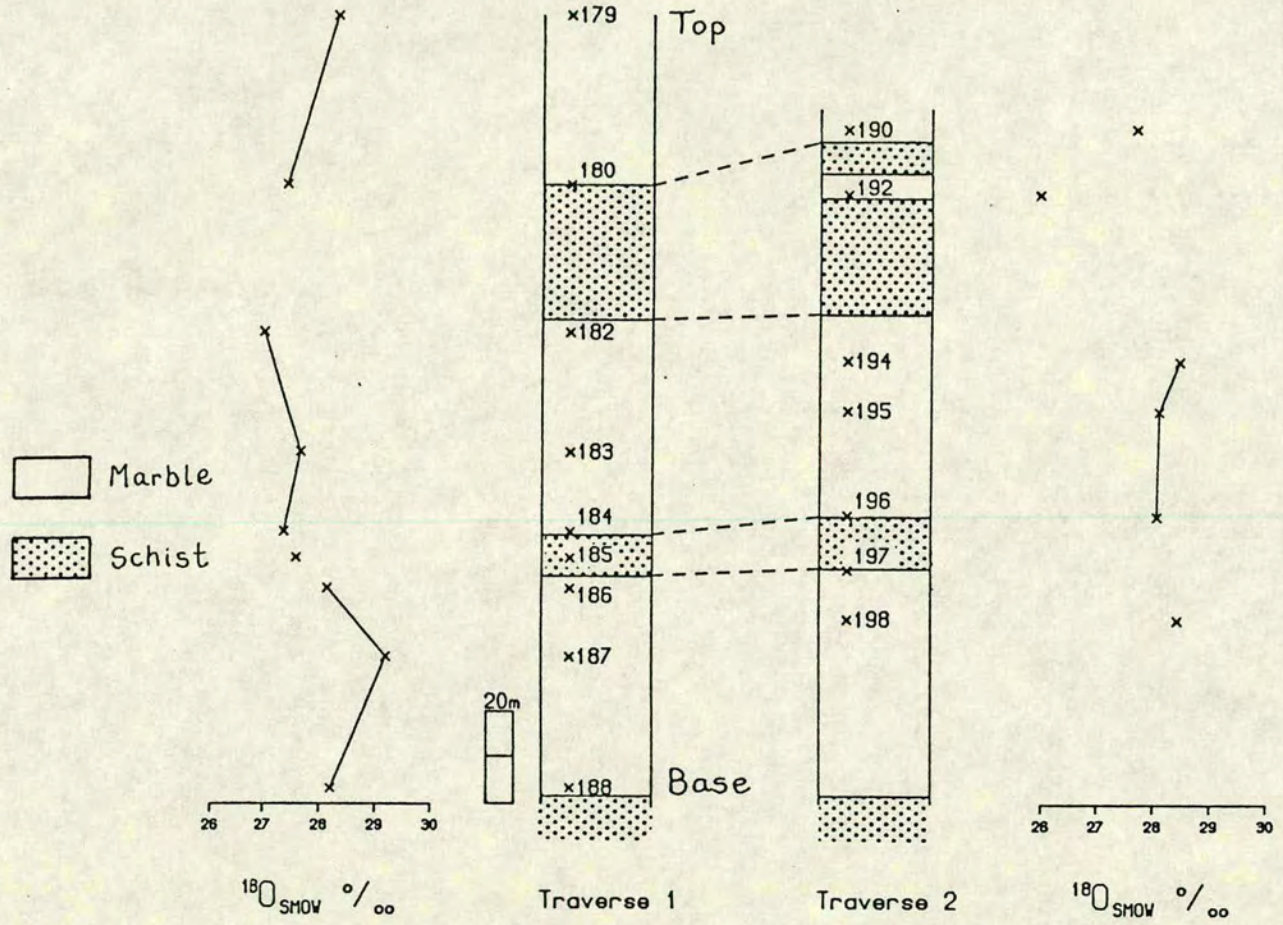

Figure 6.3 $\delta^{18}O$ data from a mixed marble-schist sequence at Oros Syringas, northern Syros. The marble units are separated by schists, and the base of the marble overlies a major schist unit. The numbers refer to sample numbers given in table 6.1. Lines connect analyses from the same unit. The sequence was sampled along two traverses 50 metres apart.

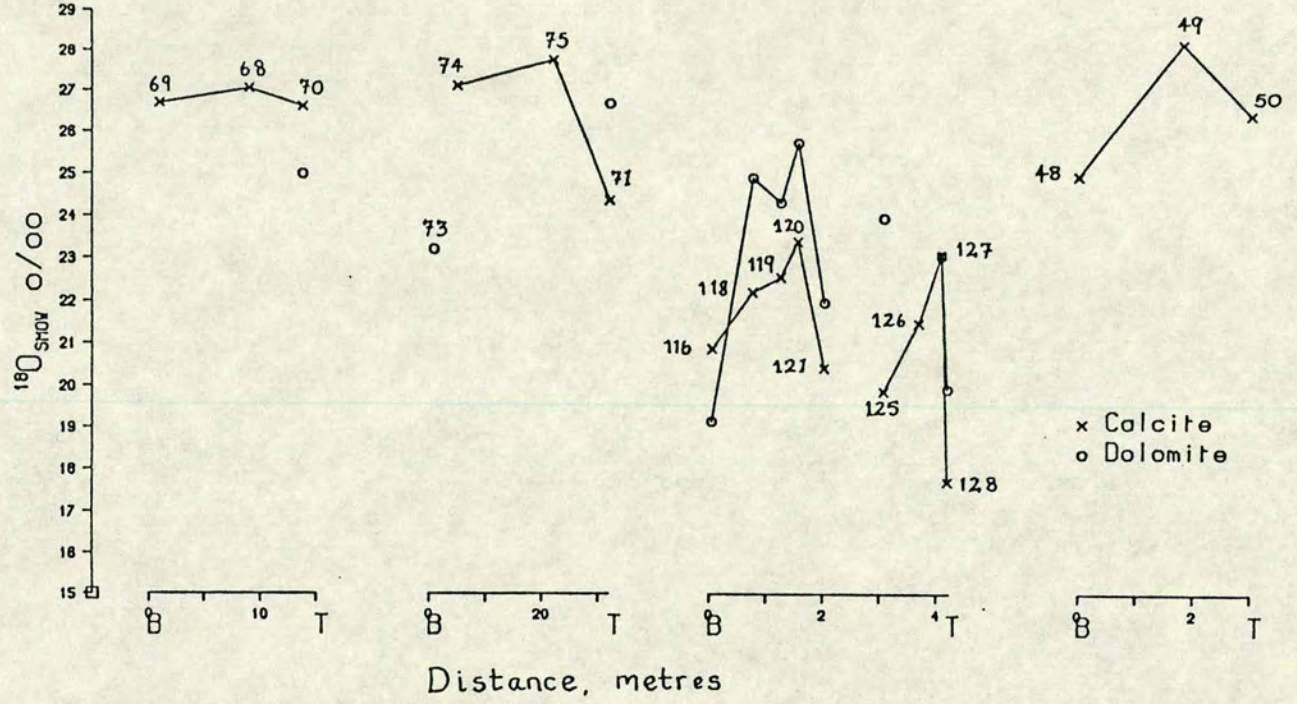

Figure 6.4 $\delta^{18}O$ variations across marble units in southern Syros. All the marbles have upper and lower contacts with schist. T and B stand for the top and bottom of the marble unit respectively. Numbers refer to sample numbers. (see table 6.2).

^{18}O depletion is associated with the formation of calc-silicate minerals (Valley 1986; Nabelek *et al.* 1984). However, the substantial loss of ^{18}O via calc-silicate producing reactions is unlikely to have been an important process on Syros because the the majority of the marbles are pure, with silicate phases composing less than 5% of the rock on average.

The ^{18}O depletions are interpreted to be the result of oxygen transport through the rocks. However, a variety of O-exchange mechanisms are possible:

- Solid state diffusion, involving O diffusion through silicate minerals or along grain boundaries.

- Diffusion through a static intergranular pore fluid.

- Active flow of an oxygen-bearing fluid through interconnected pores.

In practice a combination of these different processes may be operating.

The ^{18}O variations seen at marble/schist contacts can provide some evidence for the mechanisms of oxygen transport (Bickle and McKenzie 1987; Nagy and Parmentier 1982). Figure 6.5 (a-c) is taken from a paper by Nagy and Parmentier (1982), and shows the variation of a concentration parameter, c, across an exchange zone. Although these examples were developed to model the contact between an intrusive body and the surrounding metasediments, the profiles may be compared to the isotopic variations measured across marble/schist contacts. Examples (b) and (c) of figure 6.5 appear to match the isotope variations seen in the Syros marbles more exactly However, in general the marble bands on Syros have not been sampled in sufficient detail, particularly next to the contact zone, to define the exact form of the isotopic variations across them.

The observed width of the exchange zone, i.e the width over which $\delta^{18}O$ variations are observed, can provide some measure of the bulk oxygen diffusivity in the rock. Examining the oxygen isotope exchange at the contact between the igneous body and the surrounding host rocks, Nagy and Parmentier (1982) calculated the magnitude of oxygen diffusivity required to produce the observed 60cm wide exchange zone. They found that solid state diffusion (whether within minerals or along grain boundaries) was four or five orders of magnitude too slow to explain the width of the exchange zone, and instead they proposed that oxygen diffusion must have occurred through the medium of an intergranular aqueous fluid. $\delta^{18}O$ depletions in marble units from Syros are seen to occur over distances of at least 1 metre, and the areal extent of these effects points to the involvement of some sort of fluid phase. The question is whether this fluid is static, or moving relative to the surrounding rocks.

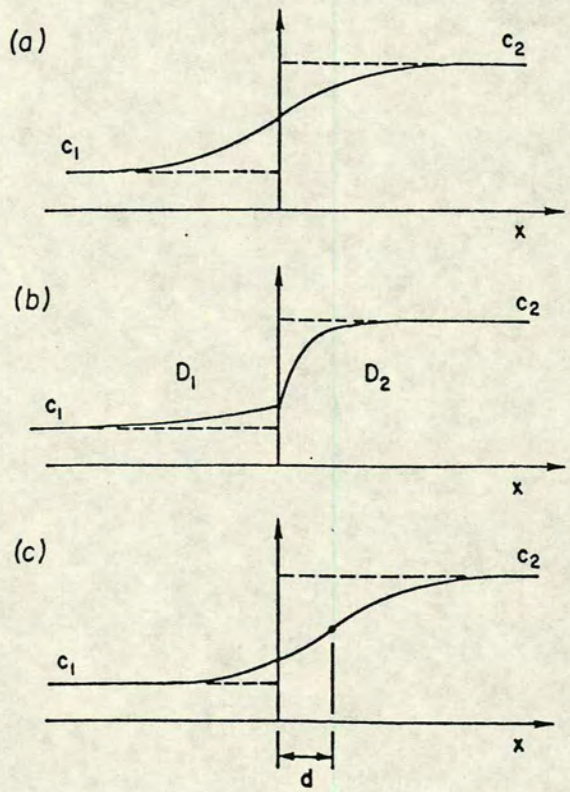

Figure 6.5 Variation of concentration, C, across an exchange zone at the contact of intrusive and host rock, with initial concentrations C_1 and C_2 respectively. (a) antisymmetric exchange zone formed by diffusion, with the same diffusivity in intrusive and host rock. (b) Asymmetric exchange zone due to larger diffusivity in intrusion than in host rock. (c) Asymmetric exchange zone due to fluid flow across intrusive/host rock contact. (from Nagy and Parmentier 1982, fig. 3).

It should be noted that fluid flow is only possible when a connected network of pores exists, at least transiently. The geometry of the fluid network is controlled by the dihedral angle, and if the dihedral angle, Θ, between two solid grains and the fluid is less than 60^{o}, then the fluid network will remain interconnected no matter how small the fluid fraction may be (Hunter 1987). Because a fluid phase is no longer present in the rocks, it is not possible to measure Θ directly from thin-section observations. However, for the sake of this discussion it will be assumed that fluid flow is possible.

The distinction between advective (fluid flow) and diffusive transport of oxygen isotopes was discussed by Bickle and McKenzie (1987). Bickle and McKenzie (1987) present non-dimensional solutions to the differential equations which express the one-dimensional transport of heat and/or matter through a rock layer. The solutions to these equations allow a distinction to be made between regimes of advective or diffusive transport of heat/matter. When the Peclet number, Pe, a dimensionless constant which describes the transport characteristics of heat or matter, is small, diffusion dominates the transport regime, but as the Peclet number increases so advection becomes important. They calculated the analytical solutions to the different equations for three concentration models. Figure 6.6 a-c is taken from Bickle and McKenzie (1987), and illustrates one type of concentration model, where the concentration (or temperature) is set to zero on both the layer boundaries. In the example shown the variation of dimensionless concentration, c', is plotted against dimensionless distance, z'. Initially concentration behaviour is dominated by diffusion (symmetric profiles), but as the Peclet number increases, so advection becomes more important, and an asymmetric profile is produced.

Although these diagrams were calculated theoretically, their application to isotope studies is clear. If consistent asymmetry is detected in $\delta^{18}O$ profiles through marble bands, then flow of an oxygen bearing fluid (advection) must have occurred in addition to diffusion. Bickle and McKenzie (1987) applied the solution of these equations to describe the $\delta^{18}O$ profiles measured on marble units from the island of Naxos. As was shown by Rye *et al.* (1976) isotopic profiles through the marble bands show asymmetric $\delta^{18}O$ distributions, with the largest ^{18}O depletions being found at the lower marble-schist contacts. Bickle and McKenzie concluded that the observed asymmetry was consistent with a combination of diffusive and advective transport of ^{18}O. Although the sampling on Syros is not detailed enough, the isotopic profiles through the marbles do not appear to be symmetrical in the majority of cases, and it is felt that the profiles are probably the result of both advective and diffusive oxygen exchange.

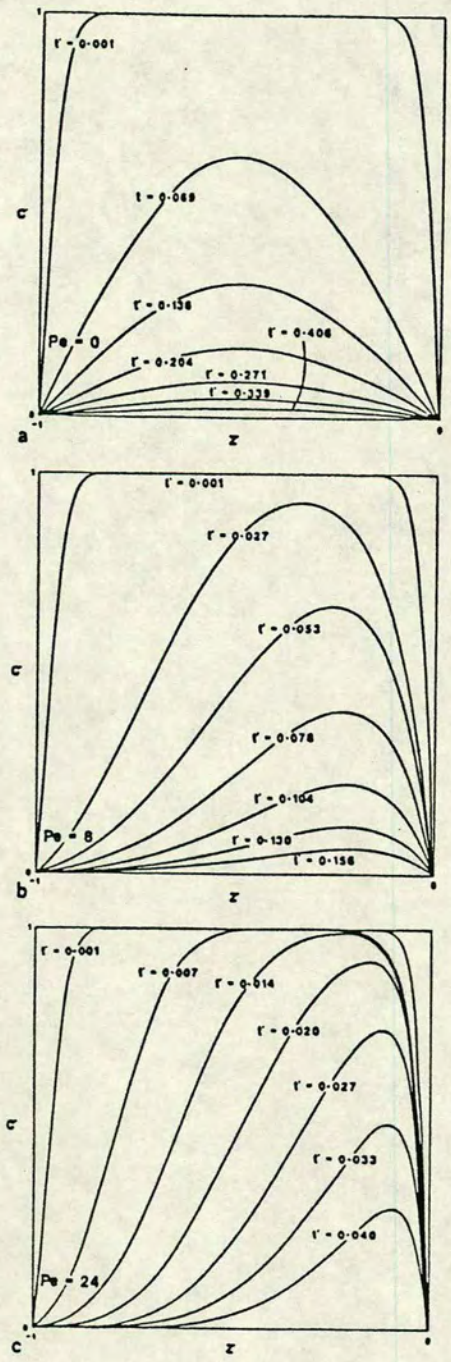

Figure 6.6 Variation of dimensionless concentration C^1 (Or temperature) plotted against dimensionless distance z^1 for a layer with initial concentration $C^1 = 1$ everywhere, and concentration $C^1 = O$ on the boundaries at $z^1 = -1$. $z+1 = O$ for all time (from Bickle and McKenzie 1987, fig. 5).

However, this may not be the case at every locality, in the northern marbles ^{18}O depletions are much less marked, with the margins having values only 1 or 2 per mil lighter than the interiors, and this may indicate that diffusive exchange alone was the dominant process.

Carbon isotopes in the marbles

Variations in $\delta^{13}C$ also occur, and figures 6.7 and 6.8 show the distribution of $\delta^{13}C$ in the same marble profiles considered in the previous section.

The carbon isotopes tend to correlate with the profiles seen in $\delta^{18}O$, with enriched values in the marble interiors, and lighter values at the margins. However, in general the values of $\delta^{13}C$ still lie within the range for unaltered Mesozoic limestones, 0-+4‰ (Keith and Weber 1964), and it is difficult to pinpoint a specific pre-metamorphic value to use as a bench mark. The marbles themselves represent the single largest source of carbon on the island, and there are only three potential ways to alter the $\delta^{13}C$ values of these marbles.

1) Decarbonation reactions within the marble.

2) Exchange with graphite.

3)Exchange with CO_2, derived from decarbonation reactions, or from deep seated sources.

The loss of isotopically heavy CO_2, enriched in both ^{18}O and ^{13}C, during decarbonation reactions would result in depletion of ^{18}O and ^{13}C in the residual marbles (Deines and Gold 1969; Valley 1986). However, as has been previously mentioned, the marbles are essentially pure, containing only small amounts of silicate phases, and the scope for alteration of the ^{13}C signature by decarbonation reactions is therefore small. Although graphite is present in the schists, it is not seen in any of the marbles, and therefore direct exchange between carbonate and graphite cannot have occurred. Oxidation of graphite in the schists would produce CO_2 with a very light $\delta^{13}C$ signature. Such light carbon is far removed from the isotopic range of $\delta^{13}C$ found in marbles, and therefore even small amounts of this isotopically light CO_2 could affect the $\delta^{13}C$ values of the marbles. However, the degree and extent of carbon isotope exchange depends to a large extent on the CO_2/H_2O ratio of the fluid. In chapters 4 and 5, it was shown that both the blueschist and greenschist assemblages are in equilibrium with a CO_2-poor fluid.

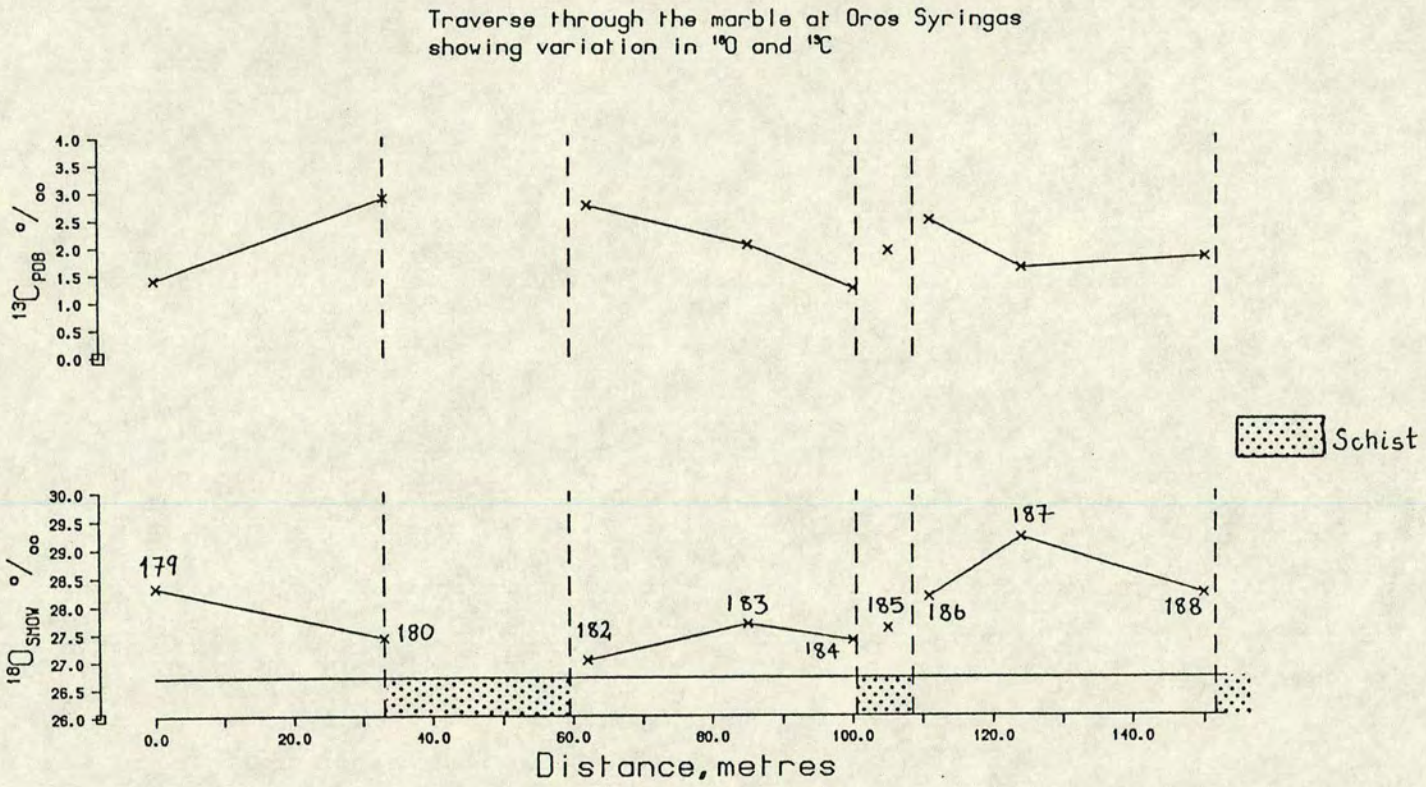

Figure 6.7 Oxygen and carbon isotopic compositions of calcite from traverse 1 at Oros Syringas, northern Syros. (see fig. 6.3)

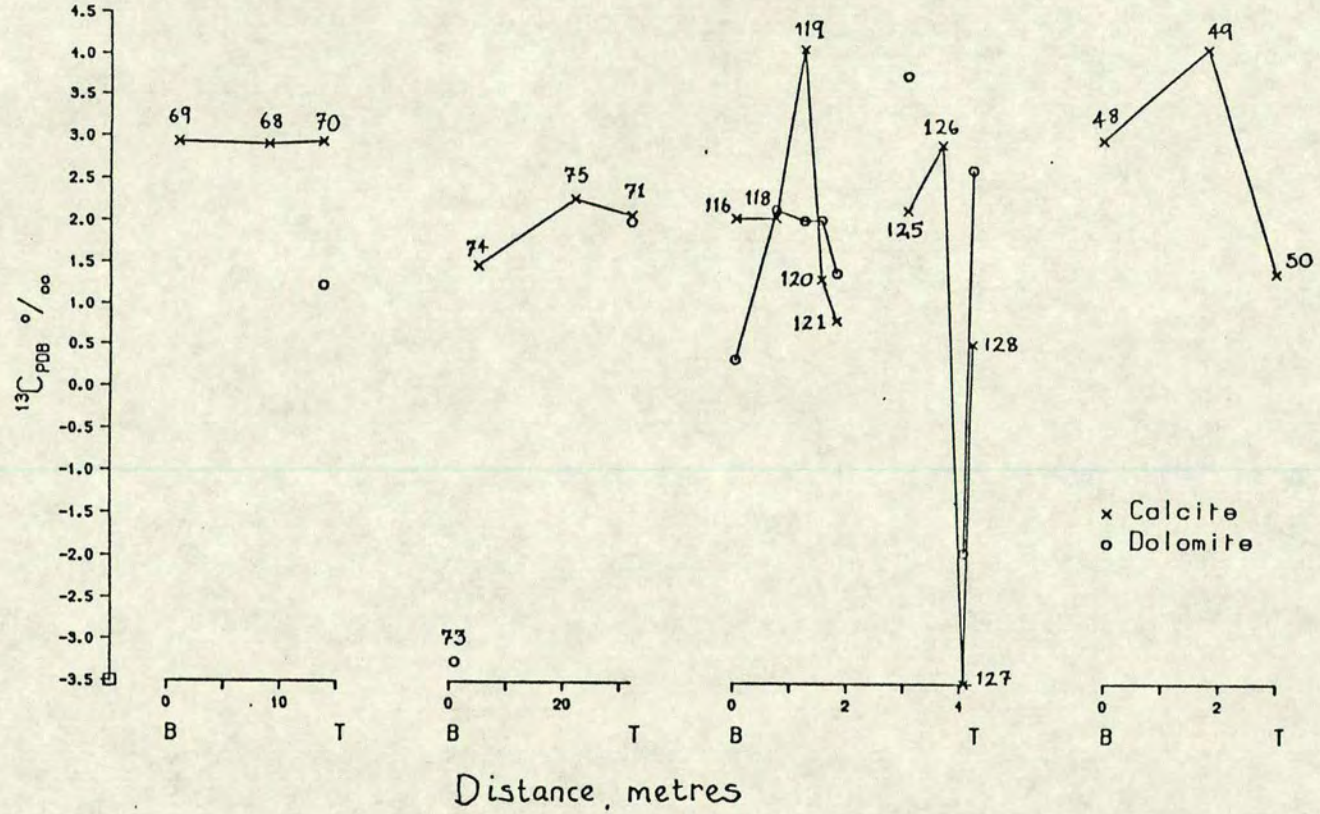

Figure 6.8 $\delta^{13}C$ variations across marble units from southern Syros. The variations in $\delta^{13}C$ appear to reflect the variation in $\delta^{18}O$. (see figure 6.4)

Thus, large-scale infiltration would be needed in order to modify the $\delta^{13}C$ signature of the marbles, which is not in agreement with the oxygen isotope data for the marbles.

It is suggested that in most cases very little modification has occurred, with the $\delta^{13}C$ values of the marbles largely reflecting original variations in the pre-metamorphic carbon. However, negative ^{13}C values may indicate interaction with a fluid containing carbon derived locally from graphite-bearing schists.

$\delta^{18}O$ variations in marbles - calculation of fluid-rock ratios.

In the previous section it was concluded that the oxygen isotope profiles in the marbles were produced by a combination of advective and diffusive transport of oxygen. This section will attempt to quantify the amount of fluid involved by calculating fluid-rock ratios. These calculations, based on an equation by Taylor (1977), provide a very rough-and-ready estimate of the fluid volume, and more sophisticated calculations now exist to estimate the amount of fluid flux in a specific direction (Bickle and McKenzie 1987). However, the lack of detail for the Syros profiles does not justify such a complicated treatment, and as a first step simple isotopic fluid-rock ratio calculations will provide an order of magnitude estimate of the amounts of fluid involved. Taylor (1977) proposed an equation which allows water-rock ratios to be calculated in situations where rocks have had their $\delta^{18}O$ values altered by interaction with an aqueous fluid. The equation is given below:

$$W/R = \frac{\delta f_{rock} - \delta i_{rock}}{\delta^{i}H_2O - \delta^{f}_{rock} + \Delta}$$

where f and i refer to the final and initial values of $\delta^{18}O$ for the rock or H_2O respectively.

Δ	$\delta f_{rock} - \delta fH_2O$
W	atom % of water oxygen
R	atom % of rock oxygen

The equation above assumes that the fluid has been continuously recycled, i.e a closed system. If the system is assumed to be open, and the fluid only makes a single pass through the rocks then the W/R ratio is given by the equation:

$$W/R = \log_e [(W/R)\text{closed system} + 1] \text{ (Taylor 1977)}$$

All the information needed to evaluate the above equation is known, except for the initial isotopic composition of the infiltrating fluid, δi_{H2O}. In order to make a sensible estimate of this unknown it is necessary to examine the possible sources for the infiltrating fluid. Devolatilisation reactions occurring in schists at depth provide the largest and most obvious source for this fluid, with the expected isotopic composition of such a fluid lying in the range of 15 - 18‰ (see section 6.7). It is impossible to give one specific value for δi_{H2O}, and thus a range of initial values will be used to calculate W/R ratios.

Before proceding to calculate W/R ratios for some localities, certain inherent assumptions must be stated:

δirock =	The interior of the marble units. These are assumed to have seen very little fluid, and will thus have retained the pre-metamorphic isotopic composition.
δfrock =	margin of the marble unit, also assumed to be in equilibrium with δf_{H2O}
δfH2O =	The final composition of the infiltrating fluid is assumed to be in equilibrium with the margin of the marble. A value is calculated using the equation for $\delta cc - \delta H_2O$ given in O'Neil *et al.* (1969), assuming some temperature.

W/R ratios will be calculated using the single pass (open system) equation, which appears to be a more realistic model of fluid flow under metamorphic conditions than closed system behaviour.

Tables 6.3a,b present estimated water-rock ratios calculated for some of the sampled marble units. The range of water rock ratios generated using the different δ^i_{H2O} values illustrates the point that the closer the initial rock and fluid compositions are in terms of ^{18}O, the larger the volume of infiltrating fluid needed to produce the desired depletion.

Table 6.3 Calculated water-rock ratios for marble units collected from the Nites region, southern Syros. At the point sampled the marble was 3m thick in case a) and 14.5m thick in case b).

δi_{rock} = 28.1 (87/49)

δf_{rock} = 25.0 (87/48)

δf_{H2O} = 23.0

δi_{H2O} ‰	minimum W/R ratio
15.0	0.33
15.5	0.34
16.0	0.36
16.5	0.39
17.0	0.42
17.5	0.44
18.0	0.48
18.5	0.52
19.0	0.57

b)

δi_{rock} = 27.04 (87/68)

δf_{rock} = 26.60 (87/70)

δf_{H2O} = 24.6

δi_{H2O} ‰	minimum W/R ratio
15.0	0.045
15.5	0.047
16.0	0.049
16.5	0.052
17.0	0.056
17.5	0.060
18.0	0.064
18.5	0.069
19.0	0.075

The marble unit sampled at Ormos Akhladhi, on the south-east coast of the island, shows some obvious differences when compared to the other sampled localities. Figure 6.9 shows a picture of the Ormos Ahkladhi locality. The marble unit is 4.23 metres thick (including a 1 metre thick mixed schist/metabasite intercalation). The main difference is that the entire unit is depleted in ^{18}O, with the maximum ^{18}O value for the interior of the unit being 25.9‰. Figure 6.10 shows a detailed profile through the marble, $\delta^{18}O$ analyses made on carbonate present in the intercalcated schist and metatuff unit, and in a cross-cutting qtz-carbonate vein are also shown. A distinctly asymmetric $\delta^{18}O$ profile is present in this marble indicating that oxygen exchange probably occurred via an advecting fluid. Do the depleted values seen at this locality indicate greater degrees of fluid-rock interaction during metamorphism, or can they be related to original $\delta^{18}O$ values in the pre-metamorphic sediment ? ^{18}O depleted limestones can be produced if ^{18}O depleted silicate phases (derived from reworked igneous or metamorphic material) are incorporated into the limestone sediment. However, this does not appear to be a viable explanation for the marble at Ormos Akhladhi, as, in common with the other Syros marbles, it contains only a few percent of silicate material. This observation also rules out decarbonation reactions as a possible mechanism to produce the $\delta^{18}O$ depletions. It is therefore proposed that the observed depletions are due to increased fluid involvement.

Interestingly the $\delta^{18}O$ values for the carbonate in the schist and metabasite are almost identical, despite the bulk compositional differences which exist between the two rock types. Indeed, there is a remarkable uniformity in the $\delta^{18}O$ values of the carbonate from the marble margins, the intercalated units and the cross-cutting vein. Ignoring the marble value from the upper contact, which appears to have exchanged with an overlying metabasite, the $\delta^{18}O$ values for the carbonates lie in the narrow range 20.3 ± 1.0‰. If the marble was originally isotopically homogeneous, with a pre-infiltration value of around 27‰, then W/R ratios can be calculated for the margins and interior of this marble.

Figure 6.9 General view of the marble unit at Ormos Akhladhi.

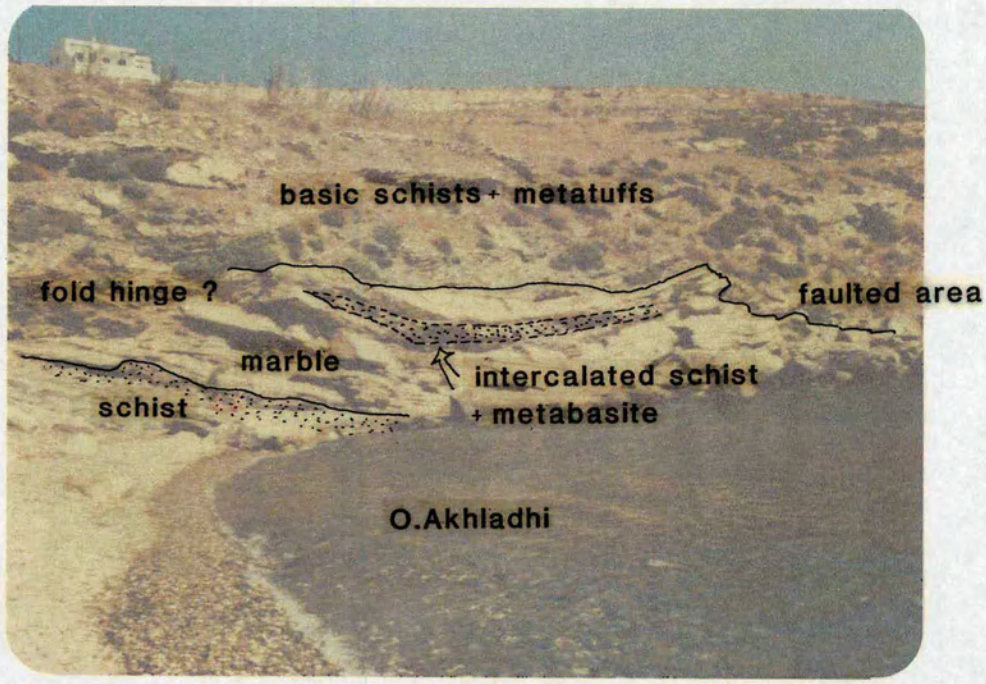

Figure 6.9 General view of the marble unit at Ormos Akhladhi.

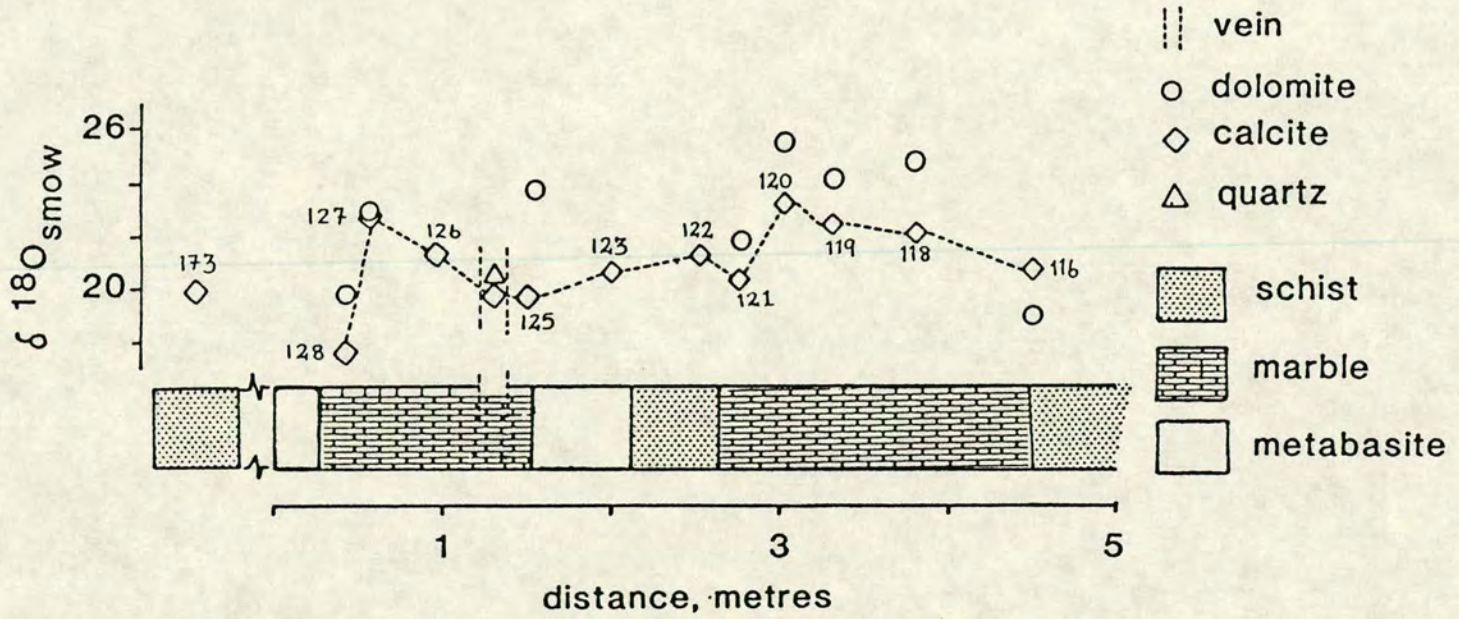

Figure 6.10 $\delta^{18}O$ variation through the composite marble unit at O. Akhladhi. The $\delta^{18}O$ values of calcite in the intercalated schist and metabasic units are also given. Sample numbers refer to those in table 6.2. The smoothing of ^{18}O gradients between the interlayered units suggests extensive exchange on a scale of at least 5 metres.

Table 6.4 W/R ratios for the Ormos Akhladhi marble unit

δi_{rock} = 27.0 average value for Mesozoic limestones

δf_{rock} (centre) = 23.4 δf_{H2O} (centre) = 21.5

δf_{rock} (edge) = 20.8 δf_{H2O} (edge) = 18.9

δi_{H2O} = 15.0 - 19.0

δi_{H2O}	W/R centre	W/R edge
15.0	0.44	0.95
15.5	0.47	1.04
16.0	0.50	1.14
16.5	0.54	1.28
17.0	0.59	1.45
17.5	0.64	1.69
18.0	0.70	2.06
18.5	0.79	2.80
19.0	0.90	

The large fluid-rock ratios suggest the presence of more fluid, particularly in the edges of the unit. Further reference to this locality will be made in section 6.9, when whole rock values for the intercalated metabasite will be used to calculate W/R ratios, these ratios will be compared to those calculated above for the marble unit.

Marbles - coexisting calcite and dolomite

Most of the marbles on Syros are calcitic. However, some do contain analysable amounts of dolomite. Using the marble unit at Ormos Akhladhi as an example (figure 6.10), it can be seen that in general dolomite is enriched in both ^{18}O and ^{13}C relative to coexisting calcite. However the isotopic fractionation between the two phases is erratic, covering a range from -0.9 to 4.9‰. Extrapolated fractionations based on high temperature experiments indicate that at 25 ^{o}C dolomite should be enriched in ^{18}O by 3 $\pm$ 1‰, and slightly in ^{13}C, relative to calcite coexisting with it at equilibrium (Land 1980), and as usual these fractionations should decrease as temperature increases. Measured isotopic fractionations on modern and ancient calcite-dolomite pairs are often at odds with these predicted experimental fractionations. Modern low temperature calcite-dolomite pairs often show a $\Delta^{18}O$cc-dol approaching zero (Degens and Epstein 1964, O'Neil and Epstein 1966),

whereas high temperature pairs show fractionations more in keeping with formation at low temperatures. Some of the unpredictable behaviour of dolomite may be related to the variable degrees of disorder in the mineral, which are not yet understood.

Table 6.5 Measured $^{18}O/^{16}O$ fractionations between coexisting calcite and dolomite.

Sample #	δ18Occ	δ18Odol	Δdol-cc
Ormos Akhladhi			
87/116	20.872	19.940	-ve
87/118	22.218	25.701	3.483
87/119	22.564	25.117	2.553
87/124a	19.365	24.727	5.362
87/125	19.863	24.745	4.882
Other mixed phase carbonates			
87/70	26.605	25.776	-ve
87/71	24.361	27.481	3.12
87/145	25.228	12.081	-ve

From table 6.5 it is apparent that the coexisting calcite-dolomite pairs do not show equilibrium isotopic fractionations. These disequilibrium fractionations may be explained in several ways:

1) Isotopic equilibrium was never established between the two phases (i.e. cc and dol are not in equilibrium)

2) Differential isotope exchange has occurred during retrograde events.

3) The closure temperature for exchange of carbon and oxygen isotopes is not the same for the two phases.

All three of the factors listed above may have been involved, to greater or lesser degrees. However, if the calcite and dolomite are assumed to have been in isotopic equilibrium prior to metamorphism, then the shifts seen may be due to the more rapid exchange of calcite with a relatively light isotopic fluid.

The impure marbles

The impure marbles contain differing amounts of silicates, varying between approximately 6 and 40%. The common silicates found are, quartz, muscovite, glaucophane and epidote group minerals, with rarer garnet and omphacite. In figures 6.11 and 6.12 the impure marbles from the southern and northern Syros can be seen to form distinct groups, depleted in both $\delta^{18}O$ and $\delta^{13}C$ compared to the pure marbles.

These depletions may be explained in a variety of ways, but the dominant processes are likely to be:

1) isotope exchange with ^{18}O depleted silicates

2) loss of isotopically enriched CO_2 via decarbonation reactions

In a large number of the impure marbles, quartz and muscovite are the dominant silicate phases, and these minerals may have been present as as detrital material in the original limestone. During diagenesis and metamorphism isotope exchange and equilibration will occur between the carbonate and silcate portions of the rock, leading to a possible overall ^{18}O depletion in the carbonate. Obviously the magnitude of this effect largely depends on the original isotopic signature of the silicate material, and some silcate sources can be ^{18}O rich, e.g. diatoms $\delta^{18}O$ = 26.5 ‰ (Valley 1986). However, consistent ^{18}O depletions in silcate-bearing marbles suggest that an isotopically light igneous or metamorphic source for the silicate material is more likely.

Oxygen isotope exchange between carbonate and silicate material will not affect the carbon isotopes, and on Syros the $\delta^{13}C$ values of the impure marbles are also seen to be depleted relative to the pure marbles. The depletions in $\delta^{13}C$ are likely to be caused by decarbonation reactions. Production of CO_2, enriched in both ^{18}O and ^{13}C, leaves the remaining marble depleted in both these isotopes. This coupled O-C depletion trend, associated with decarbonation reactions and the development of calc-silcates, is well known (Valley 1986; Nabelek *et al.* 1984).

The depletions in the impure marbles can thus be explained by a combination of the two processes discussed above.

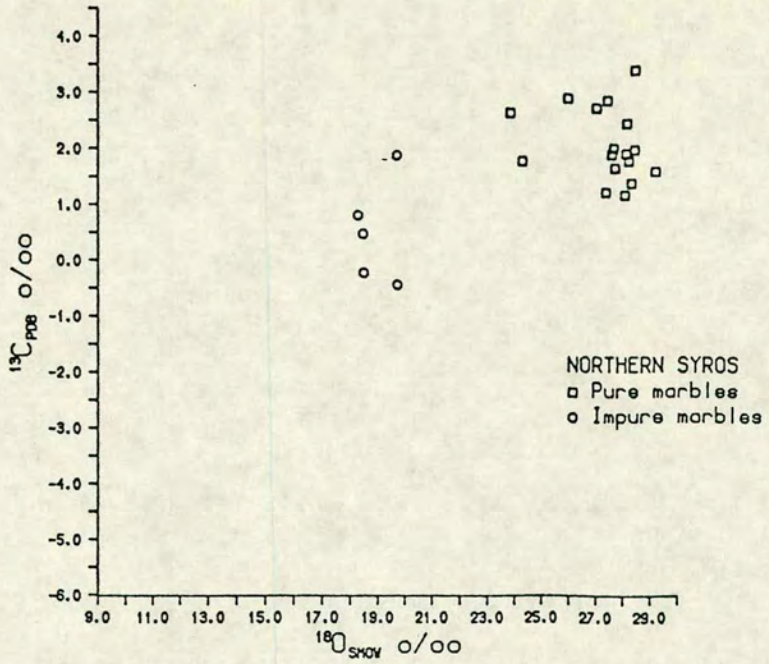

Figure 6.11 Plot of $\delta^{18}O$ versus $\delta^{13}C$ for calcite in marbles from northern Syros.

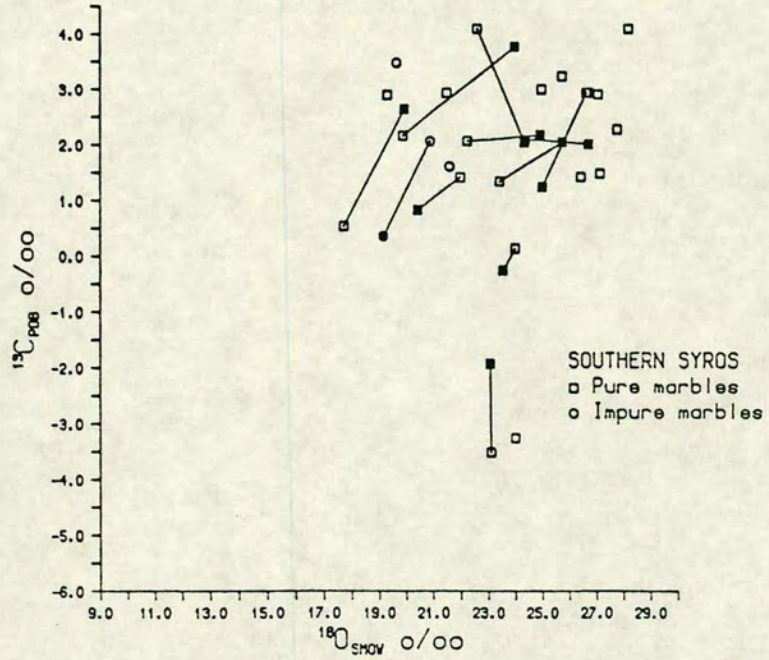

Figure 6.12 Plot of $\delta^{18}O$ versus $\delta^{13}C$ for calcite and dolomite in marbles from southern Syros. Shaded symbols refer to dolomite, and tie-lines connect analyses (of calcite and dolomite) from the same samples.

6.5 CARBONATE IN THE SCHISTS

Matrix carbonate was analysed from both blueschist and greenschist samples, partly to see if differences in the carbonate isotopic signature existed between the two groups, and partly to complement work on whole-rock silicates. The marbles have premetamorphic $\delta^{18}O$ and $\delta^{13}C$ carbonate isotope values which are known to lie within a narrow range (Hoefs 1973), but it is much harder to confidently identify a similar premetamorphic ^{18}O carbonate range for the schists. Table 6.6 presents the $\delta^{18}O$ and $\delta^{13}C$ values for the carbonates analysed, and figures 6.13 and 6.14 are plots of $\delta^{18}O$ versus $\delta^{13}C$ for the carbonates in the blueschists and greenschists respectively. Wide variations in $\delta^{18}O$ are possible for carbonates in the schists depending on the relative proportions of carbonate and silicate material in the original sediment. The initial isotopic signature of the carbonate would presumably be similar to that of unaltered limestone ($\delta^{18}O$ = 25 - 30‰ ; $\delta^{13}C$ 0 - 4‰) but the final isotopic signature will depend on the amount and source of the silicate material present in the rock. Figure 6.15 shows $\delta^{18}O$ plotted against the percentage of $CaCO_3$ present. The outlined area bounds a possible "mixing field" between a pure carbonate source, and a range of possible sedimentary sources. However, it should be stressed that not all the carbonate present in the schists will necessarily have a sedimentary origin, the negative values for $\delta^{13}C$ in particular, suggest a proportion of graphite-derived calcite.

Carbon in the schists

The previous section indicated how the presence of silicate material can modify the oxygen isotope signature of the carbonate in the metasediments by oxygen exchange. The carbon isotope ratios can be modified in a similar manner, largely through interaction with graphite, or graphite derived CO_2

The blueschists contain variable, but small amounts of graphite (see chapter 3), with $\delta^{13}C$ values clustering around -15‰. The $\delta^{13}C$ values of graphite analysed from ancient sediments of fresh-water and marine origin range from -20 to -27‰, with an average value of -22‰ (Degens 1969). The $\delta^{13}C$ values for graphite analysed from the Syros metasediments lie in a narrow band, from -16.6 to -14.3 ‰, significantly enriched in ^{13}C relative to organic matter in unaltered limestones.

Table 6.6 Oxygen and carbon isotope analyses of carbonates from blueshist and greenschist metasediments

Sample #	δ18Osmow	δ13Cpdb	wt% CaCO3	dolomite
Blueschists				
86/14	20.46	-4.06	3.0	X
86/74	24.38	-5.93	4.1	X
86/76	22.17	-3.35	5.2	X
86/95	24.72	-4.53	8.6	X
86/98B	24.80	-6.388	2.0	X
86/144	22.80	-7.00	3.9	X
86/145	21.75	1.09	18.0	X
86/191	23.09	-1.17	3.2	X
87/222	18.80	0.03	10.8	
87/kam	21.47	-7.83	1.4	X
Greenschists				
86/10	25.12	-4.06	4.6	X
86/19a	21.15	-5.93	4.1	
86/25	18.14	-3.84	3.0	
86/34	16.99	-4.02	2.0	
86/35	16.72	-3.60	3.5	
87/122	21.40	-2.82	4.6	
87/173	19.79	-4.00	5.6	
87/193	23.48	-7.82	5.0	X
87/228	16.87	-6.82	3.5	
JD17	22.57	-1.39	5.3	
JD36	15.73	-3.81	6.3	

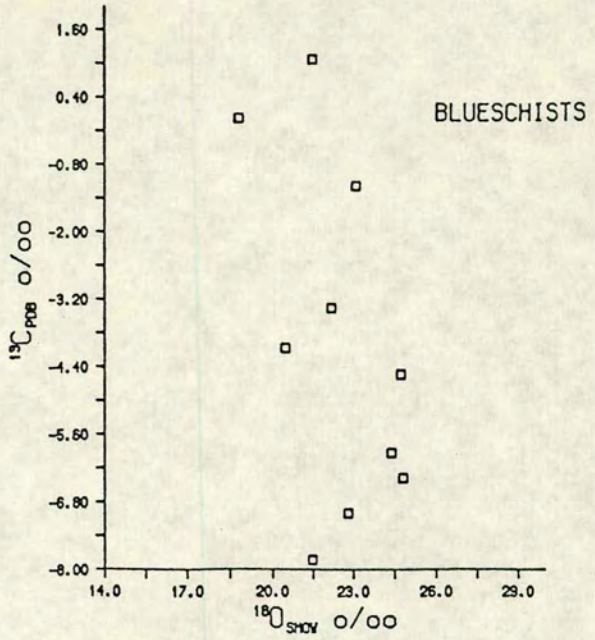

Figure 6.13 Plot of $\delta^{18}O$ versus $\delta^{13}C$ for carbonates in the blueschist metasediments.

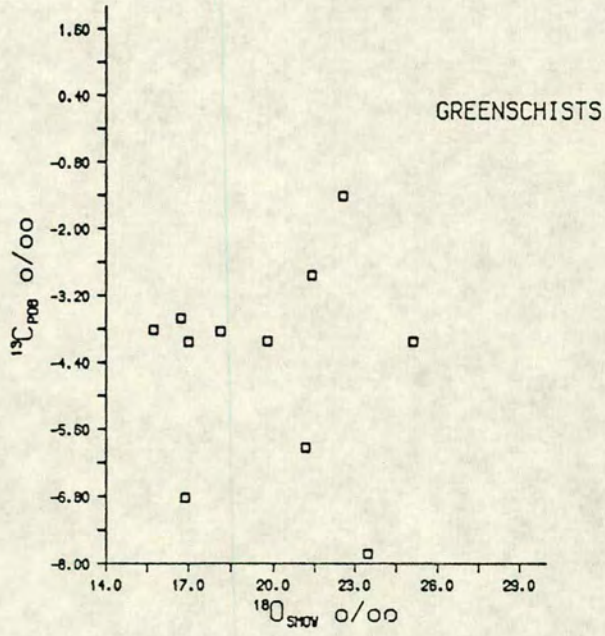

Figure 6.14 Plot of $\delta^{18}O$ versus $\delta^{13}C$ for matrix carbonate in the greenschist metasediments.

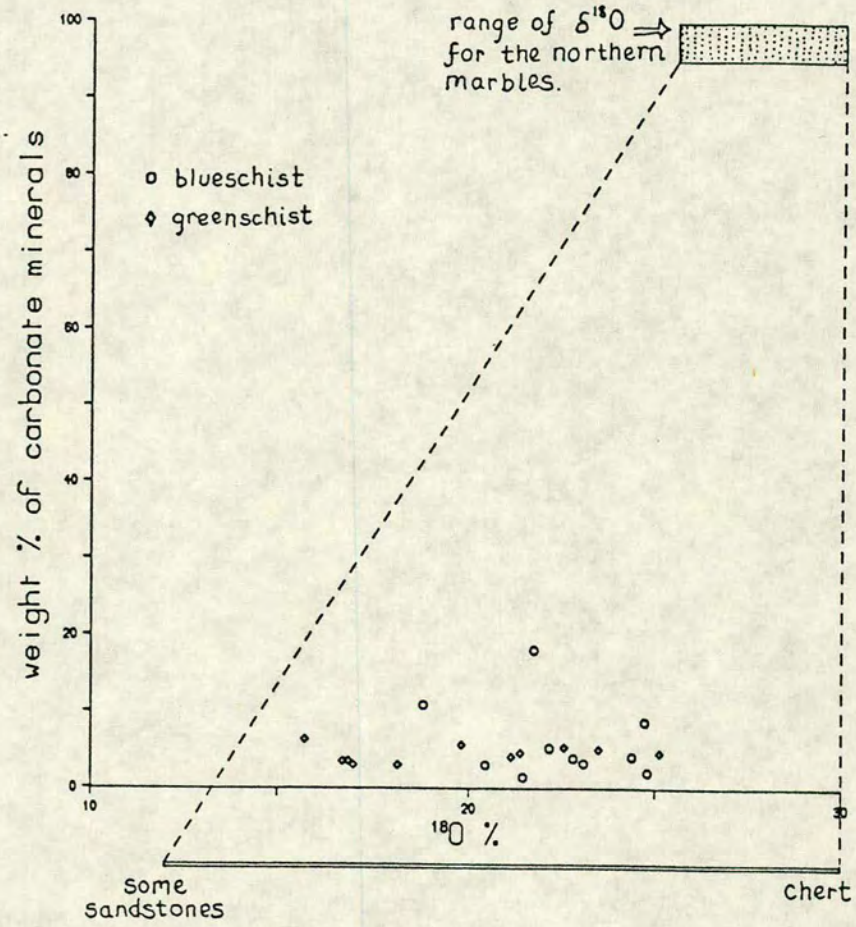

Figure 6.15 The percentage carbonate present in each sample versus $\delta^{18}O$. The scatter of samples appears quite random, and there is no obvious correlation between high $\delta^{18}O$ values and increased percentages of carbonate.

Two main processes could have caused this ^{13}C-enrichment.

1) Isotopic exchange with co-existing calcite

2) Liberation of methane

Table 6.7 shows the $\delta^{13}C$ values for coexisting calcite and graphite

Table 6.7 $\delta^{13}C$ values of coexisting calcite and graphite.

Sample #	δ13C calcite	δ13C graphite	% graphite
86/34	-4.019	-14.34	0.23
86/72	---	-16.59	0.27
86/74	-5.931	-14.42	0.24
87/217	---	-14.90	0.31

As can be seen from table 6.7, and figures 6.13 and 6.14, the $\delta^{13}C$ signature for the majority of the carbonates in the metasediments is negative. As most of the metasediments also contain graphite, it seems likely that some isotopic exchange occurred between the two phases. Since the amount of graphite is small compared to the amount of carbonate the isotope exchange reactions should have less effect on the $\delta^{13}C$ signature of the carbonate, which appears to be the case. However, graphite is seen to be enriched in ^{13}C even in those samples which do not contain carbonate, e.g 86/72 and 87/217 (Table 6.10), how can ^{13}C enrichment be explained in such cases ?

In a study of carbonaceous matter in the Swiss Alps, Hoefs and Frey (1976), related $\delta^{13}C$ enrichment in graphite to the liberation of methane.

Unlike the production of CO_2, which tends to deplete the remaining organic matter in ^{13}C, metamorphism of organic bearing metasediments under conditions of low fO_2 will drive off ^{13}C-depleted methane, leaving the residual matter enriched in ^{13}C. It seems likely that liberation of methane has occurred at some time during the metamorphism of the Syros metasediments, leaving residual graphite enriched in ^{13}C in carbonate bearing samples. Isotope exchange between coexisting graphite and carbonate could further modify the $\delta^{13}C$ signature of the two phases.

Preservation of the original carbonate phase

As was indicated in table 6.6 , in many instances the primary carbonate in the schists was dolomite-ankerite, or a mixture of this and calcite. In nearly every case the original dolomite is now replaced by calcite, with the calcitising event probably occurring quite late in the history of the terrain, (see discussion in chapter 3). It is possible that the isotope ratios measured in the blueschist carbonates today do not reflect the original isotopic signature of the dolomites. The average $\delta^{18}O$ value for quartz in the blueschists is 19‰, and at a temperature of 450 °C coexisting calcite should have an ^{18}O value of approximately 18‰ (Matthews and Schliestedt 1984). However the carbonate present in the blueschists is invariably enriched in ^{18}O relative to this value. This reversal in the order of relative ^{18}O enrichment between the phases indicates that the carbonate is not in isotopic equilibrium with the rock.

Carbonates in the greenschists

The previous discussion on ^{18}O and ^{13}C isotopes also applies to the carbonate present in the greenschists. The carbonates in the greenschists show a wider range in ^{18}O, and some is in approximate isotopic equilibrium with the coexisting silicates.

e.g.	$\delta^{18}O$quartz	$\delta^{18}O$calcite
86/25	19.6	18.1
87/173	21.5	19.8

The fact that greenschist samples contain carbonate which is in isotopic equilibrium with the rock suggests that the same fluid which caused the blueschist to greenschist transformation also deposited the carbonate. The presence of ^{18}O-enriched carbonate in some greenschist samples may indicate the involvement of a later ^{18}O-rich fluid. As the greenschist 'event', was probably protracted, it is likely that several, isotopically distinct fluids, were involved.

6.7 CARBONATE IN METABASITES

Comparatively few metabasite samples were analysed, and it is difficult to determine any overall trends with the amount of data available. Table 6.8 presents the $\delta^{18}O$ and $\delta^{13}C$ values for the carbonate analysed in the blueschist and greenschist metabasites, and these data are plotted in figure 6.16.

Table 6.8 Oxygen and carbon isotope analyses of carbonates from blueschist and greenschist metabasites

Sample #	δ^{18}Osmow	δ^{13}Cpdb
Blueschist		
86/126	12.45	-3.42
86/130	21.22	-5.89
86/208	17.88	1.25
JC13	8.35	-4.87
JO3	13.23	-2.63
IS27	14.17	-0.89
UM5	10.42	1.33
Greenschists		
87/21a	19.48	0.91
87/123	20.73	-2.21
86/201	15.47	-2.10
86/203	18.67	-3.27
86/208	11.07	-1.21

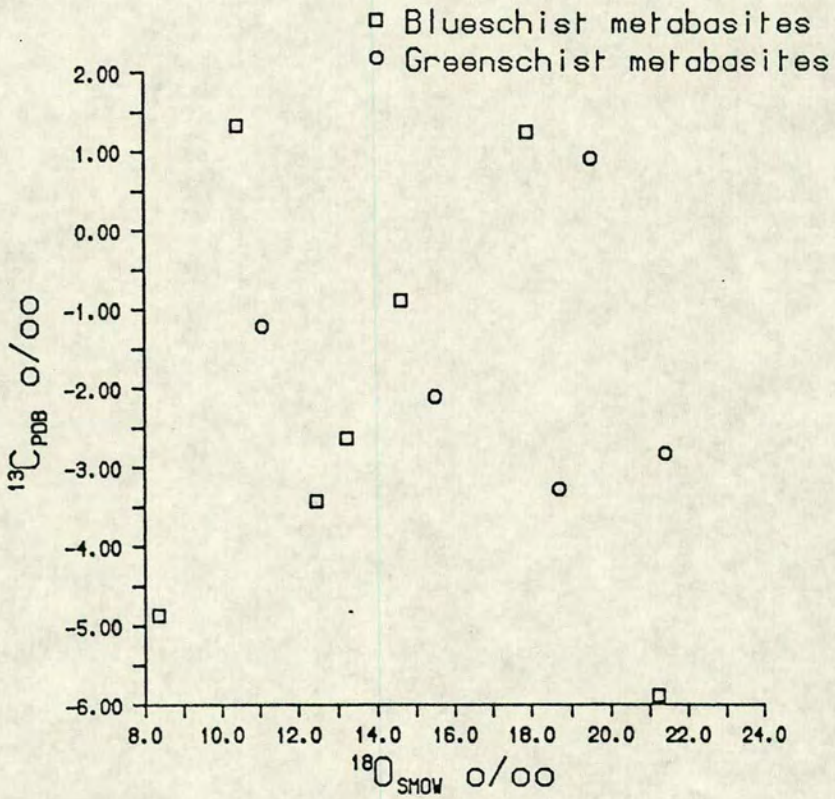

Figure 6.16 Plot of $\delta^{18}O$ versus $\delta^{13}C$ for carbonate in the metabasites (blueschist and greenschist). Despite the small number of samples the carbonates cover a wide range in $\delta^{18}O$ and $\delta^{13}C$.

Both groups show a wide scatter in $\delta^{18}O$ and $\delta^{13}C$, but, like the metasediments, most of the carbonate values are too enriched in ^{18}O to be in isotopic equilibrium with the rock. Carbonate may have appeared during sub-seafloor alteration of the basic rocks, or during metamorphism, and isotopic equilibrium with the silicate portion of the rock should have been established. The enriched values seen today either suggest that the original equilibrated low ^{18}O carbonate has been replaced by an ^{18}O enriched carbonate, or the carbonate has undergone preferential isotopic homogenisation in the solid state through the action of an ^{18}O enriched fluid.

6.8 SUMMARY

Isotopic profiles through the marble units on Syros typically show margins depleted in ^{18}O, down to 19 ‰, while the interiors retain values of around 27‰, characteristic of unmetamorphosed limestones of the same age. Although more detailed sampling is needed, the ^{18}O depletions and the apparent asymmetry in the profiles suggests that both advective and diffusive oxygen exchange was involved in their formation (Bickle and McKenzie 1987; Nagy and Parmentier 1982). Smaller ^{18}O depletions were measured in the northern marble units surrounding the blueschist unit, and this may be symptomatic of the fact that upward fluid penetration was impeded by the thick marbles of central Syros. Crude fluid-rock ratio calculations carried out on the southern marbles indicate that in most instances the volume of infiltrating fluid was low, with W/R ratios less than 0.8. However one locality (Ormos Akhladhi) shows extensive depletions throughout the marble unit and an approach towards isotopic homogenisation of carbonate between different interlayered rock types. It is suggested that this area represents a zone of high, but localized, fluid flow.

Many of the schists originally contained dolomite which is now replaced by ^{18}O-enriched calcite. The original isotopic signature of the dolomite has not been preserved, and it would be unwise to draw any conclusions about the isotopic composition of the carbonate under peak metamorphic conditions using these data.

6.9 STABLE ISOTOPE DATA - SILICATES

In order to learn more about the extent and scale of oxygen isotopic equilibration, during both metamorphic episodes, a number of whole-rock and mineral-separate samples were analysed for $\delta^{18}O$.

The specific aims of the silicate isotope study are:

- To assess whether pervasive infiltration occurred during the primary blueschist event. Mineral separates from adjacent rock layers were analysed to determine if isotopic homogenisation had occurred.

- To examine the evidence for fluid infiltration in the blueschist to greenschist transformation.

- To analyse albite crystals from the albite porphyroblast schist, in order to determine whether albites collected at different localities are isotopically homogeneous, (see discussion on albite porphyroblasts in chapter 5).

Whole-rock silicates - sample preparation and analytical techniques

Cleaned samples were ground in a Tema mill until a grain-size equivalent to 200 mesh was achieved. Approximately 1g of the ground sample was placed in a beaker and treated with concentrated HCl. The beakers were placed on a steam bath and allowed to evaporate to dryness. This procedure was followed to ensure that any relic dolomite was destroyed in addition to calcite. The samples were then washed with deionised water, and dried.

Oxygen extraction from the whole-rock samples, and the mineral separates, was carried out at the Scottish Universities Research and Reactor centre, East Kilbride. Oxygen was liberated from the samples using ClF_3, and, after purification, it was converted to CO_2 by reaction with a heated carbon rod. Oxygen yields for the samples reported here vary from 80 % or greater for the mineral separates, to 90 % or greater for the whole-rock samples. Only every fourth whole-rock sample was duplicated, as the agreement between runs was generally very good. However, all mineral-separate samples were replicated to obtain the degree of precision required. The overall reproducibility of the $\delta^{18}O$ values is $\pm$ 0.2‰, for both the whole-rock and the mineral separate samples. An NBS 28 sample (African sand) was run with each batch of 11 samples, and an average value of 9.74‰$\pm$ 0.2 was obtained.

Whole-rock analyses

Table 6.9 lists the isotopic compositions of the whole rock schists and metabasites. The isotopic ratios of whole-rock samples are strongly dependent on their mineralogy, and, before whole-rock values can be compared directly, these mineralogical effects must be removed.

A graphical method for interpretating whole-rock isotopic data

Taylor and Epstein (1962a) showed that minerals follow a consistent sequence of relative $\delta^{18}O$ enrichment under equilibrium conditions, which is related to the relative proportions of Si-O-Si, Si-O-Al and Si-O-M bond types, in the mineral phases regardless (M is a cation in six-fold co-ordination or higher) of their structure.

A list of the common minerals given in order of their ability to concentrate ^{18}O is given in table 6.10 below.

Table 6.10 The minerals are listed in decreasing tendency to concentrate ^{18}O. The table is taken from O'Neil (1980).

Quartz, dolomite,
Alkali feldspar, calcite, aragonite
Muscovite, paragonite
Anorthite
Glaucophane, staurolite
Lawsonite
Garnet, common pyroxenes and amphiboles
Biotite
Olivine, sphene
Chlorite
Ilmenite, rutile
Magnetite, hematite

In 1966 Garlick used the concept put forward by Taylor and Epstein (1962a) to propose a chemical index I, which reflects the proportion of the different bond types in a mineral.

$$I = \frac{(Si + 0.58\ Al)}{\Sigma \text{ all cations}}$$

Where Si etc. = mon-oxygen equivalents of Si

Behind this expression is the assumption that the $^{18}O/^{16}O$ ratios of the silicate phases at equilibrium are proportional to their chemical indices. This assumption appears to be justified as Garlick (1966) and other workers (Kay 1979) have shown that an approximately linear relationship exists between the $\delta^{18}O$ values and the chemical index of silicate minerals, with the slope of the line being proportional to $10^6/T^2$.

Table 6.9 $\delta^{18}O$ ratios of silicate minerals and whole rocks analysed in the present study. The chemical indices have been calculaed on a carbonate free basis. $CaCO_3$ corrected whole rock values are given for carbonate bearing samples. The uncorrected values were used to construct the Garlick plot (fig. 6.18)

Sample No	Description	Mineral	$\delta^{18}O$‰	Ca corrected values	Chemical Index, I
86/14	gl-gnt blueschist	W.R.	19.7	19.7	0.670
86/19A	cc-alb greenschist gl-pseudomorphs	W.R.	18.1	18.2	0.621
86/25	"	quartz	19.6		0.651
		w. mica	16.1		
		W.R.	18.0	18.0	
86/34	cc-chl-alb greenschist	W.R.	13.4		0.685
86/40	chl-actinolite schist	albite	16.2		
86/53H	blueschist	W.R	17.1	17.5	0.636
86/70	gl-gnt blueschist	W.R.	14.7		0.640
86/72	paragonite-bearing blueschist	W.R.	15.7		0.677
86/73	blueschist	quartz	17.5		0.672
		w. mica	15.6		
		glaucophane	13.6		
		W.R.	16.3		
86/74	blueschist	quartz	18.7		0.703
		W.R	16.8	17.8	
86/78	chloritoid blueschist	quartz	20.2		0.641
		w. mica	17.3		
		glaucophane	15.7		
		garnet	14.0		
		W.R.	16.2		
86/86	gl-ep blueschist	W.R.	11.7		0.557
86/106	blueschist at contact with serpentinite	W.R.	10.9		0.603
86/111	blueschist	W.R.	16.4		0.641
86/124	gl-ep metabasite	W.R.	5.3		0.573
87/21A	retrogressed metabasite	W.R	14.1	14.6	0.547
87/111	partly altered metabasite	W.R.	9.1		0.582
87/122	chl-alb schist	W.R.	18.8	18.9	0.65 estm.
87/123	partly altered metabasite	W.R	17.1	17.3	0.60
87/138	chl-ep-alb meta-acidite, gl pseuds.	quartz	10.6		0.753
		w. mica	6.7		
		W.R.	10.5		
87/130	gl-ep metabasite	W.R.	8.6	8.7	0.602
87/140	chl-ep-alb meta-acidite	W.R.	10.3		0.823
87/141	gl-ep-gnt meta-acidite	W.R.	7.9		0.676
87/143	chl-ep-alb meta-acidite	W.R.	9.4		0.735
87/157	gl-omphacite metabasite	W.R.	9.3		0.574
87/160	alb-ep metabasite	W.R.	9.6		0.558
87/173	chl-alb schist	quartz	21.5		0.771
		w.mica	18.0		
		W.R.	19.0	19.1	
87/193	chl-alb schist	W.R.	16.6	19.6	0.586
87/205	chl-alb schist	albite	16.1		
		w. mica	14.4		
		chlorite	11.1		
87/222	gl-gnt blueschist	W.R.	16.6	16.8	0.573
87/228	blueschist	W.R	15.6	15.7	0.702
87/KAM	blueschist	W.R.	16.8		0.667
87/SY4	gl-gnt blueschist	quartz	11.5		0.639
		glaucophane	6.6		
		W.R	9.2		

The oxygen isotope fractionation between a mineral pair at equilibrium is temperature dependent, and this dependency can be expressed by the following approximation:

$$1000 \ln\alpha \approx \delta_1 - \delta_2 \approx A(10^6/T^2)$$

Figure 6.17 (after Schliestedt and Matthews 1987) shows a plot of the chemical index, I, against $A_{Q\text{-mineral}}$. $A_{Q\text{-mineral}}$ is observed to be a linear function of I at constant temperature, and this linear relationship can be expressed by the regression equation.

$$\delta_Q - \delta_{mineral} = [\, 6.15 - 6.32\, I \,]\, 10^6/T^2 \quad \text{Schliestedt \& Matthews (1987)}$$

The major exceptions to this linear relationship are the minerals calcite and rutile. Uncorrected whole-rock analyses already refer to a decarbonated rock, but an amount of CaO equivalent to the $CaCO_3$ content of the rock must be subtracted from the X.R.F analysis before calculating the chemical index.

If all the major constituent minerals define a line, it must follow that the whole-rock co-ordinates will also lie on the line

$$\text{Since } \delta_{WR} = \Sigma\, X_{min} \cdot \delta_{min} ,$$

$$\text{then } \delta_Q - \delta_{WR} = [6.15 - 6.32.I]\, 10^6/T^2$$

Figure 6.18 shows the $\delta^{18}O$ compositions of whole-rock schists and metabasites plotted against the chemical index I. Blueschist and greenschist facies rocks are shown, together with fluid isopleths, which indicate the isotopic composition of water in equilibrium with the whole rocks, calculated for a representative temperature of 450 ^{o}C.

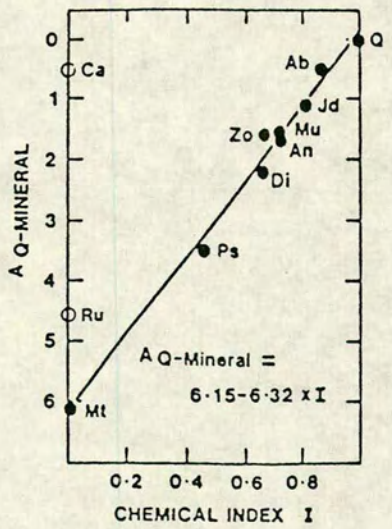

Figure 6.17 Plot of the Garlick chemical index I, against $A_{Q\text{-mineral}}$ coefficients. Excluding calcite and rutile, the other mineral phases define a reasonably linear relationship between A and I (from Schliestedt and Matthews 1987).

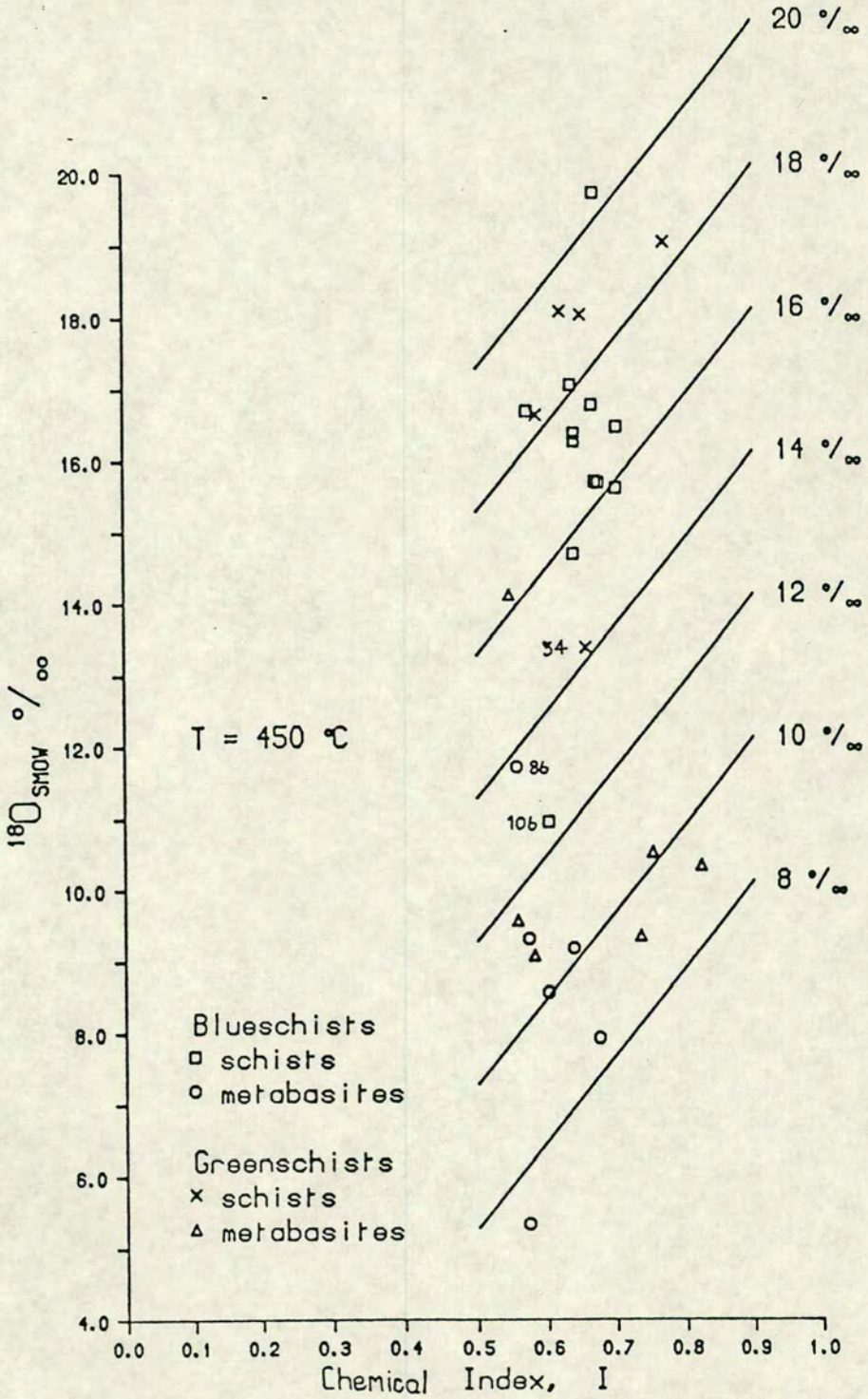

Figure 6.18 Plot of $\delta^{18}O$ against chemical index I for schist and metabasite whole rock samples. The isopleths refer to the isotopic composition of water in equilibrium with the whole rocks calculated for a temperature of 450°C. (see text for details)

The isopleths are calculated using the expression:

$$\delta_Q - \delta_{WR} = [6.15 - 6.32\ I]\ 10^6/T^2 \quad \text{Schliestedt and Matthews 1987}$$

and the quartz - water calibration of Matsuhisa *et al.* (1979):

$$\delta_Q - \delta_{H2O} = 3.13\ (10^6/T^2) - 2.94$$

From these two expressions it follows that:

$$\delta_{WR} - \delta_{H2O} = [6.32.I - 3.02]\ 10^6/T^2 - 2.94$$

As δ_{WR} is known, by taking two different values of I, the H_2O isopleths may be calculated for any temperature. On a cautionary note, recent experimental data suggest that the Matsuhisa quartz-water data may not represent an equilibium fractionation (Dr. A. Matthews pers comm. 1988). This means that the positions of the isopleths may change slightly, but as yet the revised results are not available.

If Figure 6.18 is examined in more detail some general comments can be made. The metasediments which tend to have higher whole rock values than the metabasites (largely reflecting the higher modal abundance of ^{18}O-rich quartz in the schists), plot in the upper part of the diagram, while the metabasites plot in the lower half. If a suite of chemically varied rocks equilibrates with a fluid of constant isotopic composition, then on the Garlick plot the isotopic compositions of the whole rocks should reflect their chemistry, i.e there should be a straight line correlation between increasing $\delta^{18}O_{wr}$ and increasing chemical index. The rocks should plot as a group dispersed along the appropriate fluid isopleth.

If the blueschist rocks in Figure 6.18 are considered, it is apparent that the whole-rock values for both the schists and the metabasites are dispersed vertically on the diagram, indicating that the individual rocks have equilibrated with fluids of different isotopic compositions. This suggests that the blueschist rocks have buffered the $^{18}O/^{16}O$ composition of the coexisting fluidas well as the CO_2/H_2O ratio.

Comparing blueschist and greenschist counterparts, it appears that the greenschist whole rocks are slightly enriched in ^{18}O. This implies that the greenschist rocks were in equilibrium with slightly ^{18}O enriched fluids. The fluid isopleths indicate the isotopic composition of H_2O in equilibrium with the whole rocks. Generally the range of fluid compositions in equilibrium with the schists and metabasites are distinct (15.5-20.0 ‰ and 7-11.5 ‰ respectively). However, the presence of some greenschist metabasite points within the "schist fluid" fields indicates an approach towards isotopic equilibrium at some greenschist localities.

Discussion

Some comment must be made about the 'odd' points. Samples 86/34 and 86/106 are both schists with unusually low $\delta^{18}O$ whole rock values, and it is thought that these samples have been influenced by oxygen isotope exchange with ultrabasic material.

Sample 86/106 was collected near Megas Lakkos on the northwest coast of the island, where a marble schist sequence is juxtaposed next to a serpentinite horizon, now largely altered to talc, chlorite and actinolite. 86/106 was collected 35cm from the serpentinite contact, and the low whole-rock value, for this otherwise unremarkable sample, suggests that exchange has occurred between the adjacent schists and the isotopically light ultrabasic rock and its derivatives. Similarly sample 86/34 appears to have exchanged with isotopically light oxygen. Collected at Kastri on the northeast coast the schists grade upwards into an olistostrome melange which consists of large igneous blocks held in a reacted-out serpentinite matrix. Moving up sequence towards the melange there is a gradual increase in the ultramafic input and this may explain why sample 34, collected metres from the melange, has a lower whole-rock value than other schists. In contrast sample 86/86 is a metabasite with an enriched whole-rock signature, and the reason for this is less obvious. The rock is entirely composed of glaucophane, epidote and garnet and it also comes from Kastri, collected just below the olisotrome. This sample appears to be part of a reaction zone in which glaucophane and calcite are reacting to produce omphacite, CO_2 and H_2O. Sample 86/86 may have exchanged with an ^{18}O enriched fluid derived from the adjacent marble layer, with the volume decrease accompanying the reaction allowing increased interaction between the two.

The following section uses Garlick plots to examine several different localities where the blueschist to greenschist transformation can be observed.

Agkathopes

Agkathopes forms the peninsula between the bays of Finika and Komito on the southwest coast of the island (see chapter 2). The rocks consist of an alternating sequence of basic and acidic gneisses, containing glaucophane, epidote and garnet, and an overlying marble unit. The rocks have experienced vein-controlled regression to albite-chlorite schists. The alteration zone forms around the veins, and is usually less than 1 metre wide. Figure 6.19 shows a photograph of one of these veins. Figure 6.20a is a stylised representation of the vein seen in figure 6.19. The vein was sampled in three places, at the top and bottom of the main vein and in a small veinlet.

Figure 6.19 Photograph of a large carbonate vein cross-cutting a sequence of quartz-glaucophanites, Agkathopes. A narrow retrogression halo, usually less than 1m wide is developed around the vein, and the rocks are extensively altered - albite, chlorite pseudomorphs after glaucophane.

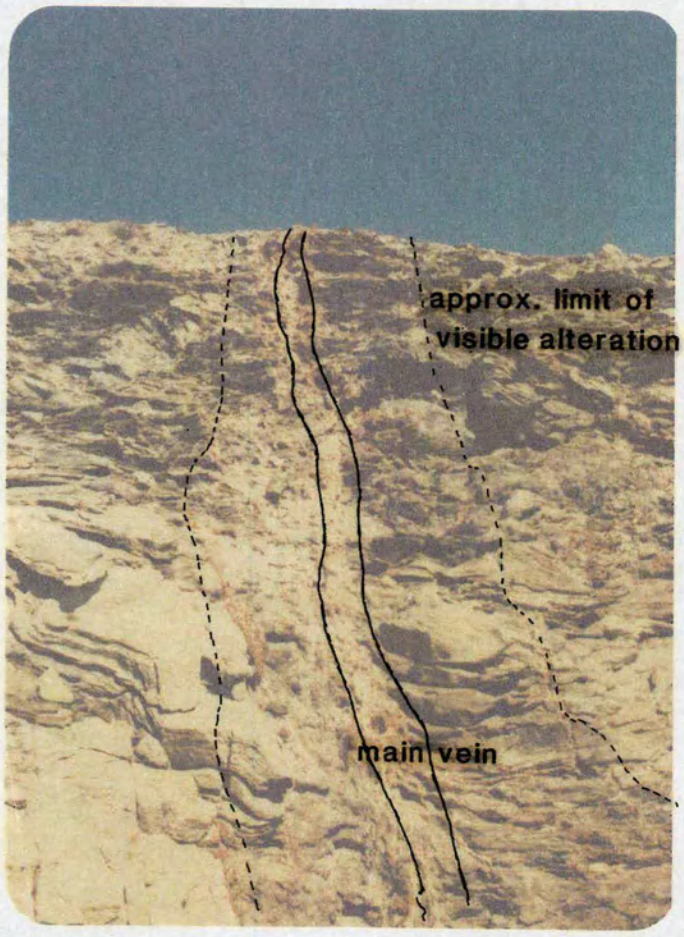

Figure 6.19 Photograph of a large carbonate vein cross-cutting a sequence of quartz-glaucophanites, Agkathopes. A narrow retrogression halo, usually less than 1m wide is developed around the vein, and the rocks are extensively altered - albite, chlorite pseudomorphs after glaucophane.

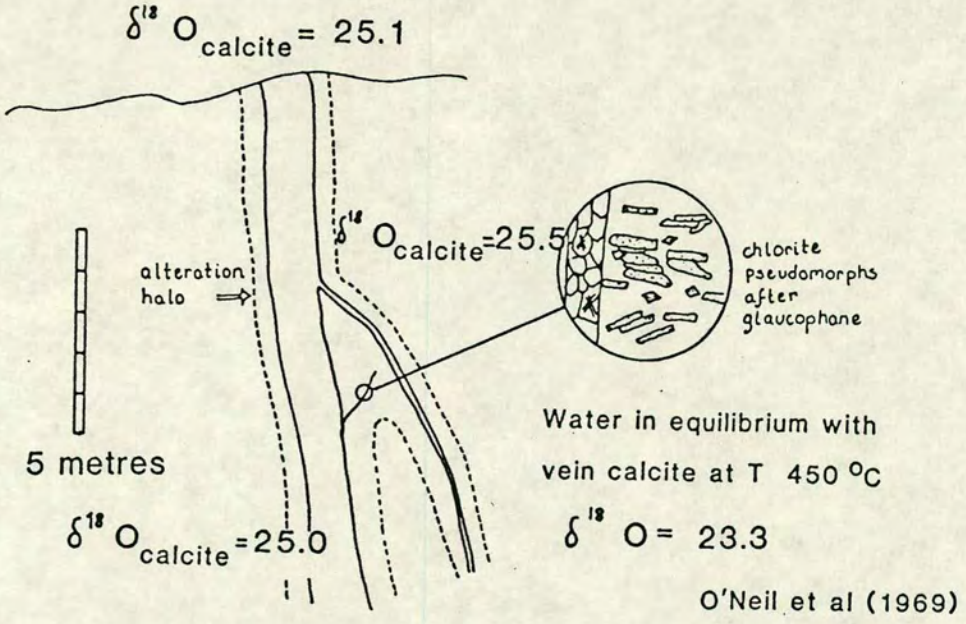

Figure 6.20a A stylized sketch of the previous photograph. The vein was sampled in three places, at the top and bottom of the main vein and in a small veinlet - the isotopic compostion of the carbonate is uniform.

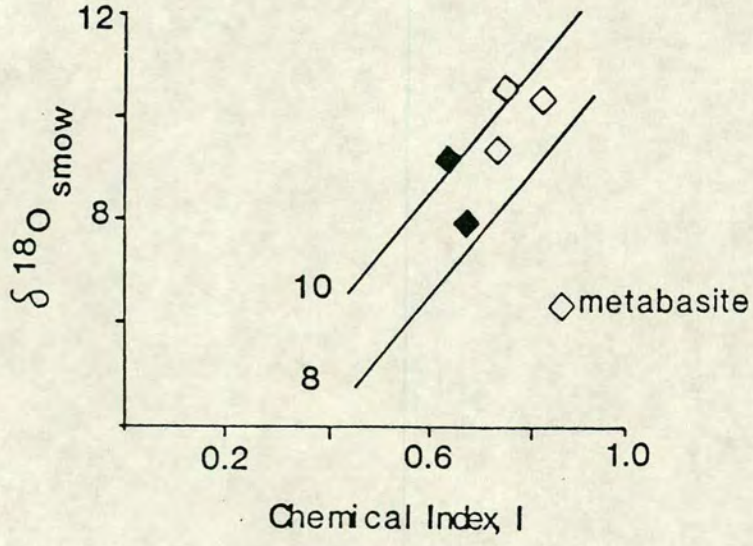

Figure 6.20b Plot $\delta^{18}O$ versus the chemical index for unaltered and altered samples, Agkathopes. Filled sybols refer to blueschist samples. There is no significant difference in the isotopic composition of the fluid associated with the blueschists or the greenschists.

The carbonate was analysed for $\delta^{18}O$ and $\delta^{13}C$ and the isotopic composition of the three samples is quite uniform, with $\delta^{18}O$ around 25‰. The isotopic composition of water in equilibrium with the carbonate can be estimated using the catcite-water fractionation of O'Neil *et al.* (1969), and this gives a value for H_2O of 23.3‰, at an assumed temperature of 450 ^{o}C. The carbon values of the vein material are negative, and range from -5.2 to -3.3, quite different from the $\delta^{13}C$ values associated with marbles, and this may indicate that the carbon values of the fluid have been influenced by isotopic interaction with graphite. Figure 6.20b is a Garlick plot for this locality, and it can be seen, from the associated fluid isopleths, that there is no significant difference in the isotopic composition of the fluid in equilibrium with the blueschists and the altered greenschists. It is very difficult to calculate meaningful fluid-rock ratios in such cases because the amount of fluid involved is so small. Attempted calculations suggest a maximum water to rock ratio of 0.18. It appears that only a small amount of fluid has infiltrated these rocks, enough to mineralogically alter the blueschists but not enough to exceed the capacity of the rocks to buffer the isotopic composition. One reason for the low volume of infiltrating fluid may be the rock chemistry. These rocks are quartz rich and have not experienced any major infiltration-driven devolatilisation reactions. Thus the rocks have remained essentially tight, with fluid flow concentrated along the vein itself.

In conclusion, at this locality the rocks appear to have experienced the rapid injection of fluid, with very limited infiltration into the surrouding host rocks.

Kouroupi gneisses

A similar case was seen in the Kouroupi gneisses near Azolimnos on the east coast of the island. Here foliated and folded glaucophane omphacite gneisses are transformed to albite-chlorite bearing rocks. The retrogression occurs in zones, with a narrow transition area usually less than 50 cms, occurring between fresh blueschists and altered rocks, (see figure 6.21). There is no obvious vein control. The retrogression is conformable with the structure, but it is not apparent whether the retrogression is early, occurring prior to folding, or late. As in the previous example calcitization is not associated with the alteration. The unaltered rocks contain glaucophane, omphacite, epidote and garnet, and these phases are largely replaced by albite and chlorite. The Garlick plot for this locality (figure 6.22), shows very little difference in the isotopic composition of the fluid in equilibrium with the altered and unaltered rocks. It appears that just enough fluid has infiltrated the rocks to mineralogically alter them, but the buffering capacity of the rocks has not been exceeded.

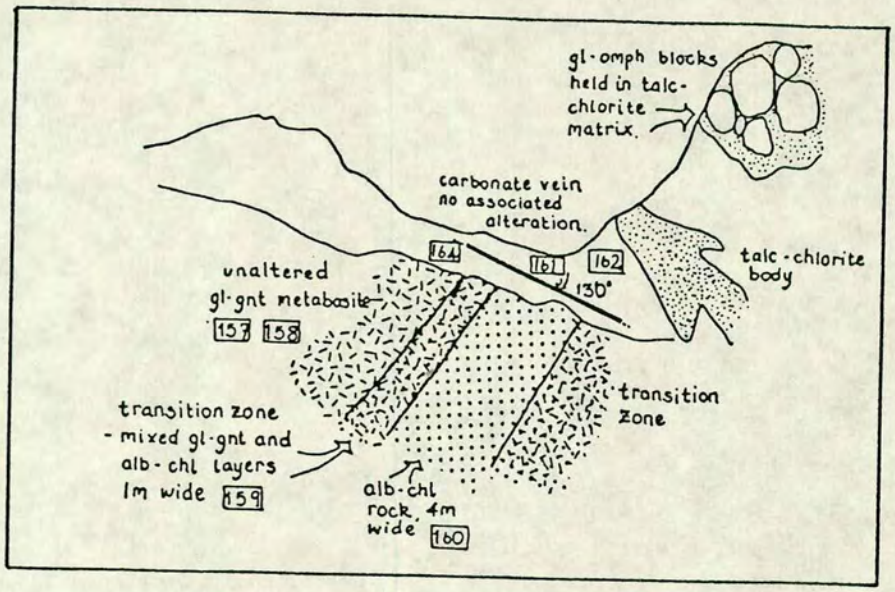

Figure 6.21 Field sketch of the Kouroupi gneisses showing the distribution of altered and unaltered rocks. The alteration occurs in zones, with no obvious vein control.

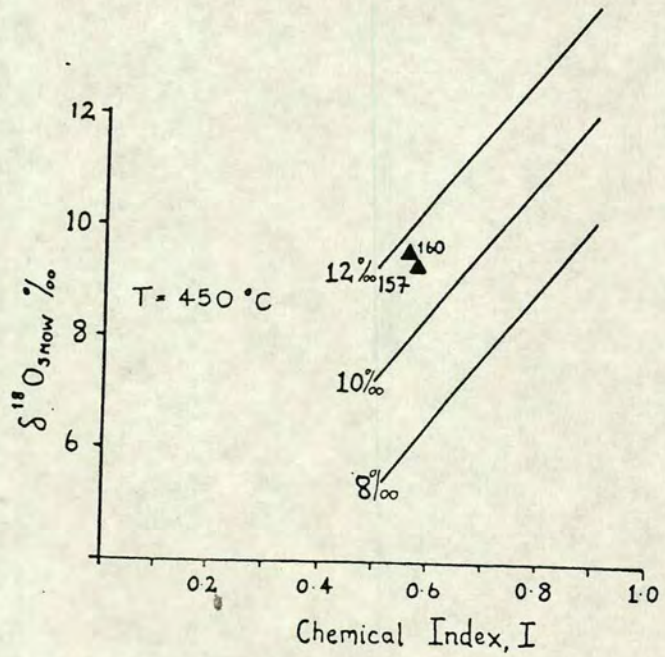

Figure 6.22 Plot of $\delta^{18}O$ versus the chemical index, I. Again, the isotopic composition of the fluid in equilibrium with the gl-gnt metabasite (87/157) and the altered chl-alb "schist", is almost identical.

Alternatively, the infiltrating fluid may have been close to isotopic equilibrium with the rocks already, thus large volumes of fluid could have infiltrated the rocks without affecting the isotopic signature.

Ormos Akhladhi

In contrast to the previous two examples Ormos Akhladhi on the south eastern coast of the island appears to be an area where fluid infiltration has been more extensive and the volume of fluid involved has been larger. At Ormos Akhladhi the sequence comprises intercalated metasediments, impure marbles, thin pure marbles and schists, and metatuffs. The area has experienced extensive post-metamorphic faulting, and the present day outcrop is composed of 3 fault-bounded components, see figure 6.23. The west side of the cove appears to be a lower part of the sequence seen on the east side, but any correlation between the two sides must be viewed cautiously. The west side of the cove is largely composed of metabasite. Relic blueschist phases can be found throughout the rock, and they are particularly well preserved around, and within, folded metachert layers. Much of the rock however now consists of albite, chlorite and calcite. Actinolite is also present, either as a separate phase or mantling glaucophanic cores.

Figure 6.24 shows the whole-rock isotopic compositions of the metabasites displayed on a Garlick plot. Also indicated is the average field for unaltered blueschist metabasites. Samples 130 and 111 have whole-rock values which lie within the general blueschist metabasite field, but samples 21a and 123 are substantially enriched in ^{18}O. The high $\delta^{18}O$ values of these metabasites relative to a fresh blueschist equivalent is evidence for the interaction of these rocks with large volumes of ^{18}O-enriched fluid.

Due to the isolated structural positions of samples 111 and 21a, these samples will not be commented on further. However sample 123, and the significance of its high whole rock value, will be discussed in more detail. Figure 6.25 examines the contact between the metabasite (87/123) and the immediately adjacent marble band in more detail. Taking an average blueschist metabasite whole-rock value as a reasonable pre-infiltration marker, the isotopic composition of the fluid in equilibrium with the metabasite has shifted from an initial value of around 10.7‰ to a final value of 19.8‰, greatly enriched in ^{18}O. It can be assumed that the marble was originally homogeneous with a pre-infiltration value similar to that of unmetamorphosed limestone of the same age, i.e. approximately 27‰. with an associated equilibrium fluid value of 25‰ (O'Neil *et al.* 1969).

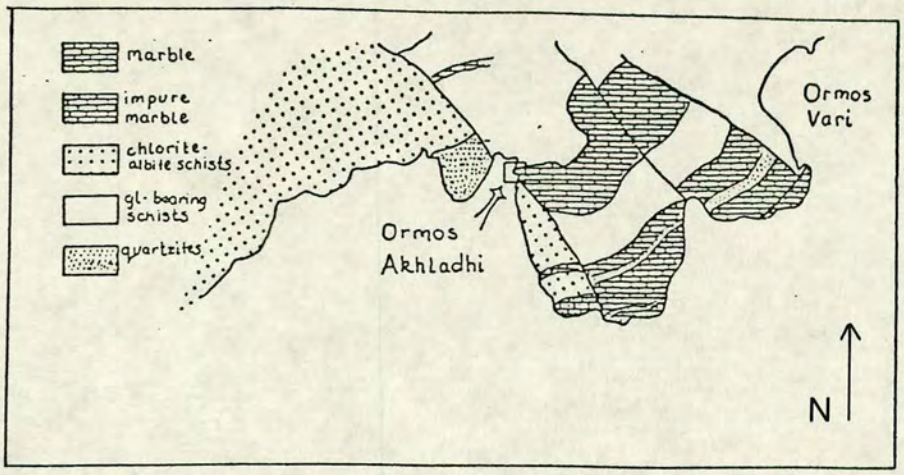

Figure 6.23 Sketch map of the area around Ormos Akhladhi. The box indicates the location of the studied marble unit. Note the occurrence of late faults dissecting the sequence.

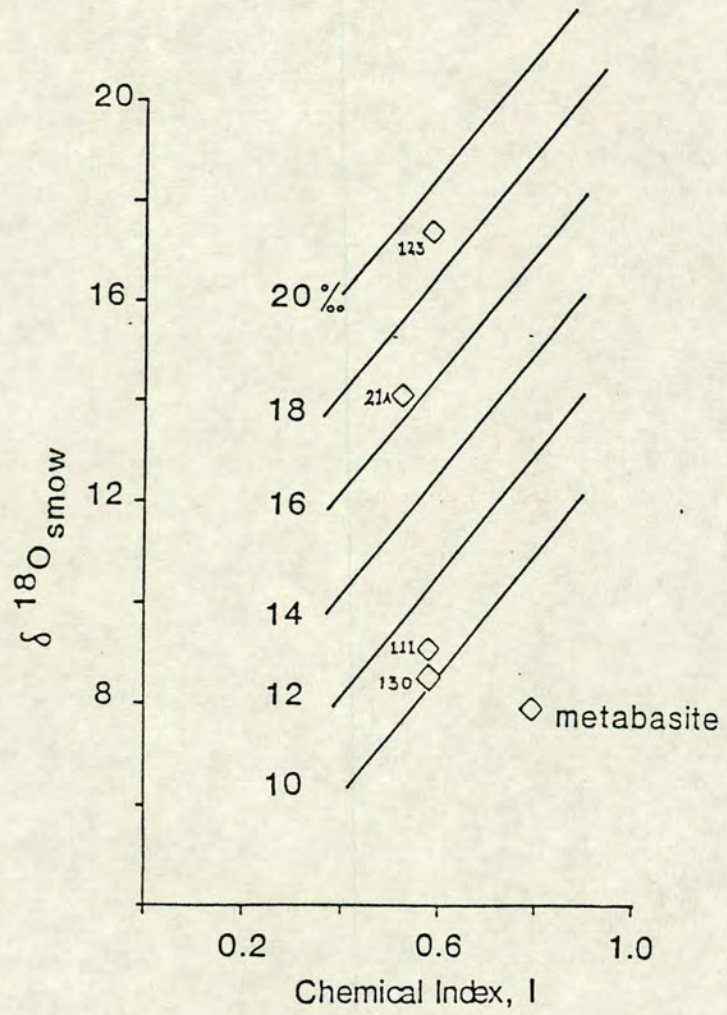

Figure 6.24 Plot of $\delta^{18}O$ versus the chemical index I for metabasites from O. Akhladhi. Shown is an unaltered blueschist metabasite (130) and several greenschist metabasites. The high $\delta^{18}O$ values of 21A and 123 suggests interaction between the rocks and ^{18}O-enriched fluids. (see text)

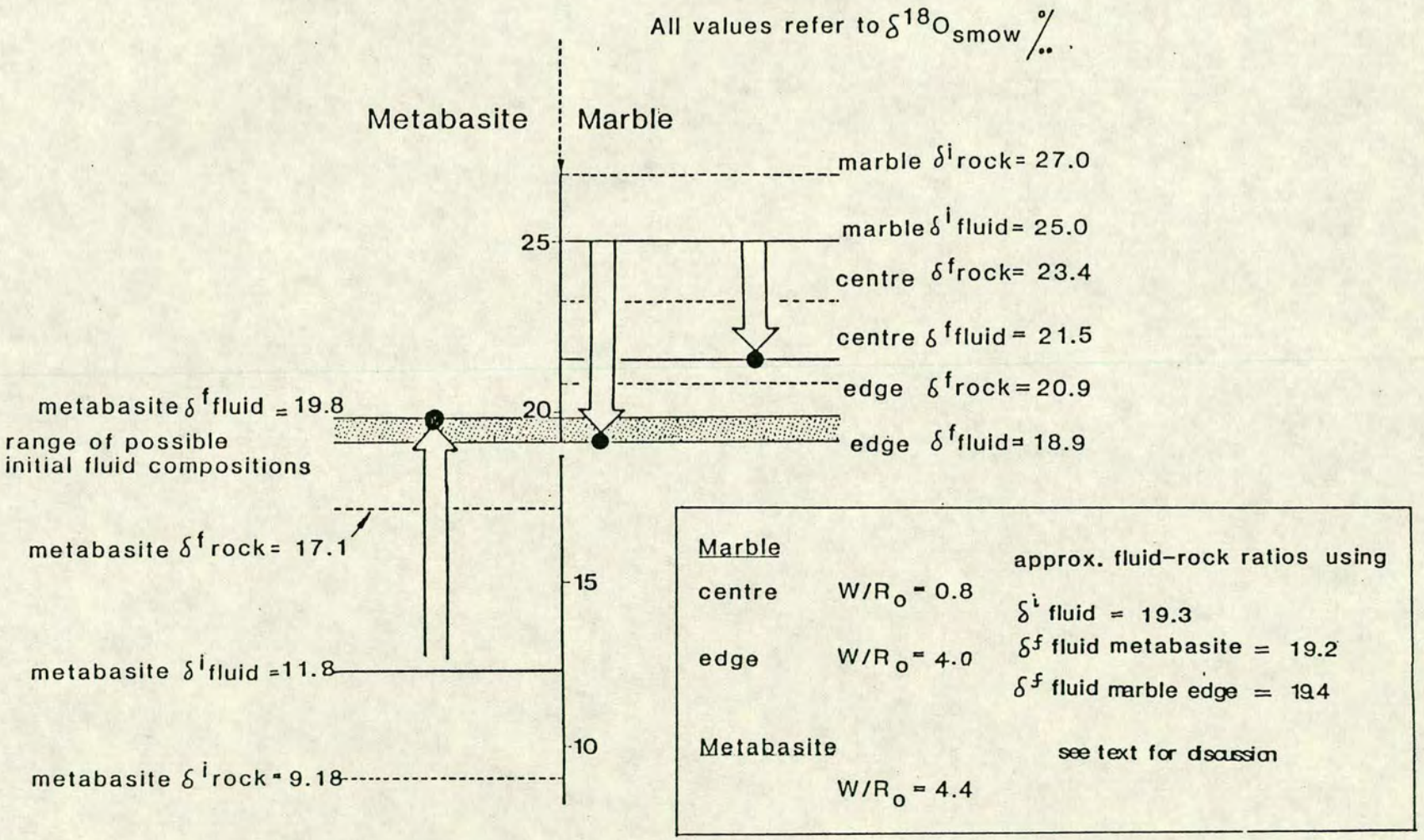

Figure 6.25 The internal marble/metabasite contact is examined in detail (see figure 6.9). Shown are whole rock isotopic compositions (dotted lines) with their associated fluids (solid lines). See text for discussion.

After infiltration the centre of the marble is in equilibrium with a fluid of composition 21.5‰, and the edge of the marble with a fluid of composition 18.9‰.

The final fluid composition in equilibrium with the metabasite is more enriched in ^{18}O than the final fluid in equilibrium with the marble edge. If the same fluid is responsible for the infiltration then this observation is difficult to explain. However, any isotope exchange process in the presence of fluid will be a mixture of both advective and diffusive exchange, and the apparent discrepency in the final fluid compositions can be explained if diffusive exchange between the two rocks continued, via a static pore fluid, after active fluid flow had ceased. In order to perform fluid-rock ratio calculations a value of 19.2‰ was used for the δ^{18}fluid (metabasite), and 19.4‰ for the marble edge. An initial fluid composition of 19.3‰ was used, (see figure 6.25). Infiltration has occurred to a variable degree, with the metabasite layer apparently having seen the most fluid. This is not surprising as the metabasite is the most chemically reactive lithology, and several studies (Rumble and Spear 1983, Rumble *et al.* 1982) have shown that there is a positive correlation between the intensity of devolatilisation reactions and the degree of fluid infiltration. The edge of the marble unit has also been infiltrated by large amounts of fluid, and in this case channelling of the fluid along the metabasite/marble contact will have facilitated exchange. In thin section a number of 'crush' zones are observed, from near the marble edge, where the grain size of the calcite is greatly reduced, and these lines of structural weakness may also have aided fluid infiltration. The centre of the marble has the lowest water-rock ratio, and the highest values for $\delta^{18}O_{calcite}$, indicating that this central portion has still acted as a partial barrier to fluid flow.

Summary

From the whole-rock isotopic data it appears that the blueschist to greenschist transformation has been accompanied by variable degrees of fluid infiltration, though in general the volume of fluid involved has been low, and the capacity of the rock to resist changes in itsisotopic composition has not been exceeded. This conclusion is reinforced by the presence of distinctly separate fluid fields for the schists and the metabasites. As the isotopic composition of the infiltrating fluid has been buffered by the rock it is difficult to determine what the initial isotopic composition of the fluid was. At Ormos Akhladhi, where larger fluid fluxes are indicated, the ^{18}O enrichment of metabasite suggests an initial composition of around 19.3‰ for the infiltrating fluid. It is difficult to assess whether this value is a representative one for the retrograde fluid as a whole, or whether the enriched fluid was only present in this area.

Examining the relationship between the fluid isopleths and the whole-rock compositions in figure 6.18, it it apparent that devolatilisation reactions in the schists could produce a fluid with an isotopic signature between approximately 17.5 and 20‰.

6.10 OXYGEN ISOTOPE DATA - MINERAL SEPARATES

The major minerals from 10 representative samples have been separated and analysed for $\delta^{18}O$. The isotopic compositions of the coexisting mineral phases are listed in table 6.11, and these are represented graphically in figures 6.26a and 6.26b.

Sample preparation

Cleaned specimens were crushed by hand using a large iron pestle and block. The crushed samples were sieved to obtain a size fraction corresponding to the grain size of the rock, generally between 90 and 170 microns. Mineral separation was achieved using standard heavy liquid and magnetic techniques. The purity of the separates was checked regularly using grain mounts and X.R.D. analysis. If necessary further purification was achieved by hand picking. The final purity of the samples was at least 90 %.

Metasediments

(samples 86/73, 86/74, 86/78, 86/25, 87/173)

The $\delta^{18}O$ values for quartz are generally high, ranging from 16.1 to 21.5. The carbonate analysed from sample 86/74 has a $\delta^{18}O$ value of 24.4‰ and is clearly out of isotopic equilibrium with the rock. Possible reasons for carbonate disequilibrium were mentioned in section 6.5, and will not be discussed here. Samples 86/25 and 87/173 are greenschists in which glaucophane is not preserved. Also shown in figure 6.26a are the ideal fractionations between the coexisting phases based on the calculated fractionation factors of Bottinga and Javoy (1975, 1973) and Javoy (1977), at a temperature of 450 ^{o}C.

Table 6.11 $\delta^{18}O(‰)$ values of mineral separates.

Sample No.	Description	Mineral	$\delta^{18}O(‰)$
BLUESCHIST METASEDIMENTS			
86/73	Blueschist	quartz	17.5
		w. mica	15.6
		glaucophane	13.6
		W.R.	16.3
86/74	Blueschist	quartz	18.7
		W.R.	16.8
86/78	Chloritoid blueschist	quartz	20.2
		w. mica	17.3
		glaucophane	15.7
		garnet	14.0
		W.R	16.2
87/SY4	gl-gnt metabasite	quartz	11.5
		glaucophane	6.6
		W.R.	9.2
GREENSCHISTS			
86/25	cc-alb greenschist	quartz	19.6
		w. mica	16.1
		W.R.	18.0
87/173	chl-alb schist	quartz	21.5
		w. mica	18.0
		W.R.	19.0
86/40	chl-actinolite schist	albite	16.2
86/205	chl-alb schist	albite	16.1
		w. mica	14.4
		chlorite	11.1
86/124	cc-chl-alb vein in blueschist metabasite	chlorite	7.6
		albite	11.2
		calcite	24.1
86/214	cc-chl-alb vein in altered metabasite	chlorite	5.8
		albite	10.0
		calcite	11.9
87/138	chl-alb meta-acidite	quartz	10.6
		w. mica	6.7
		W.R.	10.5

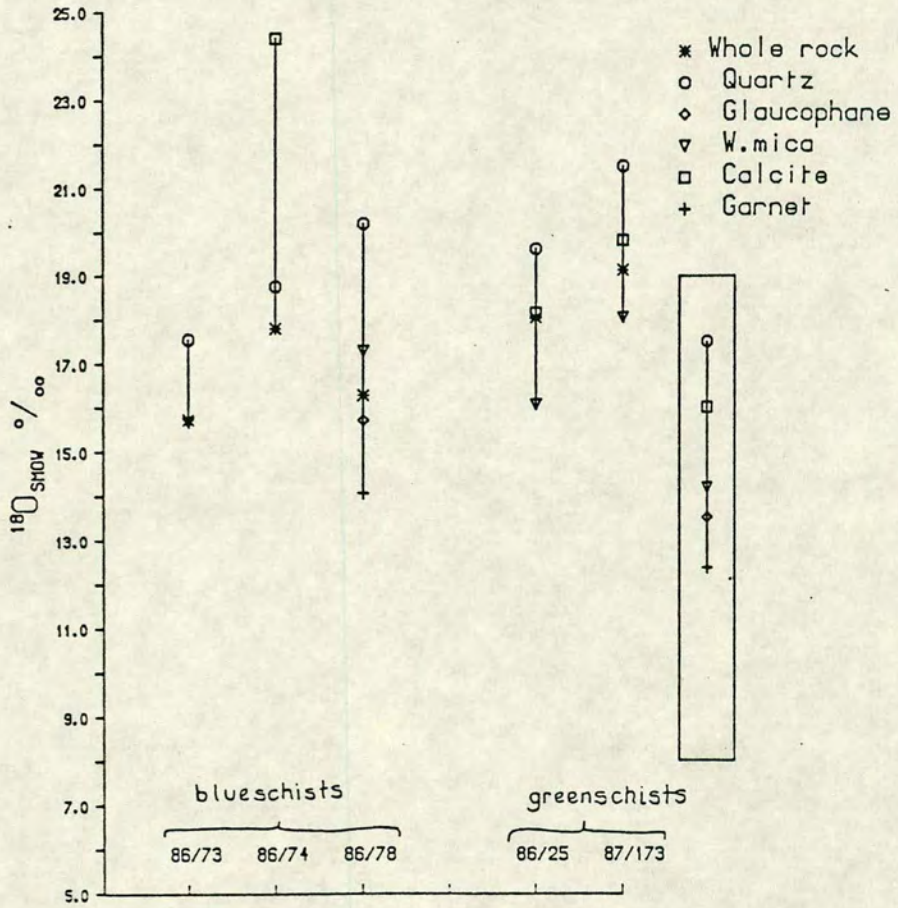

Figure 6.26a $\delta^{18}O$ values for assemblages of coexisting minerals in schists. Vertical lines connect analyses of minerals from the same sample. Note there are no isotopic reversals indicating a reasonably close approach to isotopic equilibrium. The ideal mineral fractionations for the phases encountered are shown in the box. Fractionations calculated using Bottinga and Javoy (1969) at an assumed temperature of 450°C.

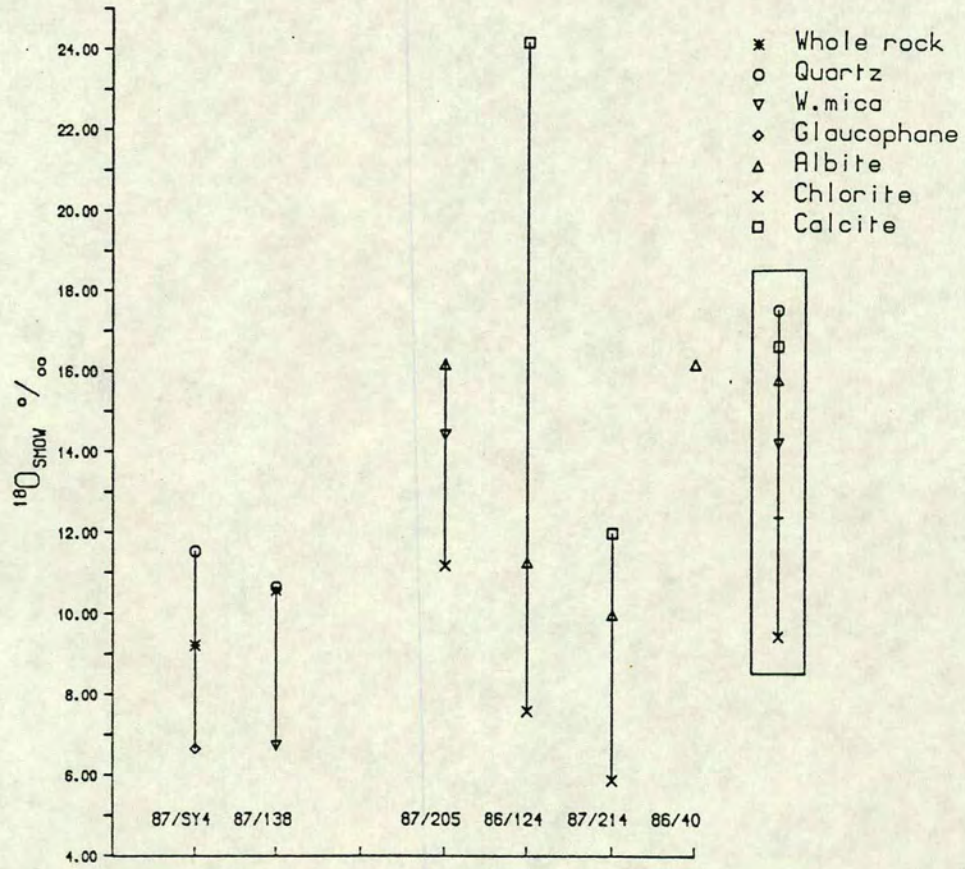

Figure 6.26b $\delta^{18}O$ values for coexisting minerals in metabasites. SY4 is a gl-gnt metabasite, 87/138 is a greenschist metabasite from the same locality, Agkathopes. Four albite-bearing samples are also plotted, note that the albite is not isotopically homogeneous. (see text for discussion)

Metabasites (samples SY4, 87/138)

87/SY4 is a pristine glaucophane-epidote gneiss, whereas 87/138, from the same locality, has experienced vein-controlled greenschist alteration, and is now composed of chlorite (pseudomorphing glaucophane), relic epidote and albite. Despite their different histories there are no significant whole-rock isotopic differences between the two samples.

Albite bearing rocks

Samples 87/205, 86/124. 87/214 and 86/40 contain albite porphyroblasts. 87/205 is a basic greenschist metasediment from Kini, containing the assemblage alb-chl-ep-qtz-sph-tour. 86/124 and 87/214 both come from cc-qtz-alb-chl veins in metabasite which have an associated retrograde halo. 86/40 comes from Kastri on the north-east coast. The rock is very magnesian in composition, and contains the assmeblage chl-act-talc-qtz-w.m-albite-cc-sph. The petrography and distribution of the albite porphyroblast schists has been discussed in chapter 5.

From the work of Watkins (1985), it was suggested that albite porphyroblast schists may delineate former zones of high fluid flux. Thus the four samples were analysed primarily to deteremine if the albites were isotopically homogeneous. It is obvious from figure 6.26b that the albite separates are not isotopically homogeneous. $\delta^{18}O$ cover a range from 9.9 to 16.2‰. Interestingly, the $\delta^{18}O$ values for rock 87/205 (16.1 ‰) and 86/40 (16.2 ‰) are almost identical, but on the small amount of data available it is not possible to say whether this represents the presence of a common albite-forming fluid, or just coincidence. It should be noted that unless vey large amounts of fluid are involved in forming the albite porphyroblast schists, homogeneous isotope values for albite are unlikely to occur. Subsequent exchange with the surrounding rock may substantially alter the isotopic signature of the albite. For instance, it may not be coincidental that samples 86/124 and 87/214, which both occur as veins in metabsites, also have the lowest $\delta^{18}O$ values for albite.

6.11 ATTAINMENT OF OXYGEN ISOTOPE EQUILIBRIUM.

The application of oxygen isotope geochemistry to geological problems depends on the assumption that isotope equilibrium has been established and preserved. The degree to which interlayered rocks have attained isotopic equilibrium can be used as a

a guide to the nature and extent of fluid-rock interaction. Two relative scales of oxygen isotope equilibrium need to be considered.

1) Local equilibrium

This implies that equilibrium has been established on the scale of a single bed, and that isotopic homogenisation has not occurred between different rock types, even for a sequence of adjacent beds. The minerals can exchange isotopes with one another within the closed system, and the final fractionation between mineral pairs will depend on the temperature of equilibration. Two criteria can be used to test for the attainment of local equilibrium, and these are:

a) Constant isotopic fractionation between coexisting mineral phases regardless of the bulk isotopic composition of the rock. This requires that there should be no reversals in the relative order of ^{18}O enrichment between the coexisting minerals.

b) Temperatures estimated from the isotopic fractionation between different mineral pairs should be internally consistent.

2) Large-scale equilibrium

In contrast to equilibrium on a local grain-to-grain scale, equilibrium may be established on an outcrop scale in the presence of a pervasive fluid.

The extent of oxygen communication between interlayered rocks can be assessed by the degree to which mineral phases in the different rock layers show uniform isotopic compositions despite original isotopic variations which existed prior to metamorphism.

Some studies have identified isotopic homogenisation on scales ranging from centimetres to hundreds of metres (Anderson 1967; Shieh and Schwarcz 1974; Taylor *et al.* 1963). Such large-scale isotopic exchange and homogenisation suggests that the rocks have been pervasively infiltrated by a large volume of isotopically homogeneous fluid. In using this criterion to establish large scale equlibrium, it is tacitly implied that the $\delta^{18}O$ values of the mineral were different prior to infiltration. Although this may seem a logical assumption for rocks of differing bulk composition, it is critical to establish the existence of pre-metamorphic/pre-infiltration isotopic heterogenity. The occurrence of local equilibrium within the rock layers has been evaluated by examining the mineral-separate isotopic data. As can be seen from figures 6.26a and 6.26b, the isotopic fractionation between the same mineral pair is not identical in every sample, and neither do the fractionations match exactly with

those calculated theoretically. However, there are no reversals in the expected order of ^{18}O enrichment, indicating a reasonably close approach to isotopic equilibrium.

The blueschist samples show greater variations in the isotopic fractionation between the various minerals than the greenschist samples. The quartz-white mica fractionations vary by more than 1‰, from 1.89‰ to 2.92‰ and the quartz-glaucophane fractionation varies from 3.9‰ to 4.5‰. In contrast, the greenschist samples show smaller variations, 3.47‰ and 3.56‰ for the quartz-white mica fractionation, and 1.48‰ and 1.69‰ for the quartz-calcite fractionation. The albite-chlorite fractionation, by contrast, varies from 3.7‰ to 5.0‰.

Although variations in the mineral-pair fractionations may indicate that isotopic equilibrium was not established during the primary event, it is equally likely that the scatter is due to retrograde isotopic exchange. Fluid infiltration during the blueschist to greenschist transformation may have allowed the affected rocks to re-equilibrate both mineralogically and isotopically, and thus the mineral fractionations in the greenschists (e.g. 86/25, 86/173) are not dispersed. Some of the more permeable blueschists may also have experienced a limited amount of fluid infiltration connected with the greenschist events. The presence of an externally derived intergranular fluid film would enhance retrograde exchange without visibly affecting the mineral assemblages. Such a process could explain the scatter in mineral-pair fractionations from the blueschist samples.

Scale of equilibration

Large-scale oxygen-isotope equilibration in the blueschists has been examined by comparing the isotopic compositions of quartz from series of interlayered rocks. Figure 6.27 illustrates one such outcrop. Within the individual layers the mineral phases show a reasonably close approach to isotopic equlibrium there is a 2.5‰ variation in the $\delta^{18}O$ values of quartz between the different units. Isotopic heterogenity on such a small scale indicates limited fluid communication across layers.

Unfortunately this is the only example where mineral-separate data are available from a series of interlayered rocks at one locality. However, the conclusion that the minerals in the different rocks have not equilibrated with a pervasive fluid of constant isotopic composition is supported by the whole rock analyses.

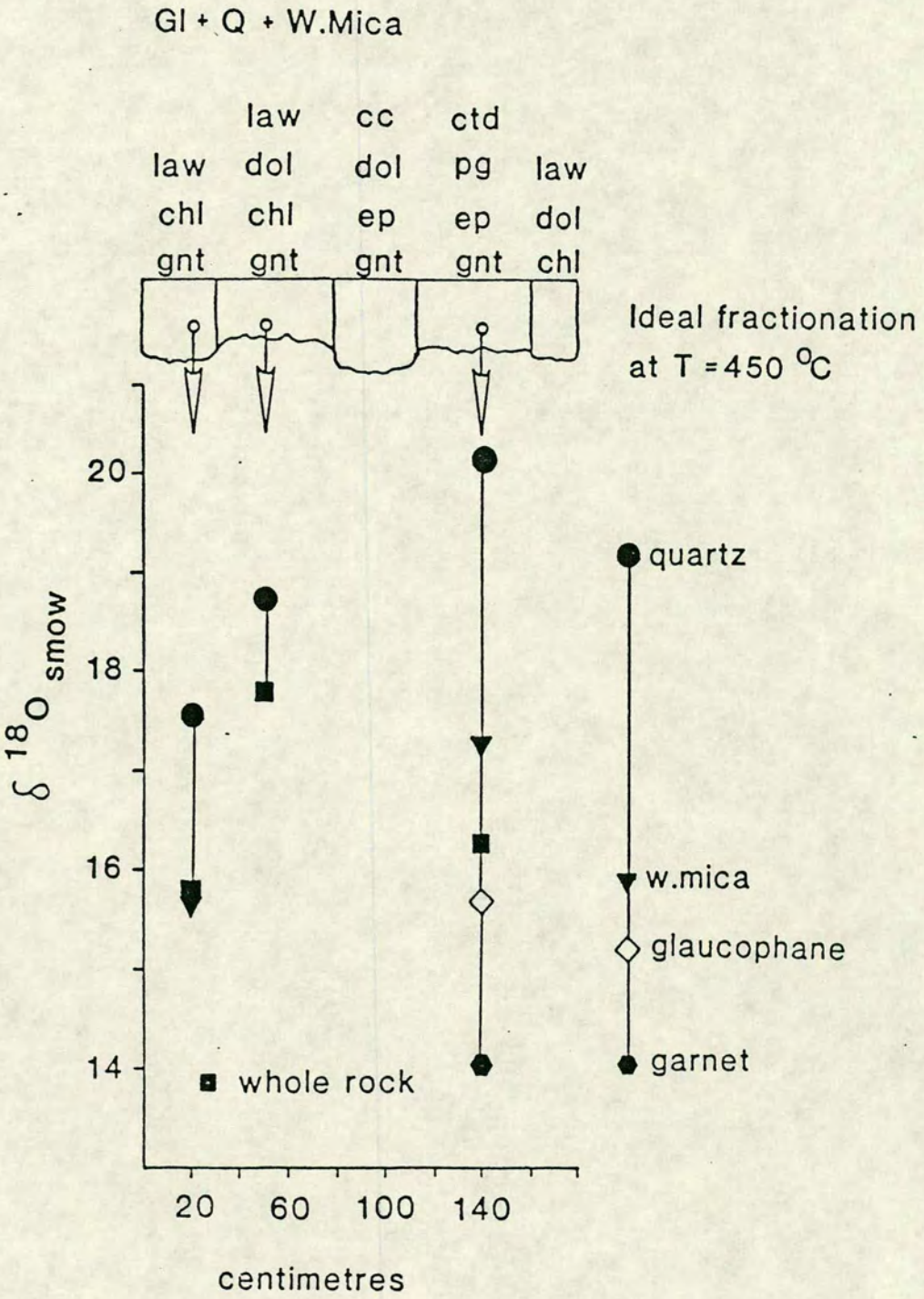

Figure 6.27 $\delta^{18}O$ values of coexisting minerals from three blueschist rocks. The assemblages present in each layer are indicated at the top of the diagram - all the rocks contain qtz, glaucophane and white mica. There are no isotopic reversals within layers, but a variation of 2.5°/∞ exists bewteen the $\delta^{18}O$ values of quartz for the 3 samples.

6.12 OXYGEN ISOTOPE GEOTHERMOMETRY

Estimates of metamorphic temperature are given in table 6.12. These estimates have been made using the mineral separate data and both calculated (Bottinga and Javoy 1973; Javoy 1977) and experimental fractionation factors (Matsuhisa *et al.* 1979; Matthews *et al.* 1983). The temperatures estimated from the theoretical calibrations are quite close to the proposed mineralogical temperatures (470 ± 30 ^{o}C), and they are 50 to 150 ^{o}C higher than the temperatures determined from the experimental calibrations. Mineral pairs that have large $\Delta^{18}O$ fractionations, e.g. quartz and magnetite, provide the most precise temperature estimates, whereas mineral pairs with small mineral-mineral $\Delta^{18}O$ fractionations are susceptible to uncertanties in the measured δ values which can produce large errors on the temperature estimates. Minimum error values have been calculated for the theoretical calibrations using the expression given by Deines (1977). The errors reflect the size of the isotopic fractionation between mineral pairs, and the experimental precision of the $\delta^{18}O$ analyses, which is 0.4‰.

Temperature estimates for the different rocks have also been made using the graphical method of Javoy *et al.* (1970). The isotopic fractionation between minerals is a function of temperature:

$$\delta_Q - \delta_{mineral} = A.10^6/T^2 + B \quad \text{where A and B are constants}$$

If all the minerals in a quartz-bearing rock are in isotopic equilibrium, then a plot of $(\delta_{Q\text{-mineral}})$-B versus A should produce a straight line passing through the origin with a slope of $10^6/T^2$. The resultant graph not only provides a visual means of assessing isotopic equilibrium, but also allows an average temperature estimate to be made for the rock as a whole. Figure 6.28 shows a number of these plots. It can be seen that the unaltered blueschists, 86/73, 86/78 and 87/SY4 have preserved higher isotopic temperatures (518-625 ^{o}C) than the equivalent greenschist rocks (456-485 ^{o}C), which may reflect the fact that the blueschists have seen less fluid after the peak metamorphic event. The lack of data for the greenschist samples means that it is impossible to draw any firm conclusions about isotopic equilibrium from this diagram. However it is intriguing that the three temperature estimates lie within a very narrow range

Rocks 86/73 and 86/78 are from the same locality and were collected just over a metre apart. 86/73 appears to be in approximate isotopic equilibrium as the qtz-mica and the qtz-amphibole pairs define a straight line with T = 625 ^{o}C. Although the qtz-mica and the qtz-amphibole pairs (in rock 86/78) define a reasonably straight line, the garnet point is displaced some distance from this.

Table 6.12 Comparison of fractination temperatures (°C) determined by experimental fractionation data and by theoretical calibrations. Errors in A. calculated using the expression in Deines (1977).

A. Theoretical fractionation data (Bottinga and Javoy (1973) and Javoy (1977).

Samples

Metasediments

	TQ-M	TQ-AM	TQ-gnt	TMU-AM	TMU-gnt	TAB-chl	TAB-MU
86/25	454±17						
86/173	462±18						
86/73	668±38	593±20		470±43			
86/78	517±22	537±17	411±56	591±68	236±19		
Metabasites							
87/138	480±19						
87/SY4		517±16					
87/205						547±12	448±30
86/124						645±17	
87/214						609±15	

B. Experimental Calibrations

Metasediments

	TQ-MU	TQ-CC	TAB-MU	TCC-MU
86/25	386	308		436
86/173	395	271		444
86/73	634			
86/78	455			
Metabasites				
87/138	414			
87/205			498	

Source of experimental fractionations:

1000 ln α_Q - H_2O = 3.13 (10^6T^{-2})-2.94 (T = 400-500°C) (Matsuhisa et al. 1979)
1000 ln α_Q - AB = 0.50 (10^6T^{-2}) (Matthews et al. 1983)
1000 ln α_Q - CC = 0.50 (10^6T^{-2}) (Matthews et al. 1983)
1000 ln α_Q - MU = 1.55 (10^6T^{-2}) (Matthews et al. 1983)

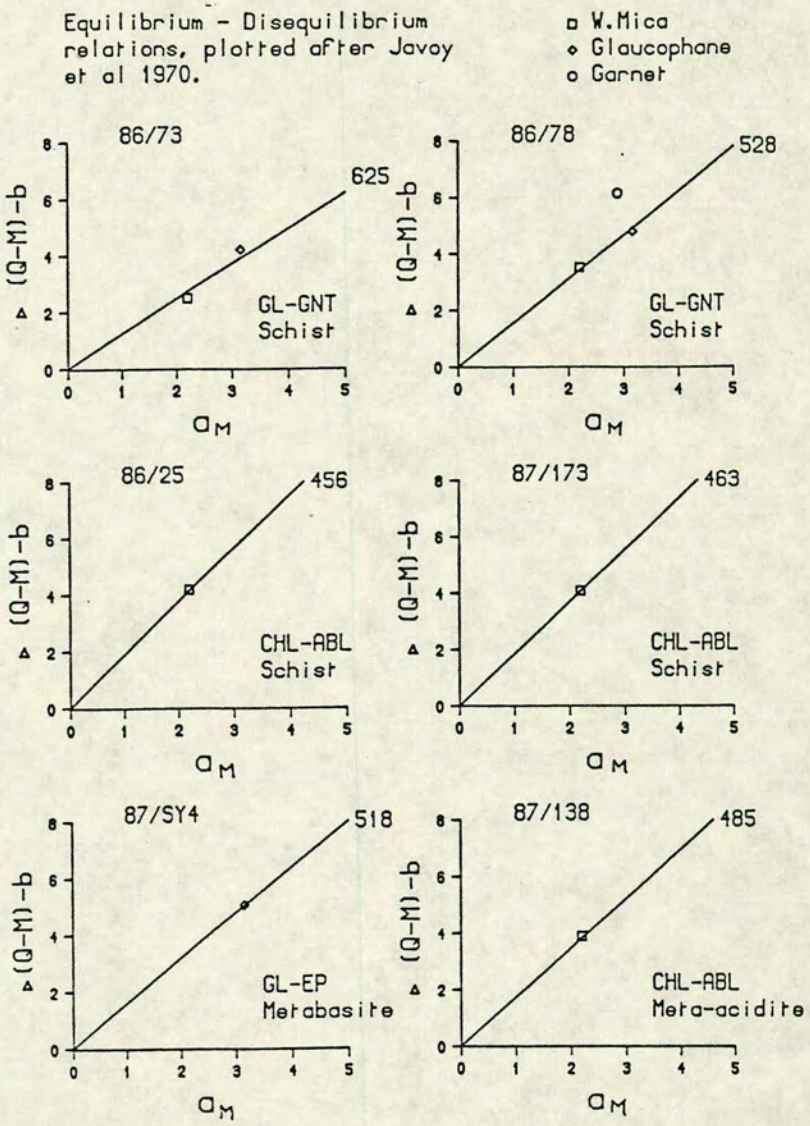

Figure 6.28 Plots of Q_M versus $\Delta(Q\text{-}M)\text{-}b_M$ for blueschist and greenschist samples showing suggsted isotherms.

A straight line from the garnet point through the origin defines an isotherm with T = 402 ^{o}C, the lowest isotopic temperature estimated. It appears that while the mica and the amphibole have retained their isotopic compositions the garnet has continued to exchange at lower temperature. This conclusion is in conflict with a number of studies which suggest that garnet is more likely to retain peak isotopic values as it is not easily reset at lower temperatures. Freer and Dennis (1982) also proposed that because of their slow diffusion rates quartz-garnet pairs are more likely to freeze-in their isotopic ratios. This discrepancy is unexplained, as the garnets in 86/78 are of typical composition (grossular rich almandines), and are virtually unaltered.

87/73 and 87/78 have similar mineralogies and modal abundances, and were metamorphosed under identical P-T conditions. Therefore it seems likely that very similar temperature estimates should be produced from the same mineral pair in the different rocks. However, figure 6.27 shows that the isotherms for the two rocks are 100 ^{o}C apart. Ignoring the fact that the isotherm for rock 73 is probably too high at 625 ^{o}C, the temperature difference suggests that rock 78 has experienced some isotopic re-equilibration.

Discussion

Over the last three decades several attempts have been made to use mineral-pair ^{18}O fractionations to estimate the maximum equilibration temperature of mineral assemblages. Clayton and Epstein (1958) suggested that the existence of isotopic equilibrium among three minerals could be verified if the three phases yielded two isotopic temperature estimates which agreed within experimental error. Applying this criterion, many mineral assemblages were discovered to be out of isotopic equilibrium (Garlick and Epstein 1967). Javoy (1977) recognised that isotopic re-equilibration was a common occurrence, and suggested that each mineral pair in a rock would give a different temperature unless all the diffusion parameters in each mineral were similar. A major breakthrough occurred in the mid-seventies when developments in analytical techniques made it possible to measure oxygen diffusion in minerals (Freer and Dennis 1982; Giletti and Anderson 1975). The interpretation of oxygen isotope geothermometry has been greatly enhanced by this new knowledge.

Oxygen diffusion rates have been determined for a variety of minerals under different P-T conditions: feldspar - Elphick *et al.* 1988, 1986; Giletti *et al.* 1978, quartz - Elphick *et al.* 1988; Elphick and Graham 1988; Giletti and Yund 1984, phlogopite - Giletti and Anderson 1975, magnetite - Castle and Surman 1969, amphibole - Farver and Giletti 1984, diopside - Farver 1989. Experiments on framework silicates

showed that under dry conditions the rate of diffusion was several orders of magnitude slower than in wet systems (Elphick *et al.* 1988; Freer and Dennis 1982; Giletti 1985).

A number of studies, discussing the petrological implications of these results, reinforced the conclusion that maximum metamorphic temperatures could only be preserved if fluid was lost from the system after the peak event. (Elphick *et al.* 1988; Elphick and Graham 1988; Giletti 1985; Graham 1981).

These ideas have been extended further in an influential paper by Giletti (1986). Giletti (1986) calculated the $^{18}O/^{16}O$ temperatures that would be measured for a rock which consisted of only three minerals (quartz, hornblende and feldspar), and cooled ideally from high temperature. The calculations take into account the diffusion rates of oxygen as a function of T, the cooling rate of the rock, the mineral grain sizes and the mode of the rock. The apparent isotopic temperatures calculated for the 3 mineral pairs were,

$\Delta_{qtz\text{-}hbl} = 605\ ^{o}C$

$\Delta_{qtz\text{-}pl} = 515\ ^{o}C$

$\Delta_{pl\text{-}hbl} = 655\ ^{o}C$

The oxygen diffusion rates in the three minerals are quite different, with feldspar exchanging very much faster than either quartz or hornblende (see fig. 6.29). The minerals also have different closure temperatures (the temperature below which O-exchange effectively ceases). Oxygen exchange will occur between a mineral pair until the temperature falls below the closure temperature for one of them. The other mineral can continue to exchange with other phases in the rock until the second last phase closes when the system must stop exchanging because the remaining phase has no other mineral to exchange with. If feldspar is present in a rock it will usually be the last mineral to close because of the rapid diffusion of oxygen in feldspars. This means that feldspar-mineral pairs will have the largest fractionation and record the lowest apparent temperature. Giletti (1986) concluded that for slowly cooled igneous and metamorphic rocks temperatures determined by mineral-pair fractionations will relate neither to the maximum equilibration temperatures nor to the mineral closure temperatures at which diffusional exchange ceases. Instead, the recorded temperatures are a function of the mineral modes in the rock, the diffusional properties of the different minerals, the grain size and the cooling rate.

Thus, in general, consistent temperature estimates from several mineral pairs in a rock may not be a reliable indicator of isotopic equilibrium.

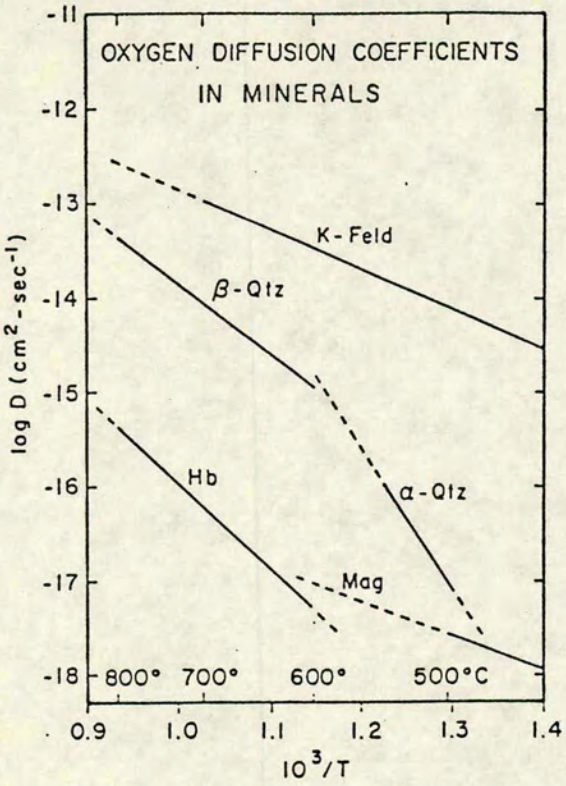

Figure 6.29 Arrhenius plots of oxygen self-diffusion coefficeints for K-feldspar, quartz, hornblende and magnetite (from Giletti 1986).

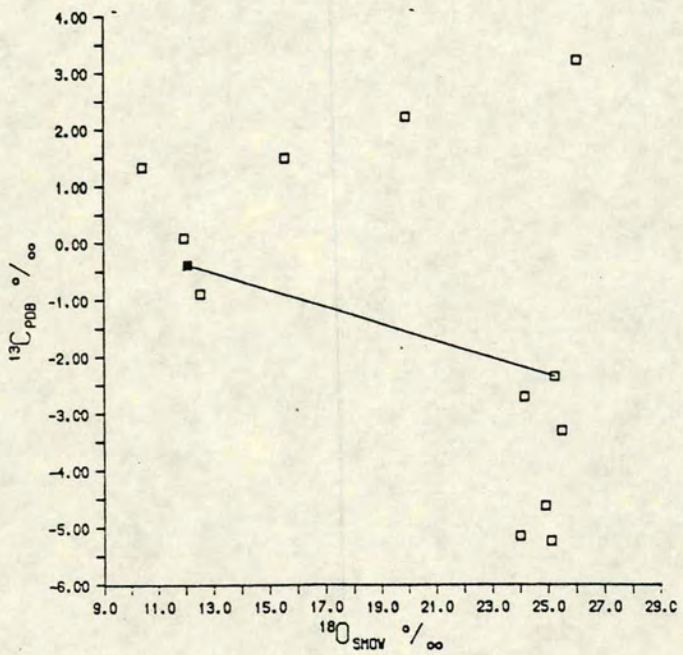

Figure 6.30 Plot of $\delta^{18}O$ versus $\delta^{13}C$ for carbonate forming veins or segretation. The line refers to sample 87/145 and connects analyses of coexisting calcite and dolomite (filled symbol).

6.13 VEINS AND SEGREGATIONS - ISOTOPIC DATA

Introduction

In any metamorphic rock a delicate balance exists between the rate of fluid production, and the permeability of the rock. If the permeability is too low, the fluid pressure will rise until the rock ultimately fractures. Thus veins and segregations can be seen as representing "fossil" fluid pathways, and it should be possible to gain more information on the isotopic composition of the fluid by analysing vein minerals.

This section presents the results of isotopic work carried out on the veins and segregations. The majority of the veins sampled occurred in metabasite, and they ranged in size from less than a centimetre, up to tens of centimetres wide. The veins are predominantly formed of carbonate, albite, quartz and chlorite, and a retrogression halo is commonly associated with them. Quartz-carbonate segregations or lenses are more common than veins in the blueschist metasediments, and these are not accompanied by any visable retrograde effects. The lenses occur parallel to the foliation and the assemblage chl+cc+(dol)+qtz$\pm$alb is commonly found. Unequivocal high pressure phases are absent.

Carbonate in veins

Table 6.13 lists the $\delta^{18}O$ and $\delta^{13}C$ values for the carbonate analysed from vein samples and this information is represented graphically in figure 6.30. A distinct bimodal grouping is present with a high ^{18}O group, ($\delta^{18}O$ around 24-25‰) and a low ^{18}O group, ($\delta^{18}O$ between 10-12‰). Despite their widely spaced geographic distribution, the veins fall in a narrow range of $\delta^{18}O$, suggesting formation from a common fluid of constant isotopic composition. This means that the fluid cannot have interacted with the host rocks to any significant degree, and fluid flow must have been focussed along the vein itself. The scatter seen in $\delta^{13}C$ may indicate low CO_2/H_2O ratios in the fluid, with the carbon signature being locally controlled. There are two alternative explanations to account for the low-^{18}O vein group. These veins may indeed constitute a separate group, and formed from an $^{18}0$-depleted fluid of roughly constant isotopic composition. Alternatively, the same fluid may have formed both the enriched and the depleted vein groups, but differing degrees of subsequent exchange with the surrounding host rocks now masks their common origin.

Table 6.13 Carbon and oxygen isotope analyses of carbonate from veins and segregations.

sample #	δ^{18}Osmow	δ^{13}Cpdb	description
86/32	24.00	-5.17	qtz-carb. segregation in partly altered blueschists, Kastri
87/Kini	15.53	1.50	5cm wide cross-cutting qtz-cc vein in retrogressed basic schist, Kinit
87/124c	19.87	2.13	qtz-cc vein in marble, O. Akhladhi
86/123	24.14	-2.728	10 cm wide cc-alb vein in blueschist metabasite, Ermoupolis, pronounced retrograde halo surrounds vein
87/161	26.02	3.22	8cm wide carbonate vein in gl-omph metabasite, Kouroupi gneisses
87/115A	12.54	-0.90	cc-qtz vein in greenschist metabasite
87/214	11.95	1.33	cc vein in metabasite, vein with retrogession halo (30cm wide) Komito
87/138	25.49	-3.32	small veinlet off main vein, extensive chloritization of host quartz glaucophanites, Agkathopes
87/136	25.10	-5.25	top of main vein associated with alteration, Agkathopes
87/142	24.89	-4.64	bottom of same vein, Agkathopes
87/145	25.23	-2.38	qtz-carb (cc+dol) segregation in qtz glaucophanites, Agkathopes, calcite analysis.
	12.08	-0.39	dolomite analysis

Another possibility is that the same fluid formed both the enriched and the depleted vein groups, however differing degrees of later exchange now masks their common origin. Based on the limited amount of data available it is impossible to narrow down the range of options on the origin and interpretation of these veins further.

In addition to the carbonate analyses quartz was separated from two mixed quartz-carbonate segregations, and one vein. The $\delta^{18}O$ ratios for these samples are given in table 6.14 below, and a rather confusing picture emerges, as in two of the three samples the quartz and carbonate portions of the rock are not in equilibrium.

Table 6.14

Sample no.	Description	$\delta^{18}O_q$ ‰	$\delta^{18}O$ carb.
86/32	qtz-carb segregation in partly altered blueschists, Kastri	11.3	24.0
87/124	cross-cutting qtz-cc vein in marble (1.5 cm wide), O. Akhladhi	20.5	19.9
87/145	qtz-carbonate (cc+dol) segregation in qtz-glaucophanites, no halo	8.6	25.2 (cc) 12.1 (dol)

There are two possible explanations for these data:

1) The veins may have acted as fluid channelways over a period of time, sampling several different fluids. Evidence for such multiple fluid events was given by Yardley (1983), following his discovery of a wide range of compositionally distinct fluid inclusions within single quartz veins in Connemara. If such processes were operating, then the quartz and calcite could have been deposited at different times from two isotopically distinct fluids. If the fluids moved relatively rapidly along the fractures then there would be little chance for re-equilibration with the earlier formed phases.

It should also be noted that in samples 86/32 and 87/145 the $\delta^{18}O$ values of the quartz are quite different from those in the surrounding host rock

Sample #	$\delta^{18}O$quartz	description
86/32	11.26	segregation in altered blueschists, Kastri.
86/25	19.62	nearby altered schist
87/145	8.56	segregation in blueschist gneisses, Akathopes.
87/138	10.60	altered gneiss
87/SY4	11.50	unaltered gl-ep gneiss

The difference in the $\delta^{18}O$ values of the quartz reaffirms the conclusion that these quartz segregations have not formed by the local dissolution and reprecipitation of quartz from the surrounding rocks, and that they do indeed represent the site of healed fractures. The isotopic differences between the vein and wall rock quartz probably indicates that the fluid in the veins did not interact isotopically with the wall rocks.

All the segregations contain carbonate in addition to quartz. In the field the carbonate is dark brown in colour, and it was assumed to be ankeritic in composition. Thin section examination reveals extensive exsolution of iron along the carbonate cleavage planes, and X.R.D. analysis shows that the carbonate present is calcite, although cathodoluminescence reveals small areas of residual dolomite. It appears that, like the carbonate in the schists, these segregations have experienced calcitization of the primary dolomite-ankerite phase. Thus the isotopic signature measured today may well not be that of the original carbonate. Sufficient dolomite remained in sample 87/145 to analyse, but the dolomite is not in isotopic equilibrium with the coexisting calcite or quartz.

Sample 87/124 is different from the other two samples in that the carbonate has apparently always been calcite, and the quartz and carbonate portions of the vein are in approximate isotopic equilibrium. $\delta_{qtz} - \delta_{cc} = 0.7‰$, and the predicted fractionation at 450 ^{o}C is 0.95‰ (Matthews *et al.* 1983a). This vein comes from the marble unit at Ormos Akhladhi where fluid fluxes are thought to be high. The initial composition of the infiltrating fluid at this locality was estimated from the fluid isopleths on the whole-rock Garlick plot to be approximately 19.5 ‰. Do the vein minerals provide a corroboratory fluid value ? The isotopic signature of the fluid was

calculated using the quartz-water fractionation of Matsuhisa *et al.* (1979) and the calcite-water fractionation of O'Neil (1969).

quartz $\delta^{18}OH2O = 17.5‰$

calcite $\delta^{18}OH2O = 17.9‰$

These values suggest a fluid slightly less enriched ^{18}O than that estimated from the whole rock isotopic data. However, the composition of the infiltrating fluid is still constrained to fall in the narrow range 17.5 to 19.5 ‰.

Further isotopic work is needed on the vein assemblages to determine a clearer picture of the fluids, and such work may provide the best information on the initial composition of the infiltrating fluid. Veins and segregations from the different metamorphic episodes may be distinguished using structural and isotopic criteria, fluid inclusions, and the presence or absence of associated alteration effects.

6.14 SUMMARY AND CONCLUSIONS

Isotopic and petrological studies suggest that the blueschist to greenschist transformation is accompanied by fluid infiltration. The volume of infiltrating fluid involved is variable, but generally appears to be low.

Comparison of variations in mineral fractionations indicates that, isotopic equilibrium, within a single layer, has been achieved, or closely approached, in both blueschist and greenschist samples. Variations seen in the blueschist samples may be due to the presence of differing amounts of a localised intergranular fluid which has enhanced oxygen diffusion and exchange during cooling. The preservation of isotopic equilibrium appears to be largely dependent on the presence or absence of a fluid phase during the later stages of metamorphism and subsequent cooling. The large variations seen in the albite-bearing rocks may reflect the fact that albite, and possibly chlorite too, continue to exchange oxygen to lower temperatures than other phases, (see figure 6.29).

Isotope temperatures will rarely determine the peak metamorphic temperature. Temperatures can be determined more easily, and accurately, using mineral geothermometers, especially as the validity of isotope temperatures are further clouded by inaccuracies in the exchange experiments used to determine the fractionation factors. Isotopic fractionations however do provide a sensitive test of isotope equilibrium between minerals. Departures from equilibrium are evident in

reversals of expected mineral-mineral fractionations and in anomalous fractionations which are either unexpectedly large or unexpectedly small.

Possible sources of infiltrating fluid

No magmatic activity is directly associated with Syros, however magmatic activity was occuring in the Cycladic area during Oligocene and Miocene times. A crystallizing magma body at depth may provide some of the fluid, or may trigger devolatilisation reaction in the surrounding rocks. The infiltrating fluid is probably linked in some way to the regional magmatic activity.

As the isotopic composition of the infiltrating fluid appears to have been largely buffered by the rocks it is difficult to propose an initial $\delta^{18}O$ value for the infiltrating fluid, and it was almost certainly quite variable, with the isotopic composition strongly dependent on what rocks the fluid had seen and interacted with on its upward path. At Ormos Akhladhi where the volume of infiltrating fluid is thought to have been greater, an initial ^{18}O value between 17.5 and 19.5‰ is indicated for the infiltrating fluid. Such an enriched ^{18}O value suggests that the fluid has exchanged isotopically with a source of heavy oxygen, and marble is the most likely source.

It is suggested that the initial isotopic composition of the infiltrating fluid is buffered locally. The fluid will infiltrate a sequence of rocks with one isotopic signature, and leave, having interacted to a greater or lesser extent with the rocks, with a different signature.

6.15 SUGGESTED FUTURE WORK

Hydrogen Isotopes

Hydrogen is an important constituent in many of the minerals found in the blueschist and greenschist facies rocks, e.g amphibole, mica and chlorite. Determination of the D/H ratios in the mineral phases may help to identify the isotopic composition of the fluid which caused the blueschist to greenschist transformation, and this information may narrow down the possible sources of this fluid. Hydrogen isotopes could also be used to examine the scales of fluid-rock interaction, presenting another way to confirm that fluid infiltration did not occur in the blueschists.

The only drawback in analysing for hydrogen isotopes is the large amount of mineral separate material required, usually 50 or 60 mg per analysis.

Mineral-pair systematics δ-δ diagrams

The application of this type of plot to metamorphic rocks has largely been overlooked, partly because its use requires a large amount of mineral separate data, which is very time consuming to produce. However, if the data are available, a number of exciting possibilities arise.

As their name suggests these diagrams plot the $\delta^{18}O$ values of one mineral against the $\delta^{18}O$ values of another coexisting phase. δ-δ plots allow mineral-pair data to be interpreted in terms of open and closed system behavior, and the exchange systematics of the oxygen isotopes in the mineral pairs can be compared. Taylor and Forrester (1969) used δ-δ plots in studying the hydrothermal alteration of the Skargaard intrusion. The plots revealed that feldspar is highly susceptible to hydrothermal ^{18}O exchange, while the $\delta^{18}O$ values of coexisting quartz only change slightly. Gregory and Taylor (1981) used this technique in investigating seawater hydrothermal circulation at ocean ridges, and again (Gregory and Taylor 1986a,b) to study metasomatic $^{18}O/^{16}O$ effects in mantle nodules.

With the introduction of ion-probe technology the amount of data on oxygen diffusion within minerals is increasing, and it may soon be possible to rank minerals according to their susceptibility to ^{18}O exchange. However, the actual mechanisms which govern the exchange rates in different minerals are not well understood. Undoubtably a number of factors are involved, and δ-δ diagrams could be used to investigate these.

Diffusion data allow predictions to be made as to which minerals should exchange ^{18}O faster. Reversals in the expected order may uncover other factors which have a control on the O diffusion rate. Factors such as rate of uplift, grain size and degree of grain deformation. Mineral separate data from a variety of metamorphic terrains which have experienced different physical conditions may help to uncover and highlight some of these factors.

The following chapter considers the formation of lawsonite in the blueschists in more detail. Various possible lawsonite-producing mechanisms are examined, and their validity is tested through mineralogical and isotopic tests.

CHAPTER 7

FORMATION OF LAWSONITE AND THE IMPLICATIONS FOR FLUID INFILTRATION DURING BLUESCHIST METAMORPHISM.

TABLE OF CONTENTS

7.0 INTRODUCTION

The mineralogical and isotopic evidence presented in chapters 4 and 6 respectively suggests that the blueschist terrain behaved as a closed system during metamorphism, however the widespread occurrence of lawsonite in the graphite-bearing schists of northern Syros challenges this conclusion.

The rocks on Syros are of one grade, they are either blueschists or their retrogressed greenschist equivalents. There are no relics of any intermediate steps taken during prograde metamorphism, and thus it is difficult to pin-point the lawsonite generating reaction which has occurred in the schists. However because lawsonite is a Ca-bearing silicate it must have formed either via a carbonate precursor or from a pre-existing Ca-silicate phase such as epidote. Examples of the two possible reaction types are given below:

1) 2 calcite + pyrophyllite = 2 lawsonite + $2CO_2$ + qtz

2) 2 epidote + $5H_2O$ + CO_2 = 3 lawsonite + calcite

The textural evidence clearly shows that lawsonite formed under blueschist facies conditions (see chapter 3), and was stable at least until the cessation of the blueschist deformation event. In reaction 1) pyrophyllite is given as the mica phase but in reality the mica involved would probably a phengitic muscovite. However, as the precise reaction is unknown pyrophyllite has been used for simplicity as this will not affect the overall conclusions.

On average the schists in northern Syros contain 4 vol% of lawsonite, although this amount can increase to as much as 40 vol% in some beds. Because of the low porosity in metamorphic rocks it would be impossible to produce the amount of lawsonite seen in the schists simply by a mechanism of internal buffering, therefore some other process must be involved. Two possible pathways exist to generate the volumes of lawsonite seen.

1) Reaction at an invariant point in a closed system.

2) Infiltration of an external fluid.

There is no mineralogical evidence to suggest the formation of lawsonite at an invariant point, and the occurrence of lawsonite bands at the margins of otherwise lawsonite-free metabasites suggests that fluid infiltration is driving mechanism behind the generation of lawsonite.

In order to estimate the possible volumes of infiltrating fluid involved some model calculations were performed, assuming lawsonite formation from a carbonate precursor.

When the position of the reaction,

2 calcite + pyrophyllite = 2 lawsonite + 2 CO_2 + 4 qtz

is calculated in T-X_{CO2} space at a pressure of 14kbars, the equilibrium fluid composition at 450 ^oC is 0.016. As the fluid generated by this reaction is pure CO_2, a fluid more water rich than the equilibrium fluid composition is required to infiltrate the system in order to maintain the fluid composition on the reaction curve. In these calculation the infiltrating fluid will be assumed to be pure H_2O, and therefore the calculated amount of fluid will be a minimum estimate.

Assuming that the initial fluid composition has a value of 0.016, then 28 cm^3 of H_2O are required per 1cc of lawsonite produced, per 100cc of rock with 0.5% porosity, (the details of this calculation are given in Appendix 7.1). Thus to generate 1 percent of lawsonite in the model rock a fluid to rock ratio of 0.28 by volume is required. Such a ratio does not seem excessive, but this value is only for 100 cm^3 of rock, and the amount of fluid required to produce lawsonite throughout the northern schists of Syros would be 28 cm^3 x a very large number.

This is because the model assumes that each packet of fluid will mix perfectly within the 100 cm^3 rock volume generating 100% of the possible lawsonite from calcite and pyrophyllite. When the fluid packet leaves the rock volume having generated 1cc of lawsonite it will have an X_{CO2} of 0.016, i.e. the equilibrium fluid composition and therefore it cannot drive the lawsonite producing reaction in the adjacent rock volume, a further 28cm^3 of H_2O is required. For any one bed, or series of beds, assuming that the fluid enters the system at one point, the part of the rock closest to the source of the fluid will "see" all of the fluid required to produce lawsonite along the bed or through a series of beds and therefore the cumulative fluid-rock ratios will be very large.

Such an infiltration mechanism implies that abrupt reaction fronts should be a common feature in the rocks, marking where the buffering power of the fluid has been exhausted before all the potential lawsonite in a bed has been produced. Such reaction fronts were not noted on Syros, but neither were they looked for, and it is possible that these features may have been overlooked.

The problem with reaction fronts could be avoided if fluid flow through the rocks occurred at a rate several orders of magnitude faster than the rate of the lawsonite

production. A situation could then be envisaged where 28 cm^3 of H_2O would pass through layer exceedingly quickly generating a small amount of lawsonite in each of the 100 cm^3 rock volumes comprising the bed. However work by Walther and Wood (1986) suggests that such a difference in flow rates and reaction rates is unlikely.

Effect of fluid infiltration on the isotopic signature of the schists

If a series of beds equilibrate with a common fluid of fixed isotopic composition then corresponding minerals in different layers should be isotopically homogeneous. It appears that the occurrence of lawsonite in a large proportion of the northern schists involves infiltration of quite large volumes of H_2O rich external fluid and yet neither the whole rock nor the mineral separate isotopic data suggests equilibrium in the presence of a pervasive fluid.

At least there is no suggestion of isotopic homogenization across layers. However, isotopic equilibration with an infiltrating fluid may have occurred within layers, although such a process would be difficult to detect. If lawsonite is formed in response to fluid infiltration along layers, then for a series of beds, those containing the most lawsonite should have seen the most fluid. If the infiltrating fluid was of fixed isotopic composition, there should be a correlation between the percentage of lawsonite present in the rock and the $\delta^{18}O$ value of quartz (or any other mineral phase). Due to the lack of mineral separate data for the blueschists this idea could only be tested at one locality. The three rocks examined all contained approximately the same amount of lawsonite, 3 vol%, yet the $\delta^{18}O$ value of quartz varied from 17.5 to 20.2‰. Although no obvious link between the percentage of lawsonite and the $\delta^{18}O$ value of quartz is apparent from this locality, a possible correlation between the two cannot be ruled out on the strength of one negative result, and further mineral separate work is required.

There is a strong correlation between the occurrence of lawsonite and the presence of graphite in the schists. The mineral assemblages in the lawsonite-bearing and the lawsonite-free schists were compared to see if any obvious difference in assemblage occurred between the two groups. The assemblages in the schists fall into three main categories.

1) lawsonite + calcite + graphite

2) lawsonite + calcite

3) epidote + calcite, sometimes with a small amount of lawsonite also present.

These groupings suggest two distinct mechanisms for generating lawsonite. In the graphite bearing schists, a process of in-situ graphite "burning" is suggested. In order to liberate the oxygen required this reaction must involve the reduction of Fe^{3+} to Fe^{2+}, and in the reaction given below Fe^{3+} bearing epidote is reduced to Fe^{2+} bearing almandine garnet.

$$24epd + 6C + 3SiO_2 = 11gross. + 9law + 8alm + 3H_2O + 6cc$$

Such a reaction implies that the garnets in the schists should be zoned with grossular rich rims. This is not the case (the grossular component in the garnets tends to maintain a constant value on moving from core to rim) and therefore a different reaction of similar type must be involved. In the graphite free schists (this also applies to the lawsonite bearing metabasites and the impure marbles) infiltration of a H_2O-CO_2 fluid is the preferred mechanism, with a possible reaction being:

$$epidote + 5H_2O + CO_2 = 3\ lawsonite + calcite$$

The CO_2 required is envisaged to be generated by graphite burning in adjacent rocks, and because of the large difference in molecular weight between 1 mole of lawsonite and 1 mole of carbon (0.509 grams of graphite will produce 40 grams of lawsonite by this reaction), the graphite in the schists will be present in excess of the amount required to generate the average of 4 vol% of lawsonite seen in the rocks.

Can evidence for these proposed reactions be found in the rocks? Figure 7.1 shows the reaction epidote $\Rightarrow$ lawsonite plotted in a T-X_{CO2} diagram at a pressure of 14 kbars. If pure clinozoisite is present then the reaction curve lies closer to the H_2O axis than if epidote is involved. The addition of Fe^{3+} to clinozoisite lowers the free energy of the phase and increases its stability field. The addition of the extra component increases the degrees of freedom by one and the univariant line in T-X_{CO2} space becomes a divariant plane in T-X_{CO2}-X_{Fe3+} space. Taking a simple case, if the reactants are favoured, i.e clinozoisite/epidote is stable, then the rocks are either Fe^{3+} rich, or the X_{CO2} of the coexisting fluid is low.

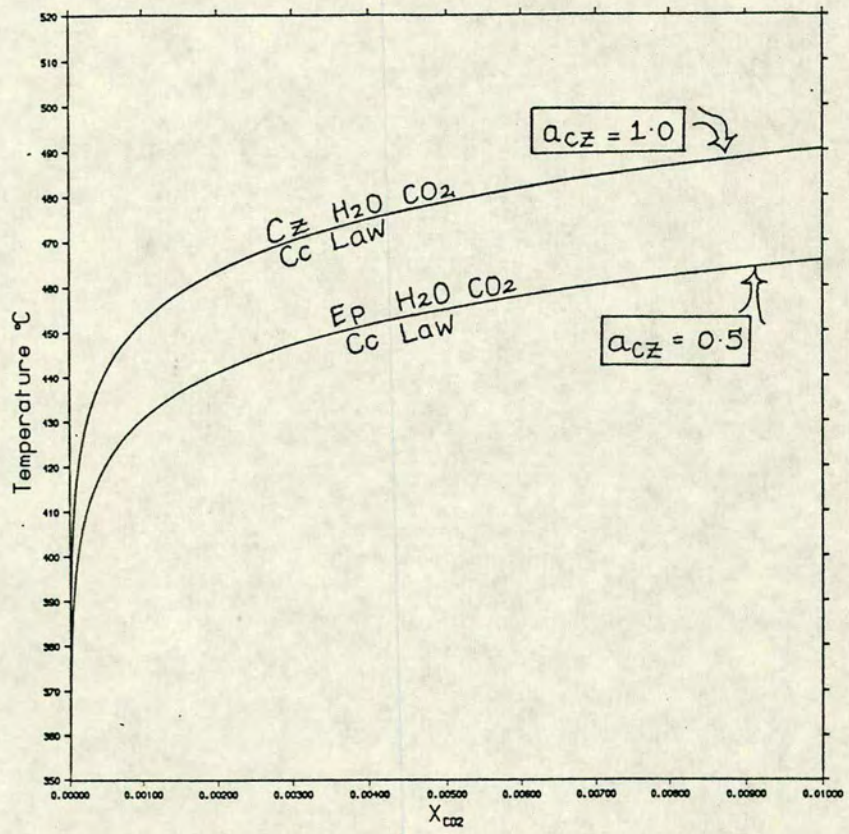

Figure 7.1 Lowering the activity of clinozoisite causes a marked shift in the position of the reaction curve, increasing the stability field of clinozoisite/epidote.

This reasoning can be applied to the rocks on Syros containing the different mineral groupings.

Group 1

Assemblage: lawsonite + calcite + graphite

Reaction mechanism: in-situ burning of graphite

Products favoured

Tests

-mineralogy: rocks should be Fe^{3+} poor, i.e low pistacite epidote, low riebeckite content in glaucophane.

-isotopes: the carbonate being formed by the reaction is produced by the oxidation of isotopically light graphite, therefore the $\delta^{13}C$ signature of the carbonate formed should also be light i.e. negative.

Group 2

Assemblage: lawsonite + calcite - no graphite

Reaction mechanism: infiltration of H_2O-CO_2 fluid

Products favoured

Tests

-mineralogy: the rocks should be Fe^{3+} poor as above, (or the X_{CO2} content of the fluid is high)

-isotopes: the infiltrating CO_2 which forms the carbonate is thought to be derived from graphite initially, but the CO_2 may have exchanged with another C source, i.e marble, before entering the schist unit, therefore the $\delta^{13}C$ signature of the carbonate formed will still probably be negative, but not as depleted as in group 1.

Group 3

Assemblage: epidote + calcite $\pm$ lawsonite

Reaction mechanism: infiltration of H_2O-CO_2 fluid
Reactants favoured

Tests

-**mineralogy:** the rocks should be Fe^{3+} rich, high pistacite epidote and high riebeckite component in glaucophane.

-**isotopes:** As for group 2, $\delta^{13}C$ signature of the carbonate should be depleted, but not as much as for group 1 carbonate.

These tests were then applied to rocks containing the appropriate mineral assemblages.

Carbon isotopes

Carbon isotope data is only available for rocks in group 1 and group 3, and this is given below.

Group 1		Group 3	
sample#	$\delta^{13}C$‰	sample#	$\delta^{13}C$‰
86/14	-3.1	86/74	-5.9
86/19a	-5.9	86/76	-5.4
86/35	-3.6		
86/32	-5.2		
86/10	-4.1		
86/98b	-6.2		
86/95	-4.5		

From the data available there does not appear to be significant difference in the $\delta^{13}C$ signature of the carbonate from the two groups. However, the schists in both groups contain more carbonate than would be produced accompanying the formation of 4% lawsonite in the rock. It is likely that the excess carbonate represents primary sedimentary carbonate. This sedimentary carbonate would be expected to have a positive $\delta^{13}C$ signature and isotopic equilibration between the two types of carbonate would tend to smooth out the difference in $\delta^{13}C$ signatures.

Riebeckitic content of glaucophane

As epidote is absent from the majority of the lawsonite bearing schists, the riebeckitic content of glaucophane was used as a crude indicator of the Fe^{3+} content of the rock. Figure 7.2 shows glaucophane analyses from schists in the three groups plotted in a miyashiro diagram (Miyashiro 1957). The schists in group 1 contain the most Fe^{3+} poor glaucophane, as was predicted, but the distinction between groups 2 and 3 is less clear.

Whatever the actual mechanism is it appears that infiltration has occurred in at least some of the blueschists to produce lawsonite. In order for this conclusion to be compatible with that based on the mineralogical and isotopic evidence which suggests that the blueschists have acted as closed systems, the infiltrating fluid must have been channellized along beds and not across them. The channellization of the fluid can be understood in terms of a model of reaction-enhanced permeability. In a sequence of metasediments some beds will have a bulk chemical and mineralogical composition favourable for the production of lawsonite. Because devolatilization reactions like this increase porosity and enhance permeability, so beds that undergo significant reaction will become loci of high fluid flow.

In order to resolve this paradoxical situation, which appears to require both internal and external buffering, further detailed work is required looking specifically at the distribution of the lawsonite bearing metasediments.

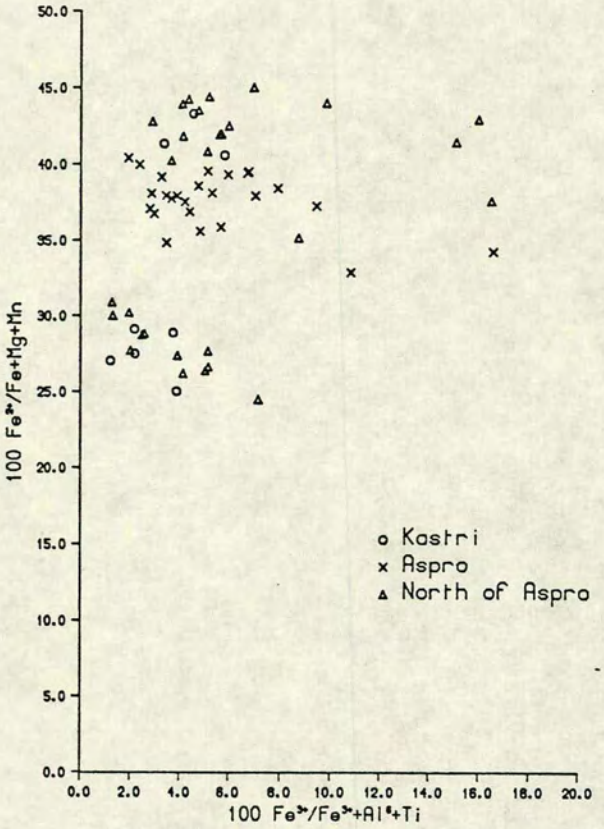

Figure 7.2. Glaucophane analyses from the three localities listed, plotted in terms of $Fe^{3+}/Fe^{3+}+Al^{VI}+Ti$ versus $Fe^{2+}/Fe^{2+}+Mg+Mn$, (Miyashiro 1957). See text for discussion.

CHAPTER 8

FLUID INCLUSION STUDIES

TABLE OF CONTENTS

8.1 INTRODUCTION AND AIMS

Fluid inclusions in minerals are trapped samples of fluids which were present at some time during the evolution of the rock. This chapter briefly describes some of the techniques used in fluid inclusion studies, and presents preliminary thermometric data on the compositions of fluid inclusions occurring in the blueschist and greenschist facies rocks.

Observations and measurements on fluid inclusions were used to answer some specific questions:

1) Have samples of the early, synmetamorphic fluid been preserved?, and can it be identified?

2) Do the fluid compositions predicted by the mineral equilibria studies correspond to the compositions of any fluid inclusions in the rock ?

3) Is there a difference in composition between the fluid inclusions associated with the unaltered blueschists and those associated with the greenschists, either in terms of the CO_2/H_2O ratio or the salinity of the fluid ?

Much of the background information for this chapter has been derived from three comprehensive reviews of fluid inclusion literature, namely: "A practical guide to fluid inclusion studies" (Shepherd *et al.* 1985); "Fluid Inclusions: applications to petrology" (L. S. Hollister, and M. L. Crawford eds 1981); and "Fluid Inclusions" E. Roedder 1984).

8.2 CHOICE OF STUDY MATERIAL

In general quartz, occurring either in the form of segregations, or within the rock matrix, has proved to be the most suitable material for study. When fluid inclusion studies are not carried out on mineral grains within the metamorphic rock it is important to determine how the segregations relate to the metamorphic history of their host rocks. As there is only one high strain deformational event documented on Syros, synchronous with the blueschist facies metamorphism (Ridley 1982), deformed and boudinaged segregations can be confidently be assigned to the blueschist event (see figure 8.1) In an attempt to pin-point possible synmetamorphic fluids in the blueschists, only small and texturally early quartz segregations were sampled.

Figure 8.1 Quartz segregations in a sequence of blueschist metasediments, Kastri. The segregation in the centre of the photograph contains brown ankeritic-carbonate (now pseudomorphed by calcite) and green fuchsite mica in addition to quartz.

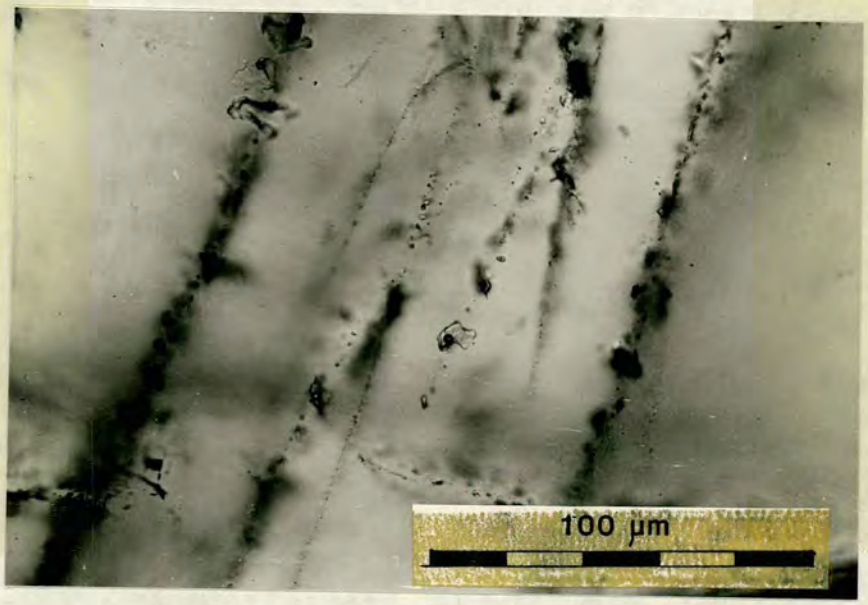

Figure 8.2 Randomly orientated trails of secondary inclusions in quartz (sample 87/190, PPL + green filter).

Inclusions trapped in synmetamorphic veins or segregations should have the same compositions and densities as inclusions trapped during growth of the minerals in the host rock (Kreulen 1980; Sisson *et al.* 1981). In this study two samples were chosen (86/77 and 87/AG1) where fluid inclusions in both quartz segregations and the surrounding host rocks were investigated. No significant compositional or density differences were detected between the fluid inclusion populations in the two settings, althoughlarger and more abundant fluid inclusions occurred within the quartz segregations.

8.3 CLASSIFICATION OF FLUID INCLUSIONS IN METAMORPHIC ROCKS

A widely adopted classification scheme for fluid inclusions is one based on their origin, i.e primary, secondary or pseudosecondary. Primary inclusions are trapped during crystal growth, whereas secondary and pseudosecondary inclusions form at some later stage, usually by the healing of fractures. The usual criteria for distinguishing between primary and secondary inclusions cannot readily be applied to metamorphic rocks because, inclusions which are secondary in relation to the rock may still be primary with respect to the deformation or recrystallization of the individual minerals. It is unlikely that all the fluid released by an average pelite during devolatilization could be accommodated by grain boundary flow (Walther and Orville 1982), and some fluid must be transported through fractures. This implies that some of the inclusions trails, so common in metamorphic rocks, should contain information about the synmetamorphic fluid. However, as pointed out by Yardley (1983), a fracture dominated transport mechanism also means that fluids may travel some distance from their site of generation. Yardley (1983) cites examples from quartz veins in Connemara where the diversity of fluid inclusion populations provides evidence that the quartz vein has seen fluids derived from several rock types.

In studies where primary inclusions can be unambiguously identified, e.g. where inclusions occur outlining growth zones in vein quartz, then fifty measurements may be sufficient to characterise the population. However, because it is difficult to identify primary and secondary inclusions in metamorphic rocks, many more measurements per sample are needed to identify possible early inclusions, and define the natural grouping of the different fluid inclusion populations.

In this study a "relative chronology" classification was adopted. It was assumed that isolated inclusions are generally earlier than those outlining fractures, and inclusions trails which do not cross grain boundaries are interpreted as being earlier than those

where the trails transect several grain boundaries. In an effort to identify possible samples of the synmetamorphic blueschist fluid, the inclusions chosen for study were either individuals, remote from trails, or inclusions forming part of intragranular clusters or trails.

8.4 INCLUSION PETROGRAPHY

Distribution of fluid inclusions

Most of the fluid inclusions in the samples examined occurred in well-defined trails along healed microfractures, see figure 8.2. Some of the trails show evidence for the migration of inclusions away from the original fracture plane causing a "blurring" of the trail. Swanenberg (1980) describes similar trail transposition features from Norwegian granulites, and he proposed that migration of the trails occurred in response to stress. Although fluid inclusions are also known to move by self-diffusion in a temperature gradient, (Wilkins and Barkas 1978), thermal gradients at a grain size scale are unlikely to have existed for long enough, or been of sufficient magnitude to cause migration of the inclusions. Inclusions have also migrated towards grain boundaries, and many of these are dark, implying that they are vapour rich and may have leaked. This migration is probably due to the ductile-deformation of the host quartz, (Wilkins and Barkas 1978). As leakage is likely to have occurred in such cases, no measurements were performed on these inclusions.

Rarer isolated inclusions were seen, randomly distributed throughout the sample. Others occurred along short intragranular trails or arranged in clusters. Some of the cluster-like configurations have been interpreted as decrepitation clusters. Decrepitation occurs when the difference between the internal pressure in an inclusion and the external pressure on the host mineral exceeds the strength of the mineral, causing the host phase to fracture. This can occur if, for example, the rock crosses the specific volume isochores of the fluid in a positive sense during uplift, causing expansion of the trapped fluid. In such a situation the inclusion can suddenly rupture and leak, leaving a star-shaped "parent" inclusion surrounded by a halo of retrapped "daughter" inclusions. The fact that autodecrepitation is not a commonly observed phenomenon in the Syros samples is probably due to the small size of most of the inclusions. Detailed work by Leroy (1979), on quartz, showed that inclusions larger than 30 microns would decrepitate at an internal pressure of 850 bars, but the internal pressure required for decrepitation increases as inclusion size decreases.

Swanenberg (1980) reports internal pressures as high as 5-6 kbars for inclusions about 1 micron in diameter.

Size and shape

Figure 8.3 is a histogram showing the size distribution of the inclusions selected for study. Most are under 12 microns in size, and the largest inclusions present in any sample are late monophase inclusions. The small inclusions commonly have a regular shape. They are often elliptical and show a general tendency to form rounded, negative crystal, shapes. Some inclusions show well developed negative crystal shapes but these are much rarer. Monophase liquid inclusions tend to be large and flat, and they commonly exhibit highly irregular shapes.

Many fluid inclusions have relatively large surface areas when they are first trapped. If the host mineral is soluble, then a process of recrystallization known as "necking down" will occur to reduce the high surface energy of the system, and the net result is the formation of several smaller equant inclusions (Roedder 1984). Although recrystallization will not affect the composition of the system, if a phase change has occurred before necking down is complete, i.e the development of a vapour bubble or daughter mineral, then the new inclusions will have very different compositions and/or densities. Although necking down is a very common phenomenon, it normally takes place close to the original temperature of formation so very little change in the vapour/liquid ratio occurs. Partially necked inclusions were identified in some of the Syros samples, where inclusions are connected by thin tubes to other nearby inclusions, (see figure 8.4a,b). Necking down has probably occurred to a large degree in these rocks, but, as long as the new inclusions preserve the same phase proportions as the original, then measurements are still valid.

8.5 THERMOMETRIC ANALYSIS OF FLUID INCLUSIONS

Thermometric analysis involves making measurements of phase transitions in inclusions as a function of temperature. By accurately measuring the temperature at which these changes occur it is possible to derive estimates of the PVTX state of the fluid at the time of trapping.

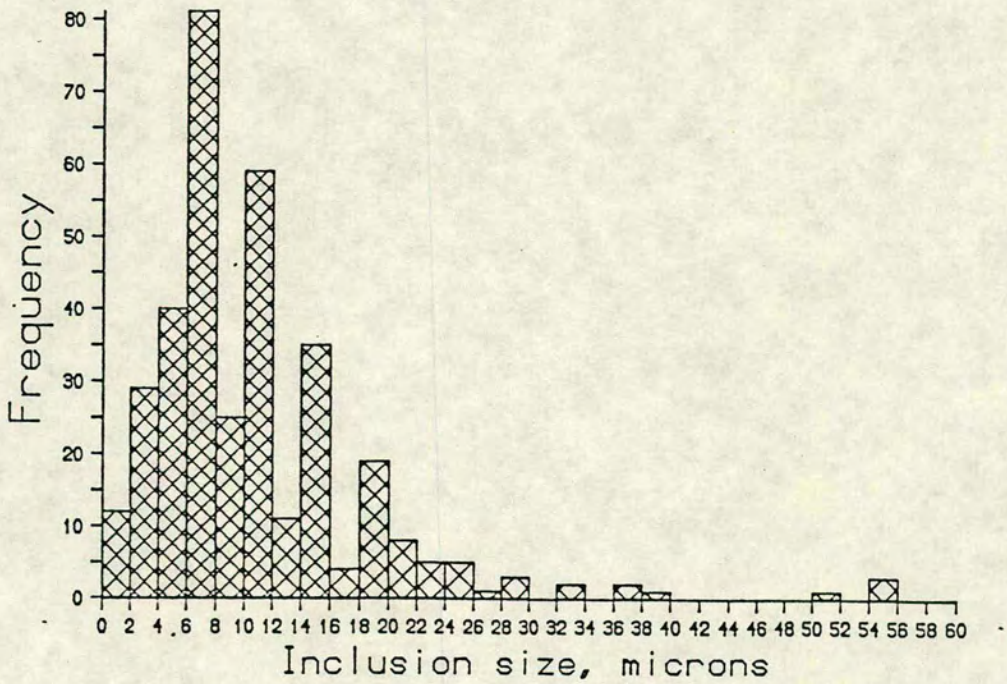

Figure 8.3 Histogram showing the size distribution of inclusions selected for thermometric analysis.

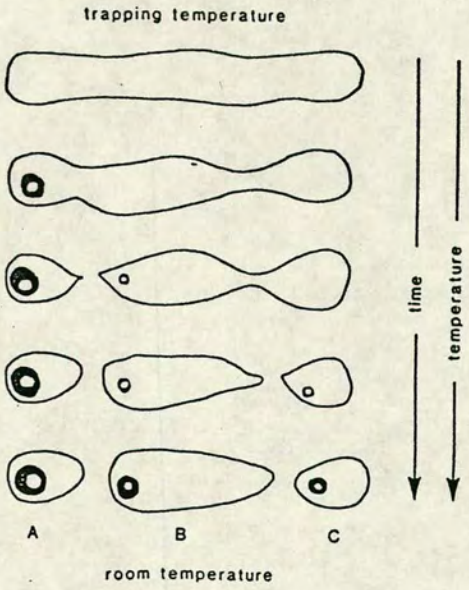

Figure 8.4a Necking down of tubular inclusions. On cooling recrystallisation occurs and the original inclusion necks down to form three separate inclusions, A, B and C. The new inclusions have variable phase proportions, and would homogenize at different temperatures (from Roedder 1962). See text for discussion.

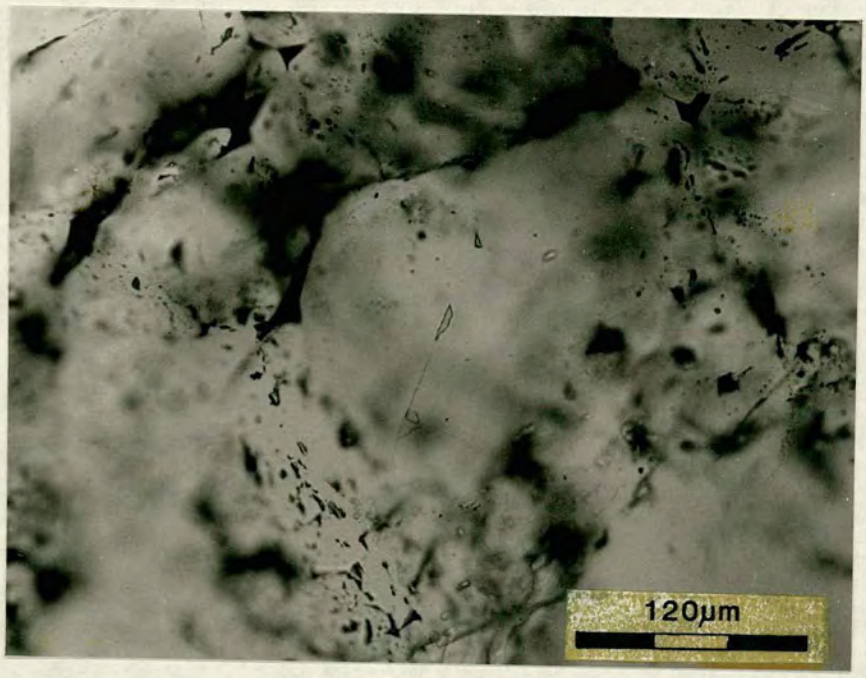

Figure 8.4b Photomicrograph showing an example of necking down. The inclusions in the centre of the photograph are connected by a thin tube. If the tube closes, forming two separate inclusions, their homogenization temperatures will be misleading because the two inclusions now have variable liquid to vapour ratios.

The equipment

Thermometric data was obtained using a Linkam TH600 heating-freezing stage, which operates over a temperature range of -180 °C to +600 °C, with a maximum temperature resolution of 0.1 °C. The Linkam stage was attached by magnetic feet to a general purpose Zeiss microscope, fitted with a long working distance objective lens and substage condenser. An overall magnification of x400 was possible.

The heating-freezing chamber contains a centrally mounted silver heating-freezing block. The temperature is raised by a resistance heater within the block, and pre-cooled nitrogen gas is circulated through the block during freezing experiments. The temperature is measured via a platinum resistor which is positioned below, and slightly offset from, the mineral fragment. See figures 8.5a and 8.5b. The temperature control unit consists of a digital temperature display and several heating control buttons. The unit can provide fully automatic programmable temperature control during both heating and freezing with direct digital temperature display. A range of heating/cooling rates can be programmed from 0.1 °C/min to 90 °C/min. The programmer includes a temperature "HOLD" facility, and a temperature limit can also be pre-set at any value between -180 and +600 °C.

Freezing experiments

This section considers freezing experiments, and the information which can be gained from them.

Inclusions must be selected for analysis before making any measurements, and this selection should be made after assessing the total population. If the inclusions to be studied are not representative of the majority, then this bias must be noted. Following selection, the inclusions are carefully described and drawn. Measurements were generally made simultaneously on groups of about six inclusions.

The data obtained during freezing experiments principally relates to fluid composition and density. The freezing point of pure water is lowered below 0 °C in proportion to the amount of dissolved salts present, therefore the final melting temperature of ice, (T_m), provides a measure of the salinity of the inclusion (figure 8.6). In practice, because fluid inclusions behave metastably when cooled, melting point measurements are made by rapidly freezing the inclusion and observing the phase transitions during controlled reheating.

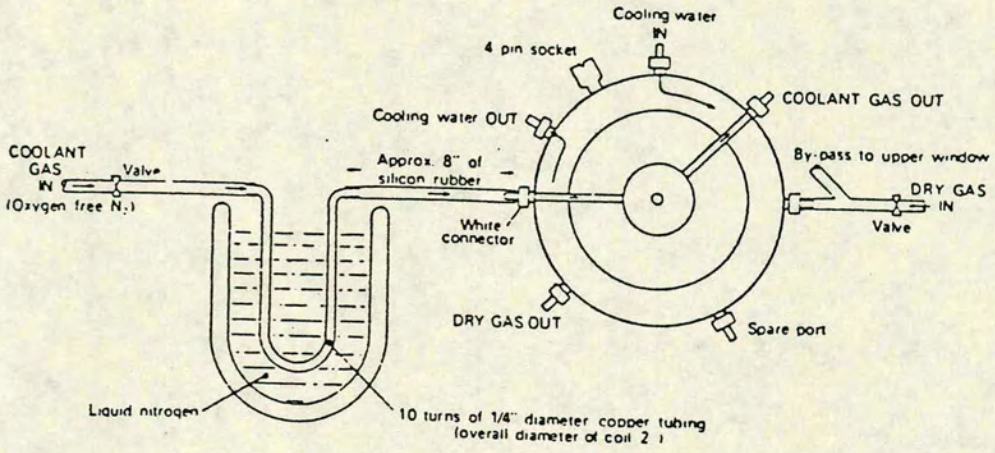

Figure 8.5a Layout of the Linkam TH600 stage.

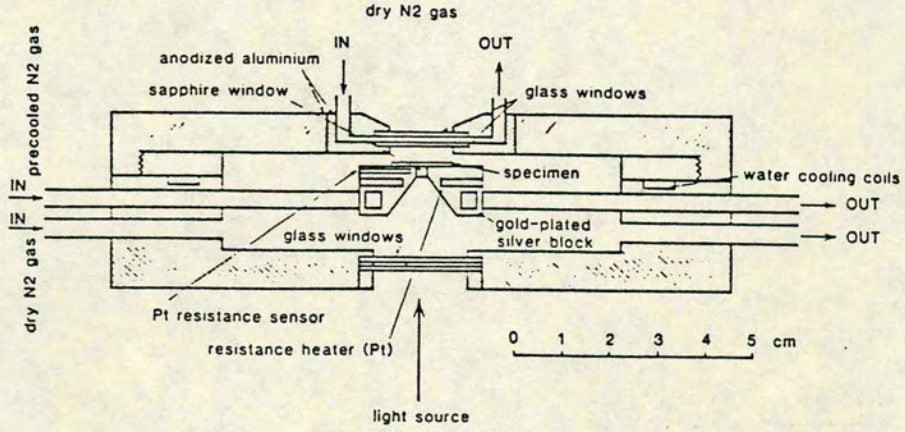

Figure 8.5b Cross-section through the Linkam TH600 heating-freezing stage.

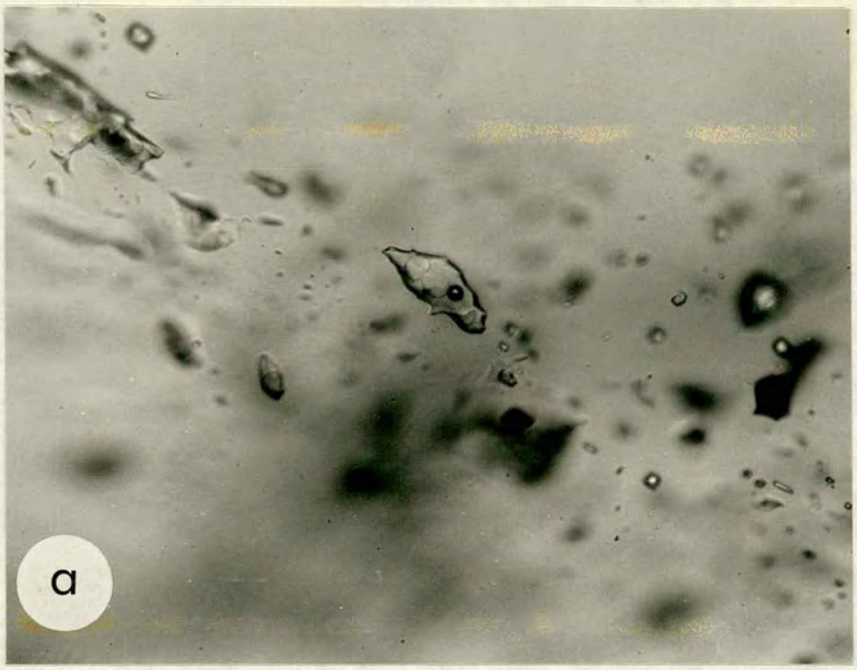

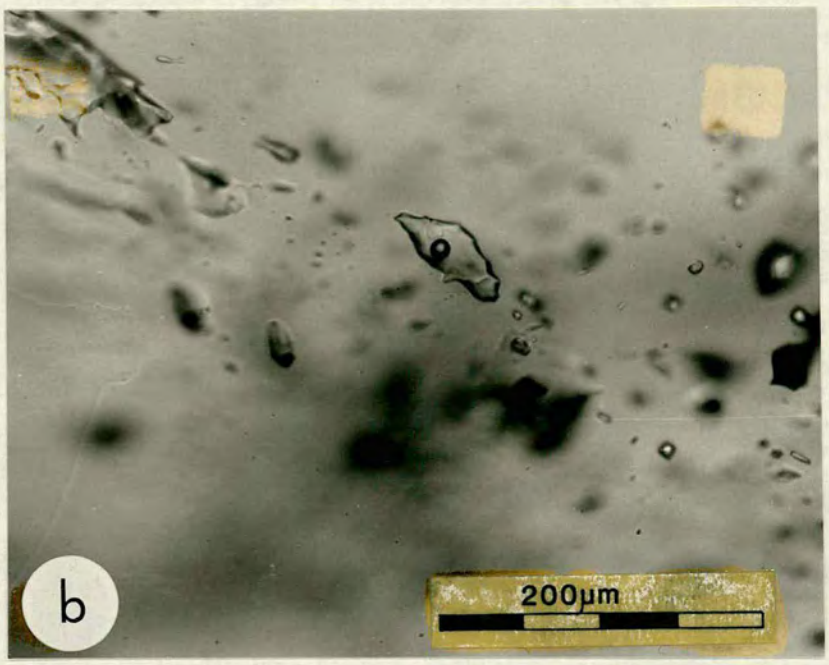

Figure 8.6 A sequence of photographs (PPL) showing the melting of ice in a two-phase aqueous inclusion in quartz. (this sample, RH8-2, was kindly donated by Dr J Kinnaird, and comes from a mineralized granite vein, Nigeria).

a) T = -2.2°C, significant melting has occurred, but 3 ice crystals remain.
b) T = -1.6°C, a single ice crystal remains attached to the vapour bubble.

Salinities are reported as "equivalent wt% NaCl", i.e the amount of NaCl which would be required to produce the observed depression of the freezing point, a practice which is justified because NaCl solutions are the most abundant. The temperature at which the first melt appears, T_{fm}, is very important, because it corresponds to the eutectic temperature of the salt-water system which is invariant. Table 8.1 is modified from Shepherd *et al.* (1985) and gives the eutectic temperatures of some common salt-water systems.

Table 8.1 Selected phase data for some common salt-water systems

System	Eutectic temperature °C	Solid phases
H_2O-NaCl-$MgCl_2$	-52	ice+NaCl.$2H_2O$+$CaCl_2$.$6H_2O$
H_2O-NaCl-$MgCl_2$	-35.0	ice+NaCl.$2H_2O$+$MgCl_2$.$12H_2O$
H_2O-NaCl-KCl	-23.5	ice+NaCl.$2H_2O$
H_2O-NaCl	-20.8	ice+NaCl.$2H_2O$
H_2O-KCl	-10.6	ice

Notable temperatures on freezing

Temperature	Comment
-20.8 °C	eutectic melting point of pure NaCl-H2O system. Aqueous inclusions showing eutectic minima below this temperature contain other salts in addition to NaCl.
-56.6 °C	Melting temperature of pure CO2 solid. Addition of other components, e.g CH4 or N2 lowers the triple point temperature.
-120 to -84 °C	Liquid-vapour transitions in this range indicates the presence of CH4.

Practical aspects of freezing experiments

Low temperature measurements are always made first, because of the possibility of inclusion decrepitation, or stretching of the host quartz, during heating runs. Cooling of the stage is achieved by passing pre-cooled nitrogen gas through the silver block. The nitrogen is pre-cooled by passing it through a series of copper coils held in a dewar of liquid nitrogen. A base temperature of -180 °C is theoretically achievable, but in practice the lowest temperature attained was -123 °C, and the usual working

limit was -90 °C. Before freezing, dry nitrogen gas must be passed through the copper coils for a few minutes to flush out any water which may have condensed there. This must be done before liquid nitrogen is added to the dewar otherwise ice can form in the coils causing blockages, and potentially explosive build-ups of back-pressure. For similar reasons nitrogen must also be passed through the sample chamber, and a small, but steady, flow is maintained during freezing to prevent moist warm air from being sucked into the chamber.

The pre-cooled gas is allowed to flow rapidly through the heating block and a temperature of -90 oC can be achieved in just over a minute. The programmer is then used to ensure a gradual and controlled reheating rate. This is done by balancing the flow rate of the gas against the heat supplied by the heating block. A re-heating rate of less than 1 °C/min should be used as phase changes are approached.

It was often difficult to observe the first melting temperature, T_{fm}, due to the small size of the inclusions, and the small quantities of melt produced at the eutectic point. To facilitate observation of this phenomenon a heat\re-freeze technique was employed. The frozen inclusion was allowed to warm up until only a single ice crystal remained. The temperature was then reduced to allow the single crystal to grow. When this crystal filled most of the inclusion, the temperature was rapidly lowered to completely refreeze the inclusion. On reheating, the first liquid was confined to one area in the inclusion which made it easier to see, and therefore permitted a more accurate determination of T_{fm}. However, even using this technique, it was very difficult to measure first melting temperatures accurately, and in many cases the temperature recorded was T_{om}, i.e the temperature of the first observed melt. Although the true first melting temperature may not have been observed, some compositional constraints can still be placed on the system, i.e melting below -21 °C indicates the presence of other dissolved salts in addition to NaCl, and melting temperatures below -35 °C can only occur in $CaCl_2$ bearing systems.

Heating experiments

When an inclusion is heated the vapour bubble gradually becomes smaller until at a certain temperature the bubble disappears (figure 8.7). This temperature is known as the homogenization temperature, T_h, and it represents the minimum trapping temperature of the inclusion. If the pressure at the time of entrapment does not exceed the equilibrium vapour pressure then the homogenization temperature will represent the true temperature of trapping, T_t.

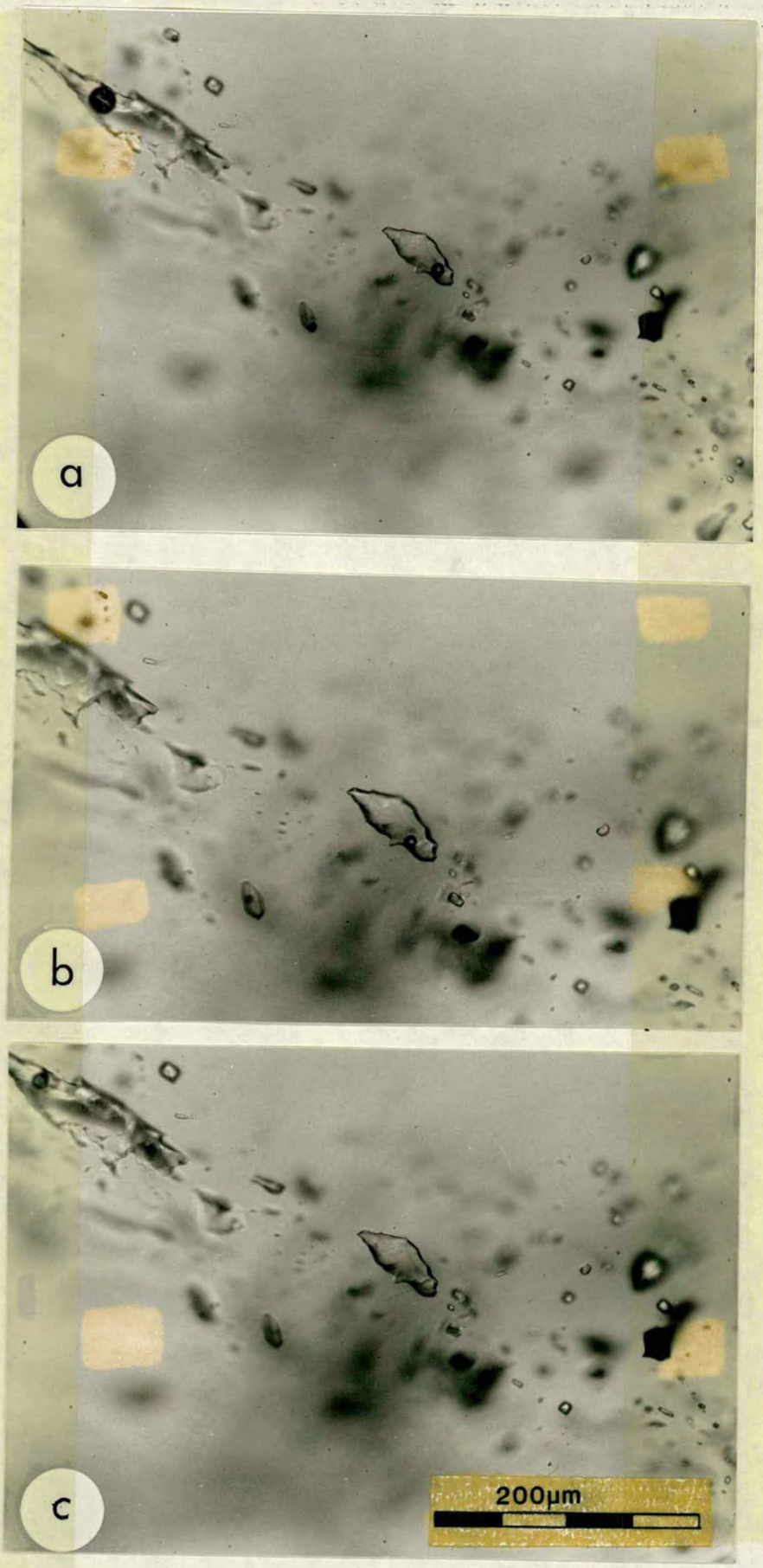

Figure 8.7 A sequence of photographs showing homogenization of a two-phase aqueous inclusion.. The sample is the same one described in fig. 8.6. a) T = 22°C, the inclusion consists of a liquid phase and a small vcapour bubble. b) T = 110°C, the vapour bubble is now visibly smaller. c) T = 147°C, Th, the vapour bubble disappeared. The inclusion has homogenised to a single, fluid phase.

However, in practice this means that all inclusions except those trapped from boiling fluids will require a pressure correction to be added to T_h to obtain T_t. Most inclusions formed under metamorphic conditions contain fluids trapped at pressures above their vapour pressure, i.e in the one-phase fluid field above the boiling curve. In order to correct homogenization temperatures the composition of the inclusion and the pressure at the time of entrapment must be known. The T_h data for the Syros samples have not been corrected because of the difficulty in estimating when, and under what pressure conditions the inclusions actually formed. Furthermore, no correction tables exist for the high pressure conditions experienced during blueschist facies metamorphism. Potter (1977) produced a series of pressure correction diagrams for different salt solutions covering the temperature range 20 to 400 °C, but these only apply for pressures up to 2 kbars.

95% of the inclusions measured homogenised to the liquid state, however this is only one of three possible modes of homogenization. Figure 8.8 is taken from Shepherd *et al.* (1985) and illustrates the three possible modes of homogenization. Although most of the inclusions examined were 2 phase, some inclusions also contained a daughter mineral. Daughter minerals are solid phases which have crystallized from the fluid after trapping. These phases can provide important information on the chemical compositions of the original parent fluid. The daughter minerals seen in the Syros samples are cubic and isotropic, and therefore the crystals were identified as being halite, NaCl. On heating, these daughter minerals begin to dissolve into the liquid, and the final solution temperature for the halite, T_sNaCl, is directly proportional to the wt% NaCl in solution.

Notable temperatures on heating

Temperature	Comments
up to +10 °C	melting of CO_2 clathrate, $CO_2.5_{3/4}H_2O$ Addition of NaCl will lower the melting temperature of CO_2 hydrate, while the presence of CH_4 will raise the upper T limit of CO_2 hydrate melting.
+31.1 °C	liquid-vapour homogenization for pure CO_2, (T_hCO_2). Addition of other non-aqueous components, e.g CH_4 or N_2, extends the range of liquid-vapour homogenization to lower T.
> 200 °C	Dissolution of daughter minerals, T_sNaCl

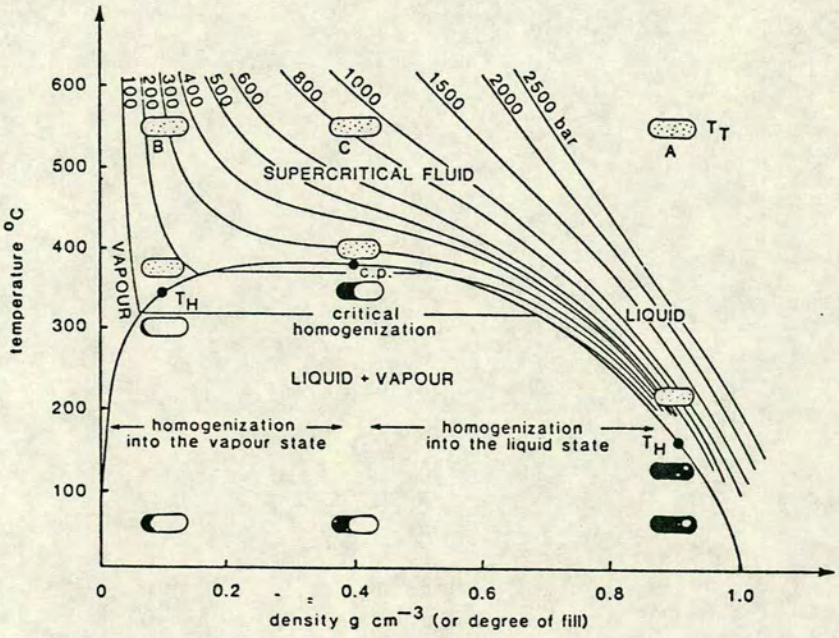

Figure 8.8 Temperature density plot for pure H_2O showing the three modes of homogenization, A) homogenization to the liquid phase, B) homogenization to the vapour phase and C) for inclusions of the critical density, homogenization by meniscus fading. Th = homogenization temperature, Tt = trapping temperature, c.p. = critical point (from Shepherd *et al.* 1985).

Practical aspects of heating experiments

The prepared wafer is broken into very small fragments each of which is used for only one heating run, due to the possible decrepitation of lower temperature inclusions. Some unused material is always retained to act as reference material. A test chip was heated rapidly (30 °C/min) to determine the general range of homogenization temperatures in the sample. Measured runs used an initial heating rate of 10-20 °C per minute (usually until T=120 °C), reduced to a rate of 3-5 °C within 10 degrees of the expected homogenization, and further reduced to a rate of less than 1 °C/min as the phase transition was approached, to ensure equilibrium. Sometimes it was difficult to tell if homogenization had occurred, especially if the bubble disappeared into a dark corner. In this case the inclusion was cooled slightly, usually 10 to 15 °C being sufficient. If the bubble was still present it would then grow in size and become visible, but if homogenization had occurred the bubble would not reappear.

8.6 FLUID INCLUSION RESULTS - BLUESCHISTS

General comments

The thermometric data for the five blueschist samples examined is presented in figure 8.9a-c. All the inclusions seen were aqueous with variable amounts of dissolved salts. At room temperature the inclusions consisted of two phases, an outer liquid phase and an inner vapour bubble. No phase transitions were observed close to +31 °C, the liquid-vapour homogenization temperature for CO_2, and homogenization temperatures were invariably greater than 100 °C, confirming the absence of two-phase CO_2-rich inclusions. All of the samples show a spread of homogenization temperatures associated with a reasonably constant salinity value, and this phenomenon probably relates to necking down of the inclusions during uplift, (Pecher 1981; Yardley 1983).

Sample 87/190 (figure 8.9a)

Location: Kaloyeros, N. Syros

Description: qtz segregation in a gl-gnt metabasite

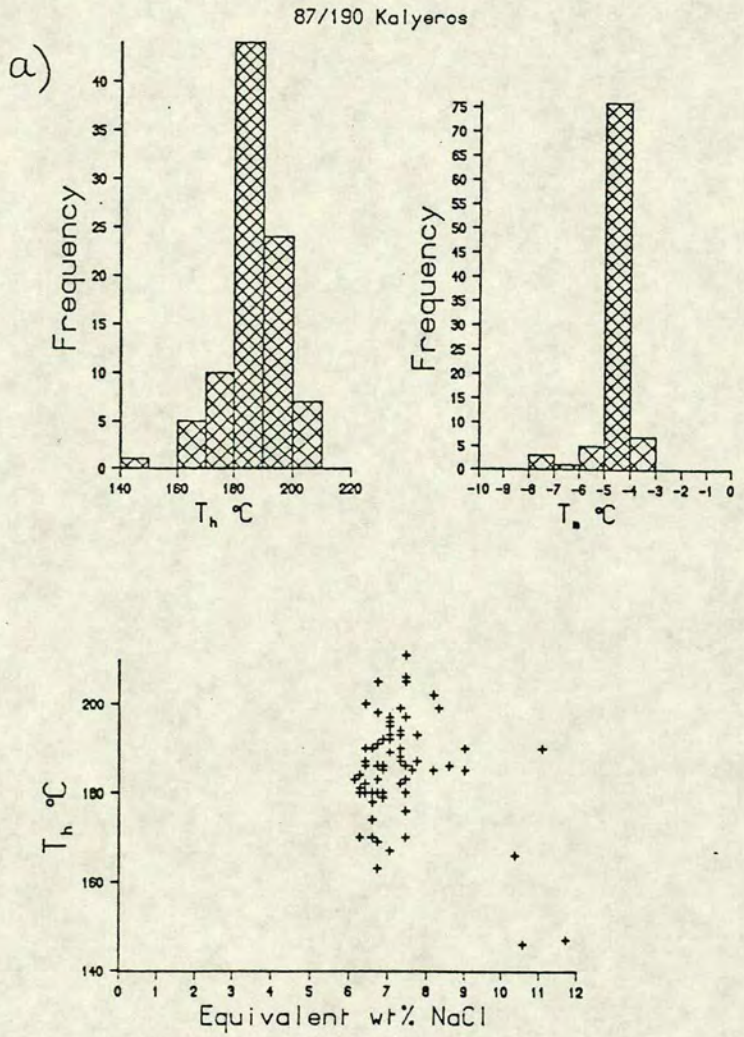

Figure 8.9a-c The following figures present the microthermometric data measured on inclusions from five blueschist samples. Each figure includes histograms showing the frequency distribution of homogenization and melting temperatures, Th and Tm respectively, and a T_h versus salinity plot. Tm measurements on inclusions containing less than 23% NaCl were converted to equivalent Wt% NaCl using the experimentally derived equation of Potter *et al.* (1978). All homogenization temperatures are to liquid unless otherwise indicated. See text for a discussion of individual samples.

b)

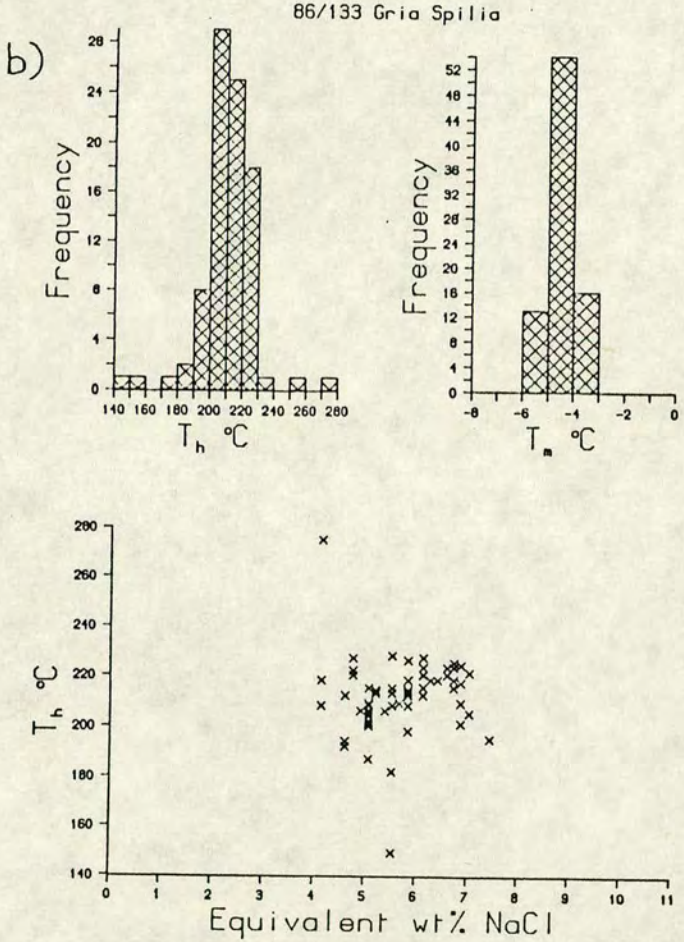
86/133 Gria Spilia
Frequency
T_h °C
Frequency
T_m °C
T_h °C
Equivalent wt% NaCl

c)

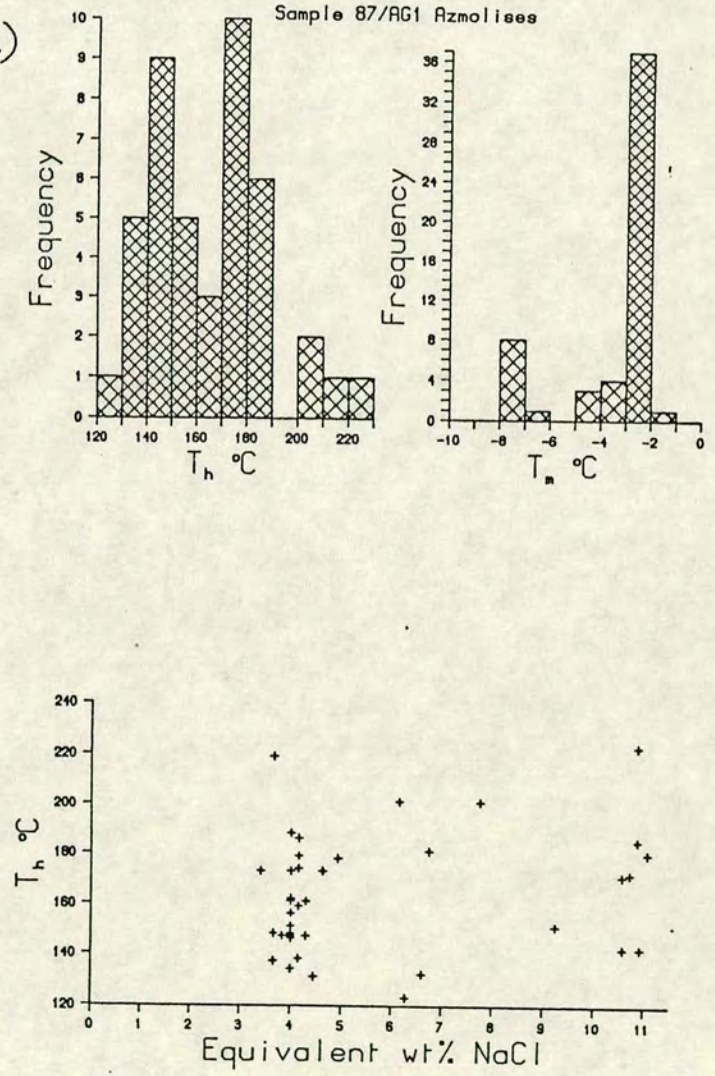
Sample 87/AG1 Azmolises
Frequency
T_h °C
Frequency
T_m °C
T_h °C
Equivalent wt% NaCl

Sample 86/133 (figure 8.9b)

Location: Gria Spilia, north-west coast

Description: Qtz segregation in gl-jadeite bearing metabasite. Mineralogy of the host rock, qtz, gl, jadeitic pyroxene, ep, gnt, sph

The fluid picture in these samples appears relatively simple, the histograms show one clear peak, suggesting a single inclusion population. Salinity values for the two samples (190 and 133) range from 6-9 and 4-7 equivalent wt% NaCl respectively, and homogenization temperatures ranging from 170-210 °C and 195-227 °C were recorded.

Sample 87/AG1 (Figure 8.9c)

Location: Kouroupi gneisses, near Azolimnos, east coast

Description: Qtz segregation and whole rock matrix quartz used. Host rock, gl-gnt metabasite

The frequency histograms of T_h and T_m are more complicated for this sample. Salinity values range from 3.5 to 11 equivalent wt% NaCl and homogenization temperatures range from 130 °C to 223 °C. Several groupings in the data appear to be present, suggesting the presence of two or possibly three distinct populations. Further measurements are required to confirm the existence of these separate populations. A large number of high density monophase liquid inclusions are present, and these are thought to represent late stage fluids trapped during the last stages of uplift. These inclusions are relatively large (>12 microns) and invariably have highly irregular shapes. A number of these inclusions disconcertingly develop vapour bubbles after freezing. As there is no vapour bubble present initially to take up the volume expansion which occurs when water freezes, it is thought that the inclusions undergo inelastic deformation causing a small volume increase and the subsequent appearance of a bubble after ice melting. No measurements were recorded from these inclusions due to their unpredictable behaviour, but where observed, their final melting temperatures were close to 0 °C, indicating that these late stage inclusions are almost pure water.

Sample 86/77 (figures 8.10,a,b)

Location: north of Aspro, N.W. coast

Description: matrix quartz from a blueschist metasediment. Mineralogy - law(psd), qtz, w.mica, gl, gnt, cc, dol(psd), chl, sph.

This sample contains inclusions which are much more saline. Figure 8.10a illustrates part of a chip containing two distinct inclusion populations, which are distinguished both spatially and compositionally. The first group are highly saline, and some of the inclusions contain a halite daughter phase. These inclusions occur either as isolated groups, or along short intragranular fractures. The second group are clearly later, occurring in apparently randomly oriented trails which transect several grain boundaries. Figure 8.10b shows the thermometric data for this sample, and, as can be seen, the fluid inclusions forming the later trails are much less saline than the earlier isolated inclusions. Some of the scatter seen in the two-phase aqueous inclusions may be due to rupturing of early saline inclusions and subsequent mixing with lower salinity fluids. Two types of homogenization behaviour were observed in the halite bearing inclusions, and these are indicated on figure 8.10b.

1) $T_h > T_s$NaCl - the vapour bubble disappeared after the halite daughter phase had dissolved, indicating that the inclusion had trapped an undersaturated solution.

2) $T_h < T_s$NaCl - the halite dissolution temperature was higher than the liquid-vapour homogenization temperature, indicating trapping of a saturated solution.

It is thought that the variation in homogenization behaviour is due to the necking down of the inclusions after development of the halite daughter phase.

First melting temperatures in the highly saline inclusions were observed at -50 °C. Although this temperature does not correspond exactly to any salt-water eutectic, the low temperature indicates the presence of $CaCl_2$ (the eutectic temperature of the system H_2O-NaCl-$CaCl_2$ is -52 °C). The presence of $CaCl_2$ was also suggested by the pinkish-brown colour of the "ice", while the low salinity inclusions remained clear. This colouration is often associated with the presence of $CaCl_2$ (or $MgCl_2$), although the exact reason for its occurrence is unknown (Shepherd *et al.* 1985). Phase transitions in addition to T_{fm} and T_m must have occurred in the saline inclusions, but these were observed. When frozen, the saline inclusions will contain ice, hydrohalite, $NaCl.2H_2O$, and antarticite, $CaCl_2.6H_2O$, and the proposed sequence of events on re-heating is as follows (see figure 8.11). At -52 °C (T_{fm}), the eutectic temperature, $CaCl_2.6H_20$ melts to leave ice and hydrohalite.

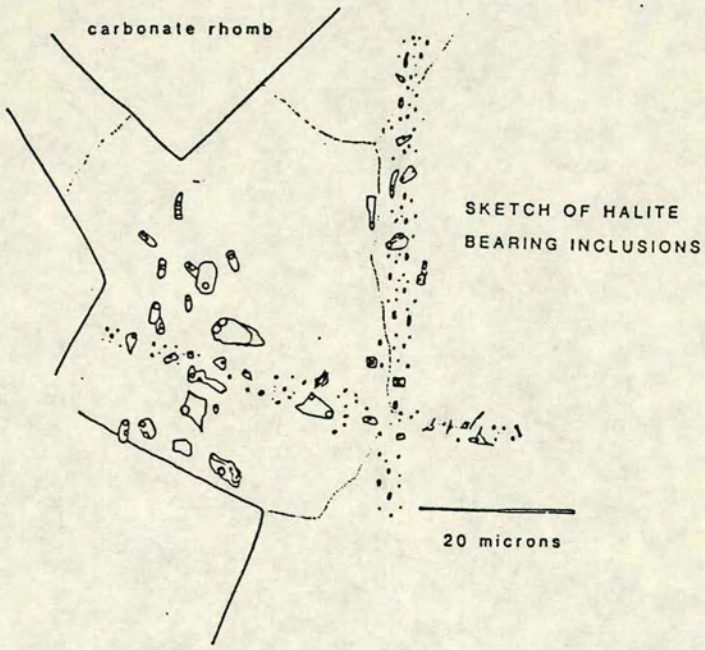

Figure 8.10a Sketch of inclusions from sample 86/77. Two distinct inclusion populations are present, an intragranular halite-saturated group (early?), and a transgranular low-salinity group

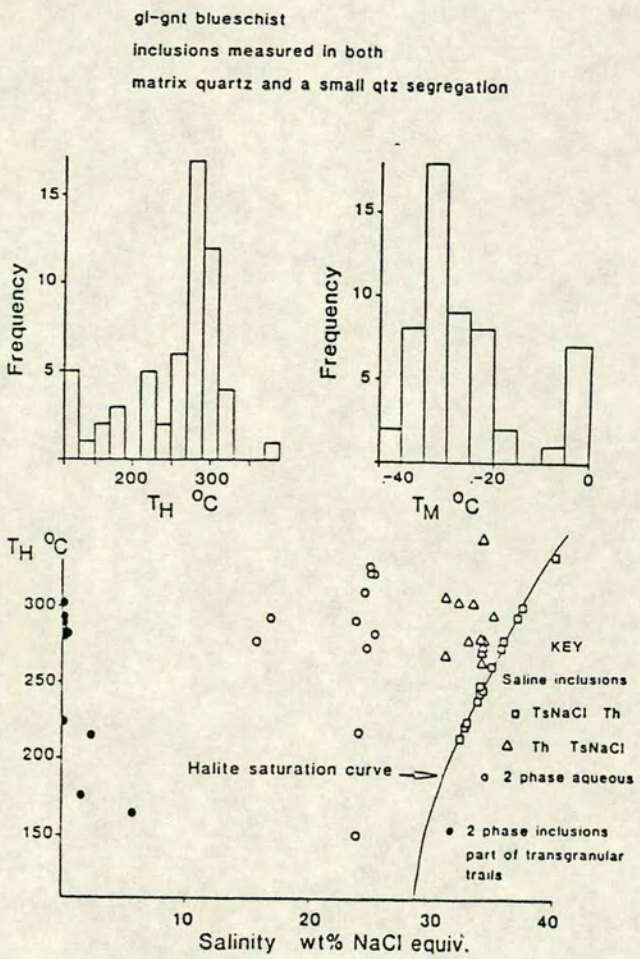

Figure 8.10b Thermometric data for sample 86/77.

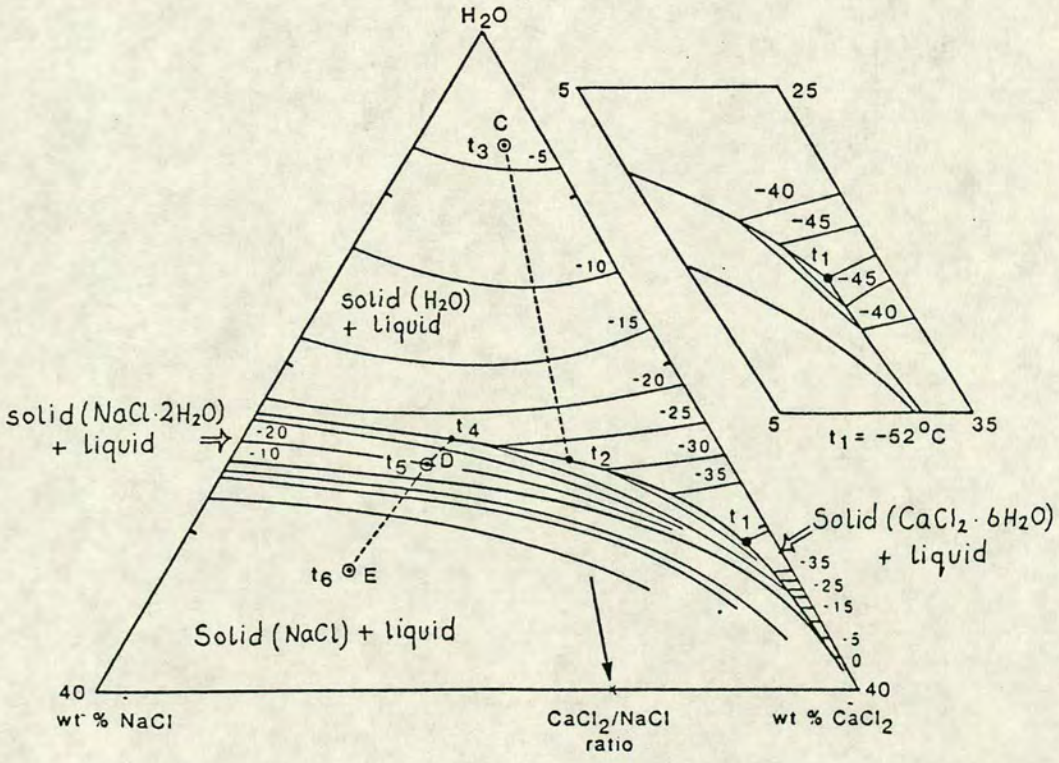

Figure 8.11 Phase relations in the ternary system H_2O-NaCl-$CaCl_2$, isotherms are labelled in °C, (from Shepherd *et al.* 1985). Shown is an example melting path for a saline inclusion containing 16 wt% $CaCl_2$ (composition point A). Melting begins at t_1, the ternary minima (-52°C). At t_1 $CaCl_2.6H_2O$ melts, and the inclusion now contains ice + hydrohalite + liquid. On further heating more liquid forms, and the inclusion follows the cotectic boundary between the ice and hydrohalite fields. At t_2 the ice melts leaving hydrhalite + liquid. The inclusion then follows a path into the hydrohalite field with the final metling point occurring at point A. The inset shows the area around the ternary eutectic, t_1, in more detail.

The inclusion will follow the cotectic boundary between the ice and hydrohalite fields as heating continues, and at some point the ice will melt (true T_m) leaving hydrohalite and liquid. The inclusion will then follow a path into the hydrohalite field moving towards the hydrohalite composition point. The final melting temperature observed (usually around -24 °C) will in fact refer to the melting of hydrohalite and should strictly be referred to as $T_m$hy. Halite-bearing inclusions will be characterised by the incongruent melting of $NaCl.2H_2O$ to produce $NaCl_{(s)}$ and liquid. In such cases the overall salinity of the inclusion cannot be determined from the final melting temperature, and instead the halite dissolution temperature, T_sNaCl, is converted into equivalent wt% NaCl using the available solubility curves for NaCl in aqueous solutions (Shepherd *et al.* 1985). It was only possible to observe T_{fm} and $T_m$hydrate in these inclusions, because ice melting was obscured due to the continued presence of hydrohalite.

The possible significance of these relatively early high-salinity inclusions will be considered in more detail in the discussion section

---

Sample 86/76 (figure 8.20-8.21)

Location: N. of Aspro, N.W coast

Description: Whole rock blueschist metasediment. Mineralogy - gl, w.mica, qtz, gnt, law(psd), cc, rut

Inclusions in garnet

Almost all the inclusions present in the blueschist rocks occur in quartz, and while quartz has the advantage of being stable in most rock types, its presence cannot be related to any specific metamorphic event, except by reference to the deformation stages affecting other minerals. However, some rare fluid inclusions were also found in garnet cores, and these are illustrated in figure 8.12. This almandine-grossular garnet grew under blueschist conditions, and therefore it is likely that these inclusions trapped samples of the synmetamorphic fluid.

The inclusions are relatively large, up to 15 microns long, elongate and quite flat. They occur as small irregularly-distributed clusters near the core of the garnet. Their habit is quite different from the negative crystal inclusion shapes described by Berglund and Touret (1976) from garnets in Madagascar, yet there is no reason to suspect that these inclusions are secondary.

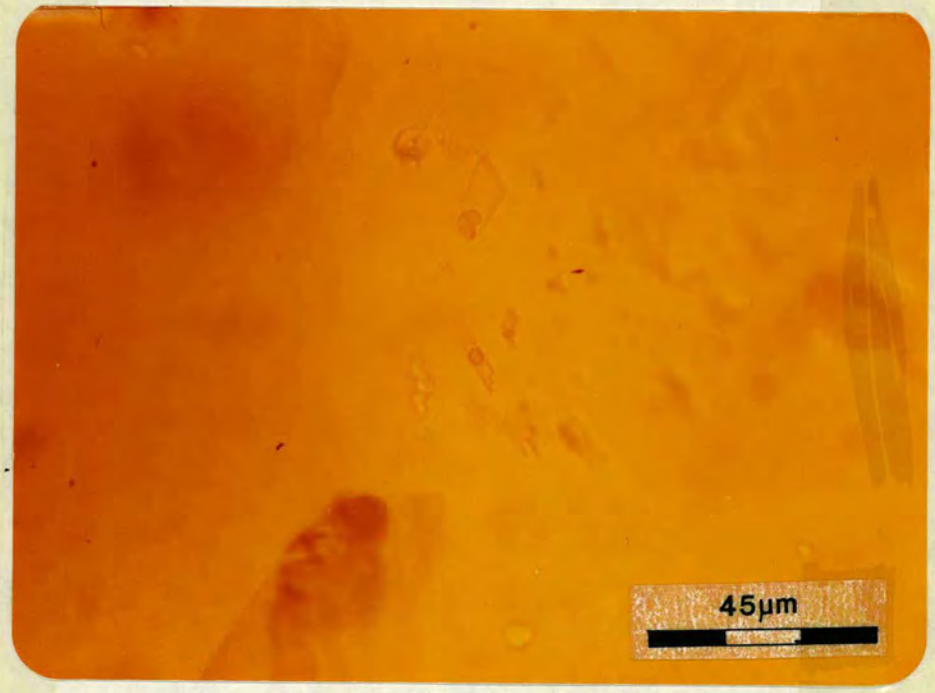

Figure 8.12 Photomicrograph of inclusions in garnet (PPL).

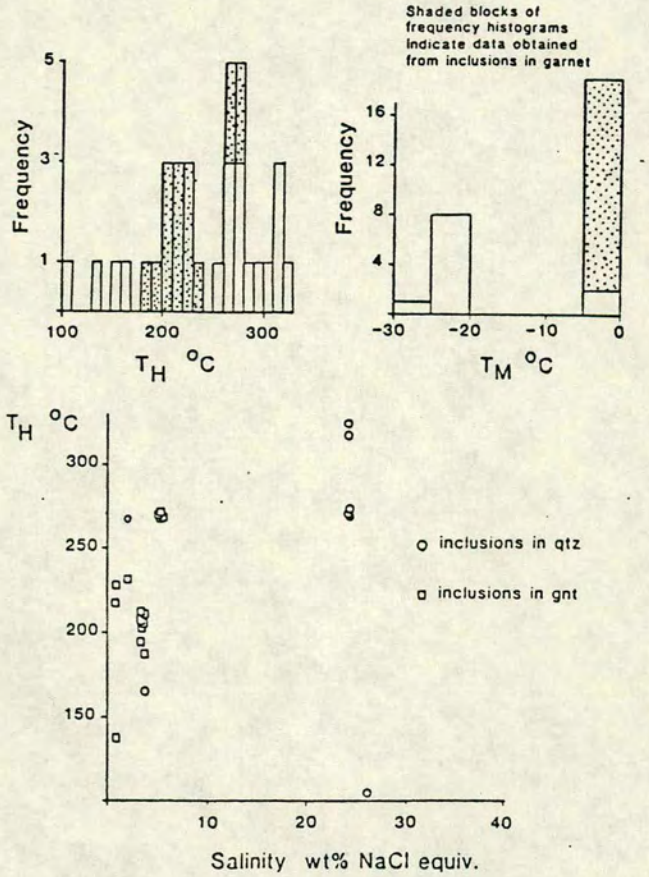

Figure 8.13 Thermometric data for sample 86/76.

The garnet inclusions contain aqueous low-salinity fluids, equivalent wt% NaCl ≈ 4 (see figure 8.13). Homogenization temperatures range from 200 to 270 °C, a similar spread to that seen in the other blueschist samples. Again, the spread of homogenization temperatures probably reflects density changes which occurred during uplift. Also shown in figure 8.13 are measurements made on isolated inclusions present in the matrix quartz. Interestingly a large proportion of these inclusions are highly saline, and similar to the inclusions seen in the previously described sample.

Dr. A. Rankin (pers. comm., 1988) suggested that the salinity of the garnet inclusions may have been underestimated if in fact the final melting temperature referred to hydrohalite not ice. This is not thought to be the case, as freezing in these inclusions occurred at around -44 °C, a typical degree of supercooling required for low salinity inclusions, whereas the saline inclusions in the matrix quartz, and those in sample 86/77, required supercooling to -80 °C in order to trigger freezing.

Summary of results

The properties of the inclusions measured in the blueschists are summarised below.

- At room temperature the inclusions consist of an outer liquid phase and an inner vapour bubble.

- Homogenization temperatures are invariably greater than 100 °C.

- Solidification of the inclusions occurs in the temperature range -25 to -80 °C.

- First melting temperatures, when observed, are lower than the eutectic temperature for the NaCl-H_2O system (Te = -20.8 °C, Crawford 1981a). The small amounts of melt produced, and the small size of the inclusions make accurate measurements of first melting difficult. Values obtained tended to cluster around -35 °C, indicating the presence of $MgCl_2$ in addition to NaCl (Crawford 1981a). Melting was observed in some of the saline inclusions at temperatures as low as -50 °C, pointing to the presence of CaCl2.

- Final melting occurs in the range -12 to 0 °C, except for the highly saline inclusions where final melting occurs at much lower temperatures, around -25 °C, and refers to the melting of hydrohalite, not ice.

Having summarised the observations for the blueschist samples, it can be stated that these inclusions, which are thought to be early, are aqueous without

microthermometrically detectable CO2, and have a variable salinity ranging from almost pure water to halite saturation.

8.8 FLUID INCLUSION RESULTS - GREENSCHISTS

Four samples showing the greenschist overprint were studied in order to make comparisons with the blueschist samples. Quartz veins or segregations were studied from samples which showed a partial or complete development of the greenschist facies overprint, and it was hoped that these might contain samples of the fluid responsible for the retrogression. The segregations sampled were significantly larger than any of those used to investigate the blueschist fluids (10's of centimetres as oppose to 10's of millimetres), and in general the inclusions were larger, and more abundant, than those seen in the blueschists. The majority of the inclusions occurred along healed fractures, but in these samples no selection bias was applied, and the inclusions studied were representative of the total population.

Sample 86/32 (figure 8.14a)

Location: Kastri, N.E. coast

Description: quartz segregation in partly altered blueschist metasediments. Mineralogy of sample - qtz, dol(psd), cc, chl, w.mica, rut

Figure 8.14a presents the thermometric data collected from this quartz segregation. The inclusions are large and abundant, and nearly all of them form part of large transgranular trails. All the inclusions seen were aqueous and the data suggests that only a single inclusion population has been sampled (see figure 8.14a). Salinity values are tightly bracketed from 6 to 9 equivalent wt% NaCl, and homogenization temperatures range from 145 to 190 °C. Melting was observed in these inclusions between -25 and -28 °C, probably indicating the presence of small amounts of $MgCl_2$ in addition to NaCl, or the occurrence of melting at the metastable eutectic, -28 °C, in the NaCl-H_2O system.

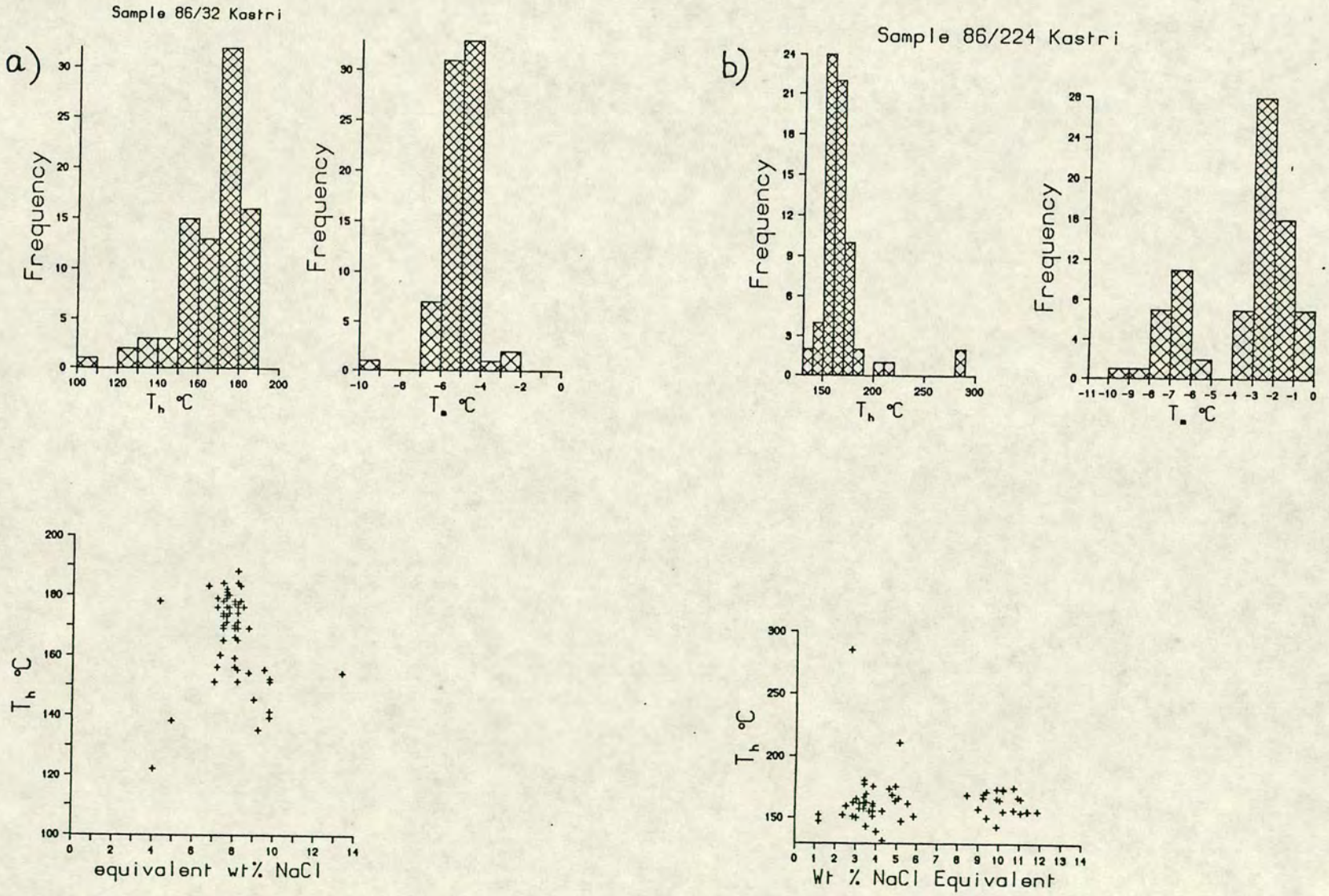

Figure 8.14a-d The following four figures present the thermometric data measured on inclusions from quartz segregations in greenschists.

c)

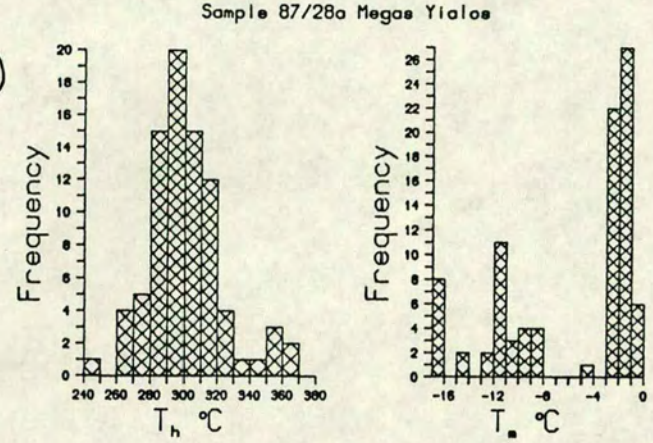
Sample 87/28a Megas Yialos
Frequency
T_h °C
Frequency
T_m °C

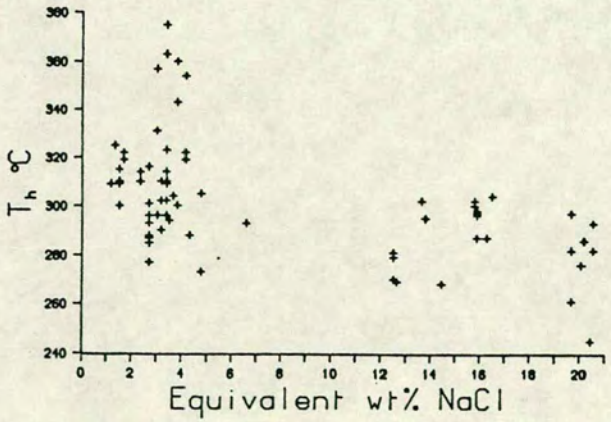
T_h °C
Equivalent wt% NaCl

d)

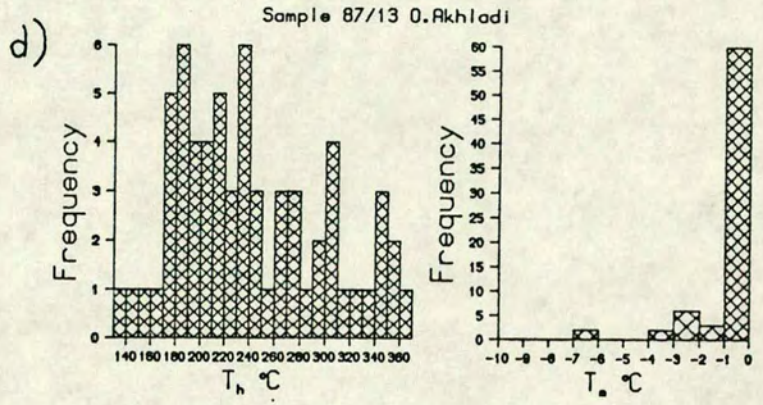
Sample 87/13 O.Akhladi
Frequency
T_h °C
Frequency
T_m °C

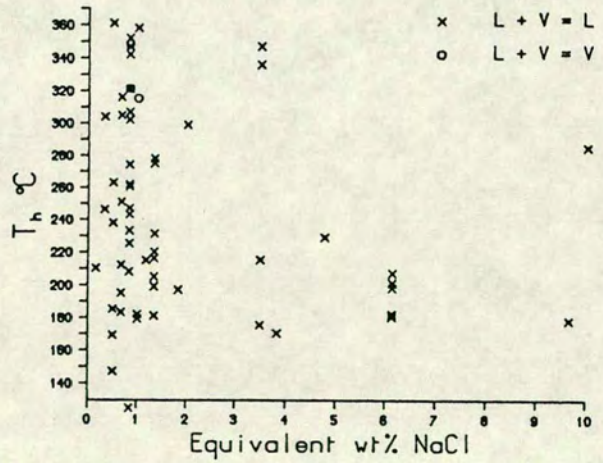
x L + V = L
o L + V = V
T_h °C
Equivalent wt% NaCl

Sample 86/224 (figure 8.23)

Location: Kastri, N.E. coast

Description: quartz vine in altered blueschist metasediment. Mineralogy of host rock - qtz, w.mica, cc, albite, chl sph

The thermometric data for this sample is shown in figure 8.14b A distinct bimodal grouping of salinities occurs, from 1.5 to 5 equivalent wt% NaCl, and from 8.5 to 12.0 equivalent wt% NaCl. There is no obvious difference, in terms of distribution and location, between the inclusions in either group. Overall the number of inclusions in this sample were low, and a relatively large proportion of those present were high density, late stage inclusions which either contained a very small vapour bubble, or were monophase liquid. Several examples of metastable behaviour were observed, the commonest of which was the failure to renucleate the vapour phase after freezing. This sometimes led to the metastable persistence of ice above 0 °C, and in one extreme case ice was still present at +8 °C. Measurements made on these inclusions are not incorporated in figure 8.14b, but final melting temperatures of less the -1 °C indicate an almost pure H_2O fluid in these very late inclusions.

Sample 87/28a (figure 8.14c)

Location: Megas Yialos, south coast

Description: qtz segregation in a series of chl-alb greenschists

This sample also shows a very definite bimodal distribution of salinities, (see figure 8.14c). There is a low salinity group which varies from 1.5 to 5 equivalent wt% NaCl, and a dispersed, higher salinity, group with values ranging from 12.5 to 20.5 equiv. wt% NaCl. The higher salinity group may represent more than one inclusion population, but more measurement would be needed to confirm this. First melting temperatures of -54 °C were recorded in some of the more saline inclusions indicating the presence of $CaCl_2$, and final melting temperatures clustered around -16 °C. First melting was observed in a number of the less saline inclusions at temperatures of -30 °C, indicating the addition of $MgCl_2$ to the simple H_2O-NaCl system. The different fluid compositions clearly indicate the presence of at least two distinct fluid inclusion populations.

Sample 87/13 (figure 8.14d)

Location: Ormos Akhladhi, south coast

Description: Qtz segregation in impure carbonate. Mineralogy of host rock - cc, qtz, w.mica, chlorite

Figure 8.14d presents the thermometric data for sample 87/13. This sample shows an exceptional range in Th, from 148 °C to 368 °C. The inclusion density was highly variable, and some chips contained almost no inclusions at all. When inclusions were present they tended to occur in clusters rather than trails, and many were concentrated along quartz grain boundaries. A number of features seen in this sample suggest that significant necking down, leakage and migration of inclusions has occurred. Small tubes were seen connecting inclusions, while others showed an expansion of the vapour phase on heating. Occasionally a small crack was seen at the edge of an inclusion, along which the fluid presumably leaked away. On heating above 270 °C, extensive decrepitation occurred, causing an abrupt darkening of the inclusion when the fluid was replaced by low-index vapour. The inclusions showed very variable phase proportions, even within single clusters. This is a commonly recognised feature in inclusions which have undergone leakage and necking down. Softer minerals with a strong cleavage, e.g. calcite, often show evidence for leakage, but quartz is usually much less susceptible to this. It is not fully understood why this sample alone should show these effects. Leakage and autodecrepitation of inclusions followed by retrapping of the fluid in "secondary" inclusions may have occurred if inclusions were subjected to temperatures higher than their temperature of formation. Such a process could account for the spread of data seen.

8.9 DISCUSSION

A number of similarities in the data are apparent for the blueschist and greenschist samples. In both cases, the inclusions are of the two phase aqueous type, and the two groups show a very similar range of homogenization temperatures, from 110 to 370 °C. The main difference is that the blueschist samples contain inclusions which are much more saline than anything found in the greenschists. Some of the greenschist samples show a clear bimodal grouping of salinities (86/224 and 87/28a), and this grouping indicates the presence of at least two distinct fluid populations. The more

saline inclusions may be a "memory population" related to the earlier blueschist event.

The saline inclusions

Until recently the sporadic occurrence of halite saturated inclusions in metamorphic rocks tended to be dismissed as an enigmatic curiosity unless they could be directly related to the presence of nearby evaporitic sequences (Rich 1979). There is certainly no evidence for the presence of an evaporite deposit at depth on Syros, but Na-bearing phases are present in the blueschists, e.g, glaucophane and paragonite, and perhaps the presence of Na-rich inclusions simply reflects the mineralogy of these host rocks. In fact the situation must be more complicated, since although the presence of Na-bearing phases means that the synmetamorphic fluid was probably saturated with respect to sodium, chloride ions must also have been present in order to form NaCl. In these rocks it is likely that the availability of the chloride ion is the most important factor in determining whether the fluid will become saturated in NaCl or not.

Participation in hydration reactions could cause low salinity fluids to become more saline, as was suggested by Crawford *et al.* (1979a) and, given that sufficient chloride ions were present, halite saturated fluids could be produced by this mechanism. A mechanism of evolving salinity with time could explain the presence of low salinity fluids in the garnet core of sample 86/76, and saline fluids in the external matrix quartz. The garnet preserving an early sample of the fluid, while subsequent hydration reactions modified the salinity of the remaining fluid later, trapped in the quartz. Although it may be coincidental, halite saturated inclusions were only seen in sample 86/77, which consists of approximately 40% lawsonite by volume. A possible link is therefore suggested between the generation of lawsonite (see discussion in chapter 7), and the presence of halite saturated inclusions. More lawsonite bearing samples would have to be examined in order to confirm this.

Relationship between fluid composition and rock type

If the fluid inclusions in the blueschists preserve samples of the fluid evolved during metamorphic reactions, a correlation between the compositions of the fluid inclusions and the host rocks should be expected. Crawford *et al.* (1979a) observed fluid inclusions in calcareous rocks which were free of CO_2, whereas the fluids contained in concordant quartz pods in semipelites were dominantly CO_2-bearing. Kreulen

(1980) reported the presence of CH_4 in inclusions from graphite bearing sediments, and as mentioned previously there is a strong correlation between the presence of evaporites and occurrence of halite saturated inclusions. The data obtained from the Syros samples , both blueschists and greenschists, shows no apparent difference in the CO_2/H_2O ratio of the fluid from samples containing different mineral assemblages. In the case of the blueschists at least, this observation may merely reflect the fact that the equilibrium CO_2/H_2O ratio is so low, that slight variations in the CO_2 content of the fluid between different samples are impossible to detect thermometrically (see results of the T-X_{CO2} grid, chapter 3.)

8.10 CONCLUSIONS

In conclusion, on the amount of data gathered so far it is not possible to state unequivocally that the fluid inclusions present in the blueschists represent samples of the synmetamorphic fluids. However, the absence of a CO_2 phase, and the abundance of aqueous inclusions is compatible with the equilibrium phase assemblages. There are very few documented cases of aqueous inclusions in high grade metamorphic rocks, largely because much of the fluid inclusion work has concentrated on CO_2-dominated granulite terrains, where H_2O-bearing inclusions are invariably dismissed in a few sentences. However examples of very early H_2O inclusions are now being reported from granulite terrains, and there are indications that these could be contemporaneous with the early CO_2-rich fluids. The recent discovery of halite cubes in decrepitated inclusions in granulites is also being interpreted as evidence for the presence of very early highly saline aqueous fluids (J. Touret pers. comm., 1989)

Unfortunately, it is not possible to calculate meaningful isochores for the blueschist samples for two reasons. Firstly, the available PVT data on aqueous saline solutions is limited to measurements made at low pressure, up to 2 kbars (Haas 1976; Potter and Brown 1977). The linear extrapolation of isochores up to 14 kbars is not justifiable. Secondly, the relatively low homogenization temperatures (< 300 ^{o}C), compared to the metamorphic temperatures estimated from phase equilibrium studies (450 ^{o}C), suggests that the inclusions have not preserved their original densities.

The inclusions present in the greenschist samples are largely of secondary origin, and whether these represent samples of the infiltrating greenschist fluid is debatable. However, in terms of a relative chronology these fluids appear to be later than the fluids sampled in the blueschists, but the greenschist samples are probably recording several fluid events which occurred during the later history of the rocks.

Possible nitrogen-bearing inclusions

In addition to the abundant aqueous inclusions there are a number of intragranular trails composed of very small dark inclusions. These, presumably vapour rich inclusions, are much too small to examine using normal thermometric techniques. Although these inclusions are insignificant, in terms of abundance, compared to the aqueous inclusions, their mode of occurrence suggests that they may be remnants of an early fluid phase. It was suggested that these inclusions may be nitrogen-rich, (J. Touret pers. comm. 1989). Recent studies have discovered nitrogen-rich inclusions in many rock types spanning a range of metamorphic grades (Schreurs 1984; Swanenberg 1980; Touret 1981; Touret and Dietvorst 1983). Although the origin and significance of these inclusions is not yet fully understood, it is thought that much of the N_2 in fluid inclusions is derived from the metamorphic breakdown of NH_4^+-bearing micas and feldspars (Guillot and Moine 1989).

Some of the potential N_2-bearing inclusions in the Syros blueschists will be analysed using the laser raman probe at the University of Amsterdam to establish their composition.

CHAPTER 9

DISCUSSION AND CONCLUSIONS

In this chapter the main results of the previous chapters are reviewed, and related to the conclusions of other blueschist workers, in order to generate a unified picture of the fluid regime operating under high-pressure, low temperature conditions.

The main conclusions arising from this thesis are:

1) The composition of the fluid coexisting with the blueschist assemblages was extremely water-rich. The mineral assemblages suggest $X(CO_2)$ values of 0.002 mol% and less. This conclusion is reinforced by fluid-inclusion studies which only detected two-phase aqueous inclusions. The salinities of the fluids are highly variable from almost pure water to halite-saturated.

2) The blueschist unit has evolved as a closed system during metamorphism. Mineral assemblages from interlayered blueschist sequences have buffered the composition of the coexisting fluid. Whole rock and mineral separate isotopic data suggest that large-scale isotopic equilibration has not occurred in the blueschist units, reinforcing the conclusion of a closed system. Mineral separate data shows that isotopic heterogeneity is preserved on a scale of centimetres.

3) The presence of lawsonite in the northern schists appears to require the infiltration of an external fluid, parallel to rock layering. Alternatively a process of coupled oxidation and graphitic burning is envisaged for the graphite-bearing lawsonite schists.

4) The blueschist to greenschist transformation occurred as a consequence of fluid infiltration during decompression. Isotopic data suggests that the volume of infiltrating fluid involved in this transformation is small. However at one locality extensive $\delta^{18}O$ depletions in marble and an approach towards isotopic homogenization between different rock types suggests fluid communication between layers. This area is interpreted as having been a zone of high, localized, fluid flow.

5) Asymmetrical $\delta^{18}O$ depletions in marble units suggests that oxygen exchange occurred via a moving fluid. Calculated isotopic fluid-rock ratios are small,

0.1 : 1 and less, except for one area (O. Akhladhi) where higher fluid fluxes are recorded.

These findings are consistent with very limited fluid flux during the peak event. This fits a low temperature regime, and indicates that the underlying subducting slab had little fluid generating potential. The development of later overprinting greenschist assemblages suggests that the blueschists interacted with some fluid after the peak metamorphic event. As was discussed in chapter 1, this fluid was probably generated at depth and channelled up-dip along planes of structural weakness. Such a mechanism will transport fluid to high levels in the wedge where it can interact with the uplifiting blueschists causing alteration.

Channellized fluid flow appears to be important during the blueschist event on Syros. The suggestion of fracture-dominated fluid transport is in agreement with the conclusions of many other workers, who emphasise the importance of syn-blueschist veining (Bebout & Barton 1989, Okay 1982). Pervasive grain boundary flow may have occurred within layers (small scale isotopic equilibrium has been approached in blueschist samples), but there is no evidence for fluid communication across layers. Each rock layer has essentially acted as a closed system, and the composition of the coexisting fluid has been buffered internally by devolatilization reactions. The very low porosity in these rocks means that fluids generated by devolatilization reactions must be expelled from the system. This expulsion is envisaged to occur through a fracture system, which effectively isolates the fluid from the surrounding rock. However, some chemically reactive layers have been pervasively infiltrated by this 'external' fluid, which has driven lawsonite-forming reactions.

The blueschist to greenschist transformation appears to be largely vein controlled, which fits with the suggestion of up-dip fluid-rich zones. However pervasive alteration has also occurred, particularly in the south of the island. The relative importance of grain boundary versus channellized fluid flow is still an unresolved question. There is a dearth of PVT data for fluids under high pressure conditions, and the study of mineral-mineral-fluid dihedral angles, which promises to provide important information on the porosities and permeabilities of metamorphic rocks is still largely in its infancy. Veins commonly form by hydraulic fracturing (Norris and Henley 1976, Wood and Walther 1986, Yardley 1983, 1986), and this process can be induced by the thermal expansion of water. An important difference exists between the behaviour of water in the blueschist and greenschist facies. Norris and Henley (1976) showed that for all geothermal gradients greater than 12°C/km thermal expansion of water will occur. However, under blueschist conditions the geothermal

gradient will generally be less than 12°C/km, and thus no thermal expansion of water will occur. This does not mean that any fluid generated under blueschist conditions will simply "sit around". The vanishingly small porosities demand that the fluid leaves the rock, but one of the main driving forces behind hydraulic fracturing will not operate in this PT regime. During uplift, the reduction in pressure, and the concomitant rise in temperature, means that thermal expansion will occur, and conditions favourable for the formation of hydraulic fractures are produced. The thermal expansion of fluids under the lower pressure greenschist conditions may lead to extensive hydraulic fracturing, enchanced permeability and a greater degree of pervasive, grain boundary fluid flow.

From these considerations, pervasive fluid flow might be expected to be more common in the greenschist/amphibolite facies than in the blueschist facies, and this appears to be true for Syros. However, Matthews and Schliestedt's data (1984, 1987) from the neighbouring Cycladic island of Sifnos can only be explained by extensive grain boundary flow. Interlayered rocks have experienced a substantial degree of isotopic homogenization, during both the blueschist and the greenschist facies events, and this suggests pervasive grain boundary flow at least over the scale sampled, $\approx$ 5 metres. Perhaps the apparent differences in fluid behaviour from two such closely associated areas should not be unexpected. As was discussed in Chapter 1, the scale over which grain bounary flow operates is probably highly variable, and the complex internal structure of subduction zones means that changes in the dominant mechanism of fluid transport could well occur over small distances.

The very water-rich nature of the blueschist fluid agrees with the available data from other high-pressure terrains (Table 9.1), and it appears that in general water-rich conditions are characteristic of subduction zones, just as CO_2-rich conditions are commonly associated with granulite terrains.

Table 9.1 Summary of blueschist fluid compositons, compiled from published data.

Author	Area	$X(CO_2)$ of fluid
Brown and Bradshaw (1979)	Franciscan formation, California	$X(CO_2)$ <0.02
Bebout and Barton (1989)	Franciscan formation, California	$X(CO_2)$ unspecified H_2O-rich
Ernst (1972)	Franciscan formation, California Sanbagawa terrane, Japan	$X(CO_2)$ <0.01 $X(CO_2)$ <0.04
Okay (1980)	Tavsanli region, Turkey	XCO_2 unspecified H_2O-rich
Holland (1979	Tauern window, Austria	$X(CO_2) = 0.02 \pm 0.02$
Ghent *et al.* (1987)	New Caledonia	$X(CO_2) = 0.1 - 0.05$
Itaya *et al.* (1985)	New Caledonia	$X(CO_2) = 0.13 - 0.04$
Schliestedt and Matthews	Sifnos, Cyclades	$X(CO_2) \approx O$
This study	Syros, Cyclades	$X(CO_2) < 0.002$

Finally, possible areas for future study are listed below;

1) More isotopic analyses of mineral separates are required from blueschist and greenschist facies sequences. As yet no detailed work has been undertaken on the greenschist rocks, and such a study is required in order to assess the degree of isotopic homogenization across layers during the greenschist event. The low fluid-rock ratios indicated by the whole rock study, suggests that for most localities only partial homogenization will have occurred, but this needs to be confirmed. Mineral separate data from blueschist localities suggests that very little, or no O exchange has occurred across layers, but further data would strengthen (or otherwise) this conclusion. Mineral separation is a slow and painstaking pursuit, and greenschist samples can be particularly difficult if albite is present intergrown with quartz. When assessing the degree of isotopic homogenization between layers quartz separates alone are quite sufficient. Two samples from each locality should be completely separated

and analysed in order to determine whether isotopic equilibration has been achieved within layers.

2) Much more data on the occurrence and distribution of veins is required, both for the prograde blueschist event, and the retrograde greenschist event. Despite being concerned with fluid-rock interaction this study has not investigated veins in any detail, and since veins represent fractures along which fluid-flow was concentrated, this is a major oversight on the part of the author. Veins were most frequently observed in metabasic rocks, where they are dominantly composed of calcite, and associated retrograde effects are seen in the host rocks. The greenschist "event" is very hard to pin down in P-T-t space, and in reality it probably consists of several diachronous events occurring during the appropriate pressure range, ≈8-5kbars. If sufficient field and isotopic data were available for the retrograde veins, it may become possible to characterise different retrograde events both through the field relationships of the different vein sets, and by the δO signature of the associated fluid. Graham *et al.* (1983) were able to characterise a widespread retrograde fluid event in the S.W. Highlands through the occurrence of associated δO-enriched carbonate. Identification of unequivocal retrograde veins would also be useful for further fluid inclusion work on the greenschists. Some isoclinally folded quartz veins were noted in the blueschist units, but quartz-carbonate segregations or lenses were more apparent, and these were not accompanied by retrogression halos. Very few veins containing definitive high pressure phases were seen, but they may have been overlooked. Further analytical and field work on the prograde veins would help constrain possible fluid transport pathways during the blueschist event, and help tighten up the isotopic and chemical characterization of the prograde fluid.

3) The occurrence and distribution of lawsonite-bearing units also requires further study. Detailed mapping following individual lawsonite-bearing beds is needed to determine if reaction fronts do occur in these rocks. Further isotopic work (mineral separates and whole rock analyses) is required to assess the extent of isotopic equilibration and homogenization both within and across lawsonite-bearing beds. Careful petrological work is also needed to find out more about when, and how, the lawsonite formed.

4) The potential for further study of fluid inclusions in the blueschist rocks is vast, and of particular merit because so little has been published in this area.

The main objectives of such a study would be to determine the properties and composition of the primary blueschist fluid. From this study it appears that the best approach to this problem would be to study inclusions in blueschist minerals, e.g. garnet and omphacite. Inclusions in quartz, where quartz forms part of the blueschist rock matrix would also be worth investigating. Initially, at least, veins and segregations should perhaps be avoided (even though the largest inclusions occur in these settings) because such obvious fluid pathways may well have been re-used at several different times during the subsequent P-T evolution of rock (e.g. Yardley 1986).

APPENDIX 1

Construction of Schreinemaker bundles

In producing any sort of petrogenetic grid some knowledge of Schreinemakers theorems (Schreinemaker 1915-1925) is required in order to position the relevant univariant reaction curves around the appropriate invariant points. In this study a matrix table method was used to assemble the univariant curves around the relevant invariant point; a method which proved to be both fast and acurate. This technique was originally derived by Niggli (1937) after Schreinemakers (Schreinemakers 1915-1925), and was later modified by Graham (pers. comm. 1986).

In the example given below the lawsonite absent invariant point [laws] is used.

a) For the particular invariant point under consideration all the relevant univariant reactions are written out and a single nondegenerate reaction is chosen at random.

$$\underbrace{\text{parag+qtz+chl+dol}}_{-} = \underbrace{\text{gl+zoi+}H_2O\text{+}CO_2}_{+} \qquad \text{[law, cc]}$$

reaction coding indicating absent phases

b) Reactants are assigned negative signs, products positive signs.

c) These signs are entered in the matrix array for the appropriate reaction [law, cc]

[LAW]	gl	parag	chl	zoi	cc	dol	H_2O	CO_2	phases
[gl]	O				-				
[parag]		O			+				
[chl]			O		+				
[zoi]				O					
[cc]	+	-	-	+	O	-	+	+	
[dol]					+	O			
[H_2O]					-		O		
[CO_2]					-			O	
reactions									

first column filled by applying the rule of opposition, see text

In terms of the matrix table this means that if the phase glaucophane has a negative sign in the reaction [cc], then the phase calcite will have a positive sign in the reaction [gl]. This is the premise, based on the principle of opposition, on which all the reaction coefficients in the matrix table are worked out.

d) The matrix is completed by filling in the appropriate signs from the other reactions involved.

[LAW]	gl	parag	chl	zoi	cc	dol	H_2O	CO_2	phases
[gl]	O	D	-	D	-	+	+	-	
[parag]	D	O	+	D	+	-	-	+	
[chl]	+	-	O	+	+	-	+	+	
[zoi]	D	O	-	O	-	+	+	-	
[cc]	+	-	-	+	O	-	+	+	
[dol]	-	+	+	-	+	O	-	-	
[H_2O]	-	+	-	-	-	+	O	-	
[CO_2]	+	-	-	+	-	+	+	O	

reactions

completed matrix for the [law] invariant point.

Notes

i D - signifies a degenerate reaction, fewer phases are involved due to the reduced number of components.

ii quartz does not appear in the matrix because it is an excess phase, the system is modelled as being silica saturated.

Drawing up the Bundle

Once the matrix is completed the bundle of univariant curves can be arranged around the invariant point. A reference curve is selected at random and drawn with arbitary slope. The next curve is placed either clockwise or anticlockwise relative to the reference curve according to the sign of this reaction in the matrix array. A sign convention is adopted whereby a positive sign indicates a clockwise position from the reference curve, and a negative sign an anticlockwise position.

In the example given below the "+" sign indicates that the [gl], [zoi], [H_2O] and [CO_2] curves lie in a clockwise position from the reference curve. The relative position of these four curves must be established by examining other rows in the matrix.

The principle of opposition

This is best demonstrated by an example. Consider the degenerate reaction which passes through the [LAW] invariant point.

$$chl+cc+CO_2 = qtz+dol+H_2O$$

According to the rule of opposition the stable parts of the chl, cc and CO_2 absent curves, i.e. [chl], [cc], [CO_2], must occur on the opposite side of the reaction line to that which the phases themselves appear. The principal of opposition follows logically because if a phase is absent from a region of T-X (or P-T etc) space it cannot take part in a reaction occurring within that space. This is illustrated in the bundle below:

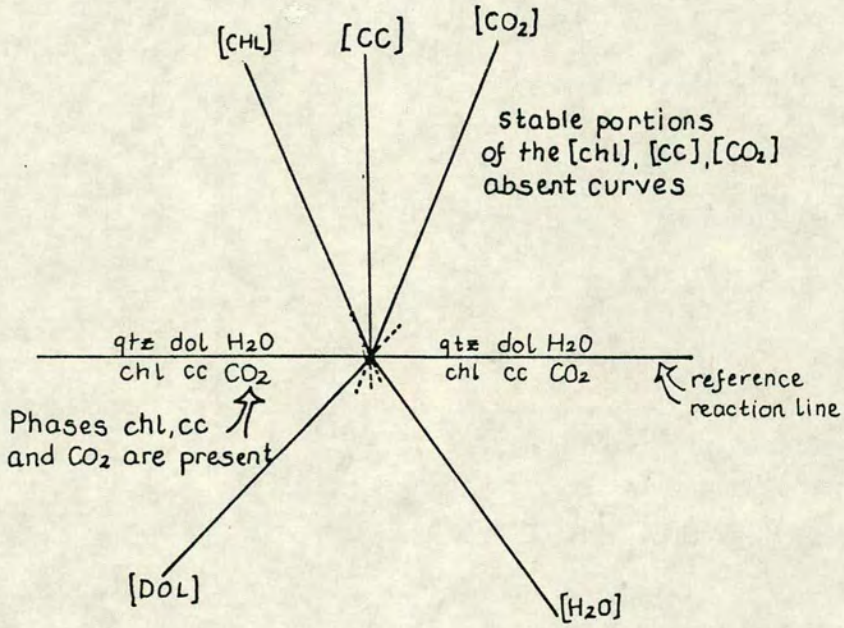

[LAW]	gl	parag	chl	zoi	cc	dol	H_2O	CO_2	
[zoi]									
[cc]	+	-	-	+	O	-	+	+	reference
[dol]									curve

The final bundle is shown below:

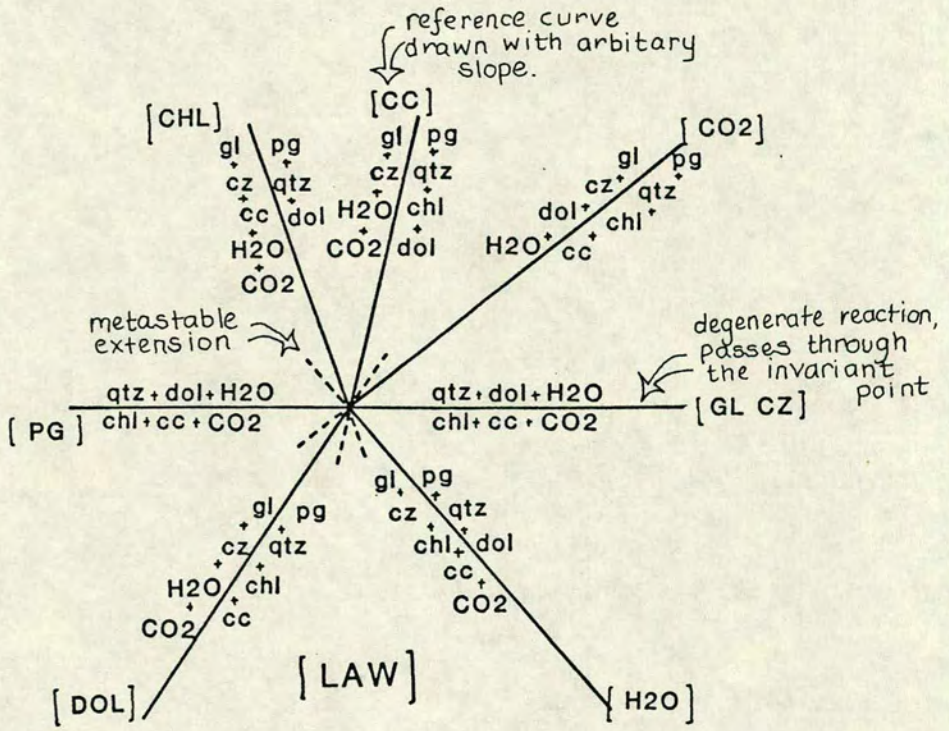

APPENDIX 2

Isotopic analysis of mixed calcite-dolomite samples

Accurate, reproducible $\delta^{18}O$ and $\delta^{13}C$ analyses of coexisting calcite and dolomite are difficult to obtain. One solution is to physically separate the two phases and analyse them separately. However, mineral separation is time consuming and not always possible, especially if the two phases have very similar physical properties. Therefore a reliable means of chemical separation would be an attractive alternative.

The carbon and oxygen isotopic signatures of carbonate present in rocks are measured by releasing CO_2 from the carbonate (calcite or dolomite) by reaction with H_3PO_4 at 25°C, and analysing CO_2 on a mass spectrometer. In the case of samples containing both calcite and dolomite chemical separation is achieved by sequential extraction of the gas released. Dolomite is more resistant to acid attack than calcite and the first CO_2 released will be derived from the breakdown of calcite. The CO_2 generated by dolomite breakdown will be released later, after most of the calcite has finished reacting. The chemical separation method is strongly dependent on the rate of reaction for the coexisting carbonates, and the reaction rate itself is governed by several factors such as:

- particle size and overall surface area
- temperature at which reaction occurs
- degree of ordering of dolomite
- degree of deformation and strain in the crystals.

Some of these factors can be controlled experimentally, e.g. the temperature of reaction, but with others it is more difficult to place limits on the reaction conditions. The uncertainties in the method, particularly related to the degree of ordering and deformation in the carbonates, mean that accuracies of greater than 1‰ cannot be expected.

Experimental Method

Samples were ground in a TEMA mill, marbles for 50 seconds, schists and metabasites for 80 seconds. The resulting powders were then passed through a 44 micron (325 mesh) sieve. In order to remove the finest material each sample was rinsed with distilled water and allowed to settle. The water and suspended fine dust was then pipetted off, and the sample was allowed to dry. This procedure should

produce samples with a restricted particle size, close to the 5-44μ fraction suggested by Walters *et al.* (1972) as the most suitable to minimise cross contamination of evolved CO_2 from calcite and dolomite.

The prepared samples were reacted with superconcentrated H_3PO_4 under vacuum. The reaction tube was placed in a water bath whose temperature was maintained at a constant 25°C. CO_2 collection times were scheduled in order to maximise the fraction of CO_2 collected separately from each carbonate following the recommendations of Walters *et al.* (1972).

The first collection of CO_2 was made one hour after the initiation of the reaction, and this fraction should contain most of the CO_2 evolved from the faster reacting calcite. The gas was extracted again after 3 hours though this portion of the gas was disregarded as it will contain a mixture of CO_2 contributed from both calcite and dolomite. The portion of CO_2 evolved from dolomite was collected from 3 hours to reaction completion.

APPENDIX 3

Bulk-rock analyses of blueschist and greenschist samples

b = blueschist, g = greenschist

	b 86/14	g86/19A	g86/25	g86/34	b 86/52	b86/53H	b86/61	b86/70	b86/72	b86/74	b86/73	b86/78
02	53.59	48.16	52.14	53.74	54.27	50.67	49.95	56.59	61.17	58.65	58.83	53.40
O3	14.91	17.42	14.40	17.40	10.55	10.89	10.07	16.18	14.65	14.95	16.08	19.59
O3	0.95	0.24	1.24	0.98	3.17	0.05	7.86	1.04	0.42	1.46	0.95	2.39
	5.31	7.68	5.13	5.45	7.82	5.93	*	6.38	6.83	5.24	5.69	5.89
	4.44	5.40	4.49	5.24	8.45	7.24	13.45	6.88	6.15	4.83	5.67	4.98
	6.50	5.95	7.32	3.19	3.25	9.42	8.01	2.01	1.39	3.59	1.91	1.58
O	1.46	2.55	1.56	2.64	5.56	1.51	1.25	3.45	1.85	1.46	2.65	2.69
	2.86	2.90	2.70	3.41	0.69	2.73	2.38	3.29	2.58	3.24	3.24	4.56
02	0.73	0.87	0.71	0.88	3.79	0.57	0.44	0.88	0.79	0.77	0.78	0.89
	0.11	0.12	0.13	0.12	0.05	0.13	0.11	0.11	0.09	0.11	0.07	0.32
05	0.10	0.08	0.11	0.13	0.05	0.09	0.01	0.10	0.12	0.12	0.11	0.20
AL	90.97	91.37	89.93	93.18	97.65	89.23	93.54	96.91	96.04	94.41	95.98	96.48
	185	228	188	217	35	433	853	379	312	245	259	282
	344	314	283	347	36	1136	3049	630	472	490	327	279
	148	187	146	183	521	140	173	172	167	154	160	221
	20	24	21	22	41	10	25	18	14	16	14	17
	38	47	33	12	18	30	27	8	32	29	18	21
	96	115	105	109	91	78	77	85	118	102	126	179
	156	150	247	82	11	110	36	46	73	89	97	117
	119	128	116	141	22	72	67	150	119	141	150	210
	142	151	144	187	75	93	33	174	147	164	176	159
	12	13	11	16	5	9	6	15	14	14	14	14
	259	392	352	395	115	596	349	388	330	327	346	558
	12	16	14	4	2	7	3	6	6	14	8	15
	11	13	10	15	*	7	3	14	11	12	14	15
	28	36	27	28	10	14	*	29	21	95	25	39
	56	74	64	74	6	39	*	70	48	60	57	102
	23	28	24	25	7	15	*	28	17	25	19	36
	22	28	21	23	24	18	10	27	19	25	21	37

	b86/86	b86/100	b86/106	b86/111	b86/124	g87/21A	g87/111	b87/130	g87/138	g87/140	b87/141	g87/143
2	51.03	60.34	51.80	53.54	50.60	42.57	49.74	47.32	65.49	73.32	60.76	65.05
O3	16.13	12.06	16.77	17.36	15.73	13.48	16.48	13.85	15.51	13.68	13.93	15.32
O3	4.91	12.04	2.58	6.60	3.06	5.31	5.38	3.28	3.99	2.33	3.58	5.25
	4.92	4.65	8.74	4.58	6.08	3.52	5.24	5.08	3.22	1.98	5.79	2.59
	7.96	1.91	4.66	4.40	6.11	6.86	5.22	4.50	2.66	1.41	5.13	2.55
	6.19	1.29	2.66	1.18	10.39	13.08	8.90	11.00	0.73	1.70	0.69	0.50
O	4.15	4.35	3.00	2.24	4.53	3.97	4.47	3.53	2.13	3.10	4.95	3.78
	1.65	0.51	4.09	4.98	0.02	0.53	0.20	0.44	1.90	0.53	0.63	1.03
2	0.90	0.46	0.69	0.65	1.78	0.77	1.19	0.83	0.58	0.36	0.69	0.96
	0.14	0.15	1.18	0.57	0.19	0.17	0.17	0.17	0.11	0.07	0.17	0.12
5	0.08	0.19	0.90	0.19	0.26	0.07	0.13	0.15	0.05	0.08	0.10	0.17
AL	98.07	97.95	97.06	96.28	98.76	90.33	97.11	90.15	96.37	98.56	96.42	97.32
	63	4	149	179	140	154	41	49	5	4	9	3
	240	5	176	188	229	392	136	136	3	1	10	4
	233	11	254	346	266	243	356	202	173	35	158	92
	37	23	12	12	31	34	43	25	23	12	29	25
	17	12	17	97	19	34	29	20	47	*	35	15
	106	307	174	208	91	74	102	59	104	27	172	122
	184	38	61	47	270	196	97	145	30	70	34	27
	33	9	153	228	*	13	4	10	53	12	13	26
	50	116	135	132	185	54	64	62	88	100	102	131
	1	2	16	10	4	1	1	3	4	3	5	5
	185	54	633	621	*	68	20	67	149	149	472	131
	9	12	28	11	4	3	9	8	4	4	3	7
	0	*	16	14	*	*	2	1	1	*	1	3
	*	20	71	51	8	0	0	8	2	4	7	10
	11	43	144	89	14	7	14	13	7	9	15	18
	4	24	70	50	11	5	6	8	7	7	9	10
	20	37	67	38	38	17	21	22	28	30	32	33

	b87/157	g87/160	g87/173	g87/193	g87/205	b87/222	g87/228	b87/KAM	b87/SY4	b87/UM3
O2	50.29	46.82	64.76	41.66	49.18	40.88	57.90	56.25	56.23	41.34
2O3	15.46	17.32	12.58	15.97	15.08	13.63	14.03	16.28	14.89	3.04
2O3	4.09	3.33	0.94	3.91	3.26	3.30	0.74	1.79	3.80	2.96
O	6.55	6.02	3.80	4.65	7.47	4.13	5.15	6.41	8.13	5.62
O	5.27	8.43	3.20	4.51	5.74	3.02	4.12	6.90	3.52	34.18
O	8.57	9.09	4.37	9.97	6.74	17.70	4.87	1.53	5.23	0.42
2O	4.56	3.38	1.27	2.11	4.44	1.67	1.98	1.50	4.32	*
O	0.95	0.19	2.00	2.33	0.08	2.95	2.35	2.51	0.30	0.00
O2	2.21	1.47	0.63	0.76	1.08	0.98	0.73	0.91	1.28	0.04
O	0.18	0.16	0.07	0.14	0.22	0.14	0.09	0.10	0.17	0.11
O5	0.32	0.15	0.12	0.12	0.16	0.29	0.14	0.13	0.11	0.00
TAL	98.45	96.35	93.74	86.12	93.45	88.68	92.10	94.30	97.99	87.69
	72	137	104	227	27	78	163	384	7	1992
	142	350	244	350	68	205	320	591	7	2900
	280	243	130	199	337	135	152	182	343	74
	28	29	15	23	32	9	21	21	47	11
	29	67	24	53	44	66	25	36	9	18
	98	78	81	104	96	102	90	131	96	57
	187	220	56	133	150	418	178	71	93	8
	12	1	73	106	2	62	105	113	7	*
	220	118	146	97	65	106	155	165	50	*
	11	5	9	10	2	9	12	15	2	0
	66	*	284	380	14	167	341	333	8	*
	*	2	5	10	10	11	10	13	12	1
	*	*	10	11	2	2	8	13	*	*
	11	5	24	29	10	1	27	29	2	3
	20	6	47	61	19	26	60	62	0	*
	16	5	20	28	7	13	21	22	4	*
	42	30	15	27	19	24	16	28	20	2

APPENDIX 4A Sample preparation for thermometric analysis

Before preparing a small number of samples as polished wafers for fluid inclusion studies, a larger number of potential samples were prepared as normal thin sections to allow the size, abundance and distribution of the inclusions to be examined. On the basis of these preliminary investigations samples were selected and small chips were cut with a surface area of approximately 3cms. One side of the chip was ground flat using 400 grade carborundum, and the sample was then mounted in expoxy casting resin. 3cm diameter rings were used for casting and these fitted round a base block prepared with silicon grease. The levelled face was placed face down on the base and the resin was added. After the resin had cured (normally 1-2) days the sample could be removed, and the uneven top face was cut to ensure that the two faces of the block were parallel. In order to remove the near-surface damage zone produced during the initial sawing, the surface of the exposed face was hand ground on a glass plate using progressively finer grades of carborundum. The final grade of carbonundum used was 1000, and in between each grade the sample was thoroughly cleaned in an ultrasonic bath.

After grinding, the sample was mounted on to a circular brass weight of the same diameter with low melting point wax to avoid overheating. Polishing was carried out using a 10" vibrolap, napped Pellon lap cloth and a slurrey of 3um alumina and water. The vibrolap worked best when 12 samples or more were polished at one time. Rubber "bumpers" were fitted to the brass weights to encourage them to rotate while walking round the lap. The polishing stage lasts for at least 24 hours, and during this time the lap was fitted with a plastic cover to prevent water evaporation.

After polishing, the sample was removed from the metal block and reverse mounted, polished face down, again using low melting point wax. A slow-speed diamond saw was used to trim off the excess material leaving a slice approximately 2mm thick. The sawn surface was then ground by hand to approximately the required thickness (0.4mm) using coarser grit (400 grade carborundum), then the lapping and polishing cycle outlined above was repeated. The final product is a doubly surfaced wafer with a high-quality polish on both sides. The wafer was removed from the resin mounting and broken into small pieces before being used for thermometric analysis.

APPENDIX 4B Calibration of the Linkam TH600 stage

Calibration of the Linkam stage using standard melting point chemicals

Before carrying out routine measurements on inclusions the heating-freezing stage was rigourously calibrated using ultra-pure chemicals with precisely known melting points. Careful calibration is particularly important for stages like the Linkam TH600 where the temperature sensor is set in the metal heating block some distance below the sample. Calibration of the stage allows discrepancies between the temperature read from the digital display and the actual temperature of the sample to be measured.

Practical procedures

For solid standards a very small amount of material was placed between two cover slips. The standard was then heated until melting occurred. Small amounts of impurities will cause a depression in the melting point, therefore the melting temperature of the last crystal was recorded, though in general melting occurred over a very narrow range.

Initially capillary tubes were used for liquid standards, but because it was very difficult to see anything due to internal reflections, this method was abandoned in favour of one using two cover slips. The cover slips were cleaned thoroughly with acetone prior to use, and were only handled with tweezers. A small drop of liquid was placed on the bottom cover slip, and this was covered with a second glass. Although this is not the recommended method for liquids, (MacDonald and Spooner 1981; Roedder 1984), the technique worked well except for very volatile liquids, e.g. chloroform and toluene, when the procedure had to be performed very quickly before evaporation occurred. The liquid standards were frozen, and the temperature of the solid⇒liquid transition was recorded on reheating.

Calibration curve

Figure A1 shows the calibration curve for the Linkam TH600 stage used in this study over a temperature of -95 °C to +400 °C. The graph relates the correction factor ΔT, which is the difference between the true melting temperature of the standard and the actual melting temperature observed, to the temperature read on the digital display. ΔT varies from -1 °C to +3 °C, and any read temperature on an inclusion was corrected for the drift in temperature simply by adding ΔT.

Table A-1 gives a list of the substances used for the temperature calibration and their melting points.

Table A-1 Substances used for calibration

Substance	Melting point oC
Toluene	-95.0
Chloroform	-63.8
Metaxylene	-47.8
Decane	-29.7
CCl4	-22.8
N-dodecane	-9.6
H2O	0.4
Phenyl benzoate	6.9
Benzil	69.0
Urea	95.0
Benzanilide	135.0
Sodium nitrate	163.0
Potassium dichromate	398.0

It is recommended that the following substances are not used for calibration purposes: acetanilide, benzoic acid, 2-chlorobenzoic acid, succinic acid and 4-chlorobenzoic acid. These substances were tested as potential standards, but they proved to be unsuitable because substantial amounts of thermal decomposition occurred prior to melting

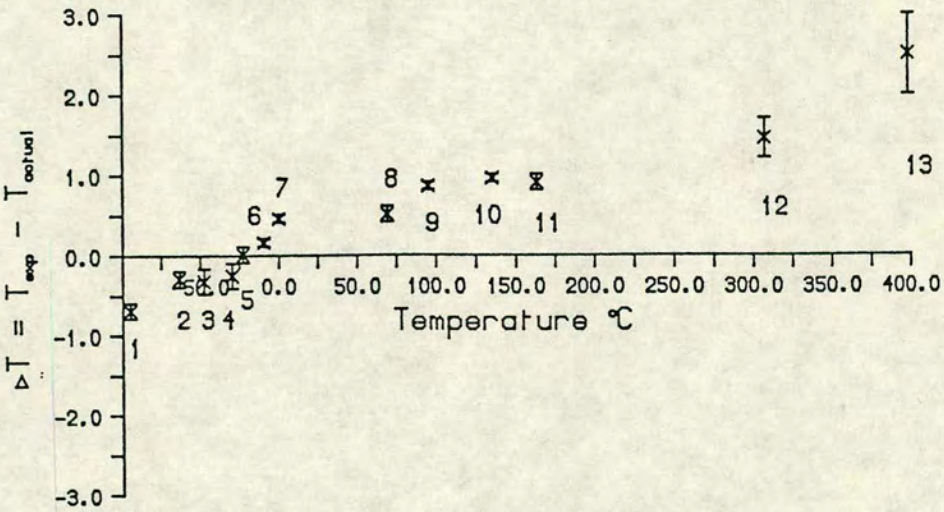

1- Toluene (-95)
2- Chloroform (-63.8)
3- Metaxylene (-47.8)
4- Decane (-29.7)
5- CCl4 (-22.8)
6- N-dodecane (-9.6)
7- H20 (0.0)
8- Phenyl Benzoate (69)
9- Benzil (95)
10- Urea (135)
11- Benzanilide (163)
12- Sodium Nitrate (306.8)
13- Pottasium dichromate (398)

Figure A1 Calibration curve for the Linkam TH600 stage. Numbers refer to the standard melting point chemicals used.

APPENDIX 5 Published work (in press)

submitted to Mineralogical Magazine,
special issue, arising from contributions
to ECROFI X, 1989.

Fluid inclusion studies in a high grade blueschist terrain, Syros, Greece.

Hazel Barr
Grant Institute of Geology, West Mains Road, Edinburgh EH9 3JW

This paper presents preliminary fluid inclusion data from a larger intergrated study combining mineral equilibria, stable isotope and fluid inclusion data in investigating fluid-rock interactions during blueschist and greenschist facies metamorphism.

Geological Setting

This study was undertaken on the Cycladic island of Syros, which is located some 150 km to the southeast of Athens in the Aegean sea. The Cycladic islands form part of a regional blueschist belt known as the Attico-Cycladic massif which stretches from mainland Greece to Turkey, and Figure 1 shows the geologic setting of the belt. $^{40}Ar/^{39}Ar$ cooling ages on micas give an Eocene date for the high pressure metamorphism (Wijbrans and Schliestedt 1988). Superimposed on the blueschist assemblages is a regional greenschist metamorphic overprint, which culminated in the local development of thermal domes, such as that seen on the neighbouring island of Naxos. Rb/Sr and K/Ar age determinations on micas give late Oligocene to early Miocene dates for this second metamorphic phase (Altherr et al 1979; Schliestedt et al 1987). Relics of the high pressure metamorphism can be found throughout the Cyclades, but some of the best preserved blueschists occur on the islands of Syros, Tinos and Sifnos.

Figure 2 shows a simplified geological map of Syros. The rocks are predominantly metasedimentary, and comprise a continuous sequence of alternating marbles and pelitic schists with some intercalated metabasites.

Metamorphic Evolution

The metamorphic conditions for the blueschist event are relatively well constrained. Figure 3 is a P-T plot indicating the critical phase equilibria for the island. The assemblages jadeite and quartz, zoisite, paragonite and quartz, and the occurrence of lawsonite without jadeite indicate temperatures between 450 to 500 ^{o}C at a minimum pressure of 14 Kbars (Dixon 1969; Ridley 1982).

Superimposed on the blueschist assemblages is a static, partial greenschist overprint associated with uplift of the terrain. Accompanying this overprint is the breakdown of

glaucophane bearing assemblages and the development of chlorite, calcite, albite and actinolite.

Isotopic evidence suggests that the blueschist to greenschist transformation is accompanied by variable degrees of infiltration, though in general the volume of infiltrating fluid involved is low.

Aims of the fluid inclusion study

Observations and measurements on fluid inclusions were used to answer some specific questions:

1. Do the blueschist metamorphic fluid compositions predicted by mineral equilibria studies correspond to the compositions of any fluid inclusions in the rocks ?

2. Have samples of an early, synmetamorphic fluid been preserved ?; and if so, can they be recognised?

3. Does a difference in composition exist between the fluid inclusions associated with the unaltered blueschists and those associated with the altered greenschists, either in terms of the CO_2/H_2O ratio or salinity of the fluid?

4. Does the retrograde fluid have a distinctive signature?

Mineral-fluid equilibria in the blueschists

This study has largely concentrated on carbonate-bearing metasediments, and detailed petrographic work has been carried out on the blueschist rocks to establish the composition of the fluid in equilibrium with the mineral assemblages. Various important reaction equilibria for the blueschist metasediments in T-X_{CO2} space are shown on figure 4. Schreinemakers analysis was used to assemble the curves around the invariant points, and shifts in the positions of the curves due to real mineral compositions have been calculated using appropriate activity-composition relationships.

Two important points can be made concerning the blueschist fluid. Firstly, individual samples, collected from a single outcrop, contain mineral assemblages which record differences in the equilibrium fluid composition. In terms of the T-X_{CO2} diagram, this means that the fluid composition in equilibrium with the different rock layers, often sampled on a scale of centimetres, will plot in separate areas of the net. Differences

existing on such a small scale suggest that the rock layers have controlled or buffered the composition of the co-existing fluid, and that very little, if any, external fluid has been involved.

The second point to emerge from the T-X_{CO2} net is that the composition of the fluid in equilibrium with the blueschist mineral assemblages is very water rich, with considerably less than 0.1 mol% CO2 present.

The question arising from these conclusions is, 'Do these predicted fluid compositions correspond to the compositions of any fluid inclusions found in the blueschists ?'

Fluid inclusion studies: techniques

After preliminary optical investigation with a standard petrological microscope, samples were selected and prepared as polished wafers with a high quality polish obtained on both sides (Shepherd et al 1985). The average thickness of the wafers is 0.3mm.

Data on homogenisation and melting temperatures of the inclusions was obtained by thermometric analysis using a Linkam TH600 stage. The stage was attached to a general purpose Zeiss petrological microscope fitted with a long working distance objective lense and substage condenser. An overall magnification of x400 was possible. Positioning of the samples was aided by x-y manipulators.

Selection of Study material

A number of the inclusions present in the blueschists are undoubtedly of secondary origin, occurring along healed fractures which cross several grain boundaries. When trying to pinpoint possible inclusions containing samples of an early or synmetamorphic fluid, a degree of screening was applied to the inclusions measured.

The inclusions chosen were either isolated from trails, occurring individually or as part of small intragranular clusters, or part of short trails which did not cross grain boundaries.

The material chosen for study was also carefully selected. Only matrix quartz material or small and texturally early quartz segregations were used when investigating the blueschist fluid. Plate 1 shows an example of one such quartz segregation. There is only one high strain deformational event on Syros which is synchronous with the blueschist facies metamorphism, and this allows deformed and boudinaged segregations, such as that shown, to be confidently assigned to the blueschist event (Ridley 1982).

Fluid inclusion results

1) Blueschists - inclusions in quartz

Figure 5 shows the thermometric data collected from a small quartz segregation in a glaucophane-garnet metabasite. The fluid picture in this sample appears relatively simple, with the histograms showing a single clear peak. Salinity values range from 6 to 9 wt% NaCl equilvalent, and homogenisation temperatures from 170 to 210 °C were recorded. The spread of homogenisation temperatures associated with a reasonably constant salinity value probably indicates necking down of the inclusions during uplift (Pecher 1981; Yardley 1983).

Some of the blueschist samples contain inclusions which are much more saline. Figure 6 illustrates one such sample containing several generations of inclusions, which can be distinguished both compositionally, and spatially.

The first group are highly saline, and some of the inclusions contain a halite daughter phase. These inclusions occur either as isolated groups, or along short intragranular fractures. The second group are clearly later, occurring in apparently randomly oriented trails which transect several grain boundaries. Figure 7 shows the thermometric data for this sample, and as can be seen, the fluid inclusions forming the later trails are much less saline than the earlier isolated inclusions. Some of the scatter seen in the two-phase aqueous inclusions may be due to rupturing of early saline inclusions and subsequent mixing with lower salinity fluids. Two types of homogenization were observed in the halite-bearing inclusions, and these are indicated on Figure 7. First melting temperatures in the highly saline inclusions were observed at -50 °C, which indicates the presence of $CaCl_2$. In these highly saline inclusions, phase transitions in addition to T_{fm} and T_m must have occurred although they were not directly observed. The final melting temperature observed (usually around -24 °C) will in fact refer to the melting of hydrohalite and should strictly be referred to as $T_m$hy. The overall salinity of these inclusions was determined from the halite dissolution temperature, T_sNaCl. The possible significance of the relatively early high-salinity inclusions will be discussed in more detail later.

Inclusions in garnet

Almost all the inclusions present in the blueschist rocks occur in quartz, and while quartz has the advantage of being stable in most rock types, its presence cannot be related to any specific metamorphic event. However some rare fluid inclusions were also found in

garnet, and one such example is illustrated in plate 2. This almandine-grossular garnet grew under blueschist conditions, and therefore there is a good chance that these inclusions may be trapped samples of the primary fluid.

The inclusions are relatively large, up to 15 microns long, and tend to be elongate and quite flat. They occur as small irregularly-distributed clusters near the core of the garnet. Their habit is quite different from the negative crystal inclusion shapes described by Berglund and Touret (1976) from garnets in Madagascar, yet there is no reason to suspect that these inclusions are secondary.

The inclusions contain aqueous fluids, though, as can be seen from Figure 8, the salinity of these fluids is quite low, at around 4 wt% NaCl equiv. Homogenisation temperatures range from approximately 200 to 270 ^{o}C, a similar spread to that seen in the other blueschist samples. Again the spread of homogenisation temperatures probably reflects density changes which occurred during uplift. Also shown in Figure 8 are measurements made on isolated inclusions present in the matrix quartz. Interestingly a large proportion of these early inclusions are highly saline, similar to the inclusions seen in the previously described samples.

2) Greenschists

Four samples showing the greenschist overprint were studied in order to make comparisons with the blueschist samples. Quartz veins or segregations were studied from samples which showed partial or complete development of the greenschist facies overprint, and it was hoped that these might contain samples of the fluid responsible for the retrogression.

Figure 9 shows data collected from a quartz segregation in altered blueschists. The inclusions in this sample are large and abundant, and nearly all of them are part of large transgranular trails. Again all the inclusions seen are aqueous and, as indicated by Figure 9, they appear to be recording a single fluid event, with salinities in the bracket 6 to 9 wt% NaCl equivalent and homogenisation temperatures from 150 to 190 ^{o}C. Other greenschist samples show a clear bimodal grouping of salinities with values up to 20 wt% NaCl equiv. being measured. This bimodal grouping indicates the presence of at least two distinct fluid populations, and the more saline inclusions may be a 'memory population' related to the earlier blueschist event.

Summary of results

The properties of the inclusions measured in the blueschists are summarised below.

- At room temperature the inclusions consisted of an outer liquid phase and an inner vapour bubble.

- Homogenisation temperatures were invariably greater than 100 °C.

- Solidification of the inclusions occured in the temperature range -25 to -80 °C.

- First melting temperatures, when observed, were lower than the eutectic temperature for the NaCl-H_2O system (Te = -20.8 °C, Crawford 1981a). The small amounts of melt produced and the small size of the inclusions, most are less than 12 microns in diameter, make accurate measurements of first melting difficult. Values obtained clustered around -35 °C, which may indicate the presence of $MgCl_2$ in addition to NaCl (Crawford 1981a). Melting was observed in some of the saline inclusions at temperatures as low as -50 °C, pointing to the presence of $CaCl_2$.

- Final melting occurred in the range -12 to 0 °C, except for the highly saline inclusions where final melting occurred at much lower temperatures, around -25 °C, and referred to the melting of hydrohalite rather than ice.

Having summarised the findings for the blueschist samples it can be stated that the inclusions which are thought to be early are dominantly two phase aqueous inclusions with a variable salinity from almost pure water to halite saturation. There is no apparent difference in the CO_2/H_2O ratio of the fluid found in schist samples containing different mineral assemblages, however it is likely that this observation merely reflects the fact that the equilibrium CO_2/H_2O ratio is so low that slight variations in the CO_2 content of the fluid between samples are impossible to detect thermometrically.

Comparing the data for inclusions measured in blueschist and greenschist samples a number of similarities between the two groups are apparent. Firstly, in both cases, the inclusions are of the two phase aqueous type. The two groups also show a very similar range of homogenisation temperatures, from 110 to 370 °C. The main difference is that the blueschist samples contain inclusions which are much more saline than anything found in the greenschists.

Discussion

The saline inclusions

The saline inclusions in the blueschists appear to be some of the earliest fluids preserved. Until recently the sporadic occurrence of halite-saturated inclusions in metamorphic

rocks tended to be dismissed as an enigmatic curiosity unless they could be directly related to the presence of nearby evaporitic sequences (Rich 1979). There is certainly no evidence for the presence of an evaporite deposit at depth on Syros, but Na-bearing phases are present in the blueschists, e.g, glaucophane and paragonite, and perhaps the presence of Na-rich inclusions simply reflects the mineralogy of the host rocks. In fact the situation must be more complicated, since although the presence of Na-bearing phases means that the synmetamorphic fluid was probably saturated with respect to sodium, chloride ions must also have been present in order to form NaCl. In these rocks it is likely that the availability of the chloride ion, presumably inherited from the original pore fluid, is the important factor in determining whether the fluid will become saturated in NaCl or not.

Participation in hydration reactions could cause low salinity fluids to become more saline, as was suggested by Crawford et al (1979a) and, given that sufficient chloride was present, halite saturated inclusions could be produced by this mechanism. Such a mechanism of evolving salinity with time could explain the presence of low salinity fluids in the garnet core of sample #76, and saline fluids in the external matrix quartz. An early sample of the fluid could have been preseved within the garnet, while subsequent hydration reactions modified the salinity of the remaining fluid later trapped in the quartz.

Conclusions

In conclusion, on the amount of data gathered so far it is not possible to state conclusively that the fluid inclusions present in the blueschists represent samples of the synmetamorphic fluids. However the absence of a CO_2 phase, and the abundance of aqueous inclusions is compatible with the equilibrium phase assemblages. There are very few documented cases of aqueous inclusions in high-grade metamorphic rocks, largely because much of the fluid inclusion work on metamorphic rocks has concentrated on CO_2-dominated granulite terrains, where H_2O-bearing inclusions are invariably dismissed as being secondary. However, examples of very early H_2O inclusions are now being reported from granulite terrains, and there are indications that these could be contemporaneous with the early CO_2-rich fluids. The recent discovery of halite cubes in decrepitated inclusions in granulites is also being interpreted as evidence for the presence of very early highly saline aqueous fluids (J. Touret 1989 pers. comm.).

Unfortunately it is not possible to calculate meaningful isochores for the blueschist samples for two reasons. Firstly, the relatively low homogenisation temperatures, compared to the metamorphic temperatures estimated from phase equilibrium studies

(450 ^{o}C), suggest that the inclusions have not preserved their original densities. Secondly, the available PVT data on aqueous saline solutions are limited to measurements made at low pressure, up to 2 kbars (Haas 1976; Potter and Brown 1977). The linear extrapolation of isochores up to 14 kbars is not justifiable.

The inclusions present in the greenschist samples are largely of secondary origin, and whether these represent samples of the infiltrating greenschist fluid is debatable. However, in terms of a relative chronology these fluids appear to be later than the fluids sampled in the blueschists, but the greenschist samples are probably recording several fluid events which occurred during the later history of the rocks.

In addition to the abundant aqueous inclusions there are a number of intragranular trails composed of very small dark inclusions. These, presumably vapour rich inclusions, are much too small to examine using normal thermometric techniques. Although these inclusions are insignificant compared to the aqueous inclusions, in terms of abundance, their mode of occurrence suggests that they may be remnants of an early fluid phase..

It is possible that these inclusions are in fact nitrogen-rich. Recent studies are discovering more and more evidence for the presence of nitrogen rich inclusions in granulite and eclogite terrains, although the origin and significance of these inclusions is not yet fully understood (Schreurs 1984; Swanberg 1981; Touret 1981; Touret and Dietvorst 1983). It is hoped that the composition of some of these inclusions in the blueschists will be established using the laser raman probe at the University of Amsterdam.

Acknowledgements

I am grateful to all the participants at ECROFI X for helpful discussion. Thanks are due to S. Elphick, B. Foster, A. Rankin and B. Yardley for encouragement and technical assistance, and to C.M. Graham and J.E. Dixon for reading early versions of the manuscript and providing constructive comments. Lastly, special thanks to J. Kinnaird, University of St. Andrews, for introducing me to fluid inclusions, and for all the subsequent time, effort and support she has given in assisting me to carry out this study.

Appendix - sample descriptions

Sample #	sample type
32	quartz segregation
Host rock:	altered blueschist metasediment
Mineralogy:	qtz-dol-cc-chl-w.mica-rutile

Sample #	sample type
76	whole rock blueschist metasediment
Mineralogy:	gl-w.mica-qtz-gnt-law(psd)-cc-rut

Sample #	sample type
77	whole rock blueschist metasediment
Mineralogy:	law(psd)-qtz-w.mica-gl-gnt-cc-dol
	chl-sphene

Sample #	sample type
190	qtz segregation
Host rock:	gl-gnt metabasite
Mineralogy:	gl-epid-omphacite-gnt-qtz-w.mica
	rutile

References

Altherr, R., Schliestedt, M., Okrusch, M., Seidel, E., Kreuzer, H., Harre, W., Lenze, H., Wendt, I. and Wagner, G.A., (1979) Geochronology of high pressure rocks on Sifnos (Cyclades, Greece) Contrib. Mineral. Petrol., 70, 245-255.

Bickle, M. J. and Powell, R. (1977) Calcite-dolomite geothermometers for the iron-bearing carbonates: the Glockner area of the Tauren Window, Austria. Contrib. Mineral. Petrol., 59, 281-292.

Berglund, L. and Touret, J. (1976) Garnet-biotite gneiss in 'Système du Graphite' (Madagascar): Petrology and fluid inclusions Lithos 9, 139-148.

Crawford, M. L., (1981a) Phase equilibria in aqueous fluid inclusions. In Short Course in Fluid Inclusions: Applications to petrology, vol. 6, (L. S. Hollister and M. L. Crawford eds.) Mineralogical Association of Canada, 157-181.

Crawford, M. L., Filer, J. and Wood, C., (1979a) Saline fluid inclusions associated with retrograde metamorphism. Bull. Mineral. 102, 562-568.

Dixon, J. E. (1969) The metamorphic rocks of Syros, Greece. Unpubl. Ph. D. thesis, University of Cambridge.

Haas, J.L. (1976) Physical properties of the coexisting phases and thermochemical properties of the H_2O component in boiling NaCl solutions (Preliminary steam tables for NaCl solutions), U.S. Geol. Surv. Bull. 1421-A.

Pecher, A. (1981) Experimental decrepitation and re-equilibration of fluid inclusions in synthetic quartz. Tectonophysics 78, 567-83.

Potter, R. W. II and Brown, D. L. (1977) The volumetric properties of aqueous sodium chloride solutions from 0o to 500 oC at pressures up to 2000 bars based on a regression of available data in the literature. U. S. Geol. Surv. Bull. 1421-C.

Powell, R. (1978) Equilibrium thermomdynamics in petrolgy: an introduction. Harper and Row: London.

Powell, R. and Holland, T. J. B. (1988) An internally consistent dataset with uncertainties and correlations: 3. Applications to geobarometry, worked examples and a computer program. J. metamorphic Geol. 6 173-204.

Powell, R. and Evans, J. (1983) A new geobarometer for the assemblage biotite-muscovite-chlorite-quartz. Contrib. Mineral. Petrol.

Rich, R. A. (1979) Fluid inclusion evidence of Silurian evaporites in south-east Vermont. Geol. Soc. Am. Bull., 90 1628-1643.

Ridley, J. R. (1982) Tectonic style, strain history and fabric development in a blueschist terrain, Syros, Greece. unpubl. Ph. D. thesis, University of Edinburgh.

Schiestedt, M., Altherr, R. and Matthews, A., Evolution of the Cyclades crystalline complex: Petrology, isotope geochemistry and geochronology. In Chemical Transport in Metasomatic Processes (H. C. Helgeson ed.), Reidel Publishing Company, (1987) 389-428.

Schreurs, J. (1984) The amphibolite-granulite transition in West Uusimaa, S. W. Finland. A fluid inclusion study. J. metamorphic geol. 2, 327-341.

Shepherd, T. J., Rankin, A. H., and Alderton, D. H. M., A practical guide to fluid inclusion studies. Blackie and Son Ltd., (1985) pp 237.

Swanenberg, H. E. C., (1980) Fluid inclusions in high-grade metamorphic rocks from S. W. Norway. Ph. D. thesis, State university of Utrecht, Geologica Ultraiectina, 25 147.

Touret, J. (1981) Fluid-inclusions in high grade metamorphic rocks. In L. S. Hollister and M. L. Crawford (eds.) Short courses in Fluid Inclusions: Applications to Petrology, vol. 6, Mineralogical association of Canada, 182-208.

Touret, J. and Dietvorst, P. (1983) Fluid Inclusions in high-grade anatectic metamorphites. J. geol. Soc. London, 140, 635-649.

Wijbrans, J. R., York, D. and Schliestedt, M., (1988) Laser probe 40Ar/39Ar age spectra of single crystals of phengite from the Cycladic blueschist belt, Greece. EOS 69, 518

Yardley, B. W. D. (1983) Quartz veins and devolatilization during metamorphism. J. Geol. Soc. London, 140, 657-663.

Figure and plate captions

Figure 1 Geologic setting of the Cycladic blueschist belt (from Blake et al, 1985), the island of Syros is highlighted.

Figure 2: Simplified geological map of Syros (after Dixon Ridley 1985).

Figure 3: Critical reaction equilibria defining the primary crystallisation field of the Syros blueschists.

Figure 4: T-X_{CO2} diagram for the system Na_2O-CaO-Al_2O_3 -MgO-SiO_2-H_2O-CO_2 calculated for 14 kbars. Shown are some reaction equilibria and phase relations amoungst the minerals glaucophane (a_{gl}=0.055[a]); paragonite(a_{pg}=0.900[b]); lawsonite (a_{law}=0.954[a]); clinochlore (a_{clin}=0.051[c]); clinozoisite (a_{ep}=0.136[b]); Ca-carbonate (a_{cc}=0.995[d]) and dolomite (a_{dol}=0.678[d]).
Source of activity formulations;
a=ideal mixing on sites; b=Powell (1978); c=Powell and Evans (1983); d=Bickle and Powell (1977).
No temperature difference between the mineral assemblages is implied.

Figure 5 Thermometric data for sample #190, a fuller description of the samples is given at end of the paper.

Figure 6: Sketch of sample #77, showing the spatial relationships between the early intragranular saline inclusions, and the later transgranular trails of low-salinity inclusions.

Figure 7: Thermometric data for sample #77. Fluid inclusions were studied in both matrix quartz and a small qtz segregation, but no significant compositional or density differences were detected between the inclusions populations in the two settings.

Figure 8: Thermometric data for sample 76. The shaded blocks in the frequency histograms refers to the thermometric data collected from inclusions in garnet, as oppose to the surrounding matrix quartz, sample #76

Figure 9: Thermometric data from a quartz-ankerite segregation in altered bluechist metasediments, sample #32

Plate 1: Field photograph of an early boudinaged quartz segregation in a blueschist metasediment.

Plate 2: Photomicrograph of fluid inclusions in garnet


Attica
Athens
Evvia
Andros
Kea
Ylaros
Tinos
Mykonos
Kithnos
Syros
Serifos
Naxos
Paros
Sifnos
Amorgos
Milos
Sikinos
Ios
Folegandros
Thira
Anafi
Astypalia
Turkey
Samos
Ikaria
Leros
blueschist facies
greenschist to amphibolite facies
granitoid plutons
allochthonous non-metamorphic units
recent volcanics
N
0
50km

1.

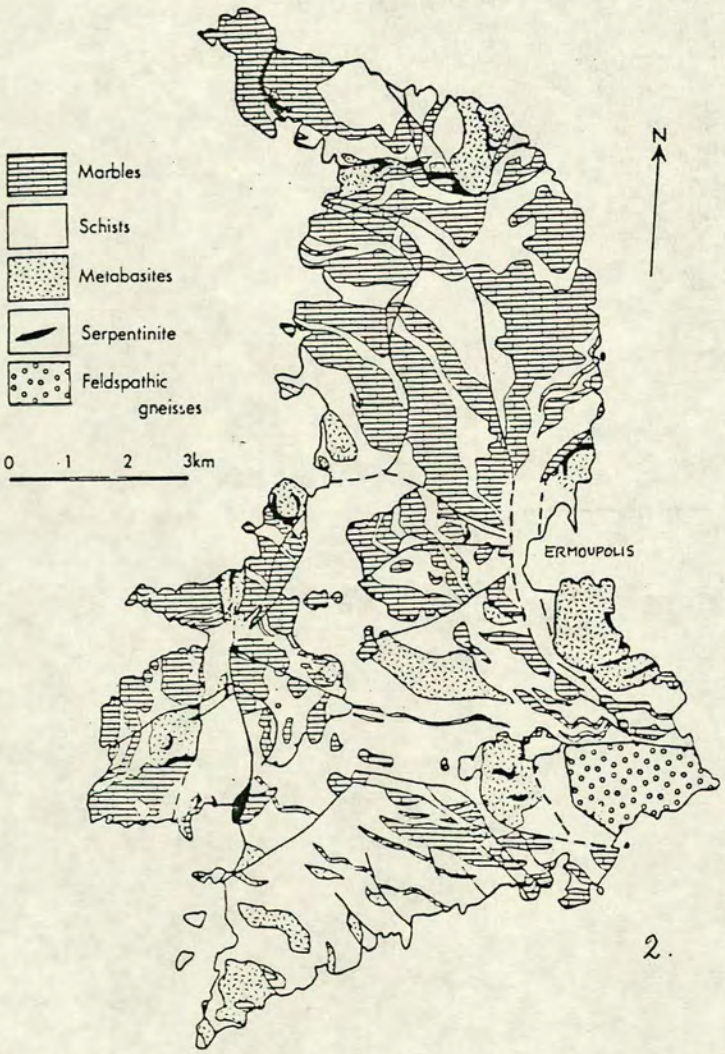
Marbles
Schists
Metabasites
Serpentinite
Feldspathic gneisses
0 1 2 3km
N
ERMOUPOLIS

2.

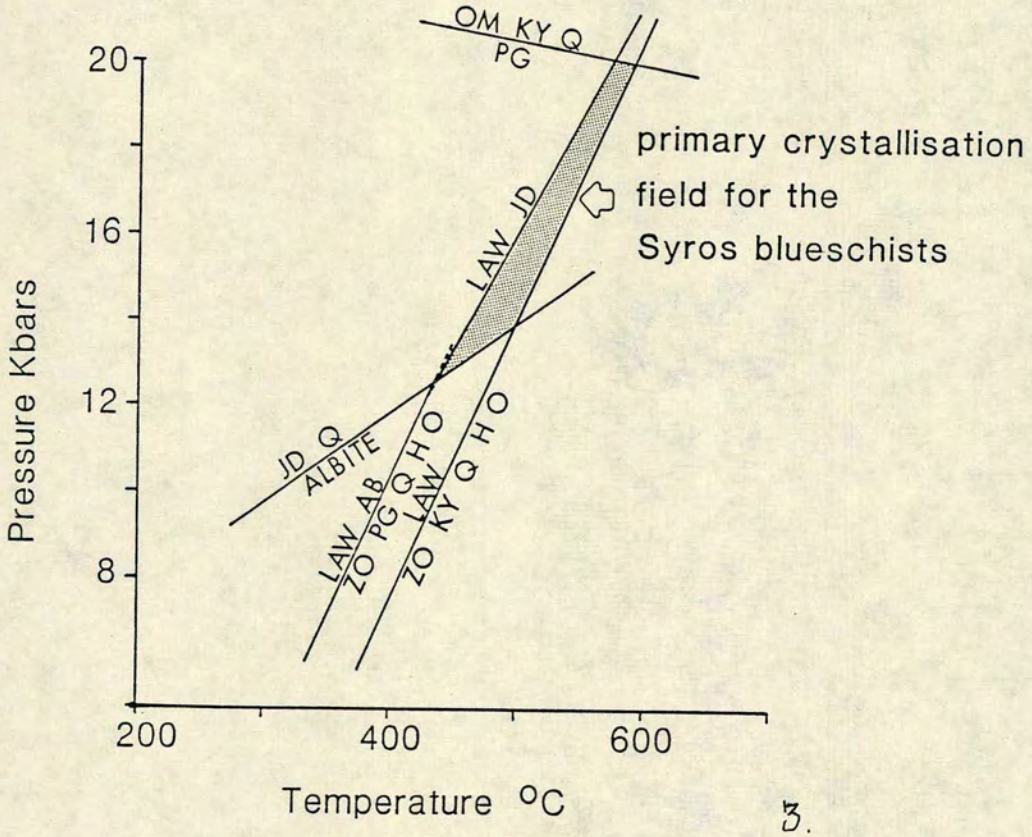
OM KY Q
PG
LAW JD
JD Q
ALBITE
LAW AB
ZO PG Q H O
LAW
ZO KY Q H O
primary crystallisation
field for the
Syros blueschists
20
16
12
8
Pressure Kbars
200
400
600
Temperature °C

3.

All assemblages plus quartz and phengite

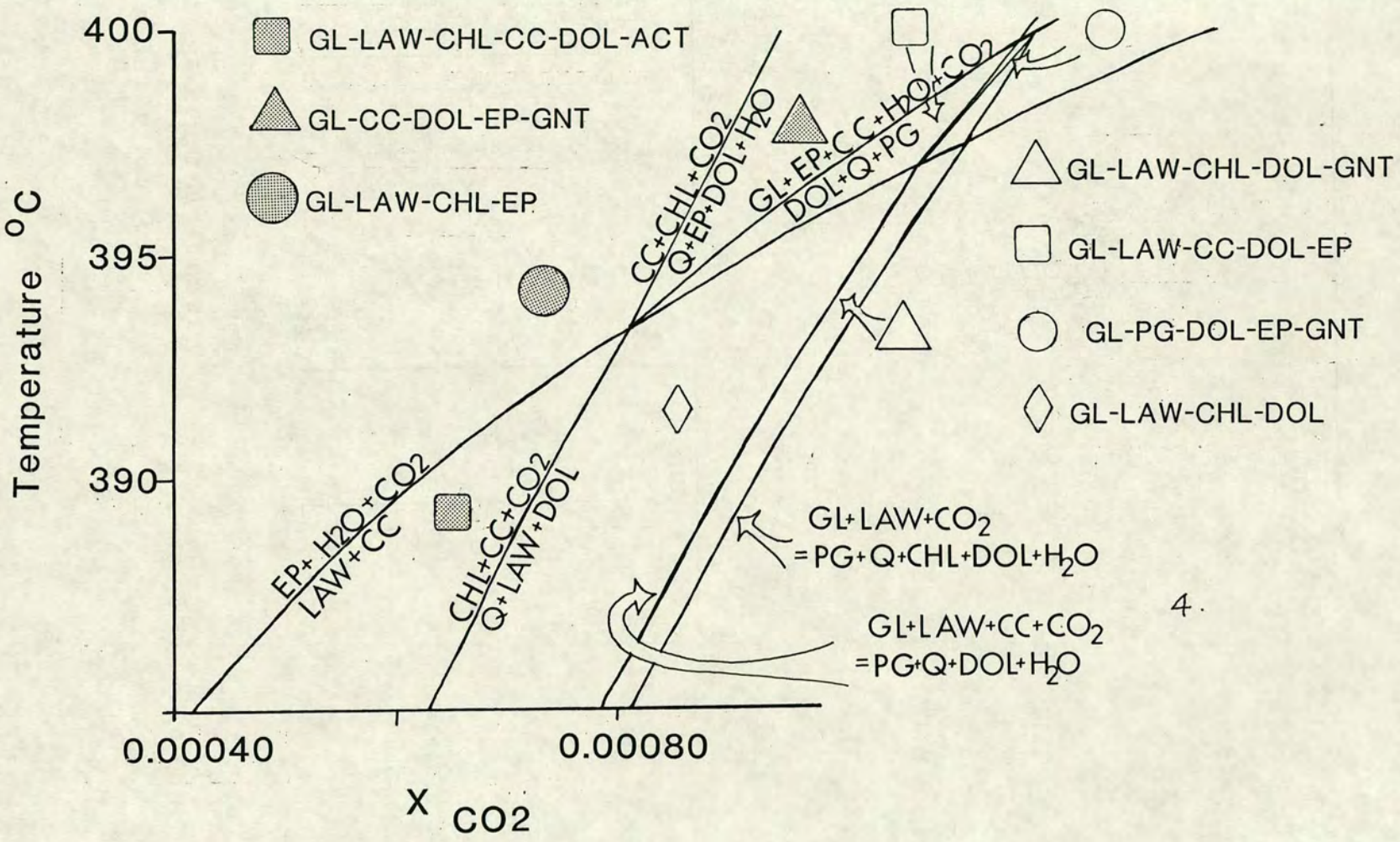

4.

qtz segregation from

gl-gnt bearing metabasite

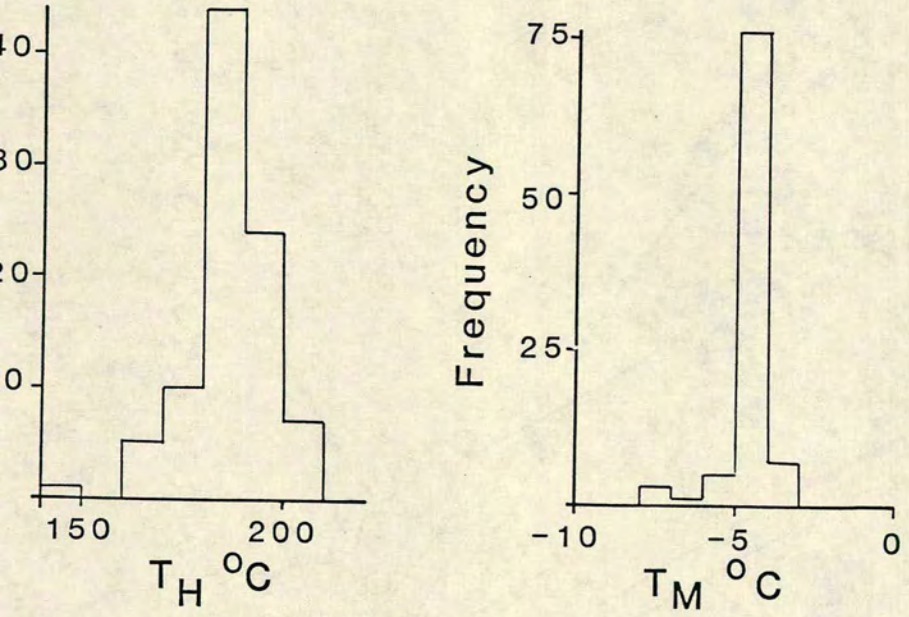

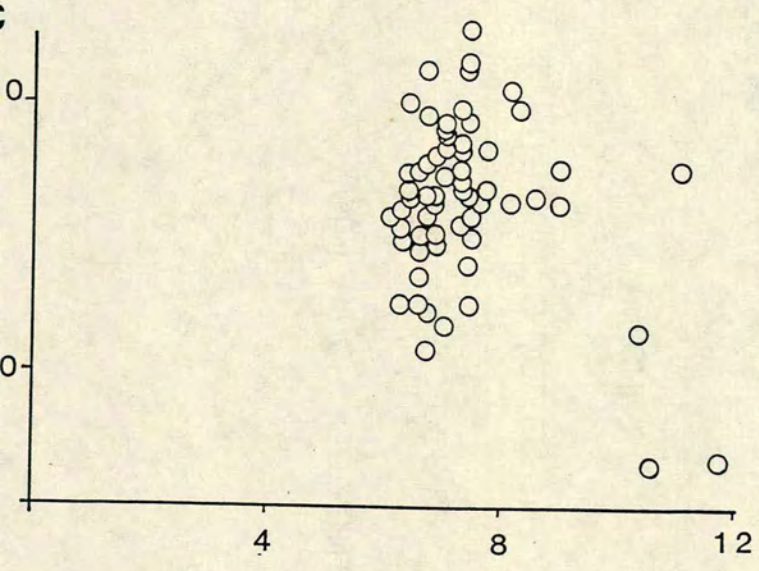

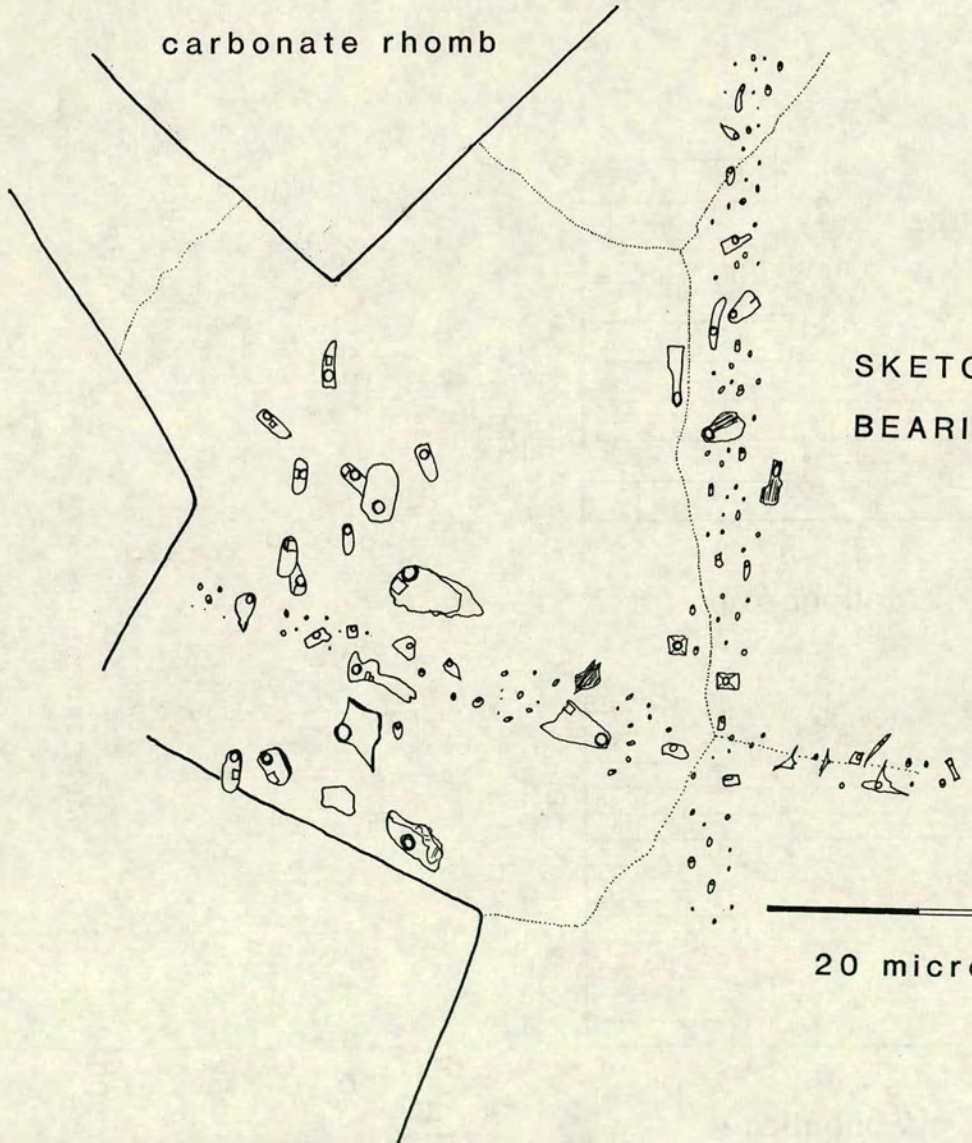

SKETCH OF HALITE
BEARING INCLUSIONS

6.

gl–gnt blueschist

inclusions measured in both

matrix quartz and a small qtz segregation

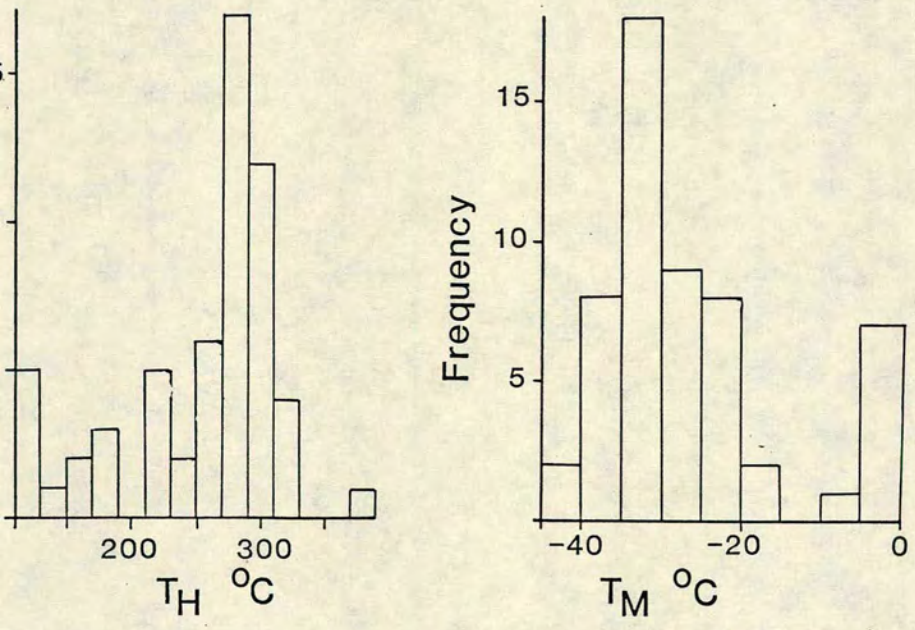

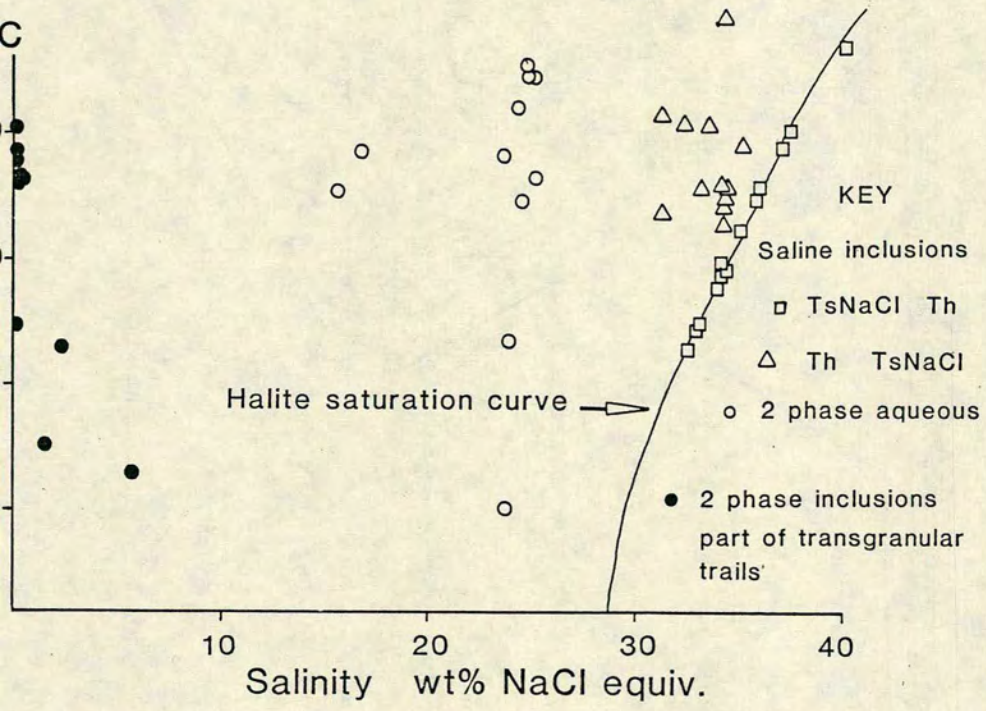

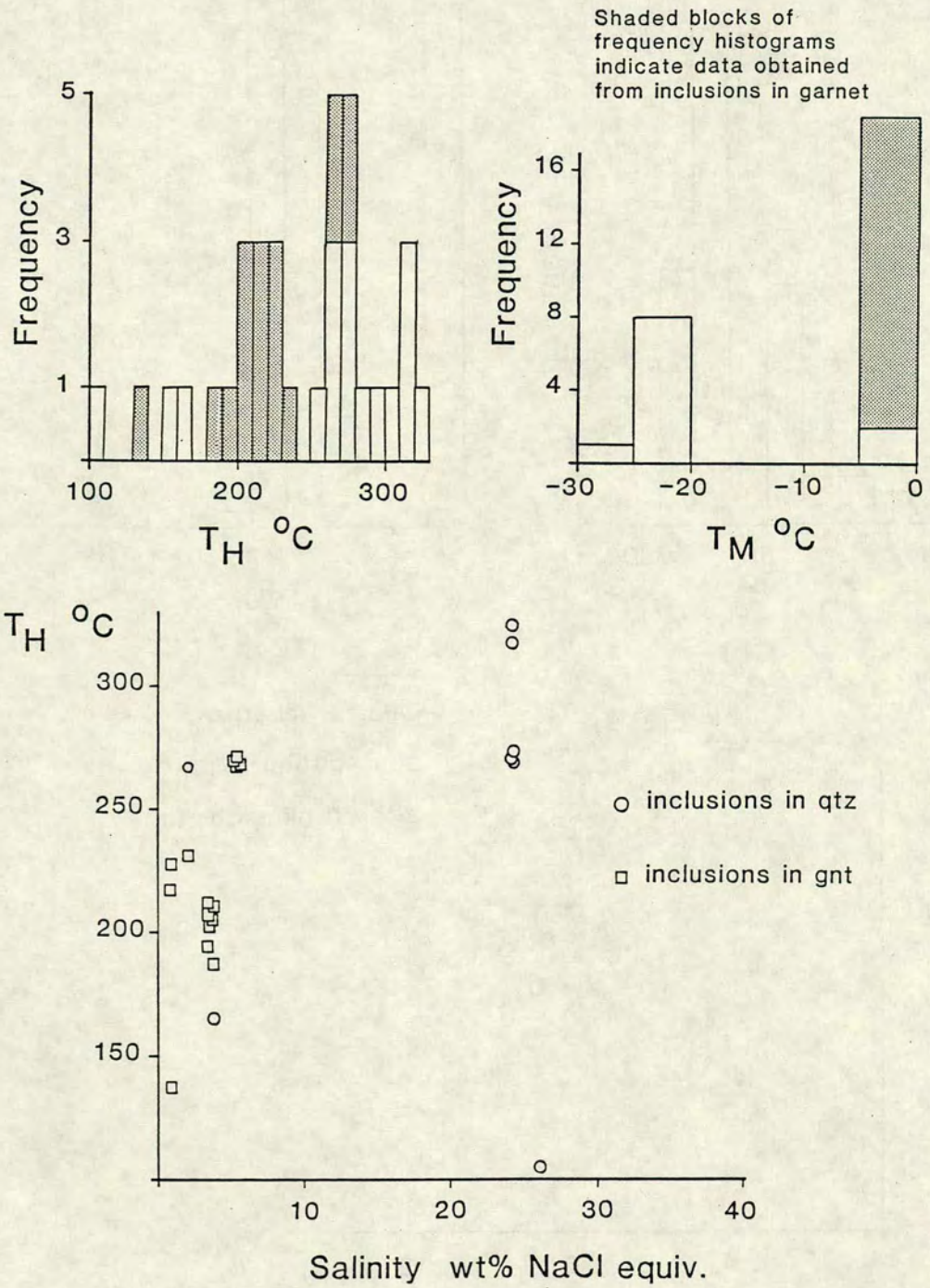
Shaded blocks of frequency histograms indicate data obtained from inclusions in garnet
Frequency
5
3
1
100
200
300
T_H °C
Frequency
16
12
8
4
−30
−20
−10
0
T_M °C
T_H °C
300
250
200
150
10
20
30
40
Salinity wt% NaCl equiv.
inclusions in qtz
inclusions in gnt

8.

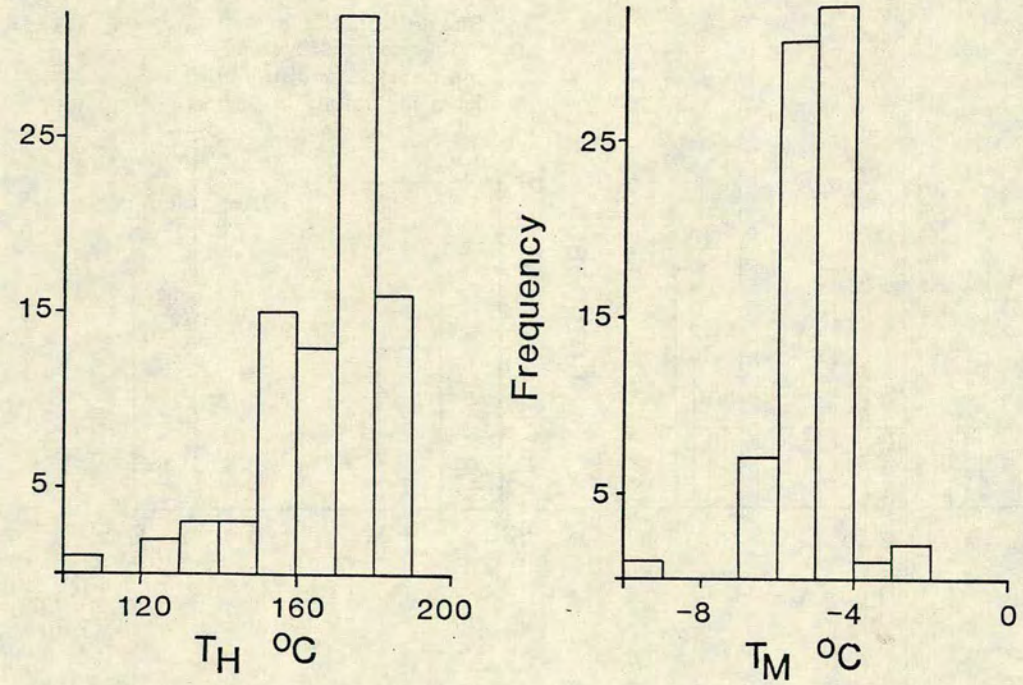

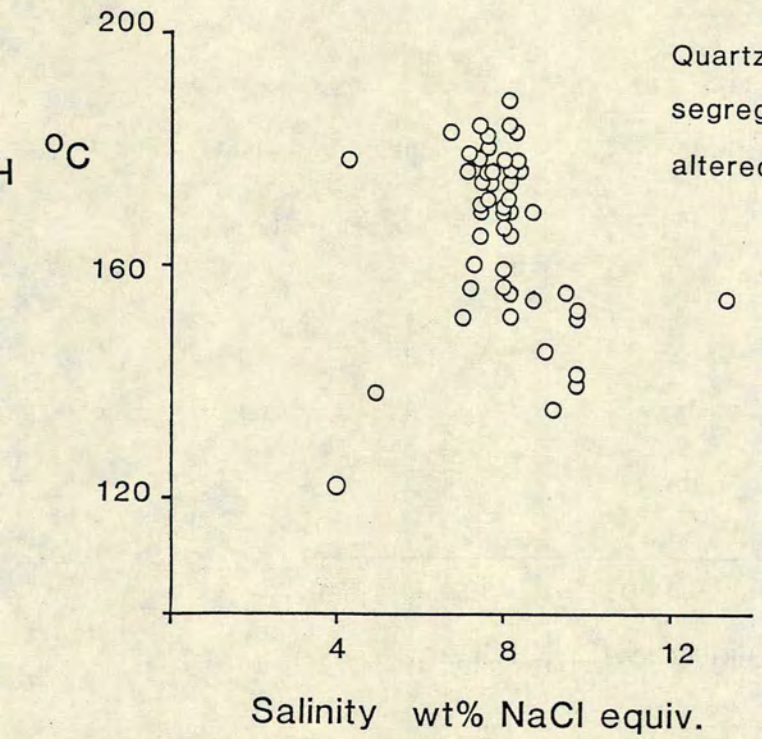

Quartz Ankerite segregation in partly altered blueschists

REFERENCES

Abraham, K. and Schreyer, W. (1976). A talc-phengite assemblage in piemontite schist from Brezovica, Servia, Yugoslavia. *J. Petrol.* **17**, 421-439.

Adams, A.E., Mackenzie, W.S. and Guilford, C. (1984). Atlas of sedimentary rocks under the microscope. Longmans 102pp.

Albee, A.L. (1965). A petrogenetic grid for the Fe-Mg silicates of pelitic schists. *Am. Jour. Sci.*, **263**, 512-536.

Altherr, R., Schliestedt, M., Okrusch, M., Seidel, E., Kreuzer, H., Harre, W., Lenz, H., Wendt, I. and Wagner, G.A. (1979). Geochronology of high-pressure rocks on Sifnos (Cyclades, Greece). *Contrib. Mineral. Petrol.* **70**, 245-255.

Anderson, A.T. (1967). The dimensions of oxygen isotopic equilibrium attainment during prograde metamorphism. *J. Geol.* **75**, 323-332.

Anderson, R.N., De Long, S.E. and Schwarz, W.H. (1977). Thermal model for subduction with dehydration in the downgoing slab. *J. Geol.* **86**, 731-739.

Anovitz, L.M. and Essene, E.J. (1987). Phase Equilibria in the system $CaCO_3$-$MgCO_3$-$FeCO_3$. *J. Petrol.* **28**, 389-414.

Baker, J., Bickle, M.J., Buick, I.S. and Matthews, A.M. (1989). Detailed isotope studies on marble bands, Naxos, Greece: Evidence for H_2O rich fluid infiltration during M2 metamorphism. Terra, abstracts **1**, 301.

Bebout, G.E. and Barton, M.D. (1989). Fluid flow and metasomatism in a subduction zone hydrothermal system: Catalina schist terrane, California. Submitted to Geology.

Bell, T.H. (1985). Deformation partitioning and porphyroblast growth in metamorphic rock: a radical reinterpretation. *J. Metamorphic. Geol.* **3**, 109-118.

Bell, T.H. (1986). Foliation development and refraction in metamorphic rocks: reactivation of earlier foliations and decrenulation due to shifting patterns of deformation partitioning. *J. Metamorphic Geol.* **4**, 421-

Bell, T.H. and Rubenach, M.J. (1983). Sequential prophyroblast growth and crenulation cleavage development during progressive deformation. *Tectonophysics*, **92**, 171-194.

Bell, T.H. Fleming, P.D., and Rubenach, M.J. (1986). Porphyroblast nucleation, growth and dissolution in regional metamorphic rocks as a function of deformation partitioning during foliation development. *J. Metamorphic. Geol.* **4**, 37-67.

Berglund, L. and Touret, J. (1976). Garnet-biotite gneiss in 'Système du Graphite' (Madagascar): Petrology and fluid inclusions. *Lithos*, **9**, 139-148.

Berman, R.G. and Brown, T.H (1985). Heat capacity of minerals in the system Na_2O-K_2O-CaO-MgO-FeO-Fe_2O_3-Al_2O_3-SiO_z-TiO_2-H_2O-CO_2 - representation, estimation and high T extrapolation. *Contrib. Mineral. Petrol.*, **89**, 168-183.

Best, N.F. (1977). Experimental studies of greenschist and amphibolite facies metamorphism of basic rocks. Unpubl. Ph.D. thesis Univ. of Edinburgh. Chpt. 3 - Activity-composition relations in epidote.

Bickle, M.J., and McKenzie, D.P. (1987). The transport of heat and matter by fluids during metamorphism. *Contrib. Mineral. Petrol*, **95**, 384-392.

Black, P.M. (1973). Mineralogy of New Caledonian metamorphic rocks II. Amphiboles from the Ouégoa District. *Contrib. Mineral. Petrol.* **39**, 55-64.

Black, P.M. (1974a). Oxygen isotope study of metamorphic rocks from the Ouégoa District, New Caledonia. *Contrib. Mineral. Petrol.* **47**, 207-214.

Black, P.M. (1974b). Mineralogy of New Caledonian Metamorphic Rocks III. Pyroxenes, and major element partitioning between coexisting pyroxenes, amphiboles and garnets from the Ouégoa District. *Contrib. Mineral. Petrol.* **45**, 281-288.

Black, P.M. (1975). Mineralogy of New Caledonian metamorphic rocks; IV sheet silicates from the Ouégoa District. *Contrib. Mineral. Petrol.* **49**, 269-284.

Blake, M.C., Banneau, M., Greyssant, J, Kienast, J.R., Lepvrier, C., Maluski, H. and Papanikolaou, D. (1981). A geologic reconnaissance of the Cycladic blueschist belt, Greece. *Geol. Soc. Am. Bull.* **92**, 247-254.

Bottinga, Y. and Javoy, M. (1975). Oxygen isotope partitioning among the minerals in igneous and metamorphic rocks. *Rev. Geophys. Space Phys.* **13**,, 401-418.

Bottinga, Y. and Javoy, M. (1973). Comments on oxygen isotope geothermometry. *Earth Planet. Sci. Lett.* **20**, 250-265.

Bowers, T.S. and Helgeson, H.C. (1983a). Calculation of the thermodynamic and geochemical consequences of nonideal mixing in the system H_2O-CO_2-NaCl on phase relations in geologic systems: Equations of state for H_2O-CO_2-NaCl fluids at high pressures and temperatures. *Geochim. Cosmochim. Acta* **47**, 1247-1275.

Bowers, T.S. and Helgeson, H.C. (1983b). Calculation of the thermodynamic and geochemical consequences of nonideal mixing in the system H_2O-CO_2-NaCl on phase relations in geologic systems: metamorphic equilibria at high pressures and temperatues. *Amer. Mineral*, **68**, 1059-1075.

Bowman, J.R., O'Neil, J.R. and Essene, E.J. (1985). Contact skarn formation at Elkhorn, Montana II. Origin and Evolution of C-O-H skarn fluids. *Am. J. Sci.* **285**, 621-600.

Brother, R.N. (1970). Lawsonite-albite schists from northern most New Caledonia. *Contrib. Mineral. Petrol.* **25**, 185-202.

Brown, E.H. (1968). The Si^{4+} content of natural phengites: A discussion. *Contrib. Mineral. Petrol.* **17**, 78-81.

Brown, E.H. (1974). Comparison of the mineralogy and phase relations of blueschists from the North Cascades, Washington and greenschists from Otago, New Zealand. *Bull. Geol. Soc. Amer.* **85**, 333-344.

Brown, E.H. and Forbes, R.B. (1986). Phase petrology of eclogitic rocks in the Fairbanks district, Alaska. In: *Blueschists and Eclogites* (Evans, B.L. and Brown, E.H. eds.) Geol. Soc. Am. Memoir, **164**, 155-167.

Brown, W.H., Fyfe, W.S, and Turner, F.J. (1962) Aragonite in Californian glaucophane schists, and the kinetics of the Aragonite-Calcite transformation. *J. Petrol.* **3**, 556-82.

Carlson, W.D. and Rosenfeld, J.L. (1981). Optical determination of topotactic aragonite. Calcite growth kinetics: metamorphic implications. *J. Geol.* **89**, 615-638.

Carman, J.H. and Gilbert, M.C. (1983). Experimental studies on glaucophane stability. *Am. J. Sci.* 283A, 414-437.

Castle, J.E., and Surman, P.L. (1969). The self-diffusion of oxygen in magnetite. The effect of anion vacancy concentration and cation distribution. *J. Phys. Chem*, **73**, 632-634.

Chapple, W.M. (1978). Mechanisms of thin-skinned fold and thrust belts. *Geol. Soc. Am. Bull.* **89**, 1189-1198.

Chatterjee, N.D. (1971). Phase equilibria in the Alpine metamorphic rocks of the Environs of the Dora-Maira-Massif, Western Italian Alps. *N. Jb. Miner. Abh.* **114**, 181-210.

Chopin, C. 1982. Magnesiochloritoid, a key mineral for the petrogenesis of high-grade blueschists. *Terra Cognita*, **2**, 331.

Chopin, C. (1981). Talc-phengite: a widespread assemblage in high-grade pelitic blueschists of the Western Alps. *J. Petrol.* **22**, 628-650.

Chopin, C. and Maluski, H. 1980. ^{40}Ar-^{39}Ar dating of high pressure metamorphic micas from the Gran Paradiso area (western Alps): evidence against the blocking temperature concept. *Contrib. Mineral. Petrol.* **74**, 109-122.

Clayton, R.N., Goldmsith, J.R., Karel, K.J., Mayeda, T.K. and Newton, R.C. (1975). Limits on the effect of pressure on isotope fractionation. *Geochim. Cosmochim. Acta.* **39**, 1197-1201.

Cloos, M. (1984). Flow melanges and the structural evolution of accretionary wedges. *Geol. Soc. Am. Spec. Paper*, **198**.

Cloos, M. 1984. Landward-dipping reflectors in accretionary wedges: Active dewatering conduits. *Geology*, **12**, 519-522.

Crawford, M.L. (1981b). Phase equilibria in aqueous fluid inclusions. In: *Mineralogical Association of Canada Short Course Handbook.* (Hollister, L.S and Carwford, M.L. eds.) **6**, 75-100.

Crawford, M.L. and Hollister, L.S. (1986). Metamorphic fluids: The evidence from fluid inclusions. In: *Fluid-Rock Interactions during metamorphism.* (Walther, J.V. and Wood, B.J. eds.). Advances in Physical Chemistry, V Springer Verlag. 1-36.

Crawford, M.L., Filer, J. and Wood, C. (1979a). Saline fluid inclusions associated with retrograde metamorphism. *Bull. Mineral.* **102**, 562-568.

Crawford, M.L., Kraus, D. and Hollister, L.S. (1979b). Petrologic and fluid inclusion study of calc-silicate rocks, Prince Rupert, British Columbia. *Am. J. Sci.* **9**, 1135-1159.

Dahlen, F.A., Suppe, J., and Davis, D., (1984). Mechanics of fold-and-thrust belts and accretionary wedges: Cohesive Coulomb theory. *J. Geophys. Res.* **89**, 10,087-10,101.

Deer, W.A., and Howie, R.A. and Zussman, J. (1966). An introduction to the rock forming minerals. Longman, London 528pp.

Deines, P. (1977). On the oxygen isotope distribution among mineral triplets in igneous and metamorphic rocks. *Geochim. Cosmochim. Acta.* **41**, 1709-1730.

Deines, P. and Gold, D.P. (1969). The change in C and O isotopic composition during contact metamorphism of the Trenton Limestone by the Mount Royal pluton. *Geochim. Cosmochim. Acta.* **33**, 421-424.

Degens, E.T. (1969). Biochemistry of stable carbon isotopes. In: *Organic geochemistry* (Eglinton, G. and Murphy, M.T.J. eds.). Springer-Verlag, New York.

Degens, E.T. and Epstein, S. (1964). Oxygen and carbon isotope ratios in coexisting calcites and dolomites from recent and ancient sediments: *Geochim. Cosmochim. Acta.* **28**, 23-44.

Dixon, J.E. (1969). The metamorphic rocks of Syros, Greece. Unpubl. Ph.D. thesis, Univ. of Cambridge.

Dixon, J.E. and Ridley, J.K. (1987). Excursion guide to the field trip on Serifos, Syros and Naxos. In: *Chemical transport in metasomatic processes* (Helgeson, H.C. ed.), 467-518. Reidel Publishing Company.

Draper, G. and Bone, R. (1981). Denudation rates, thermal evolution, and preservation of blueschist terrains. *J. Geology.* **89**, 601-613.

Dymoke, P.L. (1988). Geochronological and petrological studies of the thermal evolution of the Dalradian, South West Scottish Highlands. Unpublished Ph.D. thesis, Univ. of Edinburgh, pp444.

England, P.C. and Thompson, A.B. (1986). Pressure-temperature-time paths of regional metamorphism I. Heat trransfer during the evolution of regions of thickened continental crust. *J. Petrol.* **25**, 894-928.

Ernst, W.G. (1961). Stability relations of glaucophane. *Am. J. Sci.* **259**, 735-765.

Ernst, W.G. (1963). Petrogenesis of glaucophane schists. *J. Petrol.* **4**, 1-30.

Ernst, W.G. (1988). Tectonic history of subduction zones inferred from retrograde blueschist P-T paths. *Geology*, **16**, 1081-1084.

Essene, E.J. and Fyfe, W.S. (1967). Omphacite in Californian metamorphic rocks. *Contrib. Mineral. Petrol.* **15**, 1-23.

Etheridge, H.A., Wall, V.J., and Vernon, R.H. (1983). The role of the fluid phase during regional metamorphism and deformation. *J. Metamorphic Geol.* **1**, 205-226.

Eugster, H.P., Albee, A.L., Bence, A.E., Thompson, J.B. and Waldbaum, D.R. (1972). The two-phase region and the excess mixing properties of paragonite-muscovite crystalline solutions. *J. Petrol.* **13**, 147-179.

Evamy, B.D. (1967). Dedolomitization nd the development of rhombohedral pores in limestones. *J. Sed. Petrol.* **37**, 1204-1215.

Farver, J.R. and Giletti, B.J. (1985). Oxygen diffusion in amphiboles. *Geochim. Cosmochim. Acta.* **49**, 1403-1411.

Faure, G. (1977). Principles of isotope geology. John Wiley, New York 464pp.

Ferry, J.M. (1976). Metamorphism of calcareous sediments in the Waterville-Vassalboro areas, south-central Maine: mineral reactions and graphical analysis. *Am. J. Sci.* **276**, 841-882.

Ferry, J.M. (1980). A case study of the amount and distribution of heat and fluid during metamorphism. *Contrib. Mineral. Petrol.* **71**, 373-385.

Ferry, J.M. (1983a). Applications of the reaction progress variable in metamorphic petrology. *J. Petrol.* **24**, 343-376.

Ferry, J.M. (1983b). Regional metamorphism of the Vassalboro Formation, south central Maine, U.S.A.: a case study of the role of fluids in metamorphic petrogenesis. *J. Geol. Soc. Lond.* **140**, 551-576.

Ferry, J.M. (1983c). On the control of temperature, fluid composition and reaction progress during metamorphism. *Am. J. Sci.* **283-A**, 201-232.

Ferry, J.M. (1984). A biotite isograd in south-central Maine, U.S.A.: Mineral reactions, fluid transfer, and heat transfer. *J. Petrol.* **25**, 871-893.

Ferry, J.M. (1986). Reaction Progress: A monitor of fluid-rock interaction during metamorphic and hydrothermal events. In: *Fluid-rock interactions during metamorphism.* (Walther, J.V. and Wood, B.J. eds.). Advances in physical geochemistry **5**, 60-88.

Ferry, J.M. and Burt, D.M. (1982). Characterization of metamorphic fluid composition through mineral equilibria. In: *Characterization of metamorphic fluid composition through mineral equilibria.* (Ferry, J.M. ed.). Reviews in Mineralogy, **10**, Min. Soc. Am. 207-262.

Finger, L.W. and Burt, D.M. (1972). Reaction: a fortran IV computer program to balance chemical reactions. *Carnegie Inst. Washington Year Book.* **71**, 616-622.

Forbes, R.B., Evans, B.W. and Thurston, S.P. (1984). Regional progressive high-pressure metamorphism. Seward Peninsula, Alaska. *J. Metamorphic Geol.* **2**, 43-54.

Foster, M.D. (1962). Interpretation of the composition and classification of the chlorites. *Geol. Surv. Prof. Paper.* **414-A**.

Freer, R. and Dennis, P.F. (1982). Oxygen diffusion studies. I. A preliminary ion microprobe investigation of oxygen diffusion in some rock forming minerals. *Min. Mag.* **45**, 179-92.

Friedman, I. and O'Neil, J.R. (1977). Compilation of stable isotope fractionation factors of geochemical interest : *U.S. Geol Survey Prof. Paper.* **440K**, 12pp.

Frey, M. (1978). Progressive low grade metamorphism of a black shale formation, central Swiss Alps. *J. Petrol*, **19**, 95-135.

Frey, M., Hunziker, J.C., Jäger, E. and Stern, W.B. (1983). Regional distribution of white K-mica polymorphs and their phengite content in the Central Alps. *Contrib. Mineral. Petrol.* **83**, 185-197.

Frost, B.R. (1979). Mineral equilibria involving mixed volatiles in a C-O-H fluid phase : the stabilities of graphite and siderite. *Am. J. Sci*, **279**, 1033-1059.

Fyfe, W.S., Price, N.J. and Thompson, A.B. (1978). *Fluids in the Earth's Crust.* Elsevier, Amsterdam, 383pp.

Garlick, G.D. (1966). Oxygen isotope fractionation in igneous rocks. *Earth Planet. Sci. Lett.* **1**, 361-368.

Garlick, G.D. and Epstein, S. (1967). Oxygen isotope ratios in coexisting minerals of regionally metamorphosed rocks. *Geochim. Cosmochim. Acta.* **31**, 181-214.

Ghent, E.D., Stout, M.Z., Black, P.M. and Brothers, R.N. (1987). Chloritoid-bearing rocks associated with blueschists and ecologites, northern New Caledonia. *J. Metamorphic. Geol* **5**, 239-254.

Ghent, E.D., Robbins, D.B. and Stout, M.Z. (1979). Geothermometry, geobarometry an fluid compositions of metamorphosed calc-silicates and pelites, Mica Creek, British Columbia. *Am. Mineral.* **64**, 874-885.

Giletti, B.J. (1986). Diffusion effects on oxygen isotope temperatures of slowly cooled igneous and metamorphic rocks. *Earth Planet. Sci. Lett.* **77**, 218-228.

Giletti, B.J. (1985). The nature of oxygen transport within minerals in the presence of hydrothermal water and the role of diffusion. *Chemical. Geol*, **53**, 197-206.

Giletti, B.J. and Yund, R.A. (1984). Oxygen diffusion in quartz. *J. Geophys. Res.* **89**, 4039-4046.

Giletti, B.J. and Anderson, T.F., (1975). Studies in diffusion, II. Oxygen in phlogopite mica. *Earth Planet. Sci. Lett.* **28**, 225-238.

Graham, C.M. 1981. Experimental Hydrogen Isotope Studies III: Diffusion of hydrogen in hydrous minerals, and stable isotope exchange in metamorphic rocks. *Contrib. Mineral. Petrol.* **76**, 216-228.

Graham, C.M., Greig, K.M., Sheppard, S.M.F. and Turi, B. (1983). Genesis and mobility of the H_2O-CO_2 fluid phase during regional greenschist and epidote amphibolite facies metamorphism. *J. Geol. Soc. London.* **140**, 577-599.

Greenwood, H.J. (1975). Buffering of pore fluids by metamorphic reactions. *Am. J. Sci.* **275**, 573-593.

Gregory, R.T. and Taylor, H.P. Jr. (1981). An oxygen isotope profile in a section of Cretaceous oceanic crust, Semail Ophiolite, Oman: Evidence for $\delta^{18}O$ buffering of the oceans by Deep (>5km) seawater-Hydrothermal Circulation at Mid-Ocean Ridges. *J. Geophy. Res.* **86**, No. **B4**, 2737-2755.

Gregory, R.T. and Taylor, H.P. Jr. (1986a). Possible non-equilibrium oxygen isotope effects in mantle nodules an alternative to the Kyser-O'Neil-Carmichael $^{18}O/^{16}O$ geothermometer.

Gregory, R.T. and Taylor, H.P. Jr. (1986b). Non-equilibrium, metasomatic $^{18}O/^{16}O$ effects in upper mantle assemblages. *Contrib. Mineral. Petrol.* **93**, 124-135.

Gegory, A.R. and Backus, M.M. (1980). Geopressured formation parameters, geothermal well, Brazoria County, Texas. In: *Proceedings 4th U.S. Gulf Coast Geopressure-Geothermal Energy Conf.* (Dorfman, M.H. and Fisher, W.L. eds.), **1**, 235-311.

Guillot, C. and Moine, B. (1989). Relationships between N_2 in fluid inclusions and NH^{4+} in rocks (and micas) in the Dome de Montredon - Montagne Noire, France. In: *European Current Research on Fluid Inclusions, abstracts*, **41**. Royal School of Mines, Imperial College, London.

Haas, J.L. (1976). Physical properties of the coexisting phases and thermochemical properties of the H_2O component in boiling NaCl solutions (preliminary steam tables for NaCl solutions). *U.S. Geol. Surv. Bull*, **1421-A**.

Hausmann, J.F.L., (1845). Beiträge zur Orykrographie von Syra und ein neues Mineral, der glaucophan. *Göttingen Geologischen Anzeigen*, 193-198.

Helgeson, H.C., Delaney, J.R., Nesbitt, H.W. and Bird, D.K. (1978). Summary and critique of the thermodynamic properties of rock-forming minerals. *Am. J. Sci.* **278A**, 1-229.

Henjes-Kunst, F. and Kreuzer, H. (1982). Isotopic dating of Pre-Alpidic rocks from the island of Ios (Cyclades, Greece). *Contrib. Mineral. Petrol.* **80**, 245-253.

Hewitt, D.A. (1973). The metamorphism of micaceous limestones from south-central Connecticut. *Am. J. Sci.* **273A**, 444-469.

Hey, M.H. (1954). A new review of the chlorites. *Min. Mag.* **30**, 277-292.

Himmelberg, G.R. and Papike, J.J (1969). Coexisting amphiboles from the blueschist facies metamorphic rocks. *J. Pet.* **10**, 102-14.

Höck, V. (1974). Coexisting phengite, paragonite and margarite in metasediments of the Mittlere Hohe Tauern, Austria. *Contrib. Mineral. Petrol.* **43**, 261-273.

Hoefs, J. (1973). Stable isotope geochemistry. New York, Heidelberg, Berlin: Springer 140pp.

Hoefs, J. and Frey, M. (1976). The isotopic composition of carbonaceous matter in a metamorphic profile from the Swiss Alps. *Geochim. Cosmochim. Acta.* **40**, 945-951.

Holland, T.J. B. (1988). Preliminary phase relations involving glaucophane and applications to high pressure petrology: new heat capacity and thermodynamic data. *Contrib. Mineral. Petrol.* **99**, 134-142.

Holland, T.J.B. (1979a). High water activities in the generation of high pressure kyanite eclogites of the Tauern Window, Austria. *J. Geol.* **87**, 1-27.

Holland, T.J.B. and Powell, R. (1985). An internally consistent thermodynamic dataset with uncertainties and correlations: 2 data and results. *J. Metamorphic. Geol.* **3**, 343-370.

Holland, T.J.B. and Richardson, S.W. (1979). Amphibole zonation in metabasites as a guide to the evolution of the metamorphic conditions. *Contrib. Mineral. Petrol.* **70**, 143-148.

Holloway, J.R. (1981). Compositions and volumes of supercritical fluids in the Earth's crust. In: *Fluid inclusions : Applications to Petrology*, (Hollister, L.S. and Crawford, M.L. eds.). Mineral. Assoc. Canada., 13-38.

Hoscheck, G. (1980a). Phase relations of a simplified marly rock system with application to the Western Hohe Tauern (Austria). *Contrib. Mineral. Petrol.* **73**, 53-68.

Hoscheck, G. (1980b). The effect of Fe-Mg substitution on phase relations in marly rocks of the western Mohe Tauern (Austria). *Contrib. Mineral. Petrol.* **75**, 123-128.

Huebner, J.S. (1971). Buffering techniques for hydrostatic systems at elevated pressures. In: *Research Techniques for high Pressure and high temperature.* (Ulmer, G.C., ed.) Springer-Verlag, New York, 123-177.

Hunt, J.A. and Kerrick, D.M. (1977). The stability of sphene: experimental redetermination and geologic implications. *Geochim. Cosmochim. Acta.* **41**, 279-288.

Hunter, R.H. (1987). Textural equilibrium in layered igenous rocks. In: *Origins of igenous layering* (Parsons, I. ed.) Reidel publishing Co. 473-503.

Itaya, T., Brothers, R.N. and Black, P.M (1985). Sulphides, oxides and sphene in high pressure schists from New Caledonia. *Contrib. Mineral. Petrol.* **91**, 151-162

Jacobs, G.K. and Kerrick, D.M. 1987. Devolatilisation equilibria in H_2O-CO_2 and H_2O-CO_2-NaCl fluids : an experimental and thermodynamic evaluation at elevated pressures and temperatures. *Am. Mineral.* **66**, 1135-1153.

Jansen, J.B., and Schuiling, R.D., (1976). Metamorphism on Naxos: petrology and geothermal gradients. *Am. J. Sci.* **276**, 1225-1253.

Javoy, M. (1977). Stable isotopes and geothermometry. *J. Geol. Soc. Lond.* **133**, 609-636.

Javoy, M., Fourcade, S., and Allegre, C.J. (1970). Graphical method for examination of $^{18}O/^{16}O$ fractionations in silicate rocks. *Earth Planet. Sci. Lett.* **10**, 12-16.

Johannes, W. and Puhan, D. (1971). The calcite-aragonite transition reinvestigated. *Contrib. Mineral. Petrol.* **31**, 28-38.

Katagas, C. (1980). Ferroglaucophane and chloritoid-bearing metapelites from the phyllite series, southern Peloponnese, Greece. *Min. Mag.* **43**, 975-8.

Kay, R.L.F. (1979). Oxygen and hydrogen isotope ratio studies in Caledonian rocks of north-east Scotland. Unpubl. Ph.D. thesis, University of Aberdeen.

Keith, T.E.C., Muffler, L.J. and Cremer, M. (1968). Hydrothermal epidote formed in the Salton Sea geothermal system California. *Am. Mineral.* **53**, 1635-1644.

Keith, M.L. and Weber, J.N. (1964). Isotopic composition and environmental classification of selected limestones and fossils. *Geochim. Cosmochim. Acta.* **28**, 1787-1816.

Kerrick, D.M. (1974). Review of metamorphic mixed-volatile (H_2O-CO_2) equilibria. *Am. Mineral.* **59**, 729-762.

Kerrick, D.M. and Jacobs, G.K. (1981). A modified Redlich-Kwong equation for H_2O, CO_2 and H_2O-CO_2 mixtures at elevated pressures and temperatures. *Am. J. Sci.* **281**, 735-767.

Klein, C. (1969). Two amphibole assemblages in the system actinolite-hornblende-glaucophane. *Am. Mineral*, **54**, 212-237.

Kornprobst, J., Kienast, J. and Vilminot, J.C. (1979). The high-pressure assemblages at Milso, Greece: a contribution to the petrological study of the basement of the Cyclades Archipelago. *Contrib. Mineral. Petrol.* **69**, 49-63.

Koons, P.O. (1987). Some thermal and mechanical consequences of rapid uplift: an example from southern Alps, New Zealand. *Earth Planet. Sci. Lett.* **86**, 307-319.

Koons, P,O. (1982). An experimental investigation of the behaviour of amphibole in the system Na_2O-MgO-Al_2O_3-SiO_2-H_2O at high pressures. *Contrib. Mineral. Petrol.* **79**, 258-267.

Korzhinskii, D.S. (1959) Physico-chemical basis of the analysis of the paragenesis of minerals. New York, Consultants Bureau Inc., 142pp.

Kreulen, R. (1980). CO_2-rich fluids during regional metamorphism on Naxos (Greece): carbon isotopes and fluid inclusions. *Am. J. Sci.* **280**, 745-771.

Kreulen, R. and Schuiling, R.D. (1982). N_2-CH_4-CO_2 fluids during formation of the Dome de l'Agout, France. *Geochim. Cosmochim. Acta.* **46**, 193-203.

Land, L.S. (1980). The isotopic and trace element geochemistry of dolomite : the state of the art. *SEPM special publication.* **28**, 87-110.

Le Pichon, X. and Angelier, J. (1979). The Hellenic arc and trench system: A key to the neotectonic evolution of the eastern Mediterranean area. *Tectonophysics.* **60**, 1-42.

Leroy, J. (1979). Contribution to the evaluation of internal pressure in fluid inclusions when they decrepitate. *Bull. Mineral.* **102**, 584-593.

Liou, G. (1973). Synthesis and stability relations of epidote $Ca_2Al_2FeSi_3O_{12}(OH)$. *J. Petrol.* **14**, 381-413.

Liou, J.G. and Chen, P.Y. (1978). Chemistry and origin of chloritoid rocks from Eastern Taiwan. *Lithos*, **11**, 175-187.

McCrea, J.M. (1950). On the isotopic chemistry of carbonates and a paleotemperature scale. *J. Chem. Phys.* **18**, 849-857.

MacDonald, A.J. and Spooner, E.T.C. (1981). Calibration of a Linkam TH600 programmable heating-cooling stage for microthermometric examination of fluid inclusions. *Econ. Geol.* **74**, 1248-1258.

Maresch, W.V. (1977). Experimental studies on glaucophane: an analysis of present knowledge. *Tectonics.* **43**, 109-125.

Maresch, W.V. Hedenbach, O. and Rudolph, A. (1982). Winchite and the actinolite-glaucophane miscibility gap. *Nature.* **296**, 731-732.

Matsuhisa, Y., Goldsmith, J.R. and Clayton, R.N. (1979). Oxygen isotopic fractionation in the system quartz-albite-anorthite-water. *Geochim. Cosmochim. Acta.* **43**, 1131-1140.

Matthews, A. and Schliestedt, M. (1984). Evolution of the blueschist and greenschist facies rocks of Sifnos, Cyclades, Greece: a stable isotope study of subduction-related metamorphism. *Contrib. Mineral. Petrol.* **88**, 150-163.

Matthews, A., Goldmsith, J.R. and Clayton, R.N (1983). Oxygen isotope fractionations involving pyroxenes: the calibration of mineral-pair geothermometers. *Geochim. Cosmochim. Acta* **47**, 631-644.

Miyashiro, A. (1957b). The chemistry, optics and genesis of the alkali-amphiboles. *Tokyo Univ. Fac. Sci. J., Sec 2*, **22**, 57-83.

Miyashiro, A. and Banno, S. (1958). Nature of glaucophanitic metamorphism. *Am. J. Sci*, **256**, 97-110.

Moore, J.C. (1987). Expulsion of fluids from depth along a subduction zone decollement horizon. *Nature.* **326**, 785-788.

Muffler, L.J. and White, D.E. (1969). Active metamorphism of Upper Cenozoic sediments in the Salton sea geothermal field and Salton Trough, southeastern California. *Bull. Geol. Soc. Amer.* **80**, 157-182.

Nabelek, P.I., Labotka, T.C., O'Neil, J.R. and Papike, J.J. (1984). Contrasting fluid/rock interaction between the Notch Peak granitic intrusion and argillites and limestones in Western Utah: evidence from stable isotopes and phase assemblages. *Contrib. Mineral. Petrol.* **86**, 25-34.

Nagy, K.L. and Parmentier, E.M. (1982). Oxygen isotope exchange at an igneous intrusive contact. *Earth Planet. Sci. Lett.* **59**, 1-10.

Newton. R.C., Windley, B.F., and Smith, J.V. (1980). Carbonic metamorphism, granulites and crustal growth. *Nature.* **288**, 45-50.

Newton, R.C. and Kennedy, G.C. (1963). Some equilibrium reactions in the join $CaAl_2Si0_8$-H_2O. *J. Geophys. Res.* **68**, 2967-2983.

Nitsch, K.H (1974). Neve Erkentnisse zur Stabilität von Lawsonit. *Fortschr. Mineral.* **51**, 34-35.

Nitsch, K.H. (1972). Das P-T-X(CO_2) stabilitätsfeld von Lawsonit. *Contrib. Mineral. Petrol.* **34**, 116-134.

Norris. R.J. and Henley, R.W. 1976. Dewatering of a metamorphic pile. *Geology*, **4**, 333-336.

Northrop, D.A. and Clayton, R.N. 1966. Oxygen isotope fractionations in systems containing dolomite. *J. Geol.* **74**, 174-196.

O'Neil, J.R. (1977). Stable Isotopes in Mineralogy. *Phys. Chem. Minerals.* **2**, 105-123.

O'Neil, J.R. and Ghent, E.D. (1975). Stable isotope study of coexisting metamorphic minerals from the Esplanade Range, British Columbia. *Geol. Soc. Am. Bull.* **86**, 1708-1712.

O'Neil, J.R., Clayton, R.N. and Mayeda, T.K. (1969). Oxygen isotope fractionation in divalent metal carbonates. *J. Chem. Phys.* **51**, 5547-5558.

O'Neil, J.R. and Epstein, S. (1966). Oxygen isotope fractionation in the system dolomite-calcite-carbon dioxide. *Science*, **152**, 198-201.

Ohmoto, H. and Kerrick, D.M. (1970). Devolatilization equilibria in graphitic systems. *Am. J. Sci.* **277**, 1013-1044.

Papanikolaou, D. (1987). Tectonic evolution of the Cycladic blueschist belt (Aegean Sea, Greece). In: *Chemical transport in metasomatic processes.* (Helgeson, H.C. ed.) Reidel publishing company, 429-450.

Papanikolaou, D. (1980b). Contribution to the geology of Aegean Sea. The island of Paros. *Ann. Geol. Pays. Hellen.* **30**, 65-96.

Pattison, D.R.M. and Harte, B. (1985). A petrogenetic grid for pelites in the Ballachulish and other Dcottish thermal aureoles. *J. Geol. Soc. Lond.* **142**, 7-28.

Pecher, A. (1981). Experimental decrepitation and re-equilibration of fluid inclusions in synthetic quartz. *Tectonophysics.* **78**, 567-583.

Perkins, E.H., Brown, T.H. and Berman, R.G. (1986). PT-system, T-X-system, PX-system : three programs which calculate pressure-temperature-composition phase diagrams. *Computers & Geosciences*, **6**, 749-755.

Platt, J.P. (1986). Dynamics of orogenic wedges and the uplift of high-pressure metamorphic rocks. *Geol. Soc. Am. Bull.* **97**, 1037-1053.

Potter, R.W. II (1977). Pressure corrections for fluid inclusion homogenisation temperatures based on the volumetric properties of the system NaCl-H_2O. *J. Res. U.S. Geol. Surv.* **5**, 603-607.

Potter, R.W., Clynne, M.A. and Brown, D.L. (1978). Freezing point depression of aqueous sodium chloride solutions. *Econ. Geol.* **73**, 284-285.

Potter, R.W. II and Brown, D.L. (1977). The volumetric properties of aqueous sodium chloride solutions from O° to 500°C at pressures up to 2000 bars based on a regression of available data in the literature. *U.S. Geol. Surv. Bull.* **1421-C**.

Powell, R. (1978). Equilibrium thermodynamics in petrology. Harper and Row, London.

Powell, R. and Holland, T.J.B. (1988). An internally consistent dataset with uncertainties and correlations : 3. Applications to geobarometry, worked examples and a computer program. *J. Metamorphic Geol.* **6**, 173-204.

Powell, R. and Holland, T.J.B. (1985). An internally consistent thermodynamic dataset with uncertainties and correlations 1 Methods and a worked example. *J. Metamorphic Geol.* **3**, 327-342.

Reynard, B. and Ballèvre, M. (1988). Co-existing amphiboles in an eclogite from the Western Alps : new constraints on the miscibility gap between sodic and calcic amphiboles. *J. Metamorphic Geol.* **6**, 333-350.

Rice, J.M. (1977b). Contact metamorphism of impure dolomitic limestone in the Marysville aureole, Montana. *Am. J. Sci.* **277**, 1-24.

Rice, J.M. and Ferry, J.M. (1982). Buffering, infiltration, and the control of intensive variables during metamorphism. In: *Characterization of metamorphism through mineral equilibria.* (Ferry, J.M. ed.), pp 263-326. Mineral. Soc. Amer., Washington, DC.

Rich, R.A. (1979). Fluid inclusion evidence of Silurian evaporites in south-eastern Vermont. *Geol. Soc. Am. Bull.* **90**, 1628-1643.

Rickwood, (1968). On recasting analyses of garnet into end-member molecules. *Contrib. Mineral. Petrol.* **18**, 175-198.

Ridley, J. 1984. The significance of deformation associated with blueschist facies metamorphism on the Aegean island of Syros : In: *The Geological evolution of the eastern Mediterranean*, (Geol. Soc. Lond., spec. Publ No.17 (Dixon, J.E. and Robertson A.H.F. eds.) 545-551.

Ridley, J.R. (1982). Tectonic style, strain history and fabric development in a blueschist terrain, Syros, Greece. Unpubl. Ph.D. thesis, Edinburgh University 283pp.

Ridley, J.R. and Dixon, J.E. (1984). Reaction pathways during the progressive deformation of a blueschist metabasite: the role of chemical disequilibrium and restricted range equilibrium. *J. Metamorphic Geol.* **2**, 115-128.

Robinson, P., Spear, F.S., Schumacher, J.C., Laird, J., Klein, C., Evans, B.W. and Doolan, B.L. (1982). Phase relations of metamorphic amphiboles : natural occurrence and theory. In: *Amphiboles: petrology and experimental phase relations* (Veblen, D.R. and Ribbe, P.H. eds.). Reviews in mineralogy, 9B, Min. Soc. Am., 1-211.

Roedder, E. (1981a). Origin of fluid inclusions and changes that occur after trapping. In: *Mineralogic Association of Canada Short Course Handbook.* (Hollister, L.S. and Crawford, H.L. eds.) **6**, 101-137.

Roedder, E. (1981b). Problems in the use of fluid inclusions to investigate fluid-rock interactions in igneous and metamorphic processes. *Fortschr. Mineral.* **59**, 267-302.

Roedder, E. (1984). Fluid Inclusions. *Reviews in Mineralogy, 12.* Mineral. Soc. America.

Rodgers, J., Blake, M.C., Bonneau, M., Geyssant, J., Kienast, J.R., Lepvrier, C., Maluski, H. and Papanikolaou, D. (1984). A geologic reconnaissance of the Cycladic blueschist belt, Greece. Discussion and Reply. *Geol. Soc. Am. Bull.* **95**, 117-121.

Rumble, D. (1978). Mineralogy, petrology and oxygen isotope geochemistry of the Clough Formation, Black Mountain, Western New Hampshire, U.S.A. *J. Petrol.* **19**, 317-340.

Rumble, D. (1982). Stable isotope fractionation during metamorphic devolatilization reactions. In: *Characterization of metamorphism through mineral equilibria.* (Ferry, J.M. ed.) Reviews in Mineralogy 10, Mineral. Soc. Am., Washington, D.C., 327-353.

Rumble, D. and Spear, F.S. (1983). Oxygen-isotope equilibration and permeability enhancement during regional metamorphism. *J. Geol. Soc. London.* **140**, 619-628.

Rumble, D., Ferry, J.H., Hoering, T.C. and Boucot, A.C. (1982). Flud flow during metamorphism at the Beaver Brook fossil locality, New Hampshire. *Am. J. Sci.* **282**, 886-919.

Rye, R.O., Schuiling, R.D., Rye, D.M. and Jansen, J.B.H. (1976). Carbon, hydrogen and oxygen isotope studies of the regional metamorphic complex at Naxos, Greece. *Geochim. Cosmochim. Acta.* **40**, 1031-1049.

Salemink, J. (1987). Excursion guide to the field trip on Seriphos, Syros and Naxos. In: *Chemical transport in Metasomatic processes* (Helgason, H.C. ed.) Reidel publishing company 467-518.

Schliestedt, M. (1986). Eclogite-blueschist relationship as evidenced by mineral equilibria in the high pressure metabasic rocks of Sifnos (Cycladic Islands), Greece. *J. Petrol.* **27**, 1437-1459.

Schliestedt, M. (1980). Phasengleichgewichte in Hochdruckgesteinen von Sifnos, Griechenland. Unpubl. Ph.D. Universität Brounschweig.

Schliestedt, M. and Matthews, A. (1987). Transformation of blueschist to greenschist facies rocks as a consequence of fluid infiltration, Sifnos, (Cyclades), Greece. *Contrib. Mineral. Petrol.* **97**, 237-250.

Schliestedt, M., Altherr, R. and Matthews, A. (1987). Evolution of the Cycladic crystalline complex : Petrology, isotope geochemistry and geochronology. In: *Chemical Transport in Metasomatic Processes.* (Helgason, H.C. ed.) Reidel Publishing Company, 389-428.

Schreinemakers, F.A.H. 1915-1925. In-, mono-, and divariant equilibria (English edition): Koninkl. Akad. Wetenschappen te Amsterdam Prog. v18-28.

Schreurs, J. (1984). The amphibolite-granulite transition in West Uusimaa, S.W. Finland. A fluid inclusion study. *J. Metamorphic Geol.* **2**, 327-341.

Schreyer, W. and Baller, T. (1977). Talc-muscovite : synthesis of a new high-pressure phyllosilicate assemblage. *Neves Jahr. Mineral. Monatshefte.* **9**, 421-425.

Seidel, E., Okrusch, M. and Schubert, W. (1975). Chloritoid-bearing metapelites associated with glaucophane rocks in Western Crete, Greece. *Contrib. Mineral. Petrol.* **49**, 105-115.

Seki, Y. (1960). Jadeite in Sanbagawa crystalline schists of central Japan. *Am. J. Sci.* **258**, 705-715.

Sharma, T. and Clayton, R.N. 1965. Measurement of O^{18}/O^{16} ratios of total oxygen of carbonates. *Geochim. Cosmochim. Acta.* **29**, 1347-1353.

Shaw, D.M. 1956. Geochemistry of pelite rocks. Part III: Major elements and general geochemistry. *Bull. Geol. Soc. Amer.* **67**, 919-934.

Shepherd, T.J., Rankin, A.H. and Alderton, D.H.M. (1985). a practical guide to fluid inclusion studies. Blackie and Son Ltd. 237pp.

Sheppard, S.M.F. and Schwarcz, H.P. (1970). Fractionation of carbon and oxygen isotopes and mangesium between coexisitng metamorphic calcite and dolomite. *Contrib. Mineral. Petrol.* **26**, 161-198.

Shieh, Y.N. and Schwarcz, H.P. (1974). Oxygen isotope studies of granite and migmatite, Grenville province of Ontario, Canada. *Geochim. Cosmochim. Acta.* **38**, 21-45.

Sisson, V.B. Crawford, M.L. and Thompson, P.H. (1981). CO_2-brine immiscibility at high temperatures, evidence from calcareous metasedimmentary rocks. *Contrib. Mineral. Petrol.* **78**, 371-378.

Sorensen, S.S. (1988). Petrology of amphibolite-facies mafic and ultramafic rocks from the Catalina schist, southern California : metasomatism and migmatization in a subduction zone setting. *J. Metamorphic Geol.* **6**, 405-435.

Spear, F.S. and Kimball, K.L. (1974). RECAMP - A fortran IV program fore stimating Fe^{3+} content in amphiboles. Min. Soc. Am. Amphibole Short Course.

Spry, A. (1969). Metamorphic Textures. Pergamon Press, Oxford 350pp.

Swanenberg, H.E.C., (1980). Fluid inclusions in high-grade metamorphic rocks from S.W. Norway. Ph.D. thesis, State University of Utrecht, The Netherlands. *Geologica Ultraiectina*, **25**, 147pp.

Taylor, H.P. Jr (1977). Water/rock interactions and the origin of H_2O in granitic batholiths. *J. Geol. Soc. Lond.* **133**, 509-558.

Taylor, H.P. and Forester, R.W. (1979). An oxygen and hydrogen isotope study of the Skaergaard Intrusion and its country rocks : a description of a 55 m.y. old fossil hydrothermal system. *J. Petrol.* **20**, 355-419.

Taylor, H.P. Jr., and Coleman, R.G. (1968). $^{18}O/^{16}O$ ratios of coexisting minerals in glaucophane-bearing metamorphic rokcs. *Geol. Soc. Am. Bull.* **79**, 1727-1756.

Taylor, H.P., Jr. and Epstein, S. (1962a). Relationship between $^{18}O/^{16}O$ ratios in coexisting minerals of igneous and metamorphic rocks, parts I and II. *Bull. Geol. Soc. Amer.* **73**, 461-480; 675-694.

Taylor, H.P., Jr., Albee, A.L. and Epstein, S. (1963). $^{18}O/^{16}O$ ratios of coexisting minerals in three assemblages of kyanite-zone pelitic schist. *J. Geol.* **77**, 513-522.

Thelin, P. and Sartori, M. (1987). An occurrence of in situ synkinematic albitization (siviez-mischabel nappe, Valais, Switzerland). *Terra abstracts*, **1**, 137.

Thompson, A.B. (1983). Fluid-absent metamorphism *J. Geol. Soc. Lond.* **140**, 533-549.

Thompson, A.B. (1974). Calculation of muscovite-paragonite-alkali feldspar phase relations. *Contrib. Mineral. Petrol.* **44**, 173-194.

Thompson, A.B. and Ridley, J.R. (1987). Pressure-temperature-time (P-T-t) histories of orogenic belts. *Phil. Trans. Roy. Soc. Lond.* **A321**, 27-45.

Tómasson, J. and Kristmannsdóttir, H. (1972). High temperature alteration minerals and thermal brines, Reykjanes, Iceland. *Contrib. Mineral. Petrol.* **36**, 123-134.

Touret, J. (1981). Fluid-inclusions in high grade metamorphic rocks. In: *Short Course in Fluid Inclusions : applications to petrology*. (Hollister, L.S. and Crawford, H.L. eds.) Mineral. Association of Canada **6**, 182-208.

Touret, J. (1977). The significance of fluid inclusions in metamorophic rocks. In: *Thermodynamics in Geology*, (Fraser, C.D.G. ed.) 203-227, D. Reidel.

Touret, J. and Dietvorst, P. (1983). Fluid inclusions in high-grade anatectic metamorphites. *J. Geol. Soc. London.* **140**, 635-649.

Tracy, R.J., Rye, D.M., Hewitt, D.A. and Schiffries, C.M. (1983). Petrologic and stable isotopic studies of fluid-rock interactions, S-central Connecticut. *Am. J. Sci.* **283-A**, 589-616.

Tucker, M.E. (1981). Sedimentary Petrology: an introduction. Blackwell Scientific Publications 252pp.

Valley, J.W. (1986). Stable isotope geochemistry of metamorphic rocks. In: *Stable isotopes in high temperature geological processes* (Valley, J.W., Taylor, H.P. and O'Neil, J.R. eds.). Reviews in Mineralogy **16**, 445-490, Washington, DC.

Valley, J.W. and Essene, E.J. (1980). Akermanite in the Cascasde Slide Xenolith and its significance for regional metamorphism in the Adirondacks. *Contrib. Mineral. Petrol.* **74**, 143-152.

Van der Maar, P.A. (1981). Metamorphism on Ios and the geological history of the southern Cyclades, Greece. *Geologica Ultrajectina.* **28**, 1-142.

Velde, B. (1965). Phengite Micas : Synthesis, stability and natural occurrence. *Am. J. Sci.* **263**, 886-913.

Vrolijk, P., Myers, G. and Moore, J.C. (1988). Warm fluid migration along tectonic melanges in the Kodiak accretionary complex, Alaska. *J. Geophy. Res.* 93 10313-10324.

Walters, L.J. Jr., Claypool, G.E. and Choquette, P.W. (1972). Reaction rates and $\delta^{18}O$ variation for the carbonate-phosphoric acid preparation method. *Geochim. Cosmochim. Acta.* **36**, 129-140.

Walther, J.V. and Wood, B.J. (1984). Rate and mechanism in prograde metamorphism. *Contrib. Mineral. Petrol.* **88**, 246-259.

Walther, J.V. and Orville, P.M. (1982). Volatile production and transport in regional metamorphism. *Contrib. Mineral. Petrol.* **79**, 252-257.

Watkins, K.P. (1983). Petrogenesis of Dalradian albite porphyroblast schists. *J. Geol. Soc. London.* **140**, 601-618.

Welch, M.D. (1989). An experimental study of glaucophane-type amphiboles in the system Na_2O-MgO-Al_2O_3-SiO_2-SiF_4 (NMASF), with implications for natural systems. In press.

Wheeler, J. (1987). The significance of grain-size stresses in the kinetics of metamorphism. *Contrib. Mineral. Petrol.* **97**, 397-404.

Wickham, S.M. and Taylor, H.P. Jr. (1985). Stable isotopic evidence for large-scale seawater infiltration in a regional metamorphic terrane; the Trois Seigneurs Massif, Pyrenees, France. *Contrib. Mineral. Petrol.* **91**, 122-137.

Wickham, S.M. and Taylor, H.P. Jr. (1987). Stable isotope constraints on the origin and depth of penetration of hydrothermal fluids associated with Hercynian regional metamorphism and crustal anatexis in the Pyrenees. *Contrib. Mineral. Petrol.* **95**, 255-268.

Wilkins, R.W.T. and Barkas, J.P. (1978). Fluid inclusions, deformation and recrystallization in granite tectonites. *Contrib. Mineral. Petrol.* **65**, 293-299.

Wood, B.J. and Walther, J.V. (1986). Fluid flow during metamorphism and its implications for fluid-rock ratios. In: *Fluid-Rock interactions during metamorphism.* (Walther, J.V. and Wood, B.J. eds.). Advances in Physical Geochemistry, **5**, Springer-Verlag, New York.

Wyllie, P.J. (1987). Discussion of recent papers on carbonated peridotite, bearing on mantle metasomatism. *Earth Planet. Sci. Lett.* **82**, 391-7.

Wyllie, P.J. (1982). Subduction products according to experimental prediction. *Bull. Geol. Soc. Amer.* **93**, 468-76.

Wyllie, P.J. and Sekie, T. (1982). The formation of mantle phlogopite in subduction zone hybridisation. *Contrib. Mineral. Petrol.* **79**, 375-80.

Yardley, B.W.D. (1983). Quartz veins and devolatilization during metamorphism. *J. Geol. Soc. Lond.* **140**, 657-663.

Zen, E-An. (1966a). Construction of pressure-temperature diagrams for multicomponent systems after the method of Schreinemakers - a geometric approach: *U.S. Geol. Survey. Bull.* **1225**, 56p

Zen, E-An (1964). Coexisting muscovite and paragonite in pelitic schist. *Am. Mineral.* **49**, 904-925.

Zwart, H.J. (1962). On the determination of metamorphic mineral associations and its application to the Bosost area (Central Pyrenees). *Geol. Rundeschrau*, **52**, 38-65.